Trinity College Dublin
Coláiste na Tríonóide, Baile Átha Cliath
The University of Dublin

Limbic System Development in Children and Adolescents with Attention Deficit/Hyperactivity Disorder: A Longitudinal Multimodal MRI Analysis

Volume 1 of 2

Michael Connaughton

School of Medicine and Trinity College Institute of Neuroscience
Trinity College Dublin, University of Dublin

A thesis submitted to
Trinity College, University of Dublin
For the degree of
Doctor of Philosophy

Supervisors:
Prof. Jane McGrath
Prof. Robert Whelan
Dr. Erik O'Hanlon

2024

Declaration

I declare that this thesis has not been submitted as an exercise for a degree at this or any other university and it is entirely my own work.

I agree to deposit this thesis in the University's open access institutional repository or allow the Library to do so on my behalf, subject to Irish Copyright Legislation and Trinity College Library conditions of use and acknowledgement.

I consent to the examiner retaining a copy of the thesis beyond the examining period, should they so wish (EU GDPR May 2018).

Signed: Michael Connaughton 

Date: 14/02/24

Acknowledgments

First and foremost, I extend my heart felt gratitude to my primary supervisor, Prof. Jane McGrath. Her expertise, particularly in the realm of paediatric psychiatry, has been instrumental in shaping my academic journey. I greatly appreciate the time you gave me and the patience you showed me throughout. Our consistent weekly meetings, particularly during lockdown, were a source of calming guidance throughout this research process from start to finish. Thank you for all the advice, encouragement and support.

I also owe immense gratitude to my co-supervisors, Prof. Roberts Whelan and Dr. Erik O'Hanlon. Prof. Robert Whelan, I deeply appreciate your generosity in providing me with the resources needed to conduct this research. Your insights into statistical analyses and research methodologies have been truly invaluable. Dr. Erik O'Hanlon thank you for patiently teaching me all things MRI physics, MRI image processing and analyses, your expertise was treasured throughout this research journey.

I extend a warm thanks to my colleagues at the Whelan lab, both past and present. Special mentions go to Yihe Weng, Alannah Smyth, Tom Farnan, Jade Duffy and Julia Paterson, and Dr. Rory Boyle for their valuable contributions which have profoundly enriched my research journey. Additionally, I would like to thank my good friends Jivesh Ramduny and Michelangelo Domina, I treasured your friendship throughout my PhD experience.

A special nod of appreciation to my collaborators, Prof. Tim Silk and Prof. Alexander Leemans. Prof. Tim Silk, thank you very much for sharing the fantastic NICAP data set, this data set was incredible to work with and opened new horizons for my research. Prof. Alexander Leemans, thank you for your guidance with the ExploreDTI software, you were a constant source of neuroimaging expertise throughout my research.

Finally, my deepest appreciation goes to my family, who have supported me throughout this entire process. To my mom Maureen, my dad, Mike, and my brother Eric: your unwavering love, support, and sacrifices have sustained me throughout my unorthodox academic journey. Through thick and thin your unwavering support enabled me to pursue my passion.

I am deeply humbled by the support and guidance I've been fortunate to receive during this research endeavour. Without it, the research presented in this thesis would not be possible.

Table of Contents

List of Figures

List of Table

List of Abbreviations

A/P	Anterior/Posterior
AD	Axial Diffusivity
ADHD	Attention-Deficit Hyperactivity Disorder
ADRGL3	Adhesion G Protein-Coupled Receptor L3
AICc	Corrected Akaike Information Criterion
AK	Axial Kurtosis
ARI	Affective Reactivity Index
B	Regression Coefficient
BCT	Brain Connectivity Toolkit
BDNF	Brain-Derived Neurotophic Factor
BICc	Corrected Bayesian Information Criterion
CAI	Conner's 3 ADHD index
CDH13	Cadherin 13
CEMS	Children's Emotion Management Scales
CI	Confidence Intervals
cm	Centimeter
CNV	Copy Number Variants
CSD	Constrained Deconvolution
CSF	Cerebrospinal Fluid
DISC	Diagnostic Interview Schedule for Children
DKI	Diffusion Kurtosis Imaging
DKT	Desikan-Killiany-Tourville
dMRI	Diffusion-Weighted Magnetic Resonance Imaging
dODF	Diffusion Orientation Distribution Function
DOI	Digital Object Identifier
DSI	Diffusion Spectrum Imaging
DSM	Diagnostic and Statistical Manual of Mental Disorders
DTI	Diffusion Tensor Imaging
DWI	Diffusion-Weighted Image
ENIGMA	Enhanced Neuroimaging Genetics Through Meta-Analysis

EPI	Echo-Planar Imaging
ERC	Emotion Regulation Checklist
FA	Fractional Anisotropy
FBA	Fixel-Based Analysis
FC	Fibre Bundle Cross-Section
FDR	False Discovery Rate
FEFA	First Eigenvector-Fractional Anisotropy
FOD	Fibre Orientation Distribution
FOXP2	Forkhead Box Transcription Factor P2
FS-PFC	Frontstriatal Prefrontal Cortex
FX	Fixed Effect
GFA	Generalised Fractional Anisotropy
GRM1	Glutamate Receptor Metabotropic 1
GRM5	Glutamate Receptor Metabotropic 5
GRM7	Glutamate Receptor Metabotropic 7
GWAS	Genome-Wide Association Studies
HARDI	High Angular Resolution Diffusion Imaging
HREC	Human Research Ethics Committee
ICD	International Classification of Diseases
ICV	Intracranial Volume
IFOF	Inferior Fronto-Occipital Fasciculus
K-SADS-E	Kiddie Schedule for Affective Disorders and Schizophrenia for School-Aged Children
KA	Kurtosis Anisotropy
LMM	Linear Mixed-Effects Modeling
LPHN3	Latrophilin 3
LRT	Log-Likelihood Ratio Test
m	minute
MD	Mean Diffusivity
MEF2C	Myocyte-Specific Enhancer Factor 2C
MEMPRAGE	Multi-Echo Magnetization Prepared Rapid Gradient-Echo
MK	Mean Kurtosis
ML	Maximum Likelihood

MoCo	Motion Correction
MRI	Magnetic Resonance Imaging
ms	Millisecond
NICAP	Neuroimaging of the Children's Attention Project
NICE	National Institute for Health and Care Excellence
NMDA	N-Methyl-D-Aspartic Acid
NODDI	Neurite Orientation and Dispersion Density Imaging
NOS1	Nitric Oxide Synthase 1
OFC	Orbitofrontal Cortex
p	p-value
PARK2	Parkin RBR E3 Ubiquitin Protein Ligase
PCDH7	Protocadherin 7
PTPRF	Protein Tyrosine Phosphatase Recptor Type F
QC	Quality Control
RD	Radial Diffusivity
REM	Restricted Maximum Likelihood
RK	Radial Kurtosis
ROI	Regions of Interest
RX	Random Effect
s/mm^2	Seconds per Millimeter Squared
SD	Standard Deviation
SE	Standard Error
SEMA6D	Semaphorin 6D
SES	Socio-Economic Status
SLC6A4	Solute Carrier Family 6 Member 4
sMRI	Structural Magnetic Resonance Imaging
SNP	Single Nucleotide Polymorphism
SNR	Signal-to-Noise Ratio
SPACE	Sampling Perfection with Application Optimized Contrast with Flip Angle Evolution
ST3GAL3	ST3 Beta-Galactoside Alpha-2,3-Sialytransferase 3
t	t-score
T1	Longitudinal Relaxation Time

T2	Transverse Relaxation Time
TE	Echo Time
TIM	Total Imaging Matrix
TMCQ	Temperament in Middle Childhood Questionnaire
TR	Repetition Time
VBM	Voxel-Based Morphometry
WHO	World Health Organisation

Summary

While Attention-Deficit Hyperactivity Disorder (ADHD) is characterized by age-related changes in symptoms and brain structures during childhood and adolescence, the link between brain structure and function is less clear. Given that prior longitudinal magnetic resonance imaging (MRI) research has predominantly focused on cortical structures, there exists a compelling need for longitudinal MRI research to investigate previously unexplored brain regions and networks, specifically the limbic system. The studies described in this thesis used multimodal MRI techniques (structural and diffusion MRI) to investigate the link between limbic system structural development and ADHD symptomology at three time points, at approximately 18-month intervals, from ages 9-14.

Study 1 investigated the developmental differences in limbic system volumes among individuals with ADHD and controls using structural MRI scans processed with FreeSurfer software. The analyses of this study revealed that compared to controls, the ADHD group had lower volume in the amygdala, hippocampus, orbitofrontal cortex and cingulate gyrus across the three study time points. In the ADHD group, increased mammillary body volume growth was significantly associated with the persistence of symptom severity during mid-adolescence.

Study 2 explored the development of limbic system white matter in children and adolescents with ADHD using higher-order diffusion MRI data processed with ExploreDTI software. Manual tractography isolated the key white matter tracts of the limbic system. The analyses found that compared to controls, individuals with ADHD displayed reduced microstructural organisation in the cingulum bundle and fornix across all three study time points.

Study 3 investigated the development of topological organisation of the limbic system's structural connectivity among individuals with ADHD and controls using ExploreDTI software. Results showed that reduced routing efficiency and network density were significantly associated with increased ADHD symptom severity, suggesting that underconnectivity of the limbic system may underpin increased symptom severity in ADHD.

Overall, the results of the studies in this thesis suggest that atypical development of limbic system grey matter, white matter and subcortical nuclei may be a neurobiological feature associated with the persistence of ADHD symptoms during the transition into mid-adolescence.

List of Publications, Presentations and Awards

This thesis incorporates material already published or currently under review in the following manuscripts:

Connaughton, M., Leemans, A., Paterson, J., O'Hanlon, E., … , & McGrath, J. (2024). The Limbic System in Children and Adolescents with Attention-Deficit/Hyperactivity Disorder: A Longitudinal Structural Magnetic Resonance Imaging Analysis. Biological Psychiatry: Global Open Science. https://doi.org/10.1016/j.bpsgos.2023.10.005

Connaughton, M., Leemans, A., O'Hanlon, E., & McGrath, J. (2023). Longitudinal Analysis of Diffusion MRI Data. In *Method for analyzing large neuroimaging datasets*. Springer Nature. https://osf.io/mbyjh/

Connaughton, M., O'Hanlon, E., & McGrath, J. (2022). White matter microstructure in autism. In *The Neuroscience of Autism* (pp. 127-156). Academic Press. https://doi.org/10.1016/B978-0-12-816393-1.00012-9

Connaughton, M., Whelan, R., O'Hanlon, E., & McGrath, J. (2022). White matter microstructure in children and adolescents with ADHD. *NeuroImage. Clinical*, *33*, 102957. https://doi.org/10.1016/j.nicl.2022.102957

The following are Oral Presentations arising from this work:

Connaughton, M., Leemans, A., Silk, T., Anderson. V., O'Hanlon, E., Whelan, R., & McGrath, J. (2022). Longitudinal Neuroimaging Analysis of the Limbic System Network in ADHD. 2022. Neuroscience Ireland Young Investigator Symposium. October 2022.

Connaughton, M., Leemans, A., Silk, T., Anderson. V., O'Hanlon, E., Whelan, R., & McGrath, J. (2022). Longitudinal Neuroimaging Analysis of the Limbic System Network in ADHD. European Society for Child and Adolescent Psychiatry 2022, June 2022.

Connaughton, M., Leemans, A., Silk, T., Anderson. V., O'Hanlon, E., Whelan, R., & McGrath, J. (2021). Structural Connectivity of the Limbic System Network in ADHD. 8th World Congress on ADHD. May 2021.

The following are Awards arising from this work:

- Neuroscience Ireland (2022): Awarded Best Oral Presentation at the Young Researcher Symposium.
- ADHD World Congress (2020): Recipient of the Young Researcher Award.

1 General introduction

1.1. Overview of ADHD

Attention-Deficit Hyperactivity Disorder (ADHD) is a highly prevalent, impairing condition that significantly impacts the individual, their family, and the broader community (Gallo and Posner 2016). Like many other psychiatric conditions, the diagnosis of ADHD has been significantly refined and developed over the past 50 years (Posner, Polanczyk, and Sonuga-Barke 2020). What was once identified in the Diagnostic and Statistical Manual of Mental Disorders (second edition; DSM-II) as a "hyperkinetic reaction of childhood" has been redefined in both the DSM-5 and International Classification of Diseases (11th edition; ICD-11) as a condition that spans an individual's entire life, presenting distinct criteria for both children and adults (American Psychiatric Association and Association 2013; Organization 2004). This evolution in diagnosis has been the result of periodic review and reformulation, influenced by both research insights and clinical factors (Posner, Polanczyk, and Sonuga-Barke 2020). Historically, diagnostic systems in psychiatry have focused on a descriptive or phenomenological approach, often overlooking the underlying causes of ADHD (Posner, Polanczyk, and Sonuga-Barke 2020). However, as our understanding of the aetiology and pathophysiology of ADHD expands, there is potential for a shift in these diagnostic approaches (Posner, Polanczyk, and Sonuga-Barke 2020). By incorporating scientific discoveries, there is the possibility to expand and refine clinical approaches for people with ADHD (Posner, Polanczyk, and Sonuga-Barke 2020).

Currently, while medication-based treatments for ADHD prove efficacious and cost-effective in the short term (Pliszka et al. 2006; Scheffler et al. 2007), the long-term effectiveness of these treatment strategies on educational, vocational, and social outcomes remains unclear (Molina et al. 2009; Chang et al. 2019). Additionally, given the low adherence to these medication-based treatments, particularly in adolescence (Adler and Nierenberg 2010), there is a pressing need for the development of improved long-term ADHD treatments (Posner, Polanczyk, and Sonuga-Barke 2020). Changing the perspective on ADHD's aetiology through continued scientific advancement could pave the way for the development of innovative strategies that enhance existing treatments or novel alternatives (Posner, Polanczyk, and Sonuga-Barke 2020).

1.1.1. Classification and Diagnosis of ADHD

ADHD diagnosis requires a comprehensive evaluation of current and previous symptoms along with any functional impairments (Posner, Polanczyk, and Sonuga-Barke 2020). As per the National Institute for Health and Care Excellence (NICE), the diagnosis of ADHD should only be made by a healthcare professional with specialised training and expertise in the diagnosis of ADHD (Atkinson and Hollis 2010). The diagnosis procedures requires a comprehensive clinical and psychosocial evaluation, including a full developmental and psychiatric history as well as observer reports of the individuals mental state (Atkinson and Hollis 2010). For a diagnosis of ADHD, symptoms should meet the diagnostic criteria of the DSM-5 (Lahey et al. 2005) or ICD-11 (Reed et al. 2019), and must cause moderate to severe psychological, social and/or educational impairment to the individual (Atkinson and Hollis 2010). These impairments must also occur in 2 or more settings including social, familial, educational or occupational environments (Atkinson and Hollis 2010).

The DSM is a classification system developed in the United States of America that provides standardised criteria for the diagnosis of psychiatric disorders (Lahey et al. 2005). According to the American Psychiatric Association's DSM-5, ADHD is defined in children (< 17 years) by the presence of six or more symptoms in the domains of inattention or hyperactivity and impulsivity (Lahey et al. 2005) (see Topic Box 1). For adults, five symptoms in either domain are required to meet diagnostic criteria (Lahey et al. 2005). The DSM-5 modified the onset age criteria from before seven years in the DSM-IV to before 12 years, offering more flexibility in diagnosing adults (Lahey et al. 2005). It has also shifted from categorising ADHD into three subtypes (based on dominant symptoms) to using the term "presentation" to highlight the fluidity of symptom change as individuals mature and develop (Lahey et al. 2005) (see Topic Box 1).

The ICD is a globally recognised medical classification system maintained by the World Health Organisation (WHO), which includes both physical and mental health conditions (Reed et al. 2019). Recently the ICD has revised its diagnostic framework to align with the DSM-5, transitioning ADHD from the disruptive category to the neurodevelopmental disorder category (Reed et al. 2019). It also replaced the term "hyperkinetic disorder" with "ADHD" and recognises inattentive, hyperactive and impulsive symptom presentations (Reed et al. 2019). Unlike the DSM-5 and the ICD-10,

the ICD-11 outlines the fundamental traits of the disorder without defining a specific age of onset, duration, or number of symptoms (Reed et al. 2019) (see Topic Box 1).

Topic Box 1: ADHD diagnostic criteria according to the DSM-5 and ICD-11.

DSM-5

Inattention

- Displays careless mistakes or fails to pay close attention to details in tasks.
- Faces difficulty sustaining attention during tasks.
- Often ignores direct conversations.
- Struggles to follow instructions or finish tasks (e.g. loses focus, or gets side-tracked).
- Finds difficulty in organising tasks and activities.
- Avoids or shows reluctance in tasks requiring sustained mental effort.
- Often loses essential items for tasks and activities.
- Is easily distracted by external stimuli.
- Shows forgetfulness in daily activities.

Hyperactivity/Impulsivity

- Exhibits restless behaviours like fidgeting, tapping, or squirming.
- Inappropriately leaves a seat when expected to remain seated.
- Runs and climbs in inappropriate situations (adolescents or adults might be limited to feeling restless).
- Unable to play or engage in leisure activities quietly.
- 'On the go' or acting as if 'driven by a motor'.
- Talks excessively.
- Blurts out answer before a question has been completed.
- Has difficulty waiting their turn.
- Interrupts or intrudes on others (e.g. conversations or games).

Predominant ADHD Presentation (formally known as ADHD subtypes):

- Inattentive presentation: Individuals up to age 16 must exhibit six or more inattentive symptoms, while also having less than six hyperactivity/impulsivity symptoms (> 17 years old require 5).

- Hyperactive/Impulsive presentation: Individuals up to age 16 must display six or more hyperactivity/impulsivity symptoms, while also having less than six inattentive symptoms (> 17 years old require 5).
- Combined presentation: Individuals up to age 16 must display six or more symptoms in both inattentive and hyperactive/Impulsive categories (> 17 years old require 5).

ICD11

- Presents a persistent pattern (at least 6 months) of inattention, hyperactivity, or impulsivity.
- Symptoms typically onset in early to mid-childhood.
- Symptoms affect academic, occupational, or social functioning.

ICD11 definitions:

1. **Inattention:** Marked by difficulty in sustaining attention in non-stimulating or unrewarding tasks, distractibility, and organisational problems.
2. **Hyperactivity:** Characterised by excessive motor activity and difficulty remaining still, especially in structured situations requiring self-control.
3. **Impulsivity:** Manifested as acting on immediate stimuli without thoughtful deliberation or consideration of risks and consequences.

1.1.2. Emotional Dysregulation and ADHD

Emotional dysregulation is commonly observed in ADHD, with prevalence estimates between 24% and 50% among children with ADHD (Seymour et al. 2017; Shaw, Stringaris, et al. 2014). Emotional regulation refers to one's capacity to adjust emotional states, facilitating productive, goal-orientated behaviours (Thompson 1994). It involves the mechanisms that enable an individual to focus on, evaluate, and flexibly respond to emotionally arousing stimuli (Shaw, Stringaris, et al. 2014). These mechanisms trigger behavioural and physiological responses that can be altered to align with goal-orientated objectives (Shaw, Stringaris, et al. 2014). Emotional dysregulation emerges when these adaptive mechanisms are compromised, resulting in behaviours counterproductive to an individual's interest (Shaw, Stringaris, et al. 2014). This regulation includes 1) emotional reactions and experiences that are disproportionate or unfitting for the context compared

to societal expectations; 2) swift, unstable changes in emotion (lability); and 3) an unusual focus/fixation on emotional stimuli (Shaw, Stringaris, et al. 2014). Emotional dysregulation represents a major source of impairment among individuals with ADHD (Shaw, Stringaris, et al. 2014). Research indicates that emotional problems have a greater impact on well-being and self-esteem compared to symptoms of hyperactivity and inattention (Shaw, Stringaris, et al. 2014). In addition, the presence of childhood emotional dysregulation is associated with increased rates of anxiety disorders, mood disorders, disruptive behaviour disorders, and substance use disorders in adulthood (Althoff et al. 2010).

Building on this understanding, it is important to recognise the overlap between emotional dysregulation in ADHD and bipolar disorder. Despite their distinct diagnostic criteria, ADHD and bipolar disorder share a clinical presentation of emotional dysregulation (Shaw, Stringaris, et al. 2014). This similarity not only presents diagnostic challenges, as the emotional symptoms in ADHD can mirror those in bipolar disorder, but also challenges in pathophysiological research as MRI studies have shown both shared and distinct neurobiological mechanisms underpinning emotional regulation in these disorders (Shaw, Stringaris, et al. 2014; Seymour et al. 2015). As such, to fully understand the impact and pathophysiology of emotional dysregulation in ADHD it is important to acknowledge the potential impact of diagnostic overlap.

1.1.3. Epidemiology of ADHD

A study from 2007, which included over 100 research papers, indicated a worldwide prevalence of 5.3% (95% confidence intervals (CI): 5.01-5.56) (Polanczyk et al. 2007). Differences in results across these studies can be attributed to varying diagnostic criteria, information sources used, and the requirement of both functional impairments and symptoms for a diagnosis (Faraone et al. 2015). While adjusting for these methodological discrepancies, a later meta-analysis found no significant differences in ADHD prevalence across countries in Europe, Asia, Africa, and the Americas (Polanczyk et al. 2007). Other meta-analyses have reported varying rates but often have significant constraints, like exclusive use of DSM criteria to diagnose ADHD or simulated prevalence rates (Thomas et al. 2015; Erskine et al. 2013).

It is important to note that ADHD isn't limited to children; while many affected children do not continue to meet full ADHD diagnosis criteria in adulthood, a substantial

proportion continue to experience functional impairments or subthreshold impairing symptoms that continue to impact their lives (Faraone, Biederman, and Mick 2006). An analysis estimated adult ADHD prevalence to be 2.5% of the population (95% CI: 2.1-3.1) (Simon et al. 2009). In addition, studies focusing on older adults (aged 55-85) also found similar prevalence rates (Michielsen et al. 2012; Guldberg-Kjär and Johansson 2009), with longitudinal studies suggesting that around two-thirds of youths diagnosed with ADHD continue to experience impairing symptoms into adulthood (Faraone, Biederman, and Mick 2006).

A distinct feature of ADHD in children is the high ratio of diagnosed boys vs girls, a trend that has been supported by both population and clinical studies (Posner, Polanczyk, and Sonuga-Barke 2020). Specifically, studies have identified a boy-to-girl ADHD diagnoses ratio of 3:1 and 4:1 (Joseph Biederman et al. 2002; Cuffe, Moore, and McKeown 2005). This disparity may arise from a host of influences such as distinct symptom expression between boys and girls, biases in diagnostic criteria, or a combination of biological and environmental factors (Posner, Polanczyk, and Sonuga-Barke 2020). In adulthood, this sex ratio seemingly narrows to 1.6:1 in male vs females with ADHD (Willcutt 2012). While the causes for this shift in sex ratios across the lifespan remains unclear (Stibbe et al. 2020), research indicates varying rates of ADHD persistence in adulthood by sex. Specifically, approximately 60% of females with a childhood ADHD diagnosis continue to meet diagnostic criteria in adulthood (Biederman, Petty, Monuteaux, et al. 2010; Hinshaw et al. 2012), compared to only 35% of men (Biederman, Petty, Evans, et al. 2010).

1.2. Pathophysiology of ADHD

The pathophysiology of ADHD refers to the functional and anatomical mechanisms that underlie the disorder's symptoms and progression. While the pathophysiology of ADHD is not fully understood, research suggests a complex interplay between genetic, environmental and neuroanatomical factors in the manifestation of the disorder (Faraone et al. 2015). Given the scope of this thesis, the following section will focus on the current understanding of genetic and brain abnormalities associated with ADHD.

1.2.1. Genetics of ADHD

ADHD is a highly heritable neurodevelopmental disorder, with parents and siblings of patients with ADHD having between a fivefold and tenfold increased risk of developing the disorder compared to the general population (Biederman et al. 1992; Biederman et al. 1990). Twin studies indicate that 70-80% of ADHD cases in children and adults can be attributed to genetics (Posner, Polanczyk, and Sonuga-Barke 2020). ADHD is shaped by both stable genetic influences and those that emerge at different developmental stages across the lifetime (Chang et al. 2013). This suggests that genes contribute to the onset, persistence and remission of ADHD symptoms through both stable neurobiological abnormalities and atypical developmental processes (Faraone et al. 2015).

Two main characteristics of ADHD, inattention and hyperactivity, are separate yet interconnected areas of psychopathology (Larsson et al. 2013). The genetic correlation between these domains is around 0.6, indicating substantial overlap, but there are also unique genetic influences specific to each domain (Larsson et al. 2013). Furthermore, shared genetic factors also contribute to the presence of emotional dysregulation in ADHD (Merwood et al. 2014; Surman et al. 2011). The genetic connection between ADHD and other neurodevelopmental and psychopathological traits is also noteworthy. Family and twin studies have illustrated that common genetic influences are present between ADHD and various other conditions and traits, including conduct disorder (Christiansen et al. 2008), cognitive performance (Kuntsi et al. 2014), autism spectrum disorder (Rommelse et al. 2010) and mood disorders (Cole et al. 2009; Doyle and Faraone 2002). This genetic overlap of ADHD and other psychiatric disorders is also reflected in the Genome-Wide Association Studies (GWAS) data.

GWAS data has been used to identify single nucleotide polymorphisms (SNPs) and copy number variants (CNVs) associated with ADHD (Demontis et al. 2019; Demontis et al. 2023). These methods examine the genomes of both cases and controls for thousands of SNPs to investigate if any SNPs or CNVs correlate with the disorder (Witte 2010). Based on GWAS data, the SNP heritability (h^2_{SNP}) of ADHD is estimated to be between 0.14 and 0.22 (Demontis et al. 2019; Demontis et al. 2023), indicating that between 14-22% of the heritability of ADHD can be attributed to numerous genetic variants (loci) (Demontis et al. 2019; Demontis et al. 2023). The largest GWAS study to date (ADHD = 38,691 and control = 186,843) identified 27 ADHD-associated risk loci, highlighting 76 potential risk genes (Demontis et al. 2023). The results of this GWAS

research revealed that ADHD is highly polygenic, influenced by approximately 7,300 (Standard Deviation (SD). = 324) common genetic variants that account for roughly 90% of the disorder's h^2_{SNP} (Demontis et al. 2023). Furthermore, it emphasised that these genetic markers are not exclusive to ADHD but are shared extensively with other psychiatric disorders such as, schizophrenia, major depressive disorder, and autism (Demontis et al. 2023). The GWAS findings suggest that rather than having distinct ADHD-specific loci, there are certain genes that can impact a range of mental health disorders, but they manifest differently depending on the condition (Demontis et al. 2023).

1.2.2. Genetics and Brain Development in ADHD

Functionally, ADHD risk genes have been shown to participate in all stages of brain development (Tierney and Nelson 2009). Processes of brain development are crucial for shaping cognitive abilities, behaviours, and overall mental health, ensuring optimal functioning and adaptability throughout a life time (Tierney and Nelson 2009). If the stages of brain development are disrupted, it can lead to lasting cognitive, behavioural and neurological consequences (Tierney and Nelson 2009). These neurodevelopmental processes are orchestrated in a highly conserved sequence (Sabariego-Navarro et al. 2022). Briefly, neural progenitors located in specific neurogenic zones undergo proliferation, differentiating into distinct neuronal classes (neurogenesis) (Stiles and Jernigan 2010). These newly formed neurons then undergo a guided migration to their target locations within the neural architecture (neuronal migration) (Stiles and Jernigan 2010). Once positioned, they form intricate synaptic connections (synaptogenesis) (Dark, Homman-Ludiye, and Bryson-Richardson 2018). These synaptic connections extend to form both local and long-distance axons interconnecting different brain regions (neural connectivity) (Dark, Homman-Ludiye, and Bryson-Richardson 2018). Subsequently, synaptic refinement occurs, optimising the neuronal network through activity-dependent pruning, thereby selectively enhancing the most robust synaptic contacts and reducing neuronal redundancy (synaptic plasticity) (Dark, Homman-Ludiye, and Bryson-Richardson 2018).

Several ADHD-associated genes identified from GWAS are known to have functional significance in all stages of brain development (Dark, Homman-Ludiye, and Bryson-Richardson 2018). Genes associated with ADHD predominantly influence the formation and functioning of synapses (Dark, Homman-Ludiye, and Bryson-Richardson 2018). It has been proposed that the lower brain grey matter volume reported in ADHD

may be a consequence of reduced synaptic density rather than neuronal cell loss (Dark, Homman-Ludiye, and Bryson-Richardson 2018). As such, variants in these ADHD-associated genes have been proposed as potential contributors to the observed decrease in grey matter associated with the disorder (Dark, Homman-Ludiye, and Bryson-Richardson 2018; Hoogman et al. 2017b). Additionally, the delayed establishment of neural connections – a mechanism associated with ADHD gene variants – can lead to an underdeveloped brain (Dark, Homman-Ludiye, and Bryson-Richardson 2018). This is in line with the observed neurodevelopmental patterns of reduced and delayed development of brain structures seen in individuals with ADHD (Shaw et al. 2007; Shaw and Sudre 2021). Please see Table 1.1 for further details on the relationship between ADHD associated genes and brain development.

In summary, ADHD-associated genes play key roles in various stages of brain development, especially in the formation and function of synapses (Dark, Homman-Ludiye, and Bryson-Richardson 2018). These genetic influences may contribute to the observed reductions in grey matter and delays in brain structure development among individuals with ADHD (Friedman and Rapoport 2015).

Table 1.1 ADHD-associated genes and processes of brain development.

Neurodevelopmental process	Description	ADHD-associated genes involved in this process
Neurogenesis	Neurogenesis refers to the complex process of new neurons forming in the brain (Stiles and Jernigan 2010). In this intricate process, neural progenitor cells follow specific patterns of proliferation, differentiating into mature neurons (Dark, Homman-Ludiye, and Bryson-Richardson 2018). A balanced interplay of proliferation and differentiation is essential for proper brain development, and any deviations have profound impacts on brain development (Dark, Homman-Ludiye, and Bryson-Richardson 2018). Variants in ADHD-associated genes are hypothesised to disrupt these processes of neurogenesis, potentially contributing to the reduced brain volumes seen in the disorder (Dark, Homman-Ludiye, and Bryson-Richardson 2018).	CDH13, FOXP2, GRM1, GRM5, GRM7, MEF2C, NOS1, PARK2, SLC6A4
Synaptogenesis	Synaptogenesis is the process by which synapses are formed between neurons in the nervous system, enabling the transmission of signals and the establishment of functional neural networks (Dark, Homman-Ludiye, and Bryson-Richardson 2018). ADHD-associated genes have been shown to impact the local attractive cues guiding the location of synapse formation, disrupting the establishment of synaptic contacts between axons and dendrites (Dark, Homman-Ludiye, and Bryson-Richardson 2018). Disruption to this intricate process can not only lead to reduced synaptic formation but also decreased grey matter volume (Dark, Homman-Ludiye, and Bryson-Richardson 2018). Numerous genes associated with ADHD are involved in synaptogenesis, and a decrease in synaptic density may contribute to the observed reduction in brain volumes in individuals with ADHD (Dark, Homman-Ludiye, and Bryson-Richardson 2018).	BDNF, FOXP2, GRM5, MEF2C, PTPRF, ST3GAL3

Neuronal Migration	Neuronal migration is the process by which neurons move from their place of origin (neurogenic zone) to their final position in the brain (De Rouvroit and Goffinet 2001). This process is guided by a series of migration cues, which mainly consist of signalling molecules, including neurotransmitters and cell adhesion molecules, that influence neuronal movements via intracellular signalling pathways (De Rouvroit and Goffinet 2001). Variants in ADHD-associated genes can disrupt these migratory cues leading to abnormal brain development (Dark, Homman-Ludiye, and Bryson-Richardson 2018). It is hypothesised that in ADHD these disruptions can manifest either as a delay or mislocalisation of migrating neurons to their final location in the brain (Dark, Homman-Ludiye, and Bryson-Richardson 2018). Such disruptions may contribute to the neural phenotype of delayed neurodevelopment seen in the disorder (Dark, Homman-Ludiye, and Bryson-Richardson 2018).	FOXP2, SLC6A4
Neuronal connectivity	Neural connectivity in terms of neurodevelopment refers to the processes of neuronal pathfinding, which are essential for forming neuronal interconnections via axonal formation (Dark, Homman-Ludiye, and Bryson-Richardson 2018). Neuronal pathfinding refers to the mechanism by which the extensions of neurons, such as axons and dendrites, navigate to their appropriate target and is essential for the formation of functional neural circuits (Dark, Homman-Ludiye, and Bryson-Richardson 2018). Similar to neuronal migration, this process is driven by a series of guidance cues and cell adhesion molecules dispersed across the developing brain (Dark, Homman-Ludiye, and Bryson-Richardson 2018). Dysregulation of these guidance cues, through variants in ADHD-associated genes, can lead to a delayed establishment of neural connections (Dark, Homman-Ludiye, and Bryson-Richardson 2018). Such delays can lead to an underdeveloped brain, an observation that aligns with the developmental delays often seen in individuals with ADHD (Dark, Homman-Ludiye, and Bryson-Richardson 2018).	CDH13, LPHN3/ADRGL3, PCDH7, SEMA6D

Synaptic Plasticity	Synaptic plasticity involves changes in synaptic strength over time, leading to either strengthening (long-term potentiation) or weakening (long-term depression) of synapses and is crucial for the refinement and organisation of brain networks (Turrigiano and Nelson 2004). The ability to regulate neural connections through these processes is essential for maintaining optimal brain function (Dark, Homman-Ludiye, and Bryson-Richardson 2018). Any impairment in this regulation could lead to a reduction in brain volumes and the formation of inefficient neural networks (Dark, Homman-Ludiye, and Bryson-Richardson 2018). Interestingly, the disruption to processes of synaptic plasticity has been shown to be the most common neurodevelopmental effect of ADHD-associated genes (Dark, Homman-Ludiye, and Bryson-Richardson 2018). Specifically, it has been proposed that the decreases in brain volumes seen in ADHD may be linked to disruptions to synaptic potentiation and synaptic maintenance (Dark, Homman-Ludiye, and Bryson-Richardson 2018).	BDNF, CDH13, FOXP2, GRM5, LPHN3/ADRGL3, MEF2C, PTPRF, ST3GAL3

1.2.3. MRI research: Brain Structure in ADHD

This section will explore the current insights in relation to brain structure in children and adolescents with ADHD, specifically looking at research that investigated brain grey matter, subcortical nuclei and white matter through structural and diffusion MRI techniques. This section will also discuss current understanding of the neurodevelopmental trajectories of brain structures in ADHD.

Structural MRI

Magnetic resonance imaging (MRI) allows for high-quality anatomical images of the brain to be produced non-invasively and in vivo. MRI differentiates between grey matter, white matter, and cerebrospinal fluid, contributing to the mapping and characterisation (volume, surface area, thickness and gyrification) of cortical and subcortical structures (Symms et al. 2004). To date, six meta-analyses of structural MRI (sMRI) volumetric studies in children and adolescents with ADHD have been published (Valera et al. 2007; Hutchinson, Mathias, and Banich 2008; Ellison-Wright, Ellison-Wright, and Bullmore 2008; Nakao et al. 2011; Frodl and Skokauskas 2012; Norman et al. 2016). These examined differences in total brain volume and the volume of both cortical and subcortical brain structures.

Two sMRI meta-analyses using a region-of-interest approach investigated volumetric differences in children with ADHD and controls (Valera et al. 2007; Hutchinson, Mathias, and Banich 2008). These meta-analyses reported a reduction in grey matter volumes in the prefrontal, striatal, parietal, and cerebellar regions that were associated with individuals with ADHD compared to controls (Valera et al. 2007; Hutchinson, Mathias, and Banich 2008). The largest differences were reported in the cerebellar region, splenium of the corpus callosum, caudate and total cerebral volume (Valera et al. 2007; Hutchinson, Mathias, and Banich 2008).

Whole-brain meta-analyses of voxel-based morphometry (VBM) studies found that consistent reductions in volumes of the basal ganglia, specifically the putamen, globus pallidum and caudate nucleus, were associated with ADHD (Ellison-Wright, Ellison-Wright, and Bullmore 2008; Nakao et al. 2011; Frodl and Skokauskas 2012; Norman et al. 2016). Overall, the six meta-analyses to date have demonstrated reduced brain volume in children and adolescents with ADHD in frontal, parietal, and subcortical regions, predominantly in the basal ganglia (Valera et al. 2007; Hutchinson, Mathias, and Banich

2008; Ellison-Wright, Ellison-Wright, and Bullmore 2008; Nakao et al. 2011; Frodl and Skokauskas 2012; Norman et al. 2016). While such meta-analyses provide valuable information on brain structure in ADHD, these studies relied on published data as source material (Frodl and Skokauskas 2012; Nakao et al. 2011). This reliance posed a limitation in addressing varying covariates across studies, such as age and medication use (Frodl and Skokauskas 2012; Nakao et al. 2011). Moreover, these meta-analyses encompassed studies that differed in methods and protocols, including their choice of segmentation software and quality control measures (Hoogman et al. 2017b).

To address these limitations and increase statistical power, the ENIGMA (Enhanced Neuroimaging Genetics Through Meta-Analysis) ADHD Working Group was established in 2013 (Giedd 2019). This initiative aimed to consolidate structural MRI data from both individuals with ADHD and healthy controls across the lifespan. Two ENIGMA mega-analyses were conducted and examined between-group differences in cortical grey matter and subcortical nuclei among children and adolescents with ADHD and controls (Hoogman et al. 2017b; Hoogman et al. 2019).

One structural MRI ENIGMA mega-analysis investigated group differences in cortical brain structures among children with ADHD (n = 1081) and controls (n = 1048) aged 4-14 years old (Hoogman et al. 2019). Compared to controls, the ADHD group displayed reductions in various cortical surface areas (Hoogman et al. 2019). Specifically, among individuals with ADHD, reduced surface area was found in the frontal, temporal and cingulate regions compared to controls (Hoogman et al. 2019). Focusing on cortical thickness in children with ADHD, there were reductions in the temporal pole, fusiform gyrus, precentral gyrus and parahippocampal gyrus compared to controls (Hoogman et al. 2019).

Another structural ENIGMA MRI mega-analysis investigated group differences in subcortical brain structures among children and adolescents with ADHD (n = >600) and controls (n = >600) aged 5-14 years old (Hoogman et al. 2017b). The results found that children with ADHD had reduced grey matter volume in the accumbens, amygdala, caudate, hippocampus, pallidum, putamen, thalamus, and total intracranial volume compared to controls (Hoogman et al. 2017b). Exploratory analysis investigated age-related differences in attaining peak volume of subcortical structures between children with ADHD and controls (Hoogman et al. 2017b). The results of this analysis found that compared to controls, children with ADHD displayed a delay in attaining peak volume in

the amygdala, hippocampus and accumbens (Hoogman et al. 2017b). The authors caution that these results, limited by the study's cross-sectional design, require confirmation through longitudinal studies (Hoogman et al. 2017b).

Taken together, ADHD is associated with structural abnormalities in grey matter and subcortical nuclei during childhood and adolescence (Hoogman et al. 2017b; Hoogman et al. 2019). There are a large number of studies demonstrating reductions in volume, cortical thickness and surface area, with the most prominent differences being identified in the prefrontal, cingulate, basal ganglia, hippocampus, amygdala and total intracranial volume (Hoogman et al. 2017b; Hoogman et al. 2019). Exploratory age-stratified analysis identified a maturation delay in the development of subcortical structures among children with ADHD (Hoogman et al. 2017b), revealing exciting avenues for future longitudinal research to explore.

Diffusion MRI

Diffusion-weighted magnetic resonance imaging (dMRI) is a powerful MRI technique that investigates white matter microstructure through the degree of diffusivity of molecules within biological tissue (Jones and Leemans 2011). The diffusion of molecules in white matter is influenced by cellular membranes, specifically myelin sheaths, which determine the diffusion-weighted contrast signal (Van Hecke, Emsell, and Sunaert 2016). This signal can be used to estimate the underlying microstructure and reconstruct the organisation of white matter tracts (Van Hecke, Emsell, and Sunaert 2016). In the early 2000s, the most common technique for modelling dMRI was Diffusion Tensor Imaging (DTI) (Basser, Mattiello, and LeBihan 1994; Mori and van Zijl 2002). DTI is an important research tool for understanding white matter microstructure (Qiu, Mori, and Miller 2015; Goddings et al. 2021; Sexton et al. 2014), but it has some limitations. Most notably, it cannot accurately model voxels that contain crossing white matter fibres (Pierpaoli et al. 2001; Behrens et al. 2007; Jeurissen et al. 2011). In recent years, improvements in dMRI acquisition parameters have allowed for higher-order diffusion modelling techniques, which increase reconstruction accuracy and can overcome some of the limitations of DTI (Van Hecke, Emsell, and Sunaert 2016). High Angular Resolution Diffusion Imaging (HARDI) uses an increased number of diffusion direction gradients to estimate microstructural properties along multiple fibre populations within a single voxel,

providing improved accuracy for white matter tract reconstruction compared to traditional DTI (Descoteaux).

Another advancement in dMRI acquisition parameters is the collection and integration of multiple b-values (Pines et al. 2020; Jeurissen et al. 2014)('Advances in Cognitive Neurodynamics (V)' 2016). B-values summarise diffusion-weighting strength, duration, and amplitude during scans (Van Hecke, Emsell, and Sunaert 2016). Different strength b-values affect tissue responses, which can be used to improve the reconstruction accuracy in neurocellular environments (Van Hecke, Emsell, and Sunaert 2016). Diffusion of molecules in the brain can be better detected with higher b-values (Burdette et al. 2001), but they are also more prone to noise and artefacts than lower b-values (Kingsley and Monahan 2004). Multi-shell dMRI data combine high b-value images for increased signal and low b-value images for reduced noise, resulting in improved anatomical accuracy (Pines et al. 2020). In the context of higher-order diffusion modelling, various techniques have been developed, including constrained deconvolution (CSD), diffusion spectrum imaging (DSI), diffusion kurtosis imaging (DKI), Q-ball, and neurite orientation and dispersion density imaging (NODDI) (Jeurissen et al. 2011; Zhang et al. 2012; Tuch 2004; Tournier et al. 2004b; Dhollander et al. 2021). These techniques describe the diffusion of molecules within a voxel with greater accuracy compared to DTI (Van Hecke, Emsell, and Sunaert 2016). For example, the fibre orientation distribution (FOD) function for CSD and diffusion orientation distribution function (dODF) for DSI and Q-ball can be used to model voxels that contain crossing white matter fibres (Van Hecke, Emsell, and Sunaert 2016). As a result, metrics derived from these higher-order models have increased accuracy and yield clinically relevant information that cannot be obtained from the DTI model (Van Hecke, Emsell, and Sunaert 2016). Higher-order diffusion models offer crucial insights into neurological and psychiatric disorders by revealing detailed information about white matter tracts' microstructure and organization (Van Hecke, Emsell, and Sunaert 2016). While a detailed description of the common dMRI metrics and their clinical implications is provided in Table 3.1, a summary of the metrics that will be discussed in the following sections is provided below in Table 1.2.

Table 1.2 Diffusion MRI metrics investigated in the systematic review.

Modelling technique	Metric	Description
DTI	Fractional anisotropy	A summary measure that quantifies the directional preference of molecule diffusion within a reconstructed fibre tract (Van Hecke, Emsell, and Sunaert 2016; Zhang and Burock 2020).
	Radial diffusivity	A metric that measures the rate of diffusivity perpendicular to the principle direction of diffusion in a reconstructed fibre tract (Song et al. 2005; Van Hecke, Emsell, and Sunaert 2016).
	Axial diffusivity	A measure of the rate of diffusion along the principal direction of the reconstructed fibre tract (Alexander et al. 2007; Van Hecke, Emsell, and Sunaert 2016).
	Mean diffusivity	A metric that quantifies the total amount of diffusion in reconstructed fibre tract, regardless of direction (Alexander et al. 2007; Van Hecke, Emsell, and Sunaert 2016).
DSI	Generalised fractional anisotropy	An extension of fractional anisotropy, generalised fractional anisotropy quantifies the directional preferences of molecule diffusion within a reconstructed fibre tract (Van Hecke, Emsell, and Sunaert 2016). Unlike fractional anisotropy, generalised fractional anisotropy is derived from more complex dMRI models which can capture multiple diffusion directions in a given voxel (Van Hecke, Emsell, and Sunaert 2016).
	Return-to-orientation probability	A metric that evaluates the total diffusional cellular volume, offering insights into the cellular structure and arrangement of a reconstructed fibre tract (Assaf, Mayk, and Cohen 2000; Özarslan et al. 2013; Ning, Westin, and Rathi 2015).
	Return-to-axis probability	A measure that characterises the axonal density and packing of a reconstructed fibre tract (Assaf, Mayk, and Cohen 2000; Özarslan et al. 2013; Ning, Westin, and Rathi 2015).
DKI	Mean kurtosis	An analogue to mean diffusivity, this metric quantifies the overall non-gaussian (kurtosis) diffusion of a reconstructed fibre tract regardless of direction (Van Hecke, Emsell, and Sunaert 2016).

	Axial kurtosis	An extension of axial diffusivity, that measures the kurtosis diffusion along the principle direction of a reconstructed fibre tract (Steven, Zhuo, and Melhem 2013).
	Radial kurtosis	An analogue to radial diffusivity, this metric quantifies the kurtosis diffusion along the perpendicular direction of a reconstructed fibre tract (Steven, Zhuo, and Melhem 2013).
FBA	Fibre density	A measure of white matter microstructure, specifically focusing on the density of fibre tracts within a given region (Raffelt et al. 2012; Genc et al. 2020).
	Fibre cross-section	A fixel-wise analogue of tensor-based morphometry, this metric evaluates the cross-sectional area of individual tracts, offering insights into their morphological properties (Raffelt et al. 2012).
	Fibre density and cross-section	A fixel-wise analogue of voxel-based morphometry, this metric combines density and cross-sectional measurements to provide a comprehensive overview of white matter microstructural integrity (Raffelt et al. 2012).
Graph theory	Streamline	A measure of structural connectivity that quantifies the number, proportion and/or weighting of the streamline connections between two nodes (Yeh et al. 2016). Streamlines are virtual reconstructions of single fibre pathways (Van Hecke, Emsell, and Sunaert 2016).
	Global efficiency	A metric that quantifies the network's overall potential for efficient information transmission, determined by calculating the average inverse of the shortest path length across all pairs of nodes (Bullmore and Sporns 2009).
	Small-world network	A network characteristic that indicates efficient local and global information transfer within a network (Rubinov and Sporns 2010). This network characteristic is a key feature of the human brain (Rubinov and Sporns 2010).
	Rich club region	A network characteristic where highly connected nodes preferentially connect with each other, such architecture is characteristic of the human brain (Colizza et al. 2006).

Diffusion MRI Research in ADHD

As part of this PhD research, a systematic review was conducted, in which white matter microstructure in children and adolescents (< 18 years) with ADHD (Connaughton et al. 2022) (DOI: 10.1016/j.nicl.2022.102957). This review incorporates 46 studies in total, utilising diverse diffusion MRI imaging techniques and analytic methods (Connaughton et al. 2022). It includes whole-brain, region of interest and connectomic analyses, presenting a comprehensive overview of the dMRI research in children and adolescents with ADHD (Connaughton et al. 2022). The next section will provide an overview of the findings of this systematic review.

Publication Details:

Title: White matter microstructure in children and adolscents with ADHD

Journal: NeuroImage Clinical

DOI: 10.1016/j.nicl.2022.102957

Authors

Michael Connaughton[1], Prof. Robert Whelan[1,2], Dr. Erik O'Hanlon [3,4], Prof. Jane McGrath [1]

Affiliations

1. Department of Psychiatry, School of Medicine, Trinity College Dublin, Ireland.
2. School of Psychology, Trinity Dublin, Ireland
3. Trinity College Institute of Neuroscience, Trinity Dublin, Ireland
4. Dept of Psychiatry, School of Medicine, Royal College of Surgeons in Ireland, Dublin, Ireland

Co-authors contributions:

- RW contributed to the writing and formatting of the manuscript.
- EH offered technical support, particularly in diffusion MRI methodologies.

- JMG was involved in writing and formatting, provided clinical expertise in ADHD, and reviewed the included papers for accuracy and relevance.

Abstract

Attention deficit hyperactivity disorder (ADHD) is a common neurodevelopmental disorder. Advances in diffusion magnetic resonance imaging (MRI) acquisition sequences and analytic techniques have led to growing body of evidence that abnormal white matter microstructure is a core pathophysiological feature of ADHD. This systematic review provides a qualitative assessment of research investigating microstructural organisation of white matter amongst children and adolescents with ADHD. This review included 46 studies in total, encompassing multiple diffusion MRI imaging techniques and analytic approaches, including whole-brain, region of interest and connectomic analyses. Whole-brain and region of interest analyses described atypical organisation of white matter microstructure in several white matter tracts: most notably in frontostriatal tracts, corpus callosum, superior longitudinal fasciculus, cingulum bundle, thalamic radiations, internal capsule and corona radiata. Connectomic analyses, including graph theory approaches, demonstrated global underconnectivity in connections between functionally specialised networks. Although some studies reported significant correlations between atypical white matter microstructure and ADHD symptoms or other behavioural measures there was no clear pattern of results. Interestingly however, many of the findings of disrupted white matter microstructure were in neural networks associated with key neuropsychological functions that are atypical in ADHD. Limitations to the extant research are outlined in this review and future studies in this area should carefully consider factors such as sample size, sex balance, head motion and medication status.

Keywords

Attention Deficit Hyperactivity Disorder, children and adolescents, diffusion MRI, white matter microstructure, tractography, connectomic

Introduction

Attention deficit hyperactivity disorder (ADHD) is a neurodevelopmental disorder characterised by hyperactivity, impulsivity, and inattention, which causes significant functional impairment (Thapar and Cooper 2016). It is one of the commonest childhood psychiatric conditions with an estimated prevalence of 5.3% in children and adolescents (Polanczyk et al. 2007), and is highly heritable, with a heritability estimate of 0.76 (Faraone and Larsson 2019). While the pathophysiology of ADHD is not well understood, neuroimaging research has reported abnormalities in both brain structure (Valera et al. 2007; Frodl and Skokauskas 2012; Hoogman et al. 2017b; Hoogman et al. 2019), function (Castellanos and Proal 2012; Cortese et al. 2012a) and functional connectivity (a term describing the co-ordination of processing or communication between brain regions (Gao et al. 2019)) across widespread brain regions in children and adolescents with ADHD. The developmental periods of childhood and adolescence are of particular interest in ADHD as research has shown changes in the ADHD symptomology and neuropsychological functioning as an individual enters puberty (Dorn 2006). Furthermore, white matter is particularly sensitive to remodelling with exposure to pubertal hormones (Juraska and Willing 2017) and adolescence is a crucial period for the re-organisation of white matter in the brain (Paus, Keshavan, and Giedd 2008).

Diffusion magnetic resonance imaging is a technique that enables the assessment of the underlying architectural organisation of white matter tracts through the measurement of restricted diffusion of molecules in tissue (Jones and Leemans 2011). In early 2000's the most common diffusion MRI analysis model was Diffusion Tensor Imaging (DTI) (Basser, Mattiello, and LeBihan 1994; Mori and van Zijl 2002). DTI remains an important diffusion MRI modelling technique and frequent diffusion indices using DTI modelling are fractional anisotropy, mean diffusivity, radial diffusivity and axial diffusivity (see topic box 1 in supplemental material). DTI analysis of diffusion data

has a number of limitations, including its ability to model only a single fibre-tract per voxel (Pierpaoli et al. 2001; Behrens et al. 2007; Jeurissen et al. 2011). The limitations of DTI and the development of diffusion MRI acquisition parameters such as increased diffusion-weighted directions and multiple b-values have led to more advanced diffusion MRI imaging models. These include diffusion kurtosis imaging (DKI), diffusion spectrum imaging (DSI), constrained spherical deconvolution (CSD), Q-ball, fixel-based analyses (FBA) and neurite orientation and dispersion density imaging (NODDI) (Pierpaoli et al. 2001; Behrens et al. 2007; Jeurissen et al. 2011; Zhang et al. 2012; Alexander 2008; Broad et al. 2019; Van Hecke, Emsell, and Sunaert 2016). These diffusion modelling techniques estimate the fibre orientation distribution function for CSD, or diffusion orientation distribution function for DSI and Q-ball, parameters that can describe the direction of diffusion in voxels with multiple crossing fibres. Metrics derived from these higher order models have increased accuracy, yielding clinically relevant information that cannot be obtained from the DTI model (Van Hecke, Emsell, and Sunaert 2016). Common metrics derived from these advanced DWI methods are summarised in topic box 1 (see supplemental table).

There are many different methods of diffusion analysis, which can be broadly categorised as follows: whole brain, region of interest, and connectomic. Whole-brain analyses evaluate local voxel-wise differences across the whole brain. A common whole-brain analysis technique is tract-based spatial statistics, an automated analysis for evaluating diffusion metrics in major white matter tracts on a voxel-wise level across groups of subjects (Smith et al. 2006). Region of interest analyses are based on the delineation of predefined areas of interest in the brain. Common region of interest techniques includes atlas-based analyses and tractography. Atlas-based analysis uses a standard or population-specific atlas to evaluate differences in regions of the brain. Tractography uses the orientation of the diffusion profile to reconstruct specific white matter tracts in 3-dimensional space, allowing researchers to investigate the micro-structural organisation of white matter tracts connecting specific brain regions.

Connectomic analyses is a technique which models the human brain as a complex network (connectome) and evaluates the topological property of this network enabling the investigation of white matter organisation at the macroscopic level (Liao, Vasilakos, and He 2017; Sporns, Tononi, and Kötter 2005). Typically, in white matter connectomic research, using both structural and diffusion MRI, the brain connectome consists of nodes

comprised of nodes (grey matter) and edges (white matter) (Bullmore and Sporns 2012). Graph Theory is a mathematical framework that can be used for the assessment and representation of the human brain connectome. A variety of graph-theoretical measures can be extrapolated that provide summary information on properties of the brain network (or sub-networks) (Sporns, Tononi, and Edelman 2000; Bullmore and Sporns 2012)(see topic box 1 in supplemental material).

Previous meta-analyses of diffusion MRI research in children with ADHD reported wide-spread abnormalities in white matter microstructure. These abnormalities were in brain regions including the corpus callosum, cingulum, inferior and superior longitudinal fasciculus, inferior fronto-occipital fasciculus, uncinate fasciculus, internal capsule, cerebellum, basal ganglia and areas of the frontal, temporal, parietal and occipital lobe (van Ewijk et al. 2012; Chen et al. 2016). However, these meta-analyses only included studies that had used a whole-brain diffusion MRI approach. There has been no previous systematic review that investigated the white matter microstructure of ADHD across multiple diffusion MRI analytic techniques. This paper provides a systematic review of diffusion MRI studies that have used whole-brain, region of interest and connectomic approaches to investigate white matter microstructure in children and adolescents with ADHD. The results of this systematic review are described in the following sections: 1) whole-brain and region of interest studies, 2) connectomic studies, 3) associations between white matter and ADHD symptoms. In the discussion we explore the evidence for, and the possible impact of, disrupted white matter in the neural networks associated with the key neuropsychological functions that are atypical in ADHD.

Material and Methods

A systematic literature search of the EMBASE, Medline, PsychINFO, Web of Science, and the Cochrane Library databases was conducted on the 18th of June 2021. Reference lists of retrieved studies were also searched manually to screen for additional papers. The search strategy was prospectively registered to PROSPERO, where full details and breakdown of the search strategy are available *(PROSPERO ID:* CRD42020160401*)*. After de-duplication, the title and abstract of 1538 papers were screened, and relevant studies were selected and reviewed. Inclusion criteria were: human research that investigated between-group white matter differences using diffusion-weighted MRI, in children aged 3-18, who had a formal diagnosis of ADHD according to DSM-4, DSM-4-

TR, DSM-5 or ICD-10. Studies were included only if they included a typically developing comparison group aged 3-18, were published in English and in a peer-reviewed journal. After screening, 1323 records were excluded, and two authors (MC and JM) independently reviewed 215 studies that met inclusion criteria to confirm eligibility. 46 studies met inclusion criteria (see Figure 1).

The following information was extracted: study population characteristics (i.e., sample demographics, sample size, diagnostic criteria), diffusion MRI modelling technique, diffusion MRI analysis technique, main findings (Table 1). Data extraction was completed independently by the two authors MC and JM, and disagreements regarding extracted data or study inclusion were resolved by a mediator (EOH/RW) (see Figure 1). A qualitative review of all eligible studies was then conducted.

Figure 1: Flow diagram of selection of studies

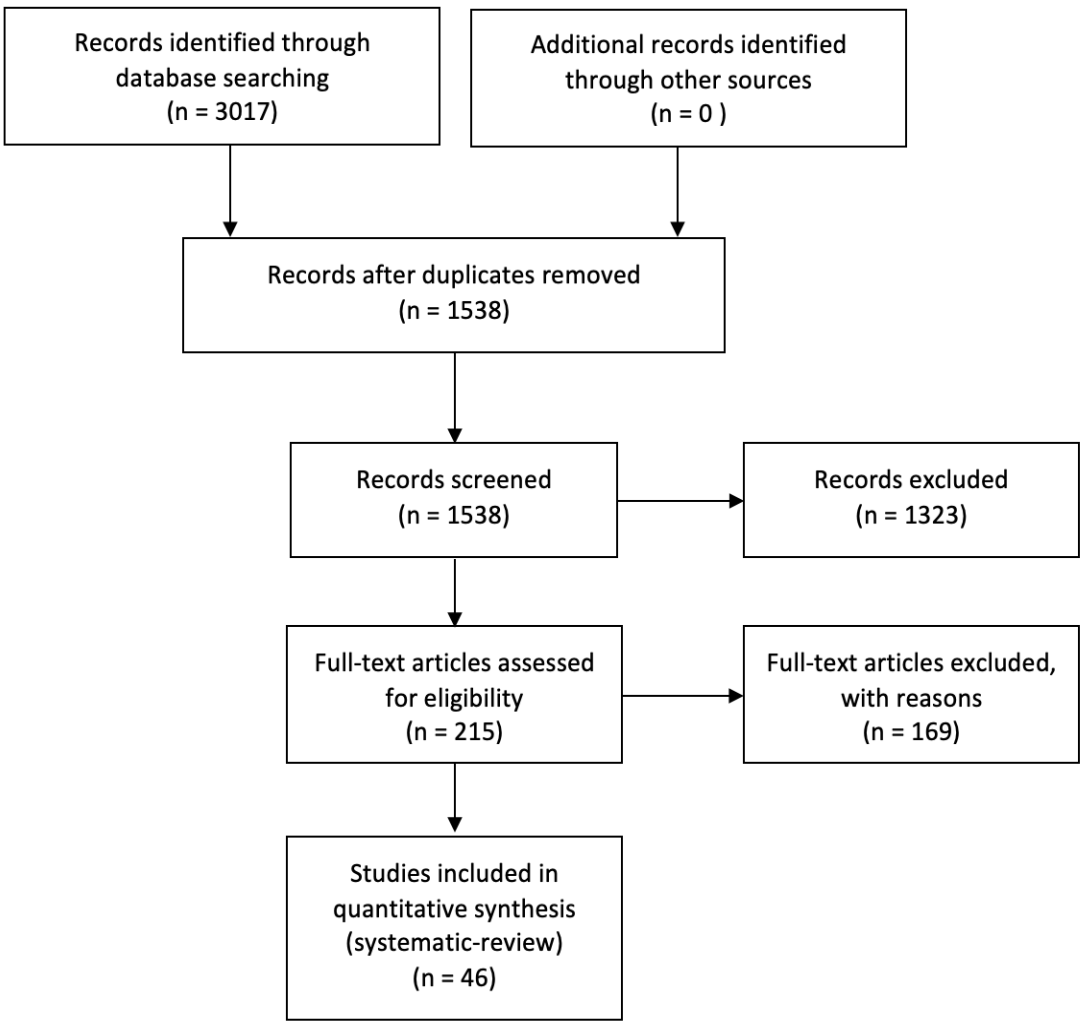

Results

Whole-brain and region of interest studies

Frontostriatal White Matter Tracts

There were nine studies that examined frontostriatal tracts. Seven studies reported reduced white matter microstructure in all four frontostriatal tracts (striatum-dorsolateral prefrontal cortex, striatum-orbitofrontal cortex, striatum-medial prefrontal cortex, and striatum-ventrolateral prefrontal cortex) (see Topic box 2 in supplemental material) in children and adolescents with ADHD, characterised by reduced generalised fractional anisotropy (Chiang et al. 2015; Chiang et al. 2016; Shang et al. 2013; Gau et al. 2015; Wu et al. 2014; Lin et al. 2014; Tung et al. 2021). Two studies did not find between-group differences in white matter organisation of these tracts (de Zeeuw, Mandl, et al. 2012; Silk, Vilgis, et al. 2016).

Corpus Callosum

Twelve studies investigated the corpus callosum in ADHD. Eight studies reported decreased organisation of white matter microstructure in regions of the corpus callosum in young people with ADHD which was characterised by reduced fractional anisotropy (Cao et al. 2010; Qiu et al. 2011; Ameis et al. 2016; King et al. 2015; Pastura et al. 2016; Wu et al. 2017) and higher mean kurtosis (Adisetiyo et al. 2014). In contrast, one study reported increased axial diffusivity (Tamm, Barnea-Goraly, and Reiss 2012). Four other studies did not report a difference in white matter organisation in this tract in ADHD (Hamilton et al. 2008; Peterson et al. 2011; Bouziane et al. 2018; Fuelscher et al. 2021).

Superior Longitudinal Fasciculus

Of the sixteen studies that examined the superior longitudinal fasciculus, twelve reported reduced white matter microstructural organisation in the superior longitudinal fasciculus in children and adolescents with ADHD. These studies included reports of decreased generalised fractional anisotropy (Chiang et al. 2015; Chiang et al. 2016), decreased fractional anisotropy (Hamilton et al. 2008; King et al. 2015; Pastura et al. 2016; Wu et al. 2017), increased mean diffusivity (Pavuluri et al. 2009; Nagel et al. 2011; Lawrence et al. 2013), increased radial diffusivity (Wu et al. 2017), increased mean

kurtosis (Adisetiyo et al. 2014) and decreased return-to-orientation probability and return-to-axis probability (Wu et al. 2020). In contrast, two other studies reported higher fractional anisotropy (Silk et al. 2009b) and lower mean diffusivity (Adisetiyo et al. 2014) in the superior longitudinal fasciculus amongst individuals with ADHD. Two studies did not find between-group differences in white matter organisation of these tracts (Peterson et al. 2011; Bouziane et al. 2018).

Cingulum Bundle

Fourteen studies investigated white matter microstructure of the cingulum. Six studies described reduced white matter organisation in the cingulum in children with ADHD characterised by reduced generalised fractional anisotropy (Chiang et al. 2015; Chiang et al. 2016; Tung et al. 2021), fractional anisotropy (King et al. 2015) and increased mean diffusivity (Pavuluri et al. 2009), and decreased return-to-orientation probability and return-to-axis probability (Wu et al. 2020). Two other studies reported conflicting results; one reported an increase in fractional anisotropy (Silk et al. 2009b), the other reported higher axial diffusivity (Svatkova et al. 2016) in the cingulum in children and adolescents with ADHD. Six other studies that isolated the cingulum bundle did not report any significant between-group difference in white matter structure (Hamilton et al. 2008; Peterson et al. 2011; Lawrence et al. 2013; Lin et al. 2014; Cooper, Thapar, and Jones 2015; Fuelscher et al. 2021).

Thalamic White Matter

Ten studies examined thalamic white matter; four of these reported a reduction in microstructural organisation of the thalamic radiation in participants with ADHD characterised by lower generalised fractional anisotropy (Tung et al. 2021), lower fractional anisotropy (Bouziane et al. 2018), higher mean kurtosis (Adisetiyo et al. 2014) and higher mean diffusivity and axial diffusivity (Lawrence et al. 2013). In contrast four studies found increased fractional anisotropy in the anterior (Tamm, Barnea-Goraly, and Reiss 2012; Svatkova et al. 2016) and posterior thalamic radiation (Peterson et al. 2011; Pastura et al. 2016) in children with ADHD. Two other studies reported atypical white matter microstructure in white matter tracts connecting the thalamus to a number of regions. Reduced fractional anisotropy was found in white matter tracts between the thalamus and striatum, hippocampus, motor cortex and prefrontal cortex (Xia et al. 2012).

Decreased return-to-orientation probability and return-to-axis probability was reported in white matter connections between the thalamus and pre-central gyrus, superior frontal gyrus and left paracentral gyrus (Wu et al. 2020). Increased return-to-orientation probability and return-to-axis probability was found between the thalamus and right paracentral gyrus (Wu et al. 2020).

Internal Capsule

Of the eight studies examining the internal capsule, seven found disrupted organisation of white matter in children with ADHD. Five reported decreased fractional anisotropy in the internal capsule (Ashtari et al. 2005; Qiu et al. 2011; Pastura et al. 2016; Wu et al. 2017) and posterior limb of the internal capsule (Nagel et al. 2011). Two other studies reported increased mean kurtosis, reflecting increased complexity in tissue microstructure (Adisetiyo et al. 2014), reduced fibre coherence and increased mean diffusivity (Pavuluri et al. 2009) in this tract. One study failed to find between-group differences in white matter organisation in the internal capsule (Peterson et al. 2011).

Corona Radiata

Eight studies investigated the corona radiata in children and adolescents with ADHD. Five of these reported disrupted organisation of corona radiata white matter. Reduced fractional anisotropy was reported in all regions of the corona radiata (anterior, superior and posterior) (Pavuluri et al. 2009; Nagel et al. 2011; Qiu et al. 2011; Wu et al. 2017), and increased radial diffusivity (Wu et al. 2017), axial diffusivity (Tamm, Barnea-Goraly, and Reiss 2012), and mean diffusivity was reported in the anterior corona radiata (Pavuluri et al. 2009). Three other studies reported contrasting findings with increased fractional anisotropy in the anterior corona radiata (Davenport et al. 2010; Tamm, Barnea-Goraly, and Reiss 2012) and reduced mean diffusivity in the superior and posterior corona radiata in children with ADHD (Adisetiyo et al. 2014).

White matter organisation in other regions

Other white matter tracts have not been as extensively studied, and for many tracts there has been mixed findings relating to white matter microstructure with some studies finding between-group differences but others failing to find a difference. Reduced organisation of white matter microstructure has been reported in the arcuate

fasciculus (Chiang et al. 2016; Tung et al. 2021), inferior longitudinal fasciculus (Pavuluri et al. 2009), uncinate fasciculus (Nagel et al. 2011; Tamm, Barnea-Goraly, and Reiss 2012; Fuelscher et al. 2021; Tung et al. 2021), inferior fronto-occipital fasciculus (Tamm, Barnea-Goraly, and Reiss 2012; Adisetiyo et al. 2014; Pastura et al. 2016; Fuelscher et al. 2021; Tung et al. 2021), corticospinal tract (Hamilton et al. 2008; Fuelscher et al. 2021), external capsule (Adisetiyo et al. 2014; Pastura et al. 2016; Wu et al. 2017), fronto-pontine tract (Fuelscher et al. 2021), parieto-occipital pontine tract (Fuelscher et al. 2021), frontal aslant tract (Tung et al. 2021), perpendicular fasciculus (Tung et al. 2021), stria terminalis (Tung et al. 2021), forceps major (Lin et al. 2020) and forceps minor (Qiu et al. 2011; Lawrence et al. 2013; King et al. 2015; Svatkova et al. 2016) as well as in white matter tracts in the parahippocampal gyrus (Peterson et al. 2011), lingual gyrus (Peterson et al. 2011), striatum (Ashtari et al. 2005; Wu et al. 2017), premotor region (Ashtari et al. 2005), motor cortex (Jacobson et al. 2015), basal ganglia (Li et al. 2010; Qiu et al. 2011), fornix (Davenport et al. 2010), fronto-parietal tracts (Nagel et al. 2011) and white matter in the medial orbitofrontal cortex (Jacobson et al. 2015), parieto-occipital region (Ashtari et al. 2005), cerebellar peduncle (Ashtari et al. 2005; Bechtel et al. 2009) and cerebellum (Nagel et al. 2011). Increased white matter microstructural organisation has been reported in the corticospinal tract (Silk et al. 2009b), uncinate fasciculus (Silk et al. 2009b; Tamm, Barnea-Goraly, and Reiss 2012), inferior fronto-occipital fasciculus (Tamm, Barnea-Goraly, and Reiss 2012), inferior longitudinal fasciculus (Silk et al. 2009b; Svatkova et al. 2016), corticospinal tract (Svatkova et al. 2016), striatum (Peterson et al. 2011), anterior forceps (Tamm, Barnea-Goraly, and Reiss 2012) and forceps minor (Tamm, Barnea-Goraly, and Reiss 2012; Lawrence et al. 2013), as well as in white matter in the frontal region (Li et al. 2010; Davenport et al. 2010), and temporo-occipital white matter (Kobel et al. 2010). A number of studies reported no-between group difference in the inferior longitudinal fasciculus (Hamilton et al. 2008), uncinate fasciculus (Hamilton et al. 2008; Lawrence et al. 2013), inferior fronto-occipital fasciculus (Hamilton et al. 2008; Lawrence et al. 2013), corticospinal tract (Cooper, Thapar, and Jones 2015), cerebellar peduncle (Fuelscher et al. 2021), forceps major (Lawrence et al. 2013) and the basal ganglia (Silk et al. 2009a).

Connectomic studies

Five studies were identified that used graph theory analysis to investigate both global and regional white matter microstructure in children with ADHD. In graph theory analysis of whole brain networks, children with ADHD displayed the same small-world network organisation seen in a neurotypical population (Cao et al. 2013; Beare et al. 2017), but decreased global, long-range connections suggesting a reduction in connections between local, functionally specialised networks in ADHD (Beare et al. 2017; Cao et al. 2013; Cha et al. 2015). The greatest reduction in efficiency was seen in the left parietal, frontal, and occipital cortices (Cha et al. 2015). Decreased white matter organisation was reported inside highly connected regions (rich-club regions) of the network amongst children with ADHD (Ray et al. 2014). These results suggest that ADHD may be characterised by under-connectivity inside highly connected regions (rich-club regions) and that this underconnectivity may be partially explained by findings of lower generalised fractional anisotropy within these regions (Ray et al. 2014). However, the white matter networks in the population with ADHD were not simply characterized by reduced connectivity; outside of highly connected regions (rich-club regions), white matter microstructure between other brain regions was increased, highlighting the complexity of the network dynamics within this disorder (Ray et al. 2014). Regional abnormalities of the connectome in children with ADHD were characterised by reduced connectivity in a network comprising frontal, striatal, and cerebellar regions (Hong et al. 2014), decreased white matter connections in prefrontal circuitry (Cao et al. 2013; Beare et al. 2017) and fronto-accumbal circuitry (Cha et al. 2015), and increased white matter connections in the orbitofrontal-striatal circuitry in children with ADHD (Cao et al. 2013).

Associations between white matter and ADHD symptoms

Several of the diffusion MRI studies included in this systematic review investigated the relationship between white matter organisation and ADHD symptom severity.

Overall ADHD severity

Greater severity of ADHD symptoms has been correlated with increased fractional anisotropy in the cingulum bundle (Cooper, Thapar, and Jones 2015) and left sagittal stratum (Peterson et al. 2011), and with greater left lateralisation of fractional anisotropy

values in white matter between the putamen and ventrolateral prefrontal cortex (Silk, Vilgis, et al. 2016). Overall severity has been associated with reduced fibre density in the left fronto-pontine tract (Fuelscher et al. 2021) and reduced axonal/cellular density and volume in the thalamus-precentral gyrus bundle (Wu et al. 2020). However, other studies have failed to find any correlation between diffusion metrics and ADHD severity scores (Ercan, Suren, Bacanlı, et al. 2016; Svatkova et al. 2016; Bouziane et al. 2018).

Inattention

Higher inattention scores were significantly associated with reduced generalised fractional anisotropy in the left striatum-orbitofrontal cortex (Wu et al. 2014), right superior longitudinal fasciculus (Chiang et al. 2015) and cerebellum (Ashtari et al. 2005), increased mean diffusivity, axial diffusivity, or radial diffusivity values in the forceps minor (Lawrence et al. 2013) and reduced network connectivity strength in a prefrontal network (Cao et al. 2013). A number of other studies have reported correlations between inattention scores and white matter organisation in the frontostriatal tracts (Shang et al. 2013; Wu et al. 2014; Chiang et al. 2015; Chiang et al. 2016), superior longitudinal tracts (Chiang et al. 2016), cingulum bundle (Chiang et al. 2015; Chiang et al. 2016), posterior corona radiata, posterior limb of the internal capsule, frontolimbic and temporo-occipital white matter (Nagel et al. 2011) however, these studies have not specified the direction of the association.

Hyperactivity/impulsivity

Higher scores on measures of hyperactivity/impulsivity have been associated with increased fractional anisotropy in the right inferior longitudinal fasciculus (King et al. 2015), corpus callosum, right superior longitudinal fasciculus and right corona radiata (Wu et al. 2017), lower fractional anisotropy in the forceps major (Lin et al. 2020) and increased network connectivity strength in the orbitofrontal-striatal portion of a defined network (Cao et al. 2013). Other studies reported significant associations between hyperactivity/impulsivity and white matter organisation in frontostriatal tracts (Shang et al. 2013; Wu et al. 2014; Chiang et al. 2015), superior longitudinal fasciculus (Chiang et al. 2015) and cingulum bundle (Chiang et al. 2015) although the direction of association has not been specified. One study did not find any correlation between white matter microstructure and hyperactivity/impulsivity scores in ADHD (Hamilton et al. 2008).

Other neuropsychological / behavioural functions

Reduced organisation of white matter microstructure in young people with ADHD has also been significantly associated with deficits in a variety of neuropsychological functions including executive function (Lawrence et al. 2013; Chiang et al. 2016; Svatkova et al. 2016), vigilance (Wu et al. 2014; Chiang et al. 2015), cognitive control (Li et al. 2010), inhibitory control (Jacobson et al. 2015), fine motor competence (Hyde et al. 2021), delayed reward (Bessette and Stevens 2019) and school dysfunction (Gau et al. 2015). Significant correlations have been reported between white matter microstructural organisation and spatial planning (Shang et al. 2013; Chiang et al. 2016), reaction time (Lin et al. 2014; Fall et al. 2015) and short-term memory (Chiang et al. 2016), but the direction of these correlations has not been specified.

Discussion

Overall Findings

The results of this systematic review highlight widespread abnormalities of white matter microstructure in both discrete white matter tracts and neural networks in children and adolescents with ADHD. Whole-brain and region of interest approaches reported atypical organisation of white matter microstructure in several white matter tracts, with the most prominent findings in the frontostriatal tracts, corpus callosum, superior longitudinal fasciculus, cingulum bundle, thalamic radiations, internal capsule and corona radiata. Connectomic approaches suggested global underconnectivity in connections between functionally specialised networks as well as regional reductions in network efficiency in frontal, parietal, striatal, occipital, and cerebellar regions. In some white matter tracts however, increased connectivity was reported and it appears that ADHD is not simply characterised by underconnectivity within neural networks, highlighting the complexity of this neurodevelopmental disorder.

From a behavioural perspective, many studies have reported significant correlations between disrupted white matter organisation and a variety of behavioural measures. However, few studies have investigated the association between the same

behavioural measure and diffusion metric in the same white matter tract, and replication is therefore required. In many studies it was not clear whether correlation analyses were exploratory or whether there was correction for multiple comparisons. In addition, a number of studies did not report the direction of the association rendering the information less clinically meaningful. Consequently, there is not yet a clear consensus on the overall impact white matter pathology has on core features of ADHD or other behavioural measures.

Research in ADHD has consistently reported deficits across a wide range of neurocognitive domains. Several neuropsychological theories postulate that the core deficits of ADHD are underpinned primarily by executive dysfunction (Barkley 1997), atypical reward processing (Sagvolden et al. 2005; Tripp and Wickens 2008; Sonuga-Barke 2011), aberrant functioning of the default mode network (Sonuga-Barke and Castellanos 2007), or delay aversion (Sonuga-Barke et al. 2008). While it is clear that there is atypical white matter microstructure in ADHD, the links between white matter pathology and these neuropsychological theories has not been well explored. In the following sections we provide a brief overview of four key neuropsychological theories of ADHD, consider their associated neural networks and explore potential links with the white matter pathology described in this review. There is overlap in certain white matter tracts which are involved in multiple neurocognitive processes (e.g. frontostriatal tract, superior longitudinal fasciculus and cingulum bundle). We synthesise the findings of this systematic review to explore if neuroimaging evidence is concordant with disrupted white matter in these networks.

Executive dysfunction theory of ADHD

The executive dysfunction theory of ADHD holds that deficits in executive function underpin the core symptoms of ADHD (Barkley 1997). There is a wealth of behavioural and neuroimaging data supporting this hypothesis (Roth and Saykin 2004; Hosenbocus and Chahal 2012; Hart et al. 2013), however this theory does not provide a unifying pathophysiological explanation for ADHD (Solanto et al. 2001; Nigg et al. 2005; Sonuga-Barke, Bitsakou, and Thompson 2010; de Zeeuw, Weusten, et al. 2012; Sjöwall et al. 2013; Coghill et al. 2014). Executive functioning is subserved by the cortico-striato-thalamo-cortical (CSTC) neural network, superior longitudinal fasciculus white matter and the cingulum bundle. The frontostriatal tracts are a key component of the CSTC and

connect the striatum to the frontal cortex. In children and adolescents with ADHD, previous research has reported reduced white matter microstructural organisation of frontostriatal tracts (Shang et al. 2013; Lin et al. 2014; Wu et al. 2014; Chiang et al. 2015; Chiang et al. 2016; Gau et al. 2015; Tung et al. 2021) was associated with inattention (Chiang et al. 2015; Chiang et al. 2016; Shang et al. 2013; Wu et al. 2014), deficits in focused attention (Chiang et al. 2015), impulsivity (Chiang et al. 2015; Wu et al. 2014), school dysfunction (Gau et al. 2015), reaction time(Lin et al. 2014), hyperactivity/impulsivity (Shang et al. 2013), executive function (Shang et al. 2013) and ADHD symptom severity (Beare et al. 2017). The superior longitudinal fasciculus, and specifically the superior longitudinal fasciculus II has also been implicated in executive functioning in ADHD. The superior longitudinal fasciculus II is thought to play a role in visuospatial awareness and attention (Chiang et al. 2015; Schmahmann et al. 2008). White matter microstructure of the superior longitudinal fasciculus II was reduced (Wu et al. 2020; Tung et al. 2021) in children with ADHD and this finding has been associated with reduced fine motor control (Hyde et al. 2021). The cingulate gyrus is associated with executive function (Schermuly et al. 2010; Bubb, Metzler-Baddeley, and Aggleton 2018) and this brain region is strongly connected to the cingulum bundle (Nolte, Vanderah, and Gould 2016). Reduced microstructural organisation of white matter in the cingulum bundle has been repeatedly reported in the ADHD literature (Nagel et al. 2011; Chiang et al. 2015; Chiang et al. 2016; King et al. 2015; Wu et al. 2020; Tung et al. 2021) and this atypical white matter has been associated with inattention (Chiang et al. 2015; Chiang et al. 2016), sustained attention (Chiang et al. 2015), impulsivity (Chiang et al. 2015), vigilance (Chiang et al. 2015), planning (Chiang et al. 2016), ADHD severity(Cooper, Thapar, and Jones 2015), reaction time(Lin et al. 2014), executive function (Svatkova et al. 2016).

Atypical reward processing theory of ADHD

Altered sensitivity to reward is considered a core element in the pathophysiology of ADHD (Sagvolden et al. 2005; Tripp and Wickens 2008; Sonuga-Barke 2011). Behaviourally, children with ADHD tend to favour small immediate rewards over larger delayed ones (Sonuga-Barke 2011). Functional MRI studies have consistently shown that individuals with ADHD show neural hyposensitivity in dopaminergic neurons in the nucleus accumbens when presented with rewarding stimuli (Baroni and Castellanos 2015;

Plichta and Scheres 2014; Furukawa et al. 2020).The main neural network subserving reward processing is the fronto-accumbal circuitry (Knutson et al. 2007; Cha et al. 2016), which originates in the nucleus accumbens and projects to prefrontal regions (orbitofrontal cortex, anterior cingulate gyrus, dorsal prefrontal cortex). Reduced white matter microstructure of the fronto-accumbal circuitry has been reported in youths with ADHD (Cha et al. 2015) and this white matter change has been associated with increased aggression (Cha et al. 2015). The frontostriatal tract (striatum-orbitofrontal cortex) is also a key component of the reward processing circuitry (Haber 2011) and in children and adolescents with ADHD, a number of studies have reported reduced white matter microstructure of this tract (Shang et al. 2013; Lin et al. 2014; Wu et al. 2014; Gau et al. 2015; Chiang et al. 2015; Chiang et al. 2016) This atypical white matter has been associated with inattention (Chiang et al. 2016; Shang et al. 2013; Wu et al. 2014), focused attention (Chiang et al. 2015), hyperactivity/impulsivity (Chiang et al. 2015; Cao et al. 2013), school dysfunction (Gau et al. 2015), reaction time(Lin et al. 2014), executive function (Shang et al. 2013).

Default mode network theory of ADHD

The default mode network (DMN) theory of ADHD suggests that many problems associated with ADHD arise from periodic lapses in attention due to spontaneous intrusions of DMN activation (Sonuga-Barke and Castellanos 2007). The DMN is a network comprised of distinct brain regions in the ventromedial and lateral prefrontal cortex, posteromedial and inferior parietal cortex, and medial and lateral temporal cortex (Andrews-Hanna et al. 2010; Kernbach et al. 2018; Lopez-Persem et al. 2019). The nodes of the DMN are connected by a number of major white matter tracts including the anterior and posterior cingulum bundles, uncinate fasciculus, superior longitudinal fasciculus II, arcuate fasciculus, and inferior longitudinal fasciculus (Alves et al. 2019). There are also structural connections between subcortical and cortical nodes of the DMN; fibres of the anterior thalamic radiation connect the thalamus and prefrontal cortex, fibres of the cingulum connect the basal forebrain with the prefrontal and cingulate cortices and fibres of the fornix connect the basal forebrain with the hippocampus (Alves et al. 2019). Reduced organisation of white matter microstructure has been described in the cingulum (Chiang et al. 2015; Chiang et al. 2016; King et al. 2015; Pavuluri et al. 2009; Nagel et al. 2011; Wu et al. 2020; Tung et al. 2021), superior longitudinal fasciculus II

(Wu et al. 2020; Tung et al. 2021), arcuate fasciculus (Chiang et al. 2016; Tung et al. 2021) and inferior longitudinal fasciculus (Nagel et al. 2011). Conversely, an increase in white matter microstructural organisation was reported in the uncinate fasciculus (Tamm, Barnea-Goraly, and Reiss 2012) and anterior thalamic radiata (Tamm, Barnea-Goraly, and Reiss 2012; Lawrence et al. 2013; Svatkova et al. 2016). White matter microstructural organisation in the DMN tracts was also significantly associated with ADHD symptoms and neuropsychological functioning; in the cingulum (inattention (Chiang et al. 2015; Chiang et al. 2016), sustained attention (Chiang et al. 2015), impulsivity (Chiang et al. 2015), vigilance (Chiang et al. 2015), planning (Chiang et al. 2016), ADHD severity (Cooper, Thapar, and Jones 2015), reaction time (Lin et al. 2014) and executive function (Svatkova et al. 2016)), superior longitudinal fasciculus II (motor response (Wu et al. 2020)), arcuate fasciculus (inattention (Chiang et al. 2016) and executive functioning (Chiang et al. 2016)) and inferior longitudinal fasciculus (delay reward (Bessette and Stevens 2019), impulsivity (King et al. 2015), executive functioning (Svatkova et al. 2016)).

Delay aversion theory of ADHD

The delay aversion theory holds that a desire to avoid delay underpins the core deficits in ADHD (Sonuga-Barke et al. 2008; Sonuga-Barke 2005), delay aversion is mediated by atypical functioning in brain regions associated with the anticipation and response to aversive outcomes. These regions are primarily the amygdala and its connections with the prefrontal cortex (specifically dorsolateral prefrontal cortex and ventrolateral prefrontal cortex), temporal pole, and insula (Sonuga-Barke 2005; Van Dessel et al. 2018). Functional MRI research findings have provided support for the delay aversion theory (Lemiere et al. 2012; Wilbertz et al. 2013; Van Dessel et al. 2018; Van Dessel et al. 2020). Research specifically investigating the white matter microstructure of the complete delay aversion network in ADHD has not yet been conducted. However significant abnormalities have been found in components of this network. The uncinate fasciculus is a major white matter tract connecting the amygdala and the ventral prefrontal cortex; greater white matter microstructure of the uncinate fasciculus predicted reduced amygdalar activation (Kim and Whalen 2009; Swartz et al. 2014). Three studies included in this systematic review reported atypical white matter organisation in the uncinate fasciculus. However the findings were mixed with two study

finding reduced generalised fractional anisotropy (Tung et al. 2021) and fractional anisotropy (Nagel et al. 2011) and the other finding increased fractional anisotropy (Silk et al. 2009b). Impairment in an individual's ability to wait for future rewards has been associated with reduced activation in brain reward circuitry, specifically in the ventral striatum and dorsolateral prefrontal cortex (Bishop 2008; Gold, Morey, and McCarthy 2015; Van Dessel et al. 2018; Bessette and Stevens 2019). Much previous research has described a reduction in white matter microstructural organisation of the frontostriatal-dorsolateral tract in children with ADHD (Shang et al. 2013; Lin et al. 2014; Wu et al. 2014; Gau et al. 2015; Chiang et al. 2015; Chiang et al. 2016) , a finding that has been associated with focused attention (Chiang et al. 2015), sustained attention (Chiang et al. 2015), hyperactivity (Shang et al. 2013), vigilance (Chiang et al. 2015), reaction time (Lin et al. 2014), school dysfunction (Gau et al. 2015).

In summary, this systematic review is the first review paper to synthesise evidence of atypical white matter microstructure in children and adolescents with ADHD in relation to the neuropsychological theories of ADHD (executive functioning, reward processing, delay aversion and default mode network functioning). Disrupted organisation of white matter may be a neurobiological feature that could potentially provide a unifying pathophysiological account for the diverse neuropsychological theories of ADHD.

Limitations of diffusion MRI research in ADHD

Key limitations include variance in sample demographics, sample size, head motion and medication status.

Sample demographics

In relation to study populations, it is important to consider sex and age range and a recent study using normative modelling to investigate white matter in ADHD and autism spectrum disorder suggested that some of the inconsistencies in findings might be explained by confounders of age and sex (Tung et al. 2021). There was a significant sex imbalance in many studies included in this systematic review, with 12/45 studies including only males in their sample. In the developing brain the effects of sex on white matter microstructure remain unclear but may influence diffusion MRI measures (Bava et al. 2011; Chiang et al. 2011). The heterogenous age ranges found in the studies included in this review may limit the ability to compare results across different studies. White matter

organisation is sensitive to remodelling in childhood and particularly in adolescence (Juraska and Willing 2017) and white matter in younger children with ADHD may have changed significantly by later adolescence.

Sample size

Small sample sizes, typical for brain-wide association studies (research linking differences in brain structure to behavioural phenotypes), may be a key element in the widespread replication failure of brain-wide association studies (Button et al. 2013b; Ioannidis et al. 2014; Botvinik-Nezer et al. 2020). It is hoped that the increased sample size facilitated by datasets from large consortia will increase the reproducibility of brain-wide association studies.

Head motion

Many diffusion MRI studies in children with ADHD have not controlled for head motion which may lead to false positive findings (Aoki, Cortese, and Castellanos 2018). Head motion has been associated with a spurious reduction in FA (Yendiki et al. 2014), a finding that raises concern that results of some diffusion MRI research may be a result of group differences in head motion. This would be particularly pertinent for a condition such as ADHD where hyperactivity is a core feature. It is important that future ADHD neuroimaging research considers the impact of head motion, controlling for head motion both during scanning and during image processing.

ADHD medication

Another factor that may contribute to the differences in findings between studies is the impact of ADHD medication on brain structure. It has been suggested that unmedicated children with ADHD display reduced white matter volume compared to both neurotypical controls and medicated children with ADHD (Castellanos, Lee, et al. 2002b). A recent clinical trial found that following four months of methylphenidate treatment, boys with ADHD had an increase in FA in several association tracts and the corpus callosum compared to non-medicated boys with ADHD (Bouziane et al. 2019). A study included in this systematic review investigated drug-naïve boys with ADHD finding no case-control differences in white matter microstructure (Bouziane et al. 2018), with the authors suggesting that previously seen case-control differences may partially be attributed to

medication use. As studies typically contain participants with mixed medication status it is important that future research considers the potential effects of medication.

Conclusion

This paper was a systematic review of diffusion MRI research in children and adolescents with ADHD. Our results showed that white matter microstructural organisation was disrupted in many major fibre tracts in young people with ADHD, however there is heterogeneity in the literature that may stem from a variety of methodological limitations. There is not yet a clear consensus about the impact of white matter pathology on core features of ADHD or other behavioural measures, but this review has shown that numerous studies have reported aberrant white matter in the neural networks associated with four key neuropsychological theories of ADHD. Atypical white matter microstructure appears to be a core neurobiological feature of ADHD which could provide a unifying pathophysiological explanation for major neuropsychological theories of ADHD.

1.2.4. MRI Research: Brain Development in ADHD

While cross-sectional MRI studies found widespread brain differences in grey matter (Hoogman et al. 2019), subcortical nuclei (Hoogman et al. 2017b) and white matter (Connaughton et al. 2022) between children and adolescents with and without ADHD. The nature of these differences – whether they are disorder specific abnormalities or delays of normal development – remains a subject of debate (El-Sayed et al. 2003; Shaw and Sudre 2021). Longitudinal MRI research has offered valuable insights into the changes in brain structure and function over time in individuals with ADHD, contributing to the formulation of the neurodevelopmental models of ADHD. Currently the two leading neurodevelopmental models of ADHD are the *maturation delay hypothesis* (Shaw et al. 2007; Shaw et al. 2012; Rubia 2007) and the *convergence model* (Shaw and Sudre 2021).

Maturation Delay Hypothesis

The maturation delay hypothesis of ADHD suggests that individuals with ADHD typically experience a delay in cortical development of approximately 3-years, particularly in the frontal, temporal, and parietal lobes (Shaw et al. 2007). Evidence for this theory comes from longitudinal studies that have found that children and adolescents with ADHD

show marked delays in the development of brain grey and white matter compared to controls (Shaw et al. 2007; Shaw et al. 2012; Rubia 2007; Chiang et al. 2023).

The original longitudinal structural MRI study conducted in 2002 investigated changes in lobar brain volume across multiple time points between the ages of 5-20 years old in unmedicated individuals with ADHD (n=152) and controls (n=139) (Castellanos, Lee, Sharp, Jeffries, Greenstein, Clasen, Blumenthal, James, Ebens, and Walter 2002). At the initial scan, children with ADHD were found to have reduced volumes across the cerebrum and cerebellum compared to controls (Castellanos, Lee, Sharp, Jeffries, Greenstein, Clasen, Blumenthal, James, Ebens, and Walter 2002). While both groups followed similar developmental trajectories for these brain structures, the ADHD group showed a persistent developmental delay in the volumetric maturation of these regions from childhood through to adulthood (Castellanos, Lee, Sharp, Jeffries, Greenstein, Clasen, Blumenthal, James, Ebens, and Walter 2002). Such consistent parallel trajectories across all structures, except for the caudate, imply that the factors influencing brain development in ADHD are stable and non-progressive (Castellanos, Lee, Sharp, Jeffries, Greenstein, Clasen, Blumenthal, James, Ebens, and Walter 2002).

A follow-up longitudinal study aimed to investigate the trajectory of sub-lobar cortical thickness across multiple time points among individuals with ADHD between the ages of 7-13 years old (n=223) and controls (n=223) (Shaw et al. 2007). The results found that although the cortical thicknesses of brain structures in children with ADHD were reduced, the developmental trajectories of these structures were similar in children with and without ADHD (Shaw et al. 2007). The study found that the age of attaining peak cortical thickness was delayed in individuals with ADHD by 3 years across most of the cerebrum (Shaw et al. 2007). The most pronounced delays were seen in the frontal lobes, with a delay of 5 years in the middle frontal cortex and a delay of 2 years in the superior and medial prefrontal cortices (Shaw et al. 2007). The second most pronounced delay was reported with children with ADHD displaying a 4 year delay in attaining peak cortical thickness in the bilateral middle and superior temporal cortex (Shaw et al. 2007).

The third longitudinal study extended the maturation delay hypothesis to map the growth curves of cortical surface area and gyrification in children with ADHD (n = 234) and controls (n = 231) during the transition from childhood into early adulthood (Shaw et al. 2012). While children with ADHD displayed a neurotypical developmental trajectory in surface area across much of the cerebrum (Shaw et al. 2012), the study found a marked

delay in the development of cortical surface area in frontal, temporal and parietal lobes in those with ADHD, mirroring the delay in cortical thickness previously reported (Shaw et al. 2012). At a lobar level, the delay seen in the ADHD group was highly regional, with the most prominent delays being found in the right prefrontal cortex (2 year delay), right parietal lobe (1.5 year delay), left parietal lobe (2 year delay), right temporal lobe (0.5 year delay), left temporal lobe (1.5 year delay) (Shaw et al. 2012). There were no group differences in the timing of attaining peak surface area in the occipital lobe (Shaw et al. 2012).

In addition to developmental abnormalities in brain grey matter and subcortical nuclei, longitudinal diffusion MRI research has found evidence of maturation delay in white matter microstructural organisation among individuals with ADHD. A longitudinal DSI study investigated changes in white matter microstructure at two time points among individuals with and without ADHD (Chiang et al. 2023). In this study, at time point 1 (mean age 10.95), individuals with ADHD displayed reduced generalised fractional anisotropy (GFA) in several white matter tracts, specifically the arcuate fasciculus, superior longitudinal fasciculus, frontal aslant tract, cingulum bundle, inferior fronto-occipital fasciculus, frontostriatal tract (connecting to the prefrontal cortex), thalamic radiation, corticospinal tracts, and the corpus callosum (Chiang et al. 2023). As individuals with ADHD showed a more rapid rate of increase in GFA, by time point 2 (mean age 15.96), these tracts had normalised to the control group's GFA (Chiang et al. 2023). This study demonstrated atypical developmental trajectories in white matter tracts in ADHD, marked by a "normalisation" process with age in ADHD from childhood to early adulthood, supporting the maturational delay theory of ADHD (Shaw and Sudre 2021; Shaw et al. 2013). Of note, as per the diagnostic procedures of this study, ADHD diagnosis was only confirmed at time point 1. Significant differences in inattentive, hyperactive, impulsivity and total ADHD severity score (as measured by the Kiddie Schedule for Affective Disorders and Schizophrenia for School-Aged Children (K-SADS-E)) were found in the ADHD group from time point 1 to time point 2. This indicated a significant decrease in ADHD symptom severity and a potential diagnostic remission within the ADHD group at time point 2. This is a crucial consideration, as the trajectories observed in this study may align with another prominent neurodevelopmental model of ADHD, the convergence model.

Convergence Model of ADHD

The convergence model proposes that the improvement or remission of ADHD symptoms is a result of atypical neural characteristics in childhood converging towards neurotypical markers in adolescence and adulthood (Shaw and Sudre 2021). This model incorporates the concept of the maturation delay hypothesis (Shaw and Sudre 2021). The fundamental distinction between the two models is that, according to the convergence model, children with ongoing ADHD symptoms exhibit continuous, non-progressing differences in brain structures throughout their lives when compared to individuals with remission of ADHD symptoms and controls (Shaw and Sudre 2021).To-date two MRI findings have provided support for the convergence model in ADHD.

The first longitudinal MRI study investigated 92 individuals with ADHD and 184 controls examining the link between trajectories of cortical grey matter development during childhood and adolescence with symptom severity outcomes in adulthood (Shaw et al. 2013). The results of this study found that differing trajectories of the medial and dorsolateral prefrontal cortex and cingulate gyrus at childhood and adolescence was associated with ADHD symptom severity in adulthood (Shaw et al. 2013). Specifically, higher rates of cortical thinning in these medial brain regions during childhood and adolescence were associated with the persistence of ADHD symptoms in adulthood (Shaw et al. 2013). Conversely, individuals that experienced ADHD diagnosis remission in adulthood displayed either cortical thickening or minimal thinning in these medial structures during childhood and adolescence, resulting in a convergence towards neurotypical cortical measures by adulthood (Shaw et al. 2013). Taken together, the results of this study suggest that a convergence towards neurotypical cortical features throughout childhood and adolescence may underpin symptom remission in adulthood (Shaw et al. 2013).

Evidence for the convergence model was also observed in dMRI research (Fuelscher et al. 2023). A longitudinal dMRI study from the Neuroimaging of the Children's Attention Project (NICAP) - the same dataset analysed in this thesis - investigated the relationship between deviations from typical white matter fibre development and the persistence or remission of ADHD symptoms during childhood and adolescence (Fuelscher et al. 2023). The study revealed that individuals with ADHD (both symptom remission and persistence), compared to controls, exhibited lower fibre bundle cross-section, indicative of fibre morphology (Fuelscher et al. 2023), in specific areas such

as thalamic pathways, striatal pathways, and the superior longitudinal fasciculus at around age 10 (Fuelscher et al. 2023). However, individuals showing remission of ADHD symptoms were associated with accelerated fibre development in the thalamic pathways, striatal pathways, and superior longitudinal fasciculus compared to individuals with persistent ADHD symptoms (Fuelscher et al. 2023). As a result, by age 14, they displayed increased progression and convergence towards non-ADHD fibre morphology, contrasting those with persistent ADHD symptoms, who continued to display ongoing neural anomalies throughout childhood and adolescence (Fuelscher et al. 2023). The findings of this study are consistent with the convergence model, suggesting that shifts in neural features towards neurotypical structures may underpin the remission of ADHD symptoms (Shaw et al. 2013).

Identifying how brain structure changes over developmental stages in ADHD and whether deviations from neurotypical trajectories of brain development are linked with differential outcomes, such as persistence or remission of ADHD symptoms, is essential to further our pathophysiological understanding of ADHD. As the neurodevelopmental models of ADHD are dependent on accurate tracking of symptom changes, maintaining robust diagnostic classification across study time points is essential for future longitudinal research.

1.3. Outstanding Issues

While there are promising advances in our understanding of the neural correlates of ADHD, there are two important outstanding issues that remain to be addressed.

Firstly, most longitudinal studies have primarily focused solely on cortical structures (Shaw et al. 2012; Shaw et al. 2007). There has been limited research into subcortical structures in ADHD, and consequently the developmental trajectories of subcortical structures and networks in ADHD remain poorly understood (Hoogman et al. 2017b; Rosch et al. 2018). To address this issue, the studies described in this thesis will investigate a previously under-explored brain network in ADHD, the limbic system. The limbic system is a group of interconnected cortical and subcortical structures involved in processes of emotion, cognition and human behaviour[17.] While atypical limbic system structure and function have been identified in various neurodevelopmental disorders (Rajmohan and Mohandas 2007), its specific role and influence within the context of ADHD remains largely unknown. This lack of understanding is surprising, given the high

prevalence of emotion dysregulation observed in individuals with ADHD (Philip Shaw et al. 2014). Additionally, some recent studies have reported that core symptoms of ADHD, such as impulsivity and attention deficits, are associated with structural and functional abnormalities within limbic system regions (Bauer et al. 2018; Hart et al. 2013; Tajima-Pozo et al. 2016). Despite these initial findings and the potential importance of the limbic system in ADHD's aetiology, there is a striking lack of research investigating the developmental trajectory of the limbic system in ADHD. Understanding the developmental trajectories of this prominent brain network could shed light on the underlying neural mechanisms responsible for both the core symptoms and associated emotional dysregulation, offering insights into the disorder's pathogenesis.

The second outstanding issues is that although ADHD is increasingly viewed as a disorder of dysfunctional neural networks involving multiple brain tissues (grey and white matter), the majority of MRI studies have deployed a single MRI modality, limiting the research to a single tissue type (Gareth Ball et al. 2019). Multimodal MRI approaches are vital in the study of complex neurobiological disorders such as ADHD, as they provide a comprehensive investigation of the brain across multiple tissue types (Gareth Ball et al. 2019). Unlike single-modality analysis, which may only offer a limited perspective, multimodal techniques combine different imaging modalities to provide better characterisation of the variability across tissue types in a given disorder (Groves et al. 2011). The studies described in this thesis will incorporate multimodal neuroimaging techniques (structural and diffusion MRI) to provide a more comprehensive investigation of the developmental trajectories of the limbic system in ADHD.

Overall, based on the research reviewed to this point in Chapter 1, there is a need for ADHD research to investigate brain development in previously unexplored regions and networks, specifically the limbic system. Given that ADHD is associated with abnormalities in brain grey and white matter, a multimodal MRI approach is required for a comprehensive investigation of this network within the disorder.

1.4. The limbic System

Emotions, behaviours, and memories emerge from the synchronised activities of brain regions interconnected by the limbic system (Catani, Dell'acqua, and Thiebaut de Schotten 2013). The concept of the limbic system has a long enduring history (Mesulam 2000; Catani, Dell'acqua, and Thiebaut de Schotten 2013). Initially introduced by Thomas

Willis (1664), the limbic system, rooted in the Latin term “limbus”, meaning “border”, was recognised for its distinctive positioning around the brainstem, suggesting a boundary between basic and advanced cognitive functions (Willis 1973). Its meaning has expanded over the years to encompass various brain regions with diverse functions (Marshall and Magoun 2013). Anatomical and physiological advancements in the early 20th century led by Christfield Jakob and James Papez led to the formulation of the first interconnected neural loop responsible for linking action, perception and memory to emotion, this circuit was known as the Jakob-Papez system (Jakob 1906; Papez 1937). This interconnected neural loop included structures such as the hippocampus, thalamus, mammillary bodies, cingulate gyrus, caudate nucleus, dentate gyrus and olfactory bulb (Jakob 1906; Papez 1937). According to Papez, emotion arises through either cognitive input channelled through the hippocampus or from visceral and somatic perceptions entering this circuit through the hypothalamus[169]. While this particular model is no longer considered fully accurate, it is important to acknowledge the foundational significance of the Jakob-Papez circuit in the formulation of the limbic system (Catani, Dell'acqua, and Thiebaut de Schotten 2013).

A decade after the formulation of the Jakob-Papez network, Paul Yakovlev proposed that the orbitofrontal cortex, insula, amygdala, and anterior temporal lobe form a neural circuit underpinning processes of emotion and motivation, known as the Yakovlev’s amygdala-orbitofrontal network (Yakovlev 1948). In two seminal papers, Paul MacLean, in 1949 and 1952, proposed a unitary model of the limbic system that consisted of both the Jakob-Papez circuit (Jakob 1906; Papez 1937) and Yakovlev’s amygdala-orbitofrontal network (Yakovlev 1948), that has remained almost unchanged since (MacLean 1949, 1952). MacLean’s model suggests that the limbic cortex, together with the limbic subcortical structures, form a functionally integrated network (MacLean 1949, 1952). This network is connected by short and long-range fibre pathways and is specialised for linking visceral states and emotions to cognition and behaviour (MacLean 1949, 1952).

While the definition of the limbic system remains a subject of debate, recent advancements in neuroimaging and tracing methods have allowed for a more precise delineation of its structures (Catani, Dell'acqua, and Thiebaut de Schotten 2013). The studies described in this thesis used a definition of the limbic system described by Catani and colleagues (2013). As per this description, the limbic system consists of both subcortical nuclei (amygdala, hippocampus, mammillary bodies, and anterior thalamic

nuclei) and cortical grey matter (cingulate gyrus and orbitofrontal cortex) interconnected by short and long-range fibre pathways (see Table 1.3 for functions of limbic system structures) (Catani, Dell'acqua, and Thiebaut de Schotten 2013). The major white matter pathways of the limbic system include the cingulum bundle, uncinate fasciculus, fornix, mammillothalamic tract, and anterior thalamic projections (see network schematic in Figure 1.1) (Catani, Dell'acqua, and Thiebaut de Schotten 2013).

Table 1.3 Brief description of the limbic system structures and functions.

Amygdala	The amygdala plays a role in emotional behaviour, particularly the processing of both aversive (LeDoux 1998) and pleasant information (Adolphs 2010; Janak and Tye 2015).
Hippocampus	The hippocampus has been shown to subserve functions of memory, attention, cognition, and emotion (Davidson, Jackson, and Kalin 2000; Davidson, Putnam, and Larson 2000; Posner and Rothbart 1998).
Cingulate gyrus	The cingulate gyrus is involved in the processing of emotions and behavior regulation (Rolls 2019a).
Orbitofrontal cortex	The orbitofrontal cortex is involved in processes of inhibition (Stalnaker, Cooch, and Schoenbaum 2015), impulsivity (Winstanley et al. 2004), and emotional control (Maia and McClelland 2004).
Mammillary bodies	Functionally, although the mammillary bodies have been shown to be involved in recollective memory, the exact function of this structure remains unclear (Vann 2010).
Anterior thalamic nuclei	The anterior thalamic nuclei is involved in alertness, learning and memory (Child and Benarroch 2013).

Figure 1.1 Schematic of the limbic system.

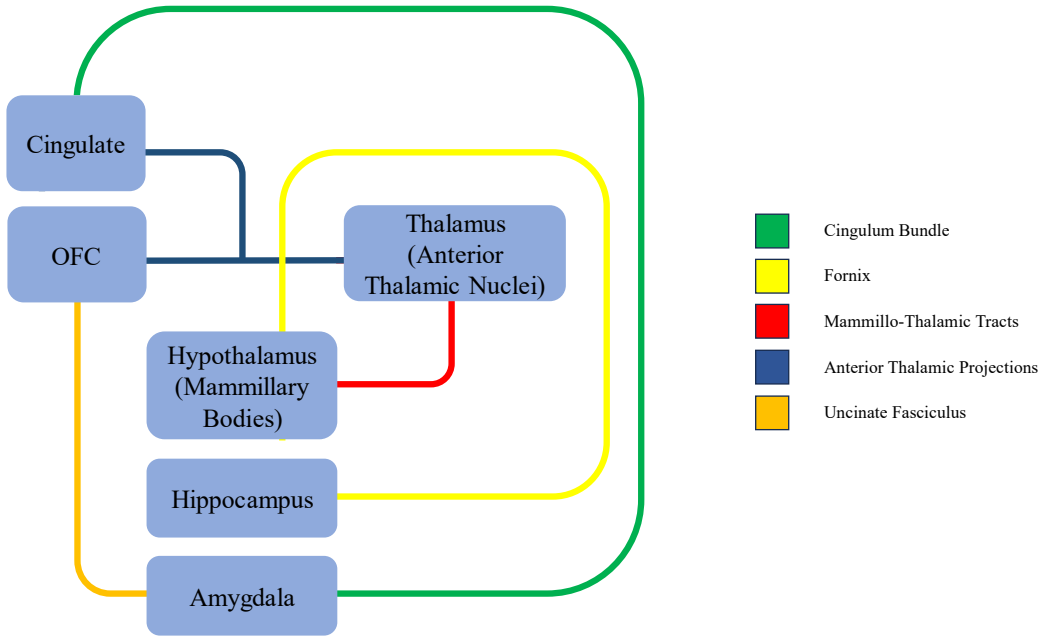

Figure 1.1: Graphical illustration of the limbic system alongside its primary pathways. The colours of the pathways match the tracts specified in the legend.

1.5. Aims and Hypotheses

The central aim of the studies described in this thesis are to investigate the link between structural changes of the limbic system and ADHD symptomology during the crucial developmental transition from childhood into mid-adolescence. This research is designed to explore three key aspects of the limbic system in individuals with ADHD compared to controls: 1) the volumes of grey matter and subcortical nuclei, 2) the microstructural properties of white matter tracts and 3) the topological organisation of the limbic system's structural connectivity.

1.5.1. Study 1: The Limbic System in Children and Adolescents with ADHD: A Longitudinal Structural MRI Analysis

The aims of Study 1 are 1) to investigate the developmental trajectories of limbic system structures (grey matter and subcortical nuclei) among individuals with ADHD during the transition from childhood into mid-adolescence and 2) to explore the relationship between changes in ADHD symptom severity and limbic system volumes among individuals with ADHD. Based on previous research (Hoogman et al. 2019; Hoogman et al. 2017b; Shaw et al. 2007; Shaw et al. 2012; Rubia 2007), the hypotheses of Study 1 are that, compared to controls, individuals with ADHD will display 1) reduced volume and 2) developmental delays in the volume of limbic system structures during the transition from childhood to mid-adolescence.

1.5.2. Study 2: Limbic System White Matter in Children and Adolescents with ADHD: A Longitudinal Diffusion MRI Analysis

The aims of Study 2 are 1) to examine the developmental differences in the microstructural organisation of limbic system white matter tracts among children and adolescents with ADHD and controls at three time points between the ages of 9 to 14 years and 2) to explore the relationship between changes in ADHD symptom severity and microstructural organisation of limbic system fibres among individuals with ADHD. Based on prior research (Connaughton et al. 2022; Fuelscher et al. 2023; Chiang et al. 2023), the hypotheses are that individuals with ADHD will display 1) lower microstructural organisation and 2) atypical development of microstructural organisation in limbic system white matter tracts during the transition from childhood to mid-adolescence compared to controls.

1.5.3. Study 3: Structural Connectivity of the Limbic System in Children and Adolescents with ADHD: A Longitudinal Network Analysis

The aims of Study 3 are 1) to characterise the developmental differences in the topological organisation of the limbic system's structural connectivity in children with ADHD and controls during the transition from childhood into mid-adolescence, and 2) to explore the relationship between ADHD symptom severity and structural connectivity of the limbic system in individuals with ADHD. Based on cross-sectional findings (Cao et al. 2013; Ray et al. 2014; Hong et al. 2014; Cha et al. 2015; Beare et al. 2017; Qian et al.

2021), the hypotheses are that, compared to controls, individuals with ADHD will demonstrate decreased network efficiency and underconnectivity in the limbic system structural connectivity connectome across the three study time points.

2 Neuroimaging of the Children's Attention Project (NICAP)

The studies presented in this thesis are based on data from the Neuroimaging of the Children's Attention Project (NICAP) (Sciberras et al. 2013; Silk, Genc, et al. 2016). This chapter offers a detailed overview of the NICAP study, including its recruitment procedures, and describes the demographic, clinical characteristics, and medication history of its participants.

2.1. The cohort

2.1.1. Children's Attention Project (CAP)

Participants for NICAP were initially recruited from the CAP study. The CAP cohort and methods have been described previously (Sciberras et al., 2013). In summary, the CAP study involved screening for ADHD among children in their second year of formal schooling, using parent and teacher reports on the Conners 3 ADHD Index (N = 6098) (Conners 2008). The screening process took place across 43 socio-economically diverse primary schools in Melbourne, Australia. Children screened positive as potential ADHD cases if parent and teacher ADHD indices were at or above the 75th percentile for boys and 80th percentile for girls. Children screened negative if both parent and teacher ADHD indices were ≥75th percentile for boys and ≥80th percentile for girls. Individuals that were screened as positive for ADHD then completed a parent face-to-face diagnostic interview to confirm ADHD status. The baseline data collection, conducted between 2011 and 2012, included a sample of 179 children diagnosed with ADHD and 212 children classified as non-ADHD controls. Following on from CAP baseline data collection, participants were followed up at 2 intervals (18 and 36 months from CAP baseline) at ages 8.5 and 10.

2.1.2. Neuroimaging of the Children's Attention Project (NICAP)

Baseline recruitment for the NICAP study coincides with the CAP 36-month follow-up data collection (age 10 years). Enrolment in the NICAP study from the CAP cohort required obtaining additional informed consent from the participants' parents or guardians. The NICAP study consists of 3 time points, at roughly 18-month intervals, between the ages of 9 and 14 years. At each data collection time-point participating

families attended a 3.5 hour assessment session at The Royal Children's Hospital, Melbourne, Australia. Assessment sessions involve a structured diagnostic interview, parent questionnaire, child cognitive assessment and MRI scanning. Questionnaires were also sent to the child's classroom teacher to ensure the child is assessed in their usual classroom condition. The research staff conducting assessments were blinded to the child's diagnostic status.

At baseline (10 years) and 36 months (13 years), a well-validated and widely used National Institute of Mental Health Diagnostic Interview Schedule for Children (DISC-IV) diagnostic interview (60–90 mins) was conducted to determine the participants' ADHD status and comorbid mental health problems including anxiety, mood and externalizing disorders. This thesis focused on individuals with persistent ADHD diagnosis across the study time points. As such, the participants included in the ADHD group received a confirmed clinical ADHD diagnosis based on a clinically administered DISC-IV interview (Shaffer et al. 2000) at each assessment (recruitment [3 years prior to imaging], wave 1 and wave 3 imaging time points). Participants in the control group did not meet the diagnostic criteria for ADHD at any study time point. Demographic and clinical characteristics of the ADHD and non-ADHD group is provided in Table 2.1

Table 2.1 Demographics and clinical variables of the NICAP data set

		Mean (SD)		***p-value***
		ADHD	***Control***	
Time point 1	**Demographic factors**			
	Scans	71	102	
	Mean FWD	0.694 (0.15)	0.688 (0.17)	0.489
	Age – years	10.40 (0.49)	10.36 (0.50)	0.626
	Female sex n (%)	15 (21.12%)	42 (41.17%)	0.009
	Left-handed n (%)	13 (18.30%)	14 (13.46%)	0.501
	Matrix reasoning raw	21.08 (5.97)	22.15 (4.68)	0.383
	SES	1019.9 (41.76)	1018 (45.72)	0.881
	Clinical factors			
	Connor's Index	11.41 (6.46)	2.26 (3.73)	<0.001

	Hyperactivity symptoms	4.90 (2.76)	0.94 (1.39)	<0.001
	Inattentive symptoms	7.08 (2.15)	1.57 (2.02)	<0.001
	Medication use (%)	28 (39.43%)	7 (6.86%)	<0.001
	Extern. Disorder n (%)	37 (52.11%)	15 (14.70%)	<0.001
	Intern. Disorder (%)	20 (28.62%)	11 (10.78%)	0.010
Time point 2	**Demographic factors**			
	Scans	70	96	
	Mean FWD	0.644 (0.18)	0.601 (0.14)	0.371
	Age – years	11.69 (0.53)	11.73 (0.55)	0.597
	Female sex n (%)	16 (22.85%)	41 (42.70%)	0.012
	Left-handed n (%)	11 (15.71%)	12 (12.50%)	0.411
	Matrix reasoning raw	23.77 (5.16)	24.55 (4.58)	0.340
	SES	1021 (40.52)	1016 (46.12)	0.519
	Clinical factors			
	Connor's Index	10.60 (6.72)	2.64 (4.19)	<0.001
	Medication use (%)	25 (35.71%)	8 (8.33%)	<0.001
Time point 3	**Demographic factors**			
	Scans	47	64	
	Mean FWD	0.694 (0.11)	0.637 (0.08)	0.885
	Age – years	13.25 (0.61)	13.15 (0.57)	0.381
	Female sex n (%)	12 (25.55%)	28 (43.75%)	0.075
	Left-handed n (%)	6 (12.76%)	6 (9.37%)	0.596
	Matrix reasoning raw	25.51 (5.08)	25.97 (4.05)	0.891
	SES	1018.4 (41.14)	1014.2 (50.07)	0.722
	Clinical factors			
	Connor's Index	9.17 (6.92)	1.48 (3.21)	<0.001
	Medication use (%)	13 (27.65%)	1 (1.56%)	<0.001
	Extern. Disorder n (%)	12 (25.53%)	5 (7.81%)	0.035
	Intern. Disorder (%)	10 (21.27%)	3 (4.68%)	0.051

2.2. NICAP procedures

2.2.1. Questionnaires

During the NICAP study, comprehensive questionnaires covering various functional domains were administered to gather data on predictor and outcome variables (see Table 2.2.). These questionnaires, completed by the child, their parents, and teachers, focused on the child's ADHD symptom severity, social, and emotional functioning. Parents provided further details through questionnaires about the child's emotional, physical, social, and school quality of life, experiences of peer victimization, symptoms indicative of autism spectrum disorders, general health, and medication history. Additionally, questionnaires pertaining to the home environment assessed family quality of life, stressful life events, and parental mental health. The study also included retrospective questions on pre- and post-natal factors such as maternal alcohol consumption and smoking during pregnancy, gestational diabetes, pre-eclampsia, stress/anxiety/depression during pregnancy, birth weight, gestational age, neonatal intensive care, and postnatal maternal depression. Teachers provided information about the child's academic competence, the student-teacher relationship, and details regarding their own teaching characteristics and education services.

Table 2.2 Summary of Assessment measures for NICAP study

Measures		**Source**	**Time Point**				
			CAP		**NICAP**		
			1	**2**	**1**	**2**	**3**
Diagnostic Interview							
ADHD & comorbidities	DISC-IV; structured clinical interview	P	✓		✓		✓
Magnetic Resonance Imaging							
	Structural T1	C			✓	✓	✓
	Structural T2	C			✓	✓	✓
	Multi-shell DWI	C			✓	✓	✓

	Resting state fMRI	C			✓	✓	✓
Cognitive Assessment							
Intellectual functioning	WASI: vocabulary, matrix reasoning	C	✓		✓	✓	✓
Language	CELF 4th edition: screening test	C	✓		✓	✓	✓
Academic Achievement	WRAT 4: word reading, numeracy	C	✓		✓	✓	✓
Working Memory	Computerised N-Back	C			✓	✓	✓
Inhibition	Computerised stop-signal task	C			✓	✓	✓
Sustained Attention	Computerised SART	C			✓	✓	✓
Spatial Attention	Landmark task	C			✓	✓	✓
Cognitive Flexibility	Computerised set-shifting task	C			✓	✓	✓
Visual-Motor	Grooved pegboard test	C			✓	✓	✓
Questionnaires							
Puberty Development	Pubertal development scale; Tanner stage charts	P			✓	✓	✓
Child Functioning							
ADHD Symptoms	Conner' 3 parent & teacher ADHD index	P,T	✓	✓	✓	✓	✓
Autism Spectrum Disorder	SCQ – lifetime version; SSIS: autism spectrum scale	P	✓	✓	✓	✓	✓
Mental Health & Social Functioning	SDQ: total problems score, emotional, conduct, peer and inattention-hyperactivity scale	P,T	✓	✓	✓	✓	✓
Social Skills	SSIS: Responsibility, self-control, bullying, communication and engagement scales	P,T	✓	✓	✓	✓	✓
Prosocial Behaviours	SDQ: Prosocial behaviour	P,T	✓	✓	✓	✓	✓
Victimisation	SEQ: Physical victimisation, relational victimisation	P		✓	✓	✓	✓
Quality of Life	Paediatric quality of life inventory (Ped QL v4)	P	✓	✓	✓	✓	✓
Health	Medication history, child global health, sustained injuries, allied health services use	P	✓	✓	✓	✓	✓
Home Environment							

Parental Mental Health	Kessler 6: psychosocial symptom screener	P	✓	✓	✓	✓	✓
Family Quality of Life	CHQ: Emotional impact, time impact, family activities	P	✓	✓	✓	✓	✓
Family Adversity	Stressful life events scale	P	✓	✓	✓	✓	✓
Parenting	LSAC parenting scales: parental warmth, hostility, consistency, parental self-efficacy	P	✓	✓	✓	✓	✓
Couple Relationship	LSAC family functioning scales: parental conflict, support, and relationship satisfaction	P	✓	✓	✓	✓	✓
Pre/postnatal Factors	LSAC prenatal & postnatal questions	P	✓				
School Environment							
Classroom performance	SSIS: Academic competence	T	✓	✓	✓		✓
Teacher-child Relationship	STRS (short form): conflict and closeness	T	✓	✓	✓		✓
Education Service	Specialised school services, individual education plans, in-class assistance and grade repetition	T	✓	✓	✓		✓
Physical Measures							
	Height, Weight	C	✓		✓	✓	✓

Legend: Child ages time points, CAP 1 - 7 years, CAP 2 - 8.5 years, NICAP 1- 10 year, NICAP 2 - 11.5 years, and NICAP 3 - 13 years

Abbreviations: Clinical evaluation of language fundamentals (CELF),child health questionnaire,(CHQ), diagnostic interview schedule for children-IV (*DISC-IV*), diffusion weighted imaging (DWI), functional magnetic resonance imaging (fMRI), longitudinal study of Australian children (*LSAC*), sustained attention to response task (*SART)*, social communication questionnaire (*SCQ*), strengths & difficulties questionnaire (*SDQ*), social experience questionnaire (*SEQ*), social skills improvement system (*SSIS*), student-teacher relationship scale (*STRS*), test of everyday attention for children (*TEA-CH*), Wechsler abbreviated scales of intelligence (*WASI*), Wechsler intelligence scale for children (*WISC*), wide range achievement test (*WRAT*). Table 2.2 is sourced from NICAP protocol publication (Silk et al., 2016).

2.2.2. Clinical features of the ADHD group

The following section will discuss the clinical features of the ADHD group investigated in this study such as presentation type, symptom severity, medication use and co-occurring comorbidities.

ADHD Symptom Presentation

ADHD Subtype

ADHD symptom count was assessed only at NICAP baseline using the DISC-IV. Among those classified as persistent-ADHD at baseline, 59.7% presented with ADHD-combined subtype, 32.8% ADHD-inattentive subtype and 7.4% ADHD-hyperactive/impulsive subtype.

ADHD Symptom Changes Across the NICAP Time Points

The Connors 3 ADHD index was conducted at all 3 time points of the NICAP study. As expected, individuals with ADHD displayed significantly higher ADHD symptom severity compared to controls (Table 2.1). Within the ADHD group, symptom severity decreased across the three study time points (see Figure 2.1). The ARI, a measure of emotional dysregulation, was conducted at study time points one and two. Compared to controls, children with ADHD had significantly higher ARI scores (Table 2.1). Within the ADHD group, ARI score reduced across study time points one and two (see Figure 2.2). These patterns are in line with previous research that indicates as individuals transition from childhood into early adolescence ADHD symptom severity reduces and emotional dysregulation issues remain relatively stable (Philip Shaw et al. 2014; Shaw and Sudre 2021).

Figure 2.1 ADHD Symptom Severity in the ADHD group across the 3 study time points

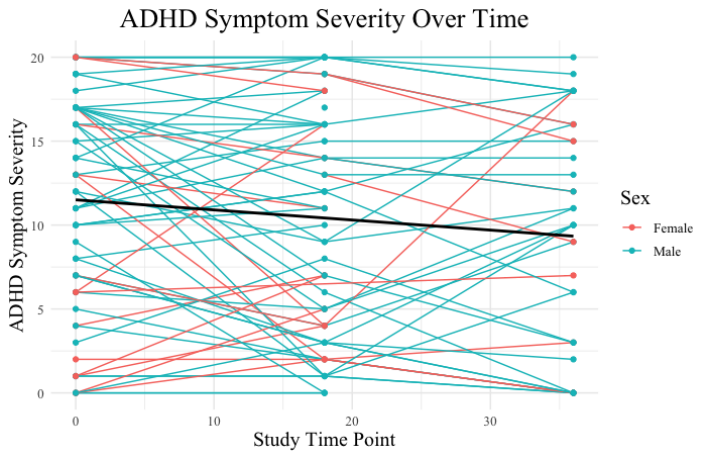

Figure 2.2 ARI scores in the ADHD group across the 3 study time points

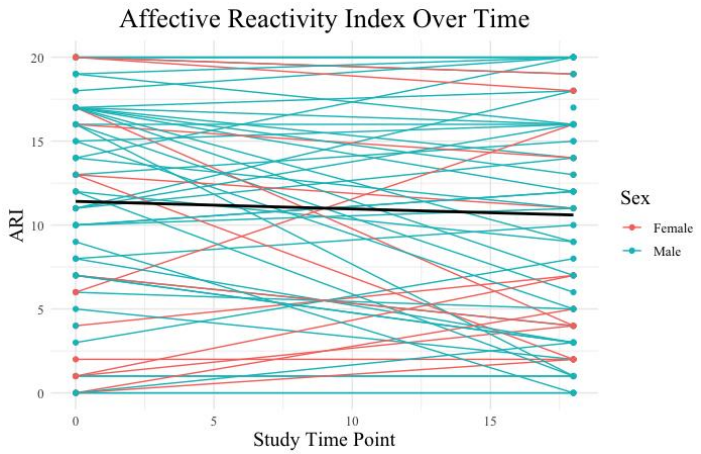

Comorbidities

During the DISC-IV, participants were assessed for the presence of internalizing and externalizing co-occurring disorders. NICAP participants were identified as presenting with an internalizing disorder if they met diagnostic criteria for depression, dysthymia, separation anxiety disorder, social phobia, generalized anxiety disorder, posttraumatic stress disorder, obsessive-compulsive disorder, hypomania, or a manic episode. NICAP participants were identified as presenting with an externalizing disorder if they met diagnostic criteria for oppositional defiant disorder or conduct disorder. As reported in Table 2.1, children in the ADHD group presented with significantly more co-occurring comorbidity (internalizing or externalizing disorders) compared to the control group at all three study time points. Importantly, as the neurobiological differences in comorbidities in ADHD remains poorly understood, sensitivity analysis was conducted to ensure the findings of this thesis were not confounded by the presence of comorbidity. Details of the sensitivity analysis used is described in section 3.2.5.

Medication Status

Medication status was collected at all three NICAP study time points. In total, 81 individual scans were performed on participants who were actively taking medication during the MRI scan. The participants were either on a single medication or a combination of multiple medications. Out of the 81 scans, 42 individuals were taking a single medication, and 39 individuals were taking multiple medications. Full details about the

type of medication use in this study is provided in Table 2.3. To ensure the case-control findings described in this thesis were not confounded by medication use, sensitivity analysis was conducted to investigate the impact of medication. Details of the sensitivity analysis used is described in section 3.2.5.

Table 2.3 Medication use during MRI scans in this thesis

Type of medication	**Name of medication**	**Number of scans**
Stimulants		
	Ritalin (Methylphenidate)	33
	Concerta (Extended-release Methylphenidate)	26
	Dexamphetamine	1
	Vyvanse (Lisdexamfetamine)	10
Non-stimulants		
	Strattera (Atomoxetine)	5
	Guanfacine (Intuniv, Tenex)	2
	Catapres (Clonidine)	14
Antidepressants		
	Lovan (Fluoxetine)	11
Antipsychotics		
	Risperdal (Risperidone)	8
Sleep Aids		
	Melatonin	20

3 The Limbic System in Children and Adolescents with ADHD: A Longitudinal Structural MRI Analysis

Publication Details:

Journal: Biological Psychiatry: Global Open Science

Chapter DOI: https://doi.org/10.1016/j.bpsgos.2023.10.005

Authors

Michael Connaughton, M.Sc.[1,2], Erik O'Hanlon, Ph.D.[3], Timothy J. Silk, Ph.D.[4,5], Julia Paterson, B.S.[1,2], Aisling O'Neill, Ph.D.[3], Vicki Anderson Ph.D.[4,6], Robert Whelan, Ph.D.[2,7], Jane McGrath, M.D., Ph.D.[1,2]

Affiliations

1. Department of Psychiatry, School of Medicine, Trinity College Dublin, Ireland
2. Trinity College Institute of Neuroscience, Trinity College Dublin, Ireland
3. Royal College of Surgeons in Ireland, Dublin, Ireland
4. Murdoch Children's Research Institute, Melbourne, Australia
5. Centre for Social and Early Emotional Development and School of Psychology, Deakin University, Geelong, Australia
6. The Royal Children's Hospital, Melbourne, Australia
7. Global Brain Health Institute, Trinity College Dublin, Ireland

Co-authors contributions:

EH contributed technical support for sMRI image processing. TS, JP, and RW were involved in manuscript writing, editing, and NICAP data collection, with RW also providing statistical analysis support. AN offered statistical analysis support. VA assisted with NICAP data collection. JMG contributed to the writing and manuscript formatting, focusing on clarity, coherence, and maintaining academic standards.

3.1. Introduction

Attention deficit hyperactivity disorder (ADHD) is a common neurodevelopmental disorder with global prevalence estimates of 5-7% in children and adolescents (Polanczyk et al. 2007). Alongside the core behavioural symptoms of inattention, hyperactivity, and impulsivity, ADHD is also associated with emotional dysregulation (Seymour et al. 2017; Shaw, Stringaris, et al. 2014). Emotional dysregulation is an individual's inability to adjust their emotional state in a manner that promotes adaptive, goal-orientated behaviours (Shaw, Stringaris, et al. 2014). In individuals with ADHD, emotional dysregulation during childhood is associated with increased rates of anxiety, mood disorders, disruptive behaviour disorders, and drug abuse in adulthood (Althoff et al. 2010). During the transition from childhood to adolescence, ADHD symptoms undergo notable change, with hyperactive and impulsive symptoms often declining (Langberg et al. 2008; Ickowicz 2002)and inattentive symptoms tending to persist (Hart et al. 1995). While the trajectories of emotional dysregulation during this period remain unclear, studies suggest that as the core symptoms of ADHD improve into adulthood, emotional dysregulation might also show parallel improvements (Althoff et al. 2010).

In parallel with these symptom changes, it is known that the human brain undergoes significant structural changes in grey matter volume, surface area, and cortical thickness (Tamnes et al. 2017; Peterson et al. 2021; Vijayakumar et al. 2016) during the transition from childhood to adolescence. Interestingly, longitudinal neuroimaging research in individuals with ADHD consistently reveals deviations in brain development. Compared to controls, individuals with ADHD exhibit reduced or delayed cortical maturation in areas associated with attention, impulse control, and executive functioning (Shaw et al. 2007; Shaw et al. 2012; Rubia 2007; Shaw and Sudre 2021). Two leading neurodevelopmental theories of ADHD include the maturation delay hypothesis (Shaw et al. 2007; Shaw et al. 2012; Rubia 2007). and the convergence model (Shaw and Sudre 2021). The maturation delay hypothesis posits that compared to controls, individuals with ADHD show a roughly 3-year delay in cortical development, particularly in the frontal, temporal, and parietal lobes(Shaw et al. 2007), with this delay being most pronounced during childhood (Shaw et al. 2012; Shaw et al. 2007). The convergence model suggests that symptom improvement or remission in ADHD is associated with the normalization of neural features that were atypical in early childhood (Shaw and Sudre 2021). This model

also integrates the concept of delayed maturation in ADHD, suggesting that it is underpinned by a correction of earlier developmental lags(Shaw and Sudre 2021). The critical difference between the two models is that according to the convergence model, children with persistent ADHD show ongoing non-progressive differences in brain structures across the lifetime compared to controls (Shaw and Sudre 2021).

Although these developmental models provide insights into the neurobiological underpinnings of ADHD symptom progression, most longitudinal studies have focused on cortical structures (Shaw et al. 2012; Shaw et al. 2007). As a result, our understanding of these models in relation to subcortical structures and networks remains largely incomplete (Hoogman et al. 2017b; Rosch et al. 2018). This gap is particularly surprising considering that functional imaging research suggests that abnormalities in subcortical brain regions may be present from the onset of ADHD and continue throughout life, irrespective of symptom change (Halperin and Schulz 2006). To further understand the neurobiological mechanisms of ADHD, it is essential to extend these neurodevelopmental models to subcortical structures and networks.

The limbic system, often termed the "emotional network" (Mesulam 2000; Catani, Dell'acqua, and Thiebaut de Schotten 2013), is a group of interconnected cortical (cingulate gyrus and orbitofrontal cortex) and subcortical (amygdala, hippocampus, mammillary bodies, and anterior thalamic nuclei) structures (see network schematic in Figure 1) (Catani, Dell'acqua, and Thiebaut de Schotten 2013). The limbic system plays a crucial role in emotional processing and regulation, as well as many other aspects of human behaviour and cognition (Catani, Dell'acqua, and Thiebaut de Schotten 2013). While the limbic system is suggested to be a central network in the pathophysiology of many neurodevelopmental disorders (Rajmohan and Mohandas 2007), its specific role in ADHD remains largely unknown. This is perhaps surprising, given the high prevalence of emotion dysregulation in people with ADHD (Shaw, Stringaris, et al. 2014). Interestingly, a small number of studies have also reported that core symptoms of ADHD are associated with structural and functional alterations within the limbic system (Bauer et al. 2018; Hart et al. 2013; Tajima-Pozo et al. 2016). Despite the links between limbic system pathology and core symptoms of ADHD, no previous studies have investigated the developmental trajectory of the limbic system in ADHD. The study aims to provide novel insights into the structural development of this crucial brain network and also further our understanding

of the relationship between ADHD symptoms and brain structure during the pivotal transition from childhood into mid-adolescence.

Using longitudinal structural MRI data, acquired across three time points, this study investigates the volumetric development of limbic system structures in children with ADHD and controls. The hypotheses are that compared to controls, individuals with ADHD will display 1) lower volumes and 2) delayed development in limbic system structures during the transition from childhood to mid-adolescence. The study also aims to investigate brain-behaviour relationships through a series of exploratory analyses in order to better understand the functional impact of the limbic system in ADHD.

3.2. Methods and Materials

3.2.1. Study Design and Participants

The data in the studies described in this thesis were collected as part of the Neuroimaging of the Children's Attention Project (NICAP) (Sciberras et al. 2013; Silk, Genc, et al. 2016). NICAP procedures and clinical characteristics have been previously described in Chapter 2. Briefly, NICAP is a single site, multimodal longitudinal neuroimaging study assessing a community-based cohort of children with and without ADHD over a 5-year period. The NICAP study consists of three study time points at approximately 18-month intervals, from ages 9-14 between 2014-2018.Multimodal MRI scanning occurred at three time points. This thesis focused on individuals with persistent ADHD diagnosis across the study time points. As such, the participants included in the ADHD group received a confirmed clinical ADHD diagnosis based on a clinically administered National Institute of Mental Health Diagnostic Interview Schedule for Children (DISC-IV) (Shaffer et al. 2000) at each assessment (recruitment [3 years prior to imaging], wave 1 and wave 3 imaging time points). Participants in the control group did not meet the diagnostic criteria for ADHD at any study time point. Written informed consent was obtained from participants' parents/guardians before enrolment. Ethical approval for the research conducted in this thesis was obtained from both the Royal Children's Hospital Melbourne Human Research Ethics Committee (HREC #34071) and the School of Psychology, Trinity College Dublin (SPRECC042021-01).

3.2.2. Structural MRI Data Acquisition

A 30-minute mock scan session was completed before scanning to familiarize each participant with the MRI environment and procedures. All neuroimaging data were collected at a single site at the Murdoch Children's Research Institute at the Royal Children's Hospital, Melbourne, on a 3-Tesla Siemens scanner using a 32-channel head coil, however while the first two waves were collected on a total imaging matrix (TIM) Trio scanner, the third wave was collected after an upgrade to a MAGNETOM Prisma scanner (previous papers on this cohort have found minimal effects of scanner upgrade (Vijayakumar, Youssef, et al. 2021)). T1-weighted volumes were collected using a multi-echo magnetization prepared rapid gradient-echo (MEMPRAGE) sequence with in-scanner motion correction (MoCo) (TR = 2530 ms, TE = 1.77, 3.51, 5.32, 7.2 ms, matrix = 256 x 232, number of slices = 176, voxel size = 0.9 mm^3, flip angle = 7^o). T2-weighted volumes were obtained using a T2-SPACE (Sampling perfection with application optimized contrast with flip angle evolution) protocol (TR = 3200 ms, TE = 532, matrix = 256 x 230, slices = 176, voxel size = 0.9 mm^3). T1 and T2-weighted volumes were used to provide optimal sensitivity and increase the accuracy of subcortical brain reconstruction (Seiger et al. 2021; Iglesias et al. 2015).

3.2.3. MRI Quality Control

MRI quality control (QC) procedures were undertaken at pre, during and post scan. Prior to the scan, a mock scanner session was completed to ensure participants were comfortable in the MRI environment and could minimise motion during live scanning session. During live scanning, Siemens in-scanner motion correction feature, adjusting the field-of-view and slice positioning in real-time to account for movement during the acquisition process (Tisdall et al. 2012). This feature significantly reduces the effect of motion artefacts and substantially improves image quality (Zaitsev, Maclaren, and Herbst 2015). This was particularly crucial for the studied population, namely with attentional and hyperactivity difficulties, where motion is a large challenge (Murillo et al. 2015). In cases where head motion was high during scan acquisition, multiple scans were acquired until a suitable image was completed. Poor images due to motion were identified by the expert on-site radiographer.

Post scan QC procedures involved a meticulous visual inspection of both raw and processed images that followed an established MRI image quality control guidelines

(Vijayakumar, Ball, et al. 2021). The inspection criteria were focused on several key aspects such as, ringing artifacts (characterised by circular or ripple-like patterns that could distort image quality), motion artifacts (marked by blurring or ghosting), image noise (variations in image intensities and/or graininess) and image truncation/ field-of-view cut-off. For the raw T1 and T2 images, a 4-point Likert scale was employed in the evaluation. A score of '1' indicated a sharply defined image with no observable artifacts. A score of '2' was assigned to images with slight blurriness or minor ringing confined to a small cortical area. Images rated '3' exhibited considerable blurriness and/or ringing throughout much of the brain, extending into white matter regions. A rating of '3' was also given if image field-of-view cut-off was present. A rating of '4', denoting extensive blurriness and/or ringing across the entire brain. If image field-of-view cut-off was present a rating of 4 was also given. Any image that received a score of '3' or higher was excluded from the study to maintain the integrity of the data. The processed images were similarly scrutinised, evaluated on a 3-point Likert scale that assessed the accuracy of anatomical structures such as white matter, cerebrospinal fluid (CSF), and pial surfaces. A score of '1' signified near-perfect reconstruction, while '2' indicated minor reconstruction issues confined to small areas of the brain. A score of '3', signifying poor reconstruction characterised by extensive or distorted areas of CSF. Any score of 3 led to the exclusion of the scan. The methodology implemented in the study included standardised viewing conditions, ensuring that all images were reviewed under consistent lighting and display settings. An experienced neuroscientist, trained in identifying and rating MRI artifacts, carried out the inspection. A sequential analysis approach was adopted, where each raw image was initially reviewed for quality before proceeding to assess the processed images. This approach ensured an unbiased evaluation.

Following this comprehensive visual inspection, a total of 380 scans were deemed suitable for analysis, with 44 scans excluded due to incomplete MRI image sets (both T1 and T2 images not present) and 27 scans being removed due to quality concerns (20 removed at pre-processing and 7 at post-processing) . Throughout this process, no manual edits were made to the remaining data.

3.2.4. Structural MRI Data Processing

FreeSurfer software (http://surfer.nmr.mgh.harvard.edu/) was used to isolate the structures of the limbic system. FreeSurfer analyses were performed using a Redhat-based

scientific Linux 7 on the high-performance computing system at Trinity College Dublin, Ireland. All MRI images were processed using FreeSurfer's *recon -all* function (version 7.2) for full cortical reconstruction and brain segmentation (Fischl et al. 2002; Fischl et al. 2004). The Desikan-Killiany-Tourville (DKT) atlas was used for brain parcellations (Desikan et al. 2006a). Additional FreeSurfer segmentation tools were used to extract the anterior thalamic nuclei (Iglesias et al. 2018) and mammillary bodies(Billot et al. 2020). The following bilateral limbic system structures were isolated: amygdala, hippocampus, mammillary bodies, anterior thalamic nuclei, cingulate gyrus (sum of cingulate gyrus parcellations), and orbitofrontal cortex (sum of orbitofrontal cortex parcellations).

3.2.5. Behavioural Measures: Conner's 3 ADHD Index and the Affective Reactivity Index

Conner's 3 ADHD Index (CAI): a rating scale questionnaire consisting of 10 items designed to evaluate the presence of the primary symptoms associated with ADHD in children aged 6 to 18 years within the past month (Conners 2008). These items are aligned with the diagnostic criteria outlined in the DSM-5 and are rated using a four-point Likert scale. At each of the three NICAP study time points, the parent-reported Conner's 3 ADHD index was administered to assess the presence of core ADHD symptoms in study participants, with a higher score indicating a greater presence of symptoms.

Affective Reactivity Index (ARI): is a psychological assessment tool for measuring emotional reactivity and irritability in children and adolescents. The ARI is a 7-item Likert scale questionnaire completed by the child's parent/guardian which has been shown to have excellent internal consistency (Stringaris et al. 2012). The ARI was completed at NICAP study time points 1 and 2, with a higher ARI score indicating increased emotional dysregulation and irritability.

3.2.6. Statistical Analysis

Prior to statistical analyses, all data points were Winsorized (Reifman and Garrett 2010; Blaine 2018) (i.e. any data points with a z-score exceeding ±3 were adjusted to ±3 standard deviations from the mean) to minimize the effects of extreme outliers. Primary statistical analyses were performed using the R software package (version 4.1.1) (Team

2013). To measure between-group differences in volume of limbic system structures, linear mixed-effects modelling (LMM) was performed using the *lme4* package in R (version 1.1-27.1) (Bates et al. 2014). A LMM is a versatile statistical approach that combines both fixed and random effects to analyse complex unbalanced data structures, such as those found in longitudinal studies (Fitzmaurice, Laird, and Ware 2012; Verbeke 1997). Fixed effects in an LMM represent the explanatory variables that are assumed to hold uniformly across the study such as sex and diagnostic group. These effects quantify the general relationships between these variables and the outcome of interest (DV), providing insights into broader patterns or tends within the data. Random effects, on the other hand, account for individual variations by allowing each subject to have their unique baseline (intercept) and rate of change over time (slope), thus capturing the inherent variability across subjects in the data.

An essential procedure of LMM is data-driven model selection, in which the goal is to identify a parsimonious model (i.e., high goodness of fit using as few explanatory variables as possible) to reduce the risk of a Type 1 error (Zuur et al. 2009). An established top-down LMM model selection was used to select the optimal model for each structure of the limbic system (Zuur et al. 2009; Harrison et al. 2018). The details of the LMM models tested in this study are presented in Table 3.1. IQ was not included as a covariate in any of the tested models as the inclusion of IQ is deemed inappropriate for neurodevelopmental disorders involving cognitive deficits such as ADHD as it can lead to overcorrected and spurious findings (Dennis et al. 2009). A top-down approach to model selection starts with the most complex model, which includes all random and fixed effects. These effects are then systematically removed in a backward fashion using a combination of fit statistics – corrected Akaike Information Criterion (AICc), corrected Bayesian Information Criterion (BICc), and Log-Likelihood Ratio test (LRT) – to identify the optimal model for each limbic system structure. Random effects were identified by comparing the fit of the models with and without the random effect of slope (RX1a vs. RX1b). The random effect of slope was included if it significantly increased the model fit and the model's boundary was not singular. The fixed effects of interest (i.e., group and group-by-age interaction) were identified by comparing the model fit of the null model (a model that only contained the covariate fixed effects: age at baseline, age, sex, and intracranial volume) against both fixed-effects models (FX1/FX2 vs. null). If a fixed-effects model significantly increased fit compared to the null model, this indicated a

significant effect on volume due to the fixed effects of interest. If both fixed effects models significantly increased model fit compared to the null model, but there was no difference in model fit between the two fixed effects models (FX1 vs. FX2), the parsimonious model (FX1) was selected, as including the interaction term was not statistically justified.

When initially comparing model fit, Maximum Likelihood (ML) was used to allow for comparability with the model fit parameters AICc and BICc. However, once the "optimal model" was identified, this model was refitted using Restricted Maximum Likelihood (REML) to increase the accuracy of estimates of the final model parameters. The covariance structure was set to "unstructured", which is the default covariance structure in R software. This structure imposes no restrictions on the covariance parameters, thus allowing the inclusion of variations in the slopes.

In all the optimal models, a robust two-stage False Discovery Rate (FDR) (Benjamini, Krieger, and Yekutieli 2006) procedure was employed to correct for multiple comparisons at q = 0.05. Two-stage FDR correction was conducted using the *MuToss* package (Team et al. 2017) in R (version 4.1.1). In line with recommendations for generating effect sizes in longitudinal LMM studies (Hoffman 2015), pseudo-standardised coefficients (β) were calculated using the *effectsize* package (Ben-Shachar, Lüdecke, and Makowski 2020) in R (version 4.1.1). These coefficients standardise according to the levels of the predictor, taking into account both within-group and between-group variants, thus offering accurate and reliable measure of effect sizes in longitudinal LMM studies.

Exploratory analyses were performed to examine the relationship between limbic system volumes and ADHD symptoms (CAI and ARI scores) in children and adolescents with ADHD. These relationships were investigated using LMM via the lme4 package in R (version 1.1-27.1) (Bates et al. 2014). The chosen LMM model, illustrated as model FX3b in Table 3.1, evaluated if changes in limbic system volumes over time varied based on ADHD symptom severity, incorporating an age-by-ADHD symptoms interaction term. This model also adjusted for covariates age, sex, and intracranial volume. To mitigate the effects of multiple comparisons, a two-stage FDR correction was applied using the MuToss package (Team et al. 2017) in R (version 4.1.1).

Sensitivity analyses were performed to assess the potential impact of confounding factors (case-control sex imbalance and ADHD medication status) on the primary statistical analyses. The first sensitivity analysis examined the potential confound caused by the case-control sex imbalance in the study sample. To investigate this, 100 LMM

iterations were run using randomly selected proportionately sex-matched case-control samples. To ensure the sex-matching in the control group was unbiased, 65 female controls scans were randomly excluded at each iteration using a script developed in R studio (see Section 12.1) (v.4.1.1). Averages of all 100 iterations were then collected to compare the results of the sensitivity analysis to the primary analysis.

The second sensitivity analysis explored the potential impact of medication use in the ADHD group. This was accomplished by conducting LMM analyses on the optimal models to compare limbic system volumes between individuals with ADHD who were taking medication and those who were not (Table 3.2). The third sensitivity analysis explored the potential impact of internalizing and externalizing comorbidities on limbic system volumes. To examine this, LMM analyses of the optimal models were conducted with an additional covariate of co-occurring disorder status (binary coded to indicate the presence or absence of an internalizing/externalizing disorder at Wave 1 and/or Wave 3).

Table 3.1 Linear mixed models tested: limbic system structures in ADHD and controls.

Random Effects Models
RX 1a
ROI ~ ICV + age at baseline + sex + diagnosis*age + (1 + age |subject)
RX 1b
ROI ~ ICV + age at baseline + sex + diagnosis* age + (1|subject)
Fixed Effects Models
Null 0a
ROI ~ ICV + age + age at baseline + sex + (1 + age | subject)
Null 0b
ROI ~ ICV + age + age at baseline + sex + (1|subject)
FX 1a

ROI ~ ICV + sex + age + age at baseline + diagnosis + (1 + age |subject)

FX 1b

ROI ~ ICV + sex + age + age at baseline + diagnosis + (1|subject)

FX 2a

ROI ~ ICV + sex + age + age at baseline + diagnosis* age + (1 + age |subject)

FX 2b

ROI ~ ICV + sex + age + age at baseline + diagnosis* age + (1|subject)

FX 3b

ROI ~ ICV + sex + age*ADHD symptom + (1|subject)

Table 3.1: RX = random effects, FX = fixed effects, ROI = regions of interest, ICV = intracranial volume, age = participant age from baseline (in months). To increase interpretability, the variables ICV and age at baseline were mean-centred. ADHD symptom = CAI and ARI score.

Table 3.2 Linear mixed models tested: limbic system and medication use in ADHD.

Random Effects Models

RX 1a

ROI ~ ICV + age at baseline + sex + medication status*age + (1 + age |subject)

RX 1b

ROI ~ ICV + age at baseline + sex + medication status*age + (1|subject)

Fixed Effects Models

Null 0a

ROI ~ ICV + age + age at baseline + sex + (1 + age | subject)

Null 0b

ROI ~ ICV + age + age at baseline + sex + (1|subject)

FX 1a

ROI ~ ICV + sex + age + age at baseline + medication status + (1 + age |subject)

FX 1b

ROI ~ ICV + sex + age + age at baseline + medication status + (1|subject)

FX 2a

ROI ~ ICV + sex + age + age at baseline + medication status * age + (1 + age |subject)

FX 2a

ROI ~ ICV + sex + age + age at baseline + medication status * age + (1|subject)

3.3. Results

3.3.1. Demographics of Study Population

The final data consisted of 380 scans from 166 individuals (children with ADHD:57, controls:109) scanned across three time points between the ages of 9-14 (Table 3.3).

Table 3.3 Study cohort characteristics.

	ADHD	**Controls**	**Test of significance**
Total scans	123	257	-
Scans wave 1	50	99	-
Scans wave 2	48	94	-
Scans wave 3	25	64	-
Medication use at any wave (%)	43	0	-
% female wave 1	20	43	p = .005
% female wave 2	22	43	p = .021
% female wave 3	33	42	p = .382
Mean age wave 1 (years)	10.35	10.38	p = .681
Mean age wave 2 (years)	11.65	11.72	p = .467
Mean age wave 3 (years)	12.98	13.16	p = .377

Table 3.3: summarises the number of scans, medication usage, sex distribution, and mean age for ADHD and control groups across the three study time points, along with the results of between-group statistical tests.

3.3.2. Limbic System Volumes in Children and Adolescents with ADHD and Controls

Model Selection Results: Limbic System Structures in ADHD and Controls

Random Effects Structure

Models that included intercept and slope as random effects were found to be the best fit for the amygdala (right) and cingulate gyrus (bilateral). The model that included only the intercept as a random effect was the best fit for the amygdala (left), hippocampus (bilateral), mammillary body (bilateral), anterior thalamic nuclei (bilateral), and orbitofrontal cortex (bilateral). For full results of the random effects model selection statistics please see Table 1 provided in the volume 2.

Fixed Effects Structures

The model that included both fixed effects (i.e., group-by-age interaction) was the best fit for the orbitofrontal cortex (left). The reduced model that only included the fixed effect of group was the best fit for the amygdala (bilateral), hippocampus (bilateral), orbitofrontal cortex (right), and cingulate gyrus (bilateral). For the mammillary bodies (bilateral) and anterior thalamic nuclei (bilateral), no significant difference in model fit was found between the fixed effects models and the null model, implying that in these structures, the null hypothesis could not be rejected due to the fixed effects of interest. For a complete overview of the fixed effects model selection statistics please see Tables 2 provided in the volume 2.

Results of Optimal Models

Full results of optimal models are presented in Table 3.7 and Table 3.8. There was a significant effect of group in volumes of the amygdala (left: β = -0.38, 95% CI = -0.66 to -0.11; right: β = -0.34, 95% CI = -0.60 to -0.08, (Figure 2.1)), hippocampus (left: β = -0.44, 95% CI = -0.73 to -0.15; right: β = -0.34, 95% CI = -0.64 to -0.04, (Figure 2.2)), cingulate gyrus (left: β = -0.42, 95% CI = -0.73 to -0.11; right: β = -0.32, 95% CI = -0.62 to -0.01, (Figure 2.3)) and orbitofrontal cortex (right: β = -0.33, 95% CI = -0.59 to -0.06, (Figure 2.4)). In all analyses, across all three time points, there was lower volume of these structures in children with ADHD compared to controls. All regions above survived two-

stage FDR correction. No significant difference in volume was observed between the groups for the bilateral mammillary bodies, anterior thalamic nuclei or left orbitofrontal cortex (Figure 2.5). There was no significant between-group difference in group-by-age interaction bilaterally in the amygdala, hippocampus, cingulate gyrus, orbitofrontal gyrus, mammillary bodies, and anterior thalamic nuclei.

3.3.3. Exploratory Analysis: The Relationship Between CAI and ARI Scores and Limbic System Volumes in Children and Adolescents with ADHD

The exploratory analysis found a significant effect of the interaction term CAI-by-age on the volume of the left mammillary body ($\beta = 0.17$, 95% CI = 0.08 to 0.25 (Figure 2.6)) in the ADHD group across the study time points. This finding survived two-stage FDR correction. After adjusting for multiple comparisons, CAI or ARI had no other significant effect on limbic system volumes in children and adolescents with ADHD (Figure 3.7-2.8; Table 3.6-3.7).

3.3.4. Sensitivity Analyses

The first sensitivity analysis examined the potential confound caused by the case-control sex imbalance in the study sample. In the 100 random sex-matched analyses, there was a slight reduction in p-value significance. This was expected given the increases in standard errors (SE) related to the reduction in sample size (Table 3.8). The right hippocampus was the only structure that no longer survived post hoc analysis following sensitivity analysis. To further understand the impact of group sex balance on right hippocampus volume, we compared beta weights and SEs of the main analysis and sex-balanced sensitivity models. Importantly, in the right hippocampus models, the beta values for the main effect of diagnosis were still within the SEs of the optimal models (see Figure 3.9), demonstrating that the overall pattern of results in the primary analysis was most likely not confounded by a sex-ratio group imbalance in the study.

The results of the second sensitivity analysis revealed no significant differences in any limbic system structure between the ADHD medication use group and the ADHD non-medication use group (Table 3.9-3.10). The results of the third sensitivity analysis are presented in Table 3.11. Importantly, the sensitivity analysis beta values of the main effect of diagnosis were still within the SEs of the optimal models (Figure 3.10). Given the beta value and SEs, the sensitivity analysis demonstrated that the overall pattern of results in

the primary analysis was most likely not confounded by the presence of internalizing and externalizing comorbidity.

Figure 3.1 Amygdala volume growth across the three study time points.

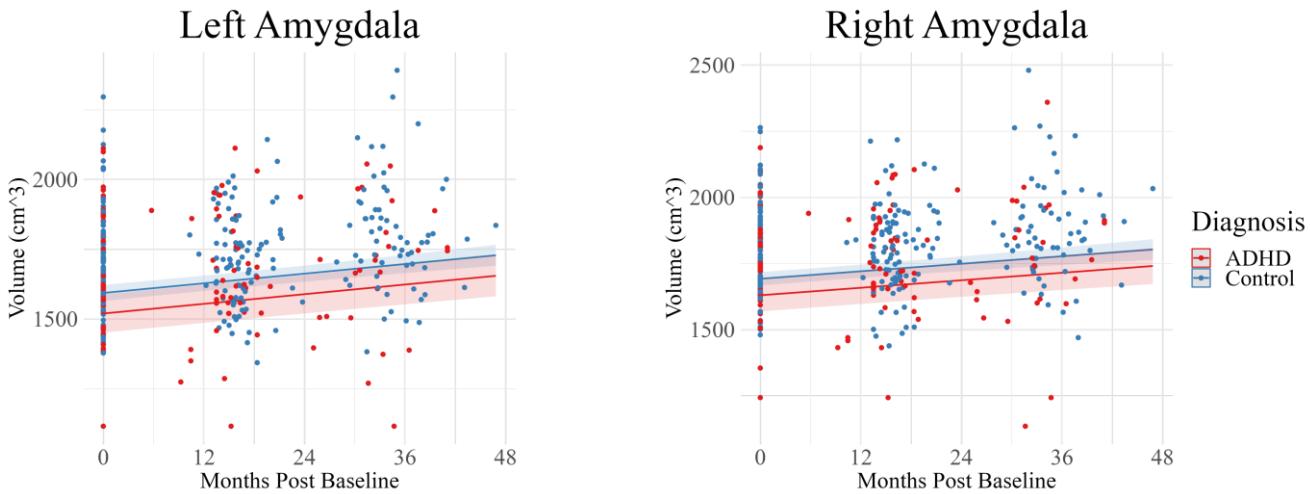

Figure 2.1: Bilateral amygdala development in the ADHD and control groups during the transition from childhood to mid-adolescence. A group effect was observed in the amygdala (bilaterally); the ADHD group displayed lower volumes compared to the control group across the three time points in this study. No significant group-by-age interactions were observed in the amygdala (bilaterally).

Figure 3.2 Hippocampus volume growth across the three study time points.

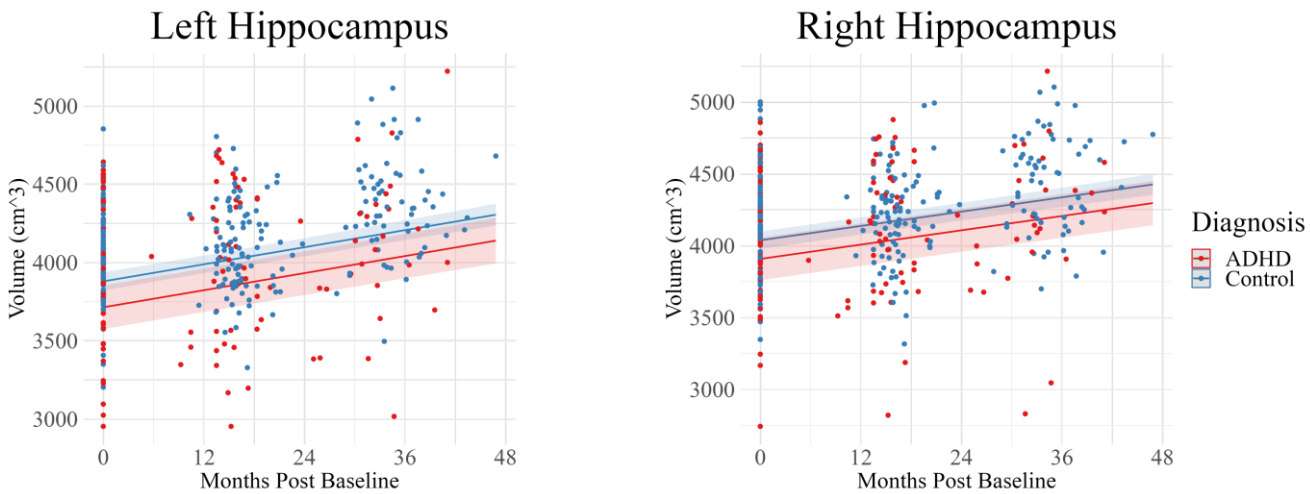

Figure 2.2: Bilateral hippocampus development in the ADHD and control groups during the transition from childhood to mid-adolescence. A group effect was observed in the hippocampus (bilaterally); the ADHD group displayed lower volumes compared to the control group across the three time points in this study. No significant group-by-age interactions were observed in the hippocampus (bilaterally).

Figure 3.3 Cingulate gyrus volume growth across the three study time points.

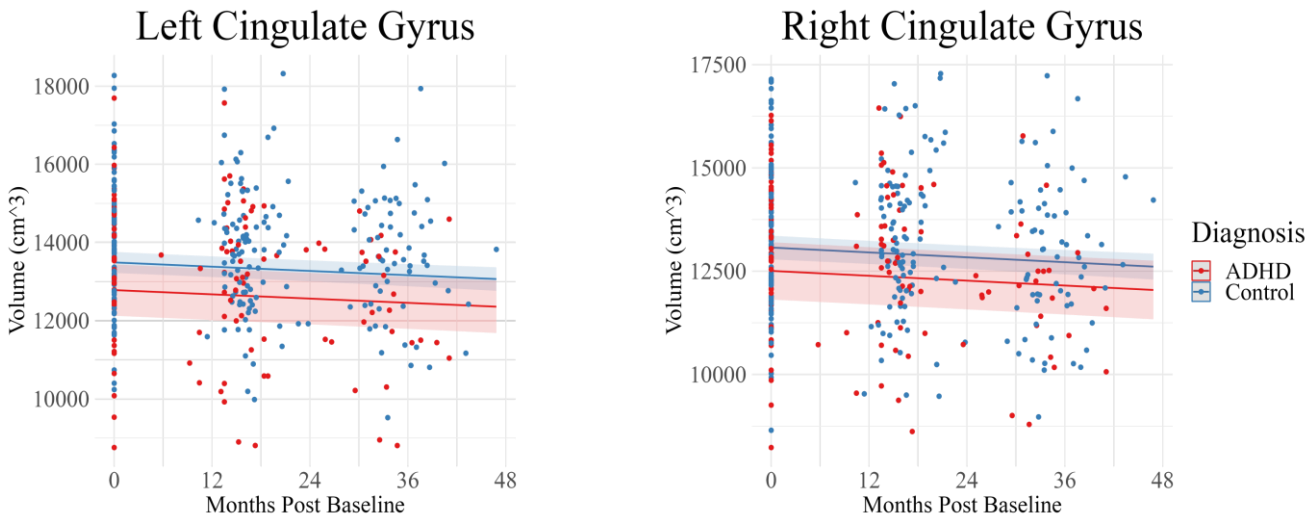

Figure 2.3: Bilateral cingulate gyrus development in the ADHD and control groups during the transition from childhood to mid-adolescence. A group effect was observed in the cingulate gyrus (bilaterally). Compared to controls, the ADHD group displayed lower volumes across the three time points in this study. No significant group-by-age interactions were observed in the cingulate gyrus (bilaterally).

Figure 3.4 Right orbitofrontal cortex volume growth across the three study time points.

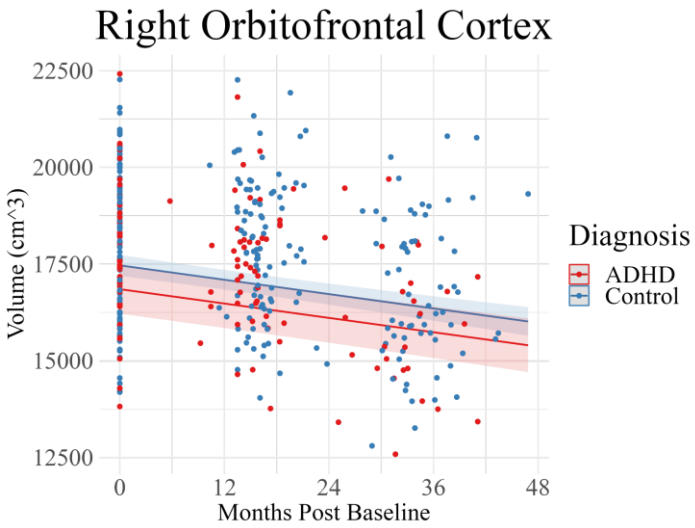

Figure 2.4: Right orbitofrontal cortex development in the ADHD and control groups during the transition from childhood to mid-adolescence. The ADHD group displayed lower volumes in the right orbitofrontal cortex compared to controls across the three time points in this study. No significant group-by-age interactions were observed in the right orbitofrontal cortex.

Table 3.4 Results of optimal mixed-effects models (without interaction term) analyses: Limbic system volumes in ADHD and Controls.

	ICV		**Sex**		**Months from baseline**		**Age at baseline**		**Diagnosis**	
	B (SE)	***t, p***	***B (SE)***	***t, p***	***B (SE)***	***t, p***	***B (SE)***	***t, p***	***B (SE)***	***t, p***
Hippocampus (Left)	4.384e-05 (7.986e-05)	0.549, 0.583	2.097e+02 (5.356e+01)	3.915, <0.000	9.093e+00 (5.875e-01)	15.476, <0.000	4.771e+01 (5.535e+01)	0.862, 0.389	-1.655e+02 (5.533e+01)	-2.991, 0.003*
Hippocampus (Right)	7.171e-05 (8.111e-05)	0.884, 0.377	1.501e+02 (5.678e+01)	2.643, 0.008	8.295e+00 (5.926e-01)	13.998, <0.000	3.665e+01 (5.894e+01)	0.622, 0.535	-1.298e+02 (5.902e+01)	-2.200, 0.029*
Amygdala (Left)	3.786e-05 (4.793e-05)	0.790, 0.430	1.557e+02 (2.688e+01)	5.792, <0.000	2.887e+00 (3.670e-01)	7.865, <0.000	3.474e+01 (2.734e+01)	1.271, 0.205	-7.368e+01 (2.716e+01)	-2.713, 0.007*
Amygdala (Right)	6.040e-05 (4.406e-05)	1.371, 0.171	1.477e+02 (2.393e+01)	6.174, <0.000	2.362e+00 (3.769e-01)	6.268, <0.000	5.469e+00 (2.451e+01)	0.223, 0.823	-6.244e+01 (2.429e+01)	-2.570 0.011*
Cingulate Gyrus (Left)	5.827e-04 (2.656e-04)	2.194, 0.029	6.041e+02 (2.358e+02)	2.562, 0.011	-9.063e+00 (2.098e+00)	-4.320, <0.000	-9.060e+01 (2.575e+02)	-0.352, 0.725	-7.073e+02 (2.619e+02)	-2.700, 0.007*
Cingulate Gyrus (Right)	1.511e-03 (2.880e-04)	5.248, <0.000	4.021e+02 (2.510e+02)	1.602, 0.110	-9.859e+00 (2.231e+00)	-4.419, <0.000	-2.778e+02 (2.720e+02)	-1.022, 0.308	-5.651e+02 (2.764e+02)	-2.044, 0.042*
Orbitofrontal Cortex (Right)	1.973e-03 (4.974e-04)	3.967, <0.000	1.008e+03 (2.513e+02)	4.011, <0.000	-3.095e+01 (3.944e+00)	-7.846, <0.000	3.735e+02 (2.535e+02)	1.473, 0.142	-6.151e+02 (2.510e+02)	-2.451, 0.015*

*= Factors that survived two-stage FDR correction

Table 3.5 Results of optimal mixed-effects models (with interaction term) analyses: Limbic system volumes in ADHD and Controls.

	ICV		**Sex**		**Months from baseline**		**Age at baseline**		**Diagnosis**		**Diagnosis * Months from baseline**	
	B (SE)	***t, p***	***B (SE)***	***t, p***	***B (SE)***	***t, p***	***B (SE)***	***t, p***	***B (SE)***	***t, p***	***B (SE)***	***t, p***
Orbitofrontal Cortex (Left)	1.905-03 (4.712e-04)	4.043, <0.000	8.154e+02 (2.503e+02)	3.258, 0.001	-2.495e+01 (3.997e+00)	-6.240, <0.000	1.024e+02 (2.533e+02)	0.404, 0.686	-3.597e+02 (2.679e+02)	-1.343, 0.180	-1.495e+01 (7.647e+00)	-1.955, 0.051
Anterior Thalamic Nuclei (Left)	1.453e-05 (5.163e-06)	2.815, 0.005	3.193e+00 (2.757e+00)	1.158, 0.248	4.410e-02 (4.383e-02)	1.006, 0.315	-5.949e-01 (2.803e+00)	-0.212, 0.832	-3.702e-01 (2.951e+00)	-0.125, 0.900	-9.513e-02 (8.386e-02)	-1.134, 0.257
Anterior Thalamic Nuclei (Right)	1.730e-05 (5.032e-06)	3.438, <0.000	3.822e+00 (2.596e+00)	-0.923, 0.357	-3.994e-02 (4.327e-02)	-0.923, 0.357	-7.995e-01 (2.632e+00)	-0.304, 0.761	-9.979e-01 (2.786e+00)	-0.358, 0.720	-7.791e-02 (8.289e-02)	-0.940, 0.348
Mammillary Bodies (Left)	3.347e-06 (3.915e-06)	0.855, 0.393	5.88e+00 (1.912e+00)	2.819, 0.005	1.392e-01 (3.214e-02)	4.330, <0.000	-9.846e-01 (1.912e+00)	-0.515, 0.607	-1.578e+00 (2.037e+00)	-0.775, 0.439	-9.730e-04 (6.157e-02)	-0.016, 0.987
Mammillary Bodies (Right)	2.338e-06 (3.899e-06)	0.600, 0.549	2.189e+00 (2.101e+00)	1.042, 0.299	2.126e-01 (3.076e-02)	6.911 <0.000	2.506e+00 (2.120e+00)	1.182, 0.239	-1.859e-01 (2.225e+00)	-0.084, 0.933	-6.136e-02 (5.872e-02)	-1.045, 0.297

Table 3.5 Results of optimal mixed-effects models (with interaction term) analyses: Limbic system volumes in ADHD and Controls.

	ICV		**Sex**		**Months from baseline**		**Age at baseline**		**Diagnosis**		**Diagnosis * Months from baseline**	
	B (SE)	***t, p***	***B (SE)***	***t, p***	***B (SE)***	***t, p***	***B (SE)***	***t, p***	***B (SE)***	***t, p***	***B (SE)***	***t, p***
Orbitofrontal Cortex (Left)	1.905-03 (4.712e-04)	4.043, <0.000	8.154e+02 (2.503e+02)	3.258, 0.001	-2.495e+01 (3.997e+00)	-6.240, <0.000	1.024e+02 (2.533e+02)	0.404, 0.686	-3.597e+02 (2.679e+02)	-1.343, 0.180	-1.495e+01 (7.647e+00)	-1.955, 0.051
Anterior Thalamic Nuclei (Left)	1.453e-05 (5.163e-06)	2.815, 0.005	3.193e+00 (2.757e+00)	1.158, 0.248	4.410e-02 (4.383e-02)	1.006, 0.315	-5.949e-01 (2.803e+00)	-0.212, 0.832	-3.702e-01 (2.951e+00)	-0.125, 0.900	-9.513e-02 (8.386e-02)	-1.134, 0.257
Anterior Thalamic Nuclei (Right)	1.730e-05 (5.032e-06)	3.438, <0.000	3.822e+00 (2.596e+00)	-0.923, 0.357	-3.994e-02 (4.327e-02)	-0.923, 0.357	-7.995e-01 (2.632e+00)	-0.304, 0.761	-9.979e-01 (2.786e+00)	-0.358, 0.720	-7.791e-02 (8.289e-02)	-0.940, 0.348
Mammillary Bodies (Left)	3.347e-06 (3.915e-06)	0.855, 0.393	5.88e+00 (1.912e+00)	2.819, 0.005	1.392e-01 (3.214e-02)	4.330, <0.000	-9.846e-01 (1.912e+00)	-0.515, 0.607	-1.578e+00 (2.037e+00)	-0.775, 0.439	-9.730e-04 (6.157e-02)	-0.016, 0.987
Mammillary Bodies (Right)	2.338e-06 (3.899e-06)	0.600, 0.549	2.189e+00 (2.101e+00)	1.042, 0.299	2.126e-01 (3.076e-02)	6.911 <0.000	2.506e+00 (2.120e+00)	1.182, 0.239	-1.859e-01 (2.225e+00)	-0.084, 0.933	-6.136e-02 (5.872e-02)	-1.045, 0.297

Figure 3.5 Volumes of limbic system structures showing no significant differences between ADHD and control groups.

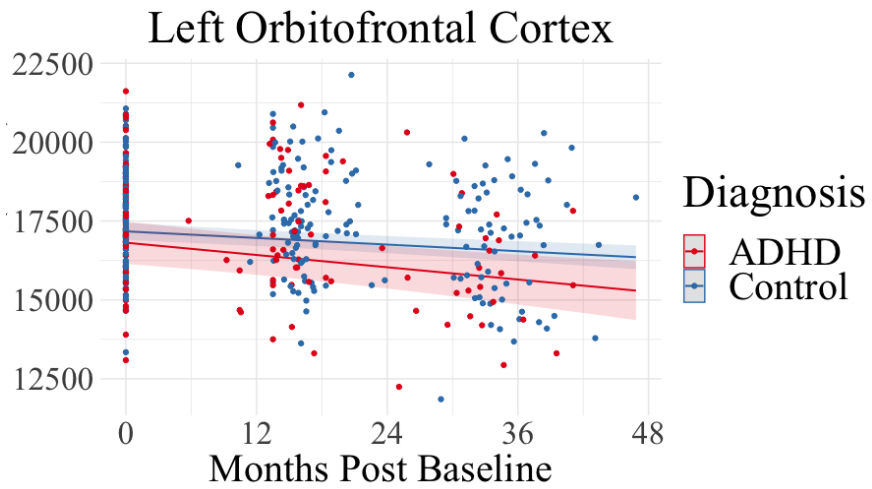

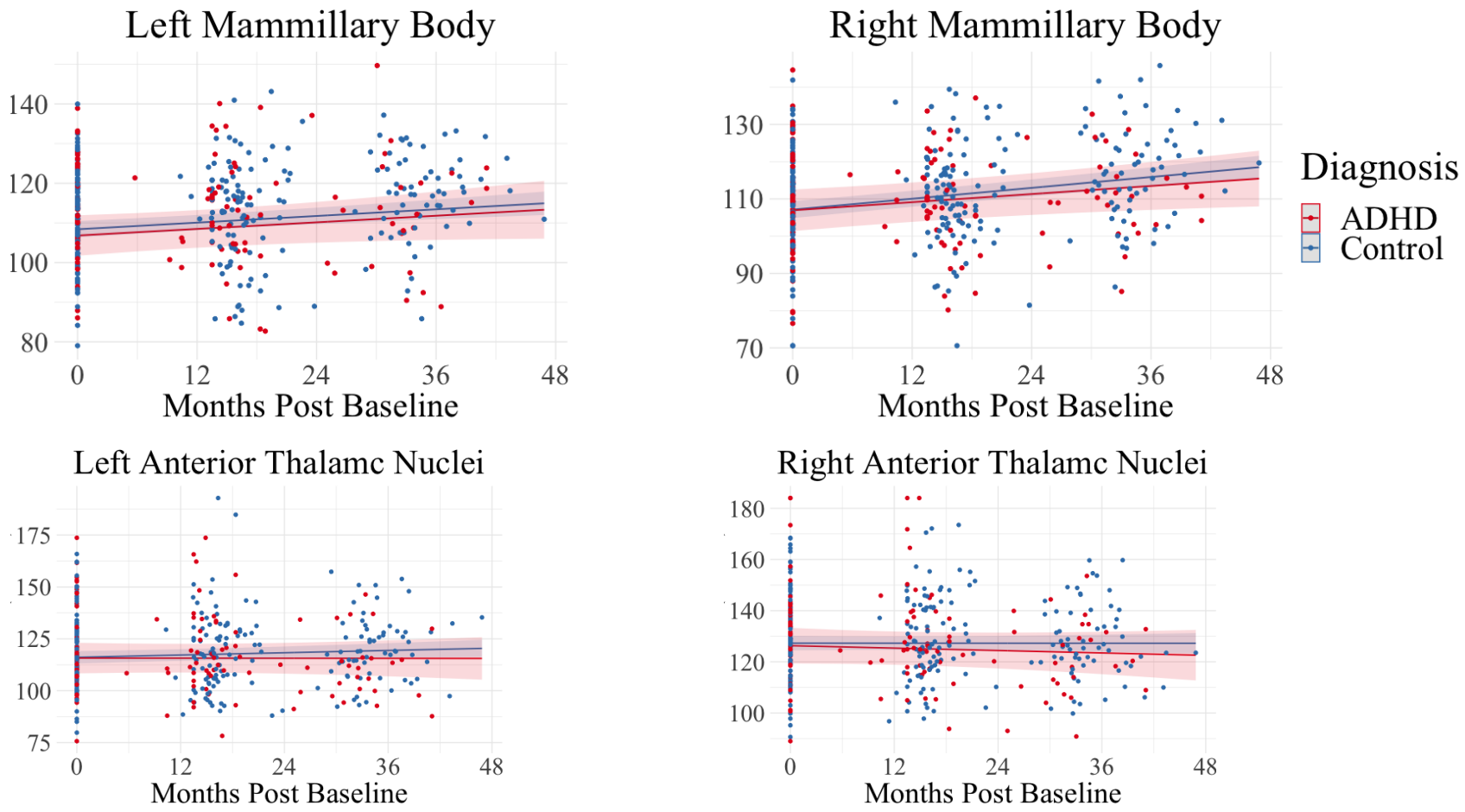
Left Mammillary Body
140
120
100
80
0
12
24
36
48
Months Post Baseline
Right Mammillary Body
130
110
90
70
0
12
24
36
48
Months Post Baseline
Diagnosis
ADHD
Control
Left Anterior Thalamc Nuclei
175
150
125
100
75
0
12
24
36
48
Months Post Baseline
Right Anterior Thalamc Nuclei
180
160
140
120
100
0
12
24
36
48
Months Post Baseline

Figure 3.6 Interaction between ADHD symptom severity and age on left mammillary body volume in ADHD.

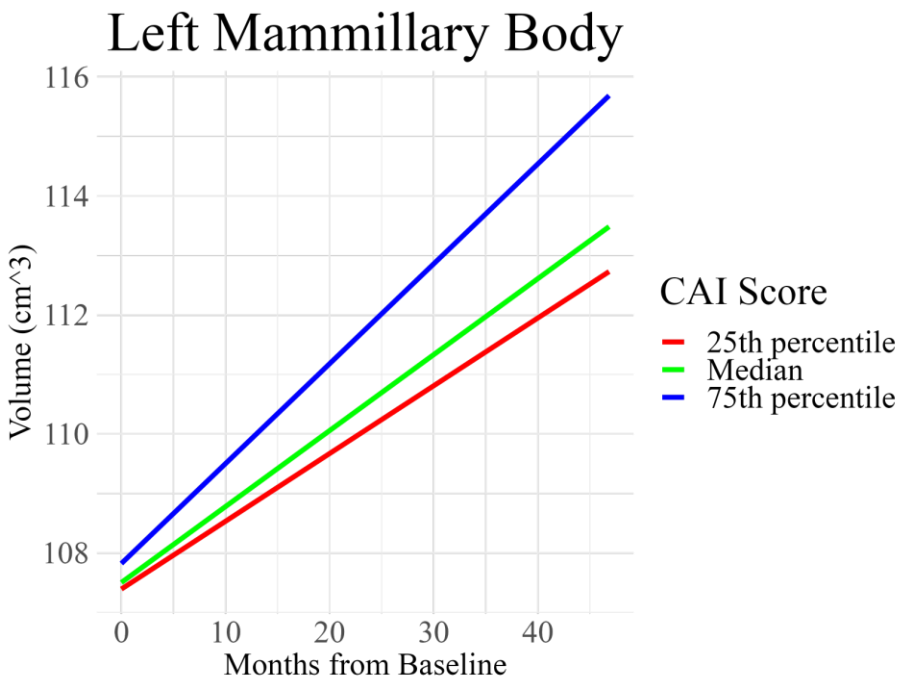

Figure 2.6: Associations between left mammillary body development and ADHD symptom severity (CAI) during the transition from childhood to mid-adolescence within the ADHD group. As individuals with ADHD age, those with more severe symptoms tend to show a slower decline or even potential growth in left mammillary body volume compared to those with milder symptoms.

Table 3.6 Results of mixed-effects models (with interaction term) analyses: limbic system volumes and CAI scores in ADHD.

	ICV		**Sex**		**Months from baseline**		**CAI**		**Months from baseline * CAI**	
	B (SE)	***t, p***	***B (SE)***	***t, p***	***B (SE)***	***t, p***	***B (SE)***	***t, p***	***B (SE)***	***t, p***
Hippocampus (Left)	-1.064e-05 (1.267e-04)	-0.084, 0.933	5.940e+02 (1.234e+02)	4.813, <0.000	7.326e+00 (2.448e+00)	2.993, 0.004	-4.095e+00 (4.632e+00)	-0.884, 0.379	-2.776e-02 (1.730e-01)	-0.160, 0.873
Hippocampus (Right)	1.143e-04 (1.438e-04)	0.796, 0.429	4.505e+02 (1.256e+02)	3.587, <0.000	7.917e+00 (2.838e+00)	2.789, 0.007	-3.554e+00 (5.265e+00)	-0.675, 0.501	-4.201e-02 (2.008e-01)	-0.209, 0.835
Amygdala (Left)	4.311e-05 (7.308e-05)	0.590, 0.556	2.738e+02 (5.406e+01)	5.064, <0.000	-6.093e-01 (1.513e+00)	-0.403, 0.688	-3.146e+00 (2.687e+00)	-1.171, 0.244	2.154e-01 (1.073e-01)	2.006, 0.049
Amygdala (Right)	9.652e-05 (6.281e-05)	1.537, 0.128	2.469e+02 (4.739e+01)	5.210, <0.000	2.019e+00 (1.291e+00)	1.564, 0.123	1.804e-02 (2.308e+00)	0.008 0.994	2.023e-02 (9.159e-02)	0.221, 0.826
Cingulate Gyrus (Left)	3.571e-04 (4.660e-04)	0.766, 0.446	1.404e+03 (5.604e+02)	2.505, 0.015	-1.073e+01 (8.750e+00)	-1.226, 0.225	-3.138e+01 (1.700e+01)	-1.846, 0.069	-1.781e-01 (6.172e-01)	-0.289, 0.773
Cingulate Gyrus (Right)	1.874e-03 (4.694e-04)	3.991, <0.000	5.378e+02 (5.649e+02)	0.952, 0.345	-5.024e+00 (8.814e+00)	-0.570, 0.571	-2.213e+01 (1.712e+01)	-1.293, 0.200	-7.817e-01 (6.217e-01)	-1.257, 0.213

Orbitofrontal Cortex (Left)	1.677e-03 (7.349e-04)	2.282, 0.024	1.041e+03 (5.445e+02)	1.912, 0.061	-5.097e+01 (1.521e+01)	-3.352, 0.001	6.317e+01 (2.702e+01)	-2.337, 0.021	1.219e+00 (1.079e+00)	1.130, 0.263
Orbitofrontal Cortex (Right)	1.855e-03 (7.714e-04)	2.405, 0.017	1.024e+03 (5.023e+02)	2.038, 0.046	-2.894e+01 (1.690e+01)	-1.713, 0.091	-1.599e+01 (2.855e+01)	-0.560, 0.576	-1.193e+00 (1.202e+00)	-0.993, 0.324
Anterior Thalamic Nuclei (Left)	6.548e-06 (8.469e-06)	0.773, 0.441	7.905e-01 (6.131e+00)	0.129, 0.898	2.037e-01 (1.768e-01)	1.152, 0.254	4.005e-01 (3.117e-01)	1.285, 0.202	-1.614e-02 (1.255e-02)	-1.287, 0.203
Anterior Thalamic Nuclei (Right)	6.548e-06 (8.469e-06)	0.773, 0.441	7.905e-01 (6.131e+00)	0.129, 0.898	2.037e-01 (1.768e-01)	1.152, 0.254	4.005e-01 (3.117e-01)	1.285, 0.202	-1.614e-02 (1.255e-02)	-1.287, 0.203
Mammillary Body (Left)	-4.143e-06 (5.186e-06)	-0.799, 0.426	9.872e+00 (3.985e+00)	2.477, 0.016	-2.404e-01 (1.060e-01)	-2.268, 0.026	-2.230e-01 (1.905e-01)	-1.171, 0.244	2.775e-02 (7.514e-03)	3.693, <0.000
Mammillary Body (Right)	5.140e-07 (5.971e-06)	0.086, 0.931	1.061e+01 (4.279e+00)	2.480, 0.016	5.295e-03 (1.251e-01)	0.042, 0.966	-7.715e-02 (2.198e-01)	-0.351, 0.726	1.449e-02 (8.883e-03)	1.631, 0.108

Figure 3.7 Scatter plot of non-significant limbic system volumes by CAI scores in ADHD.

Left Hippocampus	Right Hippocampus
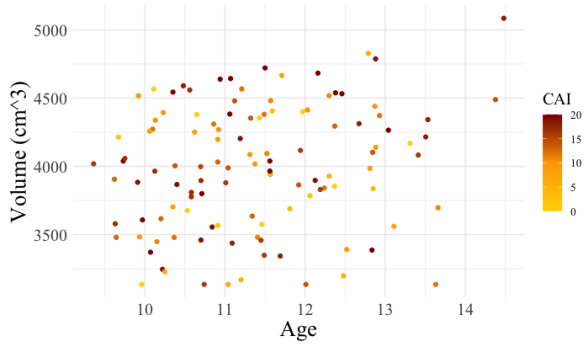	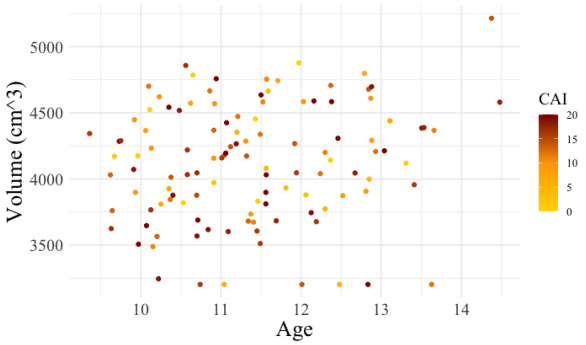
Left Amygdala	**Right Amygdala**
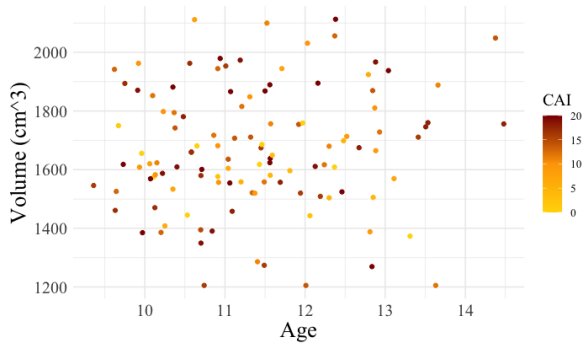	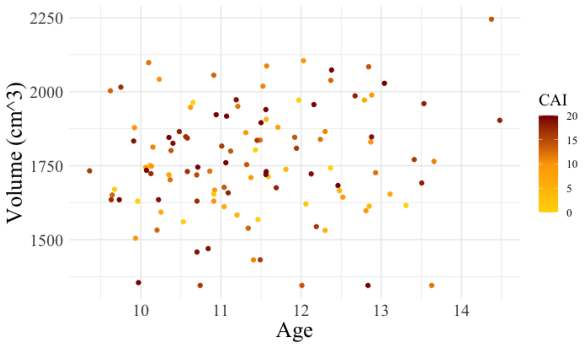
Left Anterior Thalamic Nuclei	**Right Anterior Thalamic Nuclei**
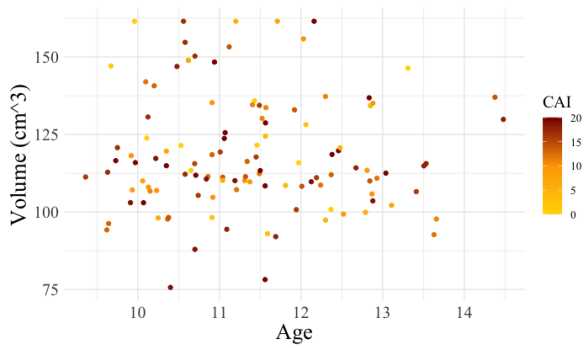	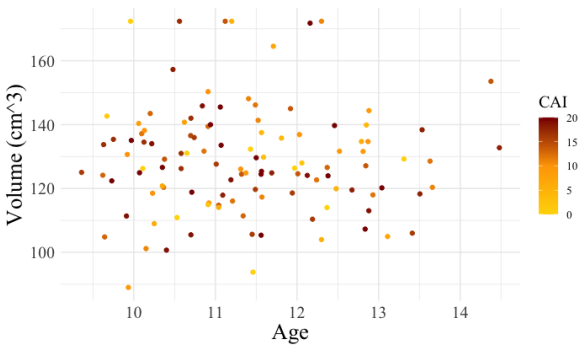

Right Mammilly Body

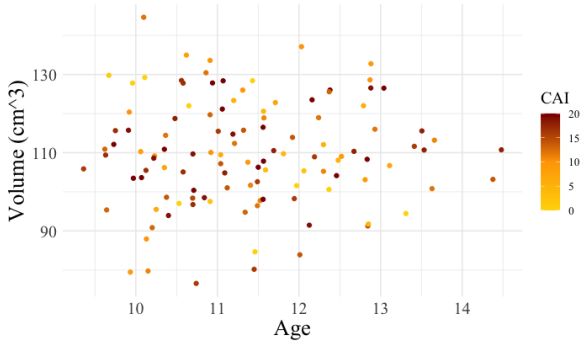

Left Cingulate Gyrus

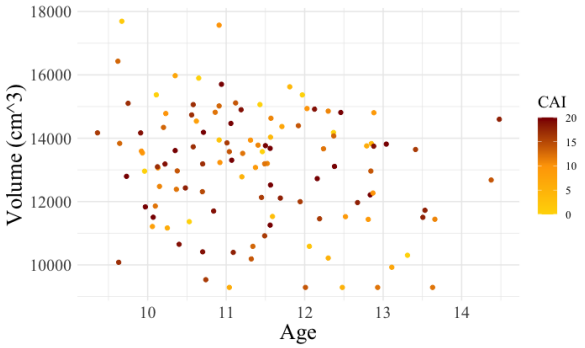

Right Cingulate Gyrus

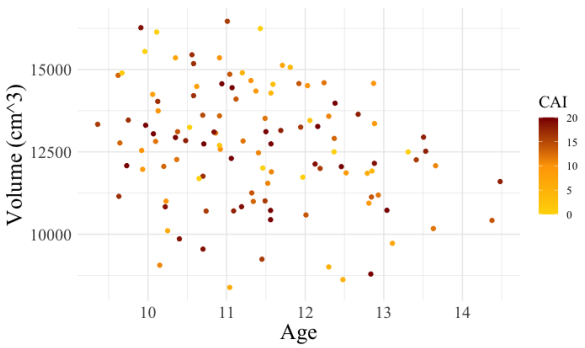

Figure 2.7: This scatter plot exclusively features non-significant limbic system network volumes (y-axis) alongside CAI scores (colour-coded) within the population. Each data point represents an individual in the study. The colour gradient used to represent CAI scores ranges from low (gold) to medium (orange) and high (dark red). Despite the absence of statistical significance, this visualization sheds light on the relationship between non-significant limbic system volumes and CAI scores across the ADHD population.

Table 3.7 Results of mixed-effects models (with interaction term) analyses: limbic system volume and ARI scores in ADHD.

	ICV		**Sex**		**Months from baseline**		**ARI**		**Months from baseline * ARI**	
	B (SE)	***t, p***	***B (SE)***	***t, p***	***B (SE)***	***t, p***	***B (SE)***	***t, p***	***B (SE)***	***t, p***
Hippocampus (Left)	4.578e-04 (2.033e-04)	2.252, 0.272	5.388e+02 (1.103e+02)	4.886, <0.000	1.477e+00 (2.326e+00)	0.635, 0.529	4.337e+00 (8.679e+00)	0.500, 0.619	3.218e-01 (4.001e-01)	0.804, 0.426
Hippocampus (Right)	8.497e-04 (2.226e-04)	3.817, 0.001	3.549e+02 (1.091e+02)	3.253, 0.002	2.405e+00 (2.779e+00)	0.866, 0.392	3.622e+00 (9.782e+00)	0.370, 0.712	2.617e-01 (4.735e-01)	0.553, 0.583
Amygdala (Left)	2.555e-04 (1.150e-04)	2.221, 0.029	2.349e+02 (5.325e+01)	4.411, <0.000	-8.680e-01 (1.537e+00)	-0.565, 0.576	2.905e+00 (5.164e+00)	0.563, 0.575	2.676e-01 (2.601e-01)	1.029, 0.309
Amygdala (Right)	3.195e-04 (9.138e-05)	3.497, <0.000	2.217e+02 (4.361e+01)	5.084, <0.000	1.190e+00 (1.174e+00)	1.013, 0.317	3.173e+00 (4.053e+00)	0.783, 0.436	4.800e-03 (1.995e-01)	0.024, 0.980
Cingulate Gyrus (Left)	3.943e-03 (7.190e-04)	5.484, <0.000	9.801e+02 (4.864e+02)	2.015, 0.049	1.138e+01 (7.375e+00)	-1.544, 0.131	-6.138e+00 (2.951e+01)	-0.208, 0.836	9.506e-01 (1.286e+00)	0.739, 0.464
Cingulate Gyrus (Right)	4.480e-03 (8.050e-04)	5.566, <0.000	2.021e+02 (5.334e+02)	0.379, 0.706	1.848e+00 (8.318e+00)	0.222, 0.825	-1.961e-01 (3.313e+01)	-0.006, 0.995	-2.094e+00 (1.449e+00)	-1.445, 0.156

Orbitofrontal Cortex (Left)	4.954e-03 (1.057e-03)	4.688, <0.000	3.766e+02 (4.799e+02)	0.785, 0.436	-2.616e+00 (1.452e+01)	-0.180, 0.858	-7.794e+01 (4.784e+01)	-1.629, 0.107	-1.463e+00 (2.450e+00)	-0.597, 0.553
Orbitofrontal Cortex (Right)	6.153e-03 (9.836e-04)	6.255, <0.000	2.379e+02 (4.073e+02)	0.584, 0.562	-3.542e+01 (1.629e+01)	-2.174, 0.035	-1.134e+02 (4.702e+01)	-2.412, 0.018	1.551e+00 (2.699e+00)	0.574, 0.568
Anterior Thalamic Nuclei (Left)	2.552e-05 (1.393e-05)	1.833, 0.070	-8.832e-01 (6.038e+00)	-0.146, 0.884	-1.974e-02 (2.074e-01)	-0.095, 0.924	-4.760e-02 (6.458e-01)	-0.074, 0.941	-5.770e-04 (3.473e-02)	-0.017, 0.986
Anterior Thalamic Nuclei (Right)	2.552e-05 (1.393e-05)	1.833, 0.070	-8.832e-01 (6.038e+00)	-0.146, 0.884	-1.974e-02 (2.074e-01)	-0.095, 0.924	-4.760e-02 (6.458e-01)	-0.074, 0.941	-5.770e-04 (3.473e-02)	-0.017, 0.986
Mammillary Body (Left)	1.321e-05 (8.443e-06)	1.565, 0.121	8.006e+00 (4.050e+00)	1.977, 0.053	-1.917e-01 (1.079e-01)	-1.777, 0.082	-2.225e-01 (3.737e-01)	-0.595, 0.553	4.039e-02 (1.834e-02)	2.203, 0.032
Mammillary Body (Right)	2.493e-05 (8.903e-06)	2.800, 0.006	7.935e+00 (4.098e+00)	1.936, 0.058	-2.251e-01 (1.200e-01)	-1.876, 0.067	-9.168e-02 (4.007e-01)	-0.229, 0.819	5.415e-02 (2.028e-02)	2.670, 0.010

Figure 3.8 Scatter plot of non-significant limbic system volumes by ARI scores in ADHD.

Left Hippocampus	Left Hippocampus
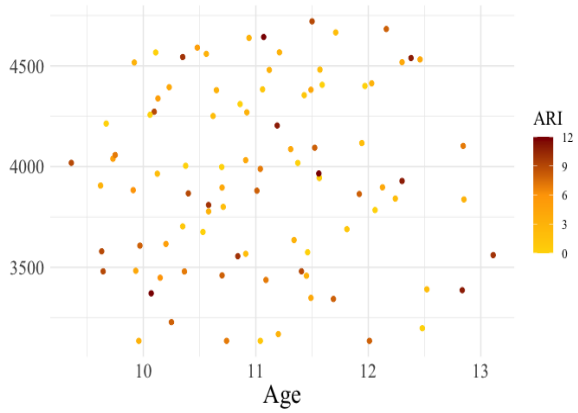	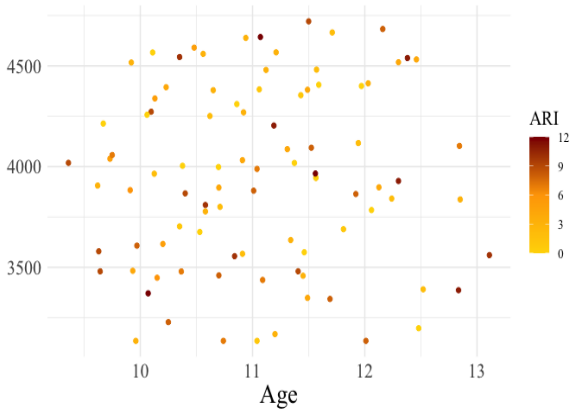
Left Amygdala	Right Amygdala
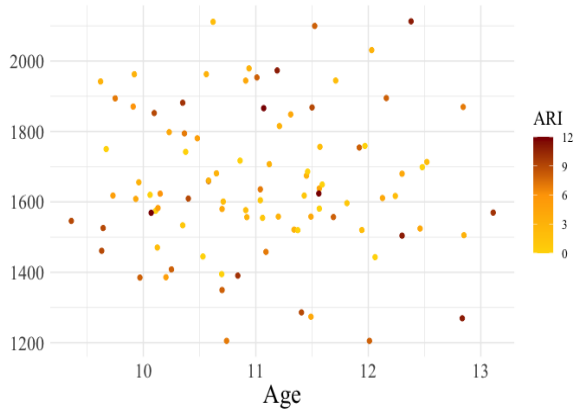	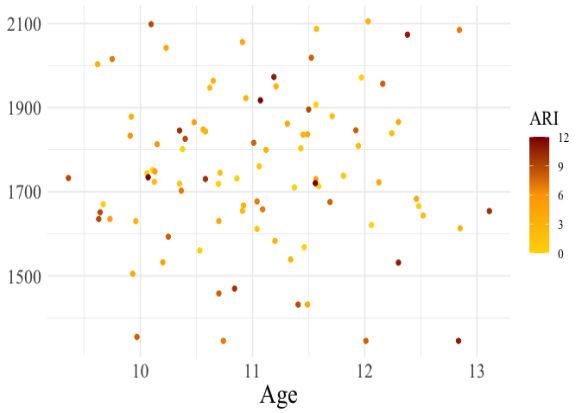
Left Anterior Thalamic Nuclei	Right Anterior Thalamic Nuclei
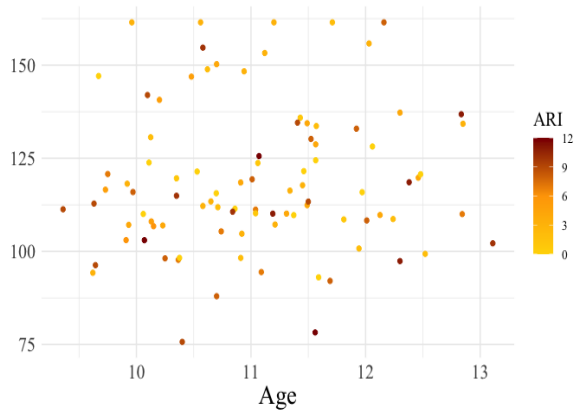	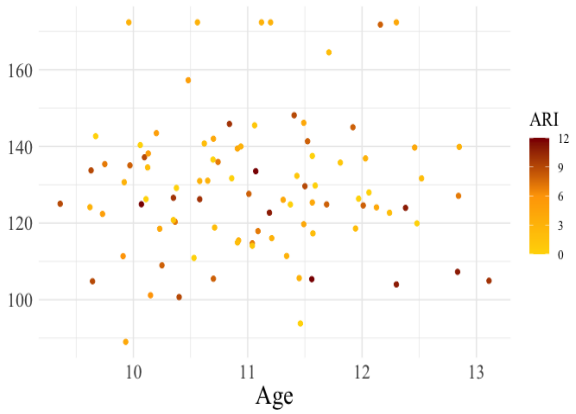
Left Mammilly Body	Right Mammilly Body

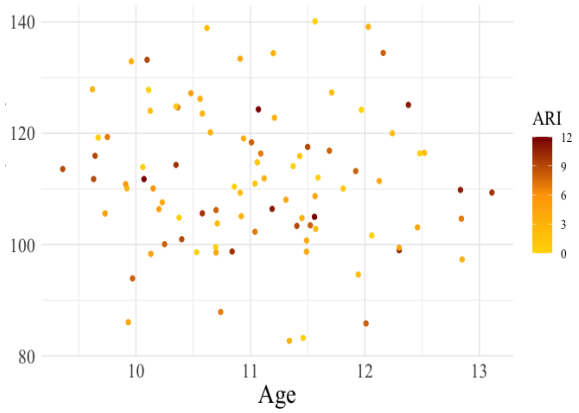

Left Cingulate Gyrus

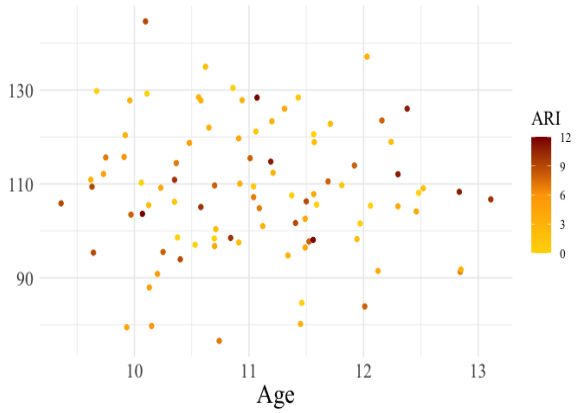

Right Cingulate Gyrus

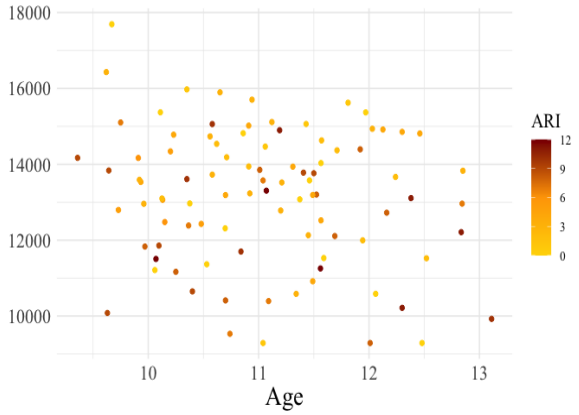

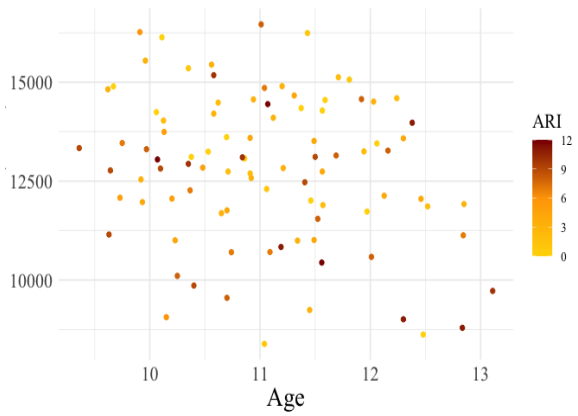

igure 2.8: This scatter plot exclusively features non-significant limbic system network volumes (y-axis) alongside ARI scores (colour-oded) within the population. Each data point represents an individual in the study. The colour gradient used to represent ARI scores nges from low (gold) to medium (orange) and high (dark red). Despite the absence of statistical significance, this visualization sheds ght on the relationship between non-significant limbic system volumes and ARI scores across the ADHD population.

Table 3.8 Mean values of the effect of diagnosis in the 100 iterations of optimal mixed-effects models analyses with sex sex-matched case-control samples.

	Diagnosis			
	B (SD)	***SE (SD)***	***t (SD)***	***p***
Hippocampus (Left)	-151.125	58.257	-2.594	**0.012***
	(9.548)	(0.857)	(0.164)	
Hippocampus (Right)	-120.955	61.591	-1.964	0.055
	(9.921)	(0.958)	(0.162)	
Amygdala (Left)	-70.055	28.397	-2.467	**0.016***
	(4.370)	(0.500)	(0.142)	
Amygdala (Right)	-61.282	24.679	-2.483	**0.015***
	(2.764)	(0.246)	(0.108)	
Cingulate Gyrus (Left)	-710.609	268.437	-2.648	**0.010***
	(51.894)	(5.313)	(0.195)	
Cingulate Gyrus (Right)	-583.268	283.561	-2.057	**0.044***
	(42.539)	(4.067)	(0.152)	
Orbitofrontal Cortex (Left)	-343.072	269.478	-1.275	0.212
	(49.202)	(6.215)	(0.193)	
Orbitofrontal Cortex (Right)	-622.017	254.495	-2.445	**0.017***
	(40.934)	(5.094)	(0.174)	
Anterior thalamic nuclei (Left)	-0.574	3.041	-0.188	0.839
	(0.490)	(0.061)	(0.161)	
Anterior thalamic nuclei (Right)	-1.418	2.921	-0.486	0.632
	(0.435)	(0.042)	(0.151)	
Mammillary bodies (Left)	-1.243	2.108	-0.590	0.562
	(0.357)	(0.027)	(0.169)	
Mammillary bodies (Right)	0.154	2.306	0.068	0.860
	(0.468)	(0.037)	(0.203)	

Table 3.8: *B* = regression coefficient, *SD* = standard deviations, *t* = t score, *p* = p-value, * = survived Two-stage FDR correction.

Figure 3.9 Beta value and SEs of the main effect diagnosis in the sex-balanced sensitivity analysis

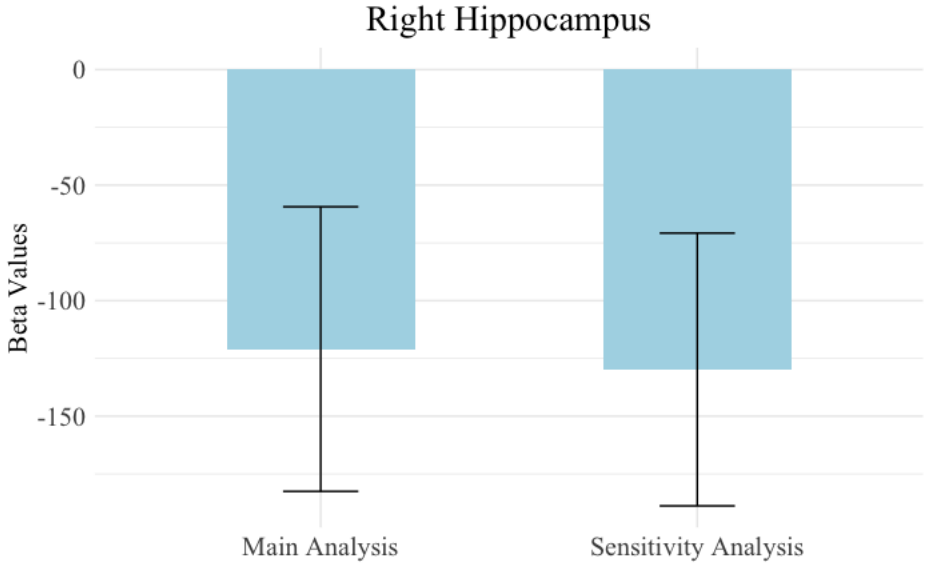

Table 3.9 Results of optimal mixed-effects models (without interaction term) analyses: Limbic system volume and medication use in ADHD.

	ICV		**Sex**		**Months from baseline**		**Age at baseline**		**Medication Status**	
	B (SE)	***t, p***	***B (SE)***	***t, p***	***B (SE)***	***t, p***	***B (SE)***	***t, p***	***B (SE)***	***t, p***
Hippocampus (Left)	-1.738e-04 (1.273e-04)	-1.365, 0.176	5.601e+02 (1.295e+02)	4.323, <0.000	6.941e+00 (1.139e+00)	6.092, <0.000	-2.004e+01 (1.020e+02)	-0.197, 0.844	1.175e+02 (5.499e+01)	2.137, 0.035
Hippocampus (Right)	2.150e-04 (1.629e-04)	1.320, 0.190	4.227e+02 (1.302e+02)	3.245, 0.002	7.918e+00 (1.330e+00)	5.953, <0.000	-5.652e+01 (1.036e+02)	-0.546, 0.587	8.538e+01 (7.056e+01)	1.210, 0.228

Table 3.10 Results of optimal mixed-effects models (with interaction term) analyses: limbic system volumes and medication use in ADHD.

	ICV		**Sex**		**Months from baseline**		**Age at baseline**		**Medication Status**		**Medication Status * Months from baseline**	
	B (SE)	***t, p***	***B (SE)***	***t, p***	***B (SE)***	***t, p***	***B (SE)***	***t, p***	***B (SE)***	***t, p***	***B (SE)***	***t, p***
Amygdala (Left)	2.833e-05 (7.736e-05)	0.366, 0.715	2.657e+02 (5.704e+01)	4.657, <0.000	2.287e+00 (8.755e-01)	2.612, 0.011	8.622e+00 (4.550e+01)	0.189, 0850	4.550e+01 (3.677e+01)	1.237, 0.218	-2.692e-01 (1.290e+00)	-0.209, 0.835

Amygdala (Right)	1.434e-04 (7.664e-05)	1.871, 0.064	2.366e+02 (4.811e+01)	4.917, <0.000	2.324e+00 (1.067e+00)	2.178, 0.035	9.393e+00 (3.845e+01)	0.244, 0.808	4.242e+01 (3.359e+01)	1.263, 0.211	-9.010e-01 (1.598e+00)	-0.564, 0.576
Cingulate Gyrus (Left)	3.437e-04 (4.791e-04)	0.717, 0.475	1.410e+03 (5.759e+02)	2.449, 0.017	-8.394e+00 (5.828e+00)	-1.440, 0.157	-2.086e+02, (4.457e+02)	-0.468, 0.641	-1.032e+02 (2.434e+02)	-0.424, 0.673	-2.804e+00 (8.877e+00)	-0.316, 0.753
Cingulate Gyrus (Right)	1.952e-03 (4.906e-04)	3.978, <0.000	5.436e+02 (5.734e+02)	0.948, 0.347	-1.204e+01, (5.058e+00)	-2.380, 0.020	-3.933e+02 (4.447e+02)	-0.884, 0.379	3.312e+00 (2.448e+02)	0.014, 0.989	-1.297e+00 (7.461e+00)	-0.174, 0.862
Orbitofrontal Cortex (Left)	2.269e-03 (8.039e-04)	2.822, 0.005	7.529e+02 (5.746e+02)	1.310, 0.196	-2.965e+01 (9.202e+00)	-3.222, 0.002	3.553e+02 (4.588e+02)	0.774, 0.442	-4.713e+02 (3.805e+02)	-1.238, 0.218	-6.564e+00 (1.356e+01)	-0.484, 0.630
Orbitofrontal Cortex (Right)	2.055e-03 (8.297e-04)	2.477, 0.014	8.571e+02 (4.983e+02)	1.720, 0.091	-3.870e+01 (1.037e+01)	-3.733, <0.000	4.434e+02, (3.999e+02)	1.109, 0.272	-4.927e+02 (3.843e+02)	-1.282, 0.202	-4.849e-02 (1.526e+01)	-0.003, 0.997
Anterior Thalamic Nuclei (Left)	1.146e-05 (9.065e-06)	1.264, 0.209	-2.426e+00 (6.254e+00)	-0.388, 0.700	3.681e-02 (1.053e-01)	0.350, 0.738	5.302e+00 (4.998e+00)	1.061, 0.294	2.341e+00 (4.271e+00)	0.548, 0.585	-1.461e-01 (1.551e-01)	-0.942, 0.350

Anterior Thalamic Nuclei (Right)	2.353e-05 (8.633e-06)	2.726, 0.007	-4.151e+00 (5.681e+00)	-0.731, 0.468	-1.879e-02 (1.024e-01)	-0.184, 0.855	4.598e+00 (4.547e+00)	1.011, 0.316	3.056e+00 (4.042e+00)	0.756, 0.451	-1.520e-01 (1.508e-01)	-1.008, 0.317
Mammillary Bodies (Left)	-4.236e-06 (5.839e-06)	-0.725, 0.469	1.142e+01 (4.110e+00)	2.778, 0.007	4.391e-02 (6.725e-02)	0.653, 0.516	-1.904e+00 (3.283e+00)	-0.580, 0.564	-3.820e+00 (2.758e+00)	-1.385, 0.168	1.567e-01 (9.909e-02)	1.581, 0.118
Mammillary Bodies (Right)	-1.643e-06 (6.151e-06)	-0.267, 0.789	1.046e+01 (4.258e+00)	2.456, 0.017	1.756e-01 (7.132e-02)	2.462, 0.016	-1.903e+00 (3.403e+00)	-0.559, 0.578	1.523e+00 (2.899e+00)	0.525, 0.600	3.605e-02 (1.051e-01)	0.343, 0.732

Table 3.11 Results of optimal mixed-effects models analyses with comorbidity status: Limbic system volumes in ADHD and Controls.

	ICV		**Sex**		**Months from baseline**		**Age at baseline**		**Diagnosis**		**Comorbidity**	
	B (SE)	***t, p***	***B (SE)***	***t, p***	***B (SE)***	***t, p***	***B (SE)***	***t, p***	***B (SE)***	***t, p***	***B (SE)***	***t, p***
Amygdala (Left)	3.458e-05	0.721	1.563e+02	5.799	2.929e+00	7.943	3.406e+01	1.242	-7.722e+01	-2.813	2.650e+01	1.038
	(4.794e-05)	0.471	(2.695e+01)	<0.000	(3.688e-01)	<0.000	(2.742e+01)	0.215	(2.745e+01)	0.005	(2.553e+01)	0.300
Amygdala (Right)	6.089e-05	1.379	1.477e+02	6.171	2.363e+00	6.224	5.468e+00	0.223	-6.241e+01	-2.545	-3.260e-01	-0.015
	(4.415e-05)	0.168	(2.394e+01)	<0.000	(3.797e-01)	<0.000	(2.453e+01)	0.823	(2.453e+01)	0.011	(2.190e+01)	0.988
Cingulate Gyrus	6.108e-04	2.305	6.160e+02	2.513	-9.031e+00	-4.788	-9.050e+01	-0.343	-7.142e+02	-2.648	-1.226e+02	-0.913
(Left)	(2.650e-04)	0.022	(2.451e+02)	0.012	(1.886e+00)	<0.000	(2.646e+02)	0.732	(2.696e+02)	0.008	(1.343e+02)	0.362
Cingulate Gyrus	1.414e-03	4.973	3.997e+02	1.550	-1.065e+01	-5.255	-2.415e+02	-0.870	-5.457e+02	-1.933	-1.458e+02	-1.010
(Right)	(2.844e-04)	<0.000	(2.580e+02)	0.123	(2.028e+00)	<0.000	(2.775e+02)	0.385	(2.823e+02)	0.055	(1.443e+02)	0.313
Hippocampus	4.547e-05	0.568	2.095e+02	3.910	9.079e+00	15.316	4.795e+01	0.866	-1.642e+02	-2.953	-9.447e+00	-0.227
(Left)	(8.010e-05)	0.570	(5.358e+01)	<0.000	(5.927e-01)	<0.000	(5.536e+01)	0.387	(5.561e+01)	0.003	(4.164e+01)	0.820
Hippocampus	7.271e-05	0.894	1.501e+02	2.642	8.292e+00	-13.868	3.667e+01	0.622	-1.295e+02	-2.184	-2.648e+00	-0.063
(Right)	(8.137e-05)	0.372	(5.680e+01)	0.008	(5.979e-01)	<0.000	(5.896e+01)	0.534	(5.930e+01)	0.030	(4.210e+01)	0.949

Orbitofrontal Cortex (Right)	2.021e-03 (4.973e-04)	4.063 <0.000	9.970e+02 (2.504e+02)	3.981 <0.000	-3.161e+01 (3.969e+00)	-7.964 <0.000	3.842e+02 (2.526e+02)	1.521 0.130	-5.601e+02 (2.525e+02)	-2.218 0.028	-4.132e+02 (2.709e+02)	-1.525, 0.128

Figure 3.10 Beta value and SEs of the main effect diagnosis in the comorbidity sensitivity analysis

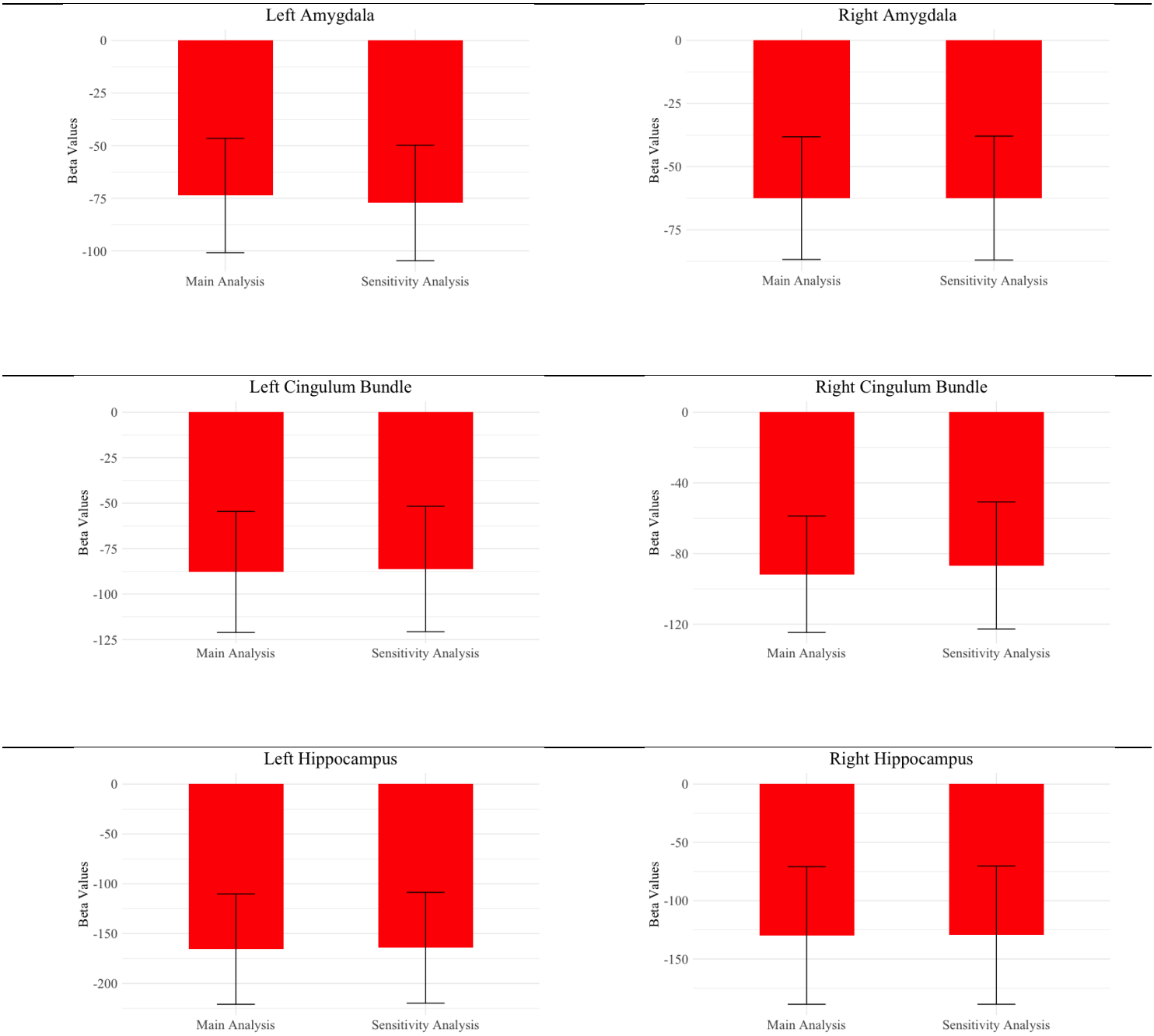

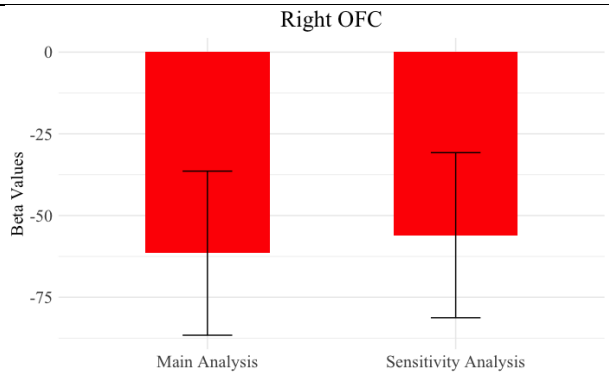
Right OFC
0
-25
-50
-75
Beta Values
Main Analysis
Sensitivity Analysis

3.4. Discussion

This longitudinal study described in this chapter investigated the volumetric development of limbic system structures in children and adolescents with ADHD. Across the three NICAP study time points, individuals with ADHD exhibited lower volume in the bilateral amygdala, hippocampus, cingulate gyrus, and right orbitofrontal cortex compared to controls. Exploratory analysis identified a significant interaction between age and symptom severity on left mammillary body volume in the ADHD group, suggesting limbic system development may play a role in the pathophysiology of ADHD. Consistent with the ENIGMA mega-analyses (Hoogman et al. 2017b; Hoogman et al. 2019) and other recent studies (Shaw, De Rossi, et al. 2014; Norman et al. 2016), the sensitivity analysis revealed no significant association between structural brain changes and ADHD medication use in children and adolescents (Tables 2.9-2.10).

3.4.1. Between-Group Differences in the Development of Limbic System Structures

To further understand the findings of the study described in this chapter, it is helpful to consider the neurotypical developmental patterns of the brain structures that comprise the limbic system. The volume of cortical structures (e.g., orbitofrontal cortex and cingulate gyrus) increases rapidly from mid-gestation before peaking during childhood (orbitofrontal cortical volume peaks at age 6-7 years (Bethlehem et al. 2022) and cingulate gyrus volume peaks at age 7-9 years (Bethlehem et al. 2022)), followed by a near-linear decrease in volume from late childhood to late adulthood (Bethlehem et al. 2022). This developmental pattern was observed in both control and ADHD groups in the cingulate gyrus (Figure 2.3) and orbitofrontal cortex (Figure 2.4), evidenced by the volumetric decrease seen across the NICAP study time points. Despite the apparent typical developmental pattern, children with ADHD had persistently lower volumes of these structures compared with controls. These findings are consistent with the 'convergence model' (Shaw and Sudre 2021), which suggests that children with persistent ADHD diagnosis display fixed, non-progressive development of neural features throughout childhood and adolescence (Shaw and Sudre 2021).

Subcortical structures (e.g., amygdala and hippocampus) increase in volume throughout childhood and early adolescence before obtaining peak volume during mid-

puberty (14-15 years) (Bethlehem et al. 2022; Herting et al. 2018), followed by a near-linear decrease in volume throughout adulthood (Bethlehem et al. 2022). This developmental pattern was seen for both control and ADHD groups in the amygdala (Figure 2.1) and hippocampus (Figure 2.2), as indicated by the increase in the volumes of these structures across the study time points. Compared to controls, however, the ADHD group showed persistently lower volume in these structures. This suggests a potential developmental "lag". While it is possible that this finding reflects a developmental delay (Shaw et al. 2007; Shaw et al. 2012; Rubia 2007), longitudinal studies employing a wider age range that captures the age of peak volume attainment are crucial to investigate if structures in the ADHD group would normalise later in development. Given that ADHD is associated with abnormalities across numerous brain structures with distinct developmental mechanisms and trajectories (Bethlehem et al. 2022; Herting et al. 2018), the pathophysiology will likely involve varied region-specific developmental patterns. In response to reviewer comments, additional supplementary analyses were conducted investigating the between-group differences in regions that are key to ADHD, such as the basal ganglia, inferior prefrontal cortex, and dorsolateral prefrontal cortex (see Section 7.6 in the appendices).

Although the underlying mechanisms that lead to the lower volume and potentially delayed neurodevelopment in ADHD remain unknown, variants of several ADHD-associated genes have been shown to play a critical role in all stages of cortical development (Dark, Homman-Ludiye, and Bryson-Richardson 2018). A recent review (Dark, Homman-Ludiye, and Bryson-Richardson 2018) investigated how these ADHD-associated genes contribute to neurodevelopment and how variants in these genes could result in the neurological phenotypes observed in the disorder. The most common effect of ADHD-associated genes on brain development is the disruption of synaptic formation and activity (Dark, Homman-Ludiye, and Bryson-Richardson 2018), and it has been suggested that lower grey matter volume in the brain may be due to the loss of synaptic density rather than neuronal cell loss (Dark, Homman-Ludiye, and Bryson-Richardson 2018). It has been proposed that variants in these ADHD-associated genes may contribute to the reduced grey matter seen in the disorder (Dark, Homman-Ludiye, and Bryson-Richardson 2018). Furthermore, the delayed establishment of neural connections – a process associated with ADHD susceptibility genes – has been shown to result in an underdeveloped brain (Dark, Homman-Ludiye, and Bryson-Richardson 2018), consistent

with the patterns of reduced volumes in various brain structures seen in individuals with ADHD (Dark, Homman-Ludiye, and Bryson-Richardson 2018).

3.4.2. ADHD Symptoms Severity and Limbic System Volumes in ADHD

While ADHD is characterised by age-related changes in symptoms and brain structure during childhood and adolescence, the link between brain structure and function is less clear. Exploratory analyses conducted in the study described in this chapter revealed a novel association between the developmental trajectory of left mammillary body volume and ADHD symptom severity. The analyses found a significant age-by-symptom severity interaction with left mammillary body volume in the ADHD group (Figure 2.6). Based on the results of this study, as individuals with ADHD progress from childhood to mid-adolescence, those with severe symptoms may show a slower decline or even a potential growth in left mammillary body volume compared to those with milder symptoms. This suggests that variations in mammillary body development may play a role in the persistence and increase of ADHD symptom severity during mid-adolescence.

While there has been a long-standing awareness of the impact of mammillary body pathology in adults, it is only recently that researchers have become aware of the significance of mammillary body pathology in younger populations (Meys et al. 2022). The mammillary bodies are an integral component of the limbic system, playing a pivotal role in encoding complex memories (McNaughton and Vann 2022). While once thought to serve primarily as a "relay" to the hippocampus, recent studies have shown that through the limbic system pathways, the mammillary bodies influence a wide range of brain regions (McNaughton and Vann 2022). The mammillary bodies have been shown to provide arousal and interoceptive information to boost and bias the iterative processing of the limbic system (McNaughton and Vann 2022). As such, the input of the mammillary bodies can significantly affect emotional regulation, memory formation and recall, and behaviour (McNaughton and Vann 2022). It has been suggested that the mammillary bodies input play a role in psychiatric and neurodevelopmental disorders, like ADHD, where memory impairments and emotional dysregulation are commonly observed (McNaughton and Vann 2022).

Mammillary body volumes are observed to increase until approximately 15 years old (Vann et al. 2022). So, while individuals with increased symptom severity might seem to converge towards a "normative" pattern, the underlying functionality or efficiency of

this region and their modulation of neural circuits, such as the limbic system, could still be compromised, contributing to the increased symptom severity. This finding underscores the belief that in ADHD, there might not just be differences in brain structure but also in how these structures modulate neural circuits to influence symptom expression (Konrad and Eickhoff 2010). Structural MRI data provides limited insight into the functional dynamics of these changes. To fully understand the link between atypical mammillary body development and ADHD symptom severity, in-depth functional imaging and histological studies are essential.

3.4.3. Limitations

A limitation of the study described in this chapter is there were significantly fewer female than male participants at study time points 1 and 2. Despite well-characterized differences in symptom profiles between girls and boys with ADHD (Mowlem et al. 2019), sex-specific differences in brain development are less clear. Research has reported no difference between girls and boys with ADHD in developmental trajectories of brain volume (Castellanos, Lee, et al. 2002a) or cortical thickness (Shaw et al. 2013). However, many studies investigating brain development in ADHD have not tested for sex differences, making it difficult to determine whether sex-specific differences in brain development are present in ADHD. The sensitivity analysis conducted in the study described in this chapter suggests that the sex imbalance between the ADHD and control groups in the sample did not significantly impact the results of the primary analysis (Table 3.8). Therefore, the findings of the primary analysis are unlikely to be confounded by this sex imbalance. Nevertheless, given that females with ADHD are often underrepresented in case-control studies, there is a need for future research to include sufficient female participants to investigate sex-specific differences in the disorder.

Another limitation of the study described in this chapter is that structural differences across the different ADHD subtypes (inattentive, hyperactive/impulsive, and combined) were not explored. While many of the smaller sample-sized studies ($n<50$) failed to identify differences in volume between subtypes (Pineda et al. 2002; Carmona et al. 2005; Vilgis et al. 2016), larger-scale studies have now suggested that there may be subtle volumetric differences across the subtypes (Al-Amin, Zinchenko, and Geyer 2018; Wu et al. 2022) . Therefore, it is important that future research should investigate

developmental differences across ADHD subtypes. Additional limitations of the studies featured in this thesis are described in Section 5.3.

3.4.4. Conclusion

The longitudinal study described in this chapter found that compared to controls, children and adolescents with ADHD had lower grey matter volume across development in key limbic system structures. Additionally, among individuals with ADHD, the developmental trajectory of the left mammillary body was significantly associated with alterations in symptom severity during the transition from childhood into mid-adolescence. Taken together, atypical development in limbic system structures appears to be a potential neurobiological feature of ADHD, advancing our pathophysiological understanding of this highly prevalent neurodevelopmental disorder.

4 Diffusion MRI Data Processing and Analysis: A Practical Guide with *ExploreDTI*

This chapter presents the detailed methodologies used for processing diffusion MRI (dMRI) data in this thesis. Originally published as a comprehensive book chapter (Connaughton M, 2023, DOI: 10.31219/osf.io/mbyjh), it serves as both a rigorous documentation of the procedures employed and a guide for future researchers in the field. The chapter outlines the principles of dMRI, followed by a step-by-step explanation of data acquisition, preprocessing, and analysis. It emphasizes the innovative techniques developed during this research, offering insights into the decision-making process behind these methods. This chapter is crucial for understanding the data processing foundation that supports the thesis' findings.

Publication Details:

Book Chapter: Methods for Analyzing Large Neuroimaging Datasets

Journal: Springer Nature

DOI: 10.31219/osf.io/mbyjh

Authors

Michael Connaughton*, M.Sc.[1,2], Alexander Leemans, Ph.D. [3], Erik O'Hanlon, Ph.D.[4], Jane McGrath, M.D. [1,2]

Affiliations

1. Department of Psychiatry, School of Medicine, Trinity College Dublin, Ireland.
2. Trinity College Institute of Neuroscience, Trinity College Dublin, Ireland.
3. Image Sciences Institute, University Medical Center Utrecht, Utrecht, Netherlands.
4. Royal College of Surgeons in Ireland, Dublin, Ireland.

Co-authors contributions:

AL: Provided technical support for ExploreDTI software

EH: Provided technical support for dMRI physics

JMG: Contributed to writing and formatting, ensuring clarity, coherence, and adherence to academic standards in the presentation of the research.

4.1. Introduction

White matter refers to the nerve fibers, also known as axons, that interconnect regions of the brain (Fields 2010). Healthy development of white matter is essential for neurotypical brain function and cognition (Lebel and Deoni 2018). This complex developmental process involves several mechanisms such as axonal growth, myelination, and synaptic pruning (Stiles and Jernigan 2010). The intricate interplay between these processes is key for the establishment of neural networks for the efficient transmission of information within the brain (Lebel and Deoni 2018). Abnormalities in white matter development have been linked to a range of cognitive functions (Lebel and Beaulieu 2011) and psychiatric impairments, including autism (Andrews et al. 2021), ADHD (Bouziane et al. 2018), and schizophrenia (Peters and Karlsgodt 2015).

Diffusion-weighted magnetic resonance imaging (dMRI) is a powerful neuroimaging technique that allows for the investigation of white matter microstructure through the diffusion measurement of molecules within biological tissue (Jones and Leemans 2011). In white matter, the diffusion of molecules is affected by cellular membranes (i.e., myelin sheaths), defining the diffusion-weighted contrast. This diffusion-weighted signal can then be mathematically modeled to estimate the underlying microstructure and reconstruct the organization of white matter tracts (Van Hecke, Emsell, and Sunaert 2016). In the early 2000s, the most common dMRI modeling technique was Diffusion Tensor Imaging (DTI) (Basser, Mattiello, and LeBihan 1994; Mori and van Zijl 2002). While DTI remains a key tool for researchers in understanding the impact of white matter microstructure (Qiu, Mori, and Miller 2015), DTI has some limitations, such as its inability to accurately model areas in which crossing white matter fibres are present (Pierpaoli et al. 2001).

In recent years, advances in dMRI acquisition parameters have enabled higher-order diffusion modeling techniques that increase reconstruction accuracy and can overcome some of the limitations of DTI. With High Angular Resolution Diffusion Imaging (HARDI), an increased number of diffusion direction gradients is acquired, which allows for the estimation of microstructural properties along multiple fiber populations within a single voxel and provides improved reconstruction accuracy of white matter tracts compared to the traditional DTI framework (Descoteaux, 2015). Another advance in dMRI for tractography is the integration of multiple b-values (Pines et al. 2020). Briefly, b-values are a summary measure of the strength, duration, and amplitude of the diffusion-weighting

applied during the scan. Different strength b-values elicit altered tissue responses which can be used to increase the reconstruction accuracy of various neurocellular environments. Higher b-values are more sensitive to detecting diffusion of molecules within brain tissues (Burdette et al. 2001), but are also more susceptible to noise and artifacts compared to lower b-values (Kingsley and Monahan 2004) As such, multi-shell dMRI data leverages the increased signal of high b-value images with the reduced noise of low b-value images to provide increased anatomical accuracy (Pines et al. 2020).

In the context of higher-order diffusion modelling, techniques have been developed, such as constrained deconvolution (CSD), Q-ball, and neurite orientation and dispersion density imaging (NODDI) among many others (Jeurissen et al., 2011). These techniques can describe the distribution of molecule diffusion within a voxel more accurately compared to DTI (e.g., the fiber orientation distribution (FOD) function for CSD and diffusion orientation distribution function (dODF) for DSI and Q-ball) and can be used to model voxels containing crossing white matter fibers. Thus, metrics derived from these higher-order models have increased accuracy, yielding clinically more relevant information that cannot be obtained from the DTI model (Van Hecke, Emsell, and Sunaert 2016). Higher-order diffusion models provide more detailed information about the microstructure and organization of white matter tracts, which can provide important insights into the pathophysiology of neurological and psychiatric disorders.

The aim of this Chapter is to introduce neuroimaging researchers to the concepts and techniques of dMRI data processing used in the field, with a focus on providing a practical step-by-step guide for processing multi-shell HARDI data and generating CSD-based tractography using the ExploreDTI software (Leemans et al. 2009). Brief explanations of the rationale behind each processing step will be provided to aid the researcher in understanding the concepts and principles involved. Potential processing pitfalls will be discussed, and tips for troubleshooting common issues will be provided. Overall, this guide aims to provide a comprehensive resource for researchers to gain the skills and knowledge necessary to process dMRI data effectively and efficiently.

4.2. Methods

4.2.1. Starting point for the data

Advanced FOD modeling techniques, such as CSD, require specific diffusion parameters. Typically for multi-shell HARDI, a minimum of two b-values images (b =

2500-3000 s/mm^2) and 45 diffusion-weighted directions (Van Hecke, Emsell, and Sunaert 2016), are required for CSD modeling for white matter tractography purposes. The Neuroimaging of the Children's Attention Project (NICAP)(Silk, Genc, et al. 2016) study diffusion parameters were used for the processing step-by-step guide provided below. Data from the NICAP cohort are available via Lifecourse (https://lifecourse.melbournechildrens.com/cohorts/cap-and-nicap/).

4.2.2. Data Storage and Computational expense

The step-by-step guide provided here was run on a Linux system with an Intel Core i7 processor and 32 GB RAM using MATLAB R2016b. A standalone version of ExploreDTI is also available. Details of the ExploreDTI instalment are provided below. It is recommended to run Steps 9 and 10 using high-performance computers, given the large processing time of these step. Table 4.1 shows the estimated processing times per participant for each step, with MATLAB parallel processing enabled.

Table 4.1 Approximate processing times for each per participant are provided below (Steps 7 and 8 are optional if multiple b-value data sets were acquired separately).

Processing Step	Name of section	Processing time (approx.)
1	Convert Bval and Bvec files into text files	< 1 min
2	Signal Drift	< 1 min
3	Sort Bvals	< 1 min
4	Gibbs Ringing	< 1 min
5	Flip Permute	< 1 min
6	Generate Mat File	5 min
7	Concatenate all b-value .mat files	2 min
8	Generate Mat File of concatenated .nii files	20 min
9	SM/EC/EPI distortion corrections	360 min
10	Whole brain Tractography	70 min

4.2.3. Step-by-step guide

In this Section, we will provide a step-by-step guide for processing multi-shell HARDI data (in BIDS format) and generating CSD-based tractography using the

ExploreDTI software. As this guide is for complete neuroimaging novices, we will use the ExploreDTI graphic user interface (GUI). A step-by-step guide to installing and using ExploreDTI is provided in the user manual. As we are using BIDS format, each subject folder containing the diffusion files should have *.json*, *.bval*, *.bvec*, and *.nii* files (see Table 4.2). Although advanced diffusion modeling is not feasible with the AOMICS datasets (https://nilab-uva.github.io/AOMIC.github.io/), we have also included step-by-step command lines to demonstrate the possibility to preprocess several subjects all at once (see supplemental material).

Table 4.2 Description of dMRI files in BIDS format

File Name	Comment
.json	This is a file containing a description of scan acquisition details.
.bval	This file contains a summary of the diffusion-weightings applied during scanning.
.bvec	These files contain details on the diffusion gradient vectors of the scan.
.nii	this is the raw diffusion scan in NIfTI format

Convert Bval and Bvec files into text files (Step 1)

The first processing step is to generate *.txt* file(s) from the *.bval* and *.bvec* files for the images you are processing. The *.txt* file is a summary file of the b-values and diffusion-weighting directions used during image acquisition and is required for image processing.

In ExploreDTI:

1. Plugins → Convert → *.bval/*.bvec to B-matrix *.txt files(s) (see Figure 4.1)
    a. Select folder containing *.bval and *.bval file(s)
    b. Select output folder for *.txt file(s)

2. The output folder now includes the converted .txt file(s)

Figure 4.1 Step 1 using the ExploreDTI GUI

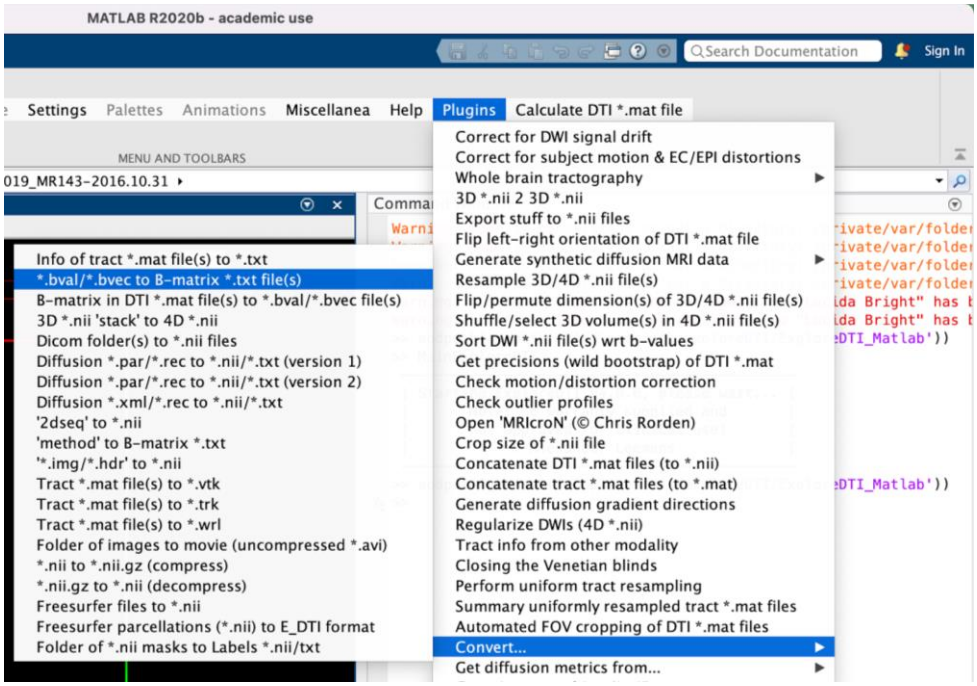

Signal Drift Correction (Step 2)

Signal drift is a phenomenon caused by scanner imperfections, which leads to an adverse alteration of the acquired signal and a bias in the estimation of diffusion measures if not corrected (Vos et al. 2017).

Note: We recommend the use of 'quadratic fit', but a signal drift fitting guide is provided in the Appendix 1 for users who want to investigate the impact of different fitting approaches (see eFigure 1).

In ExploreDTI:

1. Plugins → Correct for DWI signal drift (see Figure 4.2).
    a. Single or multiple data sets: multiple.
    b. Select the folder of .nii file(s).
    c. Select output folder.
2. The output folder now includes,
    a. *_sdc.txt file(s)

b. *_sdc.nii file(s)

c. *_sdc.png file(s)

Figure 4.2 Step 2 using the ExploreDTI GUI

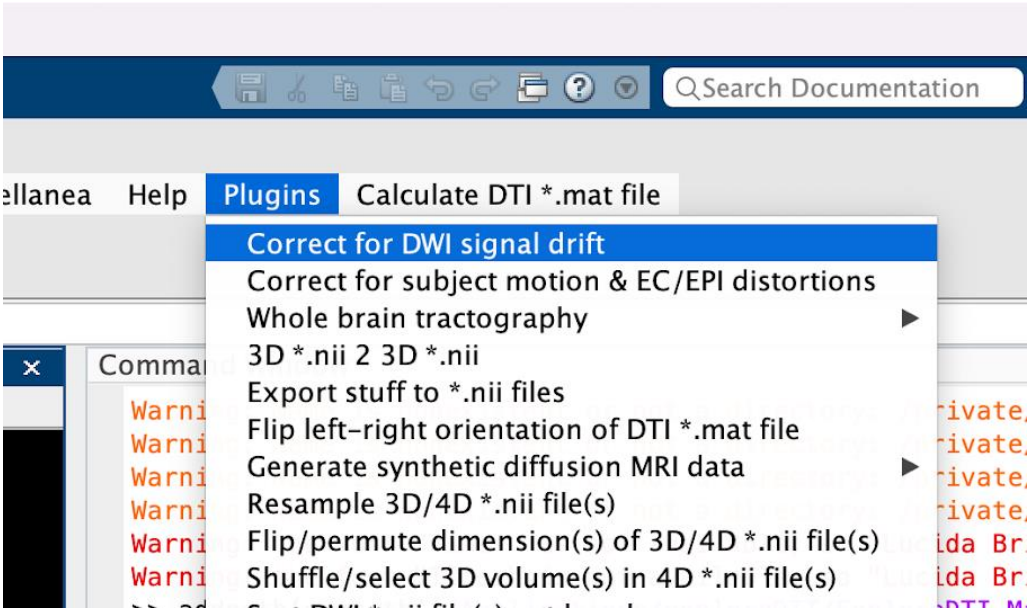

Note: As the signal drift correction uses the non-diffusion weighted (b-0) files acquired to correct for signal drift, it is crucial that signal drift correction is completed before sorting b values, which may change the order of the acquired dMRI volumes (Step 3).

Sort B-Values, Organise and remove excess b-0 files (Step 3)

For the remaining processing steps ExploreDTI requires that all b-0 files are sorted to the beginning of the diffusion files. This step quickly organizes the files to have all the b-0 files at the beginning of the *.nii* and *.txt* files.

In ExploreDTI:

1. Plugins → Sort DWI *.nii file(s) wrt b-values (see Figure 4.3)
    a. File name suffix: *_sorted.nii.
    b. Single or multiple data sets: multiple.
    c. Select the folder of *.nii file(s) and *.txt file(s).
    d. Select output folder.
2. The output folder now includes,

a. *_sdc_sorted.txt file(s)

b. *_sdc_sorted.nii file(s)

Figure 4.3 Step 3 using the ExploreDTI GUI

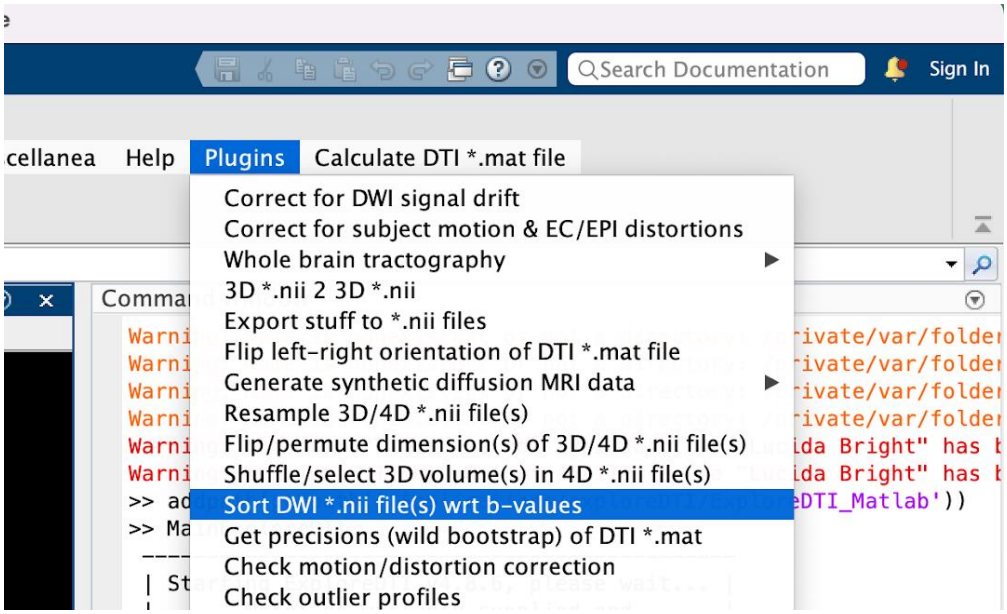

Note: Rarely, additional b-0 files are collected during scanning. To investigate if extra b-0 files are present, open the newly sorted .txt file and investigate (see Figure 4.4). If excess b-0 files are present (see red box in Figure 4), these can be removed in ExploreDTI.

Figure 4.4 Example of a sorted .txt file containing 6 b-0 images

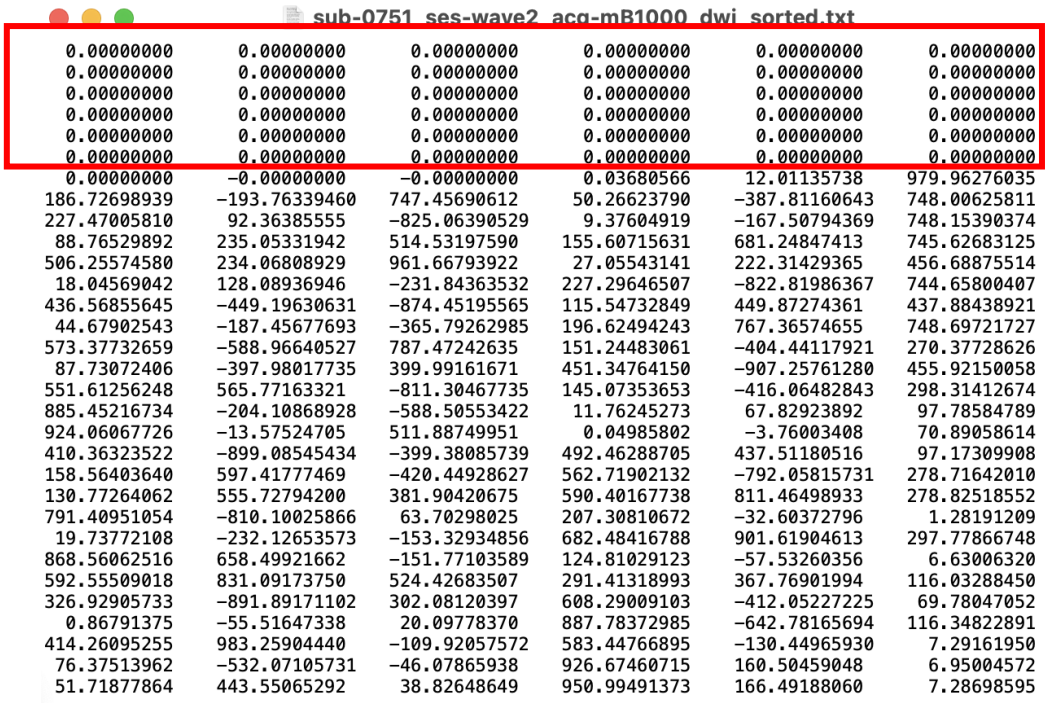

Gibbs Ringing Correction (Step 4)

A phenomenon known as Gibbs ringing may occur due to the shortening/truncation of Fourier transforms to reconstruct the MRI signal. If uncorrected, Gibbs ringing leads to artifacts that appear as multiple fine parallel lines in the image.

In ExploreDTI:

1. Plugins → TV for Gibbs ringing in non-DWI's (4D *.nii) (see Figure 4.5)
    a. Select Gibbs Ringing Correction settings (see Table 4.3).
    b. Single or multiple data sets: Multiple.
    c. Select the folder of *.nii files.
    d. Select output folder.
2. The output folder now includes,
    a. *_sdc_sorted_GR_TV.nii files.
3. Create and move *_sdc_sorted_GR_TV.nii files into a new folder.

Figure 4.5 Step 4 using the ExploreDTI GUI

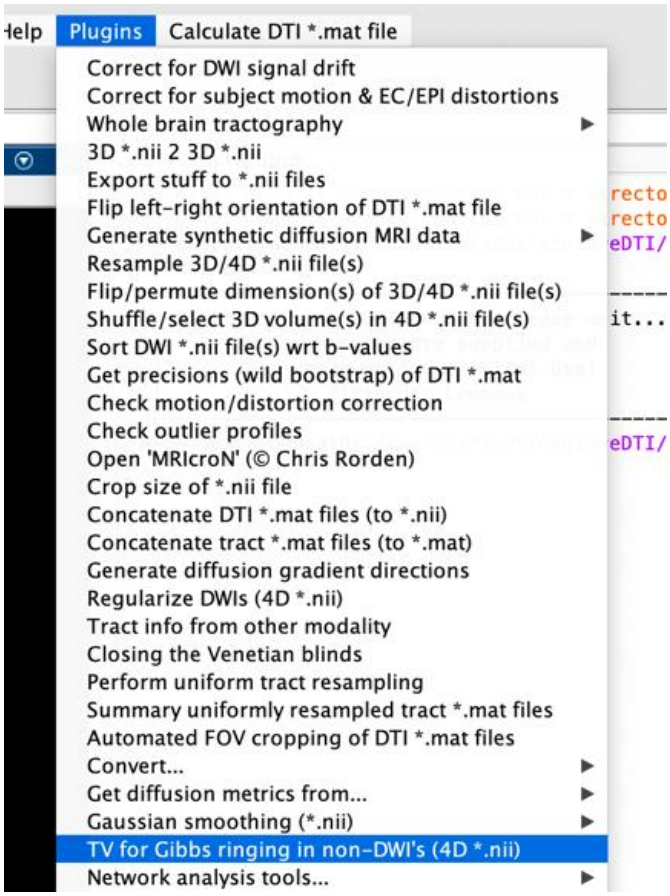

Table 4.3 Setting Gibbs ringing parameters

Parameter	Comment
Number of non-DWIs	This information is provided in the *.txt file.
Lambda ([1 200])	Lambda is a parameter that can be used to control the degree of Gibbs ringing in image reconstruction algorithms. A higher value of lambda will suppress Gibbs ringing more. However, it should be noted that a high value of lambda will also reduce the level of high-frequency information in the processed image, and therefore it is important to find a balance between reducing Gibbs ringing and preserving image quality. Recommendation: 100 (Default setting)
Number of iterations ([1 200])	The number of iterations is another parameter that controls the degree of Gibbs ringing correction. Recommendation: 100 (Default setting)
Step size ([0.001–0.1])	The step size determines the magnitude of the update applied to the image estimate at each iteration of the algorithm. A smaller step size will result in a slower convergence of the algorithm and less Gibbs ringing, while a larger step

	size will result in a faster convergence but more Gibbs ringing. The optimal value is a desired trade-off between Gibbs ringing reduction and computational time. Recommendation: 0.01 (Default setting)
Imaging plane (coronal:1, sagittal:2, axial:3)	The Gibbs ringing correction algorithm takes into account the imaging plane in which the image was acquired. This information is found in the subject specific *.json file, Phase Encoding Directions **i** left-right (sagittal) **i-** right-left (sagittal) **j** anterior–posterior (axial) **j-** posterior–anterior (axial) **k** inferior-superior (coronal) **k-** superior–inferior (coronal)

Flip Permute (Step 5)

Permutations and flips in spatial configuration and/or mismatches between spatial and diffusion coordinate systems can accidentally occur during processing and analyses across different software packages, potentially resulting in errors. The "flip/permute" tool in ExploreDTI can reorientate images and also avoid further unexpected axis flips and permutations in any following image processing step. Use default ExploreDTI settings as orientations will be inspected at the next step.

In ExploreDTI:

1. Plugins → Flip/permute dimension(s) of 3D/4D *.nii files (see Figure 4.6)
    a. Use default setting:
        i. File name suffix: _FP
        ii. Permute dimensions: 1 2 3
        iii. Flip dimensions: 0 0 0
        iv. Force voxel size: leave empty
    b. Single or multiple data sets: multiple.
    c. Select the folder of *.nii file(s).
    d. Select output folder.

The output folder now includes *_sdc_sorted_GR_TV_FP.nii files.

Figure 4.6 Step 5 using the ExploreDTI GUI

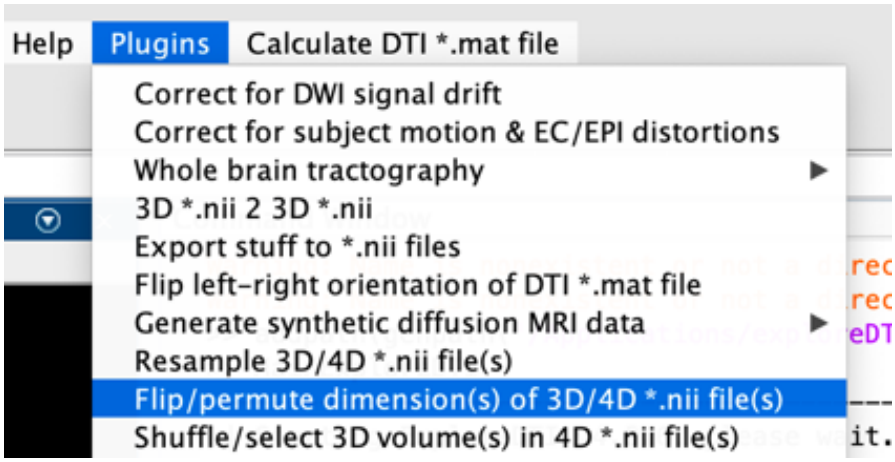

The next processing step requires each individual image to have matching .nii and .txt file names. Thus, rename *_*sdc_sorted.txt* files in the previous folder to match the current .nii file (e.g. *_*sdc_sorted_GR_TV_FP.txt*) and create a new folder containing matching .txt and .nii files.

Generate .mat file (Step 6)

It is required to generate a .mat file from the processed .nii and corresponding .txt files before tractography or other analysis tools can be applied. The DTI .mat file is a matlab format file and can be loaded into ExploreDTI for further processing and analysis.

In ExploreDTI:

1. Calculate DTI *.mat file → Convert raw data to 'DTI *.mat.(see Figure 4.7)
    a. Select settings (see Table 4.4).
    b. Select the folder of *.nii.
    c. Select folder .txt files: Press cancel if each .nii has its associated .txt file.
    d. Select output folder.

The output folder now includes *_sdc_sorted_GR_TV_FP.mat files.

Figure 4.7 Step 6 using the ExploreDTI GUI

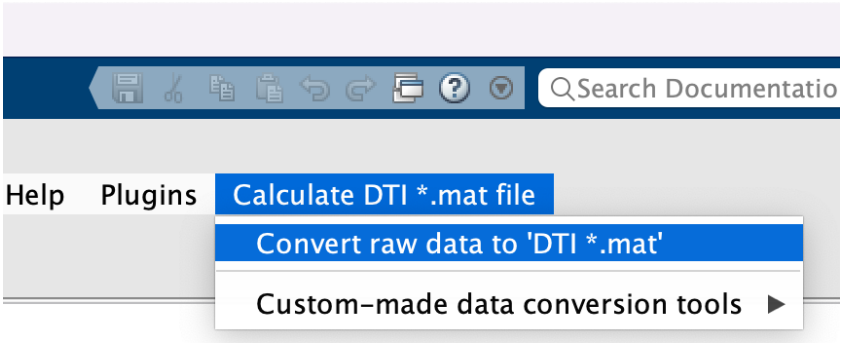

Table 4.4 Selecting .mat generation parameters

Parameter	Comment
Format diffusion weighted data	4D Nifti (*.nii)
Permute spatial dimensions	This allows you to flip spatial dimensions of image. Recommendation: Use default settings (AP RL IS) if there are no issues with spatial dimensions.
Flip spatial orientations	This step allows you flip the direction of the dimensions. This is important if your data was collected in Neurological dimensions rather than Radiological conventions. In this instance, you may need to flip dimensions from Right – Left to Left – Right. To flip, change the parameter from 'AP RL IS' to 'AP LR IS'. If your data were collected in Radiological dimensions the default setting of 'AP RL IS' should be appropriate.
Perform visual data check	This allows you to quickly visualize the orientation of the image.
Diffusion tensor estimation	The robust tensor estimation algorithms aim to minimize the impact of outliers on the final diffusion tensor estimate, leading to more reliable results. Recommendation: Robust (exclude outliers)
Format diffusion information	Text file (*.txt)
Background masking approach	Automatic
Permute gradient components	Permute gradient components should correspond to data and may require some investigation (see Note below this table).
Flip sign of gradient components	The sign of gradient components should correspond to data and may require some investigation (see Note below this table).
Data processing mode	Single or multiple data sets
b-value in units s/mm^2	E.g., 1000
Voxel size [AP RL IS] (in mm)	E.g., 2 2 2
Number of non-DW images	E.g., 3
Number of DW images	E.g., 30

Matrix size [AP RL IS]	E.g., 128 128 60

Note: A common pitfall of dMRI processing is orientation issues. During the .mat generation step you should investigate the flip/permutations to ensure appropriate orientations were selected. It is advised that you first use the default settings as ExploreDTI is able to automatically provide the correct orientation settings (Jeurissen, Leemans, and Sijbers 2014). ExploreDTI deploys the widely used color convention to ensure the orientations ('Permute gradient components') are correct (left-right: Red, top-bottom: Blue, and front-back: Green). Good tracts to investigate when checking orientations are the corpus callosum – a white matter tract that is orientated left-right (Red) and the corticospinal tracts - white matter tracts that are orientated top-bottom (Blue). To see an example of orientation checks see Figures 4.8 & 4.9.

Figure 4.8 Checking Permute Gradient Components

4.8a. 4.8b.

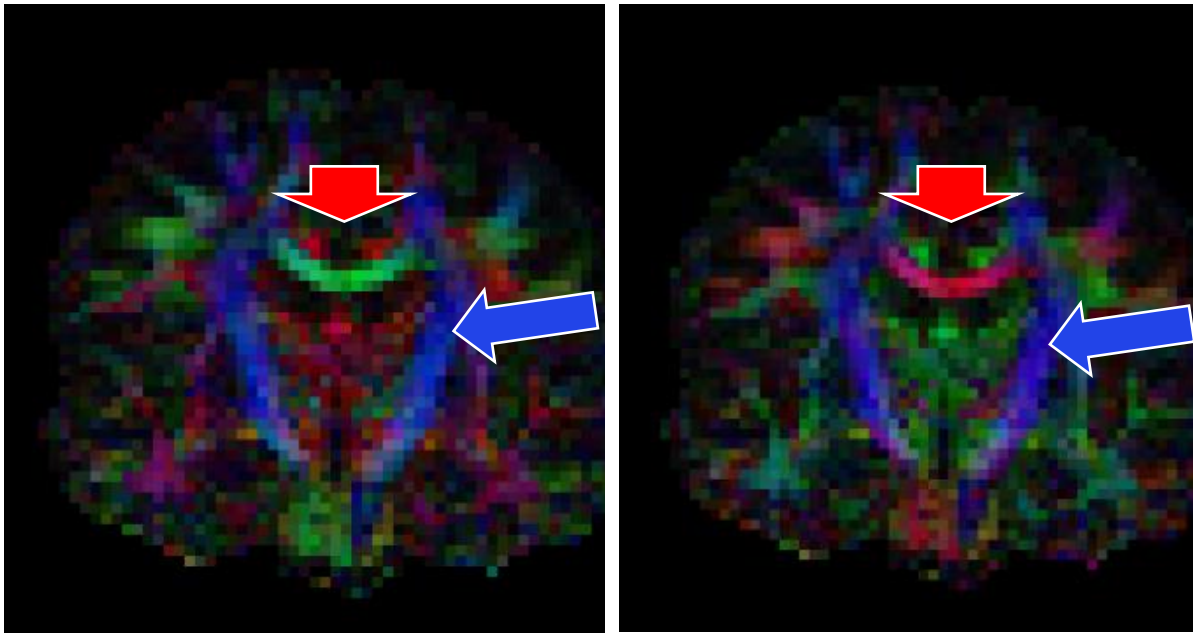

Before-and-after correct flipping of the 'Permute gradient components'. As you can see in Figure 4.8a while the corticospinal tract is the correct orientation (blue arrow) the corpus callosum (red arrow) – a white matter tract that is orientated left-right – is green. This indicates that the x and y axis need to be flipped. To do so, change the 'Permute gradient components' from *x y z → y x z* and generate a new correctly orientated .mat file (Figure 4.8b.).

Figure 4.9 Checking Flip Sign Components

4.9a. 4.9b.

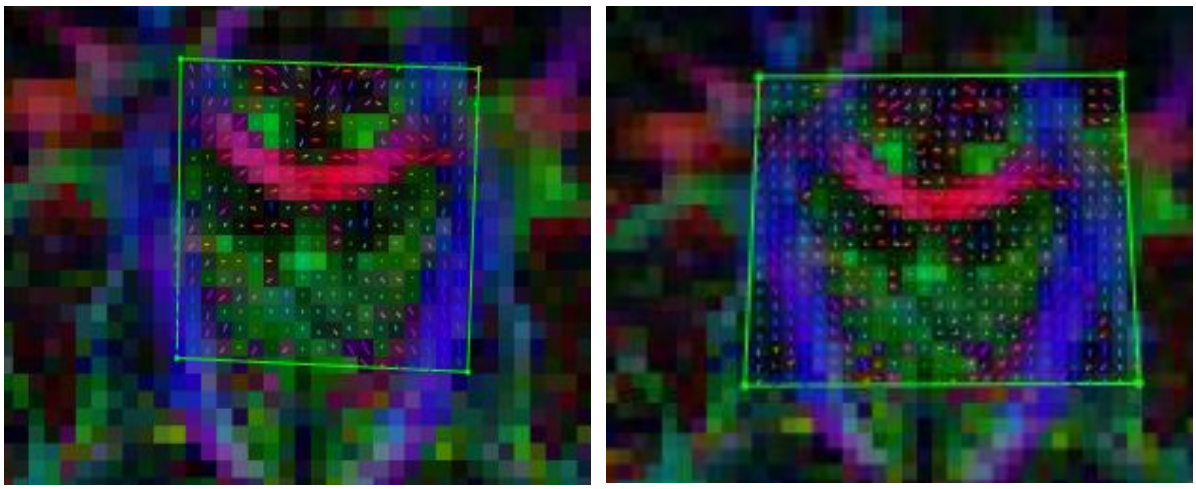

Figure 4.9 illustrates an investigation into the flip sign gradients. While the orientations of the images of both images are correct the gradient sign may be flipped. Use Glyphs (in Explore DTI: *Draw ROI → Draw Glyphs*) to inspect the signs and investigate the 'Flip sign of gradient components'. Figure 4.9a. shows an incorrect flip sign gradient as the glyphs are not following the curvature of the Corpus Callosum. To fix this the z

component must be flipped. To do so, change the 'flip sign gradients' from *x y z* → *x y -z* and generate the correct .mat file (4.9b.).

Concatenate all b-value .mat files (Step 7)

This step concatenates all the single b-values (shells) .mat files together to create a multi-shell .nii file. This enables a major benefit of multi-shell imaging; namely, leveraging the increased signal of high b-value images with the reduced noise of low b-value images to produce an image with increased anatomical accuracy.

Firstly, you should organize all your b-value .mat files into scan-specific folders (see below).

In ExploreDTI:

1. Plugins → Concatenate DTI *.mat files (to *.nii) (see Figure 4.10)
    a. Select folder of folders: select the folder containing all the scan-specific folders.
2. The output folder now includes,
    a. *_concatenated.txt file(s)
    b. *_concatenated.nii file(s).

Figure 4.10 Step 7 using the ExploreDTI GUI

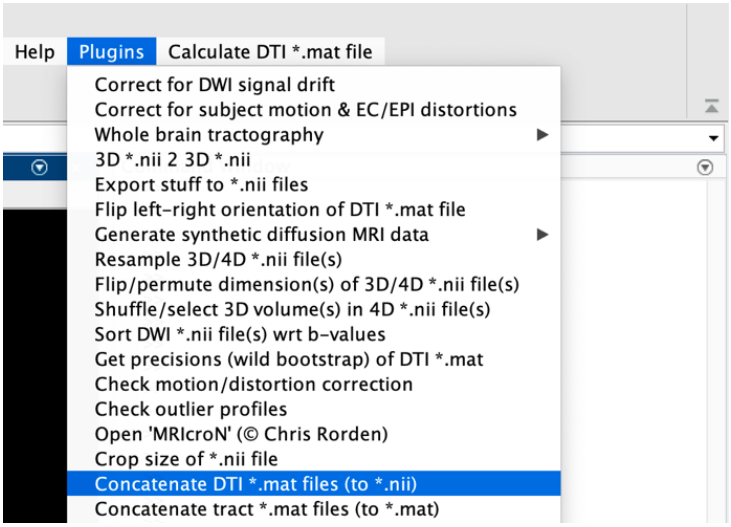

Generate concatenated .mat file (Step 8)

It is now required that you convert the concatenated .nii files into .mat files. As any orientation issues should have been resolved at Step 5, default orientation settings will be used. For processing efficiency, it is advised that you move *_concatenated.nii and *_concatenated.txt files into a folder.

In ExploreDTI:

1. Calculate DTI *.mat file → Convert raw data to 'DTI *.mat' (see Figure 4.7)
    a. Select settings (see Table 4.5).
    b. Select the folder of *_concatenated.nii files.
    c. Select folder *_concatenated.txt files: Press cancel.
    d. Select output folder.
2. The output folder now includes,
    a. *_concatenated.mat file(s).

Table 4.5 Selecting .mat generation parameters

Parameter	Comment
Format diffusion weighted data	4D Nifti (*.nii)
Permute spatial dimensions	AP RL IS
Flip spatial orientations	AP RL IS
Perform visual data check	No.
Diffusion tensor estimation	Robust (exclude outliers)

Format diffusion information	Text file (*.txt)
Background masking approach	Automatic
Permute gradient components	x y z
Flip sign of gradient components	x y z
Data processing mode	Multiple data sets
b-value in units s/mm^2	NaN (for multi-shell data) or any integer for DTI
Voxel size [AP RL IS] (in mm)	E.g., 2 2 2
Number of non-DW images	The total number of b-0 images in the concatenated images (Using the parameters in NICAP study, e.g., number of non-DW images = 16).
Number of DW images	The total number of b-value images in the concatenated images (Using the parameters in NICAP study, e.g., number of DW images = 130)
Matrix size [AP RL IS]	E.g., 128 128 60

Correcting subject motion, eddy currents, and EPI-induced distortions (Step 9)

This step corrects subject motion (SM), eddy currents (EC), and EPI-induced distortions (EPI). This is a crucial processing step, as such distortions can lead to significant changes in diffusion metric estimates. Additionally, you can use 'undistorted' structural MRI (T1 or T2) images to unwrap the deformations in the diffusion data (For more details see ExploreDTI manual). If you do not have a structural MRI this step can be conducted in native space. To process this step in ExploreDTI without a structural MRI file ensure the following setting is selected, *Settings → SM/EC/EPI correction → Also register to other data → No thanks (stay in native space).* Before beginning this step move *_concatenated.mat files (and *_nu.nii and *_mask.nii files if necessary) to a folder.

Note: Due to the large computational demand of Step 9, it is recommended to use multi-core computing support for this tool with a minimum of 32 GB RAM for dMRI data if you have more than 100 DW images.

In ExploreDTI:

1. Select settings (see Table 4.6).
2. Start MATLAB parallel pooling.
3. Plugins → Correct for subject motion & EC/EP distortions. (see Figure 4.11)
    a. Single or multiple data sets: Multiple.

b. Select the folder of *_concatenated.mat files.
    i. Include *_nu.nii and *_mask.nii for using structural MRI files for registration.
c. Select output folder.

The output folder now includes *_concatenated_trafo.mat files.

Figure 4.11 Step 9 using the ExploreDTI GUI

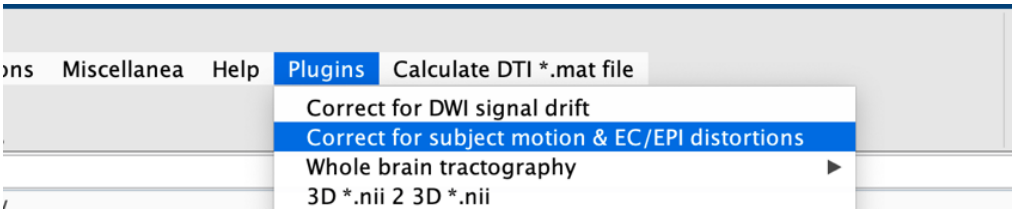

Table 4.6 Selecting SM/EC/EPI distortion parameters

Parameter	Comment
Settings → SM/EC/EPI correction → masking stuff	This setting allows you to use a mask generated from a structural MRI scan. If you do not have a structural MRI mask, do not select the 'masking stuff' setting.
Settings → SM/EC/EPI correction → Also register to other data → Yes, to do EPI correction (non-rigid)	This setting allows you to register your diffusion image to a structural MRI image during the EPI correction, enabling increased distortion correction. Recommendation: select 'orig_nu' from Freesurfer processed structural MRI files.
Settings → SM/EC/EPI correction → also register to other data → registration details → Deformation axes	By default, the non-linear deformations are allowed along any orientation. Recommendation: correction will likely improve if the registration is constrained to model deformations only along the phase encoding direction. To do this (example A-P orientation), change "Deformation axes" to [1 0 0].
Settings → SM/EC/EPI correction → Registration details for SM/EC corrections → interpolation method	Recommendation: Linear or cubic spline

Whole brain tractography (Step 10)

Whole brain tractography in ExploreDTI generates white matter tracts using a deterministic approach. Other software packages, such as FSL and MRtrix are available if

you would like to do probabilistic tractography. It is recommended that you complete whole brain tractography before reconstructing specific white matter tracts for analysis.

In ExploreDTI:

1. Plugins → whole brain tractography → CSD (see Figure 4.12)
    a. Select settings (see Table 4.7).
    b. Single or multiple data sets: multiple.
    c. Select the folder of *_trafo.mat files.
    d. Select output folder.
    e. The output folder now includes the *_trafo_Tracts_CSD.mat files (see Figure 4.13).

Figure 4.12 Step 10 using the ExploreDTI GUI

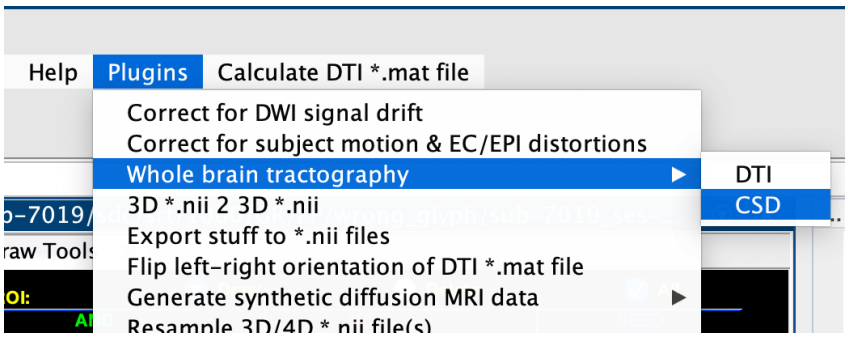

Table 4.7 Whole Brain Tractography parameters

Parameter	Comment
Seedpoint resolution (mm)	Seed point resolution is a measure of how close together the seed points are placed in the brain. A higher seed point resolution will result in a higher number of seed points used in the tractography algorithm, and therefore a higher number of the reconstructed tracts. However, this also increases the computation time. Recommendation: 2 2 2
Step size (mm)	The step size is a parameter that determines the distance between each point in the reconstructed tracts. A smaller step size will result in a higher accuracy of the reconstructed tracts, but it will also increase the computation time. Recommendation: 1
Angle threshold	The angle threshold is a parameter controls the angular deviation of consecutive steps during pathway reconstruction. A higher angular threshold will result in more or longer tracts, but it will also increase the risk of false

	positive tracts. If you are planning to exact tracts with high curvature (such as the fornix) it is advised to set this threshold higher (e.g., 60 degrees).
Fiber length range	This step allows you to set the upper and lower bound of the length of the reconstructed fibers. Change this setting if you are investigating particularly long or short white matter tracts. If you are investigating both long and short fiber it is recommended to set this setting to, 10 – 500.
Random permutations of seed points?	0 = no / 1 = yes (setting to get rid of rectilinear grid-pattern artifacts) Recommendation: 0

Figure 4.13 Complete CSD tractography (subsampled: 50)

X axis view Y axis view Z axis view

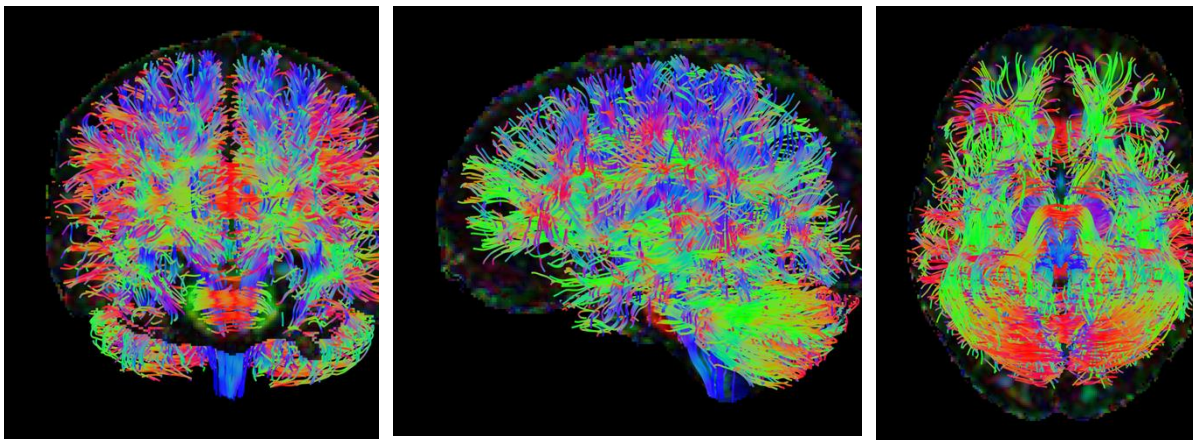

Extracting Diffusion MRI Metrics (Step 11)

At this step, you should have already extracted the white matter tracts you want to analyse. A step-by-step guide of conducting manual tractography is provided in the ExploreDTI manual. This step allows you to export diffusion metrics for the analyzed tract pathway of interest.

In ExploreDTI:

1. Plugins → convert → info. of tract *.mat file(s) to .txt. (see Figure 4.14)
    a. Select the folder of .nii.
    b. Select output folder.
2. The output folder now includes,
    a. *.txt files
3. Export *.txt file to Excel.

Figure 4.14 Step 11 using the ExploreDTI GUI

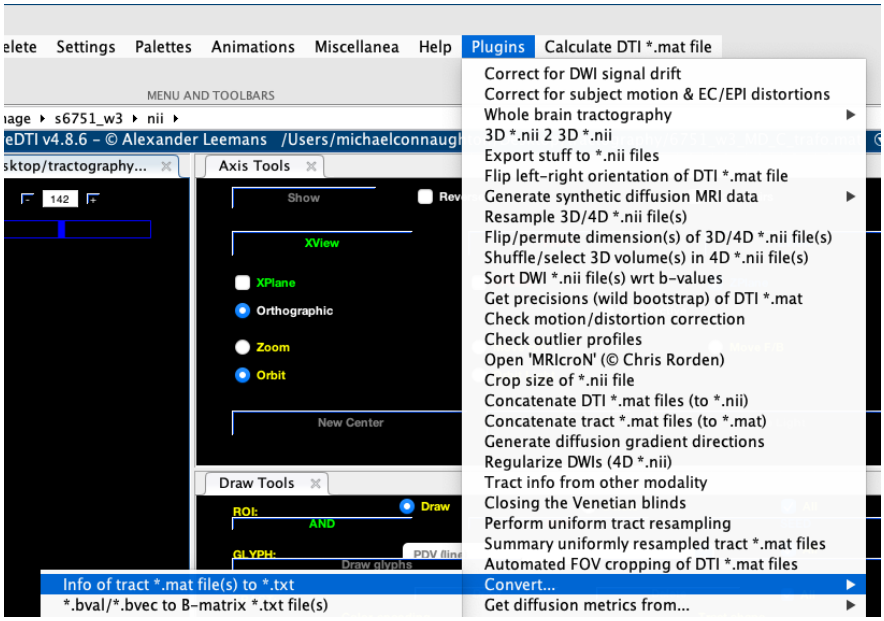

4.2.4. Conclusion

This book Chapter offers a comprehensive resource that equips researchers with the necessary skills and knowledge to effectively and efficiently process large diffusion MRI data sets. By providing practical, step-by-step guides, researchers can process both DTI and multi-shell HARDI data using the ExploreDTI software. When choosing a diffusion MRI modelling technique, it is important to consider the pros and cons of both DTI and multi-shell HARDI approaches. Multi-shell HARDI offers several advantages over DTI, including increased anatomical accuracy and the ability to model crossing fibres. However, it also comes with certain disadvantages compared to DTI that warrant careful evaluation. A significant drawback of multi-shell HARDI is that it is a highly computationally expensive technique, which results in significantly longer processing times compared to DTI. Nevertheless, steps can be taken to reduce processing time through resource optimization. Researchers can optimise the utilisation of computational resources by fine-tuning the processing parameters described in this book Chapter. When processing large data sets, it is advised to experiment with different settings parameters to find the optimal balance between reconstruction accuracy and processing time. Overall, it is crucial to assess the accessible resources, both available time and computational resources, before deciding which diffusion MRI modelling technique to employ.

5 Limbic System White Matter in Children and Adolescents with ADHD: A Longitudinal Diffusion MRI Analysis

5.1. Introduction

ADHD is increasingly viewed as a disorder of connectivity, a "dysconnectome" in which microstructural differences in white matter tracts interconnecting large-scale brain systems are associated with symptom expression (Sudre et al. 2023; Sudre et al. 2021; Konrad and Eickhoff 2010). White matter comprises nerve fibres, known as axons, that connect different regions of the brain (Fields 2010). Healthy development of white matter is crucial for efficient information transmission within the brain, leading to neurotypical brain function and cognition (Lebel and Deoni 2018). Diffusion-weighted MRI (dMRI) is a neuroimaging modality that enables the *in-vivo* exploration of white matter microstructure by measuring the diffusion of molecules within biological tissue (Van Hecke, Emsell, and Sunaert 2016). The movement of molecules in white matter is influenced by cellular membranes, such as myelin sheaths, which shape the diffusion-weighted signal (Jones and Leemans 2011). By employing mathematical modelling, this diffusion-weighted signal can be utilised to estimate and reconstruct the underlying microstructural organisation of white matter tracts (Van Hecke, Emsell, and Sunaert 2016). dMRI enables the assessment of various diffusivity metrics, which are associated with underlying microstructural organisational properties of white matter (see Table 5.1).

Table 5.1 Description and clinical implications of dMRI Metrics.

Modelling technique	Metric	Description
DTI	Fractional anisotropy (FA)	A frequently used measure that summarises the degree of white matter microstructural organization. In clinical contexts, a decrease in FA value may indicate demyelination, axonal damage, or decline of white matter coherence (Van Hecke, Emsell, and Sunaert 2016; Zhang and Burock 2020).
	Radial diffusivity (RD)	A metric used to assess the level of diffusion occurring perpendicular to the principal diffusion direction. Clinically, increased radial diffusivity could be considered a sensitive indicator for increased processes of demyelination (Song et al. 2005; Van Hecke, Emsell, and Sunaert 2016).
	Axial diffusivity (AD)	A quantitative measure that summarise the degree of diffusion along the principal diffusion direction. In clinical context, a decrease in AD has been linked to disrupted axonal integrity and organisation (Alexander et al. 2007; Van Hecke, Emsell, and Sunaert 2016).
	Mean diffusivity (MD)	A scalar metric that represents the overall extent of diffusion within a voxel, independent of direction. An elevation in MD has been linked to oedema, axonal loss, and demyelination (Alexander et al. 2007; Van Hecke, Emsell, and Sunaert 2016).
DKI	Kurtosis anisotropy (KA)	Quantifies the non-gaussian diffusion in a given voxel. KA is an analogue to the FA (Poot et al. 2010) but importantly can offer a contrast in areas where tissue complexity causes FA to fail (Hansen and Jespersen 2016). Increased KA may reflect improved myelination and axonal organisation (Maiter et al. 2021; Hansen 2019).
	Axial Kurtosis (AK)	Evaluates the non-gaussian diffusion of molecules along the axial direction and is an analogue of AD (Steven, Zhuo, and Melhem 2013). Decreases in AK have been associated with diminished axonal integrity and packing (Falangola et al. 2014).
	Radial Kurtosis (RK)	A summary measure of the non-gaussian diffusion occurring in the radial direction and is an analogue of RD (Steven, Zhuo, and Melhem 2013). Elevated RK may indicate the deterioration of myelin,

	neurofilaments and/or microtubules degeneration (Takahashi et al. 2002; Does, Parsons, and Gore 2003; Schwartz et al. 2005; Yong-Hing et al. 2005; Thelwall et al. 2006; Goryawala et al. 2018).
Mean Kurtosis (MK)	An analogue to MD and is a measure of the overall non-gaussian diffusion, independent of direction. Decreases in MK may reflect reduced structural complexity, specifically processes of myelin breakdown and reduced axonal packing (Falangola et al. 2014).

dMRI has been an essential tool in ADHD pathophysiological research, identifying atypical white matter microstructure as a potential core neurobiological feature of the disorder (Connaughton et al. 2022). Cross-sectional dMRI research has consistently identified several tracts with reduced white matter microstructure in children and adolescents with ADHD, characterised by reduced microstructural organisation (lower GFA and/or FA) in the frontostriatal tracts (Chiang et al. 2015; Chiang et al. 2016; Shang et al. 2013; Gau et al. 2015; Wu et al. 2014; Lin et al. 2014; Tung et al. 2021), corpus callosum (Cao et al. 2010; Qiu et al. 2011; Ameis et al. 2016; King et al. 2015; Pastura et al. 2016; Wu et al. 2017), superior longitudinal fasciculus (Chiang et al. 2015; Chiang et al. 2016; Pastura et al. 2016; Wu et al. 2017), cingulum bundle (Chiang et al. 2015; Chiang et al. 2016; Tung et al. 2021; King et al. 2015), internal capsule (Qiu et al. 2011; Pastura et al. 2016; Wu et al. 2017; Ashtari et al. 2005; Nagel et al. 2011), corona radiata (Qiu et al. 2011; Wu et al. 2017; Pavuluri et al. 2009; Nagel et al. 2011), and thalamic white matter (Tung et al. 2021; Bouziane et al. 2018). However, inconsistent findings have also been reported, which may be attributed to the limitations of cross-sectionally designed studies and the diffusion MRI models used (Connaughton et al. 2022). While cross-sectional studies are vital for generating hypotheses and examining associations, their inability to capture temporal changes or individual variabilities is a major limitation for pathophysiological research. Despite numerous authors emphasising the need for longitudinal case-control dMRI studies in children and adolescents with ADHD (Bouziane et al. 2018), there are two studies to-date.

The first longitudinal dMRI study used the NICAP study to investigate whether deviations from typical trajectories of white matter fibre development are associated with the persistence or remission of ADHD symptoms (Fuelscher et al. 2023). Compared to controls, individuals with ADHD displayed lower fibre bundle cross-section (FC) – a

measure of fibre morphology (Raffelt et al. 2017) – in thalamic pathways, striatal pathways, and superior longitudinal fasciculus at around age 10 but showed accelerated development of fibre morphology between ages 10 and 14 (Fuelscher et al. 2023). Within the ADHD group, individuals with remission of ADHD symptoms displayed increased convergence towards non-ADHD fibre morphology compared to individuals with persistent ADHD symptoms (Fuelscher et al. 2023). By contrast, children with persistent ADHD displayed ongoing neural anomalies throughout childhood and adolescence (Fuelscher et al. 2023). The findings if this study are consistent with the *convergence model*, a prominent neurodevelopmental model of ADHD that suggests convergence of neural features towards neurotypical brain structures is associated with remission of ADHD symptoms (Shaw et al. 2013).

The second longitudinal DSI study investigated white matter microstructure at two time points, from childhood to young adulthood (Chiang et al. 2023). Compared to controls, individuals with ADHD showed a more rapid rate of development of GFA in the left arcuate fasciculus, right SLF, left frontal aslant tract, left cingulum, left inferior fronto-occipital fasciculus (IFOF), left FS-PFC, left thalamic radiation, bilateral corticospinal tracts, and the corpus callosum (Chiang et al. 2023). The findings of this study suggest that atypical brain development in ADHD is characterised by normalisation and possible compensatory neuroplasticity processes, supporting the *maturational delay hypothesis* of ADHD (see Section 1.2.4) (Shaw and Sudre 2021; Shaw et al. 2013). Developmental models like the convergence model and maturation delay hypothesis have significantly contributed to our understanding of the neurobiological underpinnings of ADHD. However, it is essential to acknowledge that ADHD is characterised by differences across numerous brain regions, each with distinct developmental mechanisms and trajectories (Bethlehem et al. 2022; Herting et al. 2018). Consequently, it is likely that the pathophysiology of ADHD involves varied region-specific developmental patterns. Therefore, it is crucial for ongoing research to investigate under-explored regions of the brain to better understand the complex relationship between brain development and ADHD.

To date, much of ADHD white matter research has focused on components of the frontostriatal, default mode, ventral attention, somatomotor, and cortico-striato-thalamo-cortical networks (Connaughton et al. 2022). The limbic system network remains an under-investigated region of interest in ADHD research (see Section 1.3). Despite previous

cross-sectional findings of differences in structures of the limbic system in ADHD (Connaughton et al. 2022) and the high prevalence of emotional dysregulation seen in the disorder (Shaw, Stringaris, et al. 2014), the limbic system remains an under-investigated region of interest in ADHD research. To date, no longitudinal study has investigated the developmental trajectories of limbic system white matter in ADHD. As described in Section 1.4, the limbic system comprises of a collection of interconnected cortical and subcortical structures dedicated to linking visceral states and emotional cognition and behaviour (Mesulam 2000; Lövblad, Schaller, and Isabel Vargas 2014; Rolls 2019c; Messina, Grecucci, and Viviani 2021). The key white matter tracts of the limbic system include the cingulum bundle, uncinate fasciculus, fornix, anterior thalamic projections and mammillothalamic tracts (see Figure 1.1) (Catani, Dell'acqua, and Thiebaut de Schotten 2013).

Historically, reconstructing complex subcortical structures such as limbic system white matter tracts has been challenging for dMRI research. Since the early 2000s, the most common dMRI modelling technique is Diffusion Tensor Imaging (DTI) (Van Hecke, Emsell, and Sunaert 2016). While DTI has been a pioneering technique, it has some limitations, such as poor spatial resolution, low signal-to-noise ratio (SNR), high susceptibility to partial volume effects, and an inability to model crossing fibres (Pierpaoli et al. 2001; Behrens et al. 2007; Jeurissen et al. 2011). These limitations becomes particularly problematic when reconstructing complex white matter tracts associated with crossing fibres, such as those found in the limbic system (Kamali et al. 2018). However, recent advancements in dMRI acquisition parameters have led to notable progress in higher-order diffusion modelling techniques that increase white matter tract reconstruction accuracy and can overcome some of the limitations of DTI (Van Hecke, Emsell, and Sunaert 2016). High Angular Resolution Diffusion Imaging (HARDI) has emerged as an influential approach that uses additional diffusion direction gradients during acquisition (Van Hecke, Emsell, and Sunaert 2016). This allows for the estimation of microstructural properties along multiple fibre populations within a single voxel and provides improved reconstruction accuracy of white matter tracts compared to the traditional DTI framework (Van Hecke, Emsell, and Sunaert 2016).

Another significant advance in dMRI for tractography is multi-shell imaging which involves the integration of multiple b-values (Van Hecke, Emsell, and Sunaert 2016). B-values are a summary measure of the strength, duration, and amplitude of the diffusion-

weighting applied during the scan. By employing different b-values, distinct tissue responses can be elicited, enhancing the reconstruction accuracy of various neurocellular environments. Higher b-values offer greater sensitivity in detecting diffusion of molecules within brain tissues (Burdette et al. 2001) but are more prone to noise and artefacts compared to lower b-values (Kingsley and Monahan 2004). To mitigate this, multi-shell dMRI data leverages the increased signal from high b-value images with the reduced noise from low b-value images, resulting in improved anatomical accuracy for fibre reconstruction (Pines et al. 2020). The utilisation of multi-shell HARDI data offers the opportunity to employ an advanced fibre tracking technique called constrained spherical deconvolution (CSD) based tractography (Tournier et al. 2004a; Tournier, Calamante, and Connelly 2007). CSD-based tractography uses the fibre orientation distribution (FOD) function, this provides a more precise description of the distribution of molecule diffusion within a voxel and leads to increased fibre reconstruction accuracy compared to DTI (Tournier, Calamante, and Connelly 2007). This capability makes CSD especially valuable in modelling voxels that contain complex, crossing white matter fibres (Tournier, Calamante, and Connelly 2007). As Wheeler-Kingshot et al., (2009) reported, DTI tensor-based estimation cannot accurately reconstruct regions of complex fibre orientation resulting in uncertainty of the tensor derived scalar metrics. Importantly, applications of fibre orientation estimations, such as CSD tractography, have been shown to provide a more accurate tract specific metrics and are recommended in regions containing complex fibre tracts (Wheeler-Kingshott and Cercignani 2009; Reijmer et al. 2012).

Additionally, the acquisition of multi-shell HARDI data can facilitate higher-order diffusion modelling techniques, such as diffusion kurtosis imaging (DKI) (Jensen et al. 2005). DKI expands on the traditional DTI model by capturing the degree of non-Gaussian diffusion, offering a more comprehensive characterisation of the diffusion profile within a voxel (Van Hecke, Emsell, and Sunaert 2016). DKI provides several analogous but complementary quantitative measures to DTI, which are based on the kurtosis tensor (see Table 3.1). Importantly, metrics derived from these higher-order models have increased accuracy, particularly in subcortical structures (Glenn et al. 2015), yielding clinically relevant information that cannot be obtained from the DTI model (Cheung et al. 2009; Van Hecke, Emsell, and Sunaert 2016). By incorporating DKI, researchers gain a deeper insight into the microstructural complexity and heterogeneity of tissue, providing a more nuanced analysis of white matter properties.

The study described in this chapter reports an analysis of longitudinal data, using higher-order dMRI techniques, aiming to investigate the development of limbic system white matter in children and adolescents with ADHD and controls at three time points between the ages of 9 to 14 years. To investigate more complex diffusion profiles, both gaussian (DTI) and non-gaussian (DKI) metrics were compared in children with ADHD and controls. Based on cross-sectional (Connaughton et al. 2022) and longitudinal (Fuelscher et al. 2023; Chiang et al. 2023) findings, the hypotheses are that individuals with ADHD will display 1) reduced microstructural organisation and 2) atypical development in limbic system white matter during the transition from childhood to mid-adolescence compared to controls. Exploratory analyses will investigate the relationship between microstructural organisation of limbic system white matter tracts and ADHD symptom severity in children and adolescents with ADHD.

5.2. Methods and Materials

5.2.1. Study Design and Participants

The clinical assessment and diagnosis grouping procedures used in this study was previously described in Section 2.2.1. Briefly, this longitudinal analysis consisted of 169 children (72 children with ADHD and 97 controls) recruited as part of the Neuroimaging of the Children's Attention Project (NICAP) (Sciberras et al. 2013; Silk, Genc, et al. 2016). Children between the ages of 6 and 8 years were initially recruited from 43 socioeconomically diverse primary schools across Melbourne, Australia. Multimodal MRI scanning occurred at three time points (wave 1, mean = 10.39, SD = 0.46; wave 2, mean = 11.69, SD = 0.54; wave 3, mean = 13.19, SD = 0.62). This thesis focused on individuals with persistent ADHD diagnosis across the study time points. As such, the participants included in the ADHD group received a confirmed clinical ADHD diagnosis based on a clinically administered National Institute of Mental Health Diagnostic Interview Schedule for Children (DISC-IV) (Shaffer et al. 2000) at each assessment (recruitment [3 years prior to imaging], wave 1 and wave 3 imaging time points). Participants in the control group did not meet the diagnostic criteria for ADHD at any study time point.

5.2.2. Diffusion MRI Data Acquisition

As described in Section 2.2.2, multimodal MRI images were collected from a single site at the Murdoch Children's Research Institute at the Royal Children's Hospital, Melbourne, on a 3-Tesla Siemens scanner using a 32-channel head coil. dMRI data were collected using a multi-band accelerated EPI sequence protocol (CMRR, University of Minnesota) (Moeller et al. 2010), which allows for accelerated dMRI multi-shell acquisition. Multi-shell high angular resolution diffusion imaging (HARDI) data were acquired using the following protocol: 2800 s/mm^2, (60 directions, four interleaved b = 0 volumes), 2000 s/mm^2 (45 directions, 6 interleaved b = 0 volumes), and 1000 s/mm^2 (25 directions, 6 interleaved b = 0 volumes) with an anterior-posterior phase encoding direction. See Table 5.2 for description of the NICAP dMRI image acquisition protocol.

Table 5.2 Description of diffusion imaging protocol used in the NICAP study.

Parameter	Shell 1	Shell 2	Shell 3	Comment
Flip angle	90°	90°	90°	The flip angle is the degree to which the radiofrequency (RF) pulse flips the magnetization vector off the direction of the main MRI magnetic field (Currie et al. 2013). In diffusion MRI, the flip angle is typically set to 90°, to minimize the impact of T2 decay, allowing for a more accurate measurement of diffusion properties (Van Hecke, Emsell, and Sunaert 2016).
Repetition Time (TR)	3200ms	3200ms	3200ms	The TR is the time interval between successive RF pulses. A longer TR value can lead to decreased signal-to-noise ratio and reduced diffusion reconstruction accuracy (Currie et al. 2013). In dMRI the typical TR is >3ms to allow for full signal recovery (Van Hecke, Emsell, and Sunaert 2016).
Echo Time (TE)	110ms	110ms	110ms	Echo time refers to the time interval between the RF pulse and the maximum amplitude of the MRI signal (Plewes and Kucharczyk 2012). In dMRI the typical range of TE is 60-110ms (Van Hecke, Emsell, and Sunaert 2016).

Matrix size (mm^3)	110x110	110x110	110x110	The matrix size determines the spatial resolution of the reconstructed image. A larger matrix size provides increased spatial resolution but also lengthens the duration of the scan. In dMRI, the typical range of matrix size is 96-192 (mm^3) but this can vary depending on study requirements (Van Hecke, Emsell, and Sunaert 2016).
Voxel size (mm^3)	2.4	2.4	2.4	The voxel size is the cubic volume size of each voxel in the reconstructed image. It is linked to the matrix size and defines the spatial resolution of the reconstructed image. Smaller voxel size provides higher spatial resolution but also increases the computational expense and scan time. In dMRI, a voxel size of 1-6mm is typically used (Van Hecke, Emsell, and Sunaert 2016).
Phase-encoding direction	A/P	A/P	A/P	The phase encoding direction refers to the direction in which the phase of MR signal encodes spatial information in the reconstructed image. It is essential that the phase encoding direction is on the same plane for all scans of the study. If not, the diffusion metrics may be affected (Van Hecke, Emsell, and Sunaert 2016).
Slice thickness	3mm	3mm	3mm	The slice thickness refers to the thickness of each slice in the reconstructed image, lower slice thickness provides increased spatial resolution. In dMRI acquisition parameters, a range of 1-6mm is typically used (Van Hecke, Emsell, and Sunaert 2016).
Slice gap	0mm	0mm	0mm	The slice gap refers to the distance between two adjacent image slices. A slice thickness of 0mm avoids gaps and enables better fiber tracking for dMRI analysis (Van Hecke, Emsell, and Sunaert 2016).
b-value (s/mm^2)	2800	2000	1000	>2500 required for HARDI (Van Hecke, Emsell, and Sunaert 2016).

# of diffusion direction	60	45	25	Typically >40 used in HARDI (Van Hecke, Emsell, and Sunaert 2016).
# of non-diffusion	4	6	6	About 1 per 6 diffusion images (Van Hecke, Emsell, and Sunaert 2016).
Acquisition time	3.5-4m	3-3.5m	2-2.5m	These are approximations, acquisition times may vary.

Table 3.2: A/P = Anterior/Posterior, ms = millisecond, mm = millimeters, s/mm^2 = seconds per millimeter squared, # = number, m = minute.

5.2.3. Diffusion MRI Data Processing

Diffusion images were processed using ExploreDTI software (Leemans et al. 2009). A comprehensive breakdown of the dMRI processing procedures used in this study is presented in the step-by-step guide outlined in the Chapter 3. Briefly the pre-processing steps included signal drift, Gibbs ringing, echo-planar imaging (EPI) distortion and subject motion correction. To reduce the effects of EPI distortion and subject motion, each diffusion MRI scan was coregistered to a subject-specific structural MRI T1 *nu_orig* image (a volume with a normalised intensity, obtained by correcting for non-uniformity in the org.mgz volume). As recommended by Leemans and Jones (2009), b-matrices were rotated while correcting for subject motion/EPI distortion (Leemans and Jones 2009). This ensures that the diffusion gradients remain accurately aligned with the brain's anatomy to improve the integrity of the diffusion metrics (Wheeler-Kingshott and Cercignani 2009). Robust tensor estimation through the REKINDLE method was selected for its efficacy in removing outliers and maximizing tensor accuracy (Chang, Jones, and Pierpaoli 2005). Robust tensor estimations have been shown to significantly improve fibre reconstruction quality as is particularly beneficial in white matter fibres vulnerable to CSF contamination, such as the fornix, as evidenced in prior studies (Plaisier et al. 2014).

Quality control of both raw and processed dMRI scans was conducted in line with diffusion MRI quality control guidelines (Tax, Vos, and Leemans 2016). The visual inspection focused on identifying and correcting specific diffusion artifacts, including eddy currents, Gibbs ringing, chemical shifts, Nyquist ghosting, pulsations, interslice instabilities, and signal dropouts. In evaluating raw dMRI images, a 4-point Likert scale

was utilized. A score of '1' was assigned to images free of visible artifacts, representing optimal quality. Images with a score of '2' exhibited minor artifacts, such as slight motion blur or minimal eddy current distortions, while a score of '3' was given to images with moderate artifacts, including more pronounced motion blur or eddy current distortions. Images severely compromised by artifacts, indicated by a score of '4', were characterised by excessive motion blur or significant susceptibility-induced geometric distortions. Any images that received a score of 3 or greater were excluded from the study. For the post-processed images, a 3-point Likert scale was employed to assess the effectiveness of artifact corrections and the accuracy of diffusion profiles. Images with near-perfect reconstructions were scored as '1', those with minor issues confined to small brain areas received a '2', and scans with poor reconstruction, evidenced by extensive or distorted areas, were scored '3' and excluded from the study. The study's methodology encompassed standardised viewing conditions, ensuring consistent lighting and display settings for image review. An experience neuroscientist, skilled in identifying and rating MRI artifacts, conducted the inspections. A sequential analysis approach was adopted; each raw image was initially reviewed for quality, followed by the assessment of processed images, guaranteeing an unbiased evaluation.

Following this thorough visual inspection, 360 scans were found suitable for analysis, with 15 scans excluded due to incomplete MRI image sets (missing b-value images) and 5 scans excluded due to quality concerns—2 during pre-processing and 3 post-processing. No manual edits were made to the data of the remaining scans.

5.2.4. Tractography Approach

This chapter used deterministic Constrained Spherical Deconvolution (CSD) tractography to reconstruct whole brain tractography. The CSD approach was applied to the data using the concatenated multi-shell HARDI images (b = 1000, 2000, 2800 s/mm^2) using the recursive calibration of the response function (Tax et al. 2014). Whole-brain fibre deterministic tractography was performed using the following settings: seed points resolution 2x2x2 mm^3, step size 1 mm, angle threshold 60°, fibre length range, 10 – 500 mm. Detailed descriptions of each of these settings is provided in the step-by-step guide in Section 7.4.

A multiple region of interest (ROI) approach was used to ensure reliable and consistent extraction of the limbic system tracts across all participants. This approach has

previously been demonstrated to effectively isolate the major tracts in the human brain (Mori and van Zijl 2002; Wakana et al. 2007). To ensure the accuracy of the ROI gates, all tracts of interest were extracted using a subject-specific anatomic scan and colour-coded first eigenvector-fractional anisotropy (FEFA) dMRI images. Details of tract extraction protocols are provided below.

5.2.5. White matter tract extraction protocol

Cingulum Bundles

The cingulum bundle is a prominent white matter tract interconnecting frontal, parietal, and medial temporal regions, as well as linking subcortical nuclei to the cingulate gyrus (Vanderah and Gould 2016). The cingulum bundle is a key limbic system white matter tract, interconnecting the amygdala, hippocampus, cingulate gyrus as well as other regions (Catani, Dell'acqua, and Thiebaut de Schotten 2013). The 'standard cingulum' was reconstructed bilaterally using the protocol outlined by Jones and colleagues (Jones et al. 2013). To locate the rostral-caudal midpoint of the body of the corpus callosum, the midpoint between the posterior part of the curve of the genu (i.e., its most posterior part at flexion and the front of the splenium (i.e., its most anterior part at flexure) was identified. Two "AND" ROI – the term "AND" indicates that fibres must pass through this ROI – drawn five sections anterior and posterior of the identified rostral-caudal midpoint of the body of the corpus callosum. These two "AND" ROIs were separated by approximately 18mm in the anterior-posterior plane. All streamlines that passed through both "AND" ROIs were retained as 'cingulum bundle' pathways. Additional, "NOT" ROIs – the term "NOT" indicates that any fibres passing through this ROI are excluded – were used to exclude tracts that were inconsistent with known projections of the cingulum bundle. This procedure was repeated to extract the cingulum bundles in both hemispheres. A complete reconstruction of the bilateral cingulum bundles is provided in Figure 5.1.

Figure 5.1 Reconstructed cingulum bundles in a single subject with ADHD using CSD-based tractography.

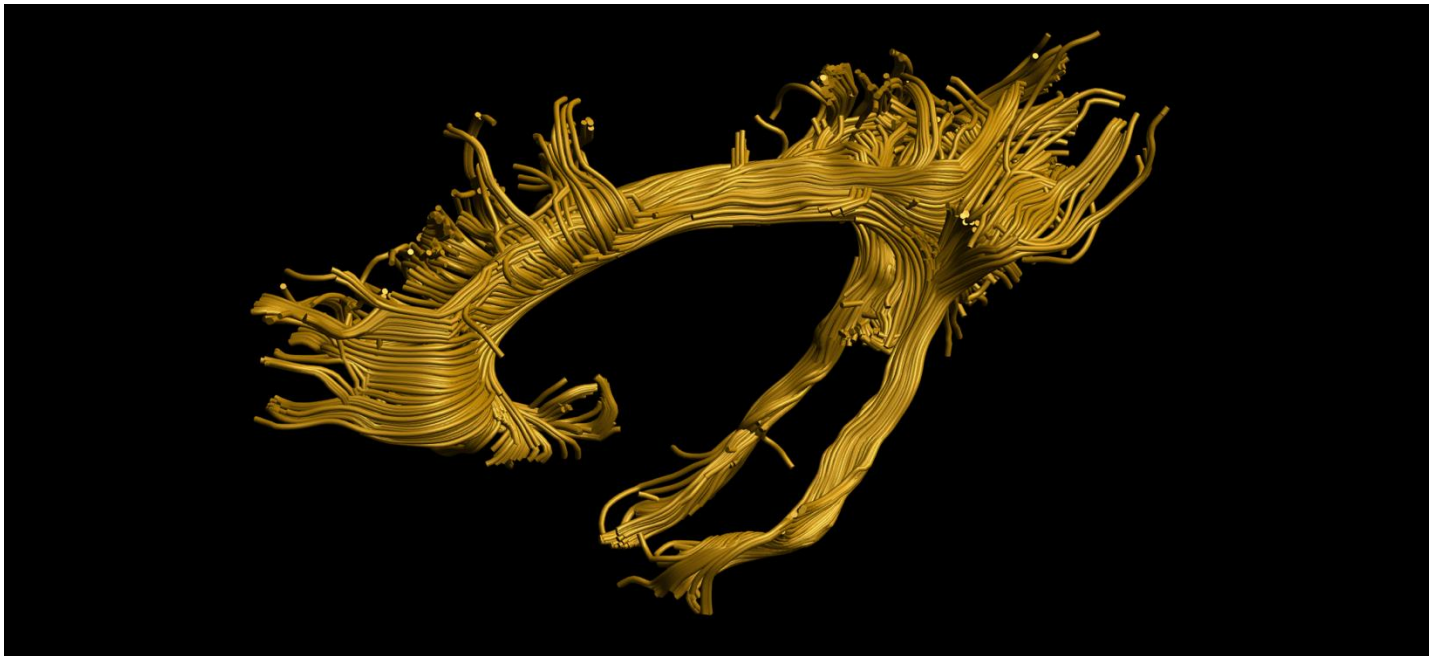

Figure 5.1: The figure shows the reconstructed cingulum bundles of a single subject in the ADHD group from this study. The cingulum bundles are highlighted in gold.

Fornix

The fornix is a key limbic system white matter bundle that interconnects the medial temporal lobe to the mammillary bodies and hypothalamus (Catani and Thiebaut de Schotten 2008; Ross 2008; Mori et al. 2000). The ROIs were manually drawn for each individual subject using landmark techniques that have been shown to be highly reproducible (Metzler-Baddeley et al. 2011). A seed ROI – a term "SEED" indicates that fibres either originated or terminated in the ROI – was placed where the anterior pillars enter the fornix body (coronal plane). Using the mid-sagittal plane as a guide, an "AND" ROI was drawn in the axial plane encompassing both the crus fornici at the lower part of the splenium of the corpus callosum. Finally, two "NOT" ROIs were drawn, 1) rostral to the anterior fornix pillars and caudal to the crus fornici (coronal slice), 2) through the corpus callosum and the upper pons (axial slice) to exclude streamlines from the corpus callosum and corticospinal tract. Once all ROIs were placed the fornix was reconstructed. This procedure was repeated to extract the fornix in both hemispheres. Figure 5.2 displays a complete reconstruction of the bilateral fornix.

Figure 5.2 Reconstructed bilateral fornix in a single subject with ADHD using CSD-based tractography.

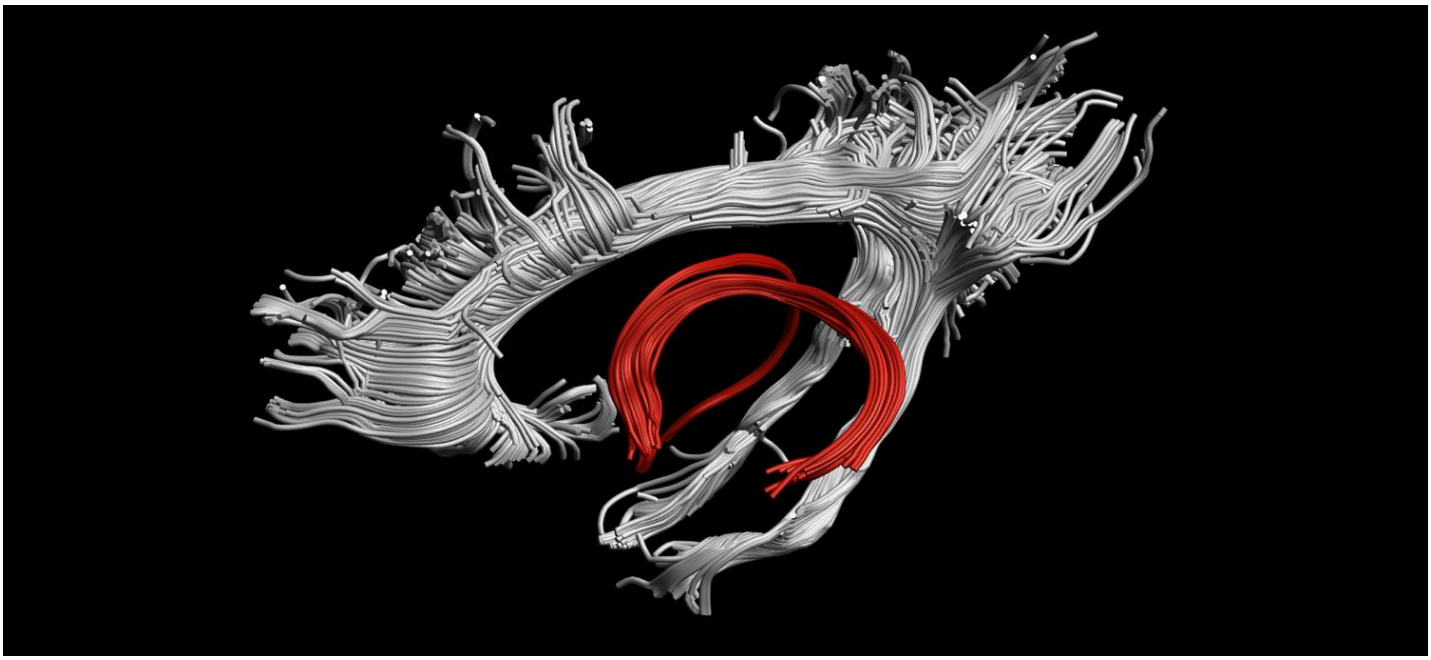

Figure 5.2: The figure shows the reconstructed bilateral fornix (red) of a single subject in the ADHD group from this study.

Mammillothalamic Tracts

The mammillothalamic tracts run inferior-superior from the mammillary bodies to the anterior thalamic nuclei and are the major connections of the anterior thalamic nuclei with the hypothalamic nuclei (Haines 2008). The multiple ROI approach to extracting the mammillothalamic tracts was described by Kamali and colleagues (2018) (Kamali et al. 2018). Using a subject-specific FEFA diffusion image the first "AND" ROI was drawn to encompass the fibres coursing through the mammillary bodies (axial plane). The second "AND" ROI was placed to contain the streamlines projecting from the medial aspect of the anterior thalamic nuclei. The addition of a second "ROI" excluded possible contamination from the stria terminalis and fornix. This procedure was repeated to extract the mammillothalamic projections in both hemispheres. An example of a reconstructed bilateral mammillothalamic projections is provided in Figure 5.3.

Figure 5.3 Reconstructed mammillothalamic tracts in a single subject with ADHD using CSD-based tractography.

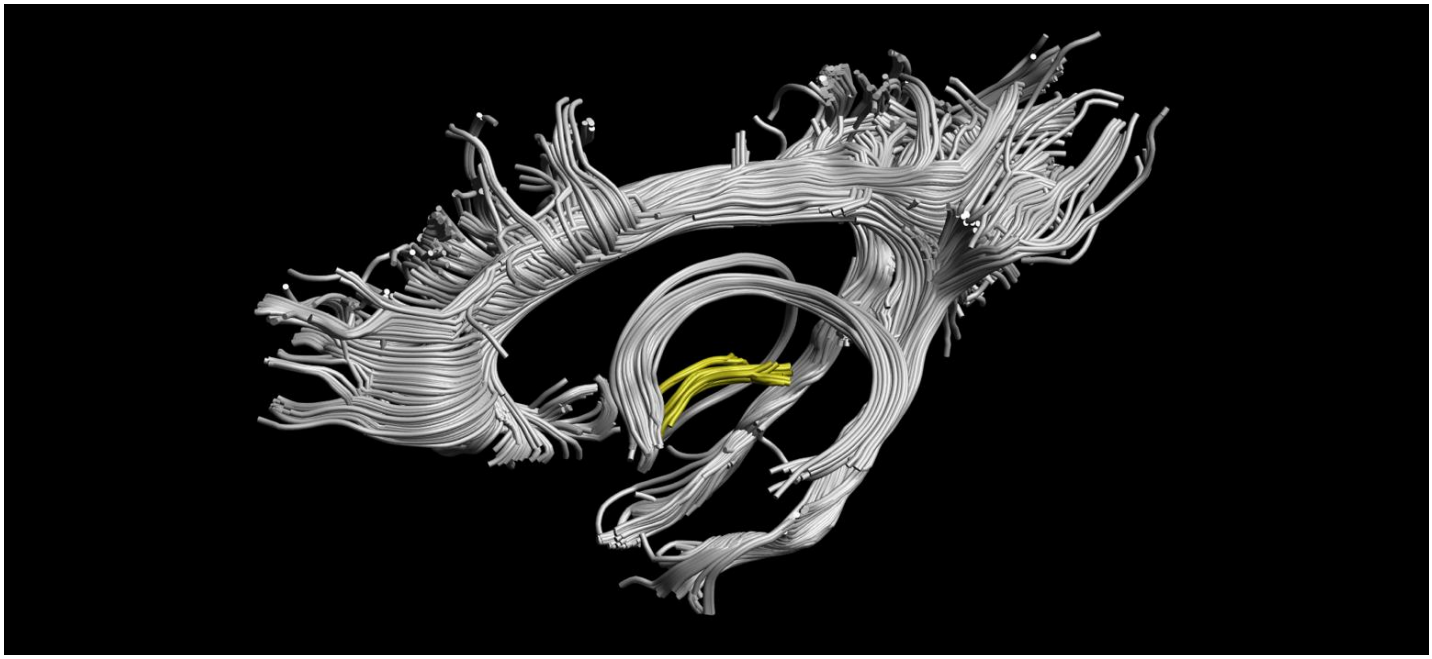

Figure 5.3: The figure shows the reconstructed mammillothalamic tracts of a single subject in the ADHD group from this study. The mammillothalamic tracts are highlighted in yellow.

Anterior Thalamic Projections

The anterior thalamic nuclei receives incoming fibres from the mammillothalamic tract and fornix and send outgoing projections via the anterior thalamic pathways to the orbitofrontal and anterior cingulate cortex (Catani, Dell'acqua, and Thiebaut de Schotten 2013). These anterior thalamic projections traverse through the anterior limb of the internal capsule, which is a dense bundle of white matter fibres that connects the thalamus to the cerebral cortex (Catani, Dell'acqua, and Thiebaut de Schotten 2013). A multiple ROI approach was used to extract the anterior thalamic projections (Niida et al. 2018; Wakana et al. 2007; Wakana et al. 2004). The first "AND" ROI was drawn that defines the anterior limb of the internal capsule (coronal plane), The second "AND" ROI was drawn and the entire thalamus was delineated (coronal slice). A "NOT" ROI passing through the midbrain, the corticospinal tract and the corticopontine tract (axial slice) were set to remove anatomically implausible fibres. This procedure was repeated to extract the anterior thalamic projections in both hemispheres. Figure 5.4 shows reconstructed bilateral anterior thalamic projections.

Figure 5.4 Reconstructed anterior thalamic projections in a single subject with ADHD using CSD-based tractography.

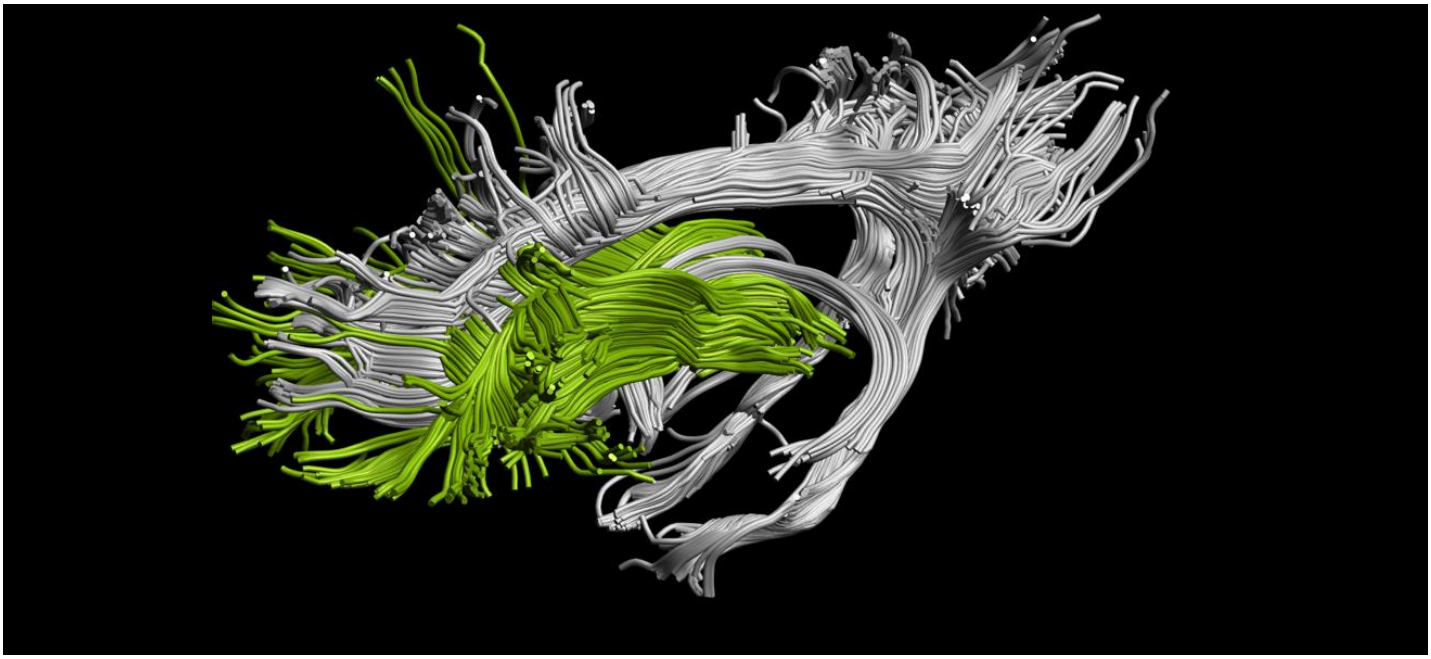

Figure 5.4: The figure shows the reconstructed anterior thalamic projections of a single subject in the ADHD group from this study. The anterior thalamic projections are highlighted in green.

Uncinate Fasciculus

The uncinate fasciculus interconnects the anterior region of the temporal lobe with the orbital and polar frontal cortex. The white matter fibres of the uncinate fasciculus originate from the temporal pole, uncus, parahippocampal gyrus, and amygdala. Projecting in a U-shaped turn, the fibres enter the floor of the external capsule (Vanderah and Gould 2016; Catani, Dell'acqua, and Thiebaut de Schotten 2013; Catani et al. 2002). Two "AND" ROIs were placed as follows: (1) at the hippocampus-amygdala region, which was drawn in the temporal lobe at the junction with the anterior part of the temporal stem (axial slice), and (2) at the anterior cingulate area was drawn in the medial frontal lobe (coronal slice) (Hernando et al. 2015; Kier et al. 2004). The two "AND" ROIs were drawn to cover a generous area to capture all possible streamlines that pass through both ROIs. This procedure was repeated to extract the uncinate fasciculi in both hemispheres. A complete reconstruction of the bilateral uncinate fasciculus is displayed in Figure 5.5.

Figure 5.5 Reconstructed uncinate fasciculi in a single subject with ADHD using CSD-based tractography.

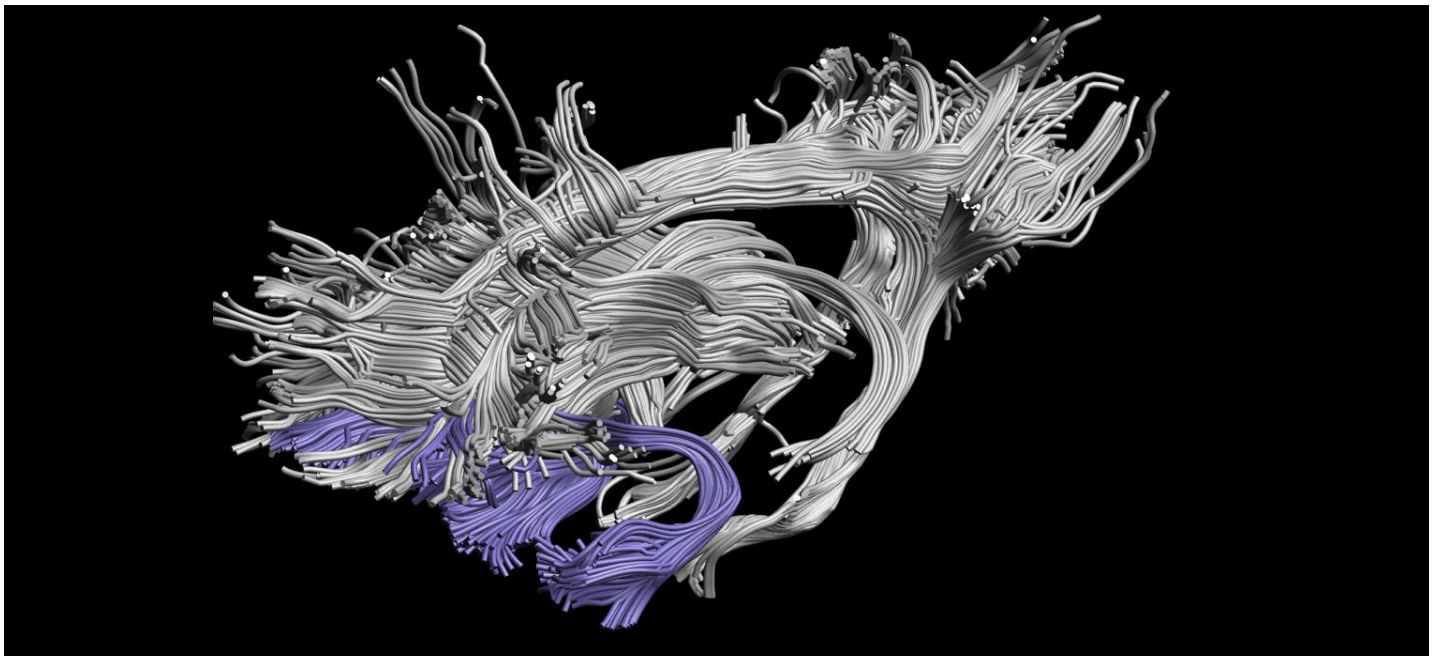

Figure 5.5: The figure shows the reconstructed uncinate fasciculi of a single subject in the ADHD group from this study. The uncinate fasciculi are highlighted in purple.

5.2.6. Behavioural Measures: Conner's 3 ADHD index (CAI) and the Affective Reactivity Index (ARI)

Conner's 3 ADHD index (CAI): As described in Section 3.2.5.

Affective reactivity index (ARI): As explained in previously in Section 3.2.5.

5.2.7. Statistical Analyses

Prior to statistical analyses, all data points underwent Winsorization procedures (Reifman and Garrett 2010; Blaine 2018) (i.e. any data points with a z-score exceeding ±3 were adjusted to ±3 standard deviations from the mean) to minimize the effects of extreme outliers. Full details of LMM procedures used in the study described in this chapter were previously presented in Section 3.2.6. Briefly, a top-down LMM model selection procedure was used to examine the between-group differences in microstructural organization of limbic system white matter tracts. The details of the LMM models tested in this study are presented in Table 5.3. Exploratory statistical analyses were conducted to

examine the relationship between microstructural organization of limbic system white matter tracts and behavioural measures (CAI and ARI) in children and adolescents with ADHD (model FX3b in Table 5.3). To mitigate the issues of multiple comparisons, a two-stage FDR correction was applied using the MuToss package (Team et al. 2017) in R (v.4.1.1). As described in Section 3.2.6., sensitivity analyses were conducted to evaluate the potential influence of confounding factors, such as case-control sex imbalance, ADHD medication status, comorbidity status, and head motion on the primary statistical analyses. To investigate the impact of head motion, a sensitivity analysis was conducted, incorporating mean frame-wise displacement as a covariate in the primary analsis optimal models.

Table 5.3 Tested models: limbic system white matter tracts in ADHD and controls.

Random Effects Models
RX 1a
ROI ~ age at baseline + sex + diagnosis*age + (1 + age |subject)
RX 1b
ROI ~ age at baseline + sex + diagnosis* age + (1|subject)
Fixed Effects Models
Null 0a
ROI ~ age + age at baseline + sex + (1 + age | subject)
Null 0b
ROI ~ age + age at baseline + sex + (1|subject)
FX 1a
ROI ~ sex + age + age at baseline + diagnosis + (1 + age |subject)
FX 1b
ROI ~ sex + age + age at baseline + diagnosis + (1|subject)
FX 2a
ROI ~ sex + age + age at baseline + diagnosis* age + (1 + age |subject)
FX 2b
ROI ~ sex + age + age at baseline + diagnosis* age + (1|subject)

FX 3b

ROI ~ ICV + sex + age* ADHD symptom + (1|subject)

Table 5.3: RX = random effects, FX = fixed effects, ROI = regions of interest, age = participant age from baseline (in months). To increase interpretability age was mean-centred at baseline.

5.3. Results

5.3.1. Demographics and Clinical Characteristics of Study Population

Full details of the demographic and clinical characteristics of this chapter's study population are provided in Table 5.4. No significant between-group difference was found in age, handedness, socioeconomic status, or matrix reasoning across all three study time points. Clinically, children with ADHD had significantly higher levels of ADHD symptom severity compared to controls. Children with ADHD were also more likely to present with externalising and internalising disorders than controls.

Table 5.4 Demographics and clinical variables.

		Mean (SD)		*p-value*
		ADHD	***Control***	
Time point 1	**Demographic factors**			
	Scans after QC	59	74	
	Age – years	10.40 (0.49)	10.37 (0.49)	0.789
	Female sex n (%)	14 (23.72%)	30 (40.54%)	0.062
	Left-handed n (%)	9 (15.25%)	11 (14.86%)	0.950
	Matrix reasoning raw	21.68 (5.55)	21.74 (4.64)	0.841
	SES	1016.3 (41.22)	1020 (43.39)	0.654
	Clinical factors			
	Connor's Index	10.98 (6.52)	2.44 (4.29))	<0.001
	Hyperactivity symptoms	4.76 (2.75)	1.08 (1.61)	<0.001
	Inattentive symptoms	7.06 (2.18)	1.70 (2.20)	<0.001
	Medication use (%)	18 (30.50%)	4 (5.40%)	<0.001

	Extern. Disorder n (%)	29 (49.15%)	15 (20.27)	<0.001
	Intern. Disorder (%)	16 (27.12%)	9 (12.16%)	0.028
Time point 2	**Demographic factors**			
	Scans after QC	55	76	
	Age – years	11.69 (0.52)	11.68 (0.56)	0.925
	Female sex n (%)	13 (23.63%)	32 (42.10%)	0.044
	Left-handed n (%)	6 (10.90%)	10 (13.15%)	0.698
	Matrix reasoning raw	24.43 (4.60)	24.36 (4.71)	0.940
	SES	1017 (40.12)	1016 (47.27)	0.892
	Clinical factors			
	Connor's Index	10.49 (6.81)	2.42 (3.80)	<0.001
	Medication use (%)	17 (30.90%)	4 (5.47%)	<0.001
Time point 3	**Demographic factors**			
	Scans after QC	40	56	
	Age – years	13.28 (0.62)	13.13 (0.59)	0.242
	Female sex n (%)	9 (22.5%)	24 (42.85%)	0.063
	Left-handed n (%)	6 (15%)	6 (10.51%)	0.531
	Matrix reasoning raw	25.98 (4.47)	25.6 (4.24)	0.614
	SES	1020.6 (39.25)	1015 (50.86)	0.649
	Clinical factors			
	Connor's Index	9.09 (6.69)	1.63 (3.91)	<0.001
	Medication use (%)	9 (22.5%)	1 (1.78)	0.004
	Extern. Disorder n (%)	8 (20%)	4 (7.14%)	0.147
	Intern. Disorder (%)	10 (25%)	2 (3.57%)	0.006

Table 3.4: *p* = p-value, SD = standard deviation, SES = socio-economic status.

5.3.2. Limbic System White Matter Tracts in Children and Adolescents with ADHD and Controls

Model Selection Procedure

Full details of the model selection fit statistics are provided in the appendices (Tables 6-21 provided in volume 2). A total of twelve fixed effects of interest models (model containing diagnosis and/or diagnosis-by-age interaction) were significantly different compared to the null models. For all other models, there was no significant difference between the fixed effects of interest models and the null models, indicating the effects of white matter microstructure due to the fixed measures of interest. The selected optimal models from the top-down LMM model selection procedure are provided in Table 5.5.

Table 5.5 Results of LMM model selection: optimal models.

	FA	**AD**	**MD**	**RD**	**KA**	**AK**	**MK**	**RK**
Cingulum Bundle (Left)	FX1A	FX1A	FX1A	FX1A	FX1A*	FX1B	FX1B	FX1A
Cingulum Bundle (Right)	FX1B	FX1B	FX1B	FX1B	FX1A*	FX1B	FX1B	FX1A
Fornix (Left)	FX1B	FX1B*	FX1B	FX2B*	FX1B*	FX1B	FX1B	FX1B
Fornix (Right)	FX1B*	FX1B	FX1B*	FX1B	FX1B*	FX1B	FX1B	FX1B
Anterior Thalamic Projections (Left)	FX1A	FX1A	FX1A	FX1A	FX1A*	FX1B	FX1B	FX2B*
Anterior Thalamic Projections (Right)	FX1B	FX1B	FX1A	FX1B	FX2B	FX1B	FX1B	FX1A
Mammillothalamic tract (Left)	FX1B	FX1B	FX1B	FX1B	FX1B	FX1B	FX1B	FX1B

Mammillothalamic tract (Right)	FX1B	FX1B	FX1B	FX1B	FX1B	FX1B*	FX1B*	FX1B
Uncinate Fasciculus (Left)	FX1B	FX1A	FX1A*	FX1A	FX1B*	FX1B	FX1B	FX1B
Uncinate Fasciculus (Right)	FX1A*	FX1B	FX1B	FX1A	FX1B	FX1B	FX1B	FX1B

Table 3.5: * = Model was significantly different to the null models

Results of Optimal Models

There was a significant effect of the diagnostic group in kurtosis anisotropy (KA) of the bilateral cingulum bundle (Left, β = -0.36, 95% CI = -0.62 to -0.09; Right, β = -0.36, 95% CI = -0.62 to -0.11, (Figure 5.6)) and left Fornix (β = -0.32, 95% CI = -0.57 to -0.06, (Figure 5.7)), characterised by reduced KA in these white matter tracts across all three study time points compared to controls. There was a significant effect of the group-by-age interaction of RK in the left anterior thalamic projection (β = 0.25, 95% CI = 0.08 to 0.42, (Figure 5.8)), organization by increased change of RK in the ADHD group compared to controls across the three study time points. There was a significant effect of the diagnostic group in RD of the left Fornix (β = 0.31, 95% CI = 0.04 to 0.58), organization by increased RD in the ADHD group compared to controls (see Figure 5.9). All regions reported above survived two-stage FDR correction. There were no other significant between-group differences in the microstructural organisation of limbic system white matter in children with ADHD and controls. All other findings are presented in Table 5.6-5.15 and Figure 5.10-5.17.

5.3.3. ADHD Symptoms Severity and Limbic System White Matter in ADHD

The exploratory analyses found no significant effect of the interaction term ADHD symptom-by-age on limbic system white matter tract microstructural organisation in in the ADHD group across the study time points (CAI, Figure 5.18-5.25; Figure 5.26-5.33). Full details of these results are provided in Table 5.16-5.31 and Figure 5.18-5.33.

5.3.4. Sensitivity Analyses

The first sensitivity analysis, using the 100 random sex-matched LMM analyses, reported an expected slight reduction in p-value significance, given the increase in standard errors (SE) related to the reduction in sample size (Table 5.32). Importantly the beta values for the main effect of diagnosis were still within the SEs of the optimal models (Figure 5.34). Given the beta value and SEs, the sensitivity analysis demonstrated that the overall pattern of results in the primary analysis was most likely not confounded by a sex-ratio group imbalance in the study.

The second sensitivity analysis found there was no significant difference in white matter microstructural organization in the bilateral cingulum bundle, left fornix, and left anterior thalamic projection among medicated ADHD and non-medicated ADHD children (Tables 5.33-5.34).

The results of the third and fourth sensitivity analyses are presented in Table 5.35 and 5.36, importantly in the sensitivity analyses the beta values for the effect of diagnosis remained within the SEs of the optimal models (see Figure 5.35-5.36). Considering the beta value and SEs, this sensitivity analysis indicated that the main findings of the primary analysis were likely not confounded by the presence comorbidity or head motion. Overall, the sensitivity analyses demonstrated that the results of the primary analysis were most likely not biased by the sex ratio per group, medication status, comorbidity status or head motion.

Figure 5.6 Kurtosis anisotropy of the bilateral cingulum bundle across the three study time points.

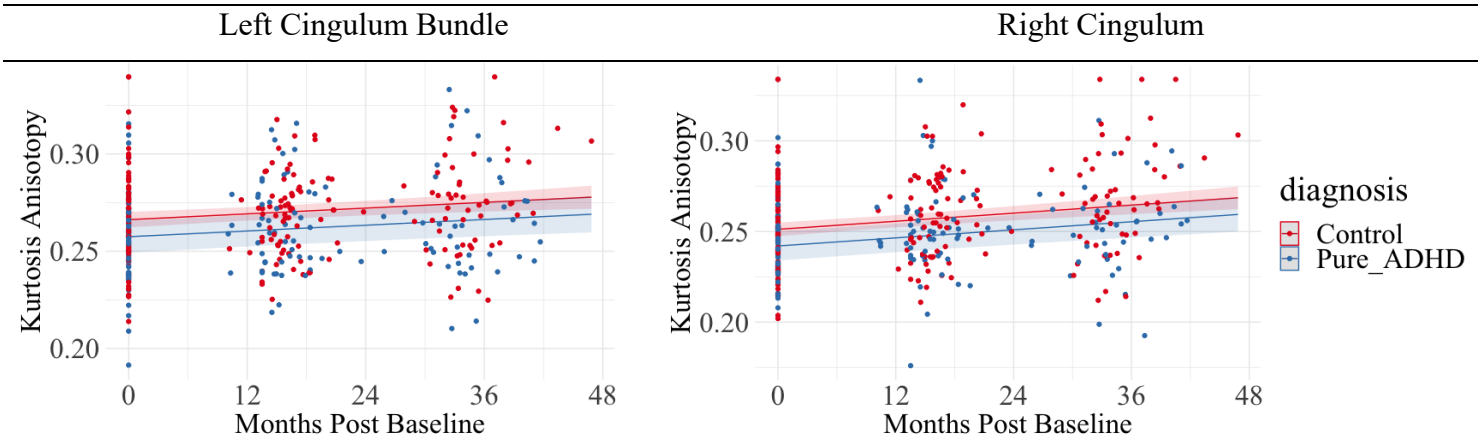

Figure 5.6: Bilateral cingulum bundle KA in the ADHD and control groups during the transition from childhood to mid-adolescence. A main effect of group interaction was observed in the bilateral cingulum; the ADHD group displayed reduced KA compared to the control group across all three study time points.

Figure 5.7 Kurtosis anisotropy of the left fornix across the three study time points.

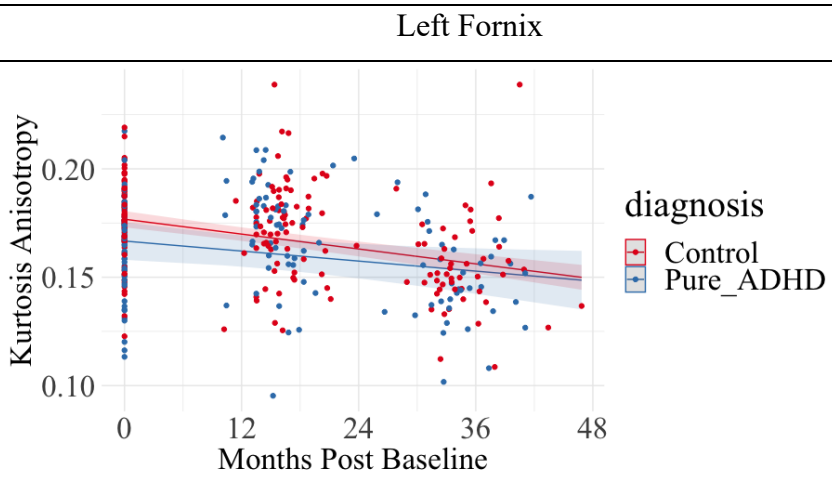

Figure 5.7: Left Fornix KA in the ADHD and control groups during the transition from childhood to mid-adolescence. A significant main effect of group was observed in the left Fornix; the ADHD group displayed reduced KA compared to the control group.

Figure 5.8 Radial Kurtosis of the left anterior thalamic projecton across the three study time points.

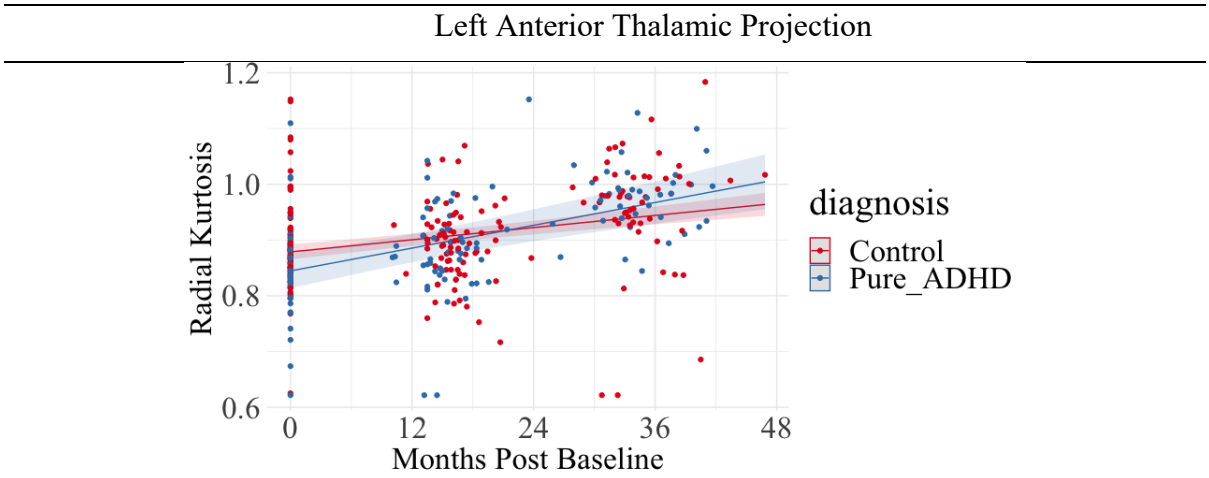

Figure 5.8: Left anterior thalamic projection RK in the ADHD and control groups during the transition from childhood to mid-adolescence. A group-by-age interaction was observed in the left anterior thalamic projection; the ADHD group displayed increased RK compared to the control group.

Figure 5.9 Radial diffusivity of the left fornix across the three study time points.

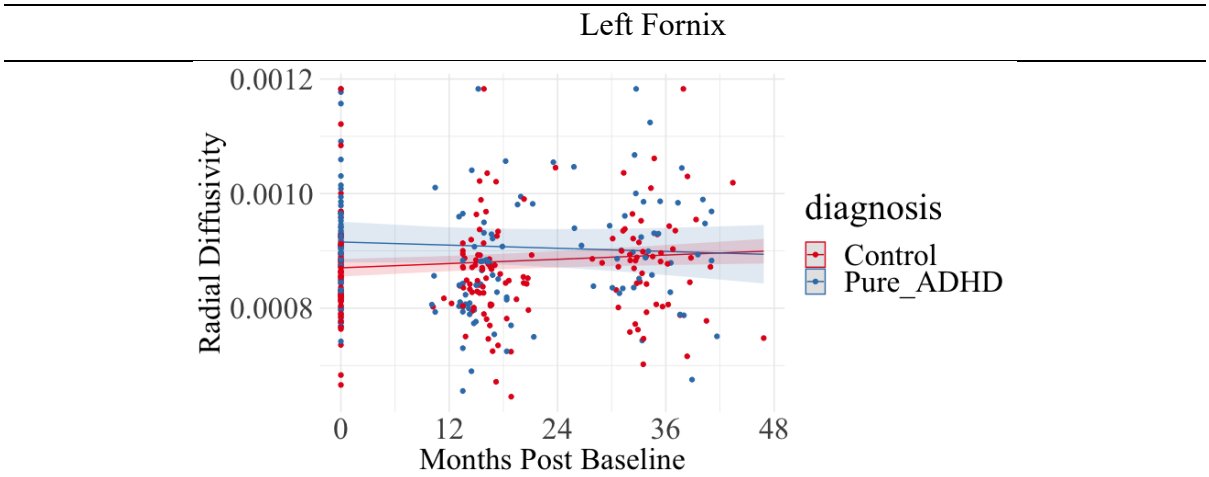

Figure 5.9: Left Fornix development in the ADHD and control groups during the transition from childhood to mid-adolescence. A group effect was observed in the left Fornix; the ADHD group displayed increased RD compared to the control group. No significant group-by-age interaction was observed.

Table 5.6 Results of optimal mixed-effects models (without interaction term) analyses: limbic system white matter KA in ADHD and controls.

	Sex		**Months from baseline**		**Age at baseline**		**Diagnosis**	
	B (SE)	***t, p***	***B (SE)***	***t, p***	***B (SE)***	***t, p***	***B (SE)***	***t, p***
Cingulum Bundle (Left)	-9.077e-04 (3.534e-03)	-0.257, 0.079	2.466e-04 (7.318e-05)	3.369 , <0.000	6.657e-03 (3.563e-03)	1.869, 0.063	-8.780e-03 (3.331e-03)	-2.635, 0.009*
Cingulum Bundle (Right)	3.054e-03 (3.483e-03)	0.877, 0.381	3.712e-04 (7.315e-05)	5.074 , <0.000	1.276e-02 (3.628e-03)	3.518 , <0.000	-9.178e-03 (3.299e-03)	-2.782, 0.006*
Fornix (Right)	-8.876e-04 (4.068e-03)	-0.218, 0.828	-1.960e-04 (7.911e-05)	-2.478, 0.014	9.841e-03 (4.117e-03)	2.390, 0.018	-4.772e-03 (3.860e-03)	-1.236 0.218
Anterior Thalamic Projections (Left)	8.212e-04 (2.619e-03)	0.314, 0.754	-1.703e-04 (5.980e-05)	-2.848, 0.005	1.927e-03 (2.642e-03)	0.729, 0.466	-5.481e-03 (2.479e-03)	-2.211, 0.028
Anterior Thalamic Projections (Right)	6.984e-04 (2.625e-03)	0.266, 0.790	1.843e-05 (5.245e-05)	0.351, 0.725	4.119e-03 (2.653e-03)	1.552, 0.122	-5.240e-03 (2.489e-03)	-2.105, 0.036
Mammillothalamic tract (Left)	-2.692e-04 (3.760e-03)	-0.072, 0.943	-7.215e-04 (1.215e-04)	-5.936, <0.000	5.136e-03 (3.866e-03)	1.329, 0.186	-5.419e-03 (3.598e-03)	-1.506, 0.134

Mammillothalamic tract (Right)	-5.522e-04 (4.232e-03)	-0.130, 0.896	-5.411e-04 (1.312e-04)	-4.124, <0.000	-2.286e-03 (4.341e-03)	-0.52, 0.599	5.953e-03 (4.041e-03)	1.473, 0.143
Uncinate Fasciculus (Left)	-1.934e-03 (3.080e-03)	-0.628, 0.530	2.293e-04 (6.918e-05)	-3.314, 0.001	6.074e-03 (3.110e-03)	1.953, 0.052	-2.538e-03 (2.922e-03)	-0.868, 0.386
Uncinate Fasciculus (Right)	1.426e-04 (3.299e-03)	0.043, 0.966	4.532e-06 (6.262e-05)	0.072, 0.942	4.192e-03 (3.315e-03)	1.265, 0.208	-1.251e-03 (3.137e-03)	-0.399, 0.691

Table 5.7 Results of optimal mixed-effects models (with interaction term) analyses: limbic system white matter tracts KA in ADHD and controls.

	Sex		**Months from baseline**		**Age at baseline**		**Diagnosis**		**Diagnosis * Months from baseline**	
	B (SE)	***t, p***	***B (SE)***	***t, p***	***B (SE)***	***t, p***	***B (SE)***	***t, p***	***B (SE)***	***t, p***
Fornix (left)	3.083e-03 (3.163e-03)	0.975, 0.331	-4.787e-04 (7.474e-05)	-6.405, <0.000	2.570e-03 (3.231e-03)	0.795, 0.042	-1.007e-02 (3.675e-03)	-2.740, 0.006*	1.870e-04 (1.496e-04)	1.250, 0.212

Table 5.8 Results of optimal mixed-effects models (without interaction term) analyses: limbic system white matter AK in ADHD and controls.

	Sex		**Months from baseline**		**Age at baseline**		**Diagnosis**	
	B (SE)	***t, p***	***B (SE)***	***t, p***	***B (SE)***	***t, p***	***B (SE)***	***t, p***
Cingulum Bundle (Left)	1.426e-03 (4.033e-03)	0.360, 0.719	1.967-03 (1.111e-04)	17.713 , <0.000	1.157e-02 (4.128e-03)	2.805, 0.005	-2.175e-03 (3.854e-03)	-0.565, 0.573
Cingulum Bundle (Right)	3.707e-04 (3.914e-03)	0.095, 0.924	2.119e-03 (1.110e-04)	19.100 , <0.000	8.917e-03 (4.008e-03)	2.225 , 0.027	-1.719e-03 (3.742e-03)	-0.459, 0.646
Fornix (Left)	5.890e-03 (5.022e-03)	1.173, 0.243	1.151e-03 (1.402e-04)	8.205, <0.000	1.986e-03 (5.165e-03)	0.385, 0.701	-2.708e-03 (4.769e-03)	-0.568 0.571
Fornix (Right)	5.373e-03 (9.350e-03)	0.575, 0.566	1.527e-03 (1.895e-04)	8.055, <0.000	1.360e-02 (9.472e-03)	1.436, 0.153	-6.686e-03 (8.881e-03)	-0.753 0.453
Anterior Thalamic Projections (Left)	8.689e-03 (3.837e-03)	2.265, 0.025	1.885e-03 (1.118e-04)	16.861, <0.000	8.626e-03 (3.923e-03)	2.198, 0.029	-1.771e-03 (3.662e-03)	-0.484, 0.629
Anterior Thalamic Projections (Right)	7.338e-03 (3.850e-03)	1.906, 0.058	2.131e-03 (1.172e-04)	18.181, <0.000	8.942e-03 (3.947e-03)	2.266, 0.024	-1.992e-03 (3.685e-03)	-0.540, 0.589

Mammillothalamic tract (Left)	1.852e-02 (7.815e-03)	2.369, 0.019	8.635e-04 (2.245e-04)	3.846, <0.000	6.913e-03 (7.993e-03)	0.865, 0.388	-5.954e-03 (7.467e-03)	-0.797, 0.426
Mammillothalamic tract (Right)	3.598e-04 (8.132e-03)	0.044, 0.964	7.370e-04 (2.505e-04)	2.94, 0.003	8.514e-03 (8.340e-03)	1.02, 0.308	1.865e-02 (7.765e-03)	2.40, 0.017
Uncinate Fasciculus (Left)	6.067e-03 (5.240e-03)	1.158, 0.249	1.582e-03 (1.317e-04)	12.014, <0.000	8.431e-03 (5.307e-03)	1.588, 0.114	-4.411e-03 (4.989e-03)	-0.884, 0.378
Uncinate Fasciculus (Right)	1.261e-02 (4.943e-03)	2.551, 0.011	2.119e-03 (1.424e-04)	14.877, <0.000	1.072e-02 (5.038e-03)	2.129, 0.035	-2.872e-03 (4.759e-03)	-0.603, 0.547

Table 5.9 Results of optimal mixed-effects models (without interaction term) analyses: limbic system white matter MK in ADHD and controls.

	Sex		**Months from baseline**		**Age at baseline**		**Diagnosis**	
	B (SE)	***t, p***	***B (SE)***	***t, p***	***B (SE)***	***t, p***	***B (SE)***	***t, p***
Cingulum Bundle (Left)	1.012e-02 (6.879e-03)	1.471, 0.143	2.559e-03 (1.635e-04)	15.653 , <0.000	1.846e-02 (7.083e-03)	2.607, 0.009	-1.078e-02 (6.558e-03)	-1.643, 0.102
Cingulum Bundle (Right)	9.482e-03 (6.822e-03)	1.390, 0.166	2.674e-03 (1.623e-04)	16.477 , <0.000	1.912e-02 (7.001e-03)	2.730 , 0.007	-1.025e-02 (6.498e-03)	-1.578, 0.116
Fornix (Left)	1.030e-03 (7.506e-03)	0.137, 0.891	1.304e-03 (1.865e-04)	6.994, <0.000	9.730e-03 (7.699e-03)	1.264, 0.208	-3.048e-03 (7.115e-03)	-0.428 0.669
Fornix (Right)	4.143e-03 (1.179e-02)	0.351, 0.726	1.587e-03 (2.353e-04)	6.743, <0.000	1.873e-02 (1.194e-02)	1.569, 0.119	-9.060e-03 (1.119e-02)	-0.809 0.419
Anterior Thalamic Projections (Left)	9.215e-03 (6.415e-03)	1.437, 0.153	2.028e-03 (1.546e-04)	13.123, <0.000	5.192e-03 (6.587e-03)	0.788, 0.432	-9.493e-03 (6.104e-03)	-1.555, 0.122
Anterior Thalamic Projections (Right)	6.471e-03 (6.847e-03)	0.945, 0.346	2.293e-03 (1.635e-04)	14.028, <0.000	1.209e-02 (7.036e-03)	1.719, 0.087	-1.146e-02 (6.524e-03)	-1.756, 0.081

Mammillothalamic tract (Left)	8.107e-03 (8.345e-03)	0.972, 0.333	1.154e-03 (2.271e-04)	5.082, <0.000	1.056e-02 (8.532e-03)	1.237, 0.218	-1.892e-03 (7.966e-03)	-0.238, 0.813
Mammillothalamic tract (Right)	-5.694e-03 (8.876e-03)	-0.641, 0.522	7.064e-04 (2.557e-04)	2.76, 0.006	9.534e-03 (9.078e-03)	1.05, 0.295	2.156e-02 (8.465e-03)	2.54, 0.011
Uncinate Fasciculus (Left)	4.347e-03 (9.027e-03)	0.482, 0.631	1.463e-03 (2.065e-04)	7.086, <0.000	1.488e-02 (9.257e-03)	1.608, 0.110	-8.326e-03 (8.589e-03)	-0.969, 0.334
Uncinate Fasciculus (Right)	1.624e-02 (7.921e-03)	2.050, 0.042	1.973e-03 (2.049e-04)	9.628, <0.000	9.146e-03 (8.111e-03)	1.128, 0.261	-5.167e-03 (7.589e-03)	-0.681, 0.497

Table 5.10 Results of optimal mixed-effects models (without interaction term) analyses: limbic system white matter RK in ADHD and controls.

	Sex		**Months from baseline**		**Age at baseline**		**Diagnosis**	
	B (SE)	***t, p***	***B (SE)***	***t, p***	***B (SE)***	***t, p***	***B (SE)***	***t, p***
Cingulum Bundle (Left)	1.259e-02 (1.290e-02)	0.975, 0.331	3.029e-03 (3.739e-04)	8.102 , <0.000	1.934e-02 (1.308e-02)	1.478,, 0.141	-9.889e-03 (1.227e-02)	-0.806, 0.421
Cingulum Bundle (Right)	2.150e-02 (1.329e-02)	1.617, 0.107	2.710e-03 (3.472e-04)	7.804 , <0.000	3.296e-02 (1.346e-02)	2.449, 0.015	-1.767e-02 (1.263e-02)	-1.400, 0.163
Fornix (Left)	1.470e-0 (1.472e-02)	0.100, 0.921	1.487e-03 (3.194e-04)	4.655,, <0.000	6.010e-03 (1.531e-02)	0.392, 0.695	1.468e-04 (1.397e-02)	0.011 0.992
Fornix (Right)	7.868e-03 (1.574e-02)	0.500, 0.618	1.437e-03 (3.268e-04)	4.397, <0.000	1.304e-02 (1.594e-02)	0.818, 0.415	-1.004e-02 (1.495e-02)	-0.672 0.503
Anterior Thalamic Projections (Right)	5.102e-04 (1.198e-02)	0.043, 0.966	2.485e-03 (3.143e-04)	7.906, <0.000	2.370e-02 (1.211e-02)	1.957, 0.052	-1.682e-02 (1.138e-02)	-1.478, 0.141
Mammillothalamic tract (Left)	4.431e-04 (1.056e-02)	0.042, 0.967	2.105e-03 (2.964e-04)	7.100, <0.000	1.652e-02 (1.081e-02)	1.528, 0.128	-3.329e-03 (1.009e-02)	-0.330, 0.742

Mammillothalamic tract (Right)	-6.837e-03 (1.113e-02)	-0.600, 0.549	1.082e-03 (3.040e-04)	3.560, <0.000	5.180e-03 (1.162e-02)	0.446, 0.656	1.615e-02 (1.085e-02)	1.488, 0.138
Uncinate Fasciculus (Left)	4.820e-03 (1.541e-02)	0.313, 0.755	1.860e-03 (3.717e-04)	5.004, <0.000	2.361e-02 (1.558e-02)	1.515, 0.132	-1.021e-02 (1.463e-02)	-0.698, 0.486
Uncinate Fasciculus (Right)	2.205e-02 (1.458e-02)	1.512, 0.133	1.943e-03 (3.603e-04)	5.393, <0.000	1.105e-02 (1.474e-02)	0.750, 0.455	-5.551e-03 (1.395e-02)	-0.398, 0.691

Table 5.11 Results of mixed-effects models (with interaction term) analyses: limbic system white matter tracts RK in ADHD and controls.

	Sex		**Months from baseline**		**Age at baseline**		**Diagnosis**		**Diagnosis * Months from baseline**	
	B (SE)	***t, p***	***B (SE)***	***t, p***	***B (SE)***	***t, p***	***B (SE)***	***t, p***	***B (SE)***	***t, p***
Anterior Thalamic Projections (Left)	3.282e-03 (1.120e-02)	0.293, 0.769	2.614e-03 (2.709e-04)	9.647, <0.000	5.270e-03 (1.135e-02)	0.464, 0.642	-3.406e-02 (1.306e-02)	-2.608, 0.009	1.591e-03 (5.427e-04)	2.93, 0.003*

Table 5.12 Results of optimal mixed-effects models (without interaction term) analyses: limbic system white matter FA in ADHD and controls.

	Sex		**Months from baseline**		**Age at baseline**		**Diagnosis**	
	B (SE)	***t, p***	***B (SE)***	***t, p***	***B (SE)***	***t, p***	***B (SE)***	***t, p***
Cingulum Bundle (Left)	4.119e-03 (3.998e-03)	1.030, 0.304	4.180e-04 (1.144e-04)	3.654 , <0.000	6.110e-03 (4.047e-03)	1.510, 0.133	-2.315e-03 (3.788e-03)	-0.611, 0.541
Cingulum Bundle (Right)	1.779e-03 (4.297e-03)	0.414, 0.679	6.988e-04 (7.156e-05)	9.765, <0.000	9.252e-03 (4.335e-03)	2.134, 0.034	-6.047e-03 (4.055e-03)	-1.491, 0.137
Fornix (Left)	7.554e-03 (5.922e-03)	1.276, 0.204	-6.713e-04 (1.139e-04)	-5.894, <0.000	5.085e-03 (5.993e-03)	0.848, 0.397	-7.863e-03 (5.614e-03)	-1.401 0.163
Fornix (Right)	7.316e-03 (4.696e-03)	1.558, 0.121	-1.882e-04 (1.130e-04)	-1.666, 0.097	2.053e-03 (4.766e-03)	0.431, 0.667	-1.035e-02 (4.466e-03)	-2.317 0.021
Anterior Thalamic Projections (Left)	2.542e-03 (3.495e-03)	0.727, 0.468	2.293e-04 (9.267e-05)	2.474, 0.014	4.416e-04 (3.541e-03)	0.125, 0.900	-7.193e-05 (3.313e-03)	-0.022, 0.982
Anterior Thalamic Projections (Right)	-2.266e-03 (3.651e-03)	-0.621, 0.533	2.920e-04 (7.469e-05)	3.910, <0.000	4.838e-03 (3.699e-03)	1.308, 0.192	-4.496e-03 (3.464e-03)	-1.298, 0.196

Mammillothalamic tract (Left)	-6.496e-03 (4.896e-03)	-1.327, 0.186	-4.426e-04 (1.342e-04)	-3.298, 0.001	1.042e-02 (4.999e-03)	2.085, 0.038	-5.286e-03 (4.671e-03)	-1.131, 0.259
Mammillothalamic tract (Right)	-4.305e-03 (4.693e-03)	-0.917, 0.360	-2.114e-04 (1.460e-04)	-1.488, 0.149	1.234e-03 (4.815e-03)	0.256, 0.798	4.918e-03 (4.489e-03)	1.095, 0.275
Uncinate Fasciculus (Left)	-3.623e-03 (5.099e-03)	-0.711, 0.478	1.861e-04 (9.763e-05)	1.907, 0.057	-3.816e-03 (5.162e-03)	-0.739, 0.460	2.665e-04 (4.822e-03)	0.055, 0.956
Uncinate Fasciculus (Right)	-4.073e-03 (4.851e-03)	-0.839, 0.402	3.820e-04 (1.315e-04)	2.906, 0.004	5.227e-03 (4.901e-03)	1.066, 0.287	-5.946e-03 (4.618e-03)	-1.288, 0.199

Table 5.13 Results of optimal mixed-effects models (without interaction term) analyses: limbic system white matter MD in ADHD and controls.

	Sex		**Months from baseline**		**Age at baseline**		**Diagnosis**	
	B (SE)	***t, p***	***B (SE)***	***t, p***	***B (SE)***	***t, p***	***B (SE)***	***t, p***
Cingulum Bundle (Left)	1.283e-05 (5.406e-06)	2.373, 0.018	-8.210e-07 (1.546e-07)	-5.312, <0.000	-1.427e-06 (5.479e-06)	-0.260, 0.794	-3.572e-06 (5.127e-06)	-0.697, 0.487
Cingulum Bundle (Right)	1.345e-05 (5.976e-06)	2.251, 0.025	-1.514e-06 (1.090e-07)	-13.890, <0.000	-5.890e-06 (6.041e-06)	-0.975, 0.331	2.384e-06 (5.657e-06)	0.421, 0.674
Fornix (Left)	-2.305e-05 (1.888e-05)	-1.221, 0.224	-3.167e-07 (3.578e-07)	-0.885, 0.377	3.905e-05 (1.911e-05)	2.044, 0.042	3.555e-05 (1.790e-05)	1.986 0.048
Fornix (Right)	1.469e-06 (1.538e-05)	0.096, 0.924	-4.347e-07 (4.095e-07)	-1.062, 0.289	1.659e-05 (1.564e-05)	1.061, 0.290	-1.452e-05 (1.465e-05)	-0.992, 0.323
Anterior Thalamic Projections (Left)	9.015e-06 (5.156e-06)	1.749, 0.082	-8.101e-07 (1.462e-07)	-5.539, <0.000	2.881e-06 (5.223e-06)	0.552, 0.581	-4.902e-06 (4.887e-06)	-1.003, 0.317
Anterior Thalamic Projections (Right)	9.705e-06 (5.420e-06)	1.790, 0.075	-1.301e-06 (1.181e-07)	-11.016, <0.000	1.548e-06 (5.477e-06)	0.283, 0.777	-3.256e-06 (5.136e-06)	-0.634, 0.527

Mammillothalamic tract (Left)	1.261e-05 (1.851e-05)	0.691, 0.497	6.785e-07 (5.379e-07)	1.262, 0.208	-7.484e-06 (1.894e-05)	-0.395, 0.693	1.551e-05 (1.768e-05)	0.877, 0.382
Mammillothalamic tract (Right)	3.848e-06 (2.491e-05)	0.154, 0.877	-2.992e-07 (6.593e-07)	-0.454, 0.650	4.296e-05 (2.541e-05)	1.691, 0.092	-2.473e-05 (2.375e-05)	-1.041, 0.299
Uncinate Fasciculus (Left)	7.794e-06 (5.680e-06)	1.372, 0.172	-1.134e-06 (1.727e-07)	-6.564, <0.000	4.100e-06 (5.770e-06)	0.710, 0.478	-3.648e-06 (5.399e-06)	-0.676, 0.500
Uncinate Fasciculus (Right)	1.591e-05 (6.338e-06)	2.511, 0.013	-8.770e-07 (1.789e-07)	-4.901, <0.000	-5.596e-06 (6.447e-06)	-0.868, 0.386	1.690e-06 (6.056e-06)	0.279, 0.780

Table 5.14 Results of optimal mixed-effects models (without interaction term) analyses: limbic system white matter AD in ADHD and controls.

	Sex		**Months from baseline**		**Age at baseline**		**Diagnosis**	
	B (SE)	***t, p***	***B (SE)***	***t, p***	***B (SE)***	***t, p***	***B (SE)***	***t, p***
Cingulum Bundle (Left)	2.410e-05 (7.341e-06)	3.283, 0.001	-6.963e-07 (2.021e-07)	-3.445, <0.000	2.210e-06 (7.443e-06)	0.297, 0.766	-6.686e-06 (6.964e-06)	-0.960, 0.338
Cingulum Bundle (Right)	1.979e-05 (7.632e-06)	2.593, 0.010	-1.342e-06 (1.567e-07)	-8.559, <0.000	3.410e-07 (7.732e-06)	0.044, 0.964	-6.223e-06 (7.246e-06)	-0.859, 0.391
Fornix (Left)	-1.590e-05 (3.328e-05)	-0.478, 0.633	-1.143e-06 (6.621e-07)	-1.726, 0.085	6.079e-05 (3.370e-05)	1.804, 0.073	3.021e-05 (3.157e-05)	0.957, 0.340
Fornix (Right)	2.026e-06 (2.627e-05)	0.077, 0.938	-7.332e-07 (7.225e-07)	-1.015, 0.311	2.894e-05 (2.672e-05)	1.083, 0.280	-5.403e-05 (2.503e-05)	-2.158 0.032
Anterior Thalamic Projections (Left)	1.452e-05 (6.340e-06)	2.290, 0.023	-6.893e-07 (1.714e-07)	-4.021, <0.000	2.813e-06 (6.418e-06)	0.438, 0.661	-1.049e-05 (6.006e-06)	-1.746, 0.082
Anterior Thalamic Projections (Right)	1.155e-05 (6.939e-06)	1.665, 0.098	-1.397e-06 (1.515e-07)	-9.224, <0.000	2.152e-06 (7.041e-06)	0.306, 0.760	-8.251e-06 (6.596e-06)	-1.251, 0.212

Mammillothalamic tract (Left)	1.240e-05 (2.331e-05)	0.532, 0.595	4.022e-07 (6.350e-07)	0.633, 0.527	5.225e-06 (2.379e-05)	0.220, 0.826	9.672e-06 (2.223e-05)	0.435, 0.664
Mammillothalamic tract (Right)	6.763e-06 (3.157e-05)	0.214, 0.830	-4.851e-07 (7.916e-07)	-0.613, 0.540	6.788e-05 (3.215e-05)	2.112, 0.036	-2.384e-05 (3.007e-05)	-0.793, 0.429
Uncinate Fasciculus (Left)	9.607e-06 (8.381e-06)	1.146, 0.254	-1.286e-06 (2.567e-07)	-5.010, <0.000	6.048e-06 (8.518e-06)	0.710, 0.479	-6.224e-06 (7.972e-06)	-0.781, 0.436
Uncinate Fasciculus (Right)	2.018e-05 (8.412e-06)	2.399, 0.017	-8.440e-07 (2.363e-07)	-3.572, <0.000	1.488e-06 (8.556e-06)	0.174, 0.862	-9.489e-06 (8.037e-06)	-1.181, 0.239

Table 5.15 Results of mixed-effects models (with interaction term) analyses: limbic system white matter tracts RD in ADHD and Controls.

	Sex		**Months from baseline**		**Age at baseline**		**Diagnosis**		**Diagnosis * Months from baseline**	
	B (SE)	***t, p***	***B (SE)***	***t, p***	***B (SE)***	***t, p***	***B (SE)***	***t, p***	***B (SE)***	***t, p***
Cingulum Bundle (Left)	7.258e-06 (5.711e-06)	1.271, 0.206	-8.479e-07 (1.647e-07)	-5.148, <0.000	-4.121e-06 (5.786e-06)	-0.712, 0.477	-7.366e-06 (6.416e-06)	-1.148, 0.253	4.068e-07 (3.299e-07)	1.233, 0.220
Cingulum Bundle (Right)	1.041e-05 (6.466e-06)	1.611, 0.109	-1.496e-06 (1.024e-07)	-14.608, <0.000	-9.180e-06 (6.525e-06)	-1.407, 0.161	4.874e-06 (6.709e-06)	0.726, 0.468	9.900e-08 (2.051e-07)	0.483, 0.630
Fornix (Left)	-2.310e-05 (1.363e-05)	-1.695 , 0.091	8.063e-08 (2.621e-07)	0.308, 0.758	3.049e-05 (1.379e-05)	2.211, 0.028	4.508e-05 (1.486e-05)	3.033, 0.002*	-1.076e-06 (5.248e-07)	-2.050 , 0.041
Fornix (Right)	-4.347e-06 (1.155e-05)	-0.376, 0.707	-2.067e-07 (3.039e-07)	-0.680, 0.497	1.010e-05 (1.175e-05)	0.860, 0.391	6.995e-07 (1.398e-05)	0.050, 0.960	2.617e-08 (6.087e-07)	-0.043, 0.966
Anterior Thalamic Projections (Left)	6.337e-06 (5.306e-06)	1.194, 0.234	-7.141e-07 (1.486e-07)	-4.807, <0.000	2.133e-06 (5.378e-06)	0.397, 0.692	-9.370e-06 (6.132e-06)	-1.528, 0.129	4.401e-07 (2.976e-07)	1.479, 0.141
Anterior Thalamic Projections (Right)	9.155e-06 (5.787e-06)	1.582 , 0.116	-1.172e-06 (1.093e-07)	-10.726 , <0.000	3.395e-07 (5.857e-06)	0.058, 0.954	-1.847e-06 (6.267e-06)	-0.295, 0.768	1.297e-07 (2.188e-07)	0.593 , 0.554

Mammillothalamic tract (Left)	1.719e-05 (1.643e-05)	1.046, 0.297	7.028e-07 (5.055e-07)	1.390, 0.166	-1.133e-05 (1.686e-05)	-0.067, 0.503	3.312e-05 (2.144e-05)	1.545, 0.123	-9.886e-07 (1.013e-06)	-0.976, 0.330
Mammillothalamic tract (Right)	4.992e-06 (2.170e-05)	0.230, 0.818	1.381e-07 (6.209e-07)	0.222, 0.824	2.945e-05 (2.220e-05)	1.327, 0.186	-4.552e-05 (2.730e-05)	-1.667, 0.096	1.425e-06 (1.244e-06)	1.145, 0.253
Uncinate Fasciculus (Left)	8.293e-06 (6.354e-06)	1.305 , 0.194	-9.336e-07 (1.716e-07)	-5.441 , <0.000	5.047e-06 (6.446e-06)	0.783, 0.435	-8.422e-06 (7.139e-06)	-1.180, 0.240	3.100e-07 (3.436e-07)	0.902 , 0.369
Uncinate Fasciculus (Right)	1.575e-05 (7.002e-06)	2.249 , 0.025	-8.544e-07 (2.078e-07)	-4.111, <0.000	-1.017e-05 (7.084e-06)	-1.435, 0.153	5.066e-06 (8.275e-06)	0.612, 0.541	-7.129e-08 (4.164e-07)	-0.171, 0.864

Figure 5.10 White matter that had no significant between-group difference in KA across the three-study time points.

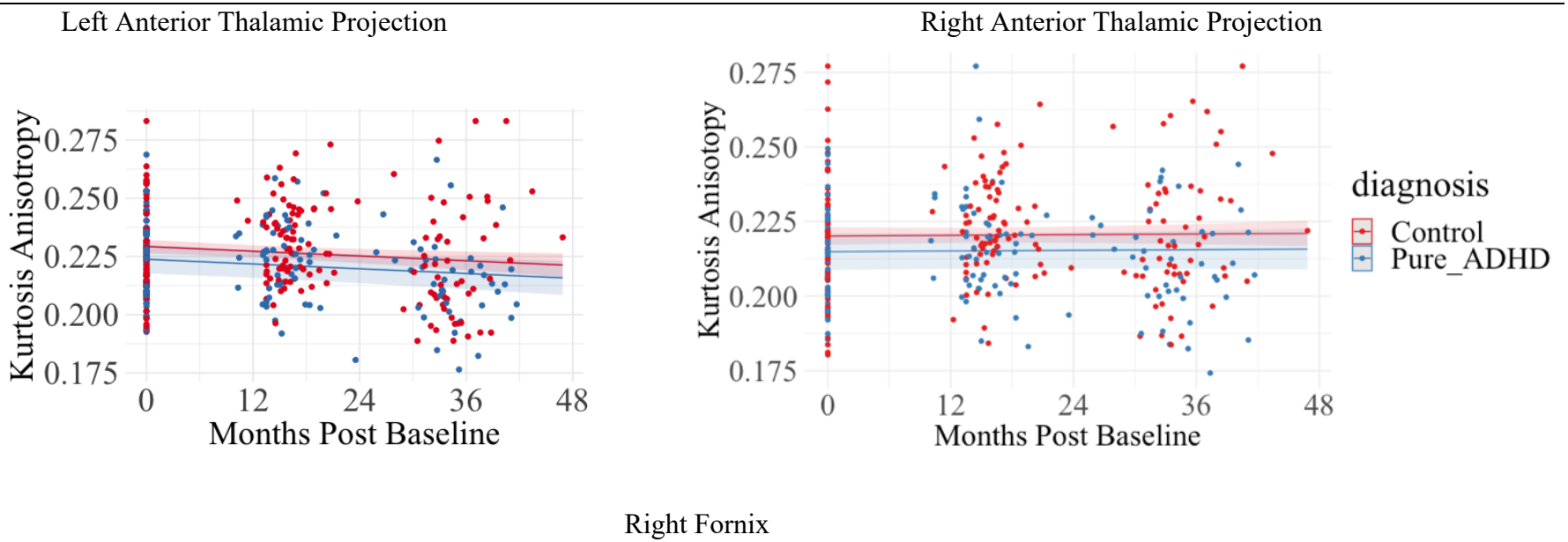

Right Fornix

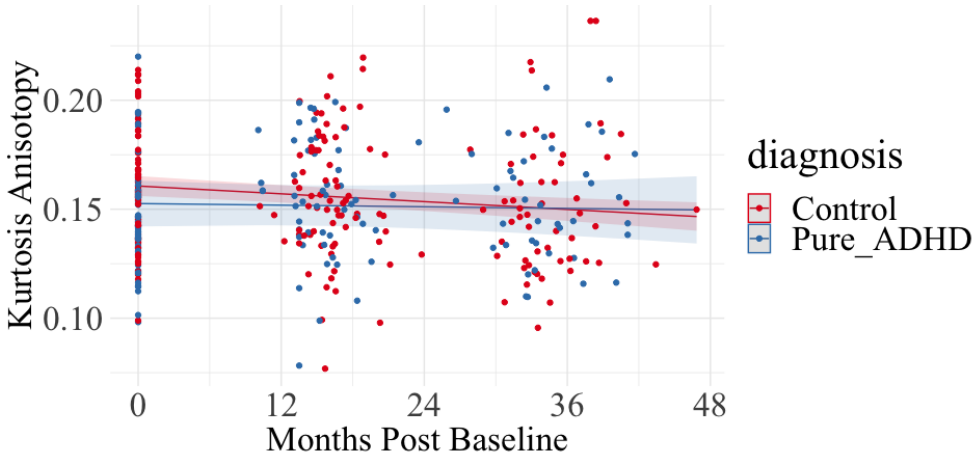

Left Mammillothalamic Tract

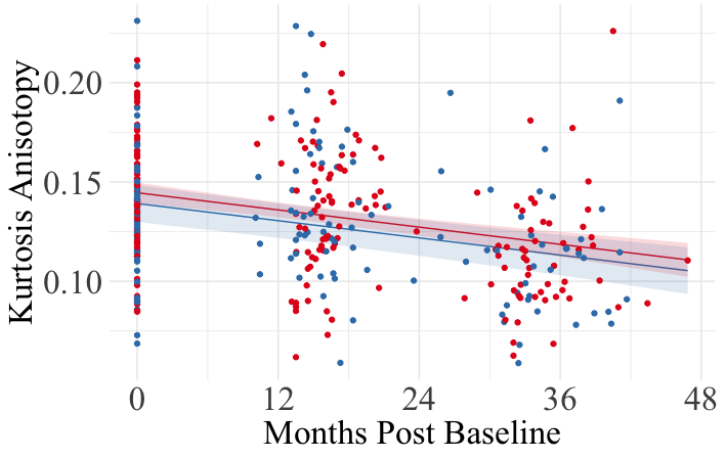

Right Mammillothalamic Tract

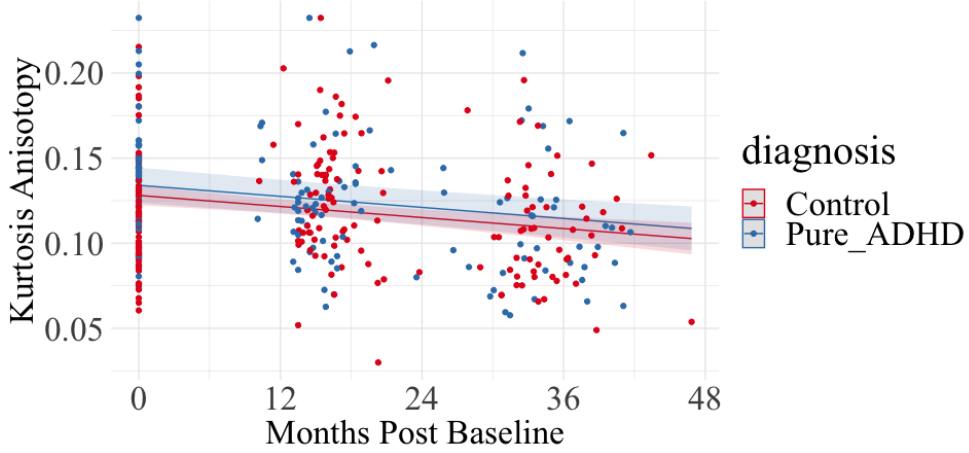

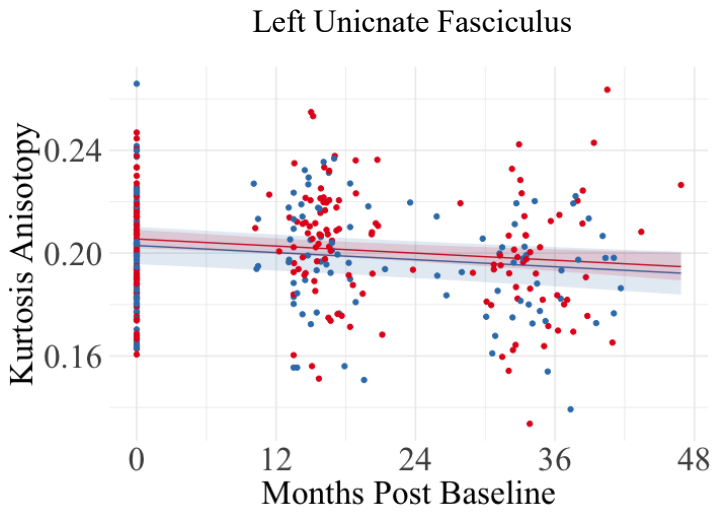
Left Unicnate Fasciculus
Kurtosis Anisotopy
0.24
0.20
0.16
0
12
24
36
48
Months Post Baseline

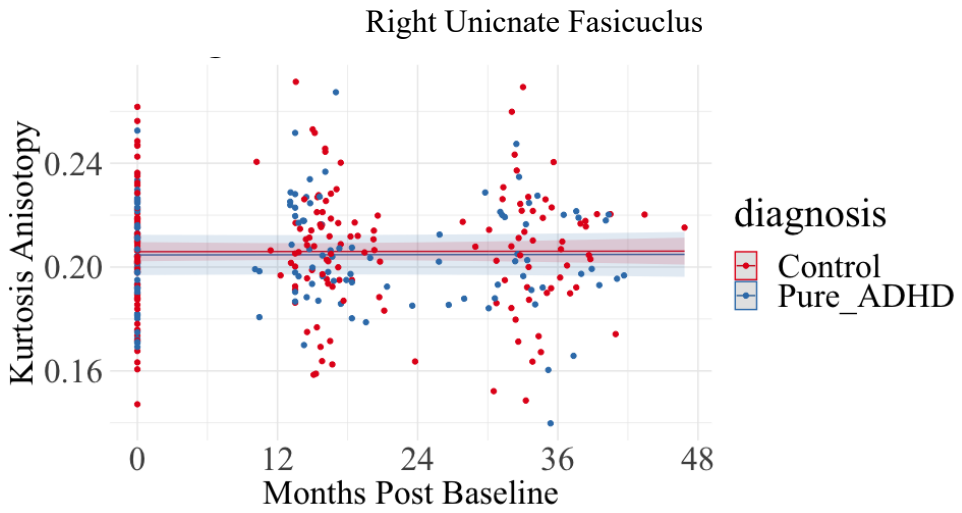
Right Unicnate Fasicuclus
Kurtosis Anisotopy
0.24
0.20
0.16
0
12
24
36
48
Months Post Baseline
diagnosis
Control
Pure_ADHD

Figure 5.11 White matter that had no significant between-group difference in AK across the three-study time points.

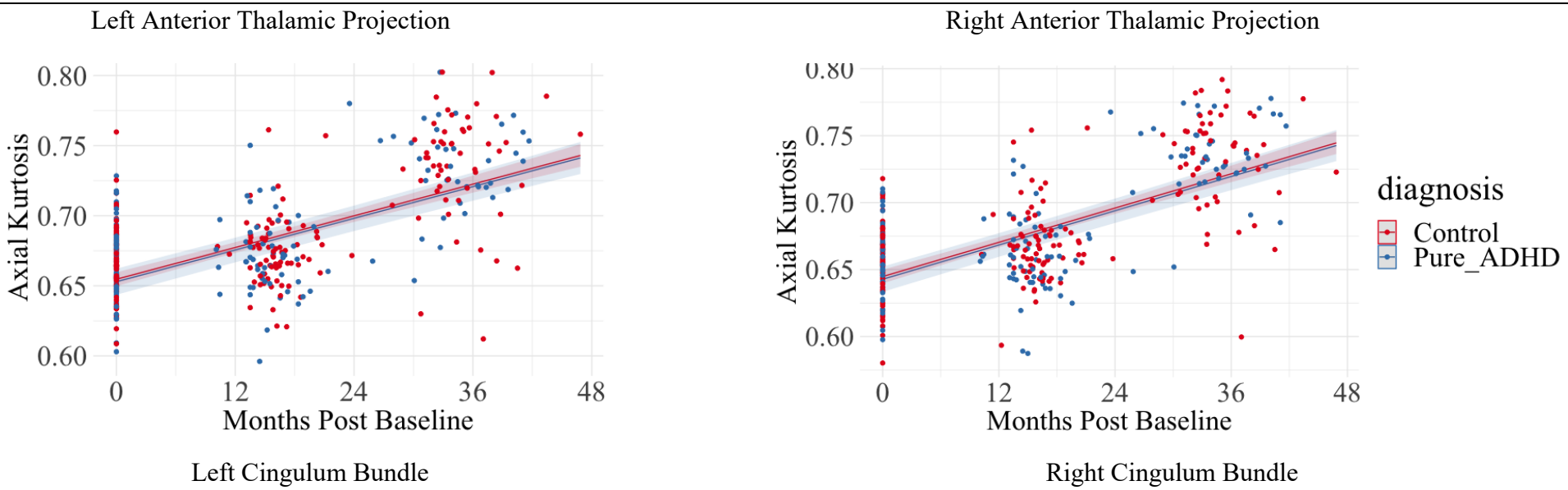

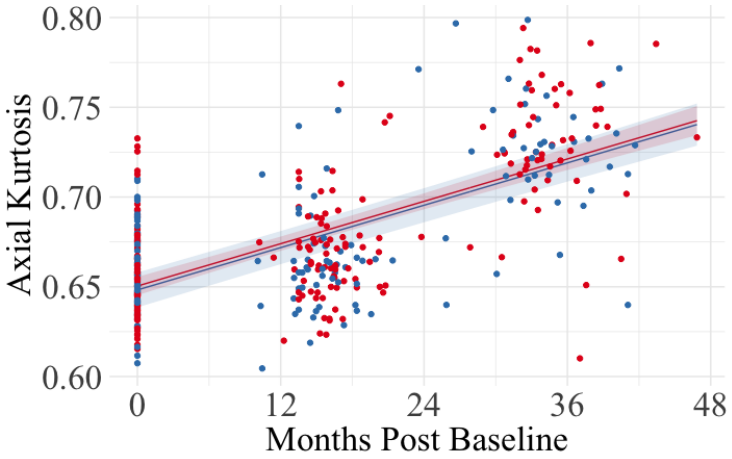

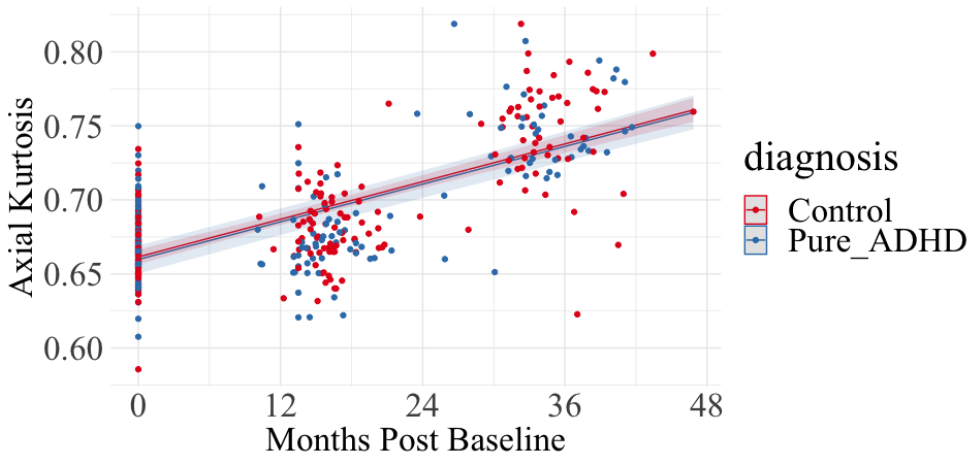

Left Fornix

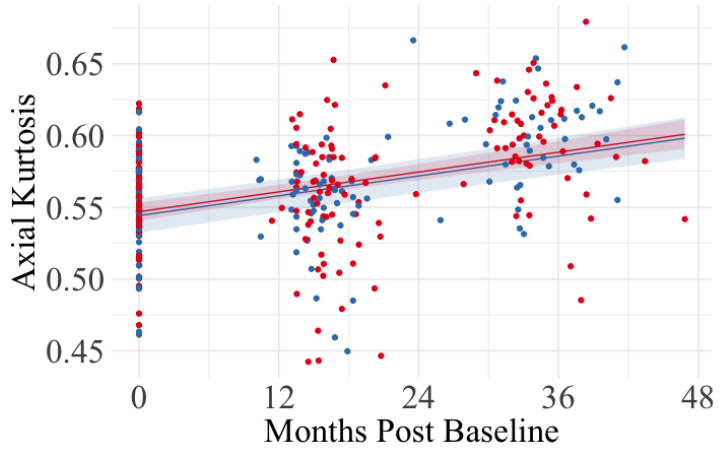

Right Fornix

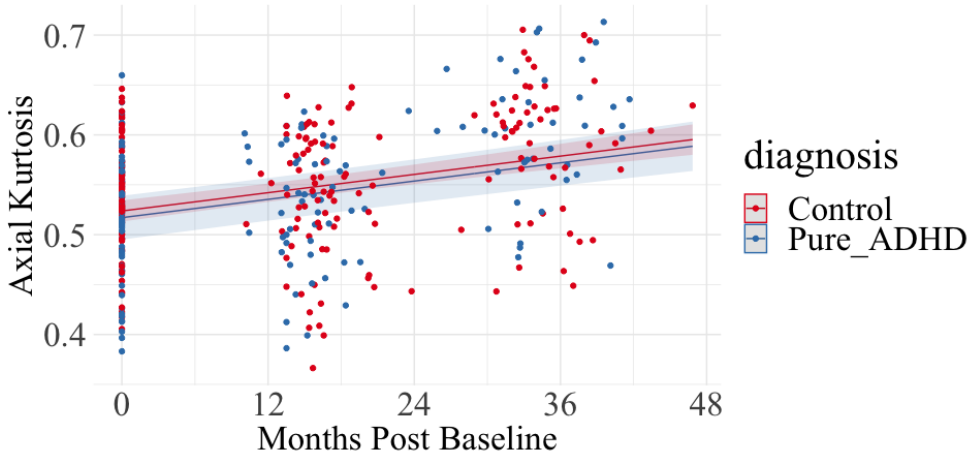

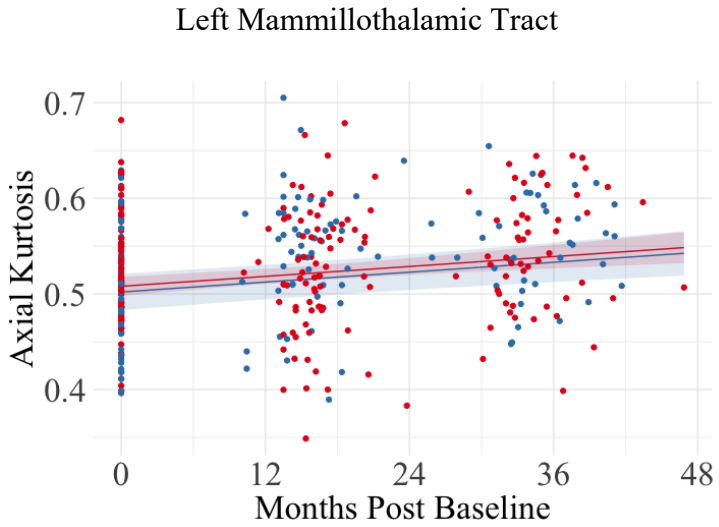
Left Mammillothalamic Tract
Axial Kurtosis
0.7
0.6
0.5
0.4
0
12
24
36
48
Months Post Baseline

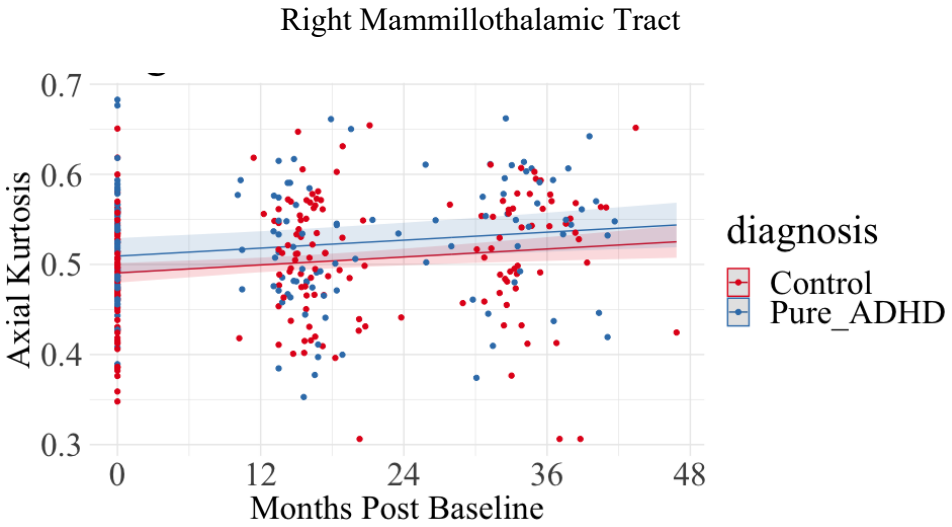
Right Mammillothalamic Tract
Axial Kurtosis
0.7
0.6
0.5
0.4
0.3
0
12
24
36
48
Months Post Baseline
diagnosis
Control
Pure_ADHD

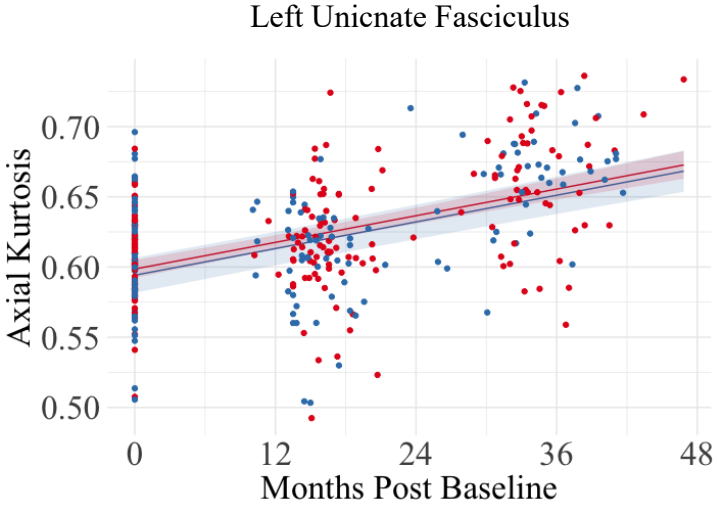
Left Unicnate Fasciculus
Axial Kurtosis
0.70
0.65
0.60
0.55
0.50
0
12
24
36
48
Months Post Baseline

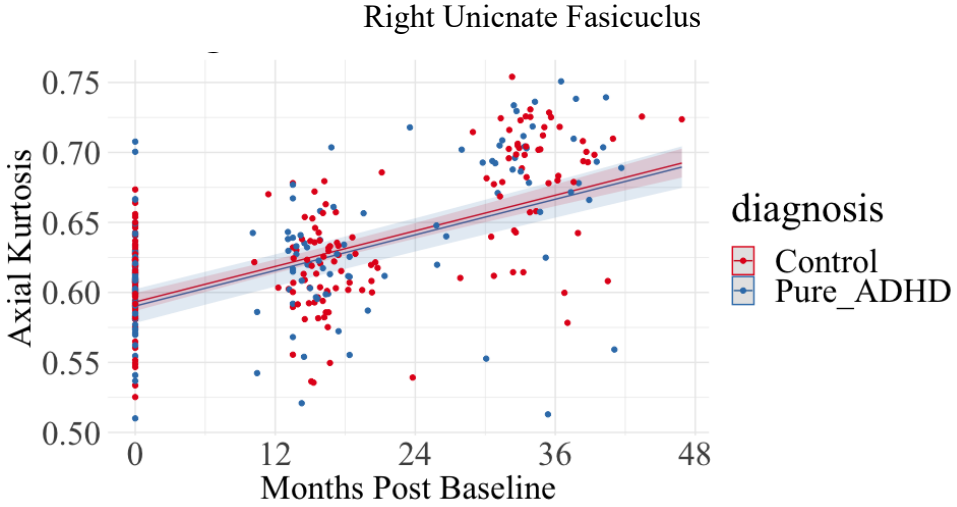
Right Unicnate Fasicuclus
Axial Kurtosis
0.75
0.70
0.65
0.60
0.55
0.50
0
12
24
36
48
Months Post Baseline
diagnosis
Control
Pure_ADHD

Figure 5.12 White matter that had no significant between-group difference in MK across the three-study time points.

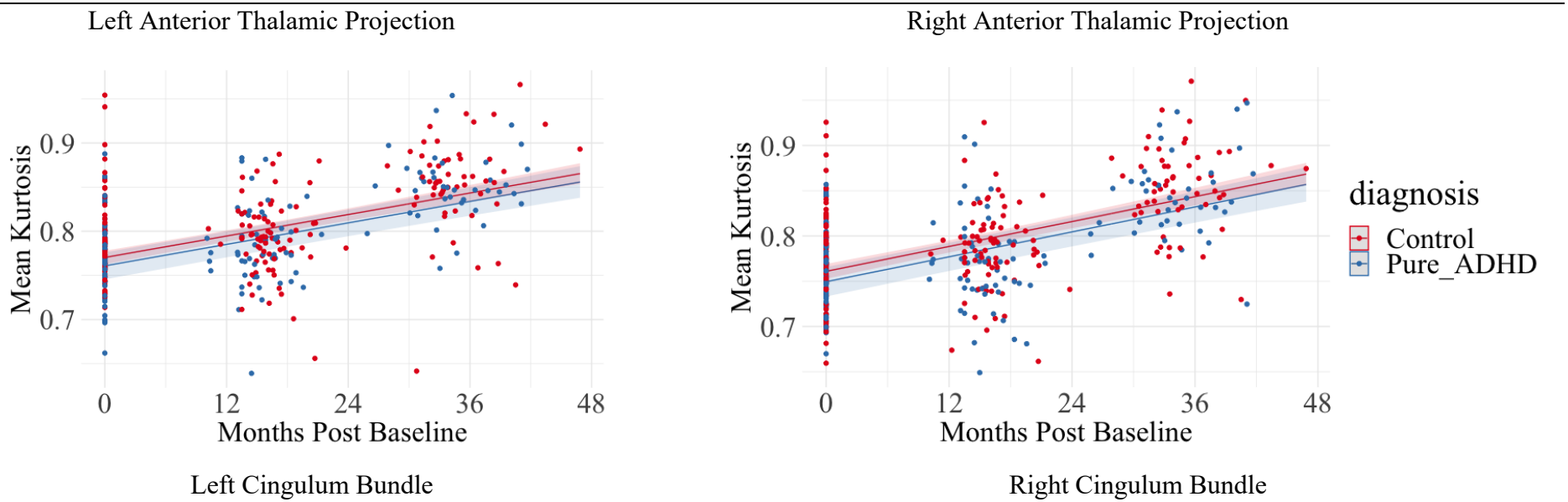

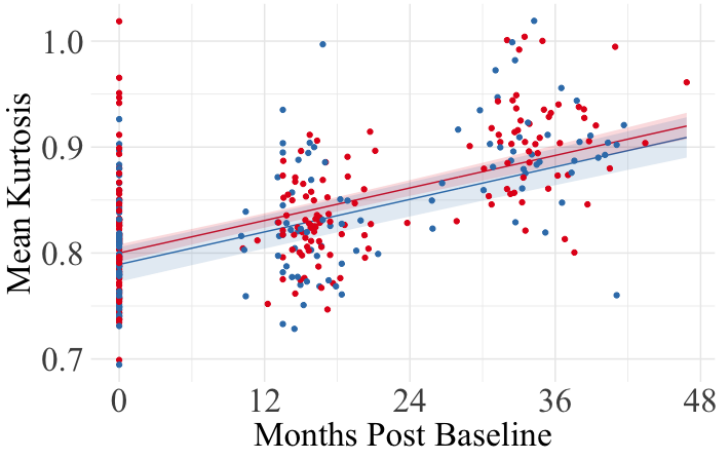

Left Fornix

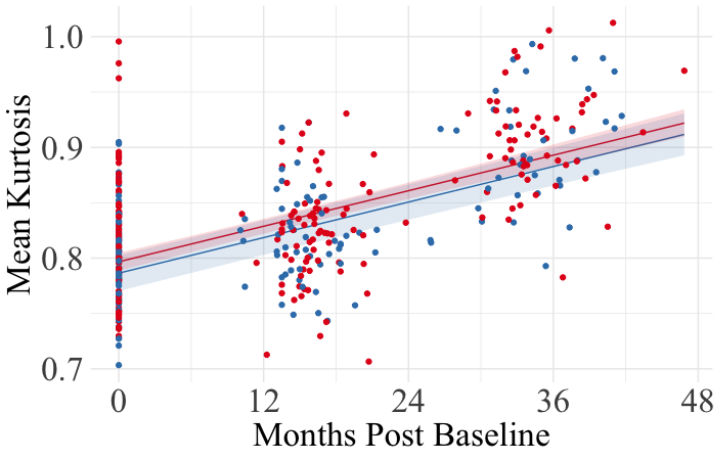

Right Fornix

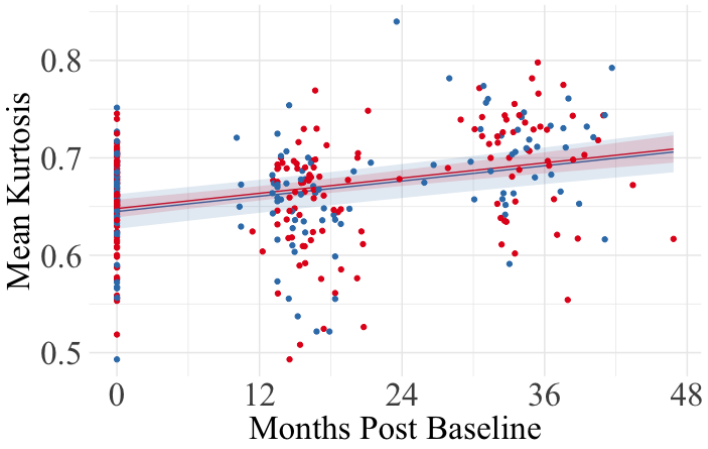

Left Mammillothalamic Tract

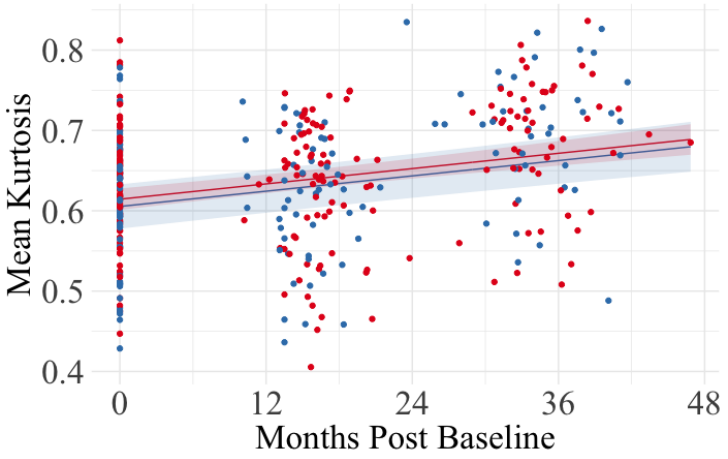

Right Mammillothalamic Tract

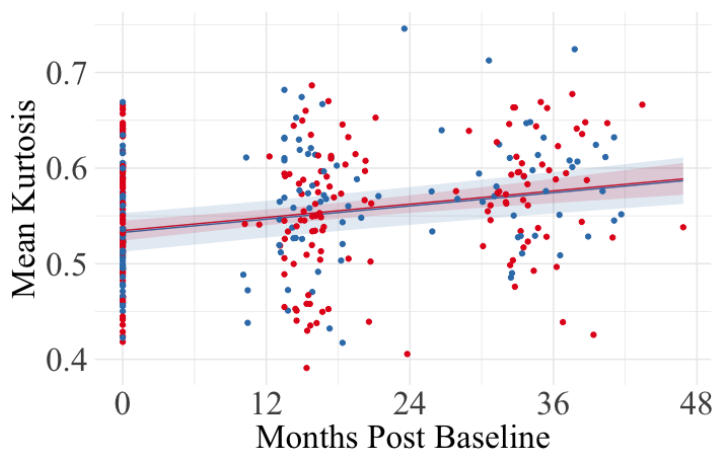

Left Unicnate Fasciculus

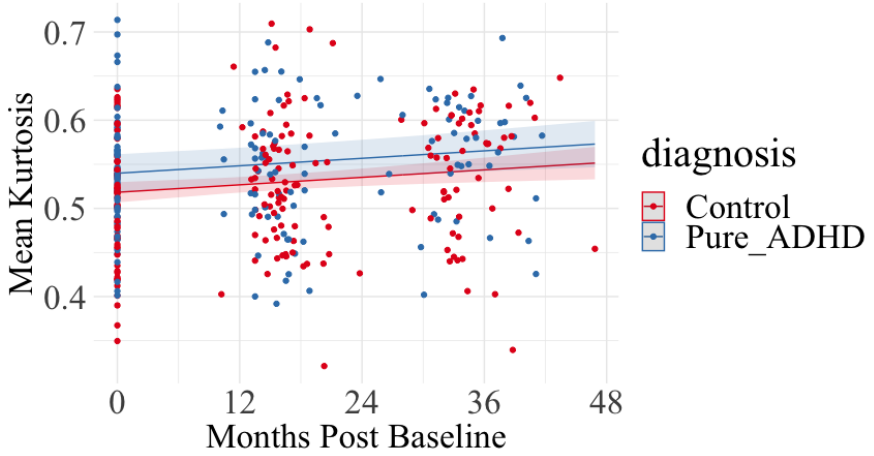

Right Unicnate Fasicuclus

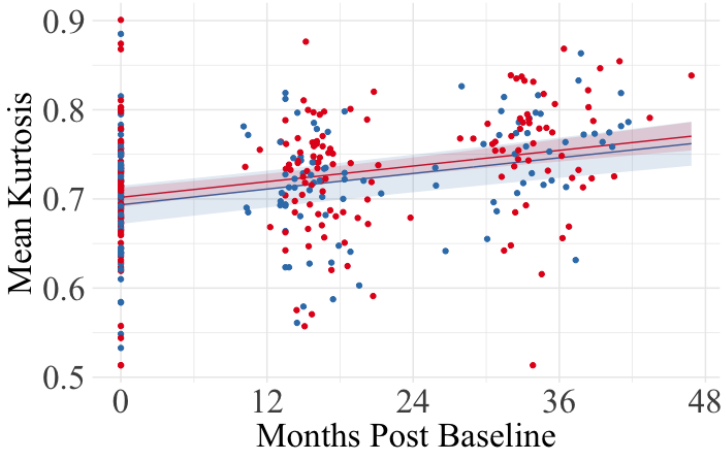

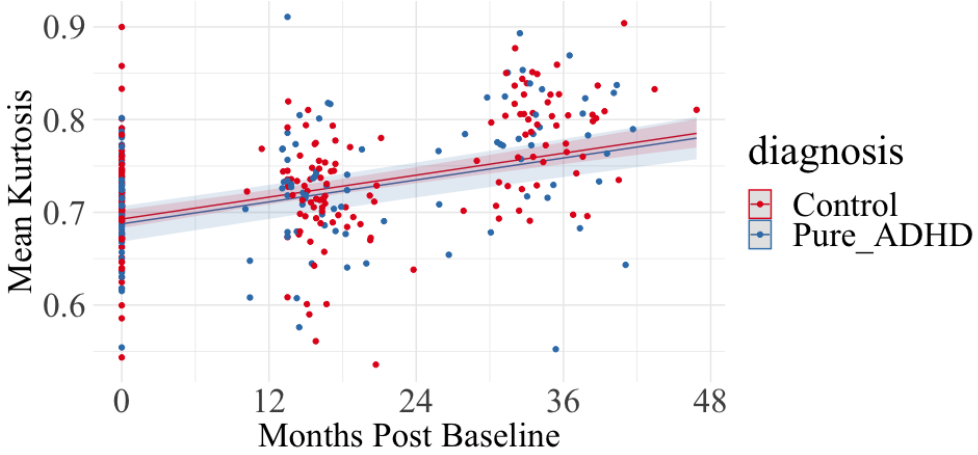

Figure 5.13 White matter that had no significant between-group difference in RK across the three-study time point.

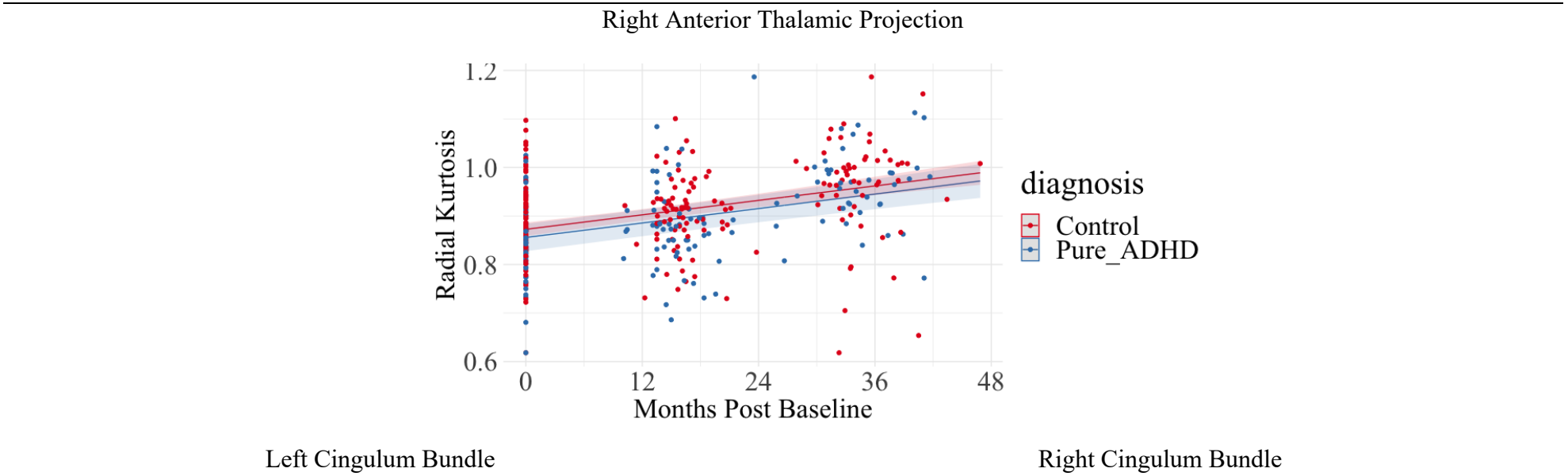

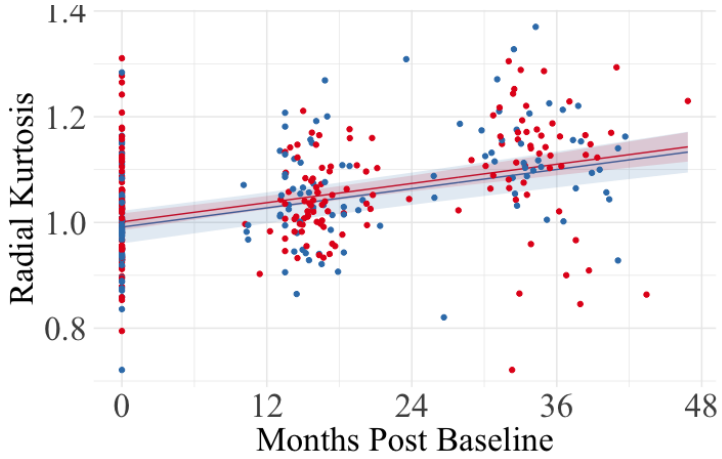

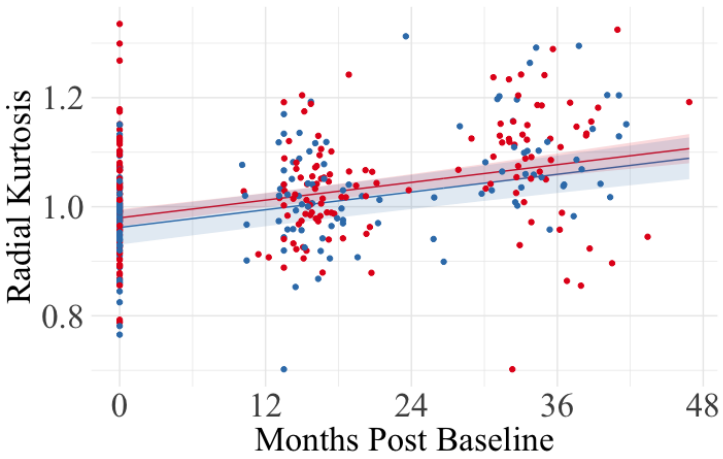

Left Fornix

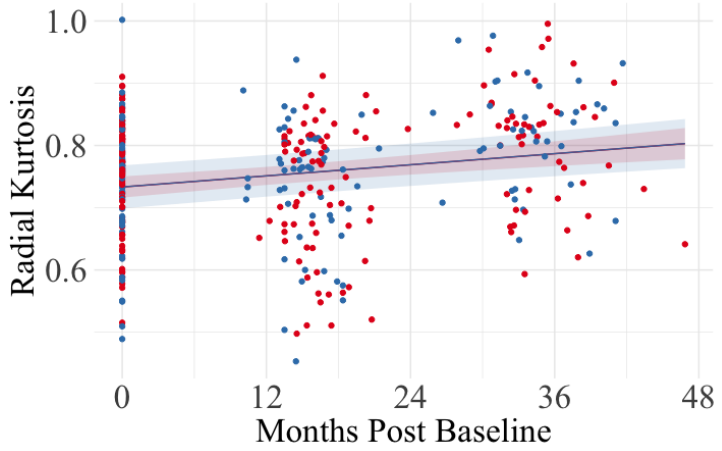

Right Fornix

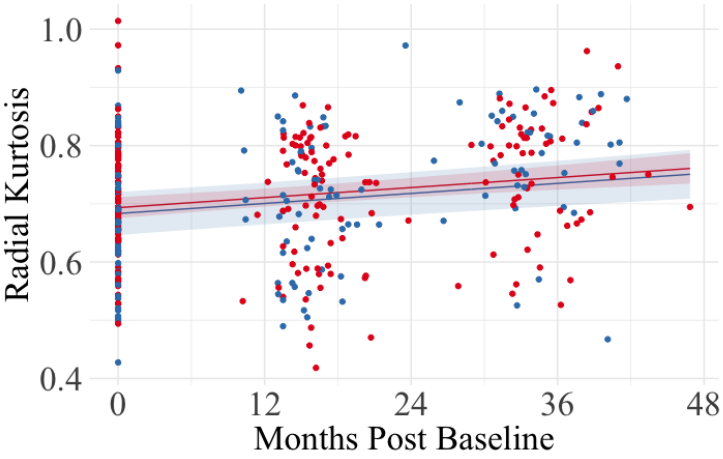

Left Mammillothalamic Tract

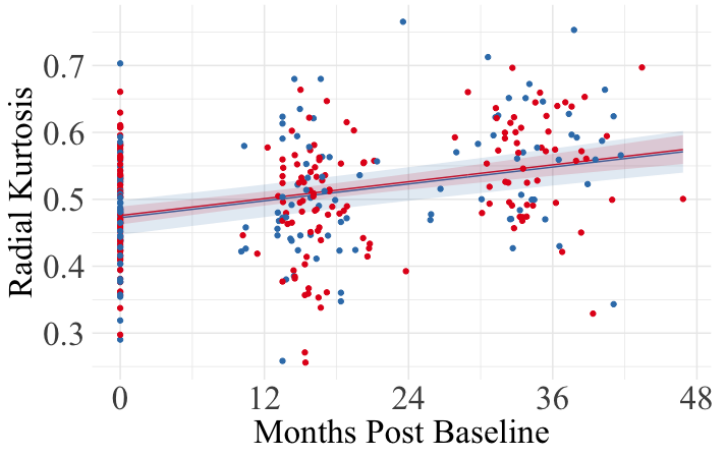

Right Mammillothalamic Tract

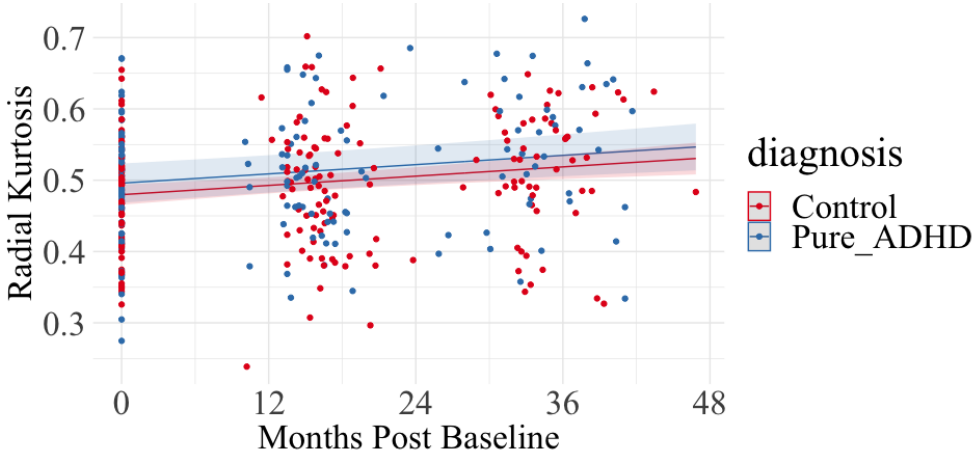

Left Unicnate Fasciculus

Right Unicnate Fasicuclus

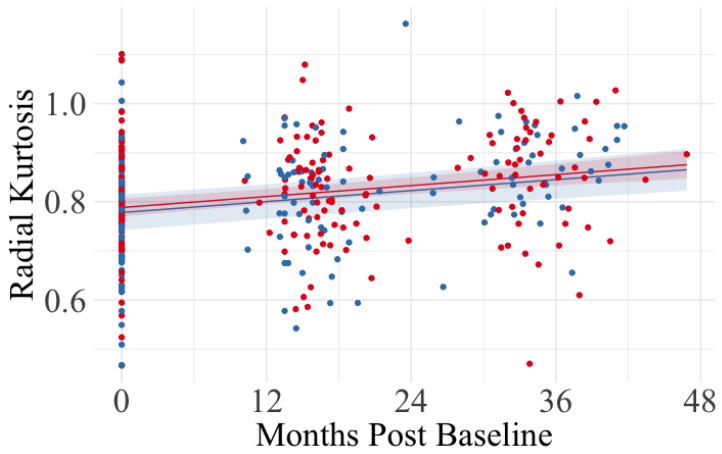
Radial Kurtosis
1.0
0.8
0.6
0
12
24
36
48
Months Post Baseline

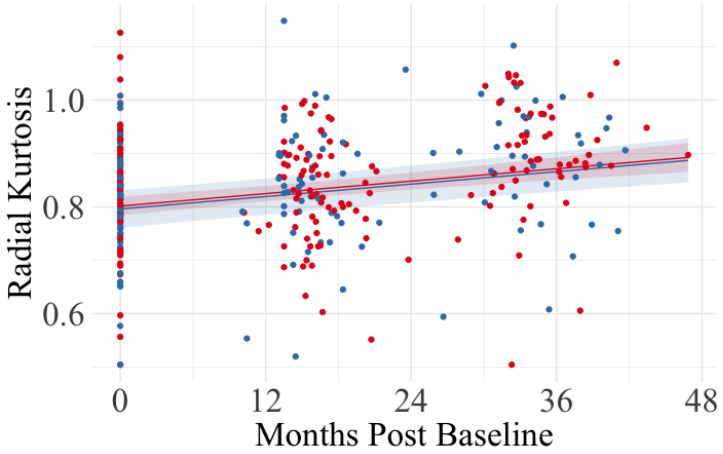
Radial Kurtosis
1.0
0.8
0.6
0
12
24
36
48
Months Post Baseline

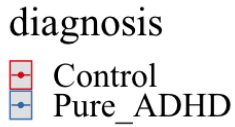
diagnosis
Control
Pure_ADHD

Figure 5.14 White matter that had no significant between-group difference in FA across the three-study time points.

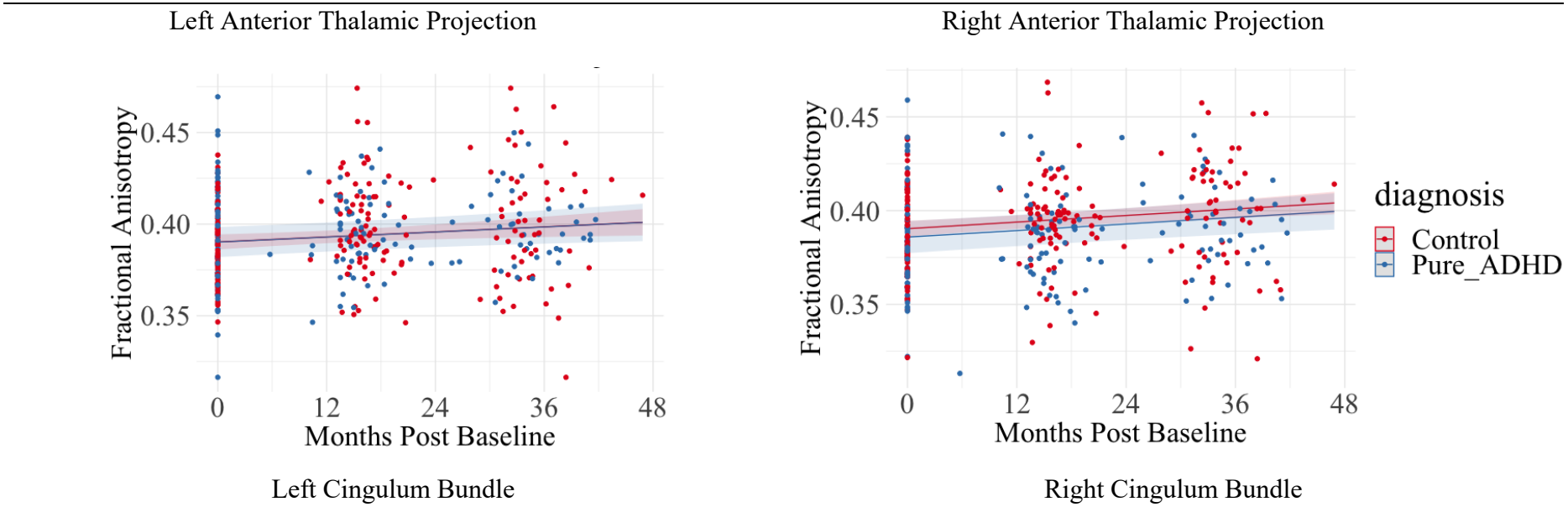

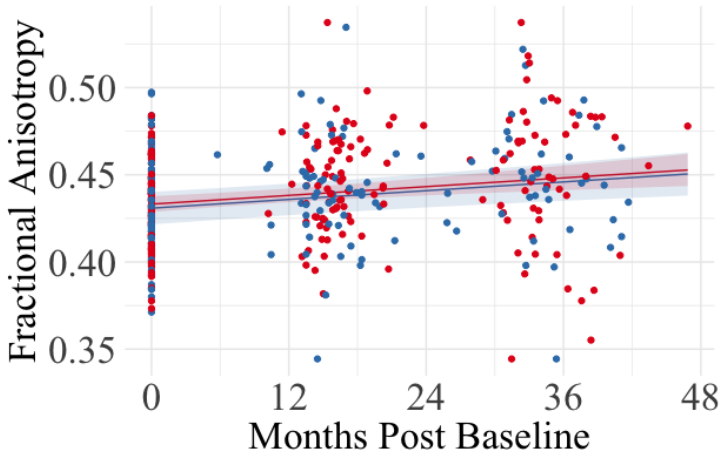

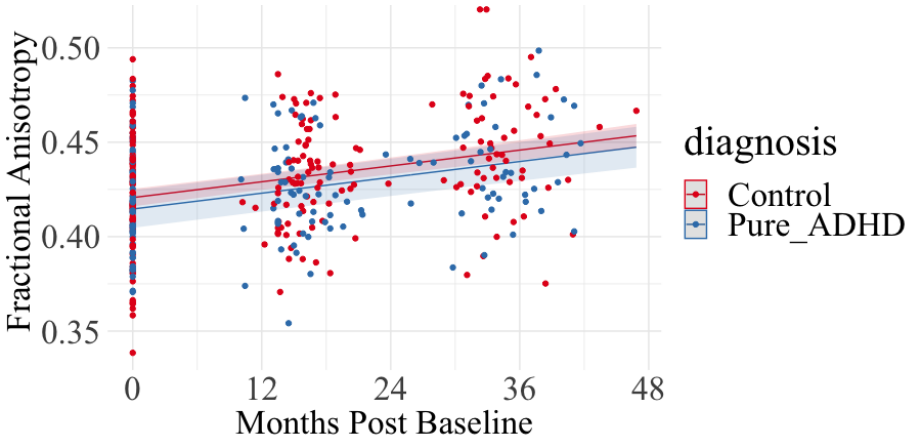

Left Fornix

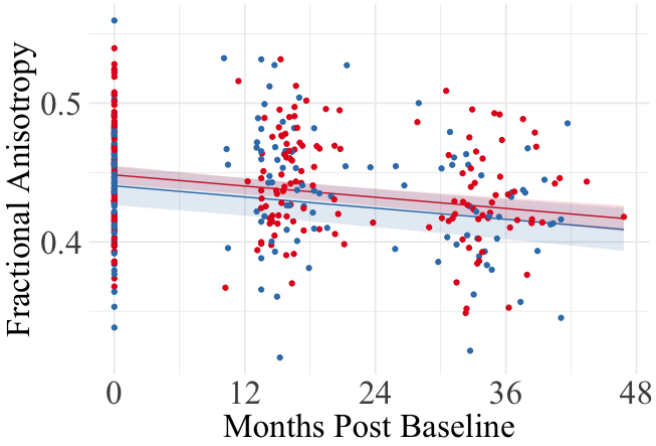

Right Fornix

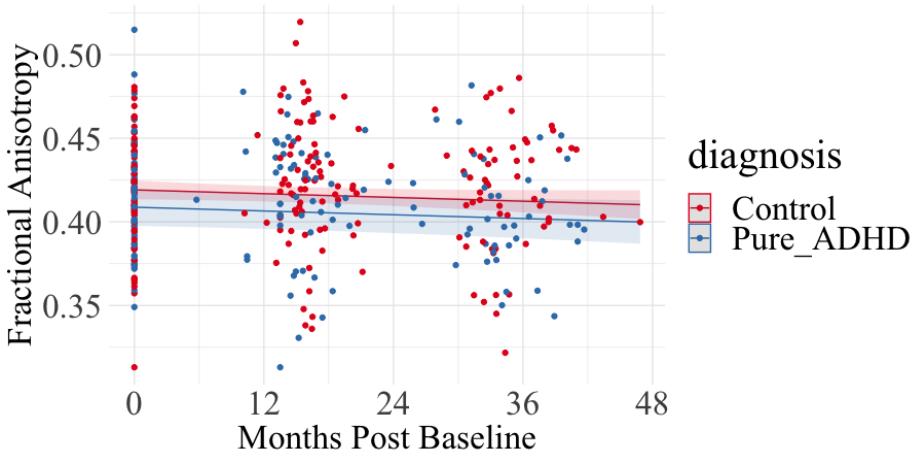

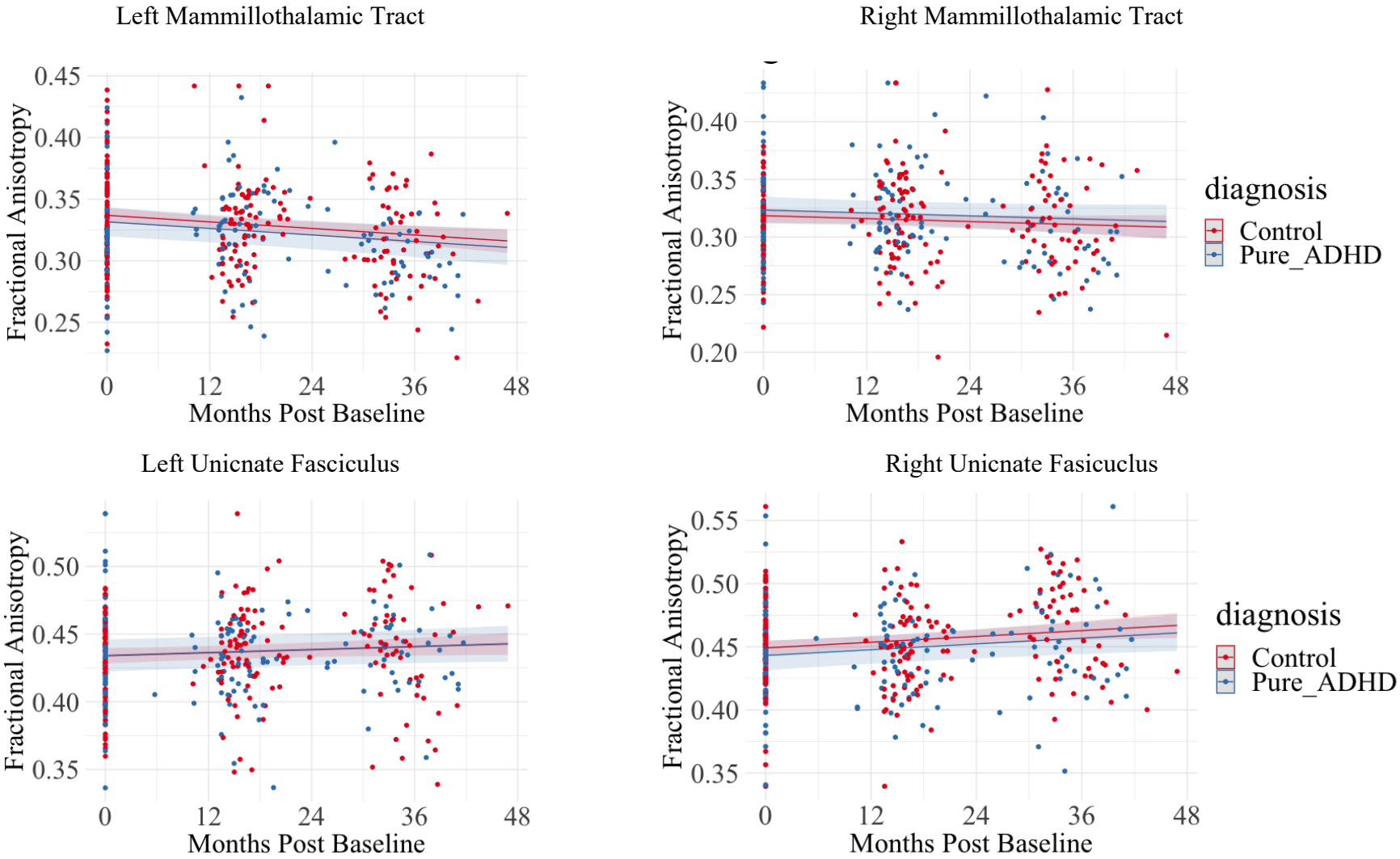
Left Mammillothalamic Tract
Fractional Anisotropy
0.45
0.40
0.35
0.30
0.25
0
12
24
36
48
Months Post Baseline
Right Mammillothalamic Tract
Fractional Anisotropy
0.40
0.35
0.30
0.25
0.20
0
12
24
36
48
Months Post Baseline
diagnosis
Control
Pure_ADHD
Left Unicnate Fasciculus
Fractional Anisotropy
0.50
0.45
0.40
0.35
0
12
24
36
48
Months Post Baseline
Right Unicnate Fasicuclus
Fractional Anisotropy
0.55
0.50
0.45
0.40
0.35
0
12
24
36
48
Months Post Baseline
diagnosis
Control
Pure_ADHD

Figure 5.15 White matter that had no significant between-group difference in MD across the three-study time points.

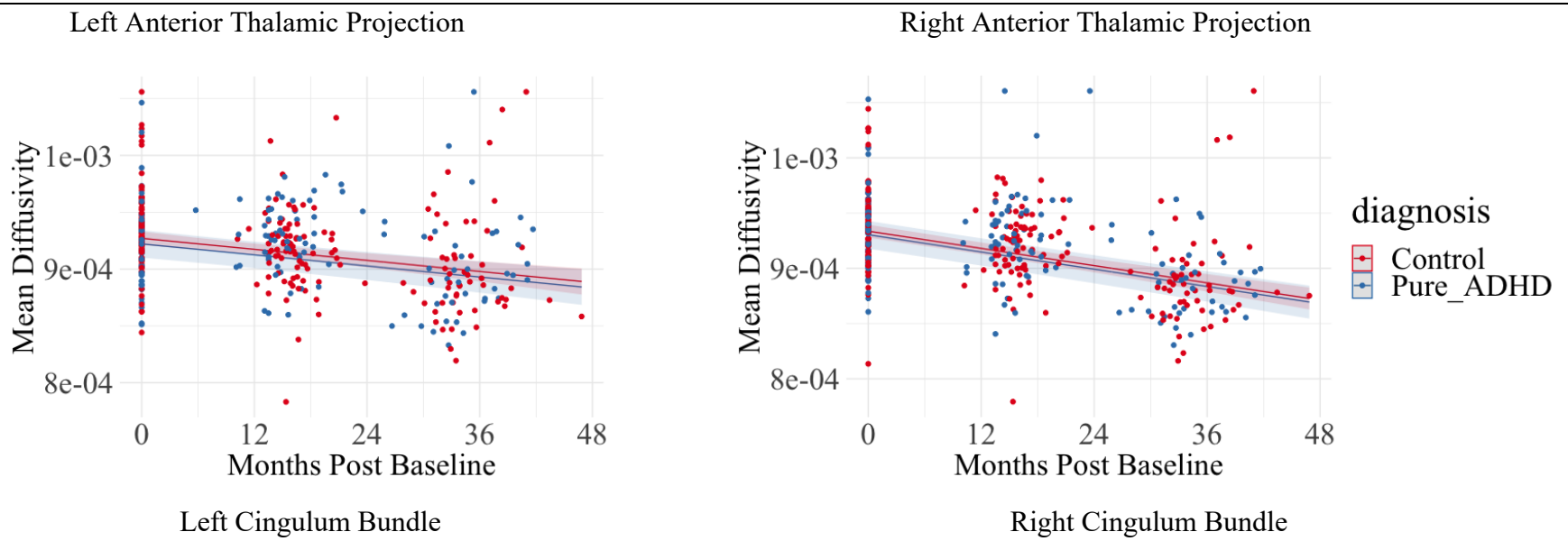

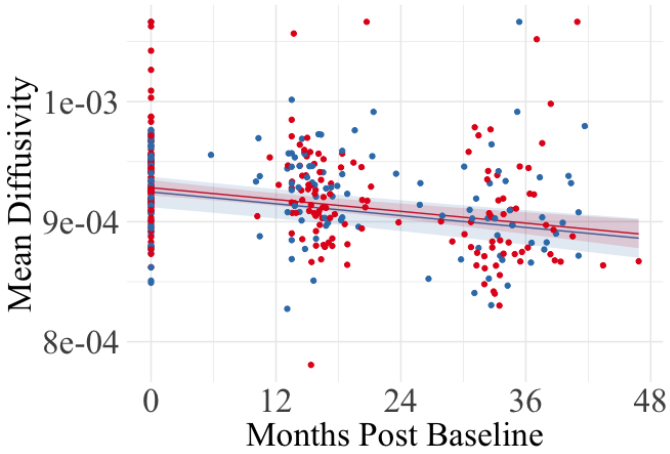

Left Fornix

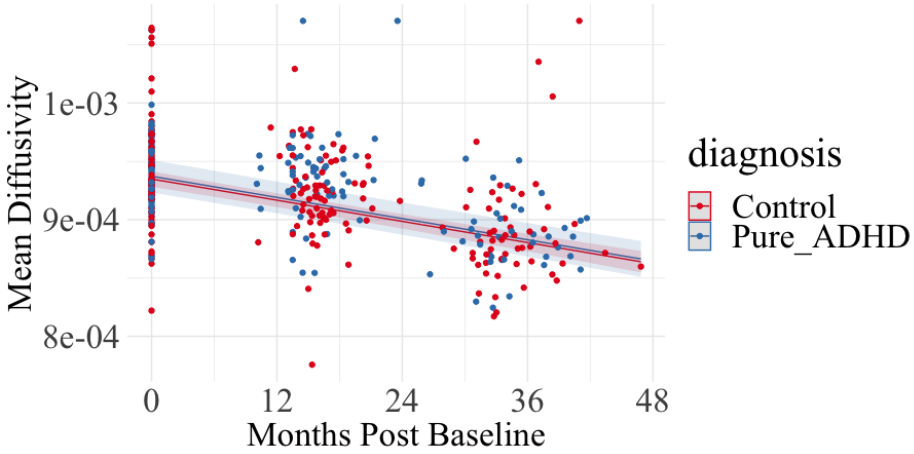

Right Fornix

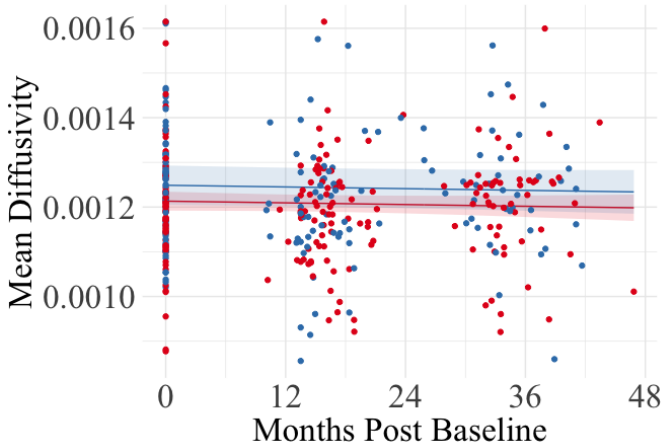

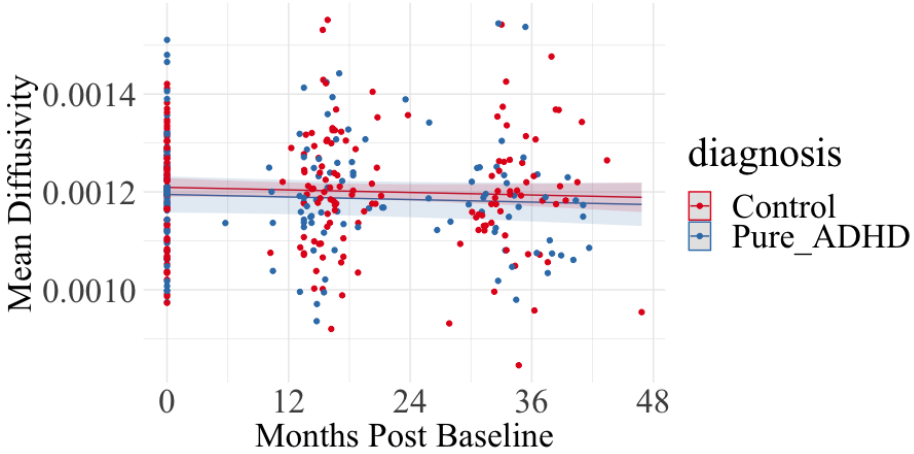

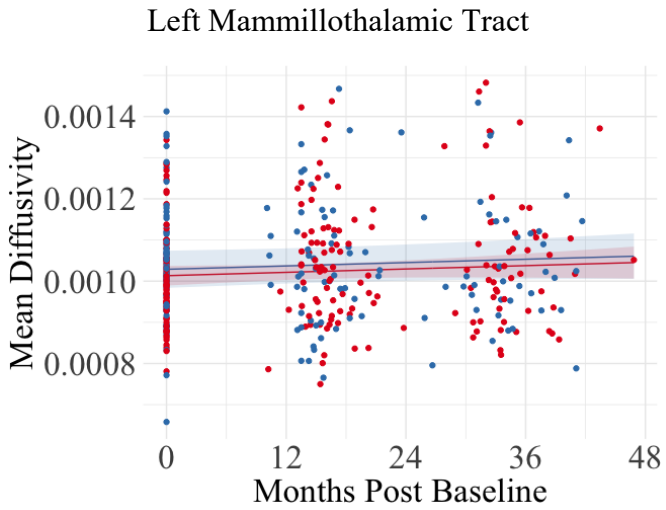

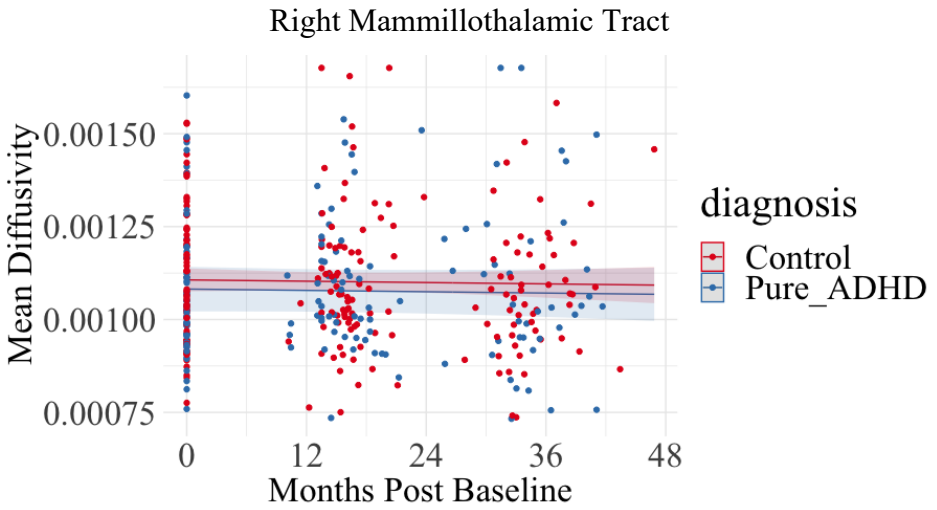

Left Unicnate Fasciculus

Right Unicnate Fasicuclus

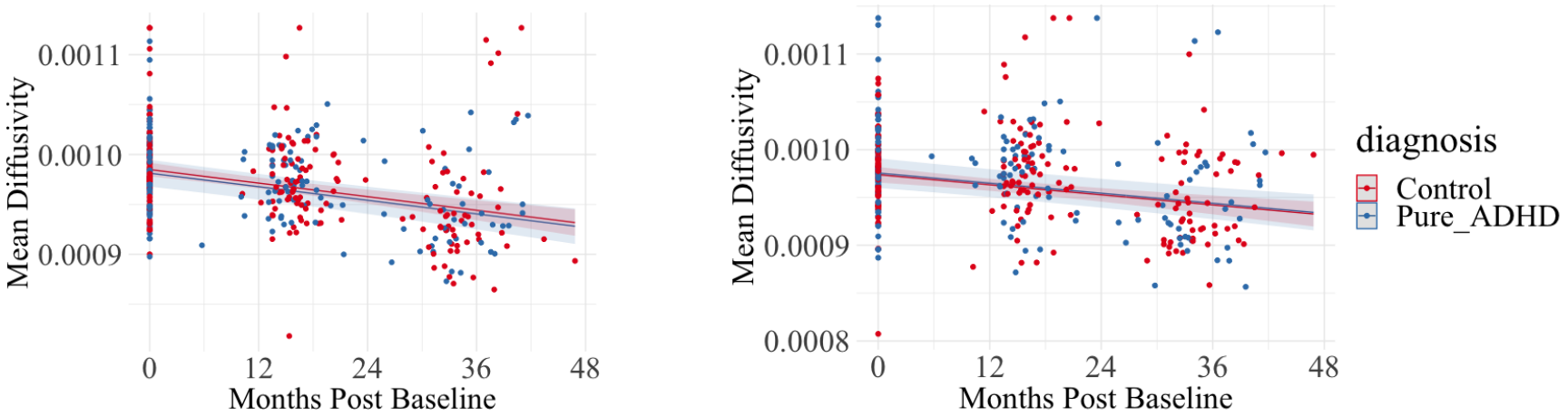
Mean Diffusivity
0.0011
0.0010
0.0009
0.0008
0
12
24
36
48
Months Post Baseline
diagnosis
Control
Pure_ADHD

Figure 5.16 White matter that had no significant between-group difference in AD across the three-study time points.

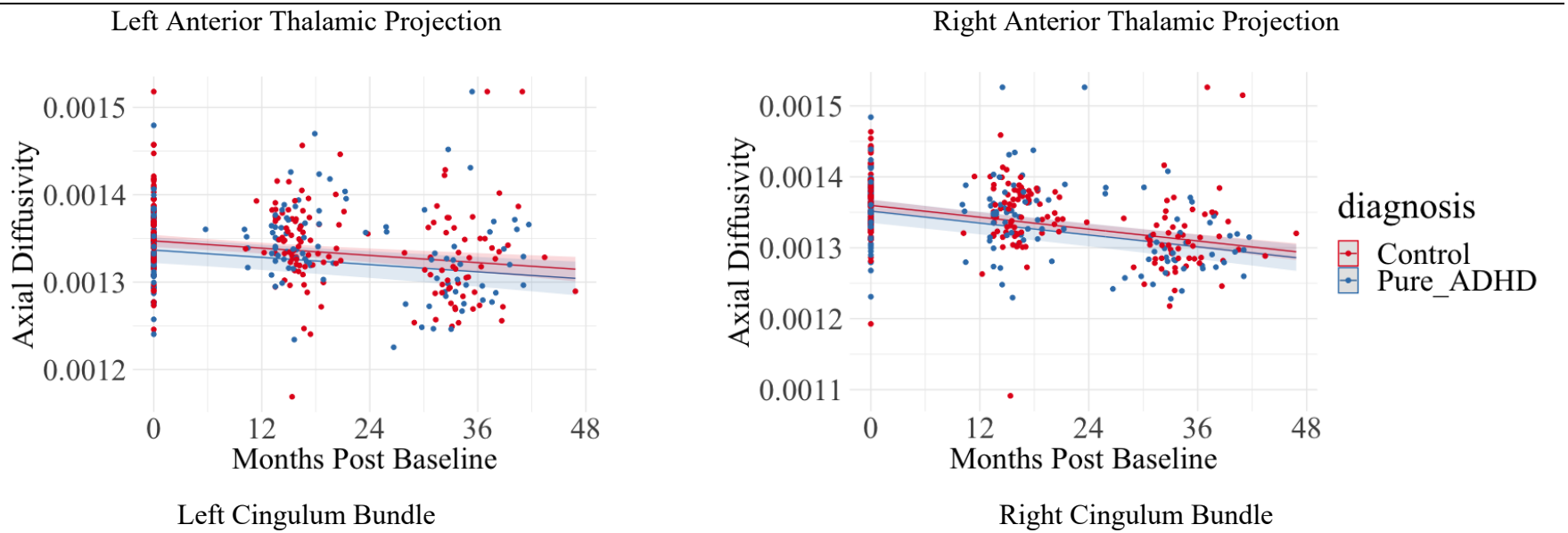

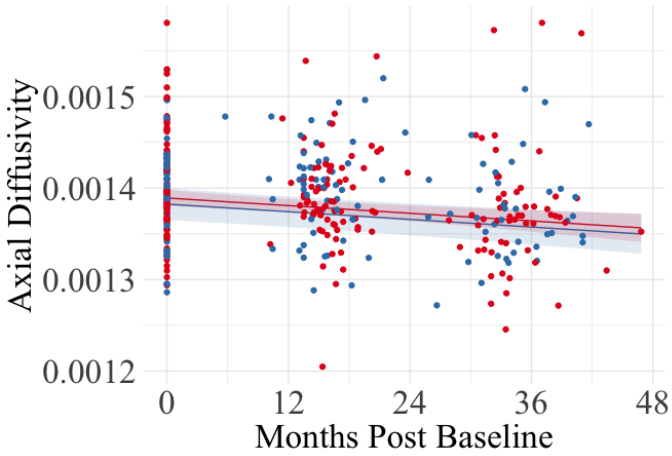

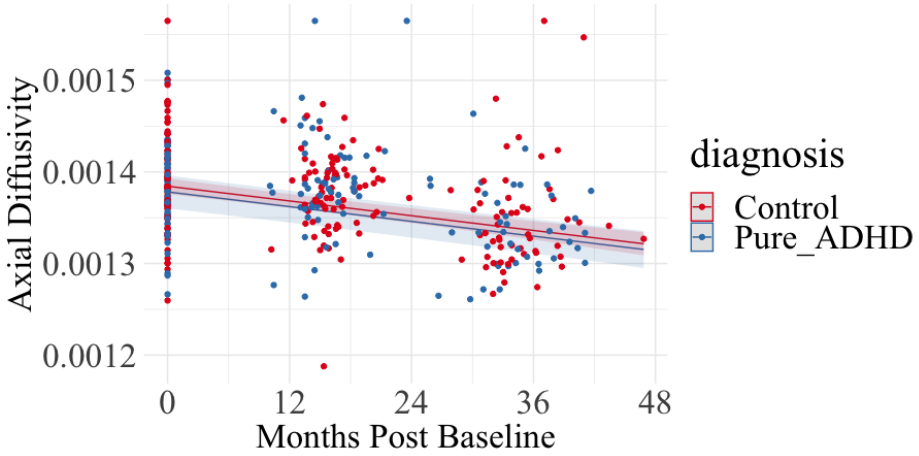

Left Fornix

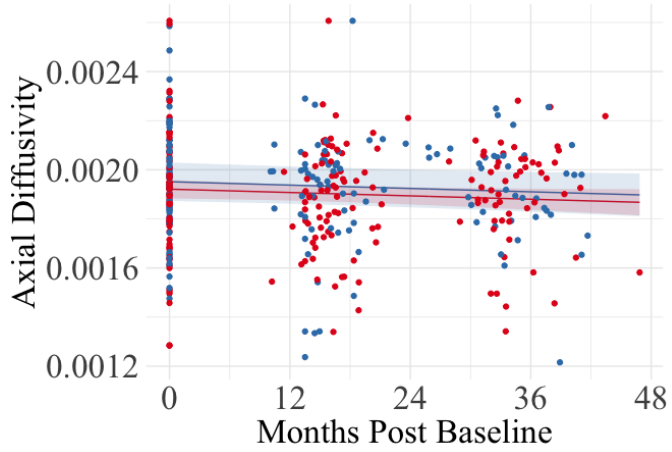

Right Fornix

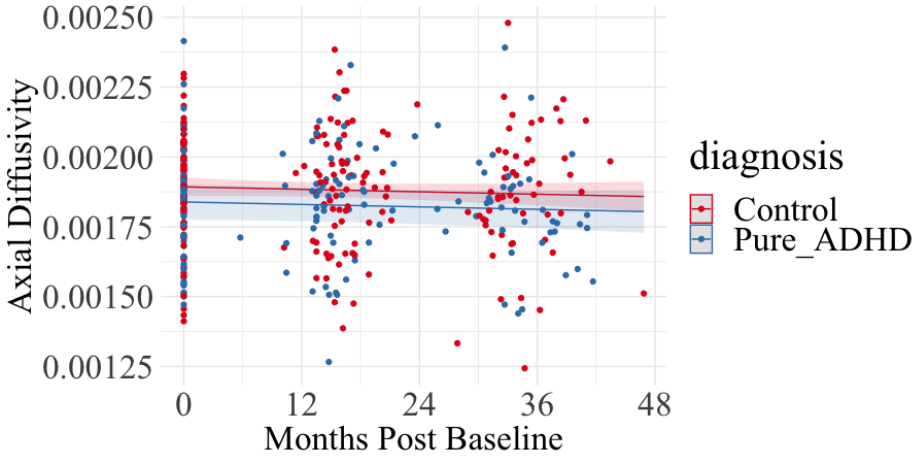

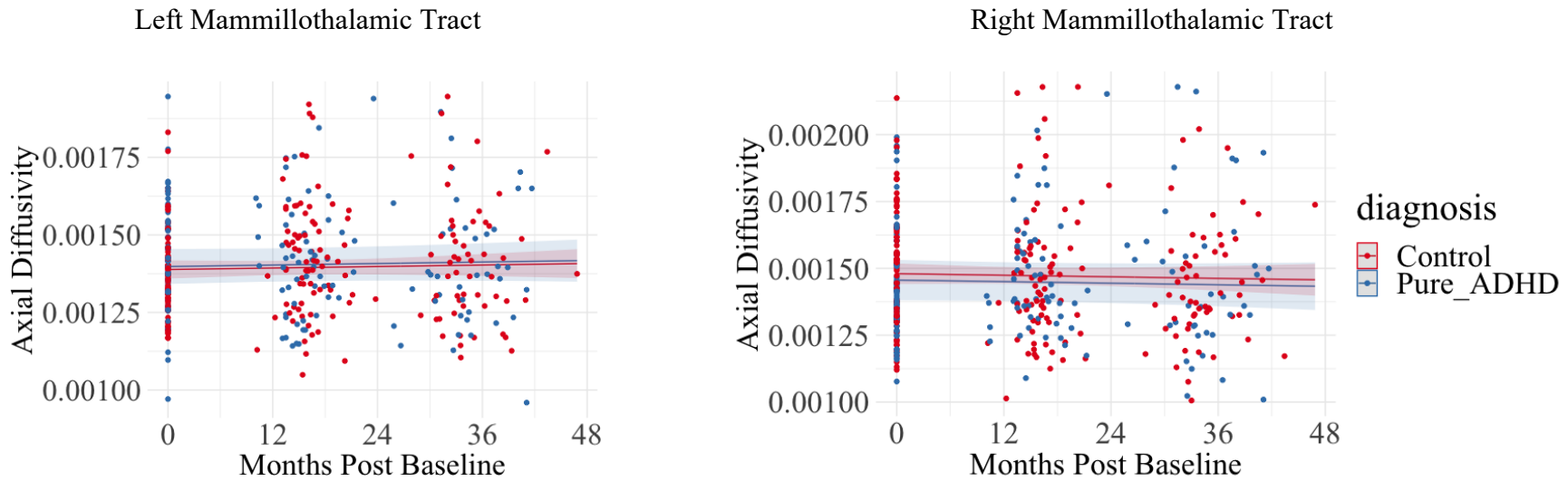
Left Mammillothalamic Tract
Axial Diffusivity
0.00175
0.00150
0.00125
0.00100
0
12
24
36
48
Months Post Baseline
Right Mammillothalamic Tract
Axial Diffusivity
0.00200
0.00175
0.00150
0.00125
0.00100
0
12
24
36
48
Months Post Baseline
diagnosis
Control
Pure_ADHD

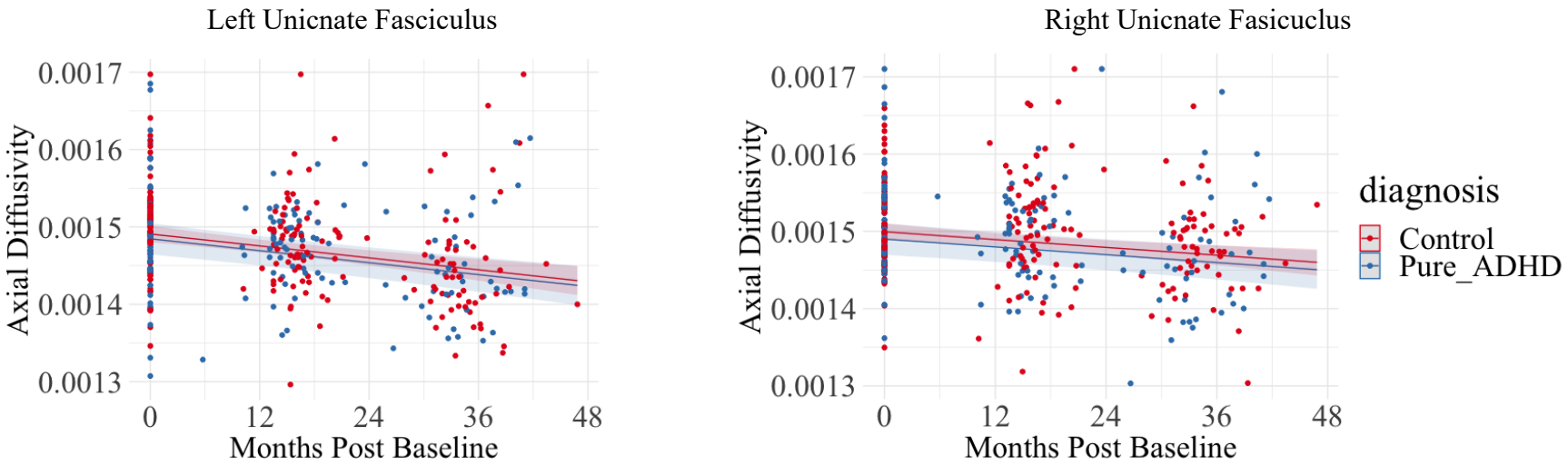
Left Unicnate Fasciculus
Axial Diffusivity
0.0017
0.0016
0.0015
0.0014
0.0013
0
12
24
36
48
Months Post Baseline
Right Unicnate Fasicuclus
Axial Diffusivity
0.0017
0.0016
0.0015
0.0014
0.0013
0
12
24
36
48
Months Post Baseline
diagnosis
Control
Pure_ADHD

Figure 5.17 White matter that had no significant between-group difference in RD across the three-study time points.

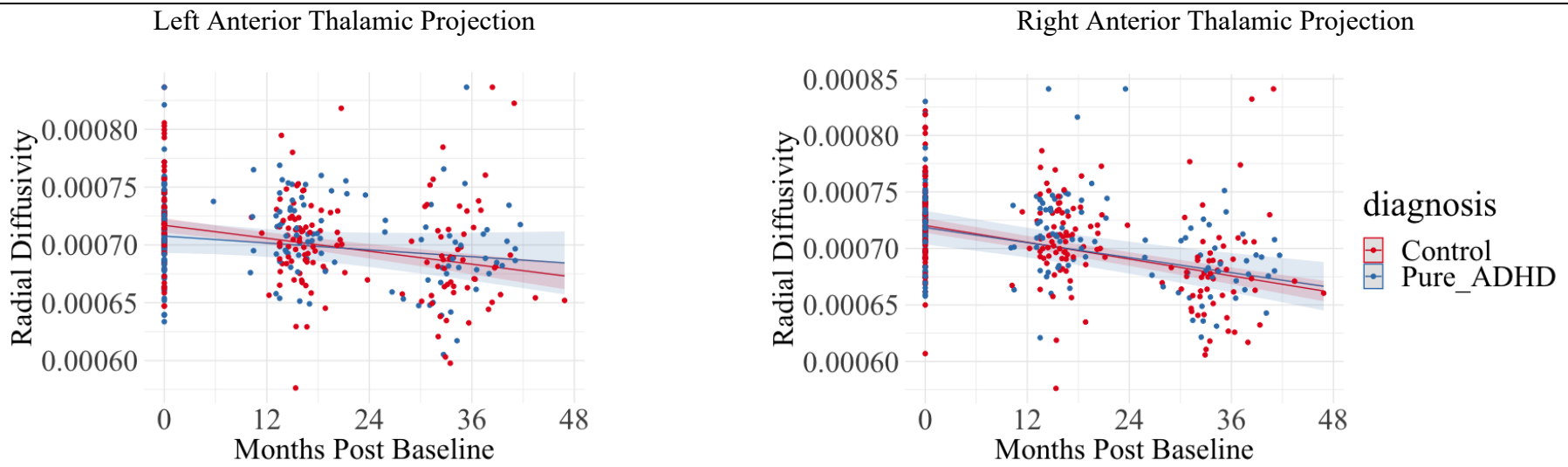

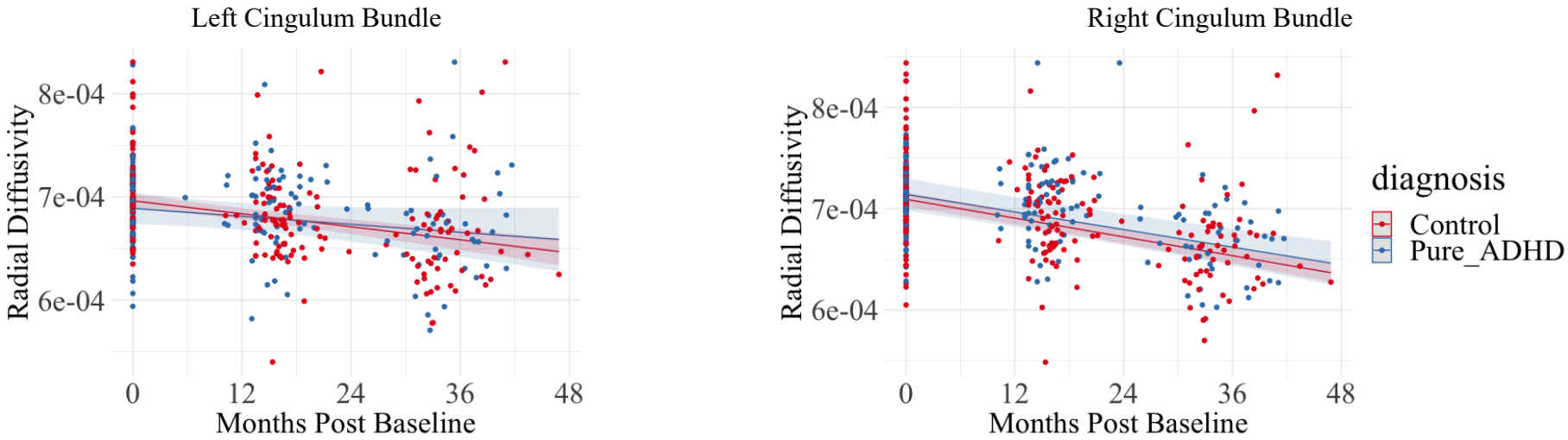
Left Cingulum Bundle
Right Cingulum Bundle
Radial Diffusivity
8e-04
7e-04
6e-04
0
12
24
36
48
Months Post Baseline
diagnosis
Control
Pure_ADHD

Left Fornix

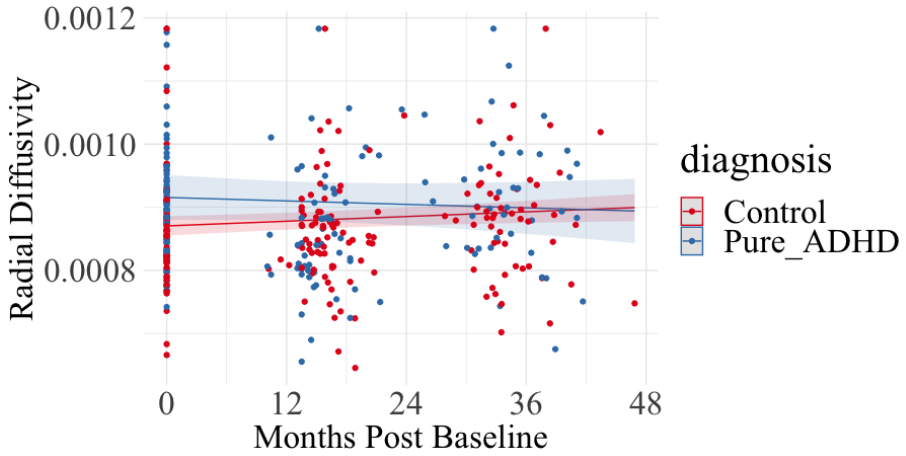

Left Mammillothalamic Tract

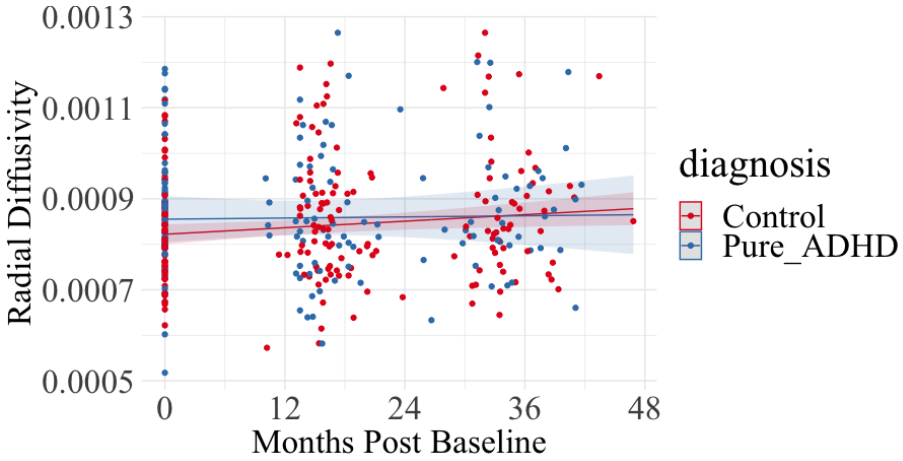

Right Mammillothalamic Tract

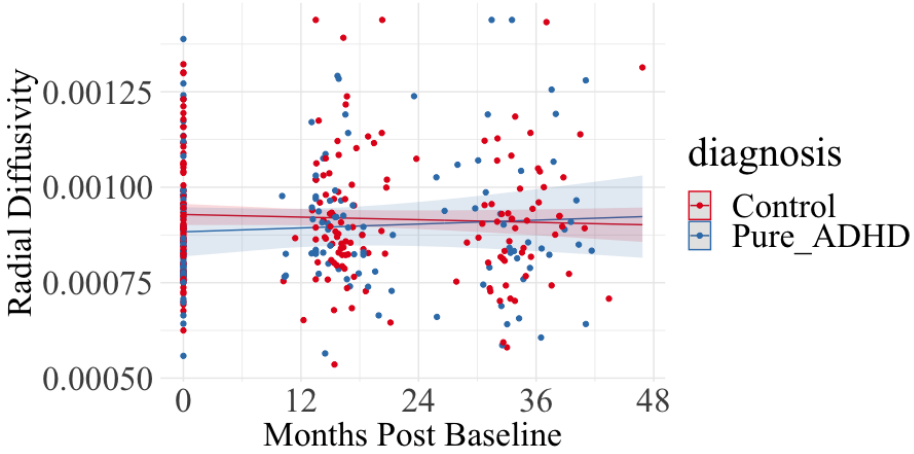

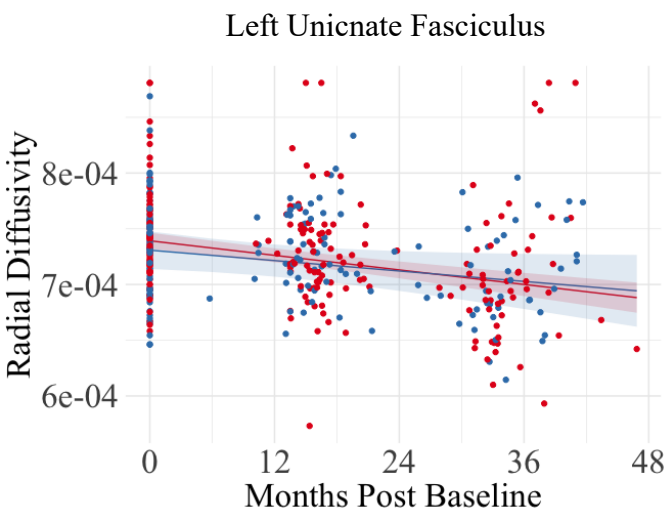
Left Unicnate Fasciculus
Radial Diffusivity
8e-04
7e-04
6e-04
0
12
24
36
48
Months Post Baseline

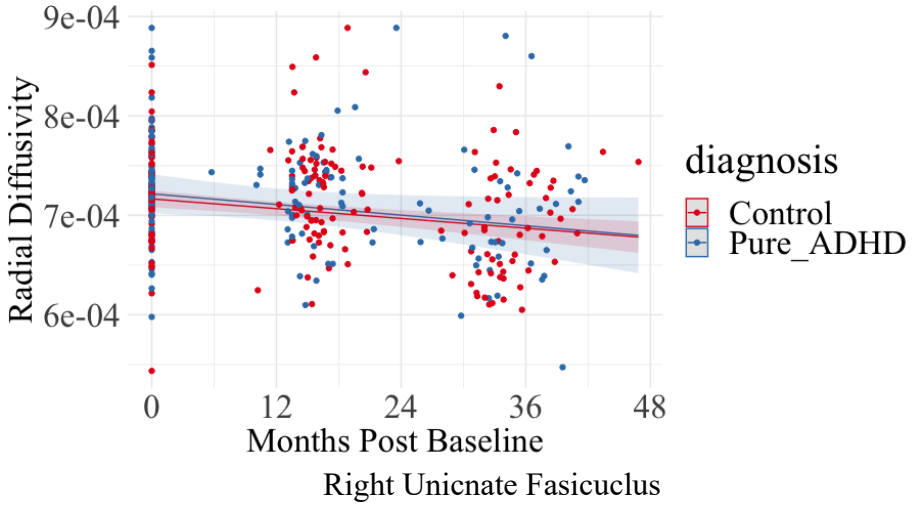
9e-04
8e-04
7e-04
6e-04
Radial Diffusivity
0
12
24
36
48
Months Post Baseline
Right Unicnate Fasicuclus
diagnosis
Control
Pure_ADHD

Figure 5.18 Scatter plot of non-significant limbic system white matter AK by CAI scores in ADHD.

Left Anterior Thalamic Projections	Right Anterior Thalamic Projections
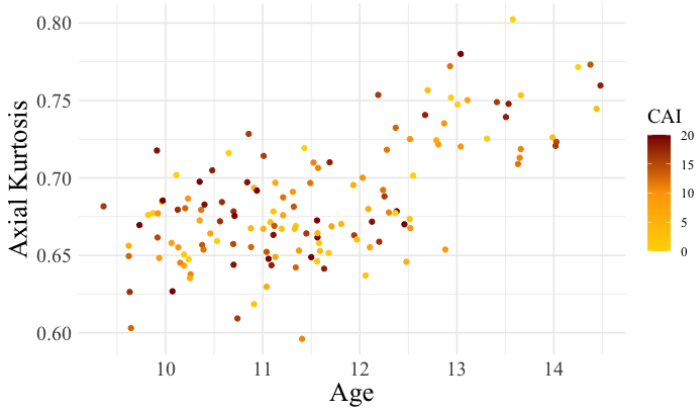	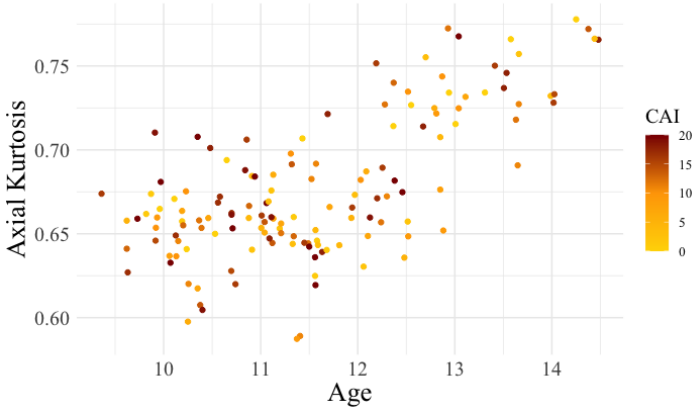
Left Fornix	Right Fornix

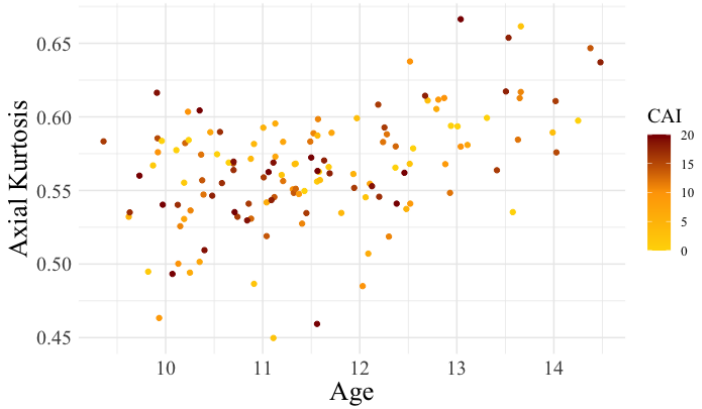

Left Uncinate Fasciculus

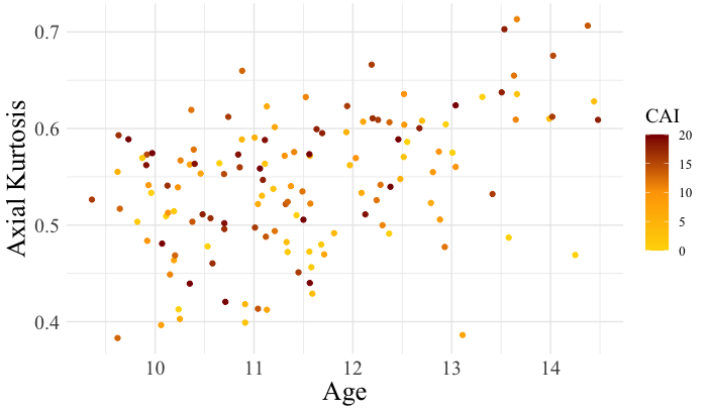

Right Uncinate Fasciculus

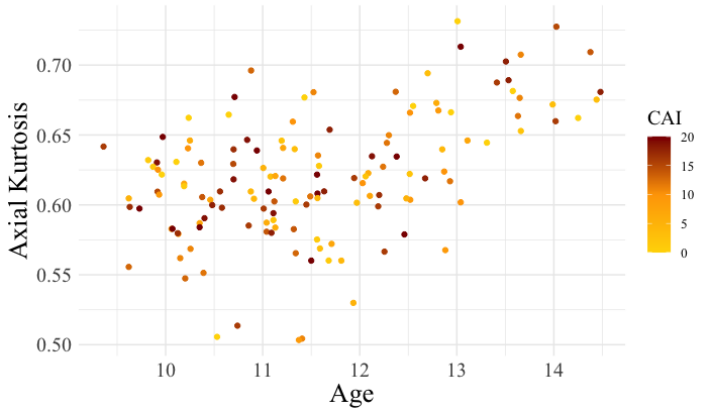

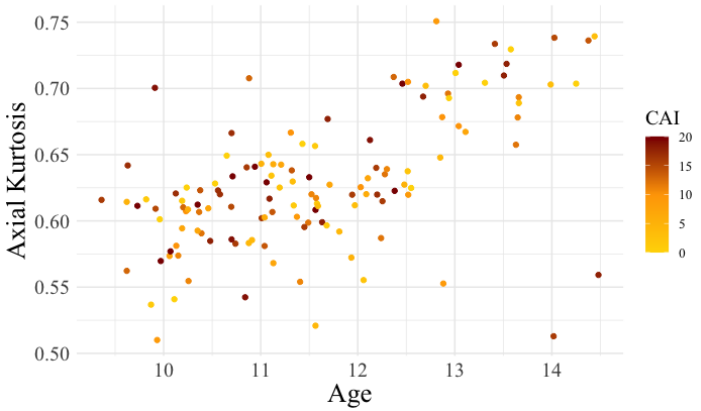

Left Mammillothalamic Tract	Right Mammillothalamic Tract
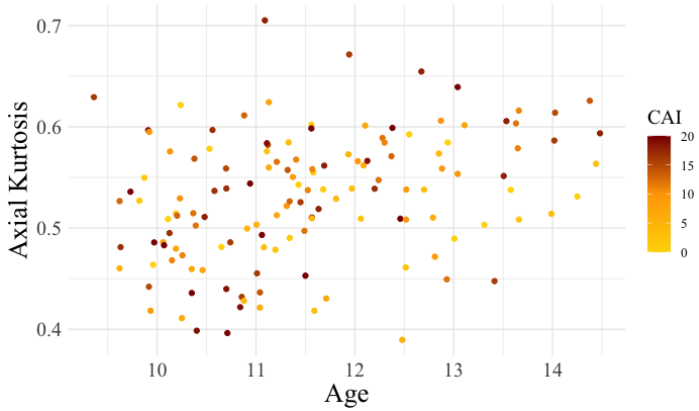	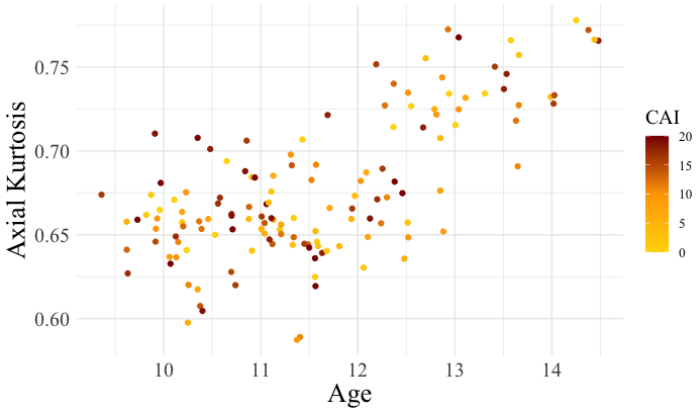
Left Cingulum Bundle	Right Cingulum Bundle

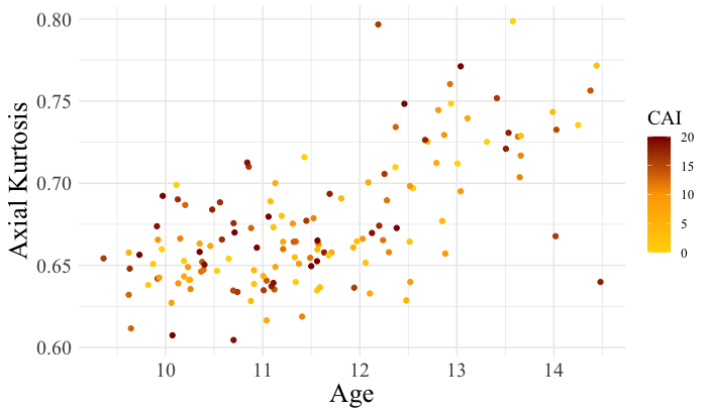
Axial Kurtosis
0.80
0.75
0.70
0.65
0.60
10
11
12
13
14
Age
CAI
20
15
10
5
0

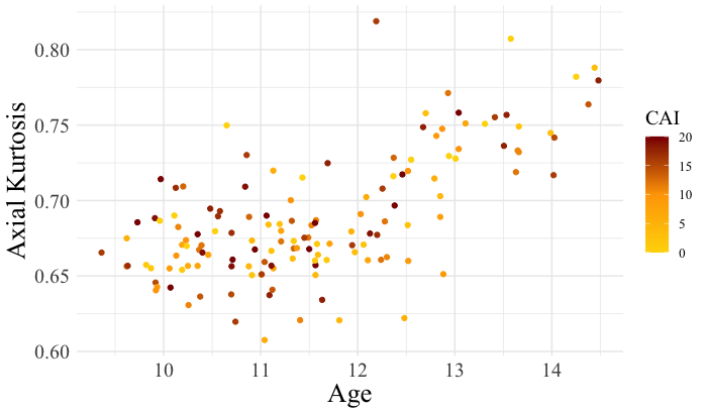
Axial Kurtosis
0.80
0.75
0.70
0.65
0.60
10
11
12
13
14
Age
CAI
20
15
10
5
0

Figure 5.19 Scatter plot of non-significant limbic system white matter KA by CAI scores in ADHD.

Left Anterior Thalamic Projections	Right Anterior Thalamic Projections
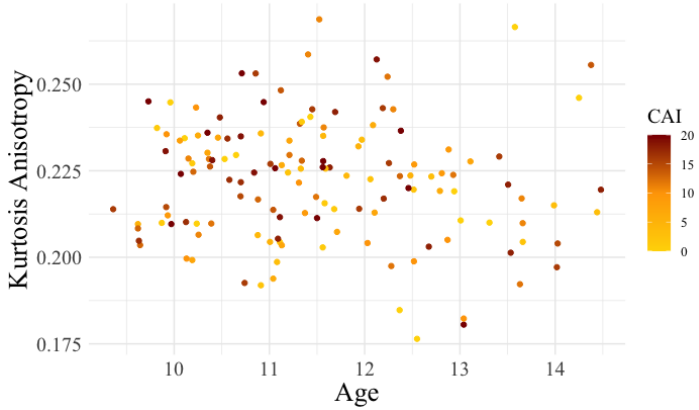	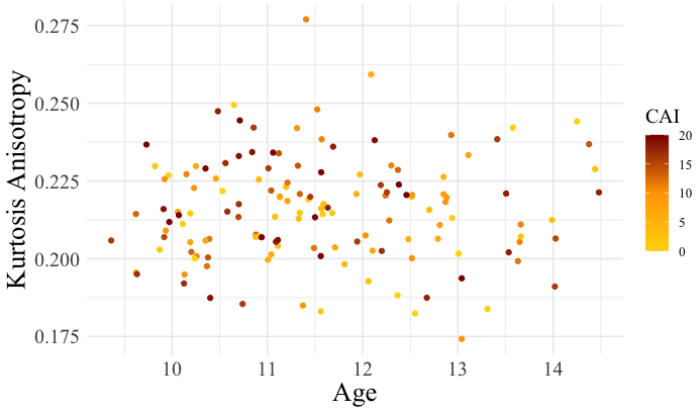
Left Fornix	Right Fornix

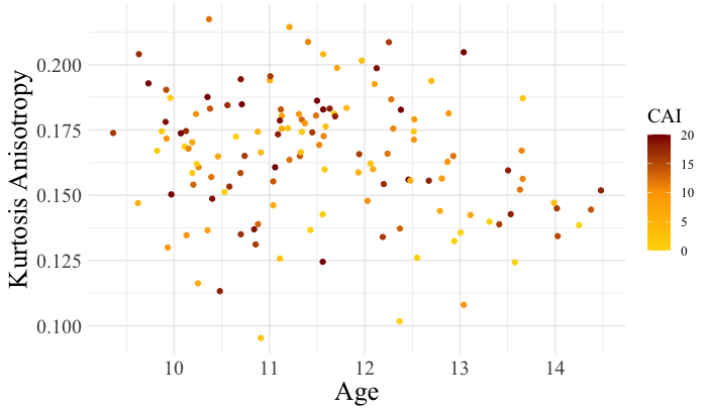

Left Uncinate Fasciculus

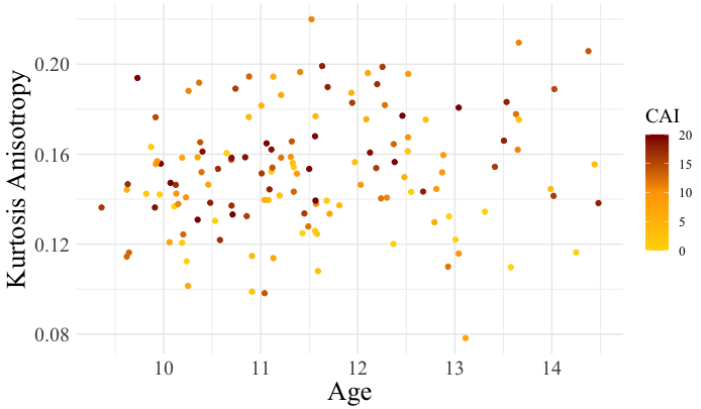

Right Uncinate Fasciculus

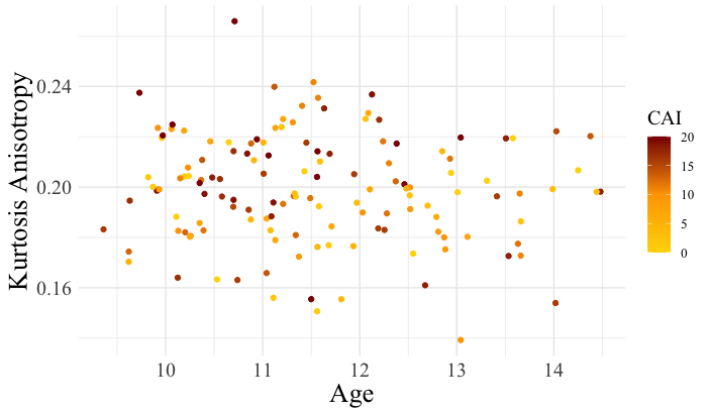

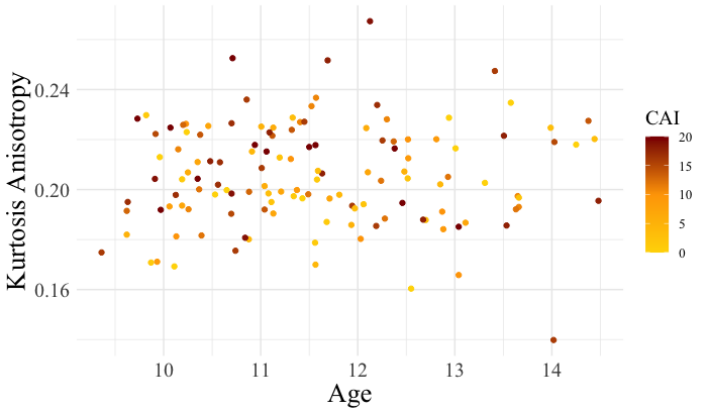

Left Mammillothalamic Tract	Right Mammillothalamic Tract
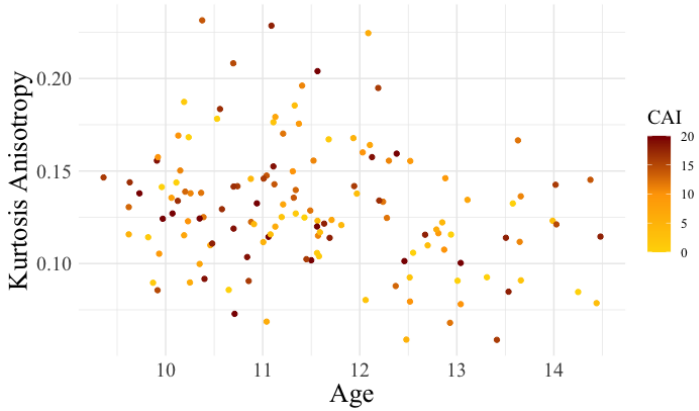	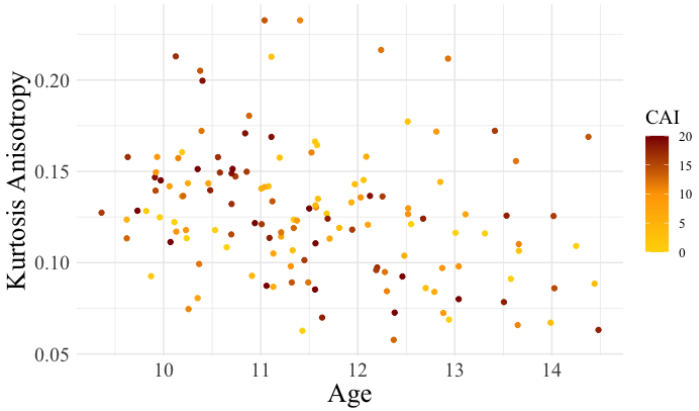
Left Cingulum Bundle	Right Cingulum Bundle

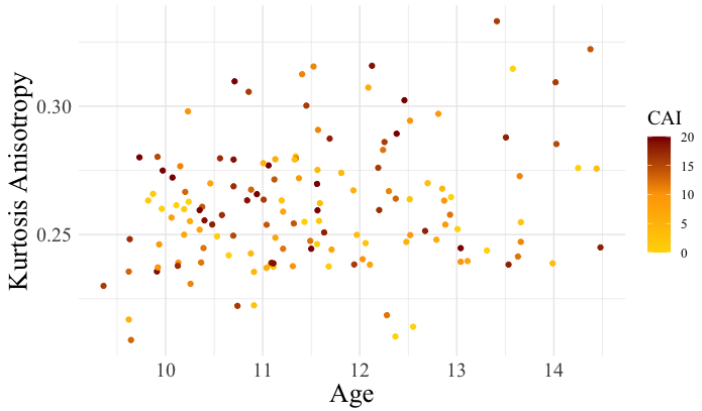
Kurtosis Anisotropy
0.30
0.25
10
11
12
13
14
Age
CAI
20
15
10
5
0

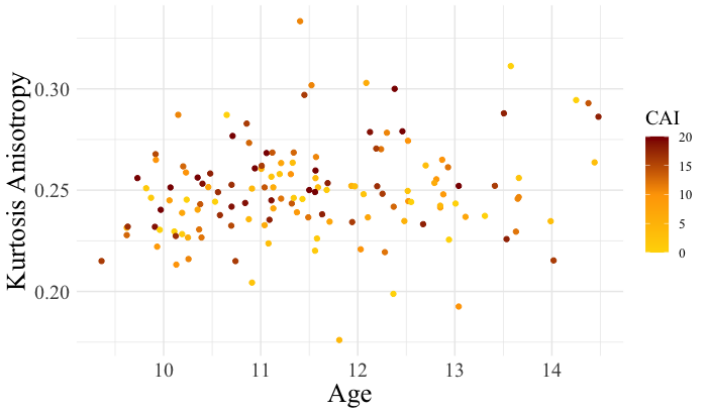
Kurtosis Anisotropy
0.30
0.25
0.20
10
11
12
13
14
Age
CAI
20
15
10
5
0

Figure 5.20 Scatter plot of non-significant limbic system white matter MK by CAI scores in ADHD.

Left Anterior Thalamic Projections	Right Anterior Thalamic Projections
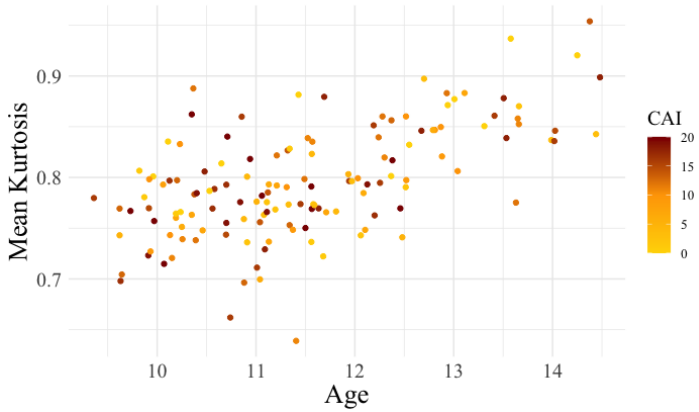	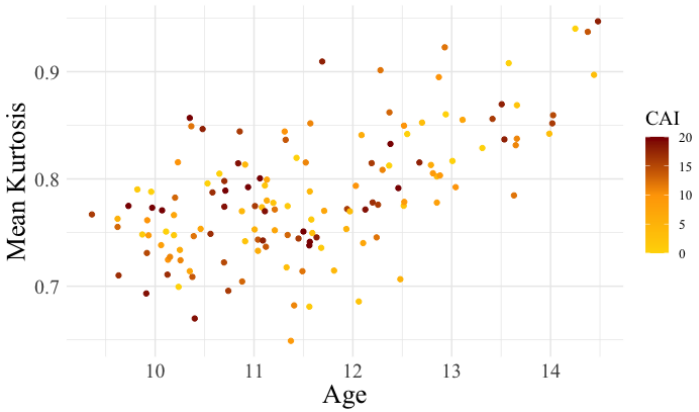
Left Fornix	Right Fornix

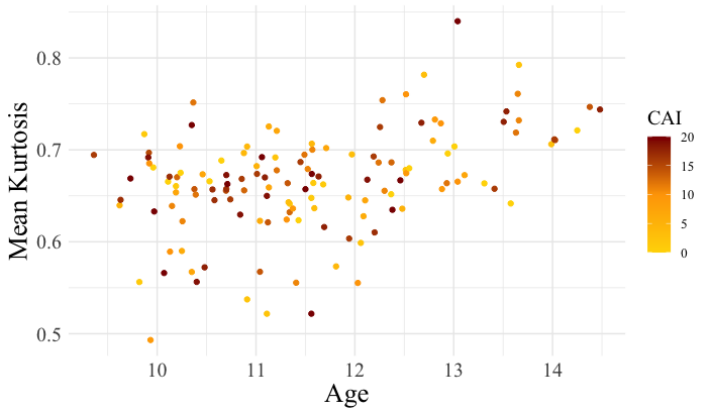

Left Uncinate Fasciculus

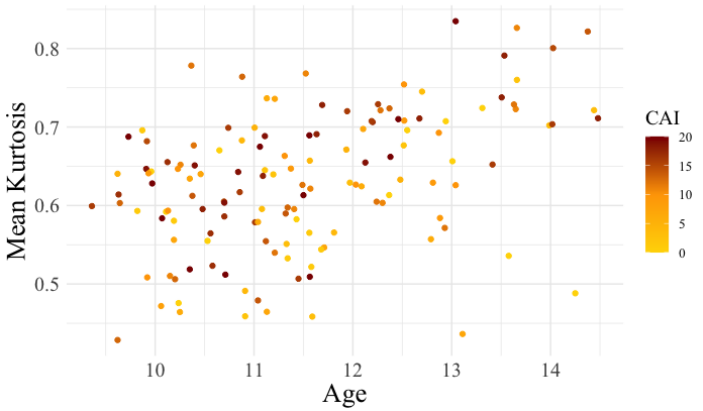

Right Uncinate Fasciculus

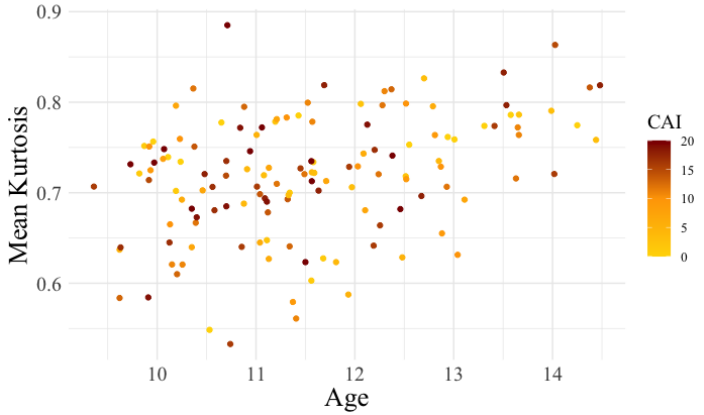

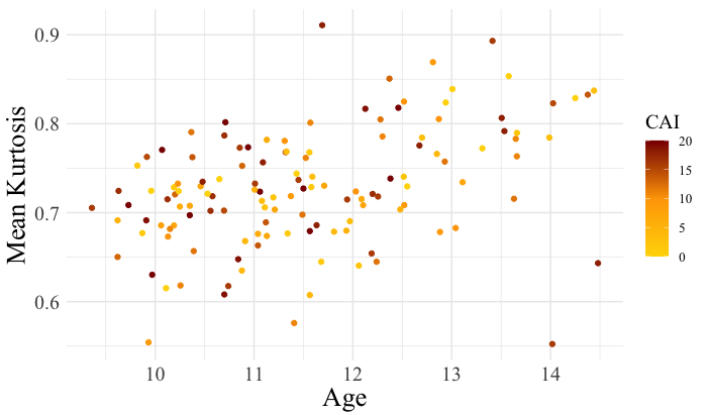

Left Mammillothalamic Tract	Right Mammillothalamic Tract
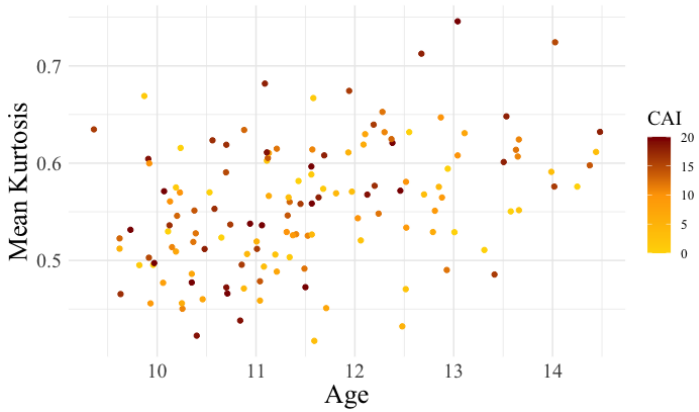	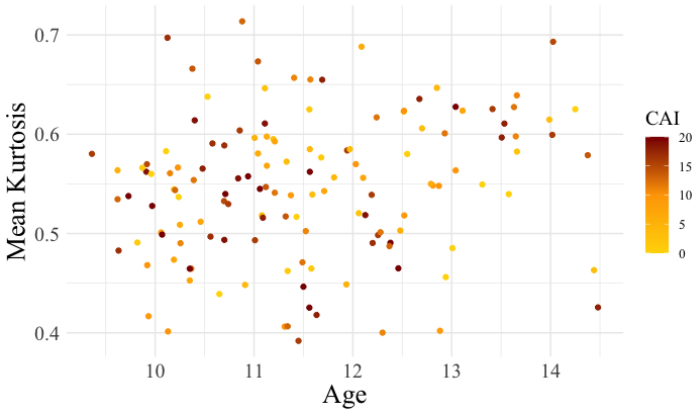
Left Cingulum Bundle	Right Cingulum Bundle

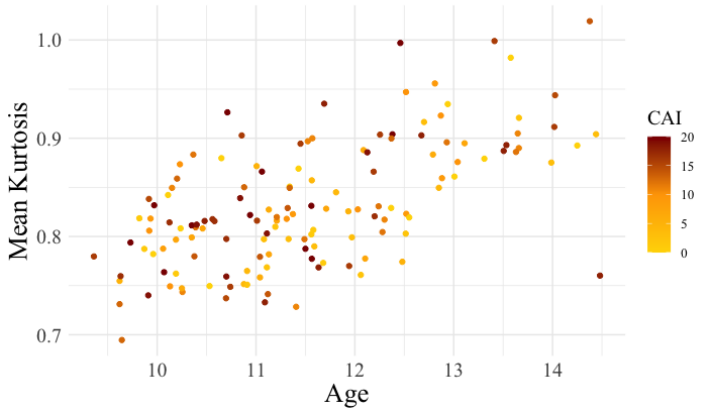
Mean Kurtosis
1.0
0.9
0.8
0.7
10
11
12
13
14
Age
CAI
20
15
10
5
0

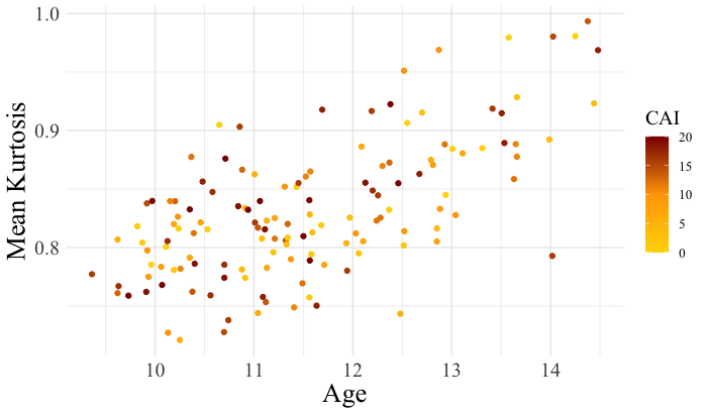
Mean Kurtosis
1.0
0.9
0.8
10
11
12
13
14
Age
CAI
20
15
10
5
0

Figure 5.21 Scatter plot of non-significant limbic system white matter RK by CAI scores in ADHD.

Left Anterior Thalamic Projections	Right Anterior Thalamic Projections
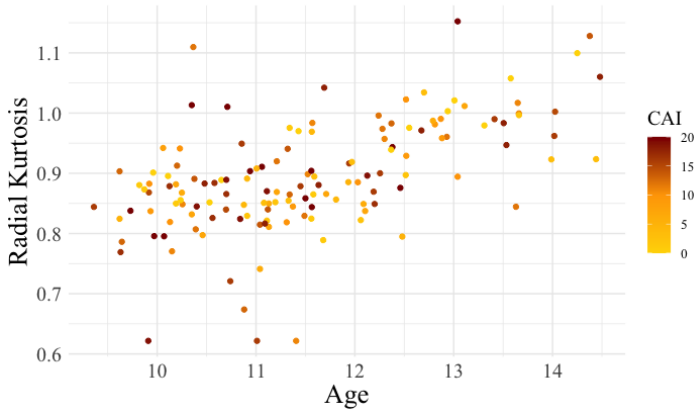	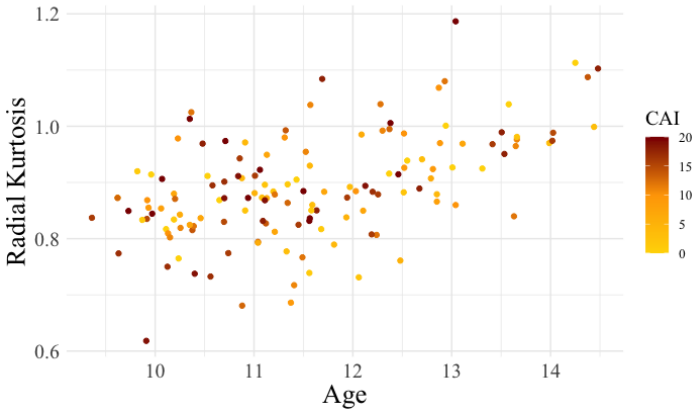
Left Fornix	Right Fornix

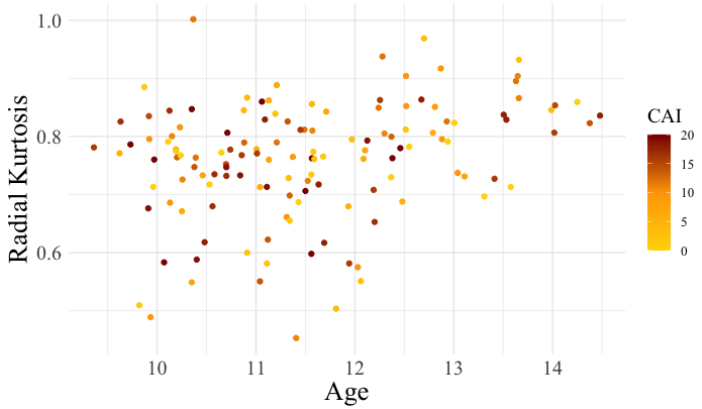

Left Uncinate Fasciculus

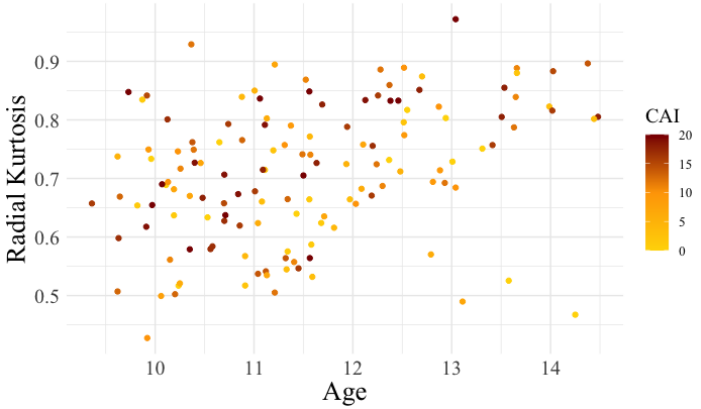

Right Uncinate Fasciculus

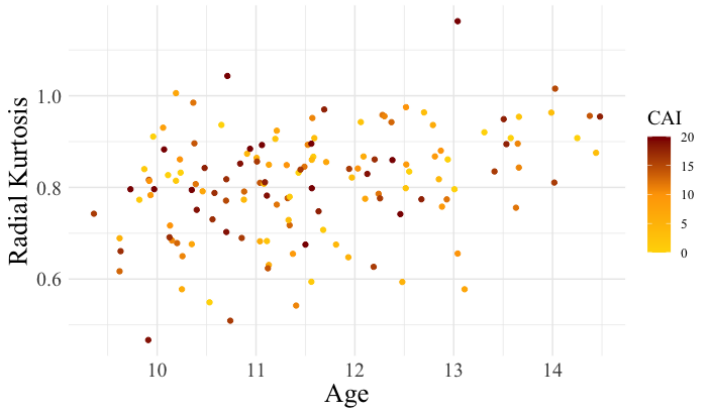

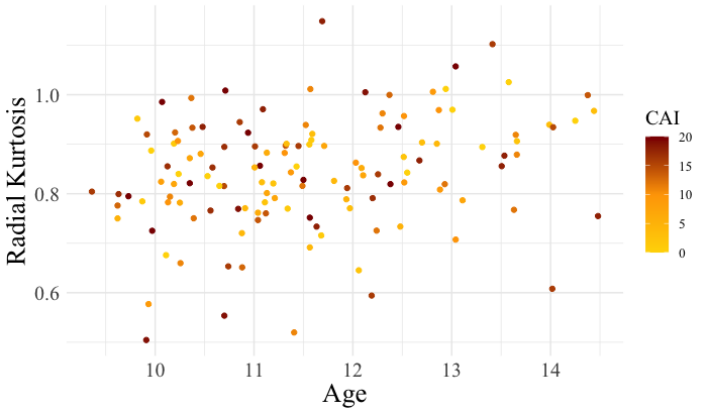

Left Mammillothalamic Tract	Right Mammillothalamic Tract
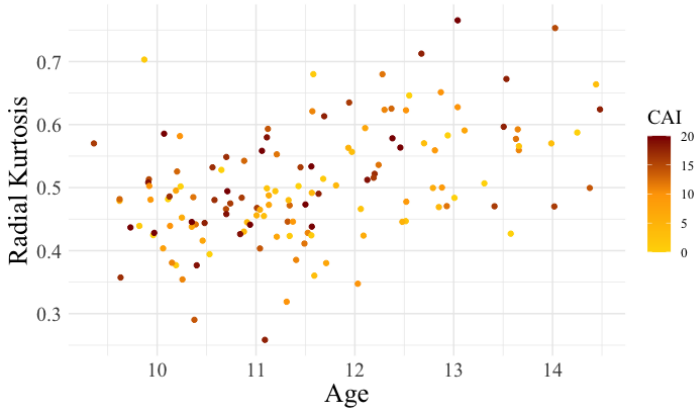	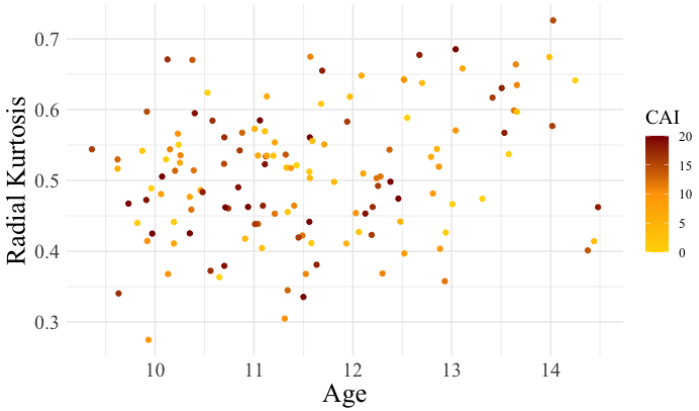
Left Cingulum Bundle	Right Cingulum Bundle

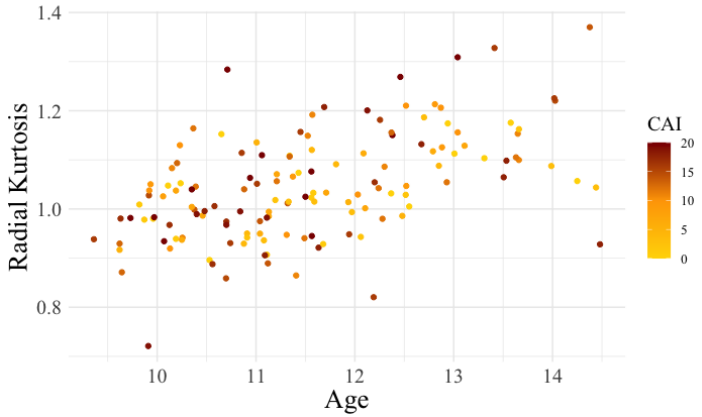
Radial Kurtosis
1.4
1.2
1.0
0.8
10
11
12
13
14
Age
CAI
20
15
10
5
0

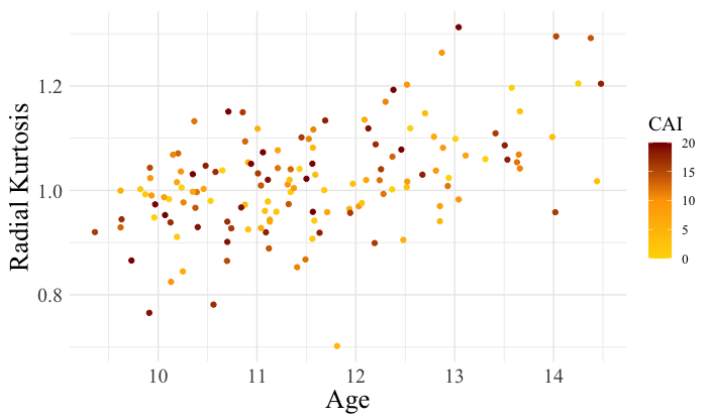
Radial Kurtosis
1.2
1.0
0.8
10
11
12
13
14
Age
CAI
20
15
10
5
0

Figure 5.22 Scatter plot of non-significant limbic system white matter AD by CAI scores in ADHD.

Left Anterior Thalamic Projections	Right Anterior Thalamic Projections
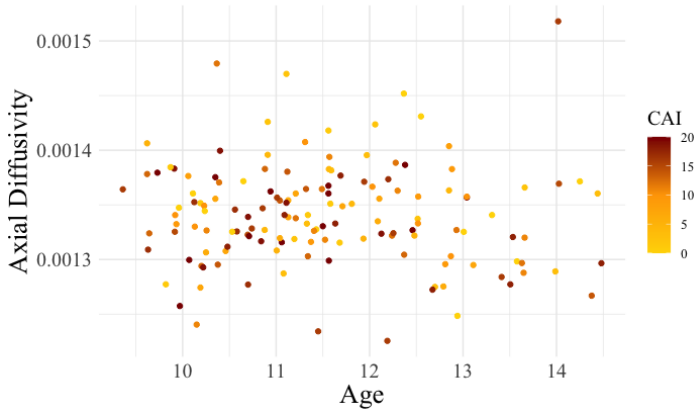	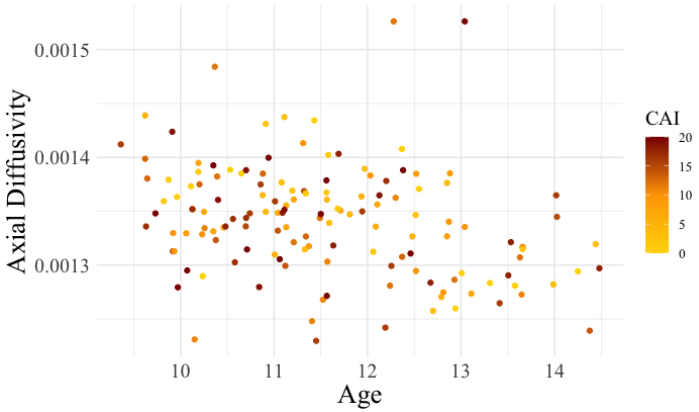
Left Fornix	Right Fornix

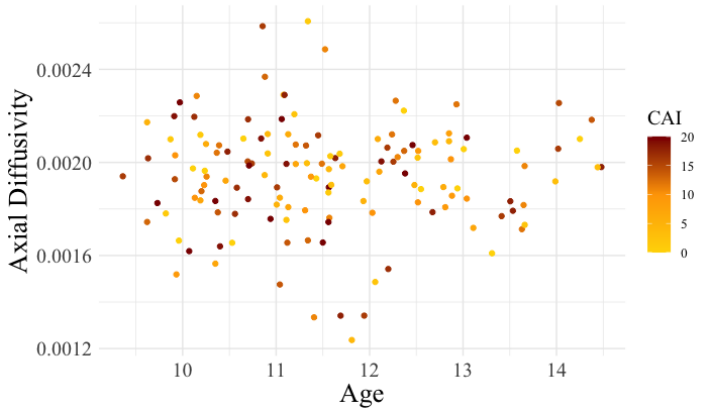

Left Uncinate Fasciculus

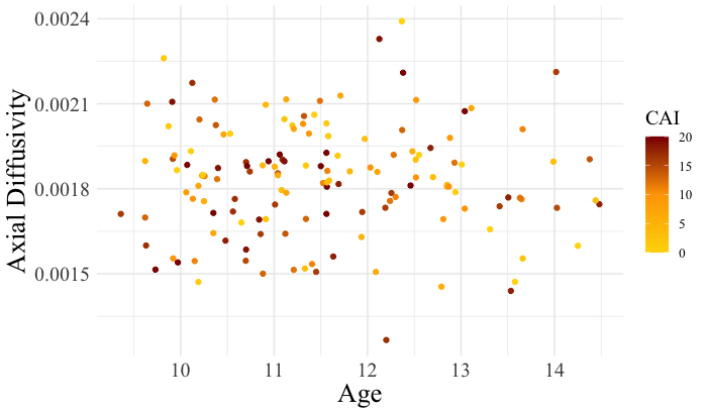

Right Uncinate Fasciculus

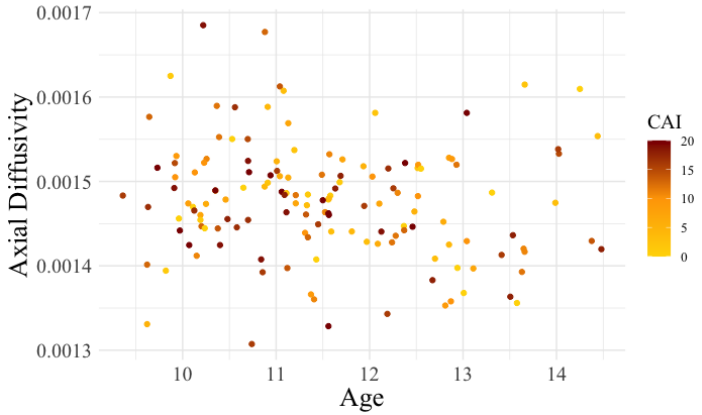

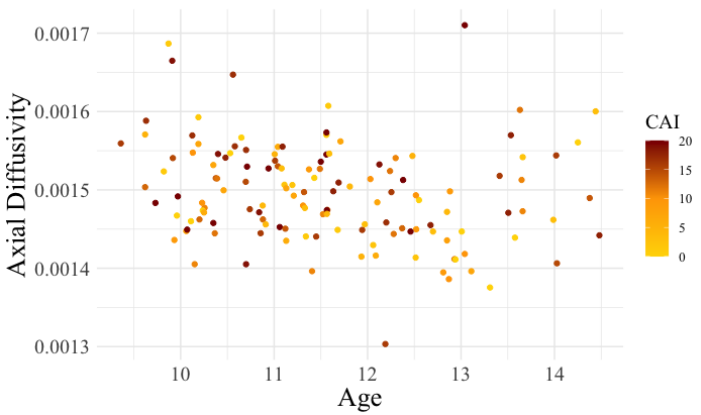

Left Mammillothalamic Tract	Right Mammillothalamic Tract
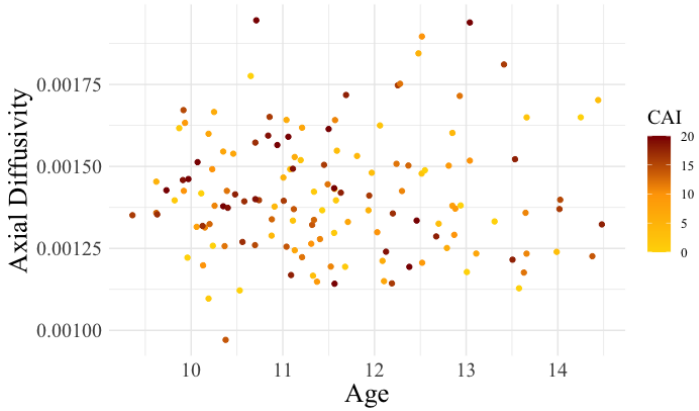	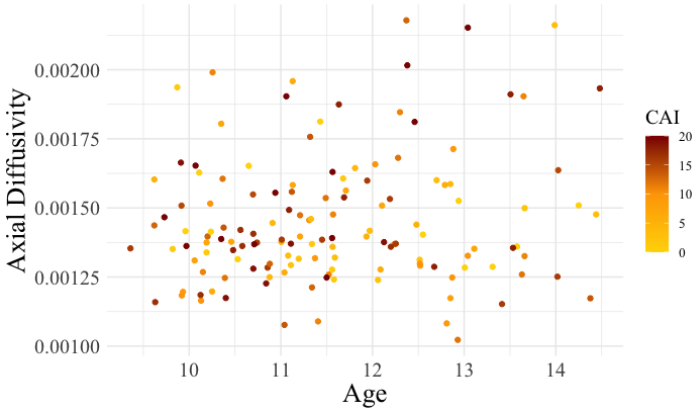
Left Cingulum Bundle	Right Cingulum Bundle

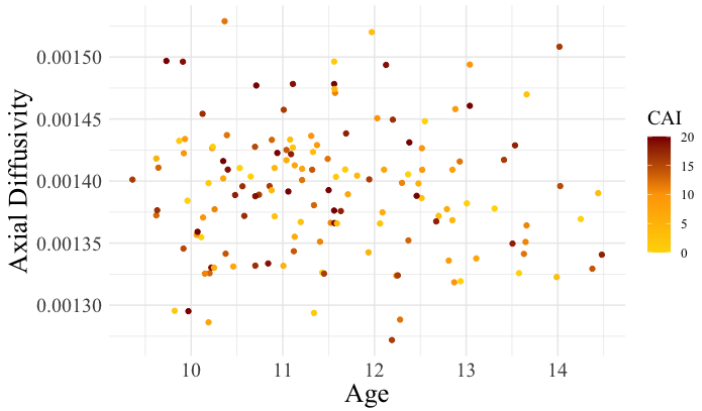
Axial Diffusivity
0.00150
0.00145
0.00140
0.00135
0.00130
10
11
12
13
14
Age
CAI
20
15
10
5
0

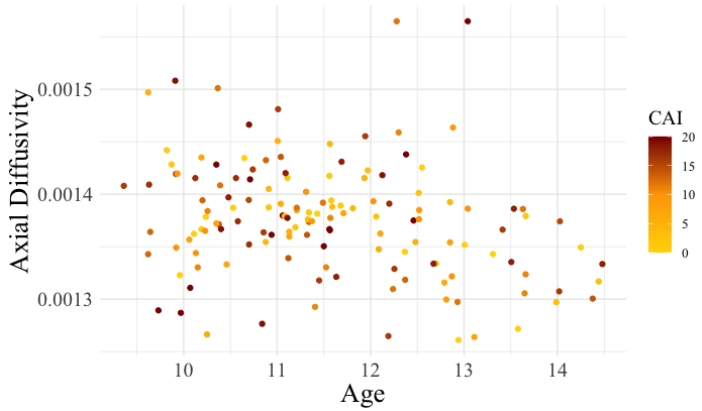
Axial Diffusivity
0.0015
0.0014
0.0013
10
11
12
13
14
Age
CAI
20
15
10
5
0

Figure 5.23 Scatter plot of non-significant limbic system white matter FA by CAI scores in ADHD.

Left Anterior Thalamic Projections	Right Anterior Thalamic Projections
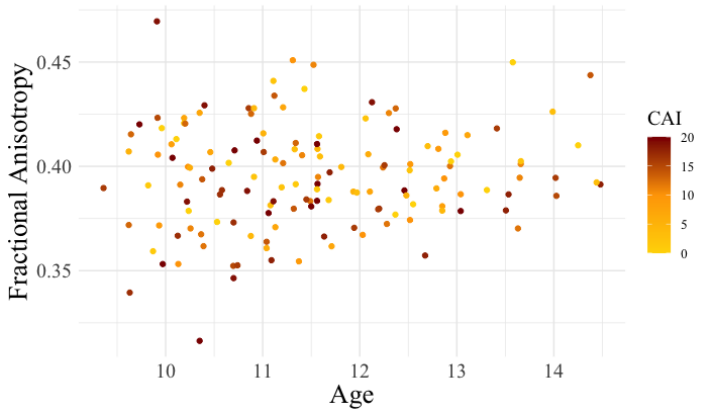	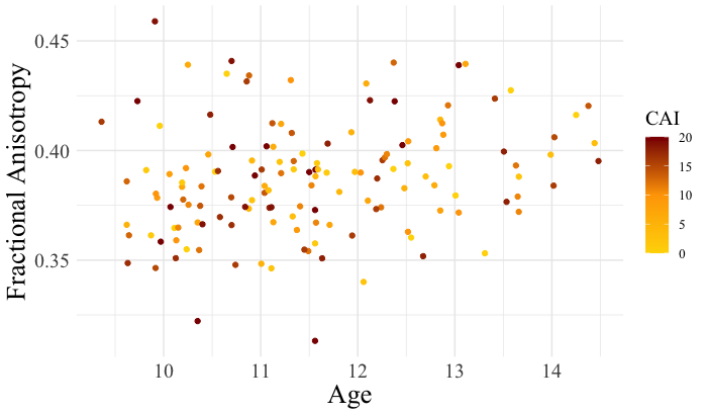
Left Fornix	Right Fornix

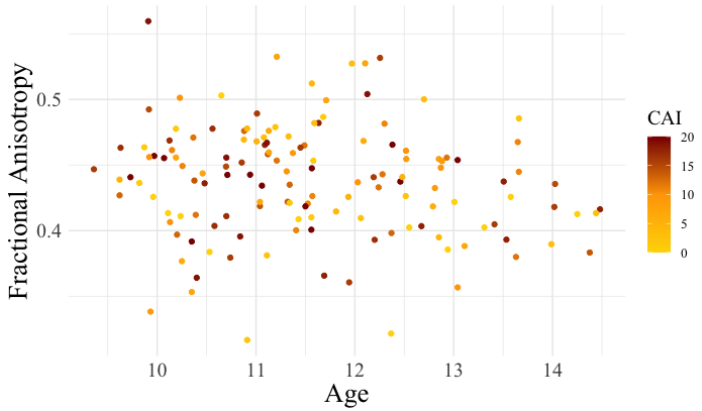

Left Uncinate Fasciculus

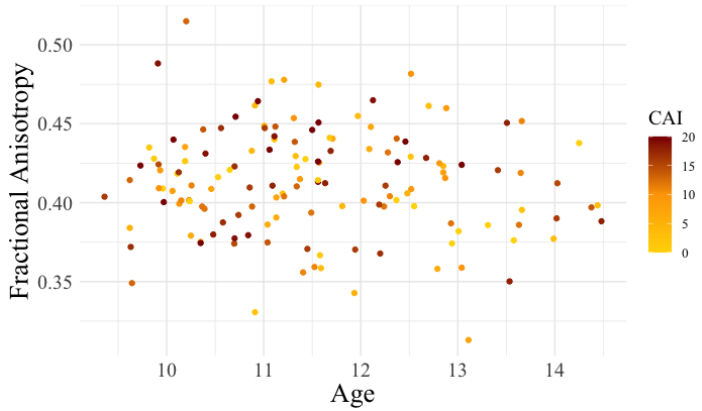

Right Uncinate Fasciculus

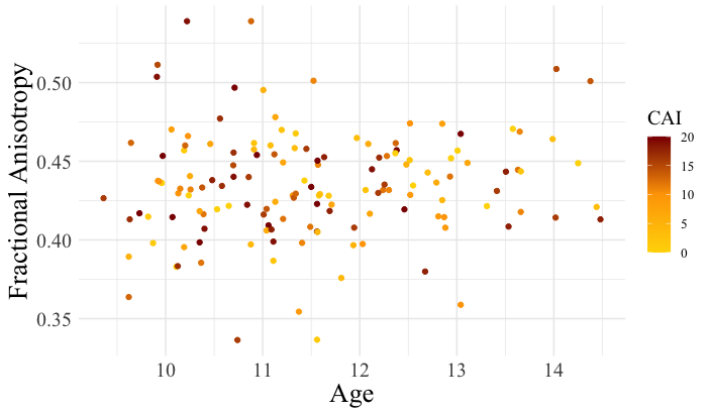

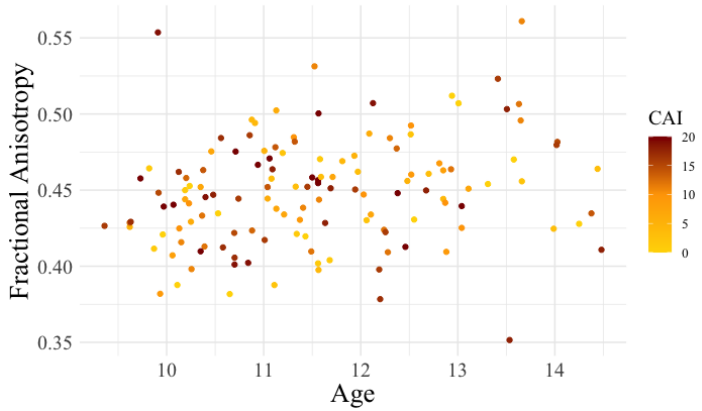

Left Mammillothalamic Tract	Right Mammillothalamic Tract
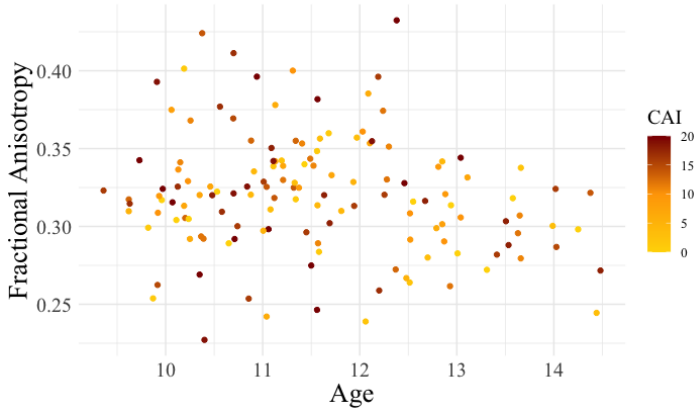	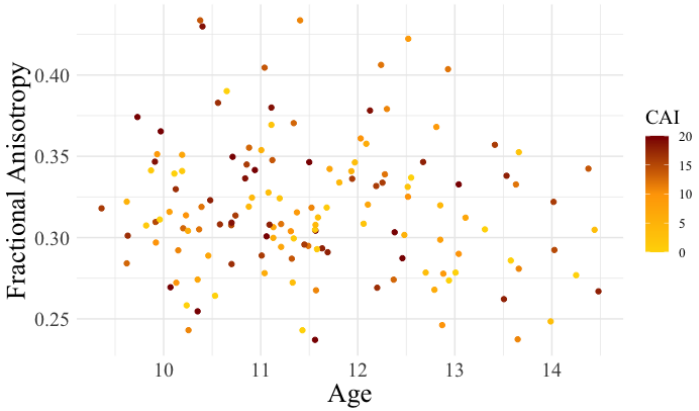
Left Cingulum Bundle	Right Cingulum Bundle

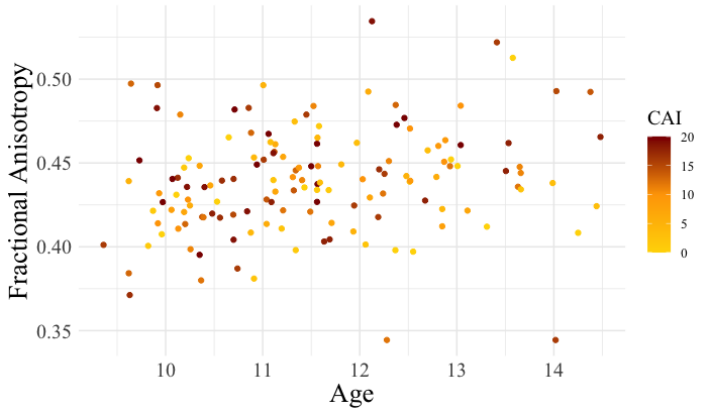
Fractional Anisotropy
0.50
0.45
0.40
0.35
10
11
12
13
14
Age
CAI
20
15
10
5
0

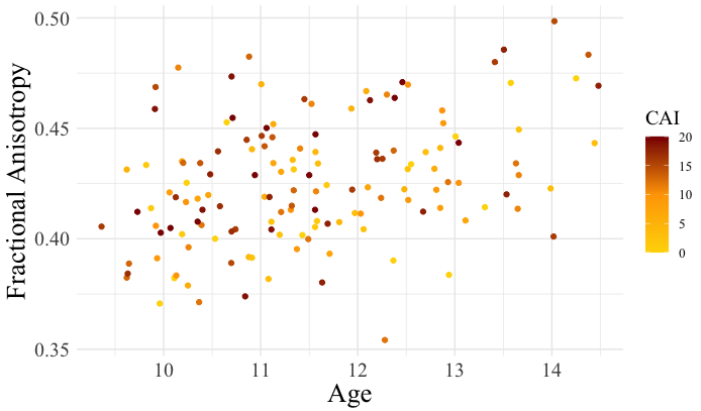
Fractional Anisotropy
0.50
0.45
0.40
0.35
10
11
12
13
14
Age
CAI
20
15
10
5
0

Figure 5.24 Scatter plot of non-significant limbic system white matter MD by CAI scores in ADHD.

Left Anterior Thalamic Projections	Right Anterior Thalamic Projections
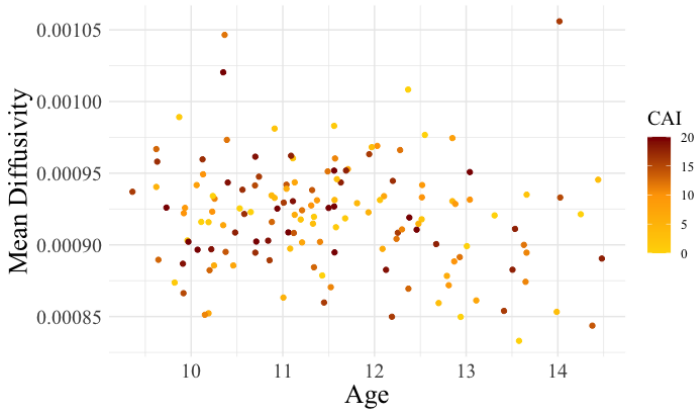	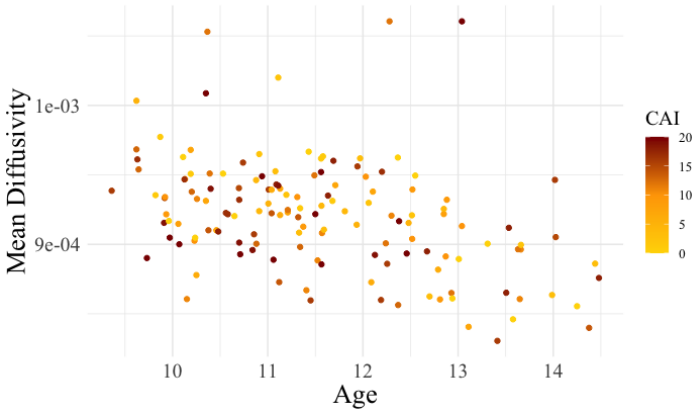
Left Fornix	Right Fornix

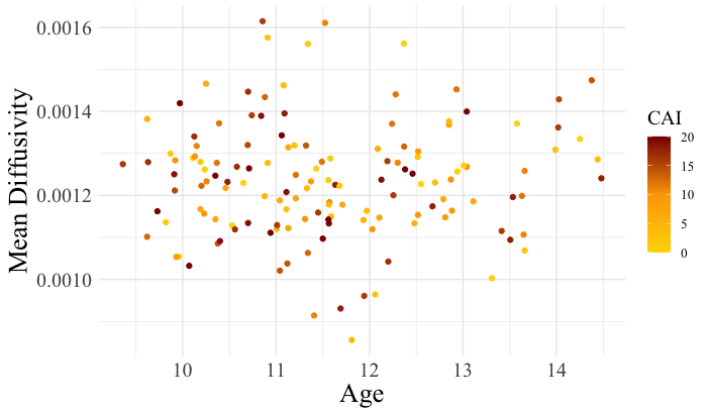

Left Uncinate Fasciculus

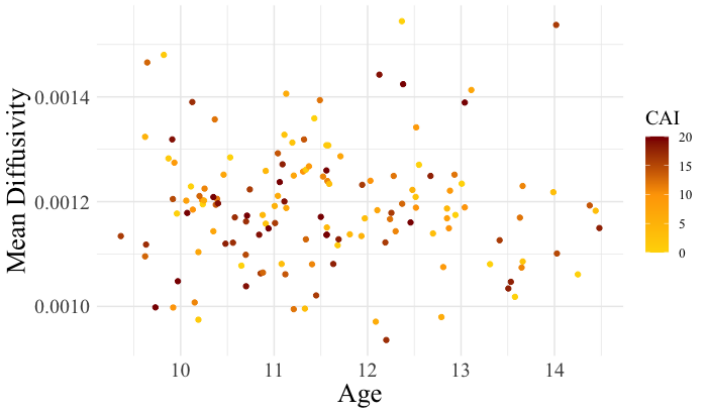

Right Uncinate Fasciculus

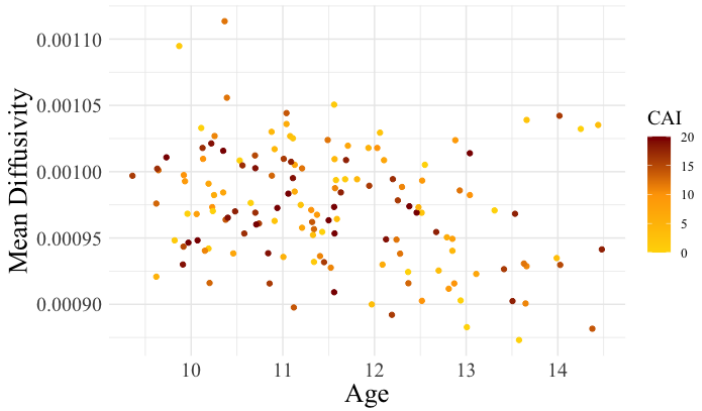

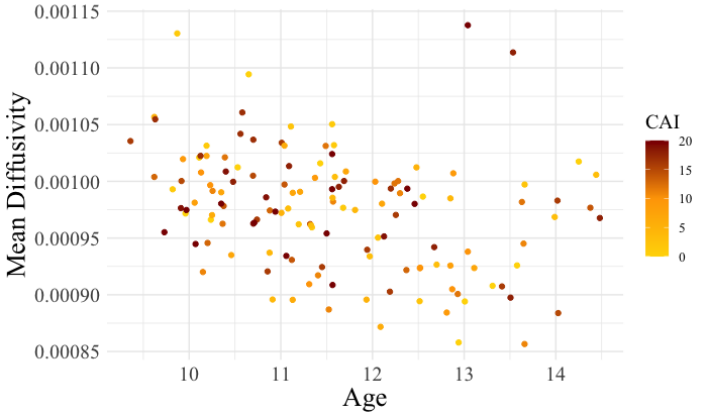

Left Mammillothalamic Tract	Right Mammillothalamic Tract
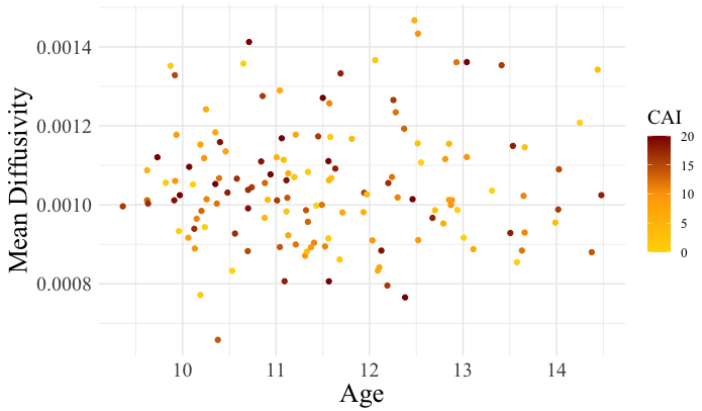	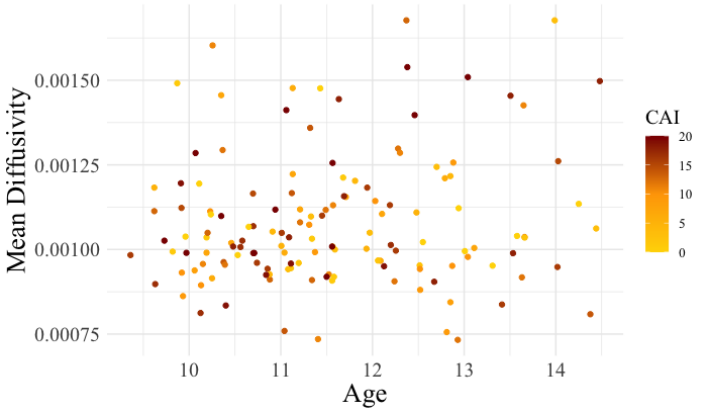
Left Cingulum Bundle	Right Cingulum Bundle

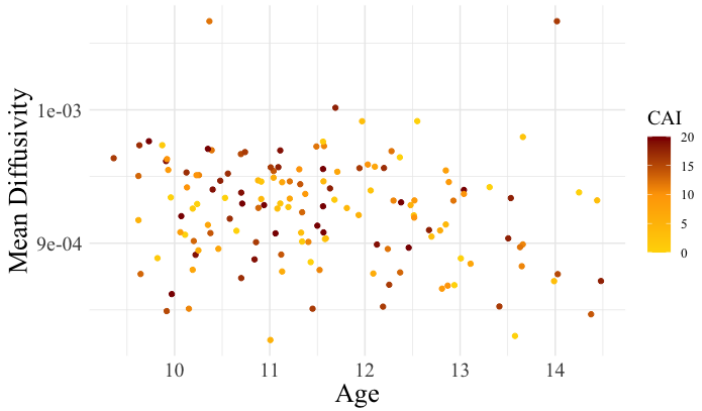
Mean Diffusivity
1e-03
9e-04
10
11
12
13
14
Age
CAI
20
15
10
5
0

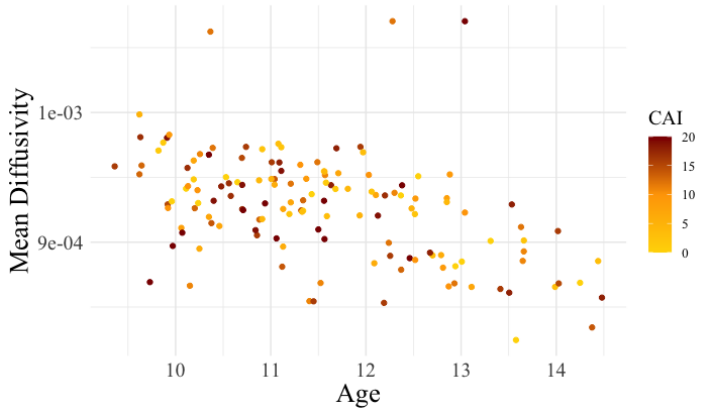
Mean Diffusivity
1e-03
9e-04
10
11
12
13
14
Age
CAI
20
15
10
5
0

Figure 5.25 Scatter plot of non-significant limbic system white matter RD by CAI scores in ADHD.

Left Anterior Thalamic Projections	Right Anterior Thalamic Projections
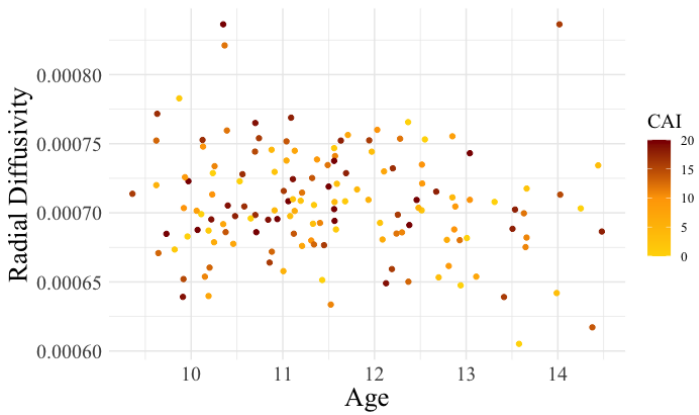	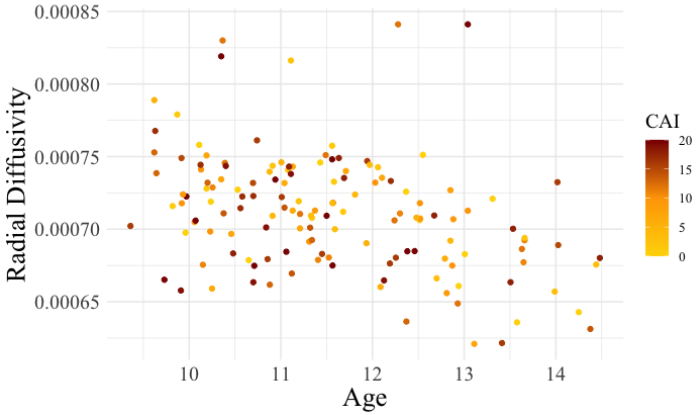
Left Fornix	Right Fornix

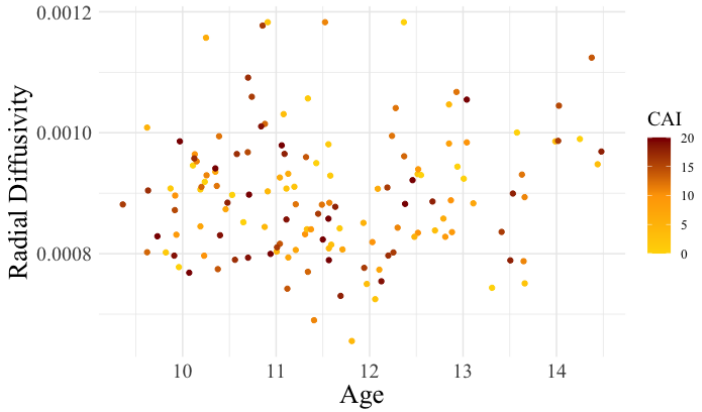

Left Uncinate Fasciculus

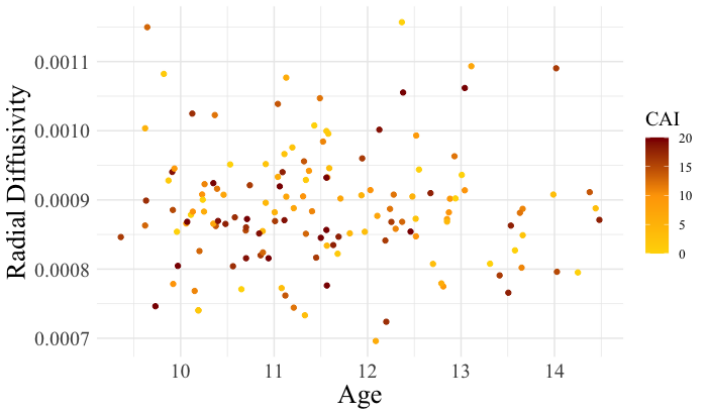

Right Uncinate Fasciculus

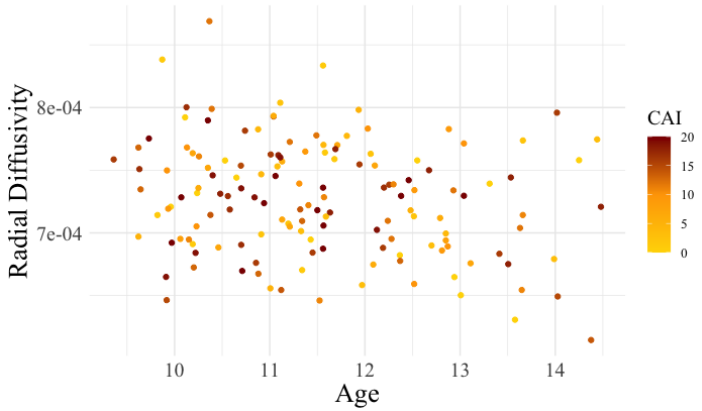

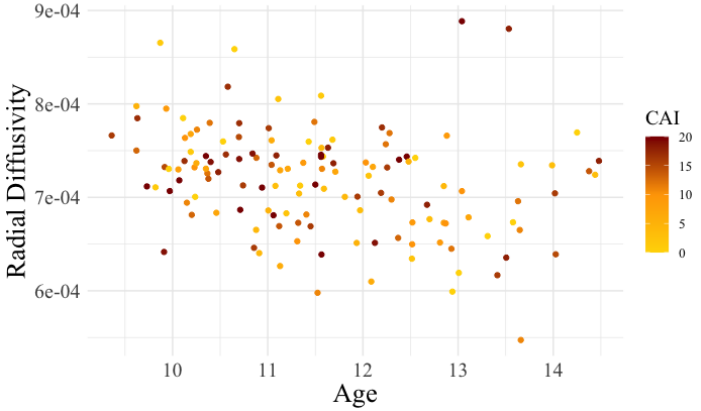

Left Mammillothalamic Tract	Right Mammillothalamic Tract
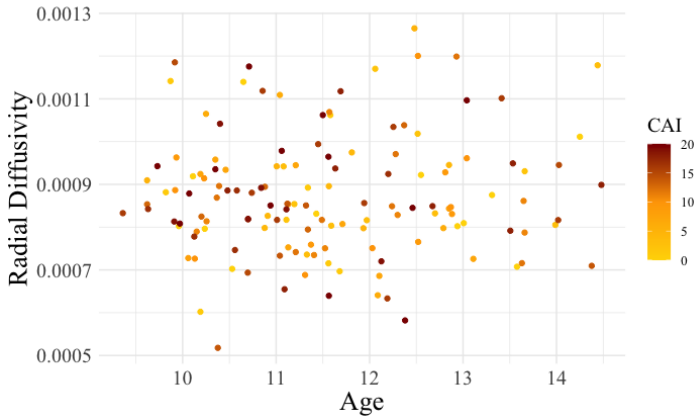	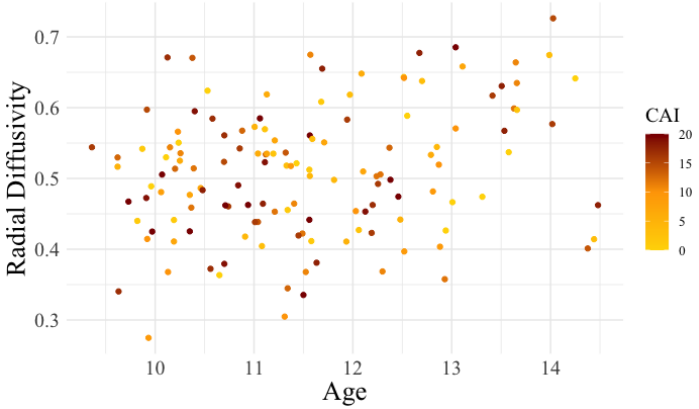
Left Cingulum Bundle	Right Cingulum Bundle

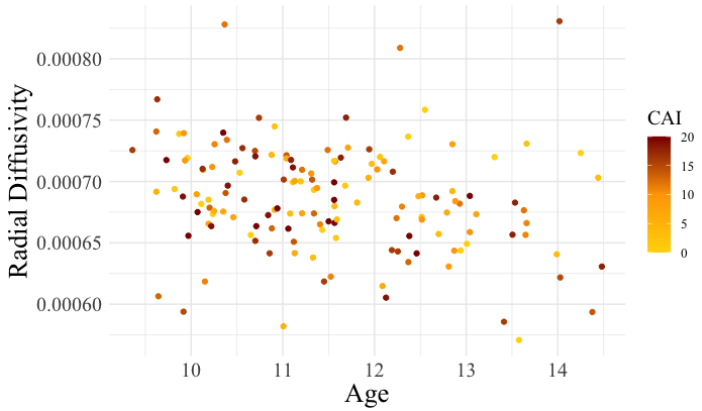
Radial Diffusivity
0.00080
0.00075
0.00070
0.00065
0.00060
10
11
12
13
14
Age
CAI
20
15
10
5
0

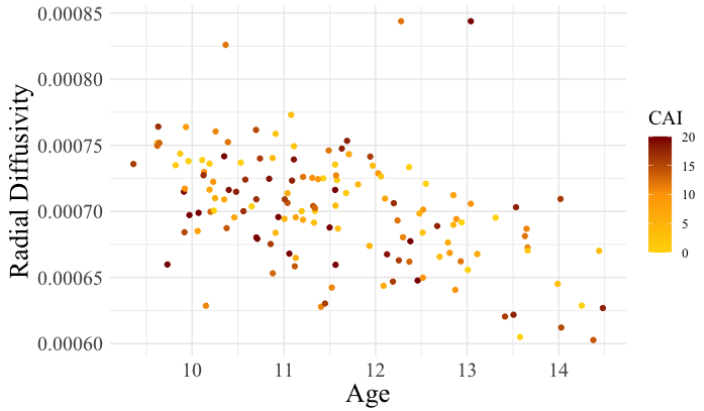
Radial Diffusivity
0.00085
0.00080
0.00075
0.00070
0.00065
0.00060
10
11
12
13
14
Age
CAI
20
15
10
5
0

Figure 5.26 Scatter plot of non-significant limbic system white matter AK by ARI scores in ADHD.

Left Anterior Thalamic Projections	Right Anterior Thalamic Projections
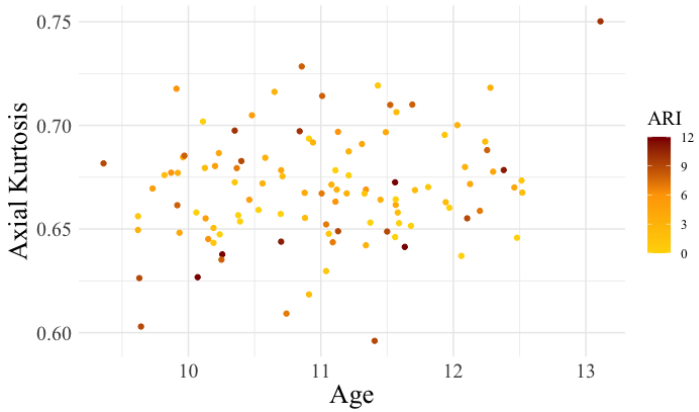	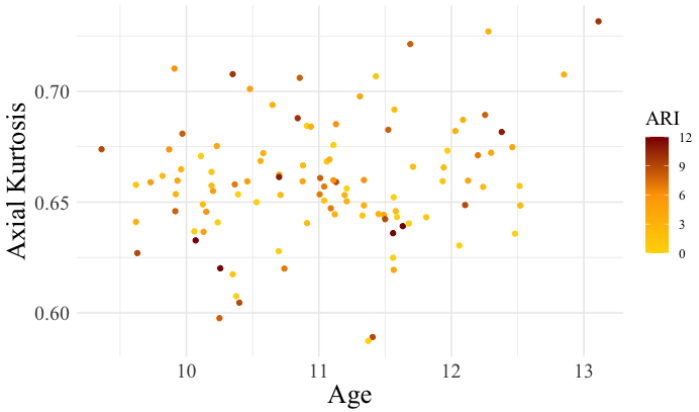
Left Fornix	Right Fornix

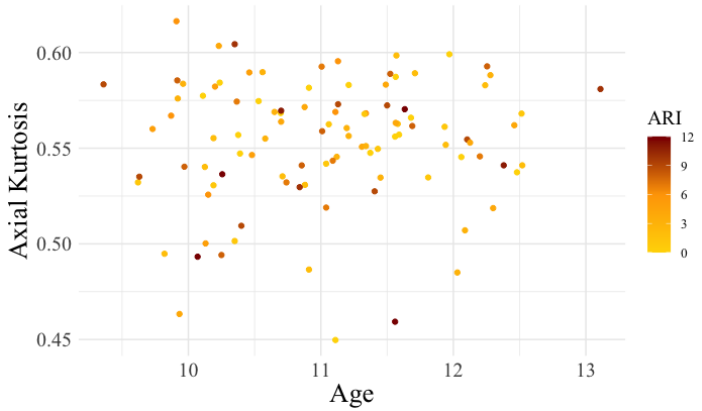

Left Uncinate Fasciculus

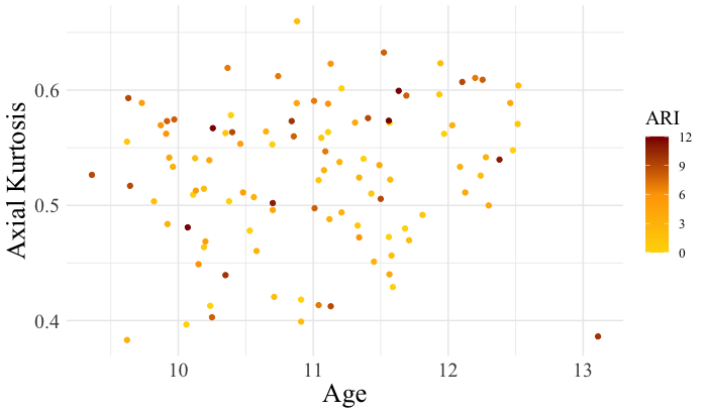

Right Uncinate Fasciculus

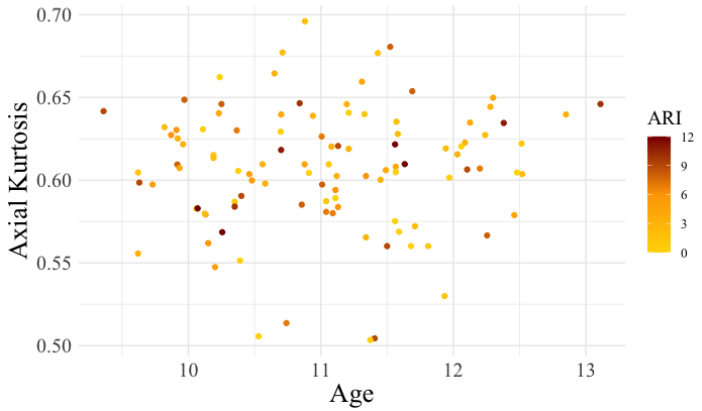

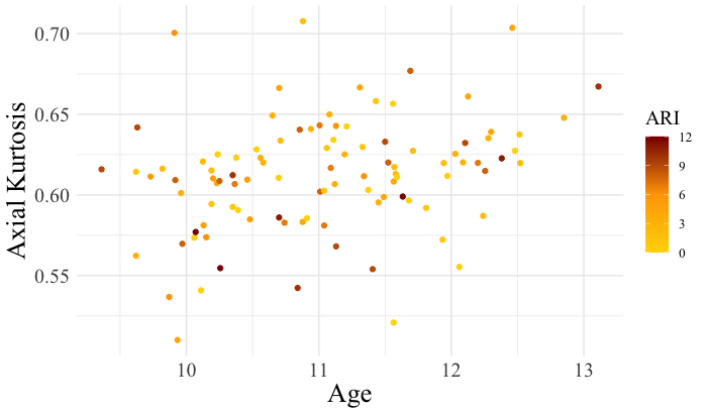

Left Mammillothalamic Tract	Right Mammillothalamic Tract
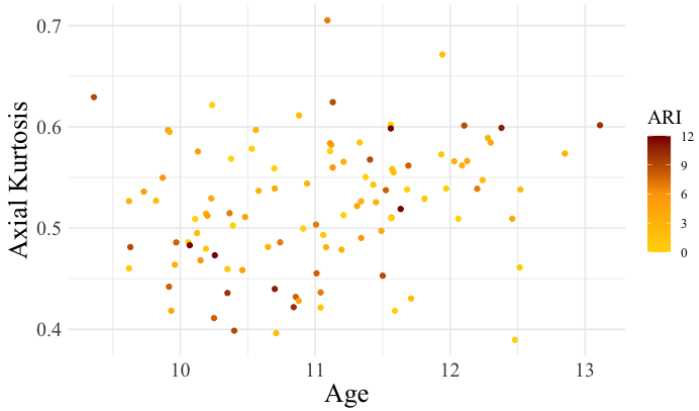	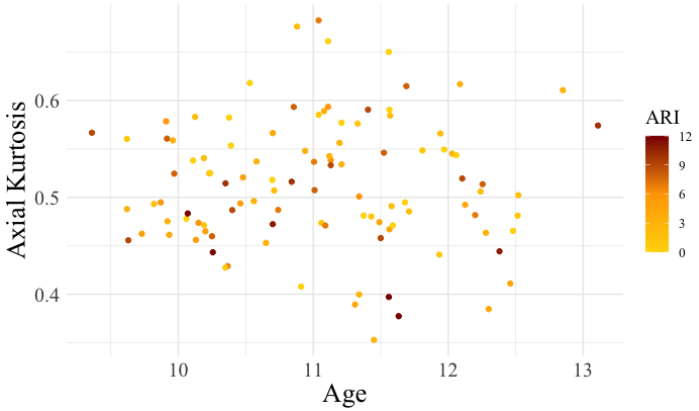
Left Cingulum Bundle	Right Cingulum Bundle

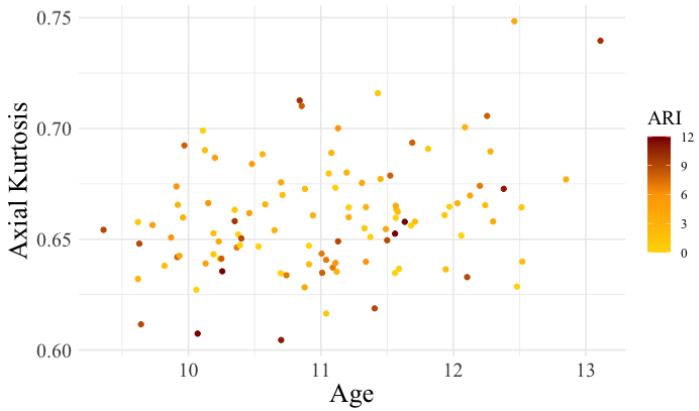
0.75
0.70
0.65
0.60
Axial Kurtosis
10
11
12
13
Age
ARI
12
9
6
3
0

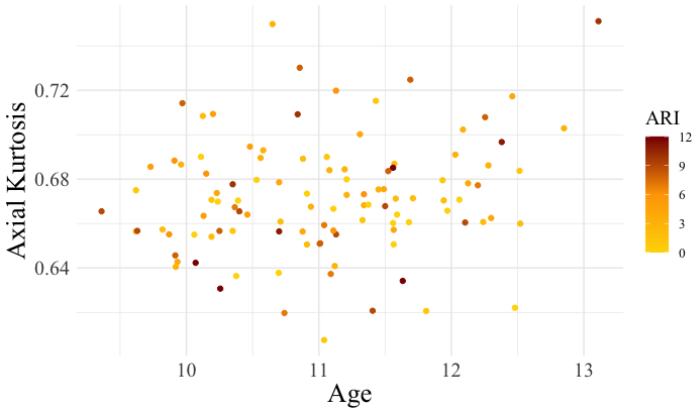
0.72
0.68
0.64
Axial Kurtosis
10
11
12
13
Age
ARI
12
9
6
3
0

Figure 5.27 Scatter plot of non-significant limbic system white matter KA by ARI scores in ADHD.

Left Anterior Thalamic Projections	Right Anterior Thalamic Projections
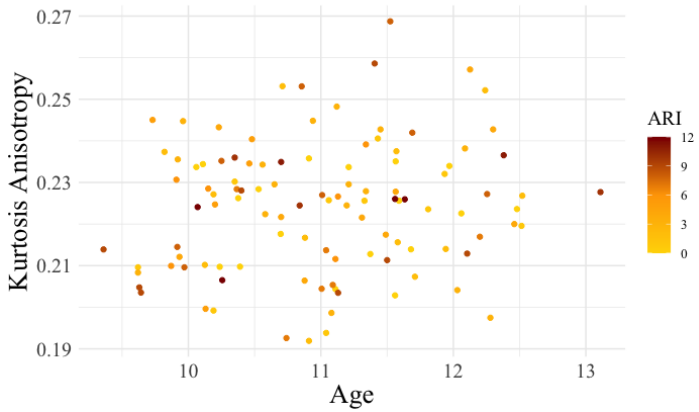	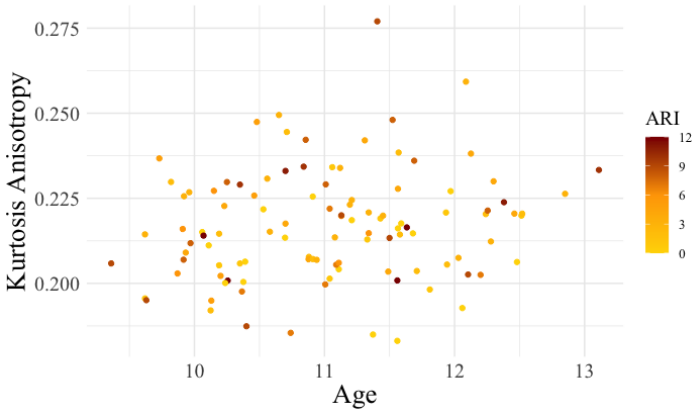
Left Fornix	Right Fornix

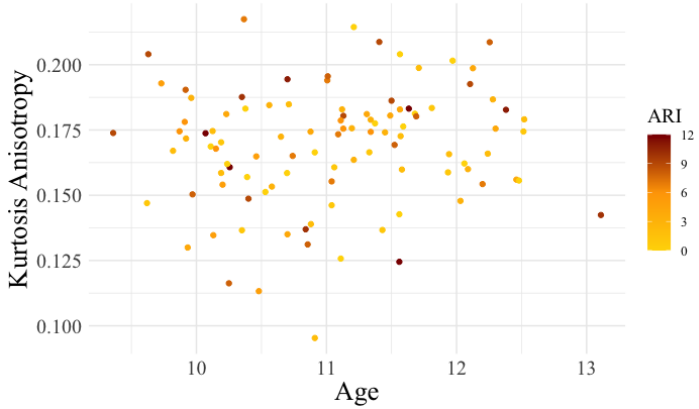

Left Uncinate Fasciculus

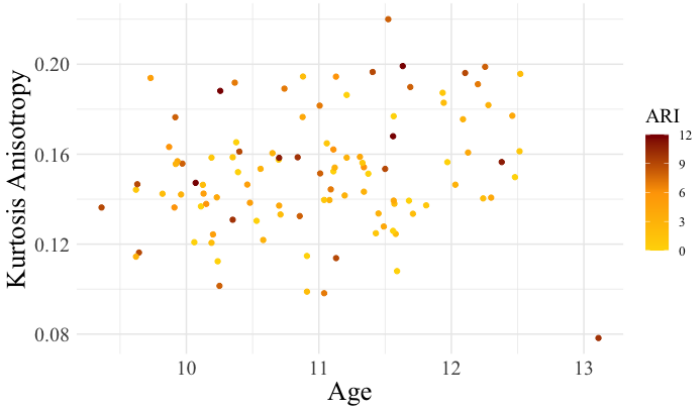

Right Uncinate Fasciculus

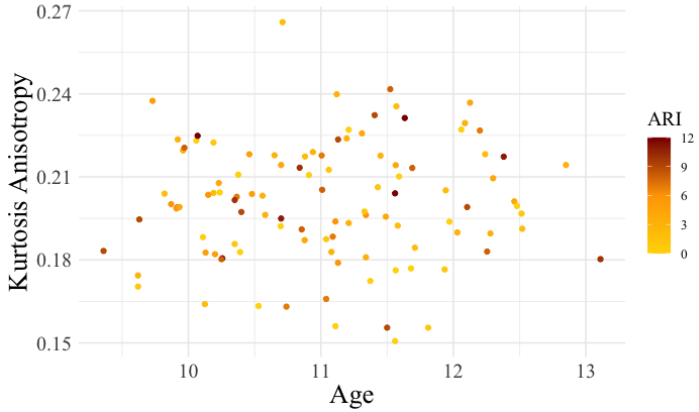

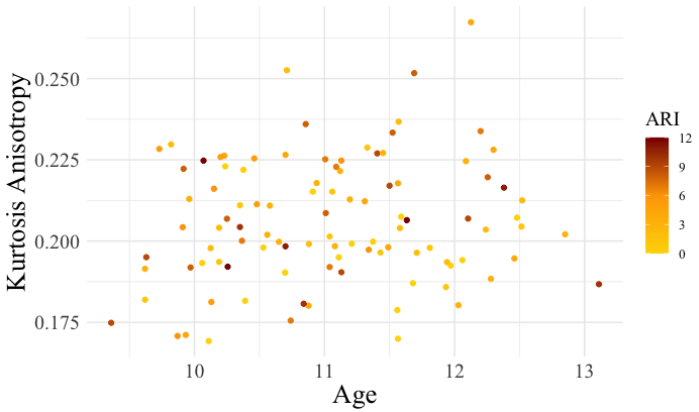

Left Mammillothalamic Tract	Right Mammillothalamic Tract
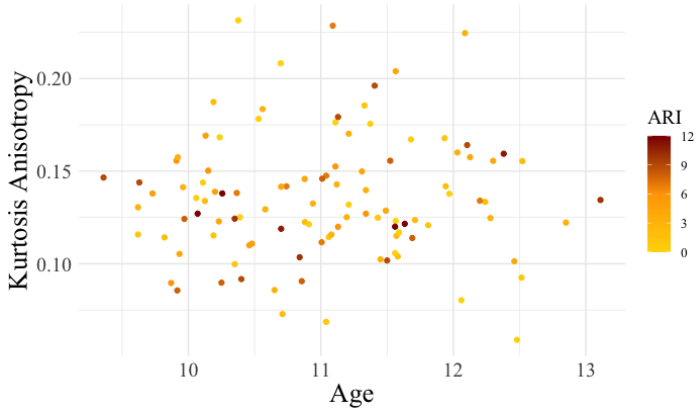	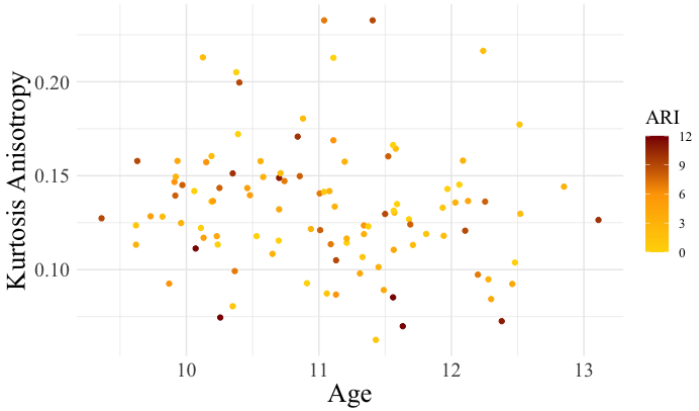
Left Cingulum Bundle	Right Cingulum Bundle

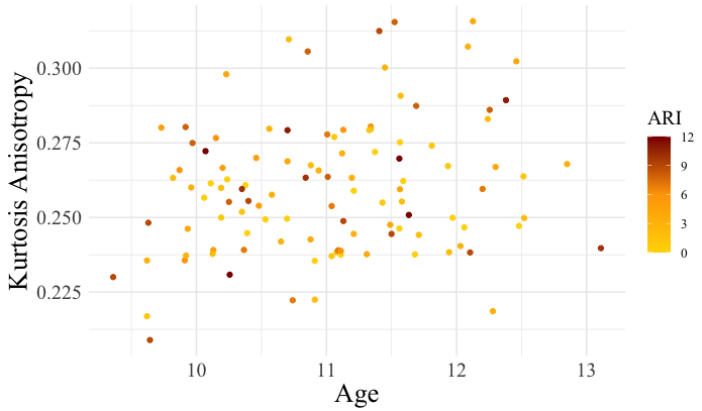
Kurtosis Anisotropy
0.300
0.275
0.250
0.225
10
11
12
13
Age
ARI
12
9
6
3
0

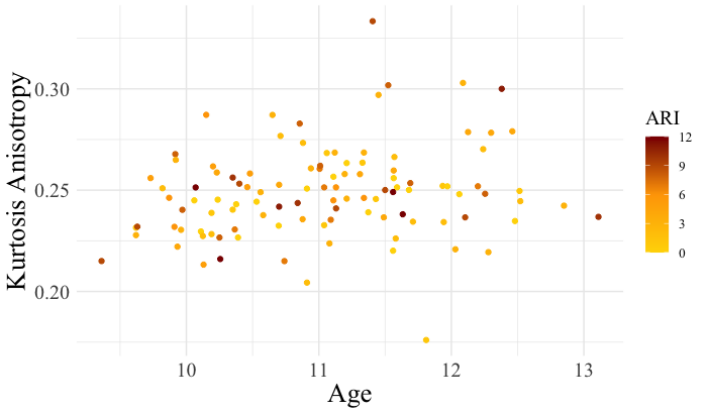
Kurtosis Anisotropy
0.30
0.25
0.20
10
11
12
13
Age
ARI
12
9
6
3
0

Figure 5.28 Scatter plot of non-significant limbic system white matter MK by ARI scores in ADHD.

Left Anterior Thalamic Projections	Right Anterior Thalamic Projections
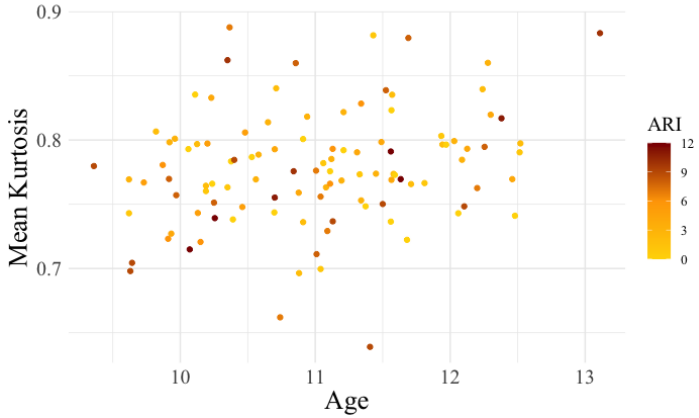	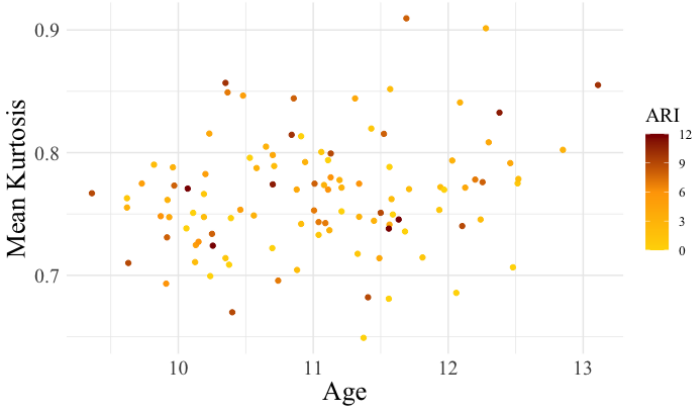
Left Fornix	Right Fornix

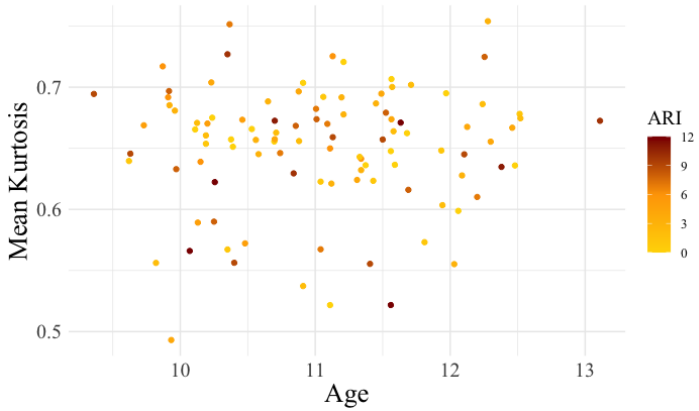

Left Uncinate Fasciculus

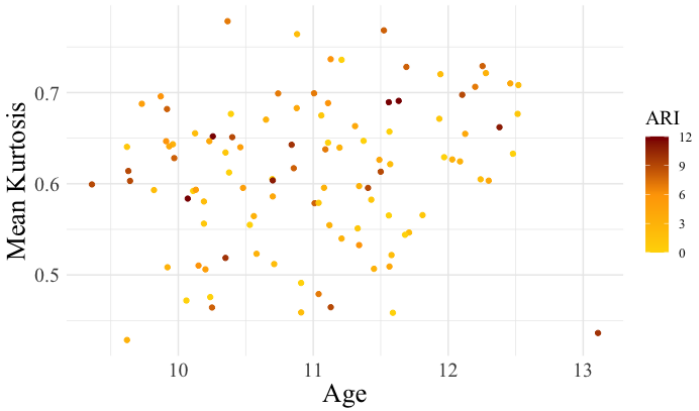

Right Uncinate Fasciculus

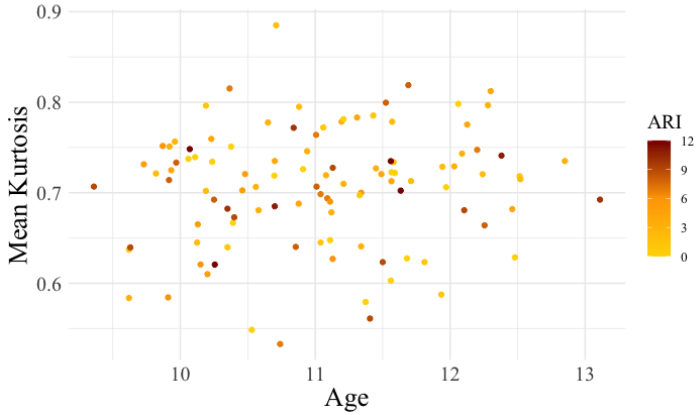

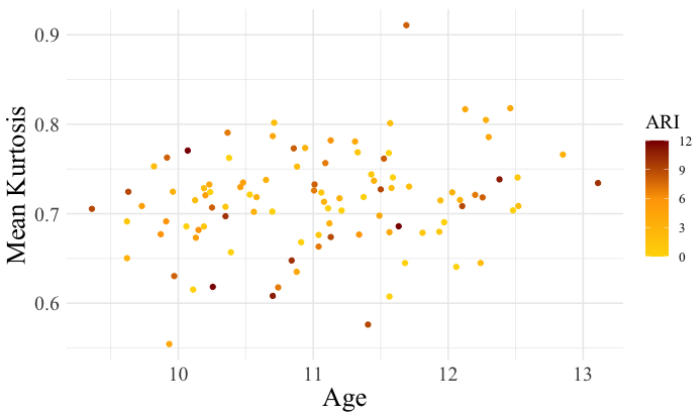

Left Mammillothalamic Tract	Right Mammillothalamic Tract
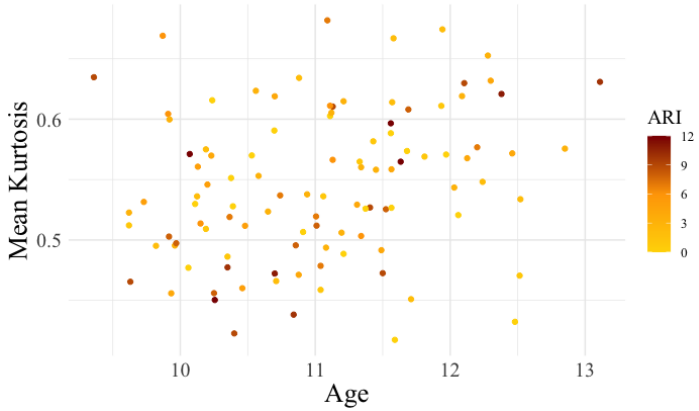	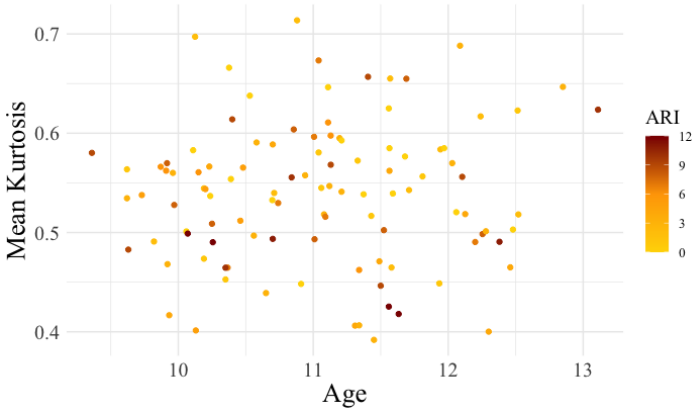
Left Cingulum Bundle	Right Cingulum Bundle

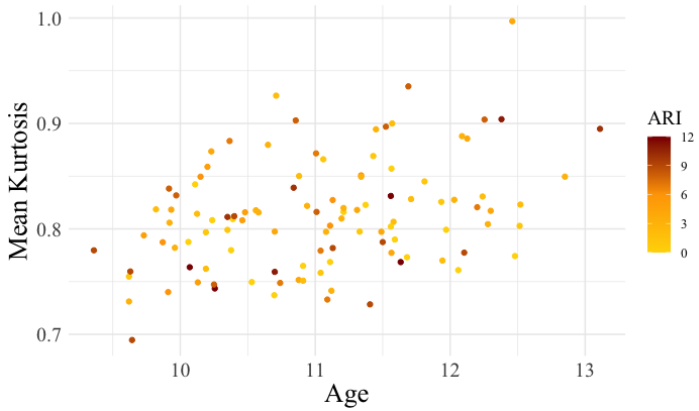
Mean Kurtosis
1.0
0.9
0.8
0.7
10
11
12
13
Age
ARI
12
9
6
3
0

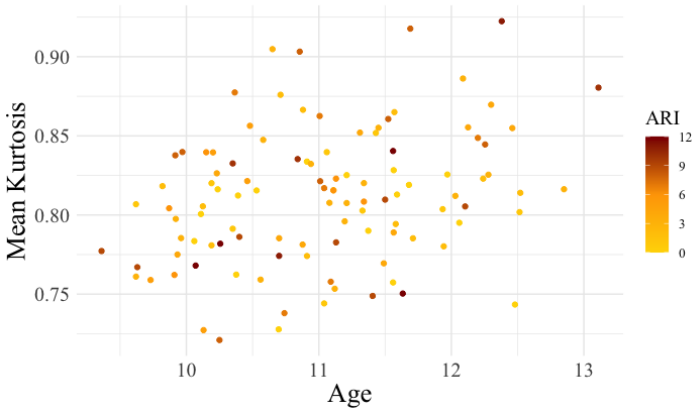
Mean Kurtosis
0.90
0.85
0.80
0.75
10
11
12
13
Age
ARI
12
9
6
3
0

Figure 5.29 Scatter plot of non-significant limbic system white matter RK by ARI scores in ADHD.

Left Anterior Thalamic Projections	Right Anterior Thalamic Projections
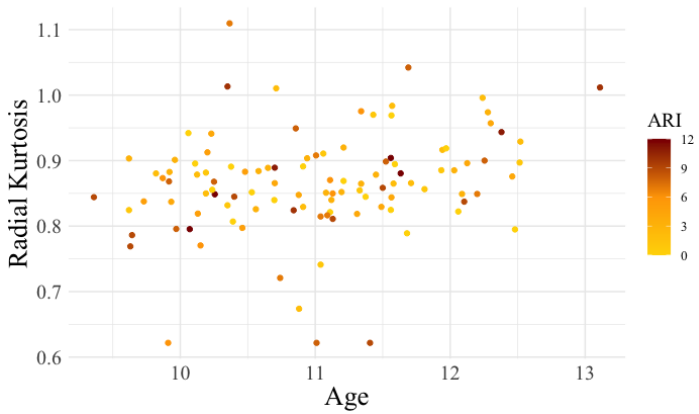	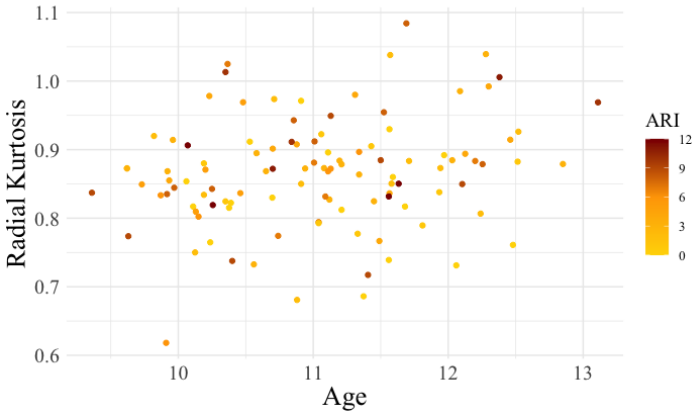
Left Fornix	Right Fornix

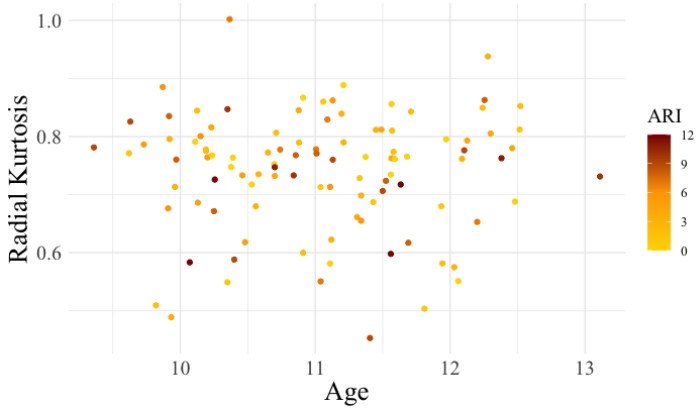

Left Uncinate Fasciculus

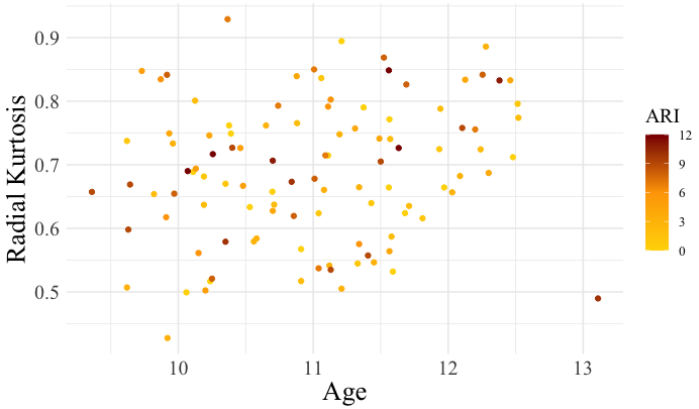

Right Uncinate Fasciculus

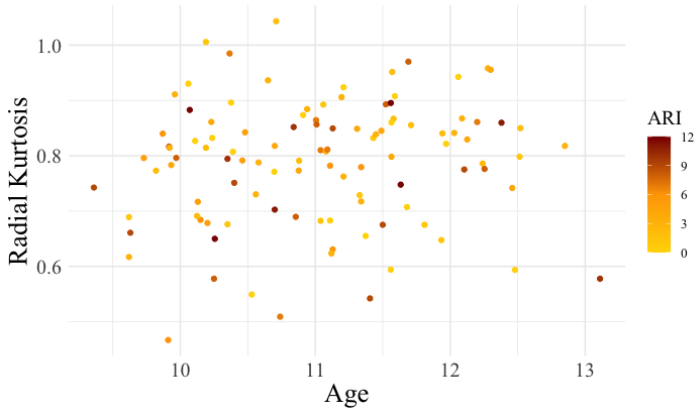

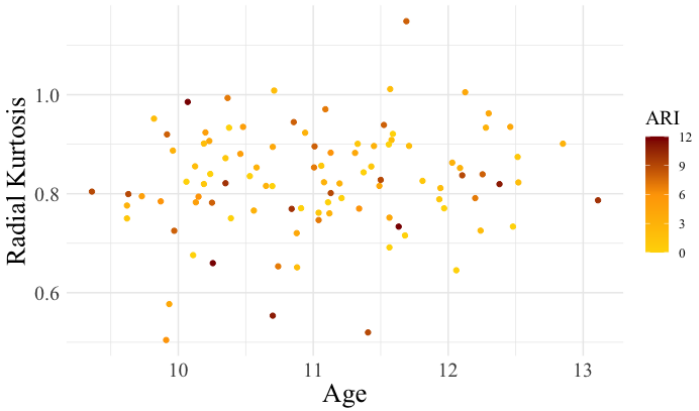

Left Mammillothalamic Tract	Right Mammillothalamic Tract
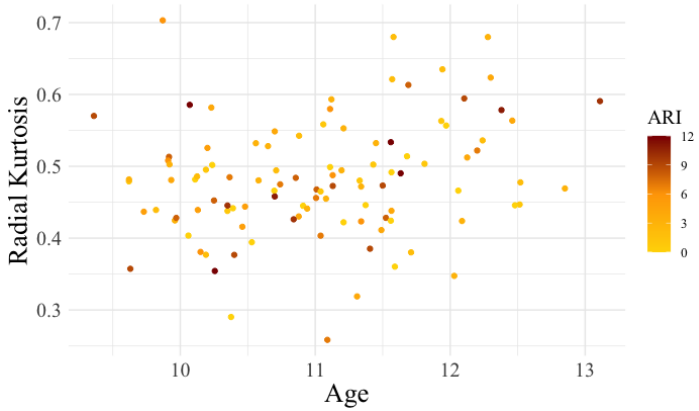	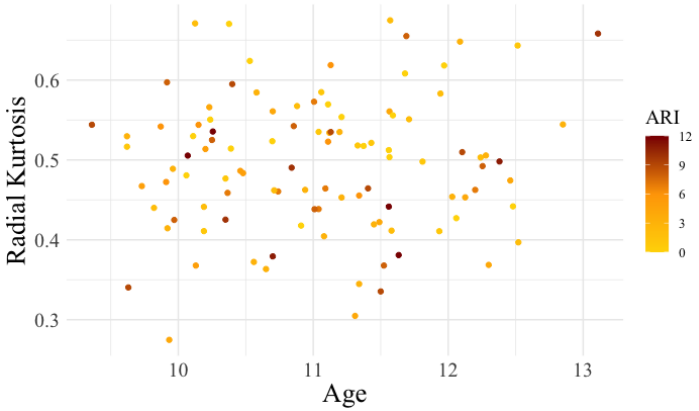
Left Cingulum Bundle	Right Cingulum Bundle

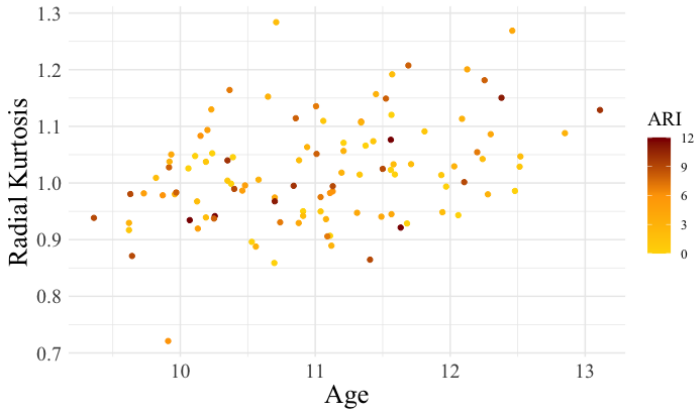
Radial Kurtosis
1.3
1.2
1.1
1.0
0.9
0.8
0.7
10
11
12
13
Age
ARI
12
9
6
3
0

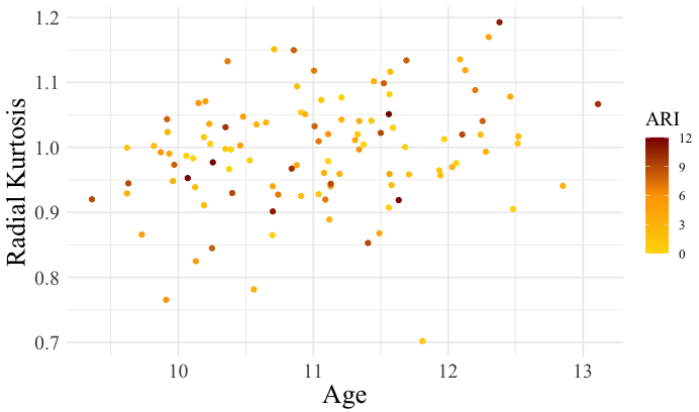
Radial Kurtosis
1.2
1.1
1.0
0.9
0.8
0.7
10
11
12
13
Age
ARI
12
9
6
3
0

Figure 5.30 Scatter plot of non-significant limbic system white matter AD by ARI scores in ADHD.

Left Anterior Thalamic Projections	Right Anterior Thalamic Projections
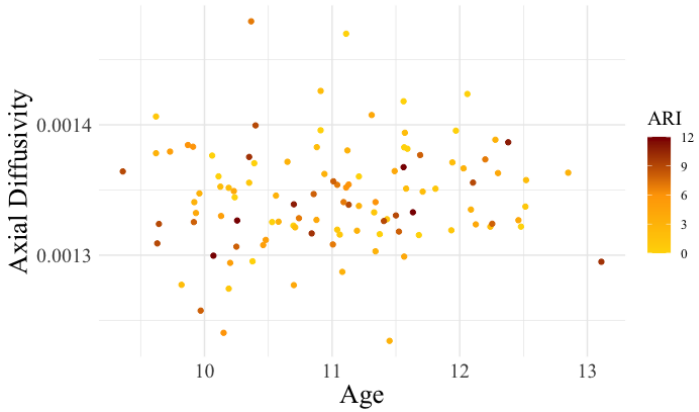	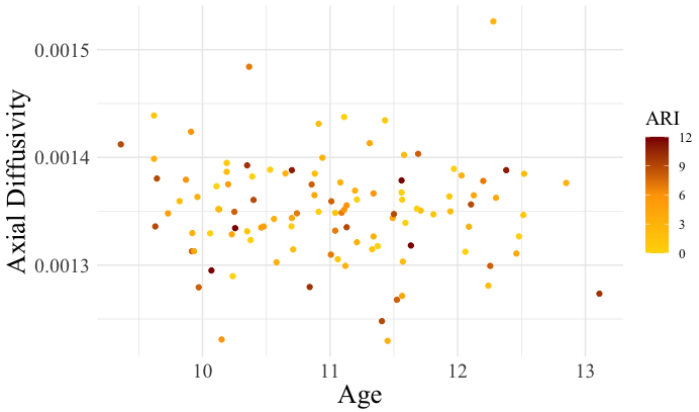
Left Fornix	Right Fornix

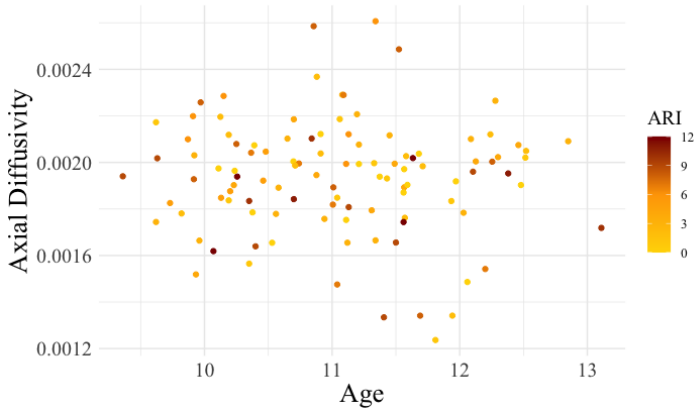

Left Uncinate Fasciculus

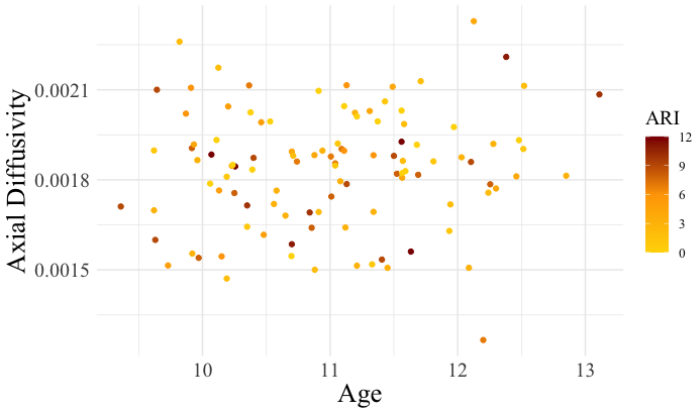

Right Uncinate Fasciculus

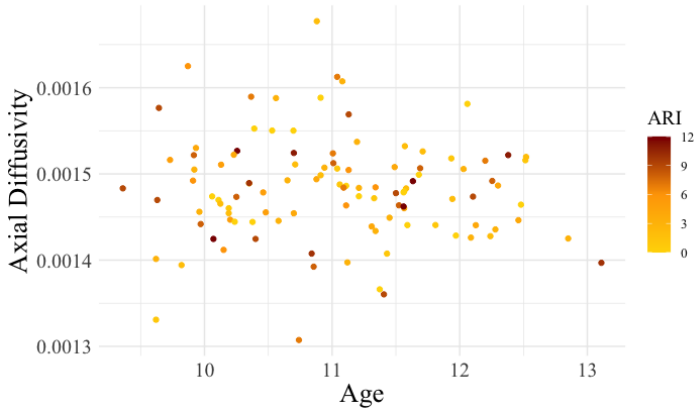

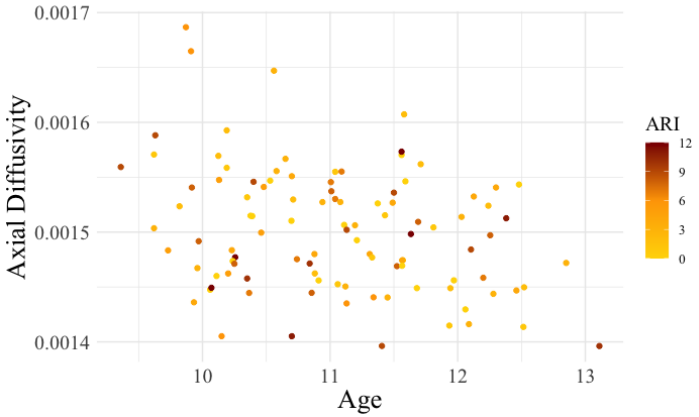

Left Mammillothalamic Tract	Right Mammillothalamic Tract
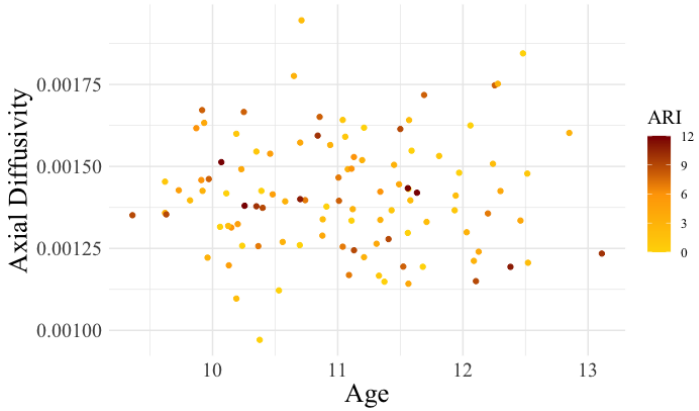	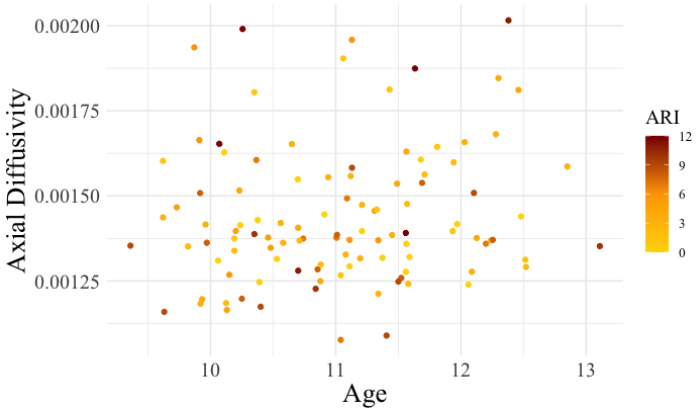
Left Cingulum Bundle	Right Cingulum Bundle

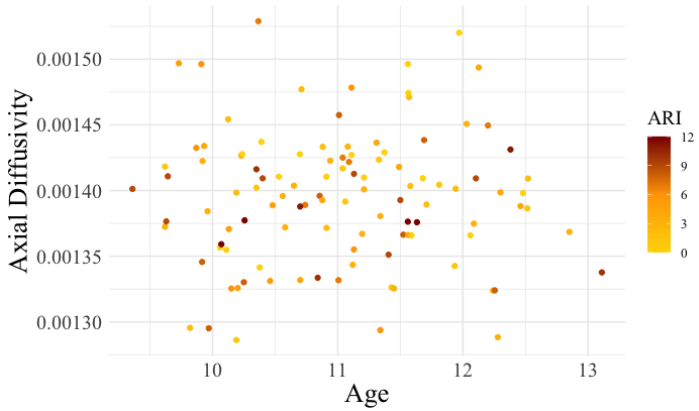
Axial Diffusivity
0.00150
0.00145
0.00140
0.00135
0.00130
10
11
12
13
Age
ARI
12
9
6
3
0

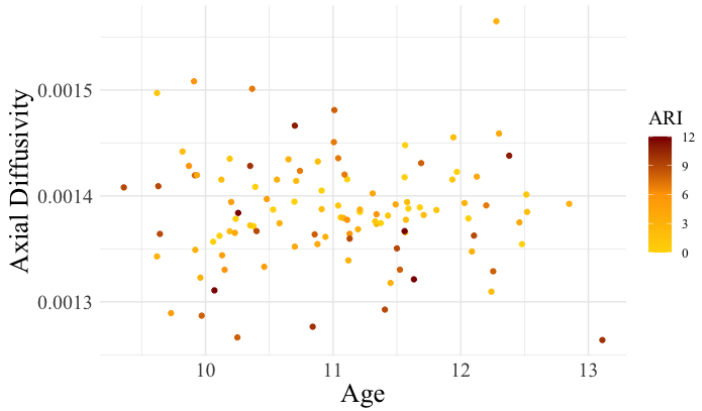
Axial Diffusivity
0.0015
0.0014
0.0013
10
11
12
13
Age
ARI
12
9
6
3
0

Figure 5.31 Scatter plot of non-significant limbic system white matter FA by ARI scores in ADHD.

Left Anterior Thalamic Projections	Right Anterior Thalamic Projections
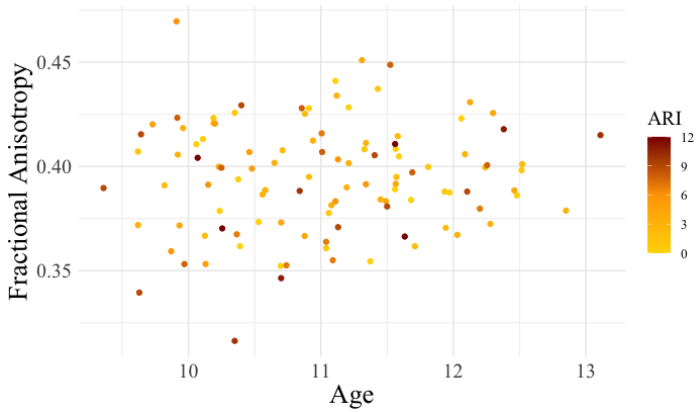	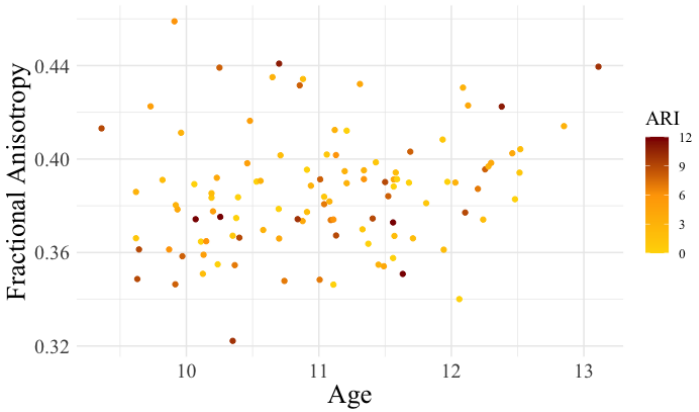
Left Fornix	Right Fornix

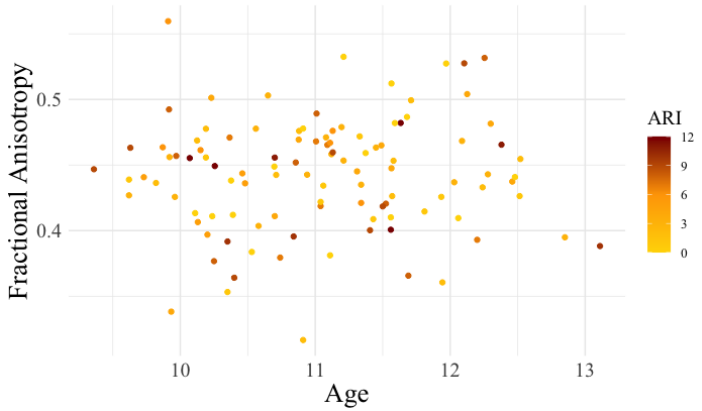

Left Uncinate Fasciculus

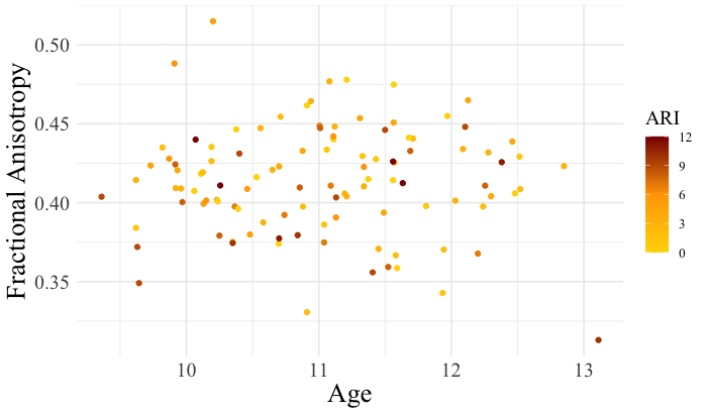

Right Uncinate Fasciculus

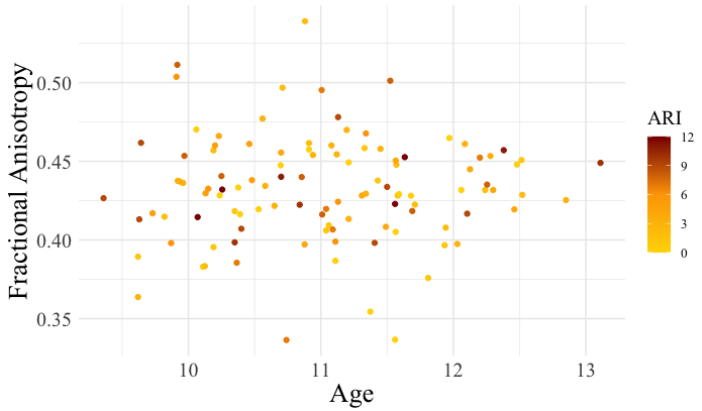

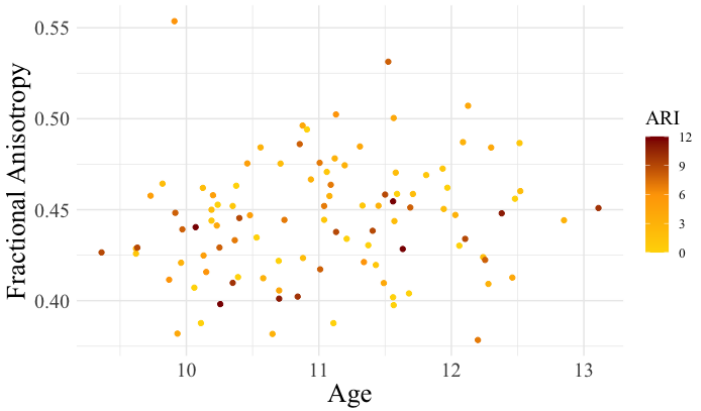

Left Mammillothalamic Tract	Right Mammillothalamic Tract
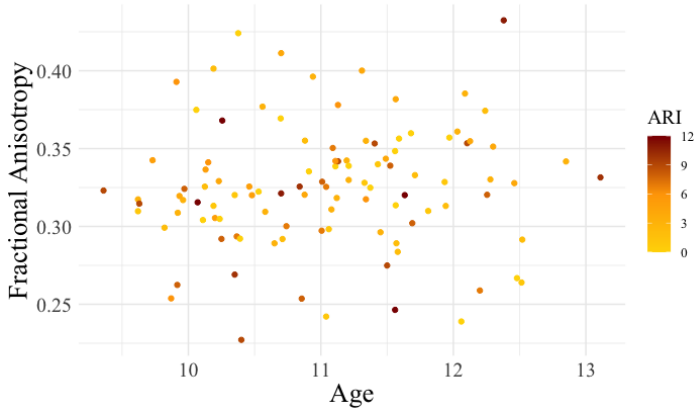	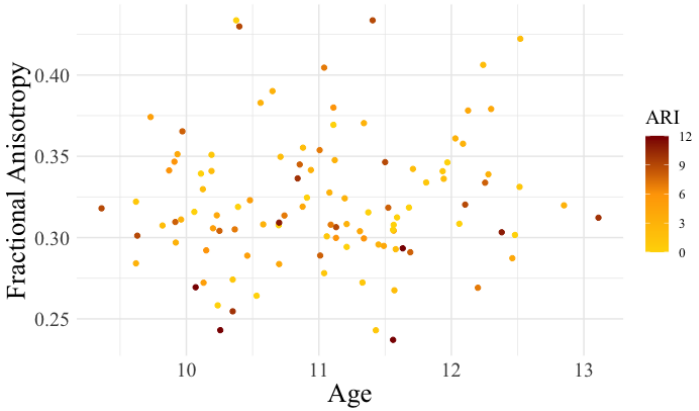
Left Cingulum Bundle	Right Cingulum Bundle

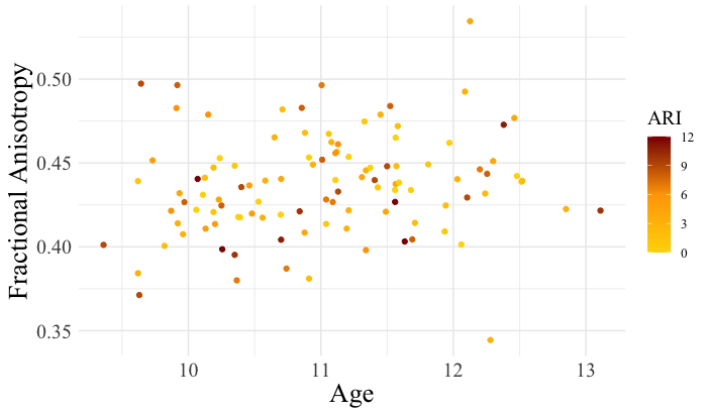
Fractional Anisotropy
0.50
0.45
0.40
0.35
10
11
12
13
Age
ARI
12
9
6
3
0

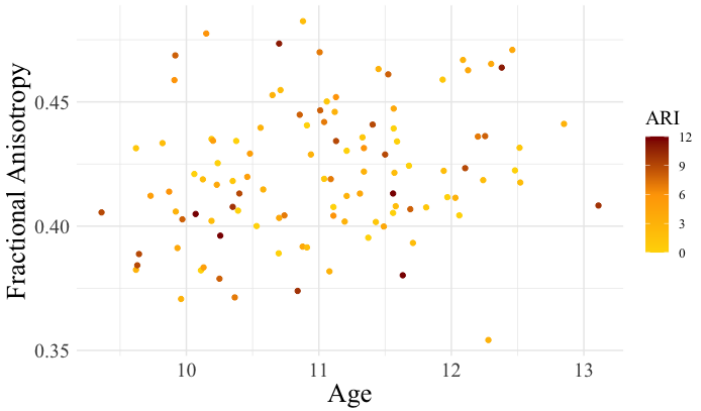
Fractional Anisotropy
0.45
0.40
0.35
10
11
12
13
Age
ARI
12
9
6
3
0

Figure 5.32 Scatter plot of non-significant limbic system white matter RD by ARI scores in ADHD.

Left Anterior Thalamic Projections	Right Anterior Thalamic Projections
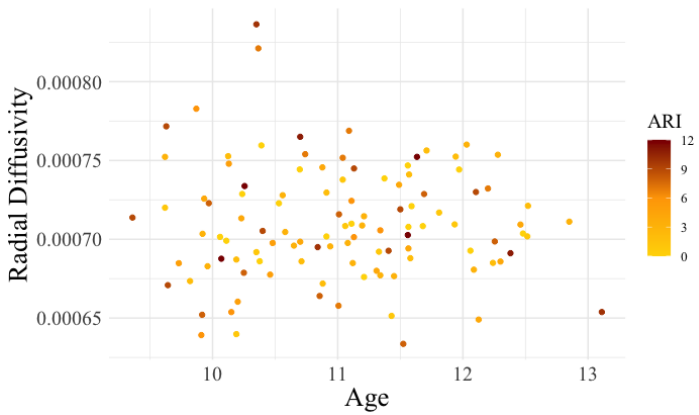	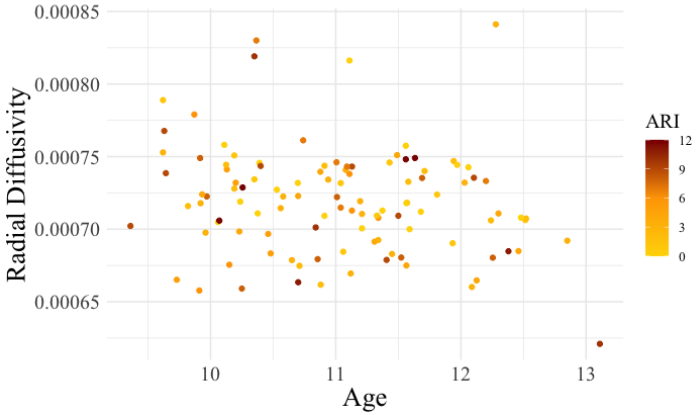
Left Fornix	Right Fornix

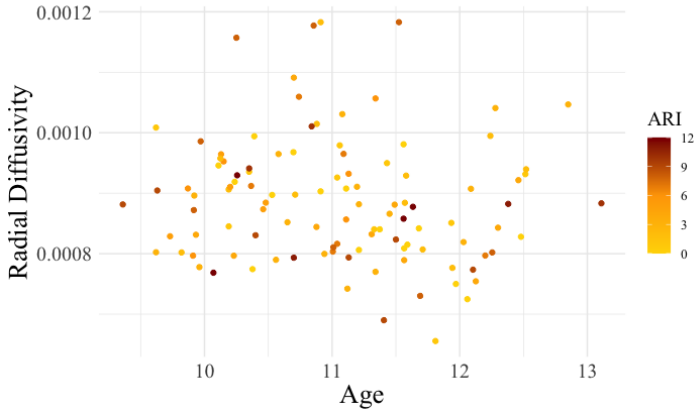

Left Uncinate Fasciculus

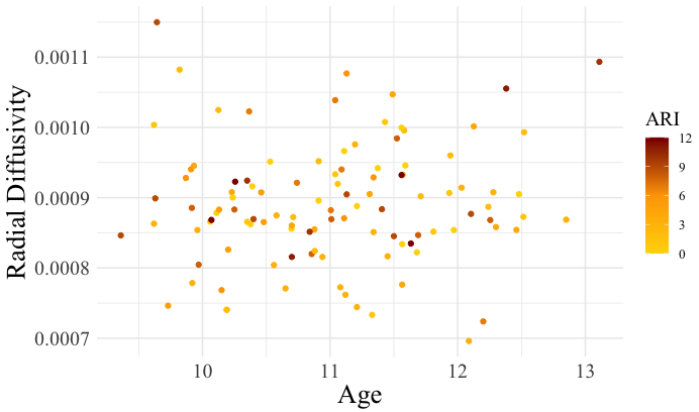

Right Uncinate Fasciculus

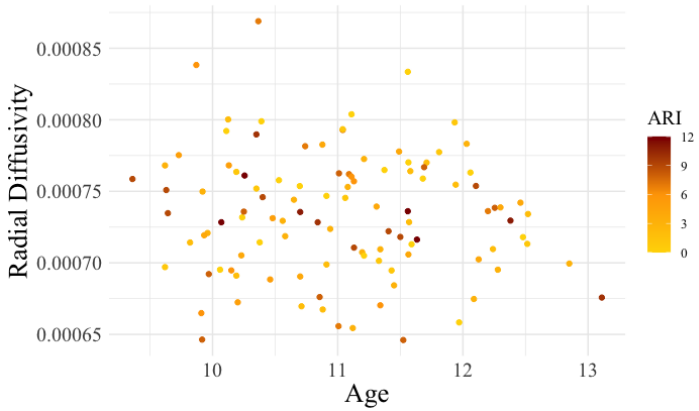

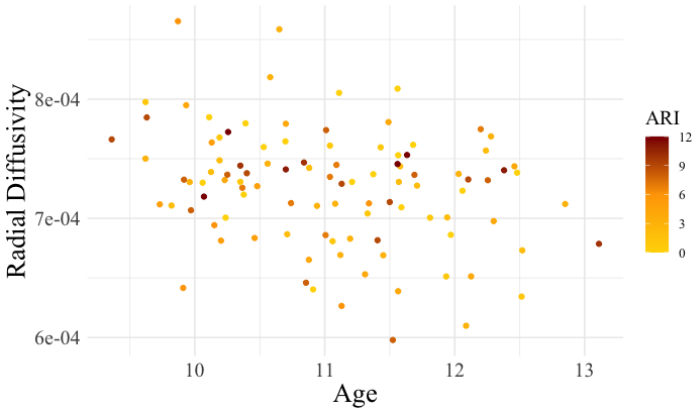

Left Mammillothalamic Tract	Right Mammillothalamic Tract
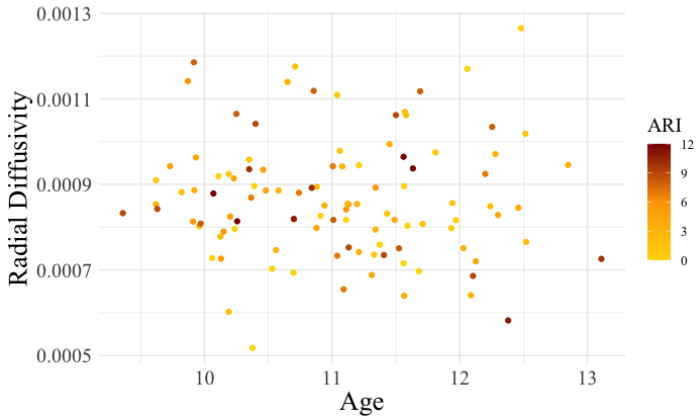	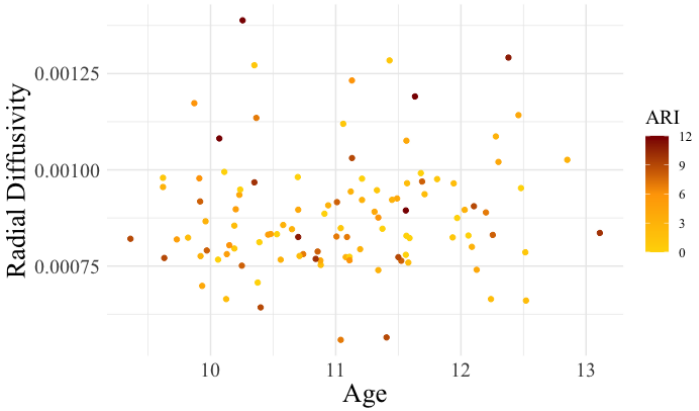
Left Cingulum Bundle	Right Cingulum Bundle

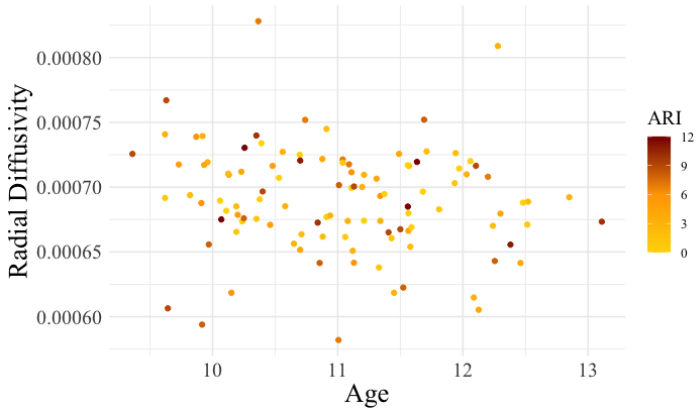
Radial Diffusivity
0.00080
0.00075
0.00070
0.00065
0.00060
10
11
12
13
Age
ARI
12
9
6
3
0

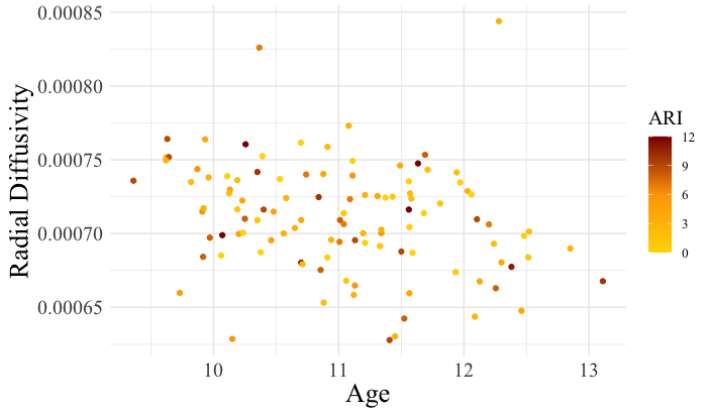
Radial Diffusivity
0.00085
0.00080
0.00075
0.00070
0.00065
10
11
12
13
Age
ARI
12
9
6
3
0

Figure 5.33 Scatter plot of non-significant limbic system white matter MD by ARI scores in ADHD.

Left Anterior Thalamic Projections	Right Anterior Thalamic Projections
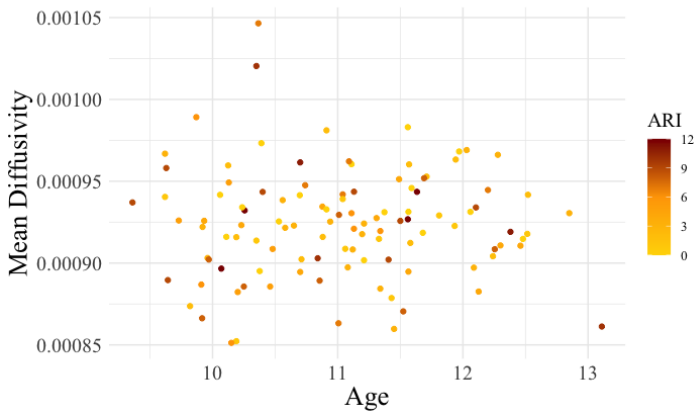	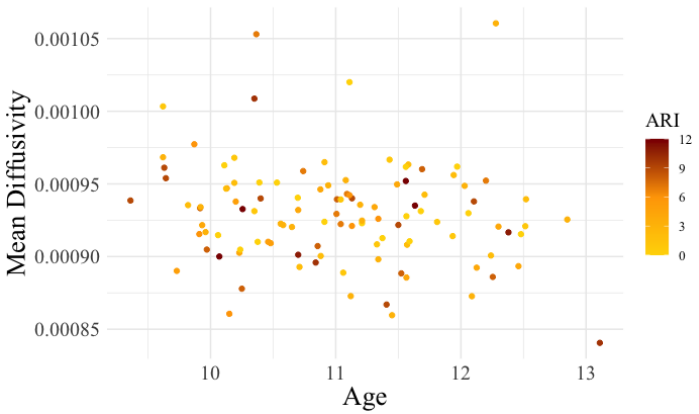
Left Fornix	Right Fornix

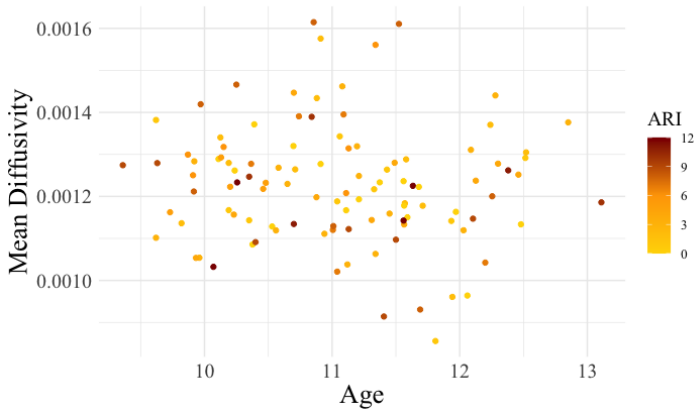

Left Uncinate Fasciculus

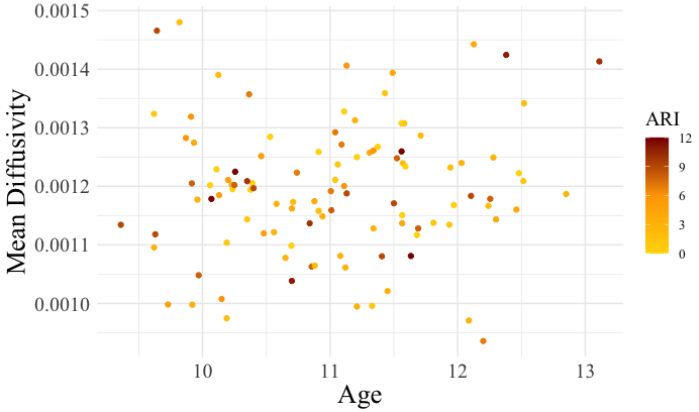

Right Uncinate Fasciculus

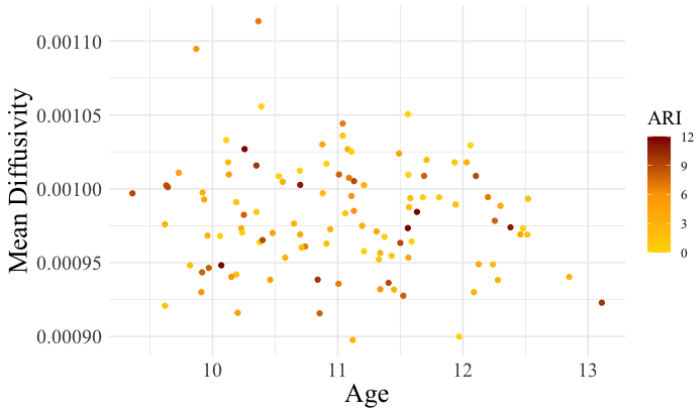

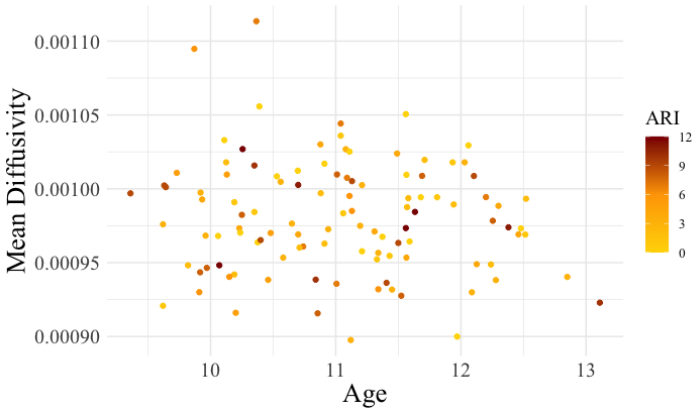

Left Mammillothalamic Tract	Right Mammillothalamic Tract
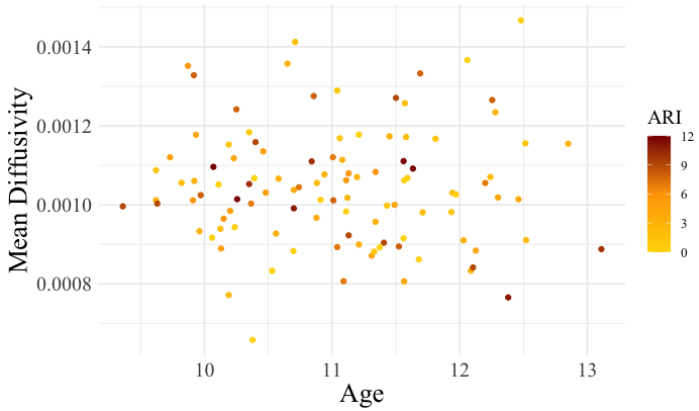	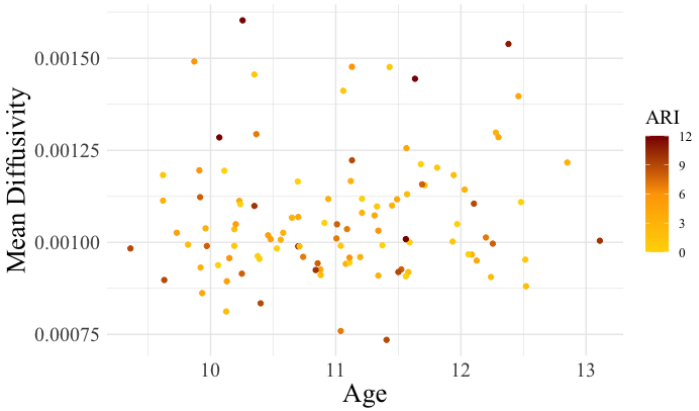
Left Cingulum Bundle	Right Cingulum Bundle

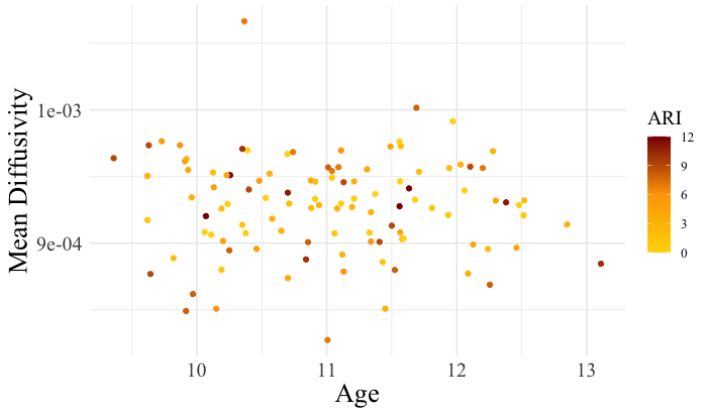
Mean Diffusivity
1e-03
9e-04
10
11
12
13
Age
ARI
12
9
6
3
0

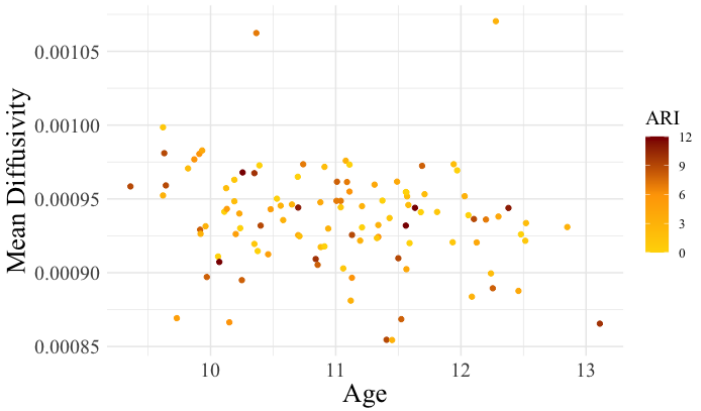
Mean Diffusivity
0.00105
0.00100
0.00095
0.00090
0.00085
10
11
12
13
Age
ARI
12
9
6
3
0

Table 5.16 Results of mixed-effects models (with interaction term) analyses: limbic system white matter tracts KA and CAI scores in ADHD.

	Sex		**Months from baseline**		**CAI**		**CAI * Months from baseline**	
	B (SE)	***t, p***	***B (SE)***	***t, p***	***B (SE)***	***t, p***	***B (SE)***	***t, p***
Cingulum Bundle (Left)	-1.095e-03 (5.887e-03)	-0.186, 0.435	1.692e-04 (1.809e-04)	0.936, 0.352	2.979e-04 (3.808e-04)	0.782, 0.435	1.123e-05 (1.555e-05)	0.722, 0.472
Cingulum Bundle (Right)	8.232e-03 (6.181e-03)	1.331, 0.187	1.536e-04 (1.870e-04)	0.822, 0.414	1.597e-04 (3.976e-04)	0.402, 0.689	1.373e-05 (1.603e-05)	0.857, 0.394
Fornix (Left)	5.097e-03 (5.875e-03)	0.868, 0.389	-4.959e-04 (2.139e-04)	-2.318, 0.023	1.820e-04 (4.189e-04)	0.434, 0.665	8.795e-06 (1.785e-05)	0.493 0.624
Fornix (Right)	1.625e-03 (6.334e-03)	0.257, 0.798	-1.265e-04 (2.098e-04)	-0.603, 0.548	5.412e-04 (4.320e-04)	1.253, 0.212	1.885e-05 (1.799e-05)	1.048 0.298
Anterior Thalamic Projections (Left)	1.167e-03 (4.433e-03)	0.263, 0.793	-1.534e-04 (1.379e-04)	-1.113, 0.269	1.125e-04 (2.905e-04)	0.387, 0.699	-3.135e-06 (1.183e-05)	-0.265, 0.792
Anterior Thalamic Projections (Right)	-7.198e-05 (4.302e-03)	-0.017, 0.987	-1.529e-04 (1.500e-04)	1.019, 0.311	-2.079e-05 (3.015e-04)	-0.069, 0.945	8.847e-06 (1.285e-05)	0.689, 0.493

Mammillothalamic tract (Left)	1.769e-03 (7.047e-03)	0.251, 0.802	-8.205e-04 (3.793e-04)	-2.163, 0.032	-3.544e-05 (6.248e-04)	-0.057, 0.954	2.413e-05 (3.201e-05)	0.754, 0.452
Mammillothalamic tract (Right)	-5.174e-03 (7.169e-03)	-0.722, 0.472	-2.709e-04 (4.031e-04)	-0.671, 0.503	8.932e-04 (6.524e-04)	1.369, 0.173	-4.725e-05 (3.388e-05)	-1.395, 0.165
Uncinate Fasciculus (Left)	3.239e-03 (5.258e-03)	0.616, 0.540	-2.616e-05 (2.075e-04)	-0.126, 0.900	6.288e-04 (3.895e-04)	1.614, 0.109	-2.170e-05 (1.765e-05)	-1.229, 0.222
Uncinate Fasciculus (Right)	-2.374e-03 (5.543e-03)	-0.428, 0.669	1.410e-04 (1.573e-04)	0.897, 0.372	5.814e-04 (3.388e-04)	1.716, 0.088	-1.507e-05 (1.341e-05)	-1.124, 0.264

Table 5.17 Results of mixed-effects models (with interaction term) analyses: limbic system white matter tracts AK and CAI scores in ADHD.

	Sex		**Months from baseline**		**CAI**		**CAI * Months from baseline**	
	B (SE)	***t, p***	***B (SE)***	***t, p***	***B (SE)***	***t, p***	***B (SE)***	***t, p***
Cingulum Bundle (Left)	-5.590e-03 (7.009e-03)	-0.798, 0.428	2.142e-03 (3.391e-04)	6.318, <0.000	7.739e-04 (5.956e-04)	1.200, 0.196	-3.390e-05 (2.891e-05)	-1.173, 0.244
Cingulum Bundle (Right)	-4.531e-03 (7.316e-03)	-0.619, 0.538	1.986e-03 (3.343e-04)	5.940, <0.000	4.062e-04 (6.003e-04)	0.677, 0.500	-8.921e-07 (2.851e-05)	-0.031, 0.975
Fornix (Left)	1.979e-03 (8.246e-03)	0.240, 0.811	1.001e-03 (3.663e-04)	2.733, 0.007	6.836e-05 (6.577e-04)	0.104, 0.917	3.091e-05 (3.052e-05)	1.013 0.313
Fornix (Right)	-6.604e-03 (1.578e-02)	-0.419, 0.676	1.492e-03 (5.545e-04)	2.690, 0.008	1.563e-03 (1.114e-03)	1.404, 0.162	5.907e-05 (4.750e-05)	1.244 0.216
Anterior Thalamic Projections (Left)	9.284e-03 (7.007e-03)	1.325, 0.190	1.809e-03 (3.267e-04)	5.538, <0.000	1.973e-04 (5.797e-04)	0.340, 0.734	4.643e-06 (2.781e-05)	0.167, 0.868
Anterior Thalamic Projections (Right)	2.273e-03 (6.883e-03)	0.330, 0.742	2.160e-03 (3.532e-04)	6.115, <0.000	4.310e-04 (6.054e-04)	0.712, 0.478	-2.665e-06 (3.004e-05)	-0.089, 0.929

Mammillothalamic tract (Left)	9.719e-03 (1.238e-02)	0.785, 0.433	4.439e-04 (6.920e-04)	0.642, 0.522	-4.843e-04 (1.124e-03)	-0.431, 0.667	1.185e-04 (5.831e-05)	2.032, 0.044
Mammillothalamic tract (Right)	-1.557e-02 (1.438e-02)	-1.083, 0.283	5.198e-04 (7.597e-04)	0.684, 0.495	-9.873e-04 (1.259e-03)	-0.784, 0.434	2.033e-05 (6.400e-05)	0.318, 0.751
Uncinate Fasciculus (Left)	9.161e-03 (9.875e-03)	0.928, 0.357	1.463e-03 (3.982e-04)	3.689, <0.000	-1.779e-05 (7.407e-04)	-0.024, 0.980	1.035e-05 (3.387e-05)	-0.306, 0.760
Uncinate Fasciculus (Right)	5.678e-03 (9.933e-03)	0.572, 0.570	2.619e-03 (4.806e-04)	5.450, <0.000	1.230e-03 (8.315e-04)	1.479, 0.142	-5.867e-05 (4.064e-05)	-1.443, 0.152

Table 5.18 Results of mixed-effects models (with interaction term) analyses: limbic system white matter tracts RK and CAI scores in ADHD.

	Sex		**Months from baseline**		**CAI**		**CAI * Months from baseline**	
	B (SE)	***t, p***	***B (SE)***	***t, p***	***B (SE)***	***t, p***	***B (SE)***	***t, p***
Cingulum Bundle (Left)	2.653e-02 (2.162e-02)	1.227, 0.224	3.177e-03 (9.631e-04)	3.299, 0.001	5.690e-04 (1.748e-03)	0.325, 0.745	5.018e-05 (8.229e-05)	0.610, 0.543
Cingulum Bundle (Right)	4.736e-02 (2.164e-02)	2.188, 0.032	2.501e-03 (8.961e-04)	2.791, 0.006	5.268e-04 (1.676e-03)	0.314, 0.753	6.679e-05 (7.656e-05)	0.872, 0.385
Fornix (Left)	3.639e-02 (2.468e-02)	1.474, 0.146	1.267e-03 (9.907e-04)	1.279, 0.205	4.993e-04 (1.859e-03)	0.269, 0.789	3.715e-05 (8.261e-05)	0.450 0.654
Fornix (Right)	9.965e-03 (2.724e-02)	0.366, 0.716	1.229e-03 (9.383e-04)	1.310, 0.194	1.505e-03 (1.900e-03)	0.792, 0.430	1.209e-04 (8.040e-05)	1.503 0.136
Anterior Thalamic Projections (Left)	2.603e-02 (1.970e-02)	1.321, 0.191	3.575e-03 (8.338e-04)	4.288, <0.000	3.658e-06 (1.542e-03)	0.002, 0.998	-7.758e-06 (7.116e-05)	-0.109, 0.913
Anterior Thalamic Projections (Right)	1.113e-02 (2.030e-02)	0.549, 0.585	2.540e-03 (8.191e-04)	3.101, 0.002	5.330e-04 (1.549e-03)	0.344, 0.731	5.927e-05 (7.000e-05)	0.847, 0.399

Mammillothalamic tract (Left)	-8.390e-03 (1.811e-02)	-0.463, 0.644	2.408e-03 (8.969e-04)	2.685, 0.008	1.148e-03 (1.527e-03)	0.752, 0.453	7.980e-05 (7.587e-05)	1.052, 0.295
Mammillothalamic tract (Right)	-1.879e-02 (2.101e-02)	-0.894, 0.375	1.471e-03 (9.473e-04)	1.553, 0.124	-3.017e-04 (1.676e-03)	-0.180, 0.857	4.592e-06 (8.018e-05)	0.057, 0.954
Uncinate Fasciculus (Left)	4.997e-02 (2.629e-02)	1.900, 0.062	1.846e-03 (1.219e-03)	1.515, 0.133	-9.080e-04 (2.138e-03)	-0.425, 0.671	7.115e-05 (1.034e-04)	0.688, 0.492
Uncinate Fasciculus (Right)	2.334e-02 (2.595e-02)	0.899, 0.372	3.197e-03 (1.198e-03)	2.668, 0.009	1.709e-03 (2.114e-03)	0.809, 0.420	-1.221e-04 (1.015e-04)	-1.203, 0.232

Table 5.19 Results of mixed-effects models (with interaction term) analyses: limbic system white matter tracts MK and CAI scores in ADHD.

	Sex		**Months from baseline**		**CAI**		**CAI * Months from baseline**	
	B (SE)	***t, p***	***B (SE)***	***t, p***	***B (SE)***	***t, p***	***B (SE)***	***t, p***
Cingulum Bundle (Left)	1.382e-02 (1.265e-02)	1.092, 0.279	2.776e-03 (5.421e-04)	5.121, <0.000	1.322e-03 (9.997e-04)	1.323, 0.188	-4.543e-06 (4.636e-05)	-0.098, 0.922
Cingulum Bundle (Right)	1.902e-02 (1.256e-02)	1.514, 0.135	2.325e-03 (5.138e-04)	4.525, <0.000	5.897e-04 (9.660e-04)	0.610, 0.543	3.763e-05 (4.390e-05)	0.857, 0.394
Fornix (Left)	1.004e-02 (1.287e-02)	0.780, 0.439	1.091e-03 (5.324e-04)	2.049, 0.043	1.685e-04 (9.861e-04)	0.171, 0.864	3.857e-05 (4.438e-05)	0.869 0.387
Fornix (Right)	-2.232e-03 (2.002e-02)	-0.111, 0.911	1.420e-03 (7.015e-04)	2.024, 0.046	1.814e-03 (1.410e-03)	1.286, 0.200	9.012e-05 (6.009e-05)	1.500 0.137
Anterior Thalamic Projections (Left)	2.004e-02 (1.089e-02)	1.840, 0.071	2.229e-03 (4.994e-04)	4.464, <0.000	8.405e-06 (8.925e-04)	0.009, 0.992	1.132e-05 (4.253e-05)	0.266, 0.790
Anterior Thalamic Projections (Right)	6.795e-03 (1.269e-02)	0.536, 0.594	2.290e-03 (5.172e-04)	4.428, <0.000	8.793e-04 (9.738e-04)	0.903, 0.368	2.778e-05 (4.419e-05)	0.629, 0.531

Mammillothalamic tract (Left)	2.777e-03 (1.283e-02)	0.217, 0.829	8.655e-04 (6.635e-04)	1.304, 0.195	6.252e-05 (1.110e-03)	0.056, 0.955	1.114e-04 (5.606e-05)	1.987, 0.049
Mammillothalamic tract (Right)	-2.309e-02 (1.605e-02)	-1.439, 0.155	7.541e-04 (7.726e-04)	0.976, 0.331	2.566e-05 (1.329e-03)	0.019, 0.985	1.256e-06 (6.528e-05)	0.019, 0.985
Uncinate Fasciculus (Left)	2.291e-02 (1.633e-02)	1.403, 0.166	1.412e-03 (6.665e-04)	2.118, 0.037	2.228e-04 (1.233e-03)	0.181, 0.856	2.035e-05 (5.667e-05)	0.359, 0.720
Uncinate Fasciculus (Right)	1.076e-02 (1.492e-02)	0.721, 0.474	2.736e-03 (6.791e-04)	4.029, <0.000	1.915e-03 (1.205e-03)	1.589, 0.114	-8.201e-05 (5.752e-05)	-1.426, 0.157

Table 5.20 Results of mixed-effects models (with interaction term) analyses: limbic system white matter tracts FA and CAI scores in ADHD.

	Sex		**Months from baseline**		**CAI**		**CAI * Months from baseline**	
	B (SE)	***t, p***	***B (SE)***	***t, p***	***B (SE)***	***t, p***	***B (SE)***	***t, p***
Cingulum Bundle (Left)	1.391e-02 (7.679e-03)	1.812, 0.074	-1.264e-04 (2.488e-04)	-0.508, 0.612	3.117e-05 (5.070e-04)	0.061, 0.951	4.544e-05 (2.121e-05)	2.142, 0.034
Cingulum Bundle (Right)	1.044e-02 (7.028e-03)	1.486, 0.142	5.712e-04 (1.902e-04)	3.004, 0.003	5.101e-04 (4.186e-04)	1.219, 0.225	8.312e-06 (1.635e-05)	0.508, 0.612
Fornix (Left)	2.751e-02 (9.971e-03)	2.759, 0.007	-7.701e-04 (3.585e-04)	-2.148, 0.034	-2.023e-04 (7.095e-04)	-0.285, 0.776	1.960e-05 (3.055e-05)	0.642 0.522
Fornix (Right)	1.515e-02 (7.479e-03)	2.026, 0.046	-5.722e-04 (3.314e-04)	-1.727, 0.087	-1.411e-04 (5.976e-04)	-0.236, 0.813	3.448e-05 (2.822e-05)	1.222 0.224
Anterior Thalamic Projections (Left)	4.663e-03 (6.281e-03)	0.743, 0.461	2.691e-05 (2.157e-04)	0.125 0.901	-3.162e-04 (4.293e-04)	-0.737, 0.463	3.851e-06 (1.838e-05)	0.210, 0.835
Anterior Thalamic Projections (Right)	1.065e-03 (6.353e-03)	0.168, 0.867	4.864e-05 (2.298e-04)	0.212, 0.833	-3.558e-04 (4.514e-04)	-0.788, 0.432	2.137e-05 (1.963e-05)	1.089, 0.279

Mammillothalamic tract (Left)	1.666e-04 (8.378e-03)	0.020, 0.984	-6.241e-04 (4.156e-04)	-1.502, 0.136	2.586e-04 (7.091e-04)	0.365, 0.716	1.057e-05 (3.518e-05)	0.301, 0.764
Mammillothalamic tract (Right)	-7.785e-04 (8.301e-03)	-0.094, 0.926	-2.722e-04 (4.687e-04)	-0.581, 0.563	8.552e-04 (7.610e-04)	1.124, 0.263	-5.595e-06 (3.951e-05)	-0.412, 0.888
Uncinate Fasciculus (Left)	2.733e-03 (8.514e-03)	0.321, 0.749	4.726e-04 (3.111e-04)	1.519, 0.132	1.052e-03 (6.038e-04)	1.743, 0.083	-3.541e-05 (2.649e-05)	-1.337, 0.184
Uncinate Fasciculus (Right)	2.707e-03 (8.359e-03)	0.324, 0.747	6.348e-04 (3.857e-04)	1.635, 0.103	6.295e-04 (6.683e-04)	0.942, 0.348	-2.456e-05 (3.238e-05)	-0.759, 0.450

Table 5.21 Results of mixed-effects models (with interaction term) analyses: limbic system white matter tracts AD and CAI scores in ADHD.

	Sex		**Months from baseline**		**CAI**		**CAI * Months from baseline**	
	B (SE)	***t, p***	***B (SE)***	***t, p***	***B (SE)***	***t, p***	***B (SE)***	***t, p***
Cingulum Bundle (Left)	3.178e-05 (1.198e-05)	2.653, 0.009	-1.336e-07 (4.855e-07)	-0.275, 0.783	7.731e-07 (9.024e-07)	0.857, 0.393	-1.894e-08 (4.128e-08)	-0.459, 0.647
Cingulum Bundle (Right)	3.245e-05 (1.297e-05)	2.501, 0.001	-1.586e-06 (4.758e-07)	-3.332, 0.001	-5.143e-07 (9.346e-07)	-0.550 0.583	1.734e-08 (4.080e-08)	0.425, 0.671
Fornix (Left)	1.126e-04 (5.574e-05)	2.021, 0.047	-1.312e-06 (2.044e-06)	-0.642, 0.522	4.219e-07 (4.012e-06)	0.105, 0.916	-7.005e-08 (1.741e-07)	-0.402 0.688
Fornix (Right)	-4.705e-07 (4.276e-05)	-0.011, 0.991	-3.472e-06 (1.985e-06)	-1.749, 0.083	-6.539e-06 (3.512e-06)	-1.862, 0.064	2.659e-07 (1.689e-07)	1.575 0.118
Anterior Thalamic Projections (Left)	1.677e-05 (1.070e-05)	1.567, 0.122	3.767e-08 (4.437e-07)	0.085 0.933	-4.690e-07 (8.170e-07)	-0.574, 0.567	-4.166e-08 (3.771e-08)	-1.105, 0.272
Anterior Thalamic Projections (Right)	1.351e-05 (1.268e-05)	1.675, 0.291	-1.836e-06 (4.191e-07)	-4.381, <0.000	-1.335e-06 (8.578e-07)	-1.556, 0.122	4.700e-08 (3.599e-08)	1.306, 0.195

Mammillothalamic tract (Left)	-2.471e-05 (4.265e-05)	-0.579, 0.564	1.163e-06 (1.971e-06)	0.590, 0.556	3.933e-06 (3.462e-06)	1.136, 0.258	-7.837e-08 (1.671e-07)	-0.469, 0.640
Mammillothalamic tract (Right)	2.140e-05 (5.636e-05)	0.380, 0.706	4.500e-07 (2.418e-06)	0.186, 0.853	1.978e-08 (4.381e-06)	0.005, 0.996	1.558e-07 (2.054e-07)	0.759, 0.450
Uncinate Fasciculus (Left)	1.555e-05 (1.590e-05)	0.978, 0.332	-5.181e-07 (6.538e-07)	-0.793, 0.430	1.222e-07 (1.208e-06)	0.101, 0.920	-5.531e-08 (5.557e-08)	-0.995, 0.322
Uncinate Fasciculus (Right)	3.403e-05 (1.438e-05)	2.367, 0.021	-1.043e-06 (6.903e-07)	-1.512, 0.133	8.633e-08 (1.176e-06)	0.073, 0.941	1.302e-08 (5.790e-08)	0.225, 0.822

Table 5.22 Results of mixed-effects models (with interaction term) analyses: limbic system white matter tracts RD and CAI scores in ADHD.

	Sex		**Months from baseline**		**CAI**		**CAI * Months from baseline**	
	B (SE)	***t, p***	***B (SE)***	***t, p***	***B (SE)***	***t, p***	***B (SE)***	***t, p***
Cingulum Bundle (Left)	6.323e-07 (1.054e-05)	0.060, 0.952	9.021e-08 (3.709e-07)	0.243, 0.808	4.310e-07 (7.311e-07)	0.589, 0.556	-7.104e-08 (3.160e-08)	-2.248, 0.026
Cingulum Bundle (Right)	5.722e-06 (1.050e-05)	0.545, 0.588	-1.526e-06 (2.795e-07)	-5.460, <0.000	-8.481e-07 (6.188e-07)	-1.371 0.173	5.362e-09 (2.405e-08)	0.223, 0.824
Fornix (Left)	2.504e-07 (2.659e-05)	0.009, 0.993	-1.593e-07 (8.914e-07)	-0.179, 0.859	4.654e-07 (1.815e-06)	0.256, 0.798	-3.375e-08 (7.600e-08)	-0.444 0.658
Fornix (Right)	-8.613e-06 (1.986e-05)	-0.434, 0.666	-1.726e-07 (8.593e-07)	-0.201, 0.841	-8.944e-07 (1.565e-06)	-0.572, 0.569	-5.893e-09 (7.321e-08)	-0.080 0.936
Anterior Thalamic Projections (Left)	2.889e-06 (9.208e-06)	0.314, 0.755	-1.314e-07 (3.787e-07)	-0.347 0.729	5.706e-07 (6.997e-07)	0.816, 0.416	-2.346e-08 (3.219e-08)	-0.729, 0.468
Anterior Thalamic Projections (Right)	7.761e-06 (1.011e-05)	0.767, 0.446	-1.346e-06 (2.930e-07)	-4.595, <0.000	-5.598e-07 (6.298e-07)	-0.889, 0.376	2.173e-08 (2.519e-08)	0.862, 0.391

Mammillothalamic tract (Left)	-9.240e-06 (3.110e-05)	-0.297, 0.767	1.075e-06 (1.573e-06)	0.684, 0.496	1.029e-06 (2.663e-06)	0.386, 0.700	-3.318e-08 (1.331e-07)	-0.249, 0.804
Mammillothalamic tract (Right)	5.316e-06 (4.050e-05)	0.131, 0.896	2.281e-07 (1.876e-06)	0.122, 0.903	-1.132e-06 (3.292e-06)	-0.344, 0.731	1.282e-07 (1.591e-07)	0.806, 0.422
Uncinate Fasciculus (Left)	4.010e-06 (1.035e-05)	0.387, 0.699	-9.041e-07 (4.392e-07)	-2.058, 0.042	-8.983e-07 (8.009e-07)	-1.122, 0.263	1.501e-08 (3.731e-08)	0.402, 0.688
Uncinate Fasciculus (Right)	1.148e-05 (1.298e-05)	0.884, 0.379	-1.415e-06 (5.798e-07)	2.441, 0.016	-8.175e-07 (1.019e-06)	-0.803, 0.423	4.874e-08 (4.869e-08)	1.001, 0.319

Table 5.23 Results of mixed-effects models (with interaction term) analyses: limbic system white matter tracts MD and CAI scores in ADHD.

	Sex		**Months from baseline**		**CAI**		**CAI * Months from baseline**	
	B (SE)	***t, p***	***B (SE)***	***t, p***	***B (SE)***	***t, p***	***B (SE)***	***t, p***
Cingulum Bundle (Left)	1.203e-05 (9.380e-06)	1.283, 0.203	3.295e-08 (3.688e-07)	0.089, 0.929	7.528e-07 (6.943e-07)	1.084, 0.280	-5.419e-08 (3.137e-08)	-1.727, 0.087
Cingulum Bundle (Right)	1.423e-05 (9.717e-06)	1.464, 0.148	-1.634e-06 (3.051e-07)	-5.357, <0.000	-7.076e-07 (6.368e-07)	-1.111 0.268	1.065e-08 (2.621e-08)	0.406, 0.686
Fornix (Left)	2.698e-05 (3.514e-05)	0.768, 0.445	-5.478e-07 (1.160e-0)	-0.472, 0.638	8.648e-07 (2.377e-06)	0.364, 0.717	-6.295e-08 (9.892e-08)	-0.636 0.526
Fornix (Right)	-1.933e-06 (2.663e-05)	-0.073, 0.942	-1.333e-06 (1.138e-06)	-1.172, 0.244	-2.472e-06 (2.083e-06)	-1.187, 0.237	7.510e-08 (9.693e-08)	0.775 0.440
Anterior Thalamic Projections (Left)	7.455e-06 (8.849e-06)	0.842, 0.402	-7.594e-08 (3.766e-07)	-0.202 0.841	2.844e-07 (6.859e-07)	0.415, 0.679	-3.513e-08 (3.199e-08)	1.098, 0.275
Anterior Thalamic Projections (Right)	1.088e-05 (9.848e-06)	1.105, 0.273	-1.556e-06 (2.903e-07)	-5.360 <0.000	-8.561e-07 (6.202e-07)	-1.380, 0.170	2.633e-08 (2.496e-08)	1.055, 0.295

Mammillothalamic tract (Left)	-1.801e-05 (3.430e-05)	-0.525, 0.601	9.324e-07 (1.689e-06)	0.552, 0.582	1.381e-06 (2.891e-06)	0.478, 0.633	-3.370e-08 (1.430e-07)	-0.236, 0.814
Mammillothalamic tract (Right)	6.738e-06 (4.655e-05)	0.145, 0.885	3.015e-07 (2.019e-06)	0.149, 0.882	-3.703e-07 (3.642e-06)	-0.102, 0.919	1.135e-07 (1.715e-07)	0.662, 0.510
Uncinate Fasciculus (Left)	7.667e-06 (9.339e-06)	0.821, 0.414	-9.113e-07 (4.344e-07)	-2.098, 0.038	-5.694e-07 (7.629e-07)	-0.746, 0.456	-9.991e-09 (3.683e-08)	-0.271, 0.786
Uncinate Fasciculus (Right)	1.903e-05 (1.177e-05)	1.617, 0.111	-1.376e-06 (5.377e-07)	-2.559, 0.012	-6.929e-07 (9.356e-07)	-0.741, 0.460	3.576e-08 (4.514e-08)	0.792, 0.430

Table 5.24 Results of mixed-effects models (with interaction term) analyses: limbic system white matter tracts KA and ARI scores in ADHD.

	Sex		**Months from baseline**		**ARI**		**ARI * Months from baseline**	
	B (SE)	***t, p***	***B (SE)***	***t, p***	***B (SE)***	***t, p***	***B (SE)***	***t, p***
Cingulum Bundle (Left)	-4.032e-04 (6.226e-03)	-0.065, 0.949	3.212e-04 (2.357e-04)	1.363, 0.180	5.595e-04 (7.399e-04)	0.756, 0.451	1.072e-05 (4.494e-05)	0.239, 0.812
Cingulum Bundle (Right)	9.679e-03 (6.159e-03)	1.571, 0.121	1.788e-04 (2.955e-04)	0.605, 0.548	7.273e-04 (8.491e-04)	0.857, 0.394	5.470e-05 (5.650e-05)	0.968, 0.338
Fornix (Left)	7.387e-03 (6.127e-03)	1,206, 0.233	3.145e-04 (3.243e-04)	0.970, 0.337	9.066e-04 (8.834e-04)	1.026, 0.307	-2.009e-06 (6.153e-05)	-0.033 0.974
Fornix (Right)	5.264e-03 (7.027e-03)	0.749, 0.457	2.029e-04 (3.402e-04)	0.597, 0.554	9.891e-04 (9.345e-04)	1.058, 0.292	2.848e-05 (6.429e-05)	0.443 0.660
Anterior Thalamic Projections (Left)	3.059e-03 (4.307e-03)	0.710, 0.480	7.709e-05 (2.086e-04)	0.370, 0.713	2.455e-04 (5.839e-04)	0.421, 0.675	9.570e-06 (3.991e-05)	0.240, 0.812
Anterior Thalamic Projections (Right)	3.434e-04 (4.270e-03)	0.080, 0.936	-2.159e-04 (2.562e-04)	-0.843, 0.403	1.035e-04 (6.546e-04)	0.158, 0.875	7.664e-05 (4.910e-05)	1.561, 0.124

Mammillothalamic tract (Left)	9.958e-03 (8.304e-03)	1.199, 0.235	-3.003e-04 (5.850e-04)	-0.513, 0.609	-1.087e-03 (1.351e-03)	-0.801, 0.425	1.175e-04 (1.133e-04)	1.037, 0.303
Mammillothalamic tract (Right)	-2.199e-03 (8.345e-03)	-0.264, 0.793	-3.443e-04 (5.860e-04)	0.588, 0.558	1.125e-03 (1.375e-03)	0.818, 0.415	-2.160e-04 (1.145e-04)	-1.887, 0.063
Uncinate Fasciculus (Left)	6.286e-03 (5.727e-03)	1.098, 0.277	-5.448e-04 (3.423e-04)	-1.192, 0.117	-9.996e-05 (8.654e-04)	-0.116, 0.908	9.882e-05 (6.594e-05)	-1.499, 0.140
Uncinate Fasciculus (Right)	6.847e-05 (5.778e-03)	0.012, 0.991	-5.437e-05 (2.043e-04)	-0.266, 0.792	-4.888e-04 (6.733e-04)	-0.726, 0.470	6.125e-05 (4.039e-05)	1.517, 0.138

Table 5.25 Results of mixed-effects models (with interaction term) analyses: limbic system white matter tracts AK and ARI scores in ADHD.

	Sex		**Months from baseline**		**ARI**		**ARI * Months from baseline**	
	B (SE)	***t, p***	***B (SE)***	***t, p***	***B (SE)***	***t, p***	***B (SE)***	***t, p***
Cingulum Bundle (Left)	-4.349e-03 (6.656e-03)	-0.653, 0.516	-1.120e-04 (4.122e-04)	-0.272, 0.787	-1.606e-03 (1.022e-03)	-1.573, 0.119	1.582e-04 (7.914e-05)	1.999, 0.050
Cingulum Bundle (Right)	-4.584e-03 (6.802e-03)	-0.674, 0.502	-4.001e-04 (4.329e-04)	-0.924, 0.358	-9.400e-04 (1.072e-03)	-0.887, 0.382	1.638e-04 (8.298e-05)	1.974, 0.052
Fornix (Left)	5.236e-04 (8.726e-03)	0.060, 0.952	-2.500e-04 (5.475e-04)	-0.457, 0.650	-1.292e-03 (1.366e-03)	-0.946, 0.347	9.827e-05 (1.043e-04)	0.942 0.350
Fornix (Right)	3.678e-03 (1.711e-02)	0.215, 0.831	8.391e-04 (8.998e-04)	0.933, 0.355	3.443e-03 (2.373e-03)	1.451, 0.150	-3.534e-05 (1.704e-04)	-0.207 0.837
Anterior Thalamic Projections (Left)	7.961e-03 (6.918e-03)	1.151, 0.254	-7.221e-05 (4.483e-04)	-0.161, 0.873	-6.451e-04 (1.086e-03)	-0.594, 0.554	1.299e-04 (8.609e-05)	1.509, 0.137
Anterior Thalamic Projections (Right)	2.350e-03 (6.918e-03)	0.340, 0.735	-2.927e-04 (4.674e-04)	-0.626, 0.533	-3.576e-04 (1.122e-03)	-0.319, 0.750	1.584e-04 (8.961e-05)	1.768, 0.081

Mammillothalamic tract (Left)	1.347e-02 (1.477e-02)	0.912, 0.365	1.857e-04 (1.042e-03)	0.178, 0.859	-4.213e-03 (2.405e-03)	-1.751, 0.082	4.335e-04 (2.019e-05)	2.147, 0.035
Mammillothalamic tract (Right)	-1.970e-02 (1.609e-02)	-1.224, 0.227	1.321e-04 (1.128e-03)	0.117, 0.907	-2.543e-03 (2.651e-03)	-0.960, 0.340	-1.381e-04 (2.205e-04)	-0.626, 0.534
Uncinate Fasciculus (Left)	8.607e-03 (1.053e-02)	0.818, 0.417	-5.328e-04 (5.341e-04)	-0.997, 0.324	-9.958e-04 (1.474e-03)	-0.676, 0.501	1.666e-04 (1.026e-04)	1.623, 0.111
Uncinate Fasciculus (Right)	1.018e-02 (9.319e-03)	1.093, 0.281	7.868e-05 (6.340e-04)	0.124, 0.902	-1.409e-03 (1.489e-03)	-0.947, 0.346	1.678e-04 (1.257e-04)	1.334, 0.188

Table 5.26 Results of mixed-effects models (with interaction term) analyses: limbic system white matter tracts RK and ARI scores in ADHD.

	Sex		**Months from baseline**		**ARI**		**ARI * Months from baseline**	
	***B* (SE)**	**t, p**	***B* (SE)**	**t, p**	***B* (SE)**	**t, p**	***B* (SE)**	**t, p**
Cingulum Bundle (Left)	2.325e-02 (2.306e-02)	1.008, 0.317	1.535e-03 (1.412e-03)	1.087, 0.281	-1.207e-03 (3.519e-03)	-0.343, 0.732	3.678e-04 (2.711e-04)	1.357, 0.180
Cingulum Bundle (Right)	4.320e-02 (2.156e-02)	2.004, 0.049	4.229e-04 (1.473e-03)	0.287, 0.774	3.285e-04 (3.517e-03)	0.093, 0.925	3.679e-04 (2.824e-04)	1.303, 0.197
Fornix (Left)	3.077e-02 (2.728e-02)	1.128, 0.264	-1.327e-03 (1.478e-03)	-0.898, 0.373	-2.537e-03 (3.979e-03)	-0.638, 0.525	1.328e-04 (2.807e-04)	0.473 0.638
Fornix (Right)	1.697e-02 (2.994e-02)	0.567, 0.573	2.978e-04 (1.486e-03)	0.200, 0.842	2.657e-03 (4.034e-03)	0.659, 0.512	1.769e-04 (2.811e-04)	0.629 0.532
Anterior Thalamic Projections (Left)	1.239e-02 (2.211e-02)	0.560, 0.577	7.765e-04 (1.308e-03)	0.593, 0.555	-2.645e-03 (3.316e-03)	-0.798, 0.427	1.707e-04 (2.510e-04)	0.680, 0.499
Anterior Thalamic Projections (Right)	-2.440e-03 (2.073e-02)	-0.118, 0.906	-7.785e-04 (1.234e-03)	-0.631, 0.530	4.617e-04 (3.165e-03)	0.146, 0.884	4.320e-04 (2.364e-04)	1.827, 0.072

Mammillothalamic tract (Left)	-1.614e-02 (2.058e-02)	-0.784, 0.436	1.271e-03 (1.335e-03)	0.952, 0.345	-9.837e-04 (3.219e-03)	-0.305, 0.761	1.807e-04 (2.586e-04)	0.699, 0.487
Mammillothalamic tract (Right)	-3.861e-02 (2.154e-02)	-1.793, 0.078	3.497e-04 (1.407e-03)	0.249, 0.804	-4.329e-03 (3.436e-03)	-1.260, 0.210	-7.278e-05 (2.758e-04)	-0.264, 0.792
Uncinate Fasciculus (Left)	4.285e-02 (2.922e-02)	1.466, 0.147	-1.146e-03 (1.936e-03)	-0.592, 0.555	-6.964e-03 (4.638e-03)	-1.501, 0.136	6.270e-04 (3.735e-04)	1.679, 0.098
Uncinate Fasciculus (Right)	2.029e-02 (2.830e-02)	0.717, 0.477	5.024e-04 (1.895e-03)	0.265, 0.792	-1.221e-03 (4.486e-03)	-0.272, 0.786	1.228e-04 (3.760e-04)	0.327, 0.745

Table 5.27 Results of mixed-effects models (with interaction term) analyses: limbic system white matter tracts MK and ARI scores in ADHD.

	Sex		**Months from baseline**		**ARI**		**ARI * Months from baseline**	
	B (SE)	***t, p***	***B (SE)***	***t, p***	***B (SE)***	***t, p***	***B (SE)***	***t, p***
Cingulum Bundle (Left)	1.639e-02 (1.319e-02)	1.243, 0.218	5.045e-04 (7.249e-04)	0.696, 0.489	-8.517e-04 (1.906e-03)	-0.447, 0.655	2.619e-04 (1.390e-04)	1.884, 0.064
Cingulum Bundle (Right)	1.812e-02 (1.132e-02)	1.601, 0.114	-2.364e-04 (7.420e-04)	-0.319, 0.751	-5.468e-05 (1.810e-03)	-0.030, 0.976	2.815e-04 (1.422e-04)	1.979, 0.052
Fornix (Left)	7.627e-03 (1.402e-02)	0.544, 0.589	-7.157e-04 (7.521e-04)	-0.951, 0.346	-1.904e-03 (2.034e-03)	-0.936, 0.352	1.328e-04 (1.427e-04)	0.931 0.357
Fornix (Right)	7.564e-03 (2.163e-02)	0.350, 0.728	5.640e-04 (1.149e-03)	0.491, 0.626	3.266e-03 (3.015e-03)	1.083, 0.281	6.049e-05 (2.176e-04)	0.278 0.782
Anterior Thalamic Projections (Left)	1.399e-02 (1.092e-02)	1.281, 0.205	2.780e-04 (7.569e-04)	0.367, 0.715	-1.282e-03 (1.775e-03)	-0.722, 0.472	1.474e-04 (1.454e-04)	1.013, 0.315
Anterior Thalamic Projections (Right)	5.312e-04 (1.216e-02)	0.044, 0.965	-5.806e-04 (7.133e-04)	-0.814, 0.419	2.133e-04 (1.844e-03)	0.116, 0.908	2.759e-04 (1.367e-04)	2.019, 0.048

Mammillothalamic tract (Left)	9.886e-04 (1.526e-02)	0.065, 0.948	3.282e-04 (9.860e-03)	0.333, 0.740	-3.485e-03 (2.383e-03)	-1.462, 0.146	3.971e-04 (1.909e-04)	2.080, 0.041
Mammillothalamic tract (Right)	-3.127e-02 (1.735e-02)	-1.802, 0.077	4.406e-04 (1.212e-03)	0.362, 0.718	-3.070e-03 (2.857e-03)	-1.075, 0.285	-1.281e-04 (2.376e-04)	-0.539 0.591
Uncinate Fasciculus (Left)	2.063e-02 (1.728e-02)	1.193, 0.237	-9.601e-04 (9.949e-04)	-0.965, 0.339	-2.806e-03 (2.566e-03)	-1.094, 0.277	3.408e-04 (1.916e-04)	1.779, 0.081
Uncinate Fasciculus (Right)	1.311e-02 (1.526e-02)	0.859, 0.394	2.551e-04 (9.253e-04)	0.276, 0.784	-7.736e-04 (2.306e-03)	-0.335, 0.738	1.531e-04 (1.835e-04)	0.834, 0.408

Table 5.28 Results of mixed-effects models (with interaction term) analyses: limbic system white matter tracts FA and ARI scores in ADHD.

	Sex		**Months from baseline**		**ARI**		**ARI * Months from baseline**	
	B (SE)	***t, p***	***B (SE)***	***t, p***	***B (SE)***	***t, p***	***B (SE)***	***t, p***
Cingulum Bundle (Left)	1.245e-02 (7.985e-03)	1.559, 0.124	4.395e-04 (4.329e-04)	1.015, 0.315	-8.362e-06 (1.146e-03)	-0.007, 0.994	-1.838e-05 (8.249e-05)	-0.223, 0.825
Cingulum Bundle (Right)	1.232e-02 (7.605e-03)	1.621, 0.110	1.481e-04 (3.000e-04)	0.494, 0.624	-4.895e-04 (9.481e+01)	-0.531, 0.597	7.556e-05 (5.703e-05)	1.325, 0.192
Fornix (Left)	3.027e-02 (1.068e-02)	2.835, 0.006	3.815e-04 (6.214e-04)	0.614, 0.541	7.807e-04 (1.619e-03)	0.482, 0.630	-3.416e-05 (1.181e-04)	-0.289 0.773
Fornix (Right)	7.564e-03 (8.542e-03)	1.605, 0.114	-2.464e-04 (5.336e-04)	-0.462, 0.646	-1.820e-03 (1.295e-03)	-1.406, 0.163	3.566e-05 (1.008e-04)	0.354 0.725
Anterior Thalamic Projections (Left)	3.520e-03 (7.173e-03)	0.491, 0.625	2.667e-04 (3.491e-04)	0.764, 0.448	-5.351e-04 (9.739e-04)	-0.549, 0.584	-6.673e-06 (6.646e-05)	-0.100, 0.920
Anterior Thalamic Projections (Right)	9.635e-04 (6.860e-03)	0.140, 0.889	-2.359e-04 (3.316e-04)	-0.711, 0.480	-9.560e-04 (9.282e-04)	-1.030, 0.305	7.078e-05 (6.313e-05)	1.121, 0.268

Mammillothalamic tract (Left)	5.547e-03 (9.852e-03)	0.563, 0.576	-1.725e-04 (6.666e-04)	-0.259, 0.797	-1.524e-03 (1.582e-03)	-0.963, 0.338	1.140e-04 (1.275e-04)	0.894, 0.375
Mammillothalamic tract (Right)	3.111e-03 (9.594e-03)	0.324, 0.746	6.835e-04 (7.321e-04)	0.934, 0.353	-6.416e-05 (1.636e-03)	-0.039, 0.969	-8.553e-05 (1.398e-04)	-0.612 0.542
Uncinate Fasciculus (Left)	5.088e-03 (8.643e-03)	0.589, 0.559	-5.431e-04 (5.442e-04)	-0.998, 0.323	8.497e-05 (2.566e-03)	0.063, 0.950	1.309e-04 (1.037e-04)	1.262, 0.213
Uncinate Fasciculus (Right)	3.262e-03 (8.994e-03)	0.363, 0.718	2.830e-04 (5.594e-04)	0.506, 0.615	1.159e-03 (1.363e-03)	0.850, 0.397	-6.669e-05 (1.059e-04)	-0.630, 0.532

Table 5.29 Results of mixed-effects models (with interaction term) analyses: limbic system white matter tracts AD and ARI scores in ADHD.

	Sex		**Months from baseline**		**ARI**		**ARI* Months from baseline**	
	B (SE)	***t, p***	***B (SE)***	***t, p***	***B (SE)***	***t, p***	***B (SE)***	***t, p***
Cingulum Bundle (Left)	2.900e-05 (1.292e-05)	2.244, 0.028	5.875e-07 (7.124e-07)	0.825, 0.413	3.792e-07 (1.871e-06)	0.203, 0.839	-1.303e-07 (1.357e-07)	-0.960, 0.341
Cingulum Bundle (Right)	3.152e-05 (1.284e-05)	2.455, 0.017	-2.257e-09 (7.108e-07)	-0.003, 0.997	-1.031e-06 (1.863e-06)	-0.553, 0.581	-1.067e-07 (1.354e-07)	-0.788, 0.434
Fornix (Left)	1.266e-04 (6.139e-05)	2.061, 0.043	-2.802e-06 (3.797e-06)	-0.738, 0.463	4.513e-06 (9.591e-06)	0.471, 0.639	3.467e-09 (7.224e-07)	0.005 0.996
Fornix (Right)	-1.278e-05 (4.731e-05)	-0.270, 0.788	3.514e-06 (3.256e-06)	1.079, 0.284	-2.218e-07 (7.530e-06)	-0.029, 0.977	-4.972e-07 (6.153e-07)	-0.808 0.422
Anterior Thalamic Projections (Left)	1.663e-05 (1.015e-05)	1.638, 0.106	1.058e-06 (6.481e-07)	1.632, 0.107	-3.120e-08 (1.584e-06)	-0.020, 0.984	-1.262e-07 (1.235e-07)	-1.022, 0.311
Anterior Thalamic Projections (Right)	8.623e-06 (1.273e-05)	0.678, 0.500	-2.074e-07 (6.339e-07)	-0.327, 0.745	-9.886e-07 (1.749e-06)	-0.565, 0.573	-1.055e-07 (1.207e-07)	-0.874, 0.386

Mammillothalamic tract (Left)	-5.789e-05 (4.211e-05)	-1.375, 0.174	1.041e-06 (3.035e-06)	0.343, 0.733	2.048e-06 (6.977e-06)	0.294, 0.770	-3.273e-07 (5.803e-07)	-0.564, 0.575
Mammillothalamic tract (Right)	2.056e-05 (5.511e-05)	0.373, 0.710	-2.615e-07 (3.023e-06)	-0.086, 0.931	-7.743e-07 (8.006e-06)	-0.097, 0.923	2.718e-07 (5.781e-07)	0.470 0.640
Uncinate Fasciculus (Left)	8.041e-06 (1.673e-05)	0.481, 0.632	-9.386e-07 (8.123e-07)	-1.155, 0.254	-4.610e-07 (2.269e-06)	-0.203, 0.839	2.912e-08 (1.547e-07)	0.188, 0.851
Uncinate Fasciculus (Right)	2.714e-05 (1.589e-05)	1.708, 0.092	-1.506e-06 (8.787e-07)	-1.714, 0.092	-2.369e-07 (2.277e-06)	-0.104, 0.917	4.549e-09 (1.664e-07)	-0.027, 0.978

Table 5.30 Results of mixed-effects models (with interaction term) analyses: limbic system white matter tracts RD and ARI scores in ADHD.

	Sex		**Months from baseline**		**ARI**		**ARI * Months from baseline**	
	B (SE)	***t, p***	***B (SE)***	***t, p***	***B (SE)***	***t, p***	***B (SE)***	***t, p***
Cingulum Bundle (Left)	1.336e-06 (1.074e-05)	0.124, 0.901	-3.015e-07 (5.932e-07)	-0.508, 0.613	1.381e-07 (1.557e-06)	0.089, 0.929	-4.554e-08 (1.130e-07)	-0.403, 0.689
Cingulum Bundle (Right)	1.725e-06 (1.026e-05)	0.168, 0.867	-3.627e-07 (4.615e-07)	-0.786, 0.436	3.692e-07 (1.337e-06)	0.276, 0.783	-1.375e-07 (8.782e-08)	-1.566, 0.124
Fornix (Left)	-3.398e-07 (2.556e-05)	-0.013, 0.989	-2.259e-06 (1.667e-06)	-1.355, 0.181	1.712e-06 (4.099e-06)	0.418, 0.677	-5.848e-08 (3.174e-07)	-0.184 0.855
Fornix (Right)	-8.386e-06 (2.145e-05)	-0.391, 0.697	1.740e-06 (1.416e-06)	1.228, 0.224	4.989e-06 (3.343e-06)	1.492, 0.139	-2.618e-07 (2.677e-07)	-0.978 0.332
Anterior Thalamic Projections (Left)	5.126e-06 (9.356e-06)	0.548, 0.586	3.636e-07 (5.760e-07)	0.631, 0.530	1.481e-06 (1.433e-06)	1.033, 0.304	-8.706e-08 (1.098e-07)	-0.793, 0.431
Anterior Thalamic Projections (Right)	5.728e-06 (9.905e-06)	0.578, 0.565	3.599e-09 (4.875e-07)	0.007, 0.994	5.786e-07 (1.353e-06)	0.428, 0.670	-1.166e-07 (9.283e-08)	-1.256, 0.215

Mammillothalamic tract (Left)	-3.521e-05 (3.300e-05)	-1.067, 0.289	1.030e-06 (2.518e-06)	0.409, 0.683	4.363e-06 (5.625e-06)	0.776, 0.440	-4.367e-07 (4.809e-07)	-0.908, 0.366
Mammillothalamic tract (Right)	5.522e-06 (4.109e-05)	0.134, 0.894	-5.142e-07 (2.481e-06)	-0.207, 0.837	1.788e-06 (6.247e-06)	0.286, 0.775	1.292e-07 (4.746e-07)	0.272 0.786
Uncinate Fasciculus (Left)	-9.956e-07 (1.040e-05)	-0.096, 0.924	3.610e-07 (7.412e-07)	0.487, 0.628	4.584e-07 (1.717e-06)	0.267, 0.790	-1.889e-07 (1.412e-07)	-1.338, 0.185
Uncinate Fasciculus (Right)	8.601e-06 (1.405e-05)	0.612, 0.543	-1.405e-06 (7.034e-07)	-1.997, 0.051	-1.938e-06 (1.921e-06)	-1.009, 0.315	1.492e-07 (1.332e-07)	1.120, 0.268

Table 5.31 Results of mixed-effects models (with interaction term) analyses: limbic system white matter tracts MD and ARI scores in ADHD.

	Sex		**Months from baseline**		**ARI**		**ARI * Months from baseline**	
	B (SE)	***t, p***	***B (SE)***	***t, p***	***B (SE)***	***t, p***	***B (SE)***	***t, p***
Cingulum Bundle (Left)	1.299e-05 (9.500e-06)	1.367, 0.176	2.033e-07 (5.199e-07)	0.391, 0.697	8.238e-07 (1.370e-06)	0.601, 0.549	-9.271e-08 (9.906e-08)	-0.936, 0.353
Cingulum Bundle (Right)	1.277e-05 (9.346e-06)	1.366, 0.177	-1.768e-07 (4.710e-07)	-0.375, 0.709	2.922e-07 (1.292e-06)	0.226, 0.822	-1.297e-07 (8.969e-08)	-1.446, 0.155
Fornix (Left)	3.002e-05 (3.574e-05)	0.840, 0.404	-2.451e-06 (2.217e-06)	-1.106, 0.274	2.646e-06 (5.591e-06)	0.473, 0.637	-2.998e-08 (4.217e-07)	-0.071 0.944
Fornix (Right)	-2.243e-06 (2.847e-05)	-0.079, 0.937	1.830e-06 (1.846e-06)	0.991, 0.325	3.919e-06 (4.397e-06)	0.891, 0.375	-3.039e-07 (3.488e-07)	-0.871 0.387
Anterior Thalamic Projections (Left)	8.809e-06 (8.438e-06)	1.044, 0.300	6.987e-07 (5.464e-07)	1.279, 0.205	8.519e-07 (1.326e-06)	0.642, 0.522	-1.222e-07 (1.041e-07)	-1.174, 0.245
Anterior Thalamic Projections (Right)	9.032e-06 (9.459e-06)	0.955, 0.343	-1.580e-07 (4.463e-07)	-0.354, 0.725	1.712e-07 (1.264e-06)	0.136, 0.892	-1.061e-07 (8.495e-08)	-1.248, 0.218

Mammillothalamic tract (Left)	-4.715e-05 (3.541e-05)	-1.331, 0.188	1.263e-06 (2.683e-06)	0.471, 0.639	3.401e-06 (6.016e-06)	0.565, 0.573	-4.336e-07 (5.125e-07)	-0.846, 0.400
Mammillothalamic tract (Right)	6.222e-06 (4.683e-05)	0.133, 0.895	-7.005e-09 (2.565e-06)	-0.003, 0.998	2.049e-06 (6.798e-06)	0.301, 0.764	6.622e-09 (4.904e-07)	0.014 0.989
Uncinate Fasciculus (Left)	9.332e-07 (9.465e-06)	0.099, 0.922	-2.004e-07 (6.309e-07)	-0.318 0.752	5.068e-08 (1.510e-06)	0.034, 0.973	-1.038e-07 (1.202e-07)	-0.864, 0.391
Uncinate Fasciculus (Right)	1.444e-05 (1.313e-05)	1.100, 0.276	-1.541e-06 (6.235e-07)	-2.471, 0.017	-1.749e-06 (1.751e-06)	-0.999, 0.320	1.198e-07 (1.180e-07)	1.015, 0.315

Table 5.32 Mean values of the effect of diagnosis in the 100 iterations of optimal mixed-effects models analyses of limbic system with sex sex-matched case-control samples.

	Diagnosis			
	B	***SE***	***T***	***p-value***
Left Cingulum Bundle (KA)	-8.50e-03	3.397e-03	-2.515	0.014
Right Cingulum Bundle (KA)	-8.89e-03	3.452e-03	-2.575	0.011
Left Fornix (KA)	-9.50e-03	3.816e-03	-2.489	0.014
Left Fornix (RD)	4.31e-05	1.57e-05	2.743	0.008
Left Anterior Thalamic Projection (RK)	1.462e-03	5.77e-04	2.531	0.014

Table 5.33 Results of medication status sensitivity analysis using optimal mixed-effects models (without interaction term) analyses: limbic system white matter KA in ADHD.

	Sex		**Months from baseline**		**Age at baseline**		**Medication Status**	
	B (SE)	***t, p***	***B (SE)***	***t, p***	***B (SE)***	***t, p***	***B (SE)***	***t, p***
Left Cingulum Bundle (KA)	-9.298e-04 (5.888e-03)	-0.158, 0.8750	2.454e-04 (9.812e-05)	2.501, 0.014	9.517e-03 (4.983e-03)	1.910, 0.060	-1.651e-03 (4.642e-03)	-0.356 0.722
Right Cingulum Bundle (KA)	7.010e-03 (5.801e-03)	1.208, 0.231	2.309e-04 (9.961e-05)	2.317, 0.022	1.208e-02 (4.907e-03)	2.462 , 0.016	-4.265e-03 (4.580e-03)	-0.931, 0.353
Left Fornix (KA)	3.272e-03 (6.003e-03)	0.545, 0.587	-4.137e-04 (1.263e-04)	-3.277, 0.001	2.593e-03 (5.255e-03)	0.493, 0.623	-7.553e-03 (5.872e-03)	-1.286, 0.200

Table 5.34 Results of medication status sensitivity analysis using optimal mixed-effects models (without interaction term) analyses: limbic system white matter RD in ADHD.

	Sex		**Months from baseline**		**Age at baseline**		**Medication status**		**Medication status*Months from baseline**	
	B (SE)	***t, p***	***B (SE)***	***t, p***	***B (SE)***	***t, p***	***B (SE)***	***t, p***	***B (SE)***	***t, p***
Left Anterior Thalamic Projection (RK)	2.758e-02 (1.707e-02)	1.616, 0.119	3.691e-03 (4.889e-04)	7.550, <0.000	2.603e-02 (1.481e-02)	1.758, 0.083	2.164e-02 (1.952e-02)	1.109, 0.269	-1.081e-03 (9.794e-04)	-1.104, 0.272
Left Fornix (RD)	3.675e-07 (2.643e-05)	0.014, 0.989	-3.899e-07 (5.477e-07)	-0.712, 0.478	3.994e-05 (2.245e-05)	1.779, 0.079	1.377e-05 (2.557e-05)	0.539, 0.591	-7.544e-07 (1.103e-06)	-0.684, 0.495

Table 5.35 Results of optimal mixed-effects models analyses with comorbidity status: limbic system white matter microstructure in ADHD and Controls.

	Sex		**Age at baseline**		**Months from baseline**		**Diagnosis**		**Comorbidity**		**Diagnosis* Months from baseline**	
	B (SE)	***t, p***	***B (SE)***	***t, p***	***B (SE)***	***t, p***	***B (SE)***	***t, p***	***B (SE)***	***t, p***	***B (SE)***	***t, p***
Left Cingulum Bundle (KA)	1.678e-04 (3.626e-03)	0.046 0.963	6.959e-03 (3.664e-03)	1.899 0.059	2.683e-04 (7.601e-05)	3.530 <0.000	-8.618e-03 (3.448e-03)	-2.500 0.013	1.765e-03 (2.629e-03)	0.671 0.502	n/a	n/a
Right Cingulum Bundle (KA)	4.022e-03 (3.756e-03)	1.071 0.285	1.070e-02 (3.801e-03)	2.816, 0.005	3.949e-04 (8.315e-05)	-4.749 <0.000	-8.679e-03 (3.601e-03)	-2.410 0.016	1.188e-03 (3.023e-03)	0.393 0.694	n/a	n/a
Left Fornix (KA)	2.491e-03 (3.017e-03)	0.826 0.410	1.241e-03 (3.089e-03)	0.402 0.688	-5.354e-04 (7.338e-05)	-7.296 <0.000	-7.385e-03 (3.565e-03)	-2.071 0.039	-6.360e-03 (2.920e-03)	-2.178 0.030	2.276e-04 (1.446e-04)	1.573 0.117
Left Fornix (RD)	-1.244e-05 (1.219e-05)	-1.020 0.309	3.249e-05 (1.240e-05)	2.620, 0.009	1.805e-07 (2.719e-07)	0.664, 0.507	3.613e-05 (1.392e-05)	2.595 0.009	1.671e-05 (1.074e-05)	1.556 0.120	-9.357e-07 (5.365e-07)	-1.744 0.082
Left Anterior Thalamic Projections (RK)	3.534e-03 (1.186e-02)	0.298, 0.766	6.248e-03 (1.205e-02)	0.519, 0.604	2.675e-03 (2.996e-04)	8.930, <0.000	-4.104e-02 (1.414e-02)	-2.903 0.003	1.625e-02 (1.168e-02)	1.391 0.165	1.775e-03 (5.885e-04)	3.016 0.002

Table 5.36 Results of optimal mixed-effects models analyses with frame-wise displacement: limbic system white matter microstructure in ADHD and Controls.

	Sex		**Age at baseline**		**Months from baseline**		**Diagnosis**		**FWD**		**Diagnosis* Months from baseline**	
	B (SE)	***t, p***	***B (SE)***	***t, p***	***B (SE)***	***t, p***	***B (SE)***	***t, p***	***B (SE)***	***t, p***	***B (SE)***	***t, p***
Left Cingulum	-1.103e-03	-0313	6.937e-03	1.947	2.672e-04	3.588	-8.955e-03	-2.689	8.961e-03	1.377	n/a	n/a
Bundle (KA)	(3.526e-03)	0.754	(3.562e-03)	0.053	(7.447e-05)	<0.000	(3.330e-03)	0.007	(6.506e-03)	0.169		
Right Cingulum	8.639e-04	0.258	1.208e-02	3.465	4.130e-04	6.818	-6.431e-03	-2.031	1.097e-03	0.191	n/a	n/a
Bundle (KA)	(3.351e-03)	0.796	(3.486e-03)	<0.000	(6.058e-05)	<0.000	(3.166e-0)	0.043	(5.749e-03)	0.848		
Left Fornix (KA)	2.773e-03	0.927	2.393e-04	0.078	-5.123e-04	-6.903	-9.285e-03	-2.625	2.097e-04	0.029	2.386e-04	1.624
	(2.992e-03)	0.355	(3.071e-03)	0.938	(7.421e-05)	<0.000	(3.537e-03)	0.009	(7.213e-03)	0.976	(1.469e-04)	0.105
Left Fornix (RD)	-1.102e-05	-0.897	3.406e-05	2.722	6.596e-08	0.240	4.220e-05	3.012	5.410e-06	0.198	-1.078e-06	-1.983
	(1.229e-05)	0.371	(1.251e-05)	0.007	(2.745e-07)	0.810	(1.401e-05)	0.002	(2.730e-05)	0.843	(5.436e-07)	0.048

Left Anterior Thalamic Projections (RK)	-2.749e-03 (1.043e-02)	-0.264 0.792	3.095e-03 (1.053e-02)	0.294 0.769	2.733e-03 (2.382e-04)	11.473 <0.000	-2.487e-02 (1.188e-02)	-2.093 0.037	5.245e-02 (2.387e-02)	2.198 0.028	1.201e-03 (4.723e-04)	2.543 0.117

Figure 5.34 Beta values and SEs of sex-group sensitivity analysis.

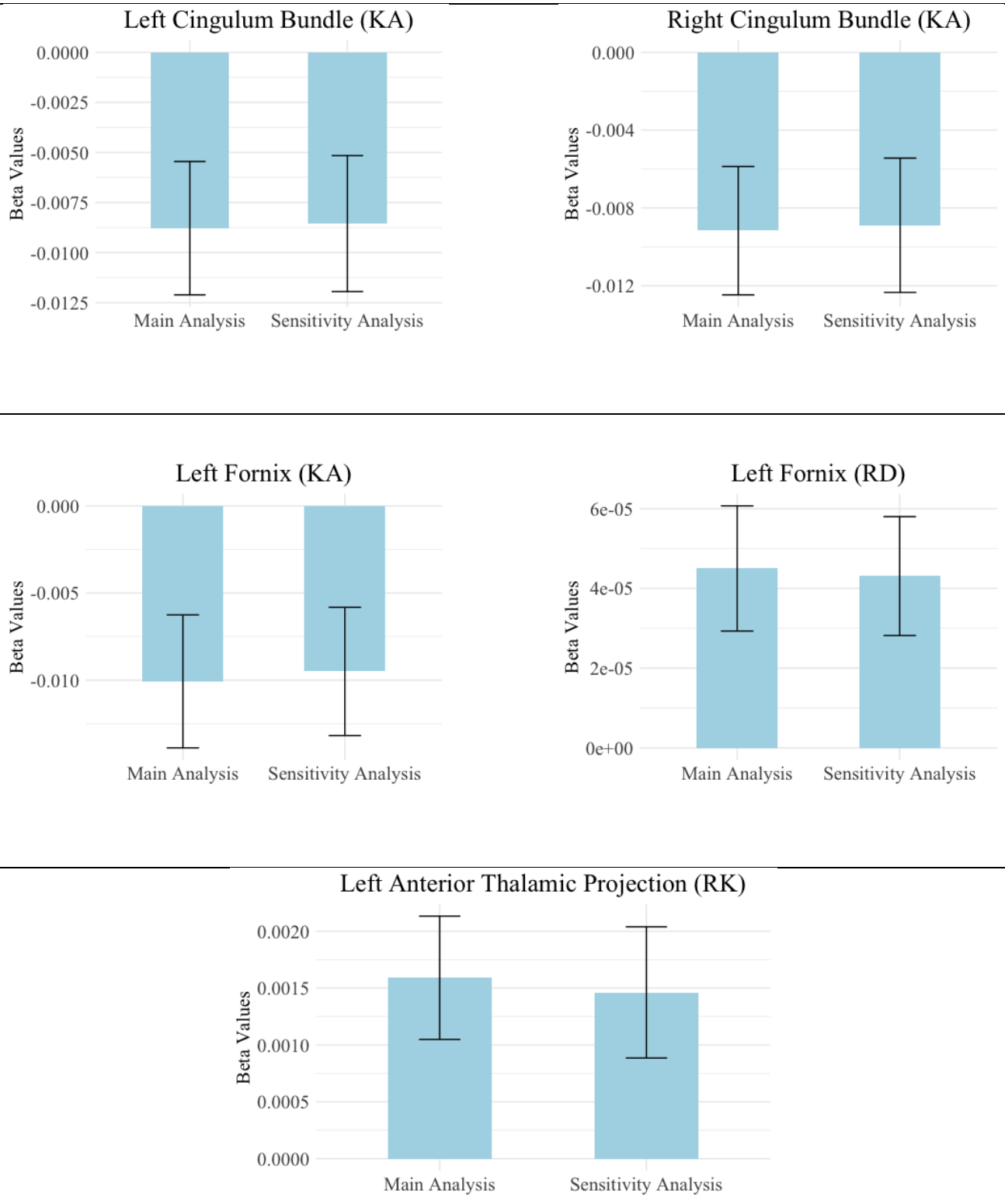

Figure 5.35 Beta values and SEs of Comorbidity sensitivity analysis.

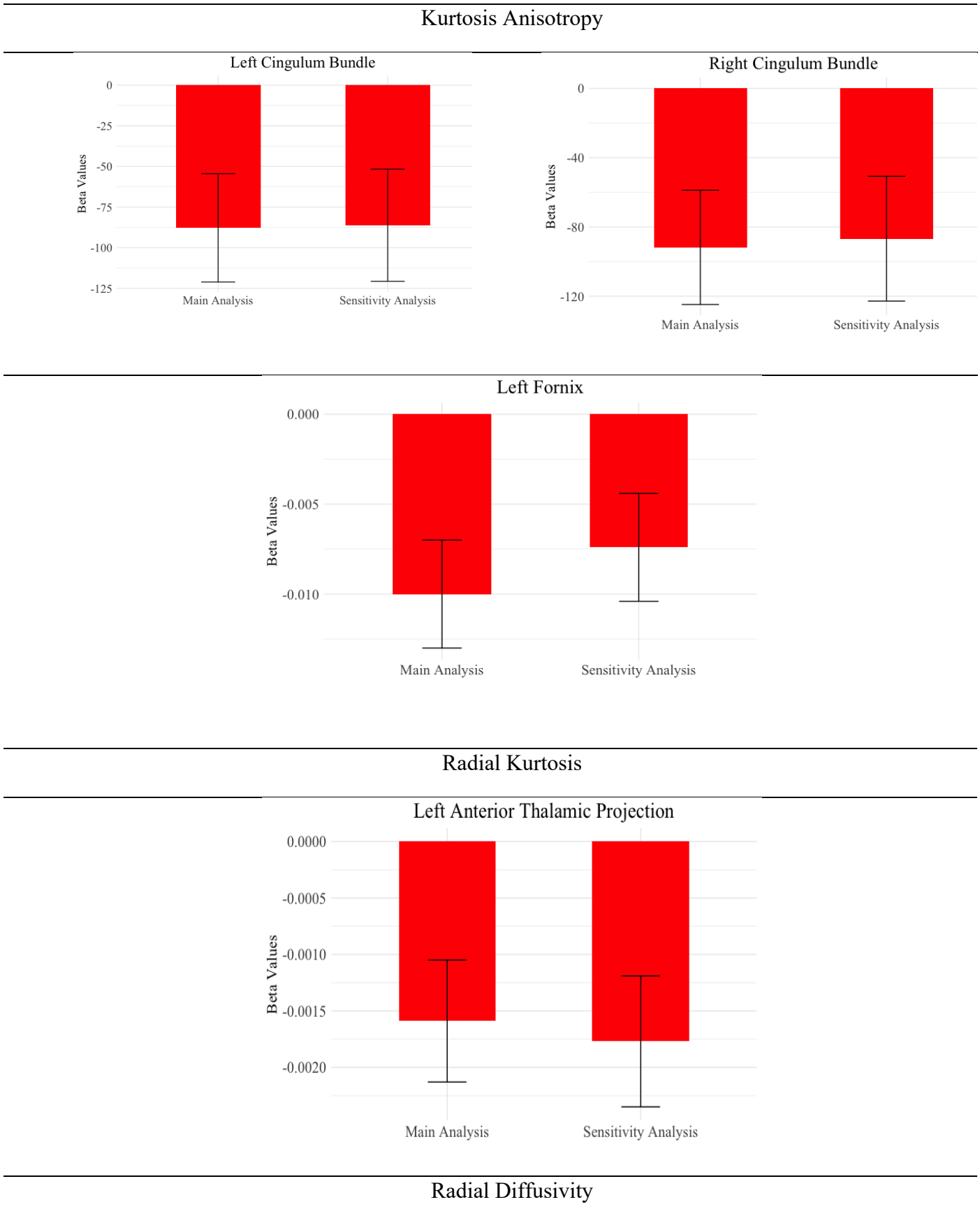

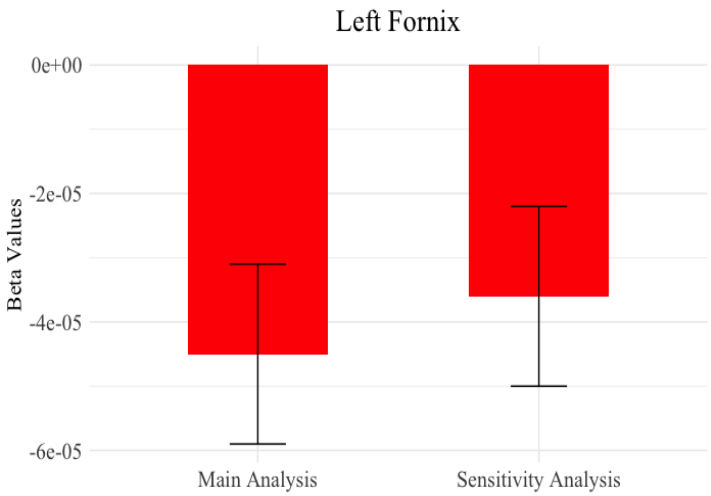
Left Fornix
0e+00
-2e-05
-4e-05
-6e-05
Beta Values
Main Analysis
Sensitivity Analysis

Figure 5.36 Beta values and SEs of FWD sensitivity analysis.

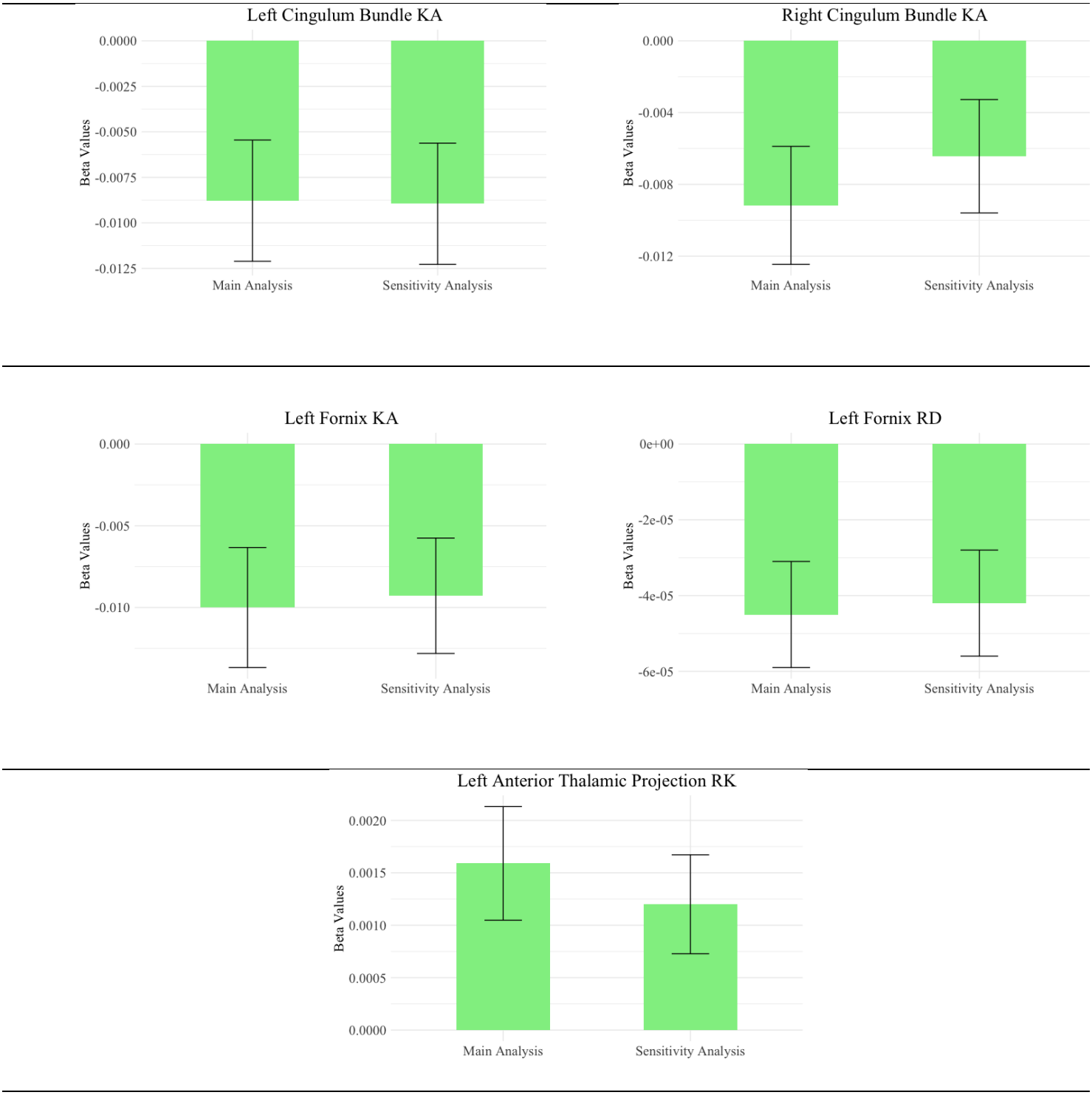

5.4. Discussion

The longitudinal dMRI study described in this chapter aimed to investigate microstructural alterations within key limbic system white matter tracts during the

transition from childhood into mid-adolescence among individuals with ADHD compared to controls. Both gaussian (DTI) and non-gaussian (DKI) metrics were investigated to provide a more complex description of the diffusion profiles. Exploratory analysis investigated associations between microstructural organisation of limbic system white matter and ADHD symptom severity in children with ADHD. The study described in this thesis presents three main findings. First, children with ADHD displayed reduced white matter microstructural organisation – decreased KA and increased RD – in the bilateral cingulum bundles and left fornix compared to controls. Second, during the transition from childhood to mid-adolescence, children with ADHD displayed an increased rate of change of RK in the left anterior thalamic projection compared to controls. Third, in children with ADHD, increased ADHD symptom severity was significantly correlated with increased KA in the right fornix.

5.4.1. Role of Limbic System White Matter Tracts Implicated in ADHD

Cingulum Bundle

The cingulum bundle is a key limbic system white matter tract which interconnects the amygdala, hippocampus, cingulate gyrus, and other brain regions (Catani, Dell'acqua, and Thiebaut de Schotten 2013). The cingulum bundle has been linked to a wide range of functions, including executive function, attention, emotional processing and regulation (Bubb, Metzler-Baddeley, and Aggleton 2018). The cingulum bundle displays an extended period of maturation through mid-adolescence and beyond, often not reaching its adult characteristics until the mid-twenties or later. With a mean age of 42 years to reach peak FA, the cingulum is considered one of the last major white matter tracts to mature by this metric (Lebel and Beaulieu 2011; Lebel et al. 2012). In the study described in this chapter, individuals with ADHD displayed reduced KA in the cingulum bundle (bilaterally) compared to controls across all three NICAP time points. In both groups, the cingulum bundle's white matter organisation increased linearly across the three NICAP study time points; a pattern consistent with neurotypical cingulum bundle maturation (Lebel, Treit, and Beaulieu 2019; Das et al. 2017). Findings of reduced KA but not FA suggest that there may be changes in the microstructural complexity or heterogeneity of the cingulum bundle without significant alterations in the overall organisation of this white matter tract. Neurobiologically, increased KA has been shown to reflect higher myelination and axonal

organisation, which are processes associated with neurotypical development of the cingulum bundle (Maiter et al. 2021; Hansen 2019). As such, the reduced KA seen in the ADHD group across all three time points may reflect atypical cingulum bundle development, specifically a fixed non-progressive disruption to neurodevelopmental processes of myelination and axonal packing, consistent with the previously mentioned convergence developmental model of ADHD.

While the cingulum bundle is one of the most prominently linked white matter tracts to ADHD, inconsistencies have also been reported. In previous cross-sectional studies, six reported reduced white matter microstructural organisation in the cingulum in children with ADHD characterised by reduced FA (King et al. 2015), GFA (Chiang et al. 2015; Chiang et al. 2016; Tung et al. 2021), decreased return-to-orientation probability and return-to-axis probability (Wu et al. 2020), and increased MD (Pavuluri et al. 2009). Two other studies reported conflicting results, characterised by findings of increased FA(Silk et al. 2009b), and AD (Svatkova et al. 2016), while five other studies found no significant between-group difference in cingulum bundle microstructure (Lin et al. 2014; Hamilton et al. 2008; Peterson et al. 2011; Lawrence et al. 2013; Cooper, Thapar, and Jones 2015).

Fornix

The fornix is a white matter bundle that interconnects the medial temporal lobe to the mammillary bodies and hypothalamus (Catani and Thiebaut de Schotten 2008; Ross 2008; Mori et al. 2000), which plays a vital role in memory formation and retrieval, spatial navigation and emotional and motivational learning (Hoffman et al. 2022; Benear, Ngo, and Olson 2020; Senova et al. 2020). The fornix is one of the earliest white matter tracts to develop, maturing during infancy and early childhood (Hoffman et al. 2022; Dimond et al. 2020). In this chapter, children with ADHD had reduced KA and increased RD in the left fornix compared to controls. This significant main effect appears to be driven by study time point one, with the ADHD group converging towards the control group at time point 3 (Figures 5.7 & 5.9). The findings of this study are consistent with the maturational delay hypothesis of ADHD (Shaw et al. 2007; Shaw et al. 2012; Rubia 2007). Reduced KA and increased RD may indicate differences in fornix microstructural organisation are associated with decreased complexity and altered myelination (Maiter et al. 2021; Xie et al. 2010; Winklewski et al. 2018). The findings of the present study support previous

research suggesting a link between ADHD and decreased microstructural organisation of the left fornix (Davenport et al. 2010; Onnink et al. 2015). It is important to note that the investigation of the fornix in ADHD has been constrained by limited research and inconsistent findings (van Ewijk et al. 2012). The fornix is a difficult white matter tract to reconstruct accurately, given its high curvature and anatomical location. It is plausible that traditional DTI metrics have struggled to capture the diffusion profile needed to investigate this white matter tract accurately. With the advancement in dMRI acquisition parameters and diffusion modelling techniques, further research is needed to explore the involvement of the fornix in children and adolescents with ADHD.

Additional information can be drawn from the previous longitudinal fixel-based analysis (FBA), a method conceptually similar to voxel-based analyses, that utilised the same NICAP dataset to investigate fibre density and fibre morphology of the cingulum bundle and fornix (Fuelscher et al. 2023). They found that compared to controls, children with ADHD displayed no significant difference in fibre density or fibre morphology of the cingulum bundle and fornix across the three NICAP study time points. FBA is a new dMRI technique that provides quantitative measures of fibre-specific populations, focusing on intra-axonal diffusion properties in a given voxel. While FBA has the benefit of providing greater biological specificity of a given white matter bundle, it does not provide information on the extra axonal diffusion properties. Extra-axonal diffusion refers to the diffusion occurring outside the axonal membranes, encompassing the spaces between axons, myelin sheaths, and other cellular components (Van Hecke, Emsell, and Sunaert 2016). Given the heterogeneous nature of biological tissues such as the brain white matter, valuable insights can be gained by investigating extra axonal diffusion profiles. Considering the findings of previous FBA analyses and the current study, differences observed in limbic system white matter microstructural organisation may be driven by atypical extra axonal diffusion. These findings indicate that children with ADHD might have diminished microstructural complexity or heterogeneity in the cingulum bundle and fornix without substantial alterations in the overall organisation or coherence of these fibre bundles.

Anterior Thalamic Projection

The anterior thalamic nuclei receive incoming fibres from the mammillothalamic tract and fornix and send outgoing projections via the anterior thalamic pathways to the

orbitofrontal and anterior cingulate cortex (Catani, Dell'acqua, and Thiebaut de Schotten 2013). The anterior thalamic projection is involved in various executive functions, such as cognitive control and emotion regulation (Niida et al. 2018; Lichenstein, Verstynen, and Forbes 2016). In this study, compared to controls, individuals with ADHD displayed a significant age-by-group interaction, with a rapid increase in RK during childhood to mid-adolescence. There are many neurobiological mechanisms that may help explain such a result. This rapid increase in non-gaussian diffusion in the radial direction may be attributed to processes of neuroinflammation, specifically an increased breakdown of myelin, neurofilaments, and microtubule degeneration associated with the ADHD group (Takahashi et al. 2002; Does, Parsons, and Gore 2003; Schwartz et al. 2005; Yong-Hing et al. 2005; Thelwall et al. 2006; Goryawala et al. 2018). Alternatively, the overshoot developmental trajectory of the anterior thalamic projections may be explained by the compensatory hypotheses of ADHD (Fassbender and Schweitzer 2006). The compensatory hypotheses of ADHD suggest certain brain regions are associated with a compensatory development of neuroplasticity processes (Chiang et al. 2020). Identifying the biological mechanisms underpinning this finding is beyond the scope of this study; however, it identifies an exciting area for future research to explore.

Overall, this study found that children with ADHD are associated with atypical development of key limbic system white matter tracts – specifically the cingulum bundle, fornix, and anterior thalamic projection – compared to controls during the transition from childhood into mid-adolescence. These findings advance our understanding of the developmental models in ADHD and suggest that the pathophysiology of ADHD will likely involve varied region-specific developmental patterns.

5.4.2. Potential Neurobiological Processes Underlying Atypical White Matter in ADHD

This section will discuss the findings of this study in the context of the prominent neurobiological theories of ADHD. Phenomenological approaches such as DTI and DKI utilise mathematical approximations of the dMRI signal without making assumptions about the specific microstructural properties of the underlying tissue (Martinez-Heras et al. 2021). While these approaches offer excellent sensitivity to microscopic diffusion alterations within a voxel, it cannot pinpoint the exact mechanisms responsible for changes in DTI and DKI metrics (Martinez-Heras et al. 2021). Therefore, interpreting dMRI

metrics in conjunction with other epigenetic, genetic and animal model research is essential, as these dMRI metrics provide complementary information rather than direct measures of neurobiological processes. The atypical microstructural organization found in this study has been linked with neurobiological mechanisms such as dysregulated myelination and processes associated with neuroinflammation.

Processes of Dysregulated Myelination

The findings of this study – particularly in the cingulum and fornix – support a long-standing hypothesis that the neurobiological phenotype seen in ADHD may be underpinned by dysregulated myelination and related changes in neuronal plasticity, particularly in the frontostriatal and limbic circuits (Dark, Homman-Ludiye, and Bryson-Richardson 2018; Lesch 2019). Myelination is a process in which the myelin sheath surrounding neurons is formed and strengthened. When myelination is delayed or disrupted, it can affect brain maturation by altering neuronal plasticity. This is because dysregulated myelination can interrupt the normal growth of neurites and axons due to abnormal production of the myelin sheath. In support of this hypothesis, a recent genome-wide association (GWAS) meta-analysis suggested that the pathophysiology of ADHD may be underpinned by a genetically driven dysregulated myelination (Demontis et al. 2019). In that study, the most significant locus was a gene encoding the beta-galactoside-alpha-2, 3-sialyltransferase-III (ST3GAL3) membrane protein. ST3GAL3 plays a key role in the sialylation of glycoproteins, a process essential for the proper formation and function of myelin sheath (Yoo et al. 2015). Animal research has found that ST3GAL-3 deficient mice displayed ADHD-like behaviours, specifically impaired cognitive function and motor coordinated gait (Yoo et al. 2015). Additionally, these behavioural phenotypes were driven by demyelination, characterised by a reduction in major myelin proteins, fewer myelinated axons, and a decrease in myelin (Yoo et al. 2015).

Other novel candidates, including FOXP2 and MEF2C identified in the GWAS meta-analysis, may also directly or indirectly be involved in the dysregulation of myelination (Dark, Homman-Ludiye, and Bryson-Richardson 2018). FOXP2 may affect myelination through its role in neuronal development and connectivity. Studies have demonstrated that reduced FOXP2 expression leads to abnormalities in the development and function of oligodendrocytes, which subsequently affect myelination processes (Lesch 2019). MEF2C is a transcription factor that plays a critical role in various aspects of brain

development, including axonal myelination. MEF2C is thought to impact myelination through its regulatory effects on the expression of genes involved in oligodendrocyte development. Studies have shown that MEF2C deficiency leads to impaired oligodendrocyte differentiation and reduced myelin formation (Li et al. 2018). The collective evidence from GWAS and neuroimaging studies suggest that variants in ADHD-associated genes may be linked to disrupted myelination, potentially contributing to the neurobiological phenotype seen in ADHD. Further research exploring this link will offer crucial insights into the pathophysiology of ADHD.

Processes of Neuroinflammation

The findings of a rapid increase in the left anterior thalamic projection RK in the ADHD group raise intriguing possibilities of a potential link with neuroinflammation in the pathophysiology of ADHD, in line with emerging evidence in this area (Pakpoor et al. 2018; Dunn, Nigg, and Sullivan 2019). Neuroinflammation is proposed to influence brain development and subsequently increase the risk of neurodevelopmental disorders by acting through mechanisms including glial activation (Réus et al. 2015), increased oxidative stress (Hassan et al. 2016), aberrant neuronal development (Belmadani et al. 2006), decreased neurotropic support (Sen, Duman, and Sanacora 2008), and altered neurotransmitter function (Kronfol and Remick 2000). Further support is found in environmental risk factors for ADHD including maternal infection, maternal tobacco smoking, fetal alcohol syndrome, and maternal obesity, all share an increased maternal inflammatory profile, raising the possibility that inflammation during neural development may play a role in the pathophysiology of ADHD (Costenbader and Karlson 2006; Shankar et al. 2011; Terasaki and Schwarz 2016). At this stage, it is essential to emphasise that these connections are speculative, further research is needed to establish any causal relationship between neuroinflammation and ADHD. This highlights the exciting potential for future research in this area.

The findings of this chapter provide additional support for dysregulated myelination in ADHD pathophysiology and further research is required to validate and elucidate the potential role of neuroinflammatory processes. ADHD is a complex and heterogeneous disorder, and dysregulated myelination and neuroinflammation are just one of many potential factors that may contribute to its aetiology. Further research is required to understand the precise link between these neurodevelopmental processes in ADHD.

Gaining insights into the neurobiological mechanisms underlying the observed neural anomalies can inform the development of targeted treatments, ultimately enhancing symptom management and outcomes for individuals with the disorder. To achieve this, incorporating kurtosis metrics in future dMRI research is recommended due to their increased sensitivity in detecting neurobiological processes compared to traditional tensor metrics (Falangola et al. 2014).

5.4.3. White Matter Microstructure and ADHD Symptom Severity

The exploratory analysis of the study described in this thesis found no significant association between ADHD symptom severity and microstructural properties of limbic system white matter in children and adolescents with ADHD. This finding aligns with the majority of case-control white matter brain-behaviour research in this population, which failed to find any association between diffusion metrics of limbic system white matter tracts and ADHD symptoms severity (Bouziane et al. 2018; Svatkova et al. 2016; Ercan, Suren, Bacanli, et al. 2016; Fuelscher et al. 2021). Notably, one of these dMRI studies using the same data set as the current study (NICAP) and employing FBA also found no significant association between the white matter morphology of the cingulum bundle, thalamic projections and uncinate fasciculus and symptom severity in children and adolescents with ADHD (Fuelscher et al. 2021). Taken together, the research suggests that individual limbic system white matter fibres do not underpin symptom severity in ADHD during childhood and mid-adolescence. As symptom expression likely arises from the complex integration and interaction between multiple neural networks and brain regions, network analysis may provide further insights into ADHD symptoms.

5.4.4. Limitations

One limitation of utilising DKI is the relatively extended time required for image acquisition compared to DTI. The longer acquisition time heightens the susceptibility to imaging artifacts and thermal noise, thereby increasing the likelihood of estimating non-physical values during the fitting process, especially in voxels characterised by low RD (Tabesh et al. 2011; Veraart, Van Hecke, and Sijbers 2011; Henriques 2012; Billiet et al. 2015; Henriques et al. 2021). Although advancements in artifacts correction, noise removal, and constrained parameter estimation techniques have minimised this issue (Tabesh et al. 2011; Veraart, Van Hecke, and Sijbers 2011; Ades-Aron et al. 2018; Veraart

et al. 2016; Mohammadi et al. 2015; Kuder et al. 2012), complete elimination has not been achieved. To minimise this limitation, a thorough visual inspection of all dMRI images was conducted. Each image was meticulously examined and evaluated for the presence of artifacts, issues related to data quality, and excessive head motion.

A further limitation of this chapter's study is the lack of understanding of how puberty affects white matter microstructure in relation to ADHD. The influence of puberty on ADHD remains uncertain. Given that the presentation of ADHD symptoms and neuropsychological functioning appear to change as an individual enters puberty (Dorn 2006), and considering white matter has been shown to be particularly sensitive to remodelling with exposure to pubertal hormones (Juraska and Willing 2017), it is important for future research to investigate the role of pubertal hormones in the development and underlying mechanisms of ADHD.

The number of female participants at study time point 2 was significantly lower compared to male participants, which represents a sex-balance limitation. While there are well-documented differences in symptom profiles between girls and boys with ADHD (Mowlem et al. 2019), the specific sex-related disparities in brain development remain less clear. Previous research revealed differences in white matter microstructure between adolescent males and females with ADHD. King and colleagues (2012) found that females with ADHD exhibited increased fractional anisotropy (FA) in major white matter tracts such as the corticospinal tract, inferior longitudinal fasciculus, and superior longitudinal fasciculus, compared to males with ADHD (King et al. 2015). In the sensitivity analysis, it was found that the sex imbalance between ADHD and controls groups did not significantly affect the results of the primary analysis (Table 3.32), thereby the findings of the primary analysis are unlikely to be confounded by this sex imbalance. However, given that numerous studies investigating brain development in ADHD have not adequately accounted for the potential sex difference, it is crucial for future research to explore how sex differences contribute to the manifestation of symptoms, response to treatment and developmental trajectories of brain networks.

A potential limitation of the study described in this chapter is that some individuals with ADHD were taking medication at certain points throughout the study. Previous research reported no significant difference in white matter microstructure between children with ADHD who have taken stimulant medication compared to no history of stimulant medication (Castellanos, Lee, Sharp, Jeffries, Greenstein, Clasen, Blumenthal,

James, Ebens, and Walter 2002). Consistent with these findings, the sensitivity analysis conducted in this study found no notable differences in white matter microstructure in ADHD individuals with and without medication use (Table 5.33-5.34). This suggests that any observed differences in white matter microstructure are unlikely to be attributed to the effect of medication use. Nevertheless, our understanding of the effects ADHD medication on white matter properties remains limited. Therefore, it is important for future ADHD research to continue investigating the potential impact of medication on brain development, as current studies often include participants with mixed medication status.

5.4.5. Conclusion

In conclusion, the study described in this chapter used higher-order dMRI modelling techniques to reveal significant developmental differences in limbic system white matter microstructure among children and adolescents with ADHD. Specifically, reduced white matter microstructural organization was observed in the bilateral cingulum bundle, left fornix, and left anterior thalamic projections during the transition from childhood to mid-adolescence. These findings contribute valuable insights into the developmental models and neurobiological mechanisms of ADHD. Furthermore, they open avenues for future research to explore the functional significance and clinical implications of these limbic system white matter microstructural changes.

6 Structural Connectivity of the Limbic System in Children and Adolescents with ADHD: A Longitudinal Network Analysis

6.1. Introduction

While univariate approaches such as structural MRI volumetric analysis (Chapter 3) and diffusion MRI tractography analysis (Chapter 5) offer valuable insights into individual regional abnormalities in ADHD, they offer limited insights into the complex interplay of multiple interconnected brain regions from which cognitive functions and behaviours emerge (Bressler and Menon 2010). The psychopathology of ADHD, along with various other psychiatric conditions, is increasingly being viewed not as abnormalities in isolated brain regions but rather as disorders stemming from various dysfunctional brain networks (Cortese et al. 2012b; Konrad and Eickhoff 2010). An important next step in furthering our understanding of brain structural changes in ADHD is in the application of *network analysis*.

Network analysis is a valuable approach that enables the investigation of complex interactions among multiple, interconnected brain regions (Bressler and Menon 2010). Connectomic analysis is a specific type of network analysis that models the human brain as a network (or connectome) (Liao, Vasilakos, and He 2017; Sporns, Tononi, and Kötter 2005). In structural connectivity network analyses, the brain network (connectome) is modelled as an integrated system of *nodes* (reconstructed representations of grey matter and/or subcortical nuclei regions) interconnected by connections known as *edges* (reconstructed representations of white matter tracts), enabling the investigation of white matter topology at a macroscopic level (Bressler and Menon 2010; Liao, Vasilakos, and He 2017; Sporns, Tononi, and Kötter 2005; Bullmore and Sporns 2012) (see Topic Box 1 for definition of structural connectivity).

Topic Box 1. Structural connectivity vs white matter microstructural integrity
Structural connectivity, as a specific type of brain connectivity, is defined by the physical interconnection of two brain regions through a fibre tract, typically measured in vivo in humans using diffusion MRI (dMRI). As such, structural connectivity is an approximation of the actual underlying fibre density or the number of axons in these tracts (Jones, Knösche, and Turner 2013). It's important to note that structural connectivity is distinct from white matter microstructural organisation, which focuses on the properties within white matter tracts, such as the degree of myelination, fibre coherence, and the integrity of axonal membranes, often

indicated by metrics like FA, MD, RD or MD (Van Hecke, Emsell, and Sunaert 2016). While structural connectivity assesses the existence and number of connections between brain regions, white matter microstructural organisation provides insight into the quality and condition of the tracts themselves (Van Hecke, Emsell, and Sunaert 2016).

The network nodes are derived from parcellations of T1 structural MRI images while the edges are derived from tractography methods using diffusion MRI (dMRI) images (Yeh et al. 2021). Typically, in structural connectivity networks, edges are generated by *streamlines* (Hagmann et al. 2008). Streamlines are virtual reconstructions of single fibre pathways through the diffusion field that are generated using tractography algorithms (Van Hecke, Emsell, and Sunaert 2016). In structural connectivity networks streamlines give an approximate measure of the number of white matter fibres connecting two nodes (Van Hecke, Emsell, and Sunaert 2016). Once the edges are generated, they can be defined either as *binary* or *weighted*. In a binary network, edges are described simply by the presence or absence of streamlines interconnecting two nodes (1 or 0) (Bullmore and Sporns 2012). In weighted networks, edges are assigned a value (weight) representing the strength, intensity, and/or capacity of the streamlines interconnecting the network nodes (Yeh et al. 2021). In structural connectivity network analyses, there are generally three methodologies employed to convert streamline counts into edge weights: raw streamline count (Yeh et al. 2016), Hagmann weighting (Hagmann et al. 2008) and streamline fraction (Cao et al. 2013). Descriptions of each approach are provided below:

Raw streamline count is a measure of structural connectivity that quantifies the number of connections between two regions (nodes) (Yeh et al. 2016). This is a basic unnormalized metric and is calculated simply by:

$$C_{ab} = Number\ of\ streamlines\ from\ region\ a\ to\ region\ b$$

Hagmann weighting is an edge weighting formula that quantifies the strength of the connection between two nodes *a* and *b* based on their streamline counts, streamline lengths, and volume of nodes (Hagmann et al. 2008). Below is a breakdown of the Hagmann weighting formula:

$$W = \frac{2C_{ab} \sum_{i=1}^{k} 1/Li}{Va + Vb}$$

- C_{ab} : This is the count of streamlines connecting region *a* and *b*, which serves as a quantitative measure of the connection strength in each direction between two regions.

- $\sum_{i=1}^{k} 1/Li$: This is the sum of the reciprocals of the lengths of the individual streamlines (Li) connecting *a* and *b*. By taking the reciprocal, shorter streamlines (which are often considered more reliable or meaningful) contribute more to the sum than longer streamlines.

- $Va + Vb$*:* These are the volumes of regions *a* and *b.* They serve as normalisation factors that account for the sizes of the connected regions. Larger regions generate more streamlines due to their increased size, so normalising by volume can make the weighting more interpretable and reliable.

- $\frac{2C_{ab} \sum_{i=1}^{k} 1/Li}{Va+Vb}$ = The final formula combines these components. The $2C_{ab}$ term essentially doubles the raw streamline count, and this is then weighted by the sum of the reciprocals of streamline lengths. This product is then normalised by the sum of the volumes of the two connected regions $Va + Vb$

Streamline fraction is an edge weighting defined as a measure of the "connection probability" between two nodes *a* and *b* based on their streamline counts (Cao et al. 2013). Below are the details of the streamline fraction equation:

$$F = 0.5 \left(\frac{C_{ab}}{C_{a\ total}} + \frac{C_{ba}}{C_{b\ total}} \right)$$

- C_{ab} and C_{ba} : These are the number of streamlines that go from region *a* to region *b* and vice versa. Similar to the term in the previous equation, it serves as a measure of the raw connection strength between two nodes.

- $C_{a\ total}$ and $C_{ba\ total}$: These terms represent the total number of streamlines leaving regions *a* and *b*. They serve as normalisation factors that account for regions with higher or lower overall connectivity.

- $\frac{C_{ab}}{C_{a\ total}}$ and $\frac{C_{ba}}{C_{b\ total}}$: These fractions represent the proportion of streamlines connecting *a* to *b* and *b* to *a* relative to the total number of streamlines leaving these regions. These values provide a normalised measure of directional strength.

- $0.5\left(\frac{C_{ab}}{C_{a\ total}}+\frac{C_{ba}}{C_{b\ total}}\right)$ = The final equation takes an average of the two directional fractions. The multiplication by 0.5 serves to normalise the sum, effectively providing an approximation of the "connection probability" between two regions.

To explore the topological organisation of brain networks, the selected edge weighting is repeated for each edge in the network to construct a structural connectivity matrix. This structural connectivity matrix describes the topological organisation of a brain network circuitry (Bullmore and Sporns 2012), which can be characterised using *graph theory*. Graph theory is a branch of mathematics that can be used to combine non-invasive imaging with statistical modelling to quantify the topological properties of a structural connectivity matrix (Farahani, Karwowski, and Lighthall 2019). Through this framework, a variety of graph-theoretical metrics can be derived to provide information about brain network properties (Bullmore and Sporns 2012; Sporns, Tononi, and Edelman 2000) (Table 6.1).

Table 6.1 Common graph theory network characteristics and metrics in dMRI neuroscience research.

Graph Theory Network Characteristics	
Shortest Path length	A network feature that refers to the minimum amount of connections needed to link two nodes (Bullmore and Sporns 2009). In a binary network, length of the shortest path is the fewest number of edges (or steps) needed to interconnect two nodes (Bullmore and Sporns 2009). In a weighted network, shortest path length is defined by the minimum summed edge weight required to interconnect two nodes (Bullmore and Sporns 2009).
Network Neighbour	A network feature typically defined as a node the that is directly connected to another node by an edge (Bullmore and Sporns 2009). Nodes are considered neighbours if there exists a direct link or edge between them in the network (Bullmore and Sporns 2009).
Network Cluster	A network feature that refers to when the nearest neighbours of a node are also directly connected to each other (Bullmore and Sporns 2009).
Small-world network	A network characterised by a high clustering coefficient (see definition below) among nodes and a short average path length between any two nodes (Rubinov and Sporns 2010). Networks with small-worldness exhibit efficient local and global information transfer and is considered a fundamental feature of the human brain's structural network (Rubinov and Sporns 2010).
Rich club region	A network feature where highly connected nodes tend to connect to other highly connected nodes, such architecture is characteristic of the human brain (Colizza et al. 2006). These regions would have a disproportionally high number of connections and would be highly interconnected, serving as central hubs for information flow and network integration (Dennis et al. 2013; McAuley, da Fontoura Costa, and Caetano 2007).
Graph Theory Metrics	
Density	A binary network metric that quantifies the extent of interconnectivity among nodes within a network (Bullmore and Sporns 2009). Network density is calculated by dividing the number of actual connections by the number of total possible connections within a network (Bullmore and Sporns 2009). A network with high density would indicate that many regions of the network are directly connected to each other via edges, suggesting a high level of integration and potential for fast information exchange between brain regions (Bullmore and Sporns 2009; Rubinov and Sporns 2010).
Characteristic Path Length	A network efficiency measure of the integration of nodes in a network (Rubinov and Sporns 2010). Characteristic path length is calculated as the average shortest path length between all possible pairs of nodes in a given network (Rubinov and Sporns 2010). In the context of brain networks, lower characteristic path length can indicate higher efficiency of information transfer between the nodes of a network (Bullmore and Sporns 2009; Bullmore and Sporns 2012).

Global Efficiency A measure of network efficiency that is calculated by the sum of the average of inverse shortest path lengths in a network (Latora and Marchiori 2001). By calculating the inverse of the shortest path length, more efficient connections (shortest paths) yield higher values, and less efficient connections (longer paths) yield smaller values (Latora and Marchiori 2001). High global efficiency indicates that information can quickly be exchanged across a network, while low efficiency suggests that the network may have bottlenecks or long paths that slow information flow (Achard and Bullmore 2007; Latora and Marchiori 2003).

Local Efficiency A measure of network fault tolerance by quantifying how network nodes communicate with its neighbouring parts when the network is damaged, or a node is removed (Latora and Marchiori 2001). Local efficiency is calculated as the average of the inverse of the shortest path lengths between all neighbours of each node in a network (Latora and Marchiori 2001). High local efficiency indicates that the nodes of a network are highly interconnected with their neighbouring nodes, enabling fast and efficient information exchange within these local subnetworks (Latora and Marchiori 2001; Latora and Marchiori 2003).

Routing efficiency A binary network measure of how efficiently information can be transferred between all nodes of a network (Avena-Koenigsberger, Misic, and Sporns 2018).. Routing efficiency is calculated as the inverse of the shortest path lengths between all node pairs in a network (Avena-Koenigsberger, Misic, and Sporns 2018). Higher routing efficiency indicates that the network has on average, shorter paths between nodes, allowing for faster and more efficient information transfer across the entire network (Goñi et al. 2013). It also suggests that the network can better integrate and handle multiple streams of information concurrently(Latora and Marchiori 2001; Goñi et al. 2013).

Network Strength A measure that quantifies the overall connectivity or ‘wiring cost’ of the network (Van Den Heuvel and Sporns 2011). This is calculated by the sum of the average edge weights across the network (Rubinov and Sporns 2010). Higher global network strength could reflect a greater capacity for information transfer across a network (Van Den Heuvel and Sporns 2011).

Clustering Coefficient A measure that quantifies the degree to which nodes in a network tend to cluster together (Bullmore and Sporns 2009). The clustering coefficient is the ratio of actual number of network clusters to the maximum number of possible clusters (Bullmore and Sporns 2009). A high clustering coefficient suggests that neighbouring nodes are likely to be interconnected, forming a tightly-knit community of interconnected nodes (Rubinov and Sporns 2010). This measure is linked to network resilience and efficient local processing (Rubinov and Sporns 2010).

Betweenness Centrality	A measure that quantifies the importance of a node within a network by measuring the fraction of all shortest paths in the network that pass through a given node (Rubinov and Sporns 2010). A higher betweenness centrality indicates that a node is more integrated and has a greater influence on the information flow within a network (Rubinov and Sporns 2010).

The majority of published MRI connectomics studies in ADHD have analysed resting-state functional MRI (Cao et al. 2013; Cao et al. 2014b; Beare et al. 2017) and focused on functional connectivity, but there is now an emerging interest in structural connectivity (see review (Cao et al. 2014a)). Using dMRI, structural connectivity connectomics are derived from the topological properties of white matter fibres connecting different brain regions (Sporns, Tononi, and Kötter 2005). At the time of writing, five prior cross-sectional studies have examined structural connectivity network properties in children and adolescents with ADHD (Cao et al. 2013; Ray et al. 2014; Hong et al. 2014; Cha et al. 2015; Beare et al. 2017). These studies employed varying methods of edge weighting, a factor that should be considered when interpreting their findings. Summaries of these studies are provided in the subsequent paragraphs.

Cao and colleagues (2013) conducted a whole-brain structural connectome (edges defined by streamline count probability) study of children with ADHD (n=30) and controls (n=30) (Cao et al. 2013). The results found that children with ADHD displayed reduced global efficiency compared to neurotypical controls, with the most pronounced efficiency decreases in the left parietal, frontal, and occipital cortices (Cao et al. 2013). Additionally, reduced structural connectivity in the prefrontal-dominant circuitry and increased structural connectivity in the orbitofrontal-striatal circuitry were significantly correlated with heightened symptoms of inattention and hyperactivity/impulsivity in children with ADHD (Cao et al. 2013).

Ray and colleagues (2014) analysed the whole-brain white matter connectome (edges defined by streamline count) in children with ADHD (n=20) and controls (n=20) (Ray et al. 2014). The results of this study found that compared to controls, children with ADHD displayed reduced connectivity inside highly interconnected regions (rich-club regions) of the network (Ray et al. 2014). Yet beyond the highly interconnected rich-club regions, white matter microstructure between brain regions displayed increased connectivity, highlighting that the network dynamics of ADHD are not solely defined by reduced connectivity (Ray et al. 2014).

Hong and colleagues (2014) investigated whole-brain white matter connectomics (edges defined by Hagmann weighting) in children with ADHD (n=71) and controls (n=26) (Hong et al. 2014). The results identified a significant reduction in the connectivity between frontal, striatal, and cerebellar regions with significantly reduced structural connectivity in children and adolescents with ADHD compared to controls (Hong et al. 2014). Additional analysis found reduced fractional anisotropy (FA) in connections inter-linking the inferior frontal gyrus, superior frontal gyrus, anterior cingulate gyrus, occipital gyrus, supplementary motor area and cerebellar regions were significantly correlated with increased inattention scores in children with ADHD (Hong et al. 2014).

Whole-brain white matter connectomics (defined by raw streamline count) research by Cha and colleagues (2015) reported that children with ADHD (n=30), relative to controls (n=31), had reduced white matter connectivity in the fronto-accumbal network (Cha et al. 2015). Interestingly, even though a reduction in network connectivity in the fronto-accumbal network was reported in those with ADHD compared with controls, a higher level of connectivity in this network was correlated with an increase in aggression in children with ADHD (Cha et al. 2015).

Beare and colleagues (2017) investigated whole-brain white matter connectomes (edges defined by Hagmann weighting) in children with ADHD (n=21) and controls (n=21) (Beare et al. 2017). The results found that while both ADHD and control groups displayed small-world network organisation typically expected in a human brain (Beare et al. 2017), individuals with ADHD were associated with decreased long-range, global connections, implying reduced communication between specialised local networks in individuals with ADHD (Beare et al. 2017). The ADHD group also exhibited a sub-network with heightened connectivity involving bilateral frontostriatal connections and left occipital, temporal, and parietal regions (Beare et al. 2017). Notably, the microstructural organisation of white matter in these regions (measured by mean FA) was positively correlated with symptom severity among children with ADHD (Beare et al. 2017).

Overall, structural connectivity whole-brain connectomics research to date has suggested ADHD may be characterised by global underconnectivity in connections between functionally specialised networks (Cao et al. 2013; Beare et al. 2017; Cha et al. 2015), along with localised reductions in network efficiency in frontal, parietal, striatal, occipital, and cerebellar regions (Cha et al. 2015; Hong et al. 2014). However, white matter

network organisation in ADHD does not appear to be simply characterised by underconnectivity, as increased connectivity has been reported in the orbitofrontal-striatal circuitry (Ray et al. 2014). While white matter network abnormalities have been associated with clinical manifestations of ADHD symptoms (Hong et al. 2014; Cao et al. 2013; Beare et al. 2017), it is important to recognise that these previous studies may be subject to limitations, such as inadequate statistical power, which increases the likelihood of false-positives.

Research on white matter in ADHD has predominantly focused on elements of the frontostriatal, default mode, ventral attention, somatomotor, and cortico-striato-thalmo-cortical networks (Connaughton et al. 2022), leaving the limbic system underexplored. The limbic system, with its intricate network of interconnected grey matter and subcortical structures – structures often atypical in ADHD (Hoogman et al. 2017a; Hoogman et al. 2019) – is central to several cognitive and emotional functions (Catani, Dell'acqua, and Thiebaut de Schotten 2013). Moreover, the limbic system is part of wider limbic-cortical networks, which have been found to be dysregulated in ADHD (Rubia 2011; Castellanos and Proal 2012). Despite the noted ADHD-related anomalies in crucial limbic system structures (Hoogman et al. 2017a; Hoogman et al. 2019), no structural connectivity network studies have specifically focused on the limbic system. A targeted network analysis of the limbic system would provide a more nuanced understanding of its potential contribution to the pathophysiology of ADHD during childhood and mid-adolescence.

Using CSD-based tractography and graph theory, the study described in this chapter will conduct a longitudinal network analysis of the limbic system among individuals with ADHD and controls during the transition from childhood to mid-adolescence. The main objectives of this study are 1) to investigate the between-group differences in limbic system network measures in children and adolescents with ADHD and controls and 2) to explore the relationship between ADHD symptom severity and limbic system network metrics among individuals with ADHD. Based on the limited cross-sectional findings (Cao et al. 2013; Ray et al. 2014; Hong et al. 2014; Cha et al. 2015; Beare et al. 2017; Qian et al. 2021), the hypothesis is individuals with ADHD will be associated with decreased network efficiency and underconnectivity within the limbic system across the three NICAP study time points when compared to controls. Exploratory analysis will explore the relationship between limbic system network metrics and ADHD symptom severity in children and adolescents with ADHD.

6.2. Methods and Materials

6.2.1. Chapter Design and Participants

The methods for clinical assessment and diagnosis grouping of the study participants have been detailed earlier in Chapter 2. Briefly, the study described in this chapter included 161 participants (36% females); 67 children with ADHD and 94 controls. Participants were recruited as part of the Neuroimaging of the Children's Attention Project (NICAP) (Sciberras et al. 2013; Silk, Genc, et al. 2016), which is described in detail in Chapter 2. Each participant completed behavioural questionnaires (Conner's 3 ADHD index and the Affective Reactivity Index), and multimodal MRI scanning occurred at three time points (wave 1, mean = 10.39, SD = 0.46; wave 2, mean = 11.67, SD = 0.53; wave 3, mean = 13.19, SD = 0.60). Details of ethical approval for the NICAP study are provided in Section 3.2.1. This thesis focused on individuals with persistent ADHD diagnosis across the study time points. As such, the participants included in the ADHD group received a confirmed clinical ADHD diagnosis based on a clinically administered National Institute of Mental Health Diagnostic Interview Schedule for Children (DISC-IV) (Shaffer et al. 2000) at each assessment (recruitment [3 years prior to imaging], wave 1 and wave 3 imaging time points). Participants in the control group did not meet the diagnostic criteria for ADHD at any study time point.

6.2.2. MRI Data Acquisition

The MRI data acquisition protocol for the NICAP study has been previously described: structural MRI in Section 3.2.2 and diffusion MRI in Section 5.2.2.

6.2.3. MRI Data Processing

The MRI data processing has been detailed previously: structural MRI in Section 3.2.3 and diffusion MRI in Section 5.2.3. Briefly, structural MRI data were processed using FreeSurfer's recon -all function (v.7.2) for motion correction, full cortical reconstruction and segmentation (Fischl et al. 2002; Fischl et al. 2004). The automated segmentation and parcellation of cortical and subcortical regions was executed using the Destrieux atlas, resulting in a total of 162 grey matter and subcortical nuclei regions (Destrieux et al. 2010).

As described in Section 5.2.3, multi-shell HARDI images were processed using ExploreDTI software (Leemans et al. 2009). The processing steps included, flip permute, quadratic signal drift, Gibbs ringing, eddy current, echo-planar imaging and subject motion corrections (Vos et al. 2017; Sarra 2006; Perrone et al. 2015; Leemans and Jones 2009; Irfanoglu et al. 2012). Crucially for network construction, subject-specific diffusion images were linearly co-registered to a subject-specific structural T1 image (*nu_orig)* during EPI distortion and subject motion correction (Irfanoglu et al. 2012). As outline in Section 5.2.3, whole brain deterministic CSD-based tractography was reconstructed using the following parameters: seed point resolution 2 x 2 x 2 mm^3, step size 1 mm, angle threshold 60°, fibre length range, 10 – 500 mm.

To ensure the precise alignment of structural and diffusion MRI images, which had already been subject to extensive QC inspections (as described in Chapters 3 & 5), a detailed visual quality control assessment was performed for each subject, following the guidelines provided in the ExploreDTI manual (Leemans et al. 2009). This essential process involved overlaying the structural image onto the diffusion first eigenvector-fractional anisotropy (FEFA) map, as depicted in Figure 6.1. The FEFA map was specifically selected for its ability to accentuate the directional orientation of diffusion fibres, enhancing the visibility of any potential misalignments between the structural and diffusion MRI images. Particular attention was paid to the alignment of the cerebrospinal fluid, pia layer, and major white matter tracts, ensuring their accurate co-registration. This meticulous cross-referencing was vital for precise alignment verification between the structural and diffusion MRI images.

Following visual inspection, 338 scans were found suitable for analysis, with a total of 22 scans removed; 17 of these were excluded due to unsuccessful connectome generation that could not be rectified, while an additional 5 were eliminated due to structural and diffusion image alignment discrepancies.

Figure 6.1 An example of an appropriate structural and diffusion image alignments

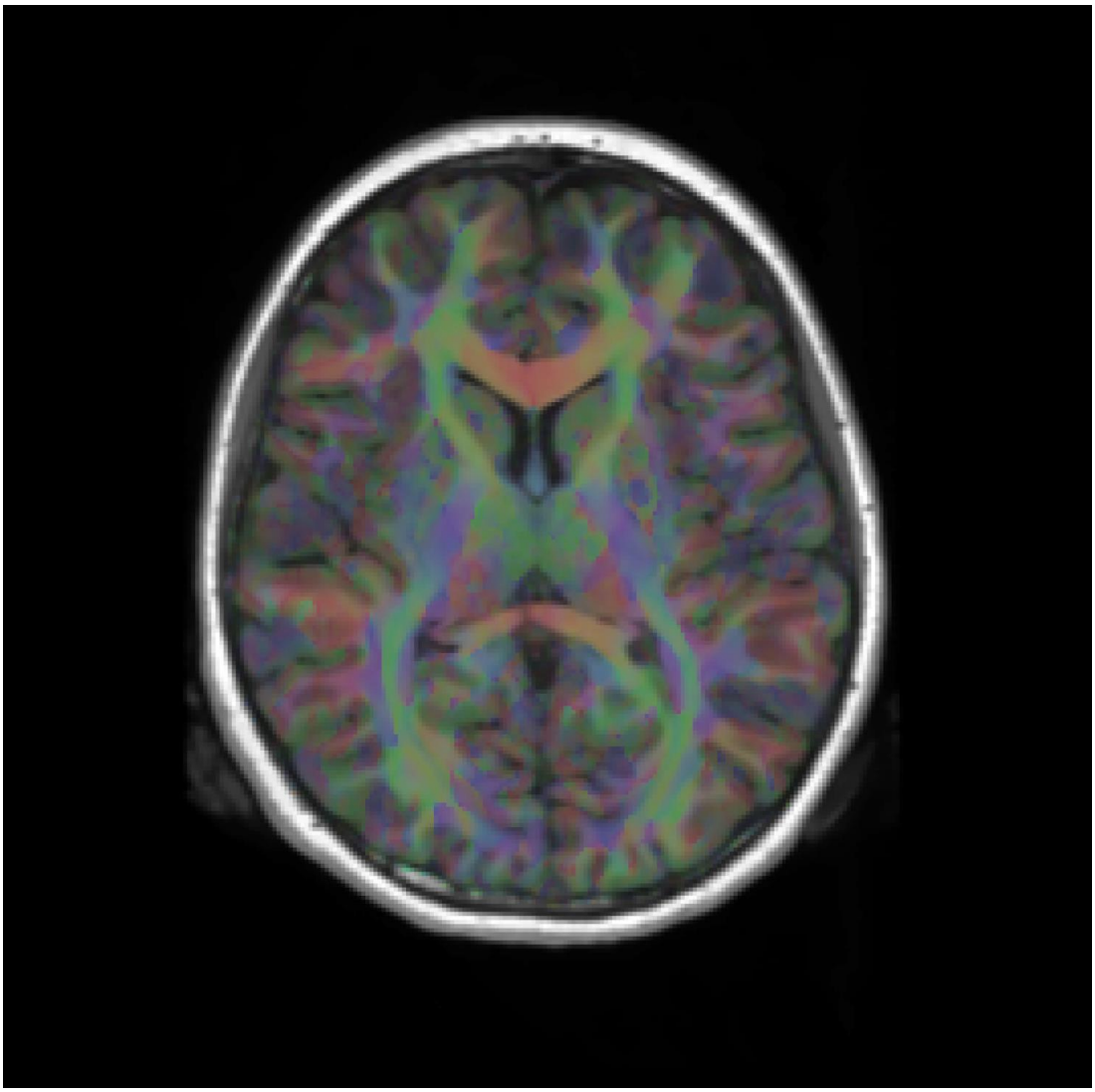

Figure 6.1: this figure shows an example of an accurate alignment of a subject's structural and diffusion MRI images. As per the visual quality control strategy, subject-specific diffusion MRI FEFA and structural MRI images were overlaid and a visual inspection to confirm alignment accuracy.

6.2.4. Connectome Construction

ExploreDTI software (Leemans et al. 2009) was used to construct subject-specific networks. The two fundamental elements of the network under investigation are nodes and edges (Sporns, Tononi, and Kötter 2005). For the network reconstruction of the limbic system, the following procedures were employed to define the nodes and edges. A visual guide of these procedures is also provided in Figure 6.2.

Node Definition

Anatomical masks were outlined using the automated segmentation and parcellation (Fischl et al. 2004) from the Destrieux Atlas (Desikan et al. 2006b) (see Figure 6.2.). In the study described in this chapter, the nodes were bilaterally defined to include the following regions: the thalamus, hippocampus, amygdala, rostral anterior cingulate gyrus, caudal anterior cingulate gyrus, posterior cingulate gyrus, isthmus cingulate gyrus, parahippocampal gyrus, lateral orbitofrontal cortex, and medial orbitofrontal cortex.

Edge Definition

Using the whole brain CSD tractography, streamlines were generated with the "pass" definition, this assigns a streamline to a pair of nodes if the streamline intersects them in its path without imposing further restrictions on its start/endpoint (Hagmann et al. 2008). The network is unrestricted, meaning every pair of nodes may potentially be connected by an edge (Hagmann et al. 2008). As discussed above, structural connectivity strength is traditionally measured by the raw streamline count (Hagmann et al. 2008). Streamline count is known to be impacted by several factors unrelated to true anatomical connectivity that may lead to spurious fibres (Sarwar, Ramamohanarao, and Zalesky 2019; Zalesky et al. 2016). These factors include, node size, connection length, and connection complexity (Hagmann et al. 2008). To mitigate these factors, the study described in this chapter incorporated a streamline density-weighted (Hagmann weighting) procedure (Hagmann et al. 2008; Sotiropoulos and Zalesky 2019). As described in the introduction, this procedure corrects for over-sampling of long tracts associated with whole-brain tractography and normalises based on node size, which is particularly important in networks containing a wide range of node volumes (Hagmann et al. 2008). Overall, Hagmann weighting streamline count provides a measure of structural connectivity in which the streamline count strength is more reflective of the underlying anatomical connectivity (Hagmann et al. 2008).

6.2.5. Global Network Metrics

Following the completion of network construction, a suite of graph theory metrics – topological measures used to quantify brain networks (Rubinov and Sporns 2010) – were computed using the Brain Connectivity Toolkit (BCT) (Rubinov and Sporns 2010). The graph theory metrics used in this chapter are global efficiency, characteristic path length,

network density, clustering coefficient, network strength, local efficiency and routing efficiency (described in Table 6.1).

Figure 6.2 Visual guide to constructing a subject-specific limbic system connectome.

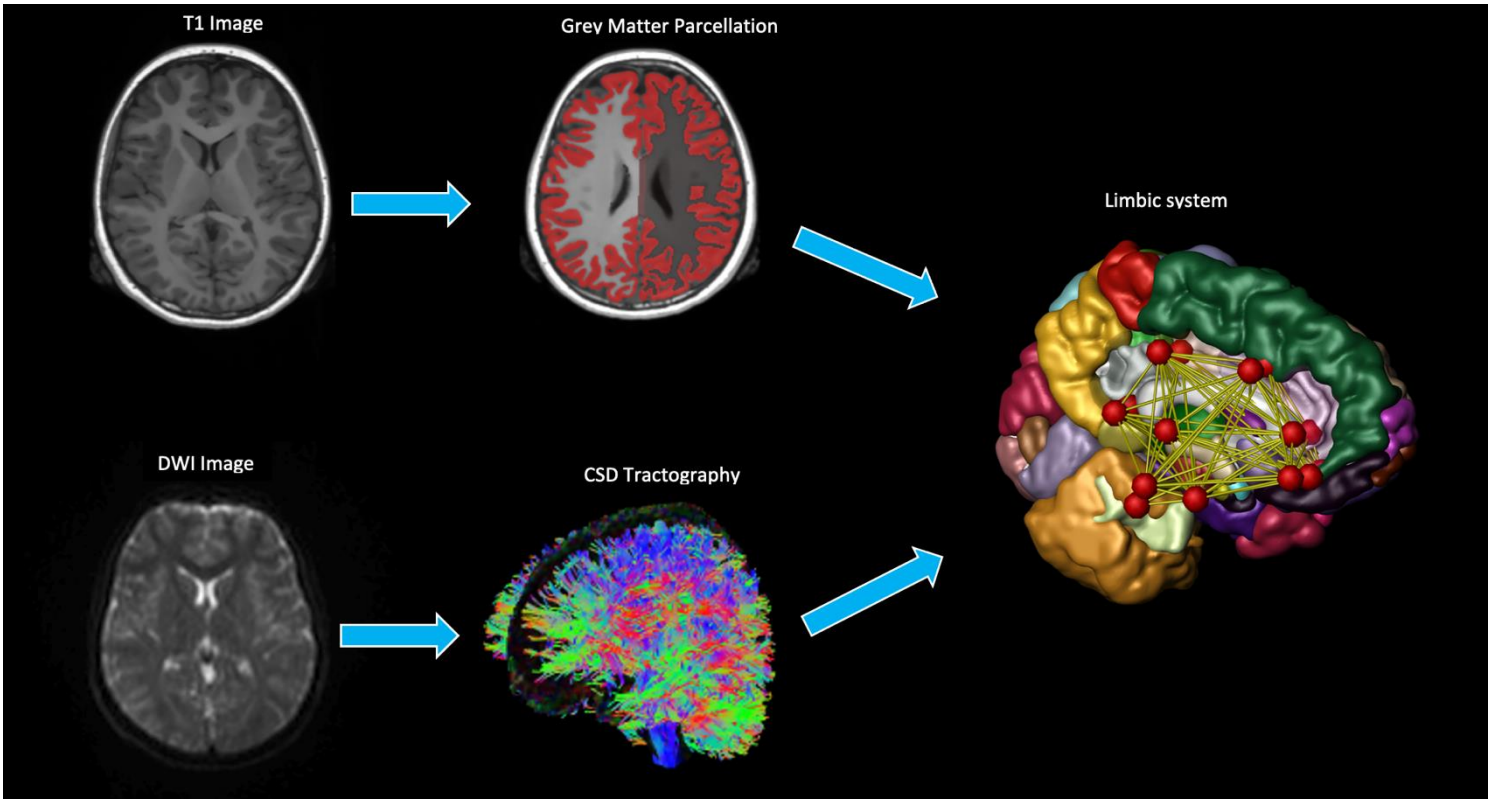

Figure 6.2: This figure outlines the key processing steps for the construction of a subject-specific limbic system connectome. After processing T1 and DWI images, full cortical parcellation and whole-brain tractography is performed. During processing the DWI image was co-registered to the T1 image, for connectomics construction it is essential that these two images are registered to the same space. Using ExploreDTI software the nodes are defined and edges are then generated using the "pass" definition, which assigns a streamline to a pair of nodes if the streamline intersects them. These procedures are repeated for each subject in the study to create subject-specific limbic system connectomes.

6.2.6. Behavioural Measures: Conner's 3 ADHD index (CAI) and the affective reactivity index (ARI)

Conner's 3 ADHD index (CAI): As described in Section 3.2.5.

Affective reactivity index (ARI): As explained in previously in Section 3.2.5.

6.2.7. Statistical Analyses

Before statistical analyses a systematic inspection of the data including outlier identification was performed. Outliers were defined as any data points diverging by ±3 standard deviations from the data mean. In line with established statistical practice outliers were removed to minimise the effect of extreme values (Iglewicz and Hoaglin 1993), which is a particular concern given the risk of "false fibres" being generated in diffusion MRI connectomics (Sotiropoulos and Zalesky 2019). Full details of top-down LMM procedures used in this study were described in 3.2.5. The specific tested LMM models are presented in Table 6.2.

Table 6.2 Tested LMMs: limbic system network measures in ADHD and controls.

Random Effects Models
RX 1a
Network Metric ~ ICV + age at baseline + sex + diagnosis*age + (1 + age |subject)
RX 1b
Network Metric ~ ICV + age at baseline + sex + diagnosis* age + (1|subject)
Fixed Effects Models
Null 0a
Network Metric ~ ICV + age + age at baseline + sex + (1 + age | subject)
Null 0b
Network Metric ~ ICV + age + age at baseline + sex + (1|subject)
FX 1a
Network Metric ~ ICV + sex + age + age at baseline + diagnosis + (1 + age |subject)
FX 1b
Network Metric ~ ICV + sex + age + age at baseline + diagnosis + (1|subject)
FX 2a
Network Metric ~ ICV + sex + age + age at baseline + diagnosis* age + (1 + age |subject)
FX 3b
Network Metric ~ ICV + sex + age + age at baseline + diagnosis* age + (1|subject)
FX 3b
Network Metric ~ ICV + sex + age* ADHD symptom + (1|subject)

6.3. Results

6.3.1. Demographics and Clinical Characteristics of Study Population

Demographic and clinical characteristics of the study populations are presented in Table 6.3. As with the previous studies described in Chapters 3 and 5, at wave 2 there were significantly fewer female participants in the ADHD group compared to the controls. No significant differences were observed between ADHD and non-ADHD control groups in age, handedness, socioeconomic status (SES), or matrix reasoning score at all three NICAP study time points. Regarding clinical characteristics, children with ADHD displayed higher levels of ADHD symptom severity compared to the control group. Additionally, children with ADHD were more likely to exhibit externalising and internalising disorders than the control group.

Table 6.3 Demographics and clinical variables.

		Mean (SD)		*p-value*
		ADHD	***Control***	
	Demographic factors			
	Scans after QC	53	69	
	Age – years	10.40 (0.49)	10.37 (0.49)	0.905
	Female sex n (%)	13 (24.52	29 (42.02)	0.068
	Left-handed n (%)	7 (13.20)	9 (13.04)	0.996
	Matrix reasoning raw	21.77 (5.62)	21.62 (4.58)	0.633
	SES	1017 (41.52)	1019 (44.62)	0.738
Time point 1	Clinical factors			
	Connor's Index	10.98 (6.33)	2.56 (4.41)	<0.001
	Hyperactivity symptoms	4.83 (2.65)	1.07 (1.64)	<0.001
	Inattentive symptoms	7.03 (2.22)	1.86 (2.34)	<0.001
	Medication use (%)	17 (30.07)	4 (5.79)	<0.001
	Extern. Disorder n (%)	26 (49.05)	12 (17.39)	<0.001
	Intern. Disorder (%)	12 (22.64)	8 (11.59)	0.11

	Demographic factors			
	Scans after QC	53	69	
	Age – years	11.67 (0.48)	11.67 (0.56)	0.972
	Female sex n (%)	11 (23.63%)	32 (42.10%)	0.022
	Left-handed n (%)	5 (9.43%)	8 (11.59%)	0.874
Time point 2	Matrix reasoning raw	24.77 (4.04)	24.40 (4.54)	0.700
	SES	1018 (40.86)	1015 (48.36)	0.739
	Clinical factors			
	Connor's Index	10.04 (6.74)	2.45 (3.88)	<0.001
	Medication use (%)	14 (26.41)	4 (5.79)	<0.001
	Demographic factors			
	Scans after QC	39	55	
	Age – years	13.25 (0.60)	13.14 (0.59)	0.385
	Female sex n (%)	9 (22.5)	30 (42.85)	0.066
	Left-handed n (%)	6 (15.38)	6 (10.90)	0.521
	Matrix reasoning raw	25.92 (4.52)	25.65 (4.26)	0.704
Time point 3	SES	1020.6 (39.78)	1015 (50.34)	0.664
	Clinical factors			
	Connor's Index	9.28 (6.71)	3.94 (3.91)	<0.001
	Medication use (%)	9 (23.07)	1 (1.81)	0.004
	Extern. Disorder n (%)	8 (20.51)	3 (5.45)	0.072
	Intern. Disorder (%)	10 (25.64)	2 (3.63)	0.006

Note: SD = standard deviation, SES = socio-economic status.

6.3.2. Between-Group Differences in Network Metrics of the Limbic System

Model Selection Procedure

Full results of the model selection fit statistics are provided in the appendix (Tables 22-23 provided in volume 2). Following outlier exclusion, some models did not have sufficient observations to support the complex random effects model (containing random intercept and random slope). No significant difference between the fixed effects of interest

models and the null models was found in any of the graph theory metrics, indicating that there was no effect of diagnosis and/or diagnosis-by-age interaction on the network metrics of the limbic system. The selected optimal models from the top-down LMM model selection procedure are provided in Table 6.4.

Table 6.4 Results of LMM Model Selection: optimal models.

	Graph Theory Metrics						
	C_{coeff}	E_{glo}	E_{loc}	E_{rout}	N_{Stren}	N_{den}	C_{pl}
Selected Optimal Model	FX1A	FX1A	FX1A	FX1A	FX1A	FX1A	FX1A

C_{coeff} = characteristic coefficient, E_{glo} = global efficiency, E_{loc} = local efficiency, E_{rout} = routing efficiency, N_{Stren} = network strength, N_{den} = network density, C_{pl} = characteristic path length

Results of Optimal Models

There were no statistically significant between-group differences in any of the graph theory measures (Table 6.5), specifically network density, global efficiency, local efficiency, routing efficiency, clustering coefficient, network strength, and characteristic path length (Figure 6.3). These findings indicate that there is no significant difference in network properties of the limbic system between children with ADHD and controls.

6.3.3. ADHD Symptoms and Limbic System Network Metrics in ADHD

An exploratory analysis found a significant effect of Conner's 3 ADHD index scores (CAI) on routing efficiency (β = - 0.29, 95% CI = -0.48 to -0.10, (Figure 6.4)) and network density (β = - 0.24, 95% CI = -0.43 to -0.05, (Figure 6.5)) in the ADHD group across the NICAP study time points. Overall, reduced routing efficiency and network density in the limbic system were significant predictors of increased ADHD symptom severity among individuals with ADHD across childhood and mid-adolescence. All results reported above survived two-stage FDR correction. There was no other significant effect of CAI or ARI on any limbic system network metric in children and adolescents with ADHD (Figure 6.7-6.8). Table 6.6-6.7 displays the full results of the exploratory analyses for all limbic system networks metrics.

6.3.4. Sensitivity Analyses

The sensitivity analysis indicated that the medication status covariate did not drive the primary findings (see Table 6.8). Due to the collinearity between CAI scores and medication use ($r = 0.337$, $p = <0.001$), an expected reduction in p-value was reported when medication status was included as a covariate. The beta coefficients of the sensitivity analyses were largely unchanged and importantly remained within the standard errors of the main analyses. This suggests that the original relationship between network metric and CAI scores was relatively robust and not substantially affected by the inclusion of the covariate. The results from the second and third sensitivity analysis are presented in Table 6.9 and 6.10. The sensitivity analyses revealed that the beta values associated with the main diagnostic effect were still within the Standard Errors (SEs) of the optimal models (Figures 6.7 & 6.8). Based on the beta value and SEs, the sensitivity analysis suggested that the results of the exploratory analysis were likely not confounded by comorbidity status or head motion. Overall, the sensitivity analyses demonstrated that the results of the exploratory analysis were most likely not biased by medication status, comorbidity status or head motion.

Table 6.5 Results of mixed-effects models (with interaction term) analyses: limbic system global metrics in ADHD and controls.

	ICV		**Sex**		**Months from baseline**		**Age at baseline**		**Diagnosis**	
	B (SE)	***t, p***	***B (SE)***	***t, p***	***B (SE)***	***t, p***	***B (SE)***	***t, p***	***B (SE)***	***t, p***
Network Efficiency	-2.929e-13 (1.895e-13)	-1.545, 0.310	-5.451e-08 (7.307e-08)	-0.746, 0.560	4.163e-09 (1.955e-09)	2.129, 0.217	-1.374e-07 (7.249e-08)	-1.895, 0.250	6.010e-08 (6.781e-08)	0.886, 0.501
Characteristic Path Length	-2.269e-13 (1.218e-13)	-1.863, 0.369	-1.896e-08 (4.609e-08)	-0.411, 0.767	1.115e-09 (1.264e-09)	0.882, 0.574	-1.023e-07 (4.551e-08)	-2.248, 0.325	4.628e-08 (4.265e-08)	1.085, 0.515
Network Density	-1.974e-08 (3.642e-08)	-0.542, 0.588	1.714e-02 (1.419e-02)	1.208, 0.228	-1.091e-03 (3.667e-04)	-2.975, 0.003	1.658e-02 (1.403e-02)	1.182, 0.239	1.987e-03 (1.315e-02)	0.151, 0.880
Clustering Coefficient	-2.429e-13 (1.556e-13)	-1.561, 0.339	-7.527e-08 (5.798e-08)	-1.298, 0.397	1.850e-09 (1.614e-09)	1.146, 0.437	-9.878e-08 (5.761e-08)	-1.715, 0.312	2.977e-08 (5.382e-08)	0.553, 0.669
Network Strength	-4.387e-12 (2.326e-12)	-1.886, 0.069	-5.460e-07 (8.818e-07)	-0.619, 0.541	1.705e-08 (2.384e-08)	0.715, 0.480	-1.831e-06 (8.724e-07)	2.099, 0.045	8.920e-07 (8.163e-07)	1.093, 0.284
Local Efficiency	-2.674e-13 (2.111e-13)	-1.267, 0.334	-1.860e-08 (7.872e-08)	-0.236, 0.835	9.586e-10 (2.203e-09)	0.435, 0.706	-1.783e-07 (7.785e-08)	-2.290, 0.152	-6.654e-09 (7.290e-08)	-0.091, 0.935

Routing Efficiency	-1.915e-09 (1.107e-09)	-1.729, 0.084	5.757e-04 (4.281e-04)	1.345, 0.180	-3.719e-05 (1.129e-05)	-3.292, 0.001	3.365e-04 (4.213e-04)	0.799, 0.425	2.412e-04 (3.954e-04)	-0.610, 0.542

Table 6.6 Results of mixed-effects models (with interaction term) analyses: limbic system network measures and CAI scores in ADHD.

	ICV		**Sex**		**Months from baseline**		**CAI**		**Months from baseline * CAI**	
	B (SE)	***t, p***	***B (SE)***	***t, p***	***B (SE)***	***t, p***	***B (SE)***	***t, p***	***B (SE)***	***t, p***
Network Efficiency	-1.647e-14 (2.752e-13)	-0.060, 0.967	-9.550e-09 (1.270e-07)	-0.075, 0.959	2.983e-09 (5.872e-09)	0.508, 0.746	-4.782e-09 (1.022e-08)	-0.468, 0.763	1.549e-10 (5.069e-10)	0.306, 0.837
Characteristic Path Length	-8.116e-14 (1.777e-13)	-0.457, 0.830	-5.459e-08 (8.279e-08)	-0.659, 0.777	2.237e-10 (3.740e-09)	0.060, 0.974	-7.791e-09 (6.625e-09)	-1.176, 0.688	8.371e-11 (3.074e-10)	0.272, 0.890
Network Density	-2.504e-08 (5.555e-08)	-0.451, 0.653	3.311e-02 (2.556e-02)	1.295, 0.200	-2.176e-03 (1.203e-03)	-1.809, 0.073	-5.197e-03 (2.091e-03)	-2.486, 0.014*	1.011e-04 (9.872e-05)	1.024, 0.308
Clustering Coefficient	-6.492e-14 (2.174e-13)	-0.299, 0.861	-1.282e-07 (1.005e-07)	-1.275, 0.603	2.688e-09 (4.358e-09)	0.617, 0.745	-2.178e-09 (7.964e-09)	-0.273, 0.871	8.823e-11 (3.670e-10)	0.240, 0.886
Network Strength	-1.878e-12 (3.352e-12)	-0.560, 0.587	-1.168e-06 (1.553e-06)	-0.752, 0.469	-2.582e-08 (6.694e-08)	-0.386, 0.707	-1.863e-07 (1.226e-07)	-1.520, 0.157	3.691e-09 (5.637e-09)	0.655, 0.526

Local Efficiency	1.051e-14	0.035,	-2.410e-08	-0.175,	-2.759e-09	-0.452,	-5.618e-09	-0.509,	4.721e-10	0.920,
	(2.999e-13)	0.980	(1.379e-07)	0.900	(6.101e-09)	0.757	(1.103e-08)	0.732	(5.131e-10)	0.583
Routing	-1.211e-09	-0.723,	9.408e-04	1.181,	-6.884e-05	-2.084,	-1.702e-04	-2.767,	2.369e-06	0.860,
Efficiency	(1.675e-09)	0.471	(7.965e-04)	0.242	(3.303e-05)	0.040	(6.153e-05)	0.006*	(2.754e-06)	0.391

Table 6.7 Results of mixed-effects models (with interaction term) analyses: limbic system network measures and ARI scores in ADHD.

	ICV		**Sex**		**Months from baseline**		**ARI**		**Months from baseline * ARI**	
	B (SE)	***t, p***	***B (SE)***	***t, p***	***B (SE)***	***t, p***	***B (SE)***	***t, p***	***B (SE)***	***t, p***
Network Efficiency	-1.740e-13 (3.906e-13)	-0.445, 0.797	4.007e-09 (1.358e-07)	0.030, 0.985	1.784e-08 (8.316e-09)	2.146, 0.486	2.529e-08 (2.100e-08)	1.204, 0.600	-3.137e-09 (1.800e-09)	-1.743, 0.525
Characteristic Path Length	-1.019e-13 (2.345e-13)	-0.435, 0.867	-3.122e-08 (8.251e-08)	-0.378, 0.881	1.277e-08 (4.996e-09)	2.556, 0.671	2.154e-08 (1.277e-08)	1.686, 0.717	-2.933e-09 (1.074e-09)	-2.731, 0.664
Network Density	-4.419e-08 (8.460e-08)	-0.522, 0.602	1.047e-03 (2.990e-02)	0.035, 0.972	-3.470e-03 (1.835e-03)	-1.891, 0.064	-1.071e-02 (4.888e-03)	-2.190, 0.031	3.668e-04 (3.996e-04)	0.918, 0.362
Clustering Coefficient	-1.219e-13 (2.895e-13)	-0.421, 0.850	-8.030e-08 (1.027e-07)	-0.782, 0.769	1.706e-08 (5.836e-09)	2.924, 0.589	3.018e-08 (1.528e-08)	-1.974, 0.640	-3.190e-09 (1.272e-09)	2.509, 0.608
Network Strength	-2.975e-12 (4.436e-12)	-0.671, 0.521	-1.077e-06 (1.518e-06)	-0.709, 0.499	1.994e-07 (9.890e-08)	2.016, 0.078	3.165e-07 (2.424e-07)	1.306, 0.227	-4.856e-08 (2.128e-08)	-2.282, 0.051
Local Efficiency	-2.176e-13 (4.298e-13)	-0.506, 0.766	-1.272e-08 (1.517e-07)	-0.084, 0.957	9.597e-09 (8.742e-09)	1.098, 0.602	1.438e-08 (2.287e-08)	0.629, 0.723	-3.436e-10 (1.801e-09)	-0.191, 0.903

Routing	-1.965e-09	-0.794,	4.810e-05	0.053,	-5.175e-05	-1.021,	-2.560e-04	-1.837,	-9.512e-07	-0.086,
Efficiency	(2.475e-09)	0.429	(9.043e-04)	0.957	(5.066e-05)	0.312	(1.394e-04)	0.069	(1.104e-05)	0.931

Figure 6.3 Between-group difference in limbic system graph theory metrics across the three NICAP study time points.

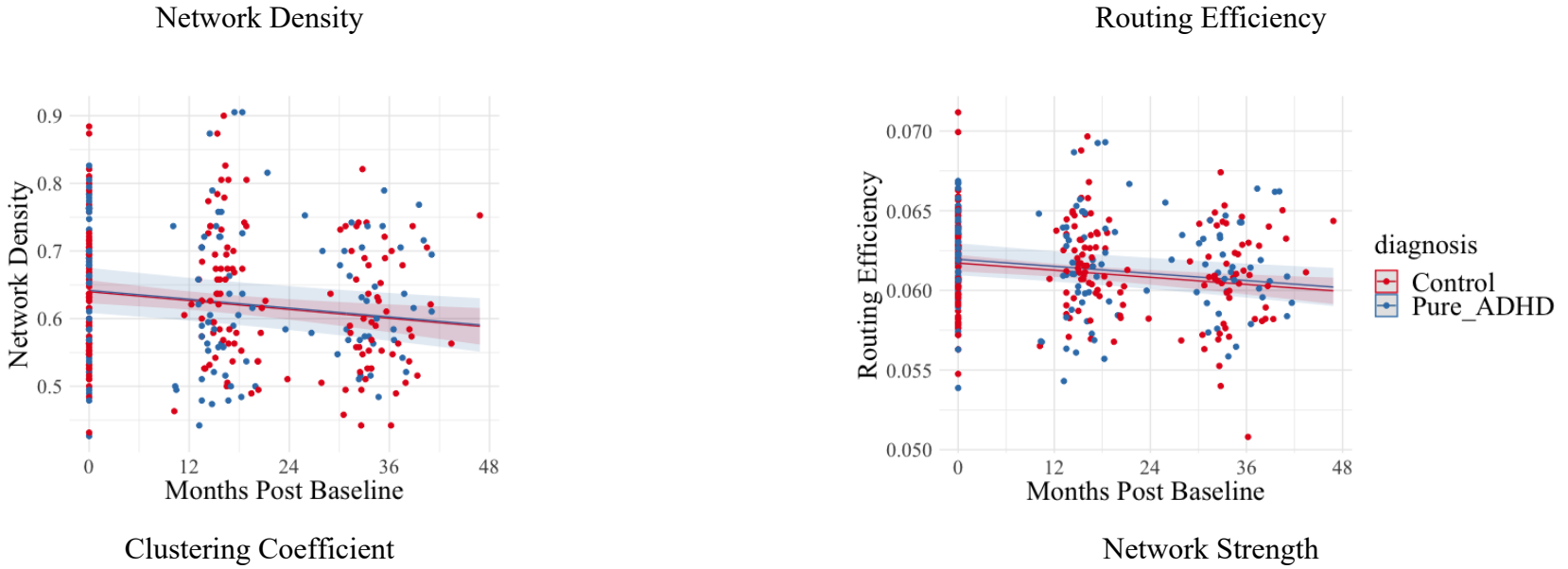

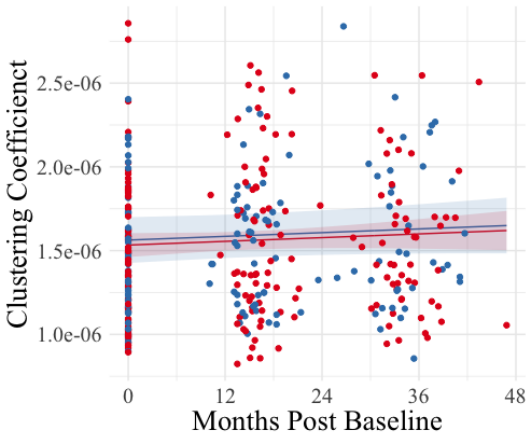

Local Network Efficiency

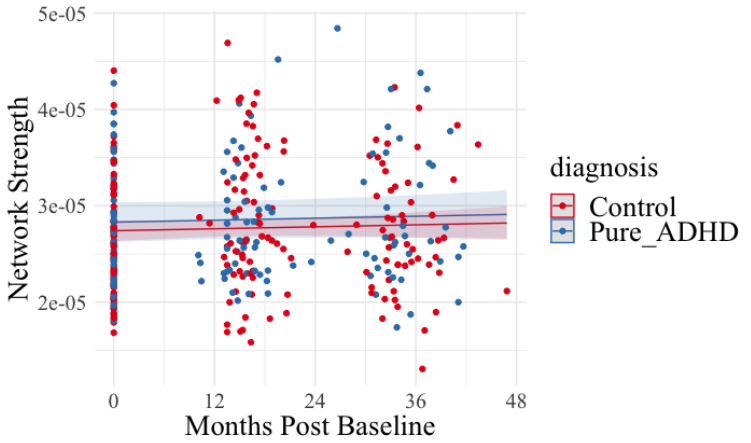

Characteristic Path Length

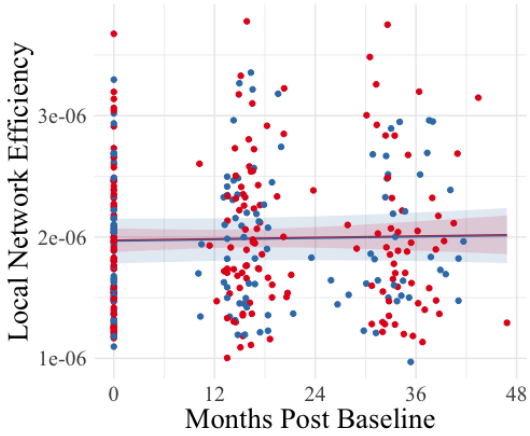

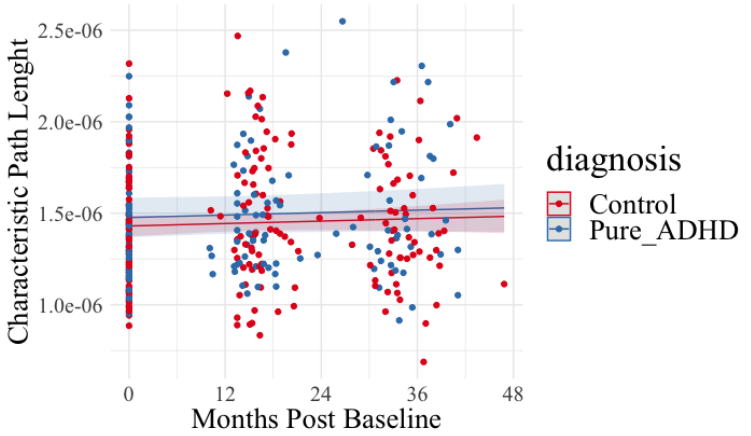

Global Network Efficiency

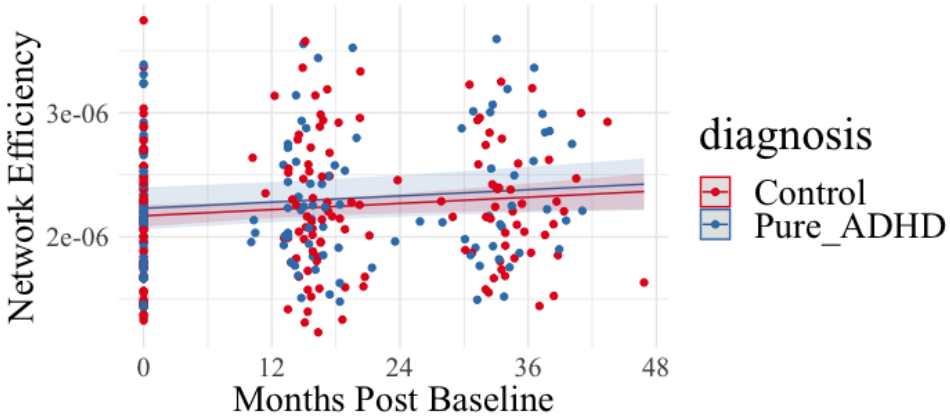

Table 6.8 Results of mixed-effects models (with interaction term) analyses: limbic system network measures and CAI scores in ADHD.

	ICV		**Sex**		**Months from baseline**		**Medication Status**		**CAI**		**Months from baseline * CAI**	
	B (SE)	***t, p***	***B (SE)***	***t, p***	***B (SE)***	***t, p***	***B (SE)***	***t, p***	***B (SE)***	***t, p***	***B (SE)***	***t, p***
Routing Efficiency	-5.264e-10 (1.678e-09)	-0.314, 0.754	1.071e-03 (7.802e-04)	1.373, 0.174	2.983e-09 (5.872e-09)	0.508, 0.746	-6.450e-05 (3.287e-05)	-1.962, 0.053	-1.239e-04 (6.444e-05)	-1.923, 0.056	2.101e-06 (2.739e-06)	0.767, 0.445
Network Density	-1.584e-08 (5.684e-08)	-0.279, 0.781	3.486e-02 (2.574e-02)	1.355, 0.180	-2.138e-03 (1.204e-03)	-1.775, 0.079	2.053e-02 (2.487e-02)	0.826, 0.411	-4.586e-03 (2.224e-03)	-2.062, 0.041	9.823e-05 (9.878e-05)	0.994, 0.322

Table 6.9 Results of mixed-effects models analyses with comorbidity: limbic system network measures and CAI scores in ADHD.

	ICV		**Sex**		**Months from baseline**		**Comorbidity**		**CAI**		**Months from baseline * CAI**	
	B (SE)	***t, p***	***B (SE)***	***t, p***	***B (SE)***	***t, p***	***B (SE)***	***t, p***	***B (SE)***	***t, p***	***B (SE)***	***t, p***
Routing Efficiency	-1.330e-09 (1.709e-09)	-0.778 0.438	9.910e-04 (8.274e-04)	1.198 0.235	-6.924e-05 (3.330e-05)	-2.079 0.040	-3.369e-04 (5.765e-04)	-0.584 0.560	-1.644e-04 (6.296e-05)	-2.611 0.010	2.206e-06 (2.774e-06)	0.795 0.428
Network Density	-3.418e-08 (5.677e-08)	-0.602 0.548	3.177e-02 (2.648e-02)	1.200, 0.234	-2.165e-03 (1.221e-03)	-1.773, 0.079	-8.249e-03 (2.003e-02)	-0.412, 0.681	-4.931e-03 (2.145e-03)	-2.298, 0.023	9.913e-05 (1.001e-04)	0.990, 0.324

Table 6.10 Results of mixed-effects models analyses with FWD: limbic system netw**o**rk measures and CAI scores in ADHD.

	ICV		**Sex**		**Months from baseline**		**FWD**		**CAI**		**Months from baseline * CAI**	
	B (SE)	***t, p***	***B (SE)***	***t, p***	***B (SE)***	***t, p***	***B (SE)***	***t, p***	***B (SE)***	***t, p***	***B (SE)***	***t, p***
Routing	-1.191e-09	-0.684	8.991e-04	1.088	-6.770e-05	-1.952	-5.236e-04	-0.267	-1.698e-04	-2.617	2.353e-06	0.815
Efficiency	(1.740e-09)	0.495	(8.267e-04)	0.281	(3.469e-05)	0.054	(1.961e-03)	0.789	(6.489e-05)	0.010	(2.887e-06)	0.417
Network	-2.246e-08	-0.391	3.027e-02	1.147	-2.107e-03	-1.681	-1.767e-02	-0.266	-5.214e-03	-2.378	1.014e-04	0.987
Density	(5.742e-08)	0.696	(2.639e-02)	0.256	(1.254e-03)	0.096	(6.632e-02)	0.790	(2.192e-03)	0.019	(1.028e-04)	0.326

Figure 6.4 Relationship between of CAI score and routing efficiency in the ADHD group over the NICAP study time points.

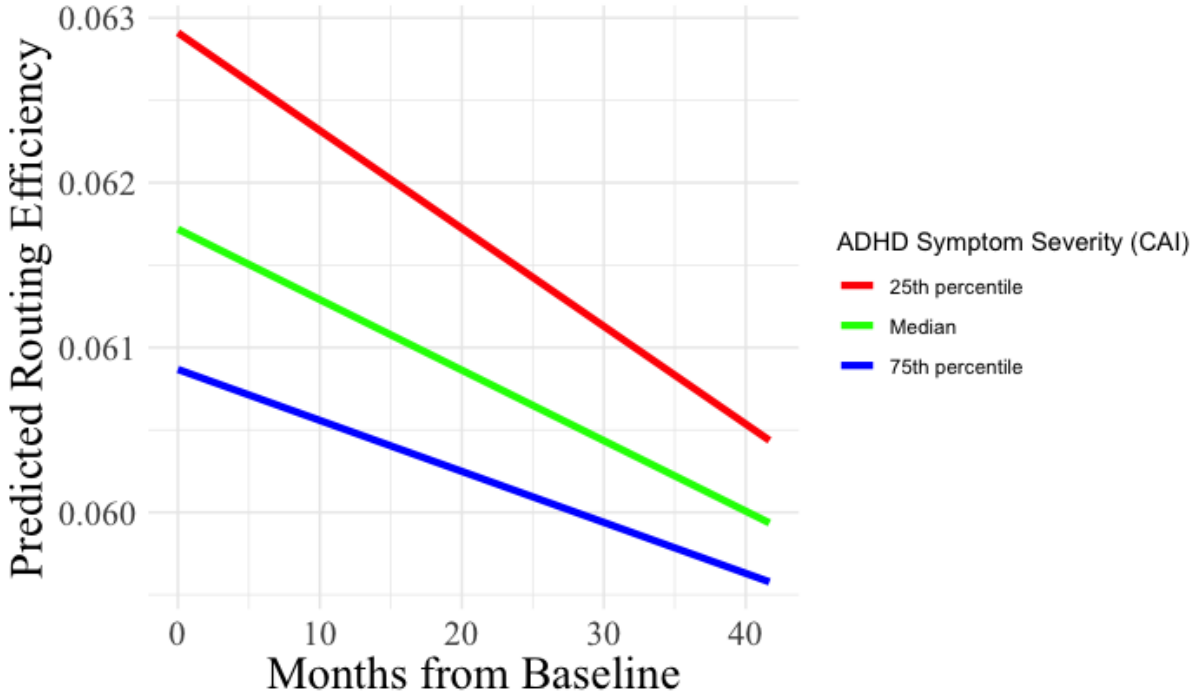

Figure 6.4: This figure illustrates the predicted change in routing efficiency of the limbic system (y-axis) as a function of age (x-axis). The colours represent different percentiles of CAI scores: 25th percentile (red), median (green), and 75th (blue). The Y axis represents the predicted routing efficiency values from the LMM model used in the exploratory analysis.

Figure 6.5 Relationship between of CAI score and network density in the ADHD group over the NICAP study time points.

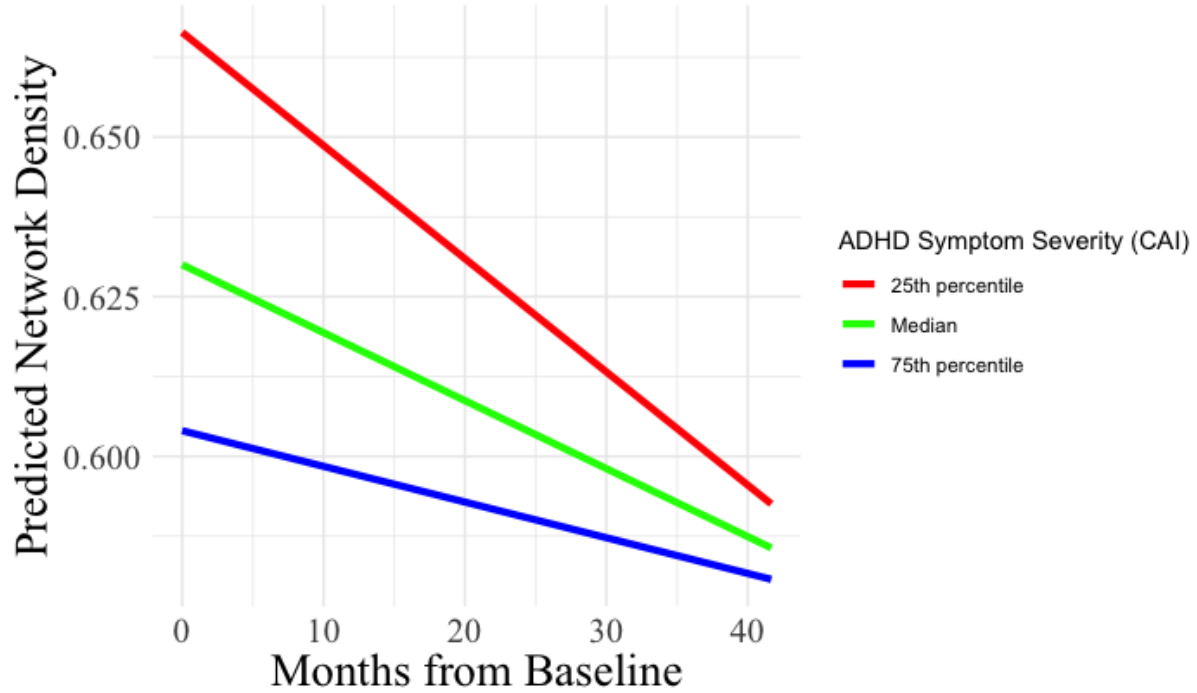

Figure 6.5: This figure illustrates the predicted change in network density of the limbic system (y-axis) as a function of Months from baseline (x-axis). The colours represent different percentiles of CAI scores: 25th percentile (red), median (green), and 75th (blue). The Y axis represents the predicted network density values from the LMM model used in the exploratory analysis.

Figure 6.6 Beta values and SEs of medication sensitivity analyses.

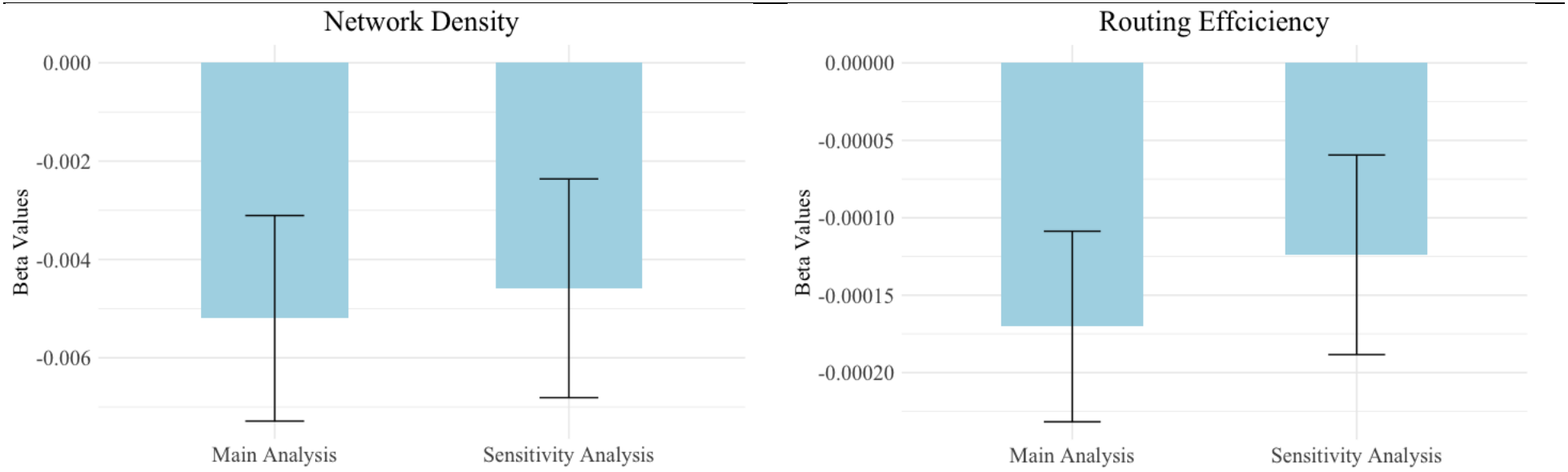

Figure 6.7 Beta values and SEs of comorbidity sensitivity analyses.

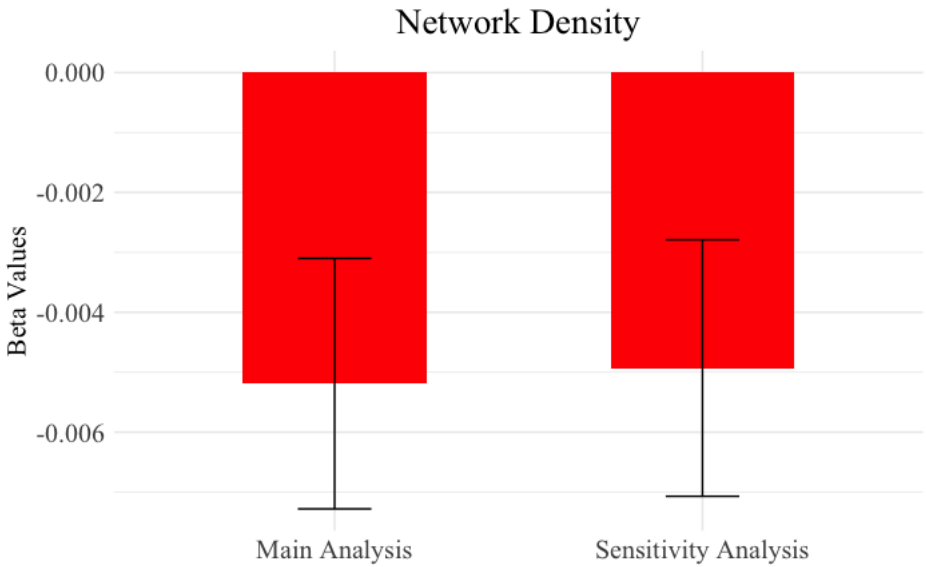

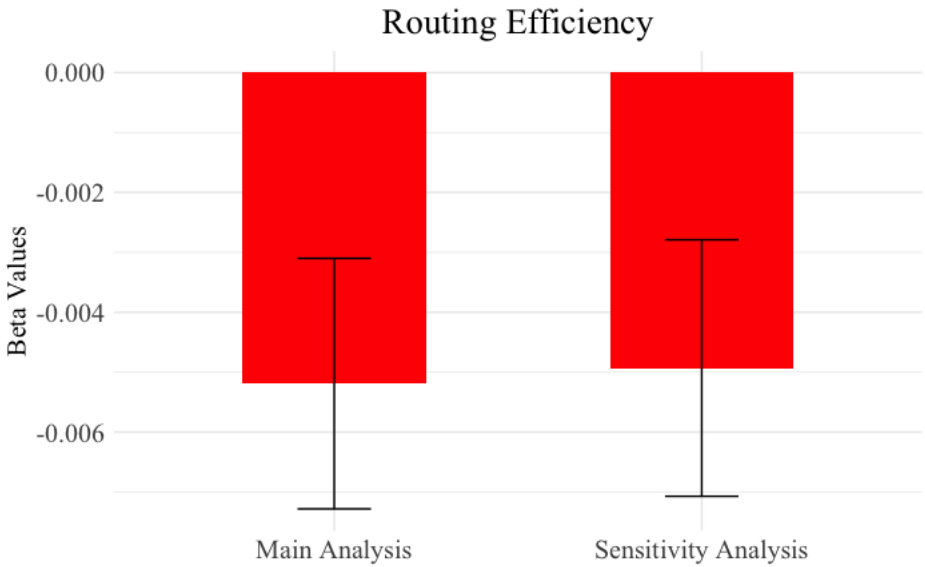

Figure 6.8 Beta values and SEs of FWD sensitivity analyses.

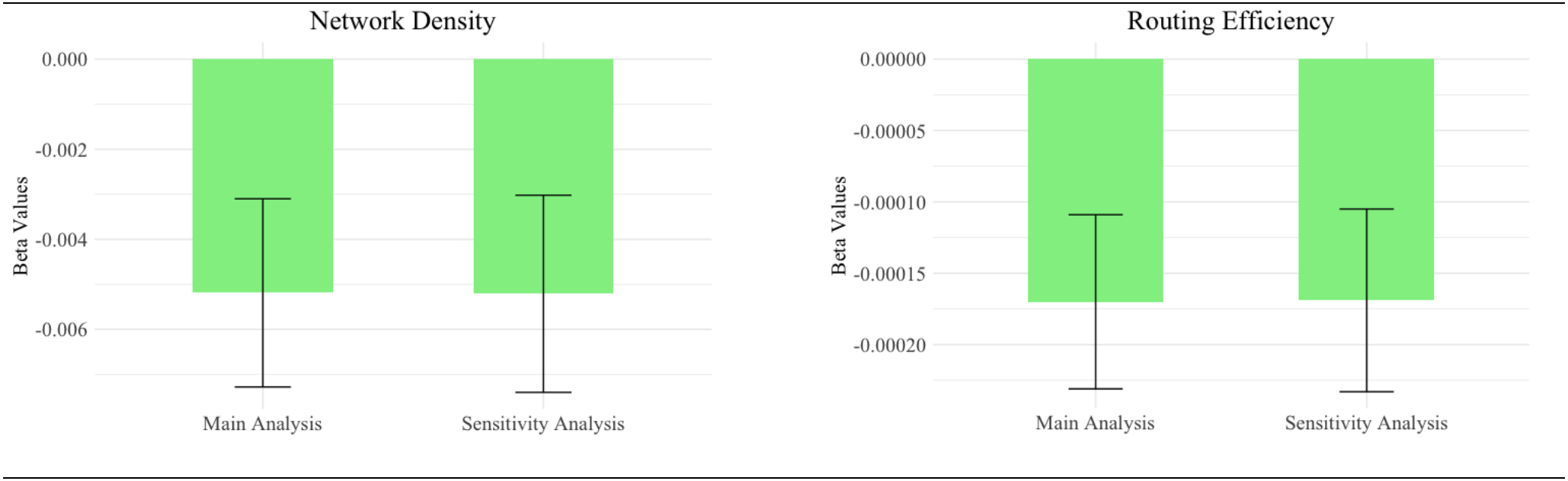

Figure 6.9 Scatter plot of non-significant limbic system network measures by CAI scores in ADHD.

Network Efficiency

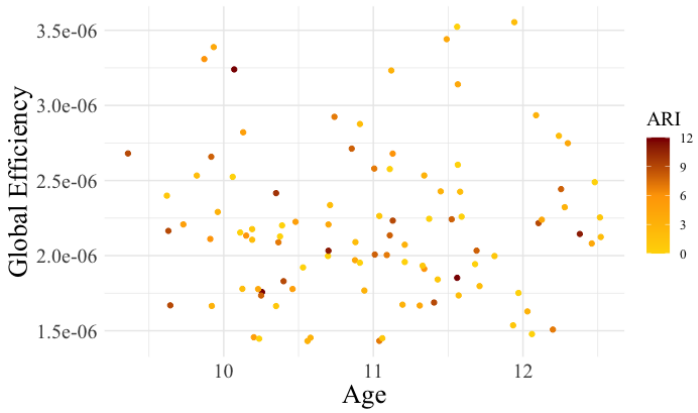

Characteristic Path Length

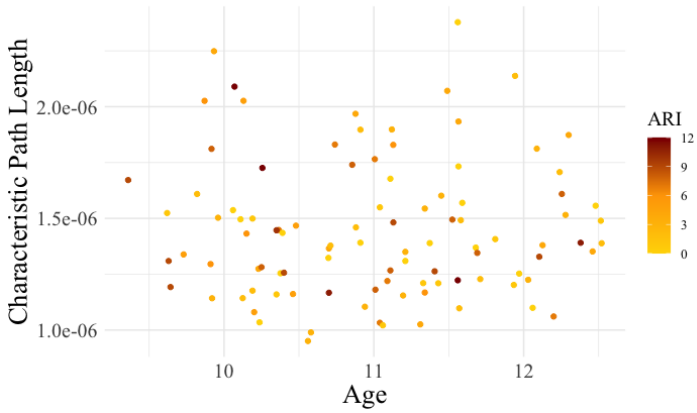

Clustering Coefficient

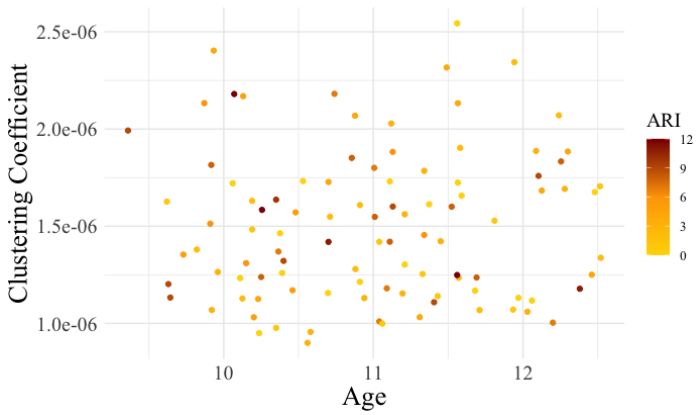

Network Strength

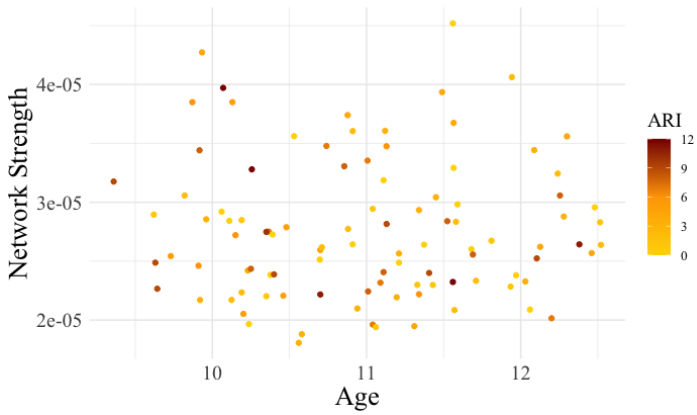

Local Efficiency

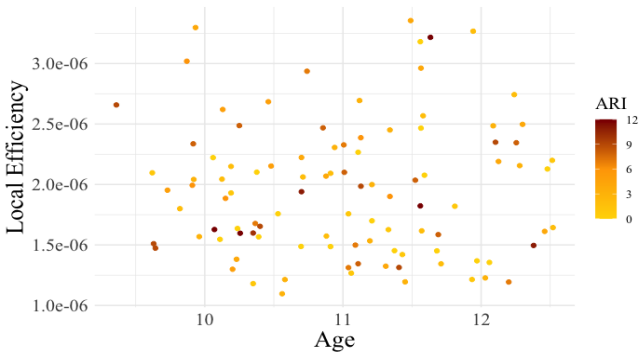

Figure 4.7: This scatter plot exclusively features non-significant limbic system network measures (y-axis) alongside CAI scores (colour-coded) within the population. Each data point represents an individual in the study. The colour gradient used to represent CAI scores ranges from low (gold) to medium (orange) and high (dark red). Despite the absence of statistical significance, this visualisation sheds light on the relationship between non-significant limbic system network measures and CAI scores across the ADHD population.

Figure 6.10 Scatter plot of non-significant limbic system network measures by ARI scores in ADHD.

Network Efficiency

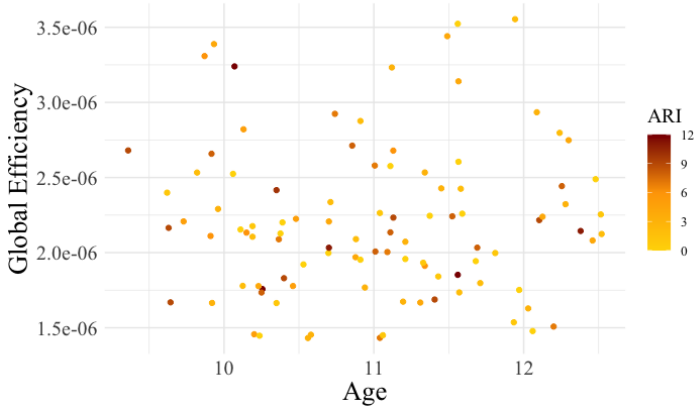

Characteristic Path Length

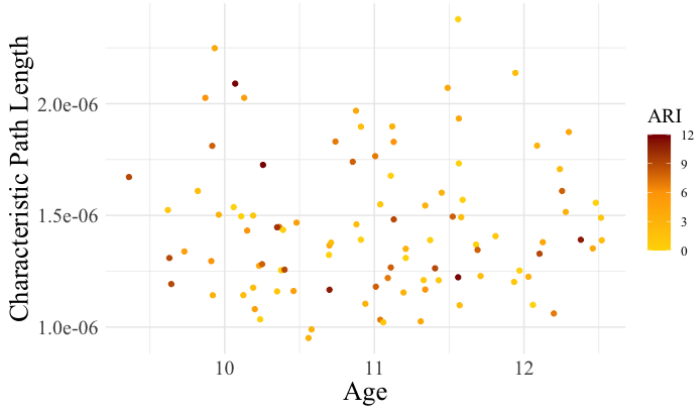

Clustering Coefficient

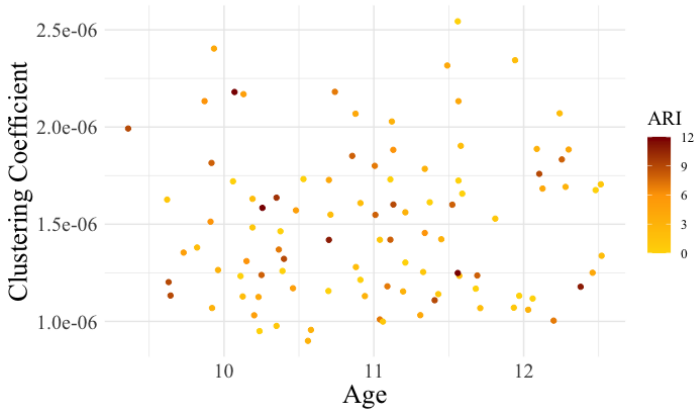

Network Strength

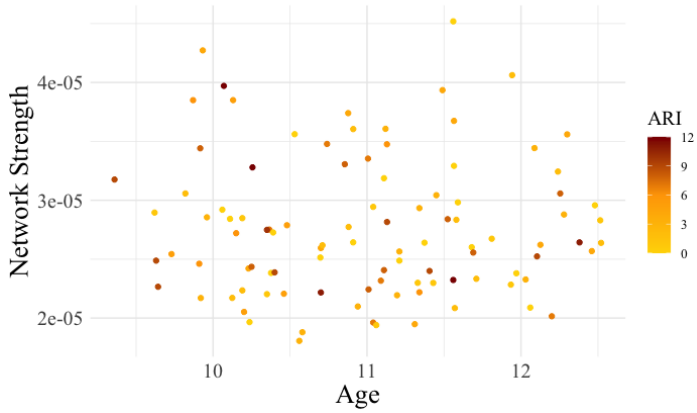

Network Density

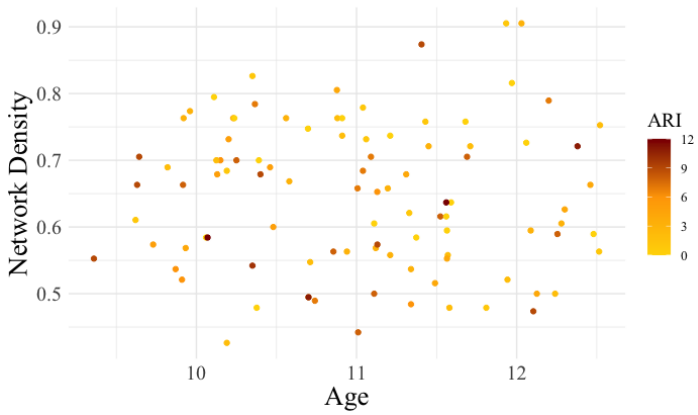

Routing Efficiency

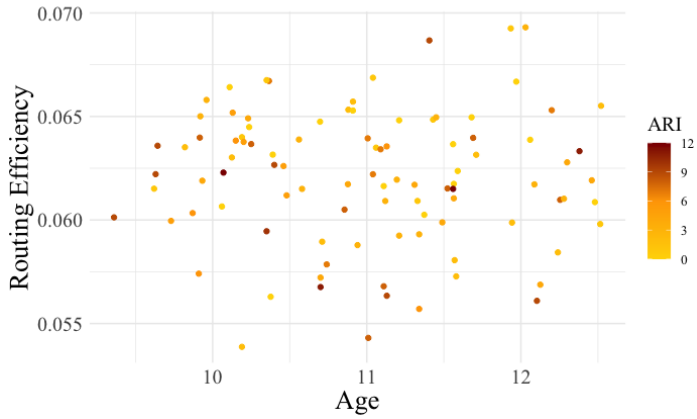

Local Efficiency

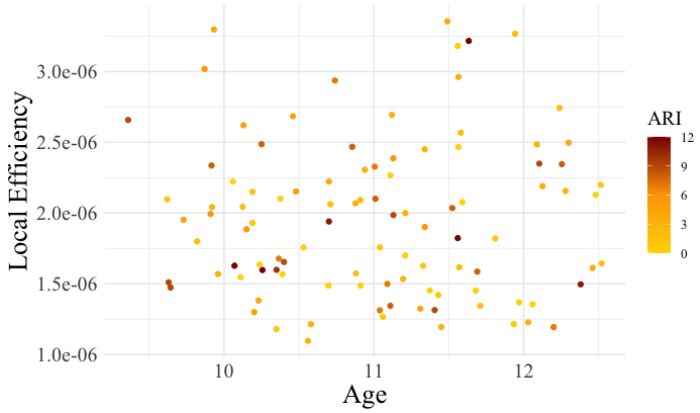

Figure 4.8: This scatter plot exclusively features non-significant limbic system network measures (y-axis) alongside CAI scores (colour-coded) within the population. Each data point represents an individual in the study. The colour gradient used to represent CAI scores ranges from low (gold) to medium (orange) and high (dark red). Despite the absence of statistical significance, this visualisation sheds light on the relationship between non-significant limbic system network measures and CAI scores across the ADHD population.

6.4. Discussion

6.4.1. Summary

The aim of the study described in this chapter was to investigate the topological organisation of limbic system connectivity in individuals with ADHD and controls during the transition from childhood to mid-adolescence. The results show that children with ADHD displayed no significant difference in network measures of the limbic system compared to controls across the three NICAP study time points. The exploratory analysis found that reduced routing efficiency and network density of the limbic system were significantly associated with increased symptom severity among individuals with ADHD. This discussion will explore the potential neurobiological mechanisms that may underpin these findings. Additionally, the findings will be discussed with respect to methodological considerations and study limitations.

6.4.2. Between-Group Differences in Network Properties of the Limbic System

The primary analysis exploring network metrics of the limbic system in ADHD and controls revealed no significant between-group differences. The findings of this study revealed an intriguing dichotomy. While the primary analysis showed no significant differences in limbic system network measures between ADHD and controls, the exploratory analysis revealed a clear association between ADHD symptom severity and limbic system network measures. Specifically, it was found that network measures – routing efficiency and network density – were significantly associated with ADHD symptom severity. This apparent paradox could be explained by the internal variability inherent to the ADHD group in this study. Despite a concerted effort to maintain consistent diagnostic profiles within the ADHD group by including only those individuals with persistently diagnosed ADHD across the NICAP study time points, it is important to acknowledge that ADHD, akin to many neurodevelopmental disorders, is recognised to exist along a spectrum (Fair et al. 2012). Within the ADHD group, there was relatively high variability in symptom severity (CAI Mean = 10.23, SD = 6.56; ARI Mean = 4.13, SD = 3.47). It is possible that alterations to the limbic system network may be more sensitive to ADHD symptom severity rather than ADHD diagnosis. As such, the heterogeneity of symptom severity within the ADHD group could essentially dilute any apparent between-group differences with averages compared between ADHD and control groups. If so, group-level comparisons between ADHD and control subjects may not reveal significant differences, yet within the ADHD group, a significant association with symptom severity might emerge. The inherent variability within the ADHD phenotype is a continuous consideration for case-control ADHD research (Silk et al. 2019) and is discussed in detail in Section 5.3.3. Future research is required to elucidate these relationships, potentially considering factors such as ADHD subtypes, symptom dimensions or the presence of comorbidities to provide a more nuanced understanding of the neurobiological underpinnings of ADHD.

6.4.3. Network Properties of the Limbic System and ADHD Symptom Severity

Understanding the dynamics between the topological organisation of brain structural connectivity and ADHD symptoms remains an essential area of research. Previous diffusion MRI connectomics research suggested links between the structural organisation of white matter and ADHD symptoms (Connaughton et al. 2022), but as all

previous studies were whole brain analyses, making comparisons with the findings of the study described in this chapter is challenging. This chapter describes the first empirical work to investigate the link between the organisation of limbic system structural connectivity and ADHD symptoms. The findings described in this chapter revealed that among individuals with ADHD, reduced network density and routing efficiency were significantly associated with increased symptom severity across the three NICAP time points (Figures 6.4-6.5). Network density and routing efficiency are both binary metrics that reflect the interconnectivity of a network Table 6.1. These metrics provide a simple measure of the efficiency of information transfer within the network (Bullmore and Sporns 2009; Goñi et al. 2013). As such, the results indicate that increased ADHD symptom severity is associated with reduced number of limbic system connections.

These findings raise an intriguing contradiction. As ADHD symptom severity, routing efficiency and network density decreased across the study time points it would be expected that reductions in ADHD symptom severity would be associated with reduction in routing efficiency and network density, but the opposite occurred. This suggests that even as the limbic system undergoes typical neural refinement, characterised by fewer interconnections across the study time points, an optimal level of interconnectedness may be essential for limbic system functioning and deviations from this may be associated with ADHD symptoms.

6.4.4. Potential Neurodevelopmental Mechanisms Contributing to the Findings

The findings of the study described in this chapter point to a link between reduced white matter connections in the limbic system and increased ADHD symptom severity. To further understand the neurobiological processes in ADHD it is essential to interpret MRI research in conjunction with other epigenetic, genetic and animal model research. As previously mentioned in Section 1.2.2, the most common effect of ADHD-associated genes on brain development involves the disruption of neuronal and synaptic formation, plasticity, and regulation (Dark, Homman-Ludiye, and Bryson-Richardson 2018; Mueller et al. 2017). Two mechanisms that can have a profound effect on the development of white matter connections are neural connectivity and synaptic plasticity. The following section will examine the current evidence for potential disruptions to these neurodevelopmental processes and the impact they might have on the ADHD phenotype.

Neural Connectivity

Neural connectivity refers to the process where environmental cues guide neuronal axons to grow and extend, ensuring the establishment of connections between neurons (De Rouvroit and Goffinet 2001). As discussed in Table 1.1, in the developing brain, guidance cues and cell adhesion molecules play a crucial role in orchestrating the formation of neural connection (Dark, Homman-Ludiye, and Bryson-Richardson 2018). Cell adhesion molecules, located on the cell surface, facilitate the establishment and maintenance of neural connectivity through their interaction with neuronal growth cones (Togashi, Sakisaka, and Takai 2009). The growth cones of developing neurons are guided to their targets (neuronal pathfinding) by attractive and repulsive cues in the extracellular environment (Thomas and Yoshikawa 2009). Cell adhesion molecules of interest in ADHD research are the cadherin molecules (Togashi, Sakisaka, and Takai 2009). Genome-wide association studies (GWAS) found risk loci for ADHD within the cadherin13 (CDH13) and protocadherin 7 (PCDH7) genes (Lasky-Su et al. 2008; Demontis et al. 2023; Demontis et al. 2019). CDH13 mediates the adhesion and interaction between neurons, guiding neuronal processes, such as axonal growth and dendritic branching, which are essential for establishing neural circuits (Drgonova et al. 2016). Disruptions in CDH13 have been demonstrated to negatively affect axonal pathfinding resulting in diminished neural connectivity between brain regions (Takeuchi et al. 2000; Bai, Ghoshal, and Jacob 2006). Similarly, the PCDH7 gene is involved in cell adhesion and signalling, helping cells stick together and communicate with each other, and plays an important role in establishing and maintaining complex neural networks (Wang et al. 2020). PCDH7 knock-out mice display stalled axonal formations suggesting that PCHD7 acts as a positive cue for axonal guidance (Leung et al. 2013; Kim et al. 2007). These findings provide compelling evidence that variants in ADHD-associated genes such as CDH13 and PCDH17 can disrupt the normal processes of formation of white matter fibres in the brain. Such disruptions may in turn lead to the structural connectivity deficits observed in ADHD.

Synaptic Plasticity

Another neurodevelopmental mechanism that impacts white matter fibre development is a process known as synaptic plasticity. Synaptic plasticity involves changes in synaptic strength over time, leading to either strengthening (long-term

potentiation) or weakening (long-term depression) of synapses and is crucial for the refinement and organisation of brain networks (Turrigiano and Nelson 2004). Potentiation and depression of synapses allow for neuronal pathways to be tuned in an activity-dependent manner to improve efficiency (Turrigiano and Nelson 2004). The inability to regulate neural connections can lead to decreased brain volumes and inefficient neural networks, a common neurological phenotype seen in ADHD (Dark, Homman-Ludiye, and Bryson-Richardson 2018). The glutamate receptor metabotropic (GRM) family play an important role in long-term potentiation and depression of synapses (Niswender and Conn 2010). The GRM genes localise to pre and postsynaptic elements, suggesting they are important to synaptic plasticity processes (Niswender and Conn 2010). Two glutamate receptor genes of particular interest in ADHD are GRM5 and GRM7 (Howells and Russell 2008; Pattij and Vanderschuren 2008; Dorval et al. 2007).

GRM 5 gene creates a protein called metabotropic glutamate receptor 5 (Lu et al. 1997). This protein belongs to a group called G protein-coupled receptors (Lu et al. 1997). When a molecule, like glutamate, attaches to this receptor, the receptor changes its shape (Lu et al. 1997). This change triggers a chain reaction inside the cell involving molecules called guanine nucleotide-binding proteins, which ultimately activate other molecules, such as phospholipase C (Tuteja 2009). This is a common way for cells to respond to signals from their environment and is essential for regulating synaptic activity and neural activity (Dark, Homman-Ludiye, and Bryson-Richardson 2018). GRM5 knockout mice have been shown to display consistent defects in long-term potentiation in N-methyl-D-aspartic acid (NMDA) in receptor-dependent pathways such as CA1 region and dentate gyrus of the hippocampus (Lu et al. 1997). Alterations in GRM5 are linked to decreased dendritic spine density, particularly in young mice (Wijetunge et al. 2008). Dendritic spines are receiving points for neural signals and a reduction in density may signify fewer available sites for synaptic connections, potentially leading to diminished neural connectivity (Runge, Cardoso, and de Chevigny 2020). Interestingly, genetic research found a deletion within GRM5 in parents and their children with ADHD (Elia et al. 2010), providing further support for the link between GRM5 variants and the disorder.

Another ADHD-associated gene of interest is GRM7 (Noroozi et al. 2019), which has also been linked to other psychiatric conditions including, bipolar disorder (Fallin et al. 2005; Tang, Thornton-Wells, and Askland 2011), autism (Noroozi et al. 2016) and major depressive disorder (Pergadia et al. 2011). GRM7 gene plays a crucial role in

protecting neurons; it is thought that neuronal overstimulation can be prevented through the regulation of both excitatory and inhibitory signalling systems (Niswender and Conn 2010; Sansig et al. 2001). It does this by suppressing certain communication pathways within the neuron, specifically by reducing the activity of a molecule called adenylate cyclase (Song et al. 2021). This in turn, dampens the function of NMDA receptors (Gu et al. 2012), which are another type of receptor involved in cell communication and can cause cell damage if they become overactive (Luo, Wu, and Chen 2011). It is believed that an inability to recruit GRM7 to synapses could lead to deficits in synaptic plasticity, leading to reduced transmission of information across synapses (Bushell et al. 2002; Goddyn et al. 2008). Through mechanisms involving neuronal damage, variants in the GRM7 gene could potentially play a role in the observed alterations in neural connectivity associated with ADHD (Noroozi et al. 2019).

In summary, the reduced white matter connections associated with ADHD symptom severity could be a result of the complex interplay between various ADHD-associated genes that are crucial for the formation and establishment of neural connections. Given their crucial role in neural connectivity (Dark, Homman-Ludiye, and Bryson-Richardson 2018), the cadherin gene family represent a promising focus of future research seeking to investigate the neurodevelopmental basis of ADHD. It is important to note that our current understanding of neural formation, regulation and plasticity in the context of ADHD is still limited, and there is a need for further research to fully understand the intricacies of this relationship and its implications for symptomology.

6.4.5. Methodological Considerations with Connectomics

In methodological terms, this study showcases significant strengths by employing an advanced MRI scan protocol coupled with a comprehensive processing pipeline. These rigorous methodologies have proven to offer significantly improved reliability in constructing structural connectomes (Roine et al. 2019). Nonetheless, despite these efforts to enhance reliability, there remain some innate challenges in connectomics analysis that warrant careful consideration (Avena-Koenigsberger, Misic, and Sporns 2018).

Node Definition

The definition of the nodes is of vital importance, particularly in smaller, function-specific brain networks (Avena-Koenigsberger, Misic, and Sporns 2018), such as the

limbic system. The anatomical boundaries of the limbic system have been a point of debate due to its complex architecture and the proximity and interaction with other critical brain regions (Catani, Dell'acqua, and Thiebaut de Schotten 2013). The specific components of the limbic system can vary according to different anatomical and functional perspectives, leading to various interpretations and node definitions (Catani, Dell'acqua, and Thiebaut de Schotten 2013). Consequently, it is important to consider these different interpretations when conducting research involving the limbic system, especially in the field of network analysis. As this is an overarching consideration across the three chapters of this dissertation, the anatomical boundaries of the limbic system are extensively discussed in Section 7.3.2. Additionally, while investigating specific brain networks may offer valuable insights, these investigations might not capture the nuances of how these localised networks are integrated within the overarching framework of the whole-brain network. For instance, in the case of structural connectivity networks, the shortest path lengths may considerably differ based on the node definition (Avena-Koenigsberger, Misic, and Sporns 2018). It is conceivable that the shortest path between two nodes in the limbic system might involve a node not defined in this study, potentially leading to a misrepresentation of communication efficiency between these two brain regions.

The study described in this thesis focused on constructing a connectome of the limbic system to investigate its role in ADHD symptomology. While this approach has provided valuable insights, a potential future exploration could employ Network Brain Statistics (NBS) to analyse the limbic system within the context of the whole-brain structural connectivity matrix. This broader approach would not only reinforce the current findings regarding the limbic system but could also unveil impactful interconnections with the limbic system that are not apparent in a limbic-specific analysis. The use of NBS in a whole-brain context might uncover how the limbic system's connectivity with other brain regions, such as the prefrontal cortex or basal ganglia, contributes to the complex symptomology of ADHD. Such research could greatly impact our understanding of the involvement of the limbic system in ADHD.

Communication Dynamics in Brain Networks

The basis for nearly all brain activities and functions lies in how neurons signal and communicate with each other (Avena-Koenigsberger, Misic, and Sporns 2018). Although network science techniques has proven useful for simulating functional brain

networks, it is important to note that these approaches are based on certain assumptions that may not accurately reflect neural systems (Avena-Koenigsberger, Misic, and Sporns 2018). The nature of graph-based inferences, or predictions, about communication patterns heavily depends on the basic assumptions or definitions regarding what constitutes an interaction or exchange of information between different brain regions (Avena-Koenigsberger, Misic, and Sporns 2018). Most analyses focusing on the transfer efficiency of information within neural networks leverage shortest-path-based metrics, such as betweenness centrality, closeness centrality and network efficiency (Van Den Heuvel et al. 2009; Bassett and Bullmore 2006; De Pasquale et al. 2016). These metrics are grounded in the assumption that neural elements can selectively route information along the shortest path (Avena-Koenigsberger, Misic, and Sporns 2018). In the context of neural systems, this assumption is being challenged (Avena-Koenigsberger, Misic, and Sporns 2018). The concept of routing communication along the most efficient (shortest) path inherently assumes that neural signals have access to information or knowledge about the global network topology (Boguna, Krioukov, and Claffy 2009; Goñi et al. 2013; Abdelnour, Voss, and Raj 2014). Although possible, this assumption seems highly improbable in a physiological system, as it is difficult to conceptualise how an action potential could encode its intended route and destination (Avena-Koenigsberger, Misic, and Sporns 2018). Additionally, an overreliance on the shortest paths for communication can leave a majority of the network's connections unused, even when these paths could offer nearly as efficient alternatives (Avena-Koenigsberger, Misic, and Sporns 2018). In the context of large-scale brain networks, this could mean overlooking more than 80% of known fibre tracts (Avena-Koenigsberger et al. 2017). As a result, measures based on shortest paths are unaffected by the targeted removal of edges, as long as the edges used in the shortest paths remain intact (Avena-Koenigsberger, Misic, and Sporns 2018). This leads to an overload of information flow on these shortest paths, resulting in network communication that is vulnerable to bottlenecks, delays, and information loss (Avena-Koenigsberger, Misic, and Sporns 2018). Consequently, shortest-path network efficiency measures could provide a distorted representation of network efficiency (Avena-Koenigsberger, Misic, and Sporns 2018).

Graph theory metrics are undeniably beneficial in offering summarised insights into network topology (Bullmore and Sporns 2009). Considering the methodological considerations mentioned above, however, it is crucial to exercise caution when inferring

complex communication dynamics from graph theory metrics (Avena-Koenigsberger, Misic, and Sporns 2018).

6.4.6. Limitations

Head motion during MRI image acquisition is a particular concern for studies involving children with ADHD (Pardoe, Kucharsky Hiess, and Kuzniecky 2016). If not appropriately managed, head motion can lead to data loss and spurious findings (van Ewijk et al. 2012; Alexander-Bloch et al. 2016). To address this concern, several measures were implemented to minimise motion-related effects. These measures included, conducting multiple initial scans when motion was high, utilising Siemens in-scanner motion correction, visually inspecting the quality of raw and processed images, and applying head motion correction on both structural and diffusion data. Considering the link between head motion, age and ADHD diagnosis, the inclusion of head motion as a covariate might result in an underestimation of the effects of interest (Dosenbach et al. 2017; Kong et al. 2014; Thomson et al. 2021). Additionally, previous research utilising the NICAP data set have indicated minimal head motion across the sample and no significant between-group difference in motion metrics between ADHD and control groups (Fuelscher et al. 2023). Nevertheless, it remains critical that ADHD research continues to minimise the impact of head motion on MRI data. Diligently addressing head motion artefacts enhances the robustness and validity of neuroimaging analyses, leading to more accurate insights into the neural correlates of ADHD.

A limitation of the study described in this chapter was that 37% of individuals included in the ADHD group had a history of taking medication during the study. While the sensitivity analysis conducted in this study indicated that medication use did not impact the primary findings of the study described in this chapter, the observed collinearity between medication use and ADHD symptom severity poses challenges in isolating their individual effects on network metrics. While no previous study has specifically investigated the impact of ADHD medication on structural connectivity connectomes, recent meta-regressions analysis found no significant effect of prior medication use and white matter properties among individuals with ADHD (Parlatini et al. 2023; Bouziane et al. 2018). Taken together, it is unlikely that the results of this study were confounded my medication use. Nevertheless, it remains essential for future ADHD research to continue investigating the potential impact of medication on brain development, such investigations

will help further our understanding of the complex interplay between medication use and neural outcomes in individuals with ADHD.

6.4.7. Conclusion

In conclusion, the study described in this chapter contributes significantly to the limited understanding of the limbic system's role in the pathophysiology of ADHD. While no notable between-group differences were found in the limbic system network measures, a significant association was found between network measures (density and routing efficiency) and ADHD symptom severity. This suggests that underconnectivity of the limbic system may underpin increased symptom severity in ADHD. While potential mechanisms were discussed, future investigations are needed to expand on this study to further understand the involvement of the limbic system in ADHD.

7 General Discussion

7.1. Review of Aims and Results

The primary aim of the research presented in this thesis was to examine the relationship between structural alteration in the limbic system and ADHD symptoms across the developmental period from childhood to mid-adolescence. The data utilized in this thesis were sourced from the Neuroimaging of the Children's Attention Project (NICAP (Silk, Genc, et al. 2016)), a longitudinal study employing multimodal MRI to assess children, both with and without ADHD, at three time points, at approximately 18-month intervals, from ages 9-14 (Silk, Genc, et al. 2016). The studies described in this thesis were designed to explore three key aspects of the limbic system in individuals with ADHD compared to controls: 1) variations in grey matter and subcortical nuclei volumes, 2) the microstructural properties of white matter tracts and 3) the topological organisation of the limbic system's structural connectivity.

7.1.1. Overview of Findings from Chapter 2

The first study in this thesis deployed longitudinal structural MRI data, acquired across three time points, to investigate the volumetric changes in limbic system grey matter and subcortical nuclei among individuals with ADHD and controls. Using Freesurfer software the following bilateral limbic system structures were isolated: amygdala, hippocampus, mammillary bodies, anterior thalamic nuclei, cingulate gyrus (sum of cingulate gyrus parcellations), and orbitofrontal cortex (sum of orbitofrontal cortex parcellations). The primary analyses of this study revealed that compared to controls, the ADHD group had lower volume of the amygdala (bilateral), hippocampus (bilateral), cingulate gyrus (bilateral), and orbitofrontal cortex (right) across development (9-14 years). Exploratory analyses revealed a significant interaction between symptom severity and age on the volume of the mammillary body (left) among individuals with ADHD, indicating that variations in mammillary body development may play a role in the persistence and increase of ADHD symptom severity during mid-adolescence. Overall, the findings of the study described in Chapter 2 suggest that atypical development in limbic system volumes may be a neurobiological feature of ADHD.

7.1.2. Overview of Findings from Chapter 3

The aim of the second study in this thesis was to explore the development of limbic system white matter in children and adolescents with ADHD between the ages of 9 to 14 years. Using multi-shell HARDI and CSD-based tractography, the major white matter tracts of the limbic system were manually isolated. These included the cingulum bundle, uncinate fasciculus, fornix, anterior thalamic projections and mammillothalamic tracts. The primary analyses found that compared to controls, individuals with ADHD displayed reduced kurtosis anisotropy in the cingulum bundle (bilateral) and fornix (left) across all three study time points. Additionally, individuals with ADHD were found to have atypical development of radial kurtosis in the anterior thalamic projection (left) compared to controls. Exploratory analyses revealed no significant association between ADHD symptom severity and microstructural organisation of limbic system white matter tracts. In conclusion, the study described in Chapter 2 revealed significant developmental differences in microstructural organisation in key limbic system white matter tracts in ADHD compared to controls, providing novel insights into the neural underpinnings of the disorder.

7.1.3. Overview of Findings from Chapter 4

The third study of this thesis aimed to investigate the topological organisation of the limbic system's structural connectivity among individuals with ADHD and controls. Using both structural and diffusion MRI scans, subject-specific limbic system structural connectivity connectomes were generated. While the primary analyses did not reveal any significant between-group differences in limbic system network measures, the exploratory analyses demonstrated a clear association between limbic system network measures and ADHD symptom severity. Specifically, among individuals with ADHD, reduced routing efficiency and network density were significantly associated with increased ADHD symptom severity. Overall, the results of this study suggest that decreased interconnectivity of this intricate network may play a role in the persistence of increased ADHD symptom severity into mid-adolescence.

7.2. Overall Implications

The studies described in this thesis add considerably to the knowledge of how the brain develops in ADHD. Specifically, it sheds new light on the role of limbic system

maturation in the manifestations of ADHD symptom expression. By exploring the structural dynamics of the limbic system and its link with ADHD symptom severity and persistence, this research advances our knowledge of the complex neurodevelopmental mechanisms underlying the disorder. Understanding the developmental trajectories of neural features in ADHD could guide clinicians in predicting the clinical course of the disorder. One of the most difficult questions that parents and young people with ADHD ask clinicians is for how long they will have ADHD symptoms. Currently the answer is frustratingly vague - "about 50% of people will not have impairing ADHD symptoms in adulthood" (Polanczyk et al. 2007; Simon et al. 2009). If a clinician had the ability to correctly predict the course of the disorder, it would have a profound impact for families. Although targeted interventions informed by these neuroanatomical findings remain a long-term goal, the ultimate aim is to refine and improve treatments by targeting the underlying neurobiological mechanisms of ADHD. The following section describes the implications of the research presented in this thesis with respect to 1) the limbic system and ADHD pathophysiology, 2) the limbic system and the neurodevelopmental models of ADHD, 3) the neural mechanisms of emotional dysregulation in ADHD and 4) the neurobiological processes underlying the neural phenotype of ADHD.

7.2.1. Limbic System and ADHD Pathophysiology

As discussed in Section 1.4, the limbic system is an important brain network involved in various processes of emotion, cognition and behaviour (Catani, Dell'acqua, and Thiebaut de Schotten 2013). While the limbic system was suggested to be a central network in the pathophysiology of many neurodevelopmental disorders (Rajmohan and Mohandas 2007), it was previously underexplored in ADHD. Using a multimodal MRI approach, the studies described in this thesis provided a novel link between disruptions to the limbic system and ADHD pathophysiology.

Synthesising the results of the multimodal approach, specifically the studies described in Chapters 3 and 5, reveal notable elements of the limbic system that may be particularly pertinent to ADHD. The cingulum bundle was associated with reduced white matter microstructural integrity in the ADHD group all three study time points. Interestingly, ADHD-associated reductions in volume were also found in the interconnected brain regions of the cingulum bundle, specifically the cingulate gyrus, orbitofrontal cortex, amygdala and hippocampus (Bubb, Metzler-Baddeley, and Aggleton

2018). To understand what was driving these structural differences in ADHD, it is important to consider the relationship between grey and white matter. While this relationship is complex, there is evidence suggesting that reduced grey matter may be driven by compromised synaptogenesis, a neurodevelopmental process associated with ADHD risk genes (Dark, Homman-Ludiye, and Bryson-Richardson 2018). As discussed in Section 1.2.2, altered synaptogenesis can disrupt the establishment of synapses formed between neurons, resulting in reduced white matter density and integrity (Dark, Homman-Ludiye, and Bryson-Richardson 2018). As such, it is plausible that the reduced white matter integrity of the cingulum bundle may be indicative of disruptions to synaptogenesis in this white matter tract, resulting in cascading impacts on the structural volume of its connected regions. These cascading effects could contribute to the observed volume reductions in the interconnected structures, potentially forming a subnetwork within the limbic system that may be central to the disrupted development seen in ADHD.

The finding of ADHD-associated reduced limbic system structural connectivity, as detailed in Chapter 6, is particularly interesting as research has shown that disrupted white matter may underpin the disrupted functional connectivity seen in the disorder (Soman et al. 2023). This interplay between structure and function in the brain highlights a crucial aspect of ADHD's pathology. Functional connectivity is scaffolded by the structural connections of the brain, disruptions to this scaffolding can result in suboptimal neural communications across a network, resulting in compromised executive and cognitive functioning (Park and Friston 2013; Baum et al. 2020). In ADHD, research has shown dysregulated myelination and axonal formation might underpin the disrupted structure-function coupling seen in the disorder (Soman et al. 2023). This disruption to the brain’s structural and functional harmony may contribute to ADHD symptom expression (Soman et al. 2023). As such, the findings of Chapter 6, which demonstrate an association between reduced limbic system interconnectivity and increased symptom severity in ADHD, likely indicate compromised structural scaffolding within this system. Such disrupted structural connectivity scaffolding could lead to impairments in the limbic system’s functional connectivity, ultimately affecting its overall functioning. This compromised functionality within the limbic system is likely a key factor contributing to the increased severity of symptoms observed in ADHD. These insights not only highlight the limbic system's role in ADHD but also the importance of structural connectivity in understanding the disorder's pathophysiology.

7.2.2. Limbic System and the Neurodevelopmental Models of ADHD

As discussed in Section 1.2.4, the neurodevelopmental models of ADHD represent a promising area of pathophysiological research that provide a framework for the relationship between the age-associated changes in brain structures and symptoms seen in ADHD (Shaw and Sudre 2021). Although these developmental models provide insights into the neurobiological underpinnings of ADHD symptom progression, most longitudinal studies have focused on cortical structures (Shaw et al. 2012; Shaw et al. 2007). As a result, our understanding of these models in relation to subcortical structures and networks is largely incomplete (Hoogman et al. 2017b; Rosch et al. 2018). This thesis expanded the neurodevelopmental models of ADHD to previously unexplored brain regions and structures. Using a multimodal MRI approach, the studies described in this thesis found that, compared to controls, there was an association between persistent ADHD diagnosis status and reduced volume, and microstructural organisation in key limbic system structures, providing novel support for the convergence model of ADHD (Shaw and Sudre 2021). The convergence model posits that individuals with persistent ADHD diagnosis will display fixed, non-progressive neural features, in contrast to those who experience symptom remission and exhibit a convergence towards neurotypical neural features (Shaw and Sudre 2021).

As highlighted in Section 1.2.2., genes associated with ADHD that play a role in brain development predominantly influence neuronal and synaptic formation (Dark, Homman-Ludiye, and Bryson-Richardson 2018). Disruptions in these processes may underlie the neurobiological mechanisms consistent with the convergence-model phenotype. The findings in the studies described in Chapters 3 and 5 underscore that while individuals with ADHD exhibit both reduced limbic system volume and white matter microstructural integrity, the developmental trajectories of these structures align with neurotypical patterns (Bethlehem et al. 2022). This suggests that the combination of early developmental disruptions in neuronal and synaptic formation (processes linked to reduced grey matter volume and white matter integrity) and no accelerated 'catch-up' phase associated with ADHD symptom remission could lead to the fixed, non-progressive neural features characteristic of persistent ADHD.

7.2.3. Limbic System and Emotional Dysregulation ADHD

While the findings of this thesis revealed a link between limbic system development and ADHD symptom severity, no significant association was found with emotional dysregulation. Emotional regulation encompasses multi-level processes, including both 'bottom-up' and 'top-down' neural regulation (Philip Shaw et al. 2014). The limbic system incorporates "bottom-up" regulation, which involves the amygdala and orbitofrontal cortex. "Bottom-up" regulation is how individuals assess emotional stimuli and value rewards, allowing quick and automatic responses to emotional stimuli (Philip Shaw et al. 2014). It is worth considering that the presence of emotional dysregulation in ADHD is a complex cognitive process that is likely influenced by various neural circuits beyond the limbic system (Philip Shaw et al. 2014).

"Top-down" regulatory processing (which involves the ventrolateral prefrontal cortex, medial prefrontal cortex and anterior cingulate gyrus), governs the allocation of attention and responses to emotional stimuli (Phillips, Ladouceur, and Drevets 2008; Ochsner and Gross 2005). This processing involves a more controlled and rational assessment of emotions, enabling individuals to modulate their reactions based on reasoned judgement (Philip Shaw et al. 2014). As this study focused on the limbic system, the structures involved in 'top-down' processing were not investigated. It is plausible that while the limbic system may play a role in emotional regulation, 'top-down' processes might be more critical for emotional dysregulation in ADHD (Philip Shaw et al. 2014).

It is also possible that the metric used to measure emotion regulation in this study, the ARI, influenced the finding of a lack of association between emotion dysregulation and limbic system structures. As discussed in Section 1.1.2, emotional dysregulation is a complex construct that can manifest in various forms, including problems with impulse control, mood swings, and an unusual fixation on emotional stimuli (Shaw, Stringaris, et al. 2014). Although the Affective Reactivity Index (ARI) is commonly used to measure emotional dysregulation, it may not fully capture this multifaceted construct (Nigg et al. 2020). The ARI primarily measures irritability and reactivity, which are just two components of emotional dysregulation (Nigg et al. 2020). It has been suggested that irritability refers to anger dysregulation whereas emotional dysregulation refers to dysregulation of both angry and positive emotions (Nigg et al. 2020). As such, the ARI may provide only a partial representation of emotional dysregulation. Considering the complex and multi-dimensional nature of emotional regulation, future research on children

with ADHD would benefit from incorporating a more comprehensive range of assessments, including but not limited to the Emotion Regulation Checklist (ERC) (Shields and Cicchetti 1997), Temperament in Middle Childhood Questionnaire (TMCQ) (Simonds and Rothbart 2004) and Children's Emotion Management Scales (CEMS) (Zeman, Shipman, and Penza-Clyve 2001; Zeman, Shipman, and Suveg 2002; Zeman et al. 2010).

7.2.4. Neurobiological Processes Underlying Atypical Brain Development in ADHD

Previous MRI research – including the findings presented in this thesis - has identified ADHD-associated macroanatomical developmental abnormalities in both subcortical and cortical regions (Shaw et al. 2012; Shaw et al. 2007). While the underlying mechanisms of these changes remains unclear, genomics studies offer an exciting direction for future research. Many risk genes for ADHD play a functional role in all stages of brain development (Dark, Homman-Ludiye, and Bryson-Richardson 2018), with a particular interest on neural formation, myelination, and synaptic regulation (Dark, Homman-Ludiye, and Bryson-Richardson 2018). It is believed that disturbances to these neurodevelopmental processes likely play a role in the neural phenotype seen in ADHD (Dark, Homman-Ludiye, and Bryson-Richardson 2018). Exploring the relationship between risk genes for ADHD and brain development provides a molecular framework for understanding the neuroanatomical changes identified through MRI research.

Among the genes of interest, members of the cadherin gene family, specifically CDH13 and PCDH7, represent a noteworthy focus. These genes are particularly intriguing due to their role in neurogenesis, synaptic formation and neural connectivity, mechanisms that appear to be altered in ADHD (see Table 1.1) (Dark, Homman-Ludiye, and Bryson-Richardson 2018). Other candidate genes of interest include GRM5 (involved in neurogenesis, synaptogenesis and synaptic plasticity), ST3GAL3 (involved in synaptogenesis and synaptic plasticity), FOXP2 (involved in neurogenesis, neuronal migration, and synaptogenesis) and MEF2C (involved in neurogenesis and synaptogenesis) (Dark, Homman-Ludiye, and Bryson-Richardson 2018). While these findings hold promise, it is important to note that our current understanding of neural formation and connectivity in the context of ADHD is still limited. Future integrated MRI,

genomic and animal model studies are imperative for delineating the precise mechanisms underpinning the neural phenotype seen in ADHD.

7.3. Limitations and Future Directions of this Thesis

Each study within this thesis has specific limitations, which are discussed in their respective chapters. In addition to these, there are some overarching limitations that apply more broadly to the type of work presented in this thesis.

7.3.1. Limitations of MRI-Based Studies

While the findings of the studies described in this thesis make a significant contribution to our understanding of the pathophysiology of ADHD, it is important to acknowledge an inherent limitation of MRI research. MRI data provides reconstructed representations of brain regions and networks. The accuracy of these brain reconstructions has been shown to be influenced by various factors, such as imaging parameters and processing steps (Despotović, Goossens, and Philips 2015; Van Hecke, Emsell, and Sunaert 2016). It has been demonstrated that suboptimal imaging parameters and image processing has been shown to lead to inaccurate and potentially false reconstructions (Despotović, Goossens, and Philips 2015; Van Hecke, Emsell, and Sunaert 2016). To maximise the quality and validity of the MRI reconstructions, the current work employed advanced MRI techniques, such as multi-shell HARDI (Van Hecke, Emsell, and Sunaert 2016) and CSD-based tractography (Tournier et al. 2004a; Tournier, Calamante, and Connelly 2007). These techniques have been shown to significantly improve reconstruction and segmentation accuracy (Van Hecke, Emsell, and Sunaert 2016). Nevertheless, it is important to recognise that even with these advanced techniques, MRI data are ultimately approximations of brain structures that are subject to artifacts and inaccuracies (Van Hecke, Emsell, and Sunaert 2016). As such, careful interpretation of MRI research findings is needed, particularly when trying to infer underlying neurobiological mechanisms.

For a more thorough understanding of structural brain changes in ADHD, complementing *in vivo* MRI findings with *ex vivo* histological research is necessary. Both *in vivo* MRI and *ex vivo* histological approaches have their respective strengths and weaknesses. MRI research provides valuable but indirect anatomical and functional insights into large samples across multiple time points. This lack of direct anatomical

measurement can limit the completeness and accuracy of the underlying neurobiological mechanisms. Conversely, *ex vivo* histological research offers high resolution, direct observations of brain structures, but is often constrained by limited sample sizes and an inability to capture developmental changes across time (Hillman 2000). The integration of both *in vivo* MRI and *ex vivo* histological techniques is essential for advancing our understanding of the neurobiological underpinnings of ADHD.

7.3.2. Anatomical Boundaries of the Limbic System

While the studies of this thesis used a scientifically defined limbic system (Catani, Dell'acqua, and Thiebaut de Schotten 2013) (see schematic Figure 1.1), it needs to be acknowledged that there is currently no universally accepted anatomical definition of the limbic system (Stephani 2014). Definitions vary, with some incorporating structures like the septal nucleus, insula and parahippocampal gyrus(Michael-Titus, Revest, and Shortland 2010). Beyond these anatomical inconsistencies, the conceptualisation of the limbic system as a single functional unit has been challenged (Rolls 2015). Rather the limbic system may be comprised of multiple functionally distinct networks (Rolls 2015). For example, it has been proposed that the limbic system is composed of two functionally distinct networks. The first includes the hippocampus and its connected structures and is involved in episodic memory (Kesner and Rolls 2015; Rolls 2018b, 2021) and navigation (Rolls and Wirth 2018). The second network involves the amygdala and its connected structures, particularly the orbitofrontal cortex, and is primarily involved in processes of emotion and regulation (Rolls 2018a, 2019b). In this dual model approach, the cingulate gyrus adds an additional layer of complexity, as it appears to play a role in both functional networks (Rolls 2019c). This variability in both structural and functional definitions presents a limitation of limbic system research, hindering the formation of a unified body of literature and a coherent understanding of limbic system functions.

Future research aimed at better understanding the limbic system can focus on two key areas: 1) investigating how the limbic system is integrated into the broader whole brain network, and 2) elucidating the interactions and functions of the limbic system's subnetworks. The ultimate objective should be the reconciliation of diverse anatomical and functional definitions, facilitating a more cohesive and unified understanding of this vital neural system.

7.3.3. Limitation of Heterogeneity of ADHD Group in Case-Control MRI Research

ADHD is a highly heterogeneous disorder (Li et al. 2021), with symptoms varying widely in presentation, severity and duration across individuals with the disorder (Faraone et al. 2015). This heterogeneity is particularly relevant during adolescence as individuals with ADHD have been shown to fluctuate in their diagnostic status across this period (Margaret H. Sibley et al. 2022). In MRI case-control research, in which the overarching goal is to isolate stable and reliable neurobiological differences between the case and control groups (Marquand et al. 2016), heterogeneity within the ADHD group is a common limitation (Faraone et al. 2015). Therefore, having diagnosis and symptom stability in both ADHD and control groups is beneficial for isolating reliable neurobiological between-group differences. As discussed in Section 2.2.1, the studies described in this thesis made a concerted effort to maintain consistent diagnostic profiles within the ADHD group by including only individuals with persistently diagnosed ADHD across the NICAP study time points. Despite this, variability of symptom severity within the ADHD group still remained, highlighting the heterogeneity in the disorder.

This limitation of ADHD research emphasises the need for future studies to investigate the neurodevelopmental processes of ADHD subtypes, symptom dimensions or the presence of comorbidities to provide a greater understanding of the neurobiological underpinnings of ADHD.

7.3.4. Linear Growth Curves

All three studies in this thesis investigated changes in brain structure across three time points using linear mixed-effects models. Although these time points provide valuable insights, the application of linear models may not fully encapsulate the intricate patterns of brain development. Alternative modelling techniques such as quadratic or cubic polynomial curves may provide a more nuanced portrayal of the trajectories of brain changes across time (Elhakeem et al. 2022). Quadratic and cubic curves offer more flexibility than linear models because they can capture non-linear trends in developmental trajectories (Elhakeem et al. 2022). The studies in this thesis deployed linear modelling due to the limited time points in the NICAP data set. With three time points, there were insufficient degrees of freedom to reliably estimate polynomial curves (Francis et al. 1991). Alternatively, Generalized Additive Mixed Models (GAMM) represent an

advanced statistical technique that allows for flexible modelling of non-linear relationships within longitudinal data. GAMM can handle complex patterns by incorporating smooth functions, making it particularly useful in studies where relationships between variables are not strictly linear. However, while GAMM offers advanced modelling capabilities for non-linear relationships, a limitation compared to LMM is its increased complexity and potential for overfitting, especially in studies with a limited number of time points or participants (Wood 2017). As such, the studies described in this thesis deployed LMM over GAMM as LMM provided the necessary balance between simplicity and accuracy for this context, ensuring clear interpretation of linear trends in brain development and behaviours.

While linear models could arguably be a reasonable approximation for capturing brain changes in this specific developmental period (Bethlehem et al. 2022), it's important to acknowledge the limitation imposed by the restricted number of study time points. More complex models, such as GAMM higher-order mixed modelling, that incorporate additional time points would provide a more detailed understanding of the changes in brain structure throughout development (Elhakeem et al. 2022). There is a pressing need for extended longitudinal studies featuring multiple time points to adequately map ADHD-specific brain growth curves across various life stages. These studies could not only deepen our understanding of the disorder's developmental trajectory but could also aid in the formulation of age-specific treatment plans. Future research should therefore prioritise developing longitudinal MRI research with more extensive temporal ranges to fully appreciate the complexities of brain development in populations with ADHD.

7.3.5. Limitation of Sample Sizes in Brain-Behaviour Studies

A common limitation in brain-behaviour association studies is small sample sizes (Button et al. 2013a; Schönbrodt and Perugini 2013; Boekel et al. 2015). In the studies described in this thesis, the sample sizes in the brain-behaviour association analyses are relatively small. Small sample sizes in brain-behaviour association studies can compromise statistical power, generalisability and reproducibility, thereby limiting the reliability of the findings (Button et al. 2013a; Schönbrodt and Perugini 2013; Boekel et al. 2015). To minimise this limitation, the studies described in this thesis deployed a focused brain-behaviour study approach (Gratton, Nelson, and Gordon 2022). This methodological choice involves a more concentrated participant group but places a higher

emphasis on precise classification and measurement of both brain structure and behaviour, utilising advanced MRI techniques and rigorous diagnostic classification (Gratton, Nelson, and Gordon 2022). This focused approach, though it includes fewer participants, is designed to enhance the quality and reliability of data, enabling more detailed and accurate correlations between brain structures and behavioural outcomes. Notably, as Gratton et al. (2022) suggest, such a focused approach can yield effect sizes comparable to those found in larger consortia studies, demonstrating its effectiveness in capturing significant brain-behaviour relationships even within a smaller cohort (Gratton, Nelson, and Gordon 2022).

Both focused samples and large consortia studies play valuable roles in psychiatric research. Large consortia studies offer heightened statistical power and generalisability due to their larger sample sizes (Marek et al. 2022), while focused sample approaches, leveraging their precision and sensitivity, provide valuable insights into the nuanced brain-behaviour relationships (Gratton, Nelson, and Gordon 2022). Given the emerging conclusion that real, reproducible associations between individual differences in complex biological systems and heterogeneous disorders such as ADHD are likely to involve small effect sizes (Bernanke et al. 2022), future research can benefit from the application of both methodologies.

7.3.6. Limitation of a Single Data Source

This study's reliance on a single data source – the NICAP dataset –is a limitation. While the NICAP dataset, with its comprehensive phenotyping, advanced MRI techniques and longitudinal design, is an extremely valuable dataset, these same unique features limited the feasibility of cross-dataset reproducibility testing. As such, there is a lack of external replication of the findings, a significant concern in ADHD MRI research (Stikov, Trzasko, and Bernstein 2019; Button et al. 2013a; Hoogman et al. 2019).

7.4. Future Directions of ADHD Pathophysiological Research

A critical focus of future pathophysiology ADHD research lies in deciphering the neurobiological mechanisms underpinning the convergence model of ADHD. Specifically, understanding the mechanism underpinning the apparent 'catch-up' developmental phase associated with symptom remission in ADHD. Unravelling this aspect is paramount because it could reveal key insights into why some individuals experience a reduction in ADHD symptoms over time, while others continue to exhibit

persistent symptoms. Understanding these mechanisms could lead to the development of targeted interventions or treatments aimed at promoting this 'catch-up' phase in those with persistent ADHD. Such advancements hold the potential to significantly improve long-term outcomes and quality of life for individuals affected by ADHD.

For these advancements to materialise, a collaborative integration of genetic studies, animal model research, and neuroimaging investigations is essential. This multidisciplinary approach would allow for a more comprehensive understanding of ADHD pathophysiology, combining insights from various levels of analysis—from genetic underpinnings to brain structure and function. Ultimately, this integrative approach could pave the way for breakthroughs in ADHD research, transforming our ability to manage and treat this complex disorder effectively.

7.5. Conclusion

Extensive converging evidence from genetic, animal model and neuroimaging research suggests that abnormal development of brain structures may underpin symptom expression in ADHD. The central aim of this thesis was to investigate an underexplored brain network in ADHD, the limbic system. Using longitudinal MRI data and advanced multimodal MRI techniques, the studies in this thesis have provided novel insights into the developmental changes of the limbic system in ADHD. Overall results suggest that atypical development of limbic system grey matter, white matter and subcortical nuclei may be a neurobiological feature associated with the persistence of ADHD symptoms during the transition into mid-adolescence.

8 References

Abdelnour, Farras, Henning U Voss, and Ashish Raj. 2014. 'Network diffusion accurately models the relationship between structural and functional brain connectivity networks', *Neuroimage*, 90: 335-47.

Achard, Sophie, and Ed Bullmore. 2007. 'Efficiency and cost of economical brain functional networks', *Plos Computational Biology*, 3: e17.

Ades-Aron, Benjamin, Jelle Veraart, Peter Kochunov, Stephen McGuire, Paul Sherman, Elias Kellner, Dmitry S Novikov, and Els Fieremans. 2018. 'Evaluation of the accuracy and precision of the diffusion parameter EStImation with Gibbs and NoisE removal pipeline', *Neuroimage*, 183: 532-43.

Adisetiyo, V., A. Tabesh, A. Di Martino, M. F. Falangola, F. X. Castellanos, J. H. Jensen, and J. A. Helpern. 2014. 'Attention-deficit/hyperactivity disorder without comorbidity is associated with distinct atypical patterns of cerebral microstructural development', *Human Brain Mapping*, 35: 2148-62.

Adler, Lisa D, and Andrew A Nierenberg. 2010. 'Review of medication adherence in children and adults with ADHD', *Postgraduate medicine*, 122: 184-91.

Adolphs, Ralph. 2010. 'What does the amygdala contribute to social cognition?', *Annals of the New York Academy of Sciences*, 1191: 42-61.

Al-Amin, M., A. Zinchenko, and T. Geyer. 2018. 'Hippocampal subfield volume changes in subtypes of attention deficit hyperactivity disorder', *Brain Research*, 1685: 1-8.

Alexander, Andrew L, Jee Eun Lee, Mariana Lazar, and Aaron S Field. 2007. 'Diffusion tensor imaging of the brain', *Neurotherapeutics*, 4: 316-29.

Alexander, D. C. 2008. 'A general framework for experiment design in diffusion MRI and its application in measuring direct tissue-microstructure features', *Magn Reson Med*, 60: 439-48.

Alexander-Bloch, Aaron, Liv Clasen, Michael Stockman, Lisa Ronan, Francois Lalonde, Jay Giedd, and Armin Raznahan. 2016. 'Subtle in-scanner motion biases automated measurement of brain anatomy from in vivo MRI', *Human Brain Mapping*, 37: 2385-97.

Althoff, Robert R, Frank C Verhulst, David C Rettew, James J Hudziak, and Jan van der Ende. 2010. 'Adult outcomes of childhood dysregulation: a 14-year follow-up study', *Journal of the American Academy of Child & Adolescent Psychiatry*, 49: 1105-16. e1.

Alves, P. N., C. Foulon, V. Karolis, D. Bzdok, D. S. Margulies, E. Volle, and M. Thiebaut de Schotten. 2019. 'An improved neuroanatomical model of the default-mode network reconciles previous neuroimaging and neuropathological findings', *Commun Biol*, 2: 370.

Ameis, Stephanie H., Jason P. Lerch, Margot J. Taylor, Wayne Lee, Joseph D. Viviano, Jon Pipitone, Arash Nazeri, Paul E. Croarkin, Aristotle N. Voineskos, Meng-Chuan Lai, Jennifer Crosbie, Jessica Brian, Noam Soreni, Russell Schachar, Peter Szatmari, Paul D. Arnold, and Evdokia Anagnostou. 2016. 'A Diffusion Tensor Imaging Study in Children With ADHD, Autism Spectrum Disorder, OCD, and Matched Controls:

Distinct and Non-Distinct White Matter Disruption and Dimensional Brain-Behavior Relationships', *American Journal of Psychiatry*, 173: 1213-22.

American Psychiatric Association, DSMTF, and American Psychiatric Association. 2013. *Diagnostic and statistical manual of mental disorders: DSM-5* (American psychiatric association Washington, DC).

Andrews, D. S., J. K. Lee, D. J. Harvey, E. Waizbard-Bartov, M. Solomon, S. J. Rogers, C. W. Nordahl, and D. G. Amaral. 2021. 'A Longitudinal Study of White Matter Development in Relation to Changes in Autism Severity Across Early Childhood', *Biol Psychiatry*, 89: 424-32.

Andrews-Hanna, Jessica R, Jay S Reidler, Jorge Sepulcre, Renee Poulin, and Randy L Buckner. 2010. 'Functional-anatomic fractionation of the brain's default network', *Neuron*, 65: 550-62.

Aoki, Y., S. Cortese, and F. X. Castellanos. 2018. 'Research Review: Diffusion tensor imaging studies of attention-deficit/hyperactivity disorder: meta-analyses and reflections on head motion', *Journal of Child Psychology & Psychiatry & Allied Disciplines*, 59: 193-202.

Ashtari, M., S. Kumra, S. L. Bhaskar, T. Clarke, E. Thaden, K. L. Cervellione, J. Rhinewine, J. M. Kane, A. Adesman, R. Milanaik, J. Maytal, A. Diamond, P. Szeszko, and B. A. Ardekani. 2005. 'Attention-deficit/hyperactivity disorder: a preliminary diffusion tensor imaging study', *Biological Psychiatry*, 57: 448-55.

Assaf, Yaniv, Adi Mayk, and Yoram Cohen. 2000. 'Displacement imaging of spinal cord using q-space diffusion-weighted MRI', *Magnetic Resonance in Medicine: An Official Journal of the International Society for Magnetic Resonance in Medicine*, 44: 713-22.

Atkinson, M, and C Hollis. 2010. 'NICE guideline: attention deficit hyperactivity disorder', *Archives of Disease in Childhood-Education and Practice*, 95: 24-27.

Avena-Koenigsberger, Andrea, Bratislav Mišić, Robert XD Hawkins, Alessandra Griffa, Patric Hagmann, Joaquín Goñi, and Olaf Sporns. 2017. 'Path ensembles and a tradeoff between communication efficiency and resilience in the human connectome', *Brain Structure and Function*, 222: 603-18.

Avena-Koenigsberger, Andrea, Bratislav Misic, and Olaf Sporns. 2018. 'Communication dynamics in complex brain networks', *Nature Reviews Neuroscience*, 19: 17-33.

Bai, Shoumei, Kalpana Ghoshal, and Samson T Jacob. 2006. 'Identification of T-cadherin as a novel target of DNA methyltransferase 3B and its role in the suppression of nerve growth factor-mediated neurite outgrowth in PC12 cells', *Journal of Biological Chemistry*, 281: 13604-11.

Barkley, Russell A. 1997. 'Behavioral inhibition, sustained attention, and executive functions: constructing a unifying theory of ADHD', *Psychological bulletin*, 121: 65.

Baroni, A., and F. X. Castellanos. 2015. 'Neuroanatomic and cognitive abnormalities in attention-deficit/hyperactivity disorder in the era of 'high definition' neuroimaging', *Current Opinion in Neurobiology*, 30: 1-8.

Basser, P. J., J. Mattiello, and D. LeBihan. 1994. 'MR diffusion tensor spectroscopy and imaging', *Biophys J*, 66: 259-67.

Bassett, Danielle Smith, and ED Bullmore. 2006. 'Small-world brain networks', *The neuroscientist*, 12: 512-23.

Bates, Douglas, Martin Mächler, Ben Bolker, and Steve Walker. 2014. 'Fitting linear mixed-effects models using lme4', *arXiv preprint arXiv:1406.5823*.

Bauer, J., A. Werner, W. Kohl, H. Kugel, A. Shushakova, A. Pedersen, and P. Ohrmann. 2018. 'Hyperactivity and impulsivity in adult attention-deficit/hyperactivity disorder is related to glutamatergic dysfunction in the anterior cingulate cortex', *World J Biol Psychiatry*, 19: 538-46.

Baum, Graham L., Zaixu Cui, David R. Roalf, Rastko Ciric, Richard F. Betzel, Bart Larsen, Matthew Cieslak, Philip A. Cook, Cedric H. Xia, Tyler M. Moore, Kosha Ruparel, Desmond J. Oathes, Aaron F. Alexander-Bloch, Russell T. Shinohara, Armin Raznahan, Raquel E. Gur, Ruben C. Gur, Danielle S. Bassett, and Theodore D. Satterthwaite. 2020. 'Development of structure–function coupling in human brain networks during youth', *Proceedings of the National Academy of Sciences*, 117: 771-78.

Bava, Sunita, Veronique Boucquey, Diane Goldenberg, Rachel E Thayer, Megan Ward, Joanna Jacobus, and Susan F Tapert. 2011. 'Sex differences in adolescent white matter architecture', *Brain Research*, 1375: 41-48.

Beare, Richard, Chris Adamson, Mark A. Bellgrove, Veronika Vilgis, Alasdair Vance, Marc L. Seal, and Timothy J. Silk. 2017. 'Altered structural connectivity in ADHD: a network based analysis', *Brain Imaging and Behavior*, 11: 846-58.

Bechtel, N., M. Kobel, I. K. Penner, M. Klarhofer, K. Scheffler, K. Opwis, and P. Weber. 2009. 'Decreased fractional anisotropy in the middle cerebellar peduncle in children with epilepsy and/or attention deficit/hyperactivity disorder: a preliminary study', *Epilepsy & Behavior*, 15: 294-8.

Behrens, Timothy EJ, H Johansen Berg, Saad Jbabdi, Matthew FS Rushworth, and Mark W Woolrich. 2007. 'Probabilistic diffusion tractography with multiple fibre orientations: What can we gain?', *Neuroimage*, 34: 144-55.

Belmadani, Abdelhak, Phuong B Tran, Dongjun Ren, and Richard J Miller. 2006. 'Chemokines regulate the migration of neural progenitors to sites of neuroinflammation', *Journal of Neuroscience*, 26: 3182-91.

Ben-Shachar, Mattan S, Daniel Lüdecke, and Dominique Makowski. 2020. 'effectsize: Estimation of effect size indices and standardized parameters', *Journal of Open Source Software*, 5: 2815.

Benear, S. L., C. T. Ngo, and I. R. Olson. 2020. 'Dissecting the Fornix in Basic Memory Processes and Neuropsychiatric Disease: A Review', *Brain Connect*, 10: 331-54.

Benjamini, Yoav, Abba M Krieger, and Daniel Yekutieli. 2006. 'Adaptive linear step-up procedures that control the false discovery rate', *Biometrika*, 93: 491-507.

Bernanke, Joel, Alex Luna, Le Chang, Elizabeth Bruno, Jordan Dworkin, and Jonathan Posner. 2022. 'Structural brain measures among children with and without ADHD in the Adolescent Brain and Cognitive Development Study cohort: a cross-sectional US population-based study', *The Lancet Psychiatry*, 9: 222-31.

Bessette, K. L., and M. C. Stevens. 2019. 'Neurocognitive Pathways in Attention-Deficit/Hyperactivity Disorder and White Matter Microstructure', *Biological Psychiatry : Cognitive Neuroscience and Neuroimaging*, 4: 233-42.

Bethlehem, R. A. I., J. Seidlitz, S. R. White, J. W. Vogel, K. M. Anderson, C. Adamson, S. Adler, G. S. Alexopoulos, E. Anagnostou, A. Areces-Gonzalez, D. E. Astle, B. Auyeung, M. Ayub, J. Bae, G. Ball, S. Baron-Cohen, R. Beare, S. A. Bedford, V.

Benegal, F. Beyer, J. Blangero, M. Blesa Cábez, J. P. Boardman, M. Borzage, J. F. Bosch-Bayard, N. Bourke, V. D. Calhoun, M. M. Chakravarty, C. Chen, C. Chertavian, G. Chetelat, Y. S. Chong, J. H. Cole, A. Corvin, M. Costantino, E. Courchesne, F. Crivello, V. L. Cropley, J. Crosbie, N. Crossley, M. Delarue, R. Delorme, S. Desrivieres, G. A. Devenyi, M. A. Di Biase, R. Dolan, K. A. Donald, G. Donohoe, K. Dunlop, A. D. Edwards, J. T. Elison, C. T. Ellis, J. A. Elman, L. Eyler, D. A. Fair, E. Feczko, P. C. Fletcher, P. Fonagy, C. E. Franz, L. Galan-Garcia, A. Gholipour, J. Giedd, J. H. Gilmore, D. C. Glahn, I. M. Goodyer, P. E. Grant, N. A. Groenewold, F. M. Gunning, R. E. Gur, R. C. Gur, C. F. Hammill, O. Hansson, T. Hedden, A. Heinz, R. N. Henson, K. Heuer, J. Hoare, B. Holla, A. J. Holmes, R. Holt, H. Huang, K. Im, J. Ipser, C. R. Jack, A. P. Jackowski, T. Jia, K. A. Johnson, P. B. Jones, D. T. Jones, R. S. Kahn, H. Karlsson, L. Karlsson, R. Kawashima, E. A. Kelley, S. Kern, K. W. Kim, M. G. Kitzbichler, W. S. Kremen, F. Lalonde, B. Landeau, S. Lee, J. Lerch, J. D. Lewis, J. Li, W. Liao, C. Liston, M. V. Lombardo, J. Lv, C. Lynch, T. T. Mallard, M. Marcelis, R. D. Markello, S. R. Mathias, B. Mazoyer, P. McGuire, M. J. Meaney, A. Mechelli, N. Medic, B. Misic, S. E. Morgan, D. Mothersill, J. Nigg, M. Q. W. Ong, C. Ortinau, R. Ossenkoppele, M. Ouyang, L. Palaniyappan, L. Paly, P. M. Pan, C. Pantelis, M. M. Park, T. Paus, Z. Pausova, D. Paz-Linares, A. Pichet Binette, K. Pierce, X. Qian, J. Qiu, A. Qiu, A. Raznahan, T. Rittman, A. Rodrigue, C. K. Rollins, R. Romero-Garcia, L. Ronan, M. D. Rosenberg, D. H. Rowitch, G. A. Salum, T. D. Satterthwaite, H. L. Schaare, R. J. Schachar, A. P. Schultz, G. Schumann, M. Schöll, D. Sharp, R. T. Shinohara, I. Skoog, C. D. Smyser, R. A. Sperling, D. J. Stein, A. Stolicyn, J. Suckling, G. Sullivan, Y. Taki, B. Thyreau, R. Toro, N. Traut, K. A. Tsvetanov, N. B. Turk-Browne, J. J. Tuulari, C. Tzourio, É Vachon-Presseau, M. J. Valdes-Sosa, P. A. Valdes-Sosa, S. L. Valk, T. van Amelsvoort, S. N. Vandekar, L. Vasung, L. W. Victoria, S. Villeneuve, A. Villringer, P. E. Vértes, K. Wagstyl, Y. S. Wang, S. K. Warfield, V. Warrier, E. Westman, M. L. Westwater, H. C. Whalley, A. V. Witte, N. Yang, B. Yeo, H. Yun, A. Zalesky, H. J. Zar, A. Zettergren, J. H. Zhou, H. Ziauddeen, A. Zugman, X. N. Zuo, C. Rowe, G. B. Frisoni, A. Pichet Binette, E. T. Bullmore, A. F. Alexander-Bloch, Brain R, Aibl, Initiative Alzheimer's Disease Neuroimaging, Investigators Alzheimer's Disease Repository Without Borders, Calm Team, C. A. N. Cam, Ccnp, Cobre, cVeda, Enigma Developmental Brain Age Working Group, Project Developing Human Connectome, FinnBrain, Study Harvard Aging Brain, Imagen, Kne, Aging The Mayo Clinic Study of, Nspn, Pond, Prevent- A. D. Research Group The, and Vetsa. 2022. 'Brain charts for the human lifespan', *Nature*, 604: 525-33.

Biederman, Joseph, Stephen V Faraone, Kate Keenan, Jonathan Benjamin, Belinda Krifcher, Cindy Moore, Susan Sprich-Buckminster, Karen Ugaglia, Michael S Jellinek, and Ronald Steingard. 1992. 'Further evidence for family-genetic risk factors in attention deficit hyperactivity disorder: Patterns of comorbidity in probands and relatives in psychiatrically and pediatrically referred samples', *Archives of General Psychiatry*, 49: 728-38.

Biederman, Joseph, Stephen V Faraone, Kate Keenan, Debra Knee, and Ming T Tsuang. 1990. 'Family-genetic and psychosocial risk factors in DSM-III attention deficit disorder', *Journal of the American Academy of Child & Adolescent Psychiatry*, 29: 526-33.

Biederman, Joseph, Carter R Petty, Maggie Evans, Jacqueline Small, and Stephen V Faraone. 2010. 'How persistent is ADHD? A controlled 10-year follow-up study of boys with ADHD', *Psychiatry Research*, 177: 299-304.

Biederman, Joseph, Carter R Petty, Michael C Monuteaux, Ronna Fried, Deirdre Byrne, Tara Mirto, Thomas Spencer, Timothy E Wilens, and Stephen V Faraone. 2010. 'Adult psychiatric outcomes of girls with attention deficit hyperactivity disorder: 11-year follow-up in a longitudinal case-control study', *American Journal of Psychiatry*, 167: 409-17.

Billiet, Thibo, Mathieu Vandenbulcke, Burkhard Mädler, Ronald Peeters, Thijs Dhollander, Hui Zhang, Sabine Deprez, Bea RH Van den Bergh, Stefan Sunaert, and Louise Emsell. 2015. 'Age-related microstructural differences quantified using myelin water imaging and advanced diffusion MRI', *Neurobiology of aging*, 36: 2107-21.

Billot, Benjamin, Martina Bocchetta, Emily Todd, Adrian V. Dalca, Jonathan D. Rohrer, and Juan Eugenio Iglesias. 2020. 'Automated segmentation of the hypothalamus and associated subunits in brain MRI', *Neuroimage*, 223: 117287.

Bishop, S. J. 2008. 'Neural mechanisms underlying selective attention to threat', *Ann N Y Acad Sci*, 1129: 141-52.

Blaine, Bruce E. 2018. 'Winsorizing', *The SAGE encyclopedia of educational research, measurement, and evaluation*: 1817.

Boekel, Wouter, Eric-Jan Wagenmakers, Luam Belay, Josine Verhagen, Scott Brown, and Birte U Forstmann. 2015. 'A purely confirmatory replication study of structural brain-behavior correlations', *Cortex*, 66: 115-33.

Boguna, Marian, Dmitri Krioukov, and Kimberly C Claffy. 2009. 'Navigability of complex networks', *Nature physics*, 5: 74-80.

Botvinik-Nezer, Rotem, Felix Holzmeister, Colin F. Camerer, Anna Dreber, Juergen Huber, Magnus Johannesson, Michael Kirchler, Roni Iwanir, Jeanette A. Mumford, R. Alison Adcock, Paolo Avesani, Blazej M. Baczkowski, Aahana Bajracharya, Leah Bakst, Sheryl Ball, Marco Barilari, Nadège Bault, Derek Beaton, Julia Beitner, Roland G. Benoit, Ruud M. W. J. Berkers, Jamil P. Bhanji, Bharat B. Biswal, Sebastian Bobadilla-Suarez, Tiago Bortolini, Katherine L. Bottenhorn, Alexander Bowring, Senne Braem, Hayley R. Brooks, Emily G. Brudner, Cristian B. Calderon, Julia A. Camilleri, Jaime J. Castrellon, Luca Cecchetti, Edna C. Cieslik, Zachary J. Cole, Olivier Collignon, Robert W. Cox, William A. Cunningham, Stefan Czoschke, Kamalaker Dadi, Charles P. Davis, Alberto De Luca, Mauricio R. Delgado, Lysia Demetriou, Jeffrey B. Dennison, Xin Di, Erin W. Dickie, Ekaterina Dobryakova, Claire L. Donnat, Juergen Dukart, Niall W. Duncan, Joke Durnez, Amr Eed, Simon B. Eickhoff, Andrew Erhart, Laura Fontanesi, G. Matthew Fricke, Shiguang Fu, Adriana Galván, Remi Gau, Sarah Genon, Tristan Glatard, Enrico Glerean, Jelle J. Goeman, Sergej A. E. Golowin, Carlos González-García, Krzysztof J. Gorgolewski, Cheryl L. Grady, Mikella A. Green, João F. Guassi Moreira, Olivia Guest, Shabnam Hakimi, J. Paul Hamilton, Roeland Hancock, Giacomo Handjaras, Bronson B. Harry, Colin Hawco, Peer Herholz, Gabrielle Herman, Stephan Heunis, Felix Hoffstaedter, Jeremy Hogeveen, Susan Holmes, Chuan-Peng Hu, Scott A. Huettel, Matthew E. Hughes, Vittorio Iacovella, Alexandru D. Iordan, Peder M. Isager, Ayse I. Isik, Andrew Jahn, Matthew R. Johnson, Tom Johnstone, Michael J. E. Joseph, Anthony

C. Juliano, Joseph W. Kable, Michalis Kassinopoulos, Cemal Koba, Xiang-Zhen Kong, Timothy R. Koscik, Nuri Erkut Kucukboyaci, Brice A. Kuhl, Sebastian Kupek, Angela R. Laird, Claus Lamm, Robert Langner, Nina Lauharatanahirun, Hongmi Lee, Sangil Lee, Alexander Leemans, Andrea Leo, Elise Lesage, Flora Li, Monica Y. C. Li, Phui Cheng Lim, Evan N. Lintz, Schuyler W. Liphardt, Annabel B. Losecaat Vermeer, Bradley C. Love, Michael L. Mack, Norberto Malpica, Theo Marins, Camille Maumet, Kelsey McDonald, Joseph T. McGuire, Helena Melero, Adriana S. Méndez Leal, Benjamin Meyer, Kristin N. Meyer, Glad Mihai, Georgios D. Mitsis, Jorge Moll, Dylan M. Nielson, Gustav Nilsonne, Michael P. Notter, Emanuele Olivetti, Adrian I. Onicas, Paolo Papale, Kaustubh R. Patil, Jonathan E. Peelle, Alexandre Pérez, Doris Pischedda, Jean-Baptiste Poline, Yanina Prystauka, Shruti Ray, Patricia A. Reuter-Lorenz, Richard C. Reynolds, Emiliano Ricciardi, Jenny R. Rieck, Anais M. Rodriguez-Thompson, Anthony Romyn, Taylor Salo, Gregory R. Samanez-Larkin, Emilio Sanz-Morales, Margaret L. Schlichting, Douglas H. Schultz, Qiang Shen, Margaret A. Sheridan, Jennifer A. Silvers, Kenny Skagerlund, Alec Smith, David V. Smith, Peter Sokol-Hessner, Simon R. Steinkamp, Sarah M. Tashjian, Bertrand Thirion, John N. Thorp, Gustav Tinghög, Loreen Tisdall, Steven H. Tompson, Claudio Toro-Serey, Juan Jesus Torre Tresols, Leonardo Tozzi, Vuong Truong, Luca Turella, Anna E. van ‘t Veer, Tom Verguts, Jean M. Vettel, Sagana Vijayarajah, Khoi Vo, Matthew B. Wall, Wouter D. Weeda, Susanne Weis, David J. White, David Wisniewski, Alba Xifra-Porxas, Emily A. Yearling, Sangsuk Yoon, Rui Yuan, Kenneth S. L. Yuen, Lei Zhang, Xu Zhang, Joshua E. Zosky, Thomas E. Nichols, Russell A. Poldrack, and Tom Schonberg. 2020. 'Variability in the analysis of a single neuroimaging dataset by many teams', *Nature*, 582: 84-88.

Bouziane, C., M. W. A. Caan, H. G. H. Tamminga, A. Schrantee, M. A. Bottelier, M. B. de Ruiter, S. J. J. Kooij, and L. Reneman. 2018. 'ADHD and maturation of brain white matter: A DTI study in medication naive children and adults', *Neuroimage Clin*, 17: 53-59.

Bouziane, Cheima, Olena G. Filatova, Anouk Schrantee, Matthan W. A. Caan, Frans M. Vos, and Liesbeth Reneman. 2019. 'White Matter by Diffusion MRI Following Methylphenidate Treatment: A Randomized Control Trial in Males with Attention-Deficit/Hyperactivity Disorder', *Radiology*, 293: 186-92.

Bressler, S. L., and V. Menon. 2010. 'Large-scale brain networks in cognition: emerging methods and principles', *Trends Cogn Sci*, 14: 277-90.

Broad, R. J., M. C. Gabel, N. G. Dowell, D. J. Schwartzman, A. K. Seth, H. Zhang, D. C. Alexander, M. Cercignani, and P. N. Leigh. 2019. 'Neurite orientation and dispersion density imaging (NODDI) detects cortical and corticospinal tract degeneration in ALS', *J Neurol Neurosurg Psychiatry*, 90: 404-11.

Bubb, Emma J, Claudia Metzler-Baddeley, and John P Aggleton. 2018. 'The cingulum bundle: anatomy, function, and dysfunction', *Neuroscience & Biobehavioral Reviews*, 92: 104-27.

Bullmore, E., and O. Sporns. 2012. 'The economy of brain network organization', *Nat Rev Neurosci*, 13: 336-49.

Bullmore, Ed, and Olaf Sporns. 2009. 'Complex brain networks: graph theoretical analysis of structural and functional systems', *Nature Reviews Neuroscience*, 10: 186-98.

Burdette, Jonathan H, David D Durden, Allen D Elster, and Yi-Fen Yen. 2001. 'High b-value diffusion-weighted MRI of normal brain', *Journal of computer assisted tomography*, 25: 515-19.

Bushell, Trevor J, Gilles Sansig, Valerie J Collett, Herman van der Putten, and Graham L Collingridge. 2002. 'Altered short-term synaptic plasticity in mice lacking the metabotropic glutamate receptor mGlu7', *TheScientificWorldJOURNAL*, 2: 730-37.

Button, Katherine S, John PA Ioannidis, Claire Mokrysz, Brian A Nosek, Jonathan Flint, Emma SJ Robinson, and Marcus R Munafò. 2013a. 'Power failure: why small sample size undermines the reliability of neuroscience', *Nature Reviews Neuroscience*, 14: 365-76.

Button, Katherine S., John P. A. Ioannidis, Claire Mokrysz, Brian A. Nosek, Jonathan Flint, Emma S. J. Robinson, and Marcus R. Munafò. 2013b. 'Power failure: why small sample size undermines the reliability of neuroscience', *Nature Reviews Neuroscience*, 14: 365-76.

Cao, Miao, Ni Shu, Qingjiu Cao, Yufeng Wang, and Yong He. 2014a. 'Imaging Functional and Structural Brain Connectomics in Attention-Deficit/Hyperactivity Disorder', *Molecular Neurobiology*, 50: 1111-23.

———. 2014b. 'Imaging functional and structural brain connectomics in attention-deficit/hyperactivity disorder', *Molecular Neurobiology*, 50: 1111-23.

Cao, Qingjiu, Ni Shu, Li An, Peng Wang, Li Sun, Ming-Rui Xia, Jin-Hui Wang, Gao-Lang Gong, Yu-Feng Zang, Yu-Feng Wang, and Yong He. 2013. 'Probabilistic Diffusion Tractography and Graph Theory Analysis Reveal Abnormal White Matter Structural Connectivity Networks in Drug-Naive Boys with Attention Deficit/Hyperactivity Disorder', *Journal of Neuroscience*, 33: 10676-87.

Cao, Qingjiu, Li Sun, Gaolang Gong, Yating Lv, Xiaohua Cao, Lan Shuai, Chaozhe Zhu, Yufeng Zang, and Yufeng Wang. 2010. 'The macrostructural and microstructural abnormalities of corpus callosum in children with attention deficit/hyperactivity disorder: a combined morphometric and diffusion tensor MRI study', *Brain Research*, 1310: 172-80.

Carmona, S, O Vilarroya, A Bielsa, V Tremols, JC Soliva, M Rovira, J Tomas, C Raheb, JD Gispert, and S Batlle. 2005. 'Global and regional gray matter reductions in ADHD: a voxel-based morphometric study', *Neuroscience Letters*, 389: 88-93.

Castellanos, F Xavier, Patti P Lee, Wendy Sharp, Neal O Jeffries, Deanna K Greenstein, Liv S Clasen, Jonathan D Blumenthal, Regina S James, Christen L Ebens, and James M Walter. 2002. 'Developmental trajectories of brain volume abnormalities in children and adolescents with attention-deficit/hyperactivity disorder', *JAMA*, 288: 1740-48.

Castellanos, F. X., P. P. Lee, W. Sharp, N. O. Jeffries, D. K. Greenstein, L. S. Clasen, J. D. Blumenthal, R. S. James, C. L. Ebens, J. M. Walter, A. Zijdenbos, A. C. Evans, J. N. Giedd, and J. L. Rapoport. 2002a. 'Developmental trajectories of brain volume abnormalities in children and adolescents with attention-deficit/hyperactivity disorder', *JAMA*, 288: 1740-8.

Castellanos, F. Xavier, Patti P. Lee, Wendy Sharp, Neal O. Jeffries, Deanna K. Greenstein, Liv S. Clasen, Jonathan D. Blumenthal, Regina S. James, Christen L. Ebens, James M. Walter, Alex Zijdenbos, Alan C. Evans, Jay N. Giedd, and Judith L. Rapoport.

2002b. 'Developmental Trajectories of Brain Volume Abnormalities in Children and Adolescents With Attention-Deficit/Hyperactivity Disorder', *JAMA*, 288: 1740-48.

Castellanos, F. Xavier, and Erika Proal. 2012. 'Large-scale brain systems in ADHD: beyond the prefrontal-striatal model', *Trends in Cognitive Sciences*, 16: 17-26.

Catani, M., F. Dell'acqua, and M. Thiebaut de Schotten. 2013. 'A revised limbic system model for memory, emotion and behaviour', *Neurosci Biobehav Rev*, 37: 1724-37.

Catani, Marco, Robert J. Howard, Sinisa Pajevic, and Derek K. Jones. 2002. 'Virtual in Vivo Interactive Dissection of White Matter Fasciculi in the Human Brain', *Neuroimage*, 17: 77-94.

Catani, Marco, and Michel Thiebaut de Schotten. 2008. 'A diffusion tensor imaging tractography atlas for virtual in vivo dissections', *Cortex*, 44: 1105-32.

Cha, J., T. Fekete, F. Siciliano, D. Biezonski, L. Greenhill, S. R. Pliszka, J. C. Blader, A. K. Roy, E. Leibenluft, and J. Posner. 2015. 'Neural Correlates of Aggression in Medication-Naive Children with ADHD: Multivariate Analysis of Morphometry and Tractography', *Neuropsychopharmacology*, 40: 1717-25.

Cha, Jiook, Jaime S Ide, F Dubois Bowman, Helen B Simpson, Jonathan Posner, and Joanna E Steinglass. 2016. 'Abnormal reward circuitry in anorexia nervosa: A longitudinal, multimodal MRI study', *Human Brain Mapping*, 37: 3835-46.

Chang, L, Derek K. Jones, and Carlo Pierpaoli. 2005. 'RESTORE: Robust estimation of tensors by outlier rejection', *Magnetic Resonance in Medicine*, 53: 1088-95.

Chang, Z., P. Lichtenstein, P. J. Asherson, and H. Larsson. 2013. 'Developmental twin study of attention problems: high heritabilities throughout development', *Jama Psychiatry*, 70: 311-8.

Chang, Zheng, Laura Ghirardi, Patrick D Quinn, Philip Asherson, Brian M D'Onofrio, and Henrik Larsson. 2019. 'Risks and benefits of attention-deficit/hyperactivity disorder medication on behavioral and neuropsychiatric outcomes: a qualitative review of pharmacoepidemiology studies using linked prescription databases', *Biological Psychiatry*, 86: 335-43.

Chen, L., X. Hu, L. Ouyang, N. He, Y. Liao, Q. Liu, M. Zhou, M. Wu, X. Huang, and Q. Gong. 2016. 'A systematic review and meta-analysis of tract-based spatial statistics studies regarding attention-deficit/hyperactivity disorder', *Neuroscience and Biobehavioral Reviews*, 68: 838-47.

Cheung, M. M., E. S. Hui, K. C. Chan, J. A. Helpern, L. Qi, and E. X. Wu. 2009. 'Does diffusion kurtosis imaging lead to better neural tissue characterization? A rodent brain maturation study', *Neuroimage*, 45: 386-92.

Chiang, H. L., Y. J. Chen, Y. C. Lo, W. Y. I. Tseng, and S. S. F. Gau. 2015. 'Altered white matter tract property related to impaired focused attention, sustained attention, cognitive impulsivity and vigilance in attention-deficit/hyperactivity disorder', *Journal of Psychiatry & Neuroscience*, 40: 325-35.

Chiang, H. L., Y. J. Chen, C. Y. Shang, W. Y. I. Tseng, and S. S. F. Gau. 2016. 'Different neural substrates for executive functions in youths with ADHD: a diffusion spectrum imaging tractography study', *Psychological Medicine*, 46: 1225-38.

Chiang, H. L., W. I. Tseng, W. L. Tseng, Y. H. Tung, Y. C. Hsu, C. L. Chen, and S. S. Gau. 2023. 'Atypical development in white matter microstructures in ADHD: A longitudinal diffusion imaging study', *Asian J Psychiatr*, 79: 103358.

Chiang, Huey-Ling, Yung-Chin Hsu, Chi-Yuan Shang, Wen-Yih Isaac Tseng, and Susan Shur-Fen Gau. 2020. 'White matter endophenotype candidates for ADHD: a diffusion imaging tractography study with sibling design', *Psychological Medicine*, 50: 1203-13.

Chiang, M. C., Katie L McMahon, Greig I de Zubicaray, Nicholas G Martin, Ian Hickie, Arthur W Toga, Margaret J Wright, and Paul M Thompson. 2011. 'Genetics of white matter development: a DTI study of 705 twins and their siblings aged 12 to 29', *Neuroimage*, 54: 2308-17.

Child, Nicholas D., and Eduardo E. Benarroch. 2013. 'Anterior nucleus of the thalamus', *Functional organization and clinical implications*, 81: 1869-76.

Christiansen, H., W. Chen, R. D. Oades, P. Asherson, E. A. Taylor, J. Lasky-Su, K. Zhou, T. Banaschewski, C. Buschgens, B. Franke, I. Gabriels, I. Manor, R. Marco, U. C. Müller, A. Mulligan, L. Psychogiou, N. N. Rommelse, H. Uebel, J. Buitelaar, R. P. Ebstein, J. Eisenberg, M. Gill, A. Miranda, F. Mulas, H. Roeyers, A. Rothenberger, J. A. Sergeant, E. J. Sonuga-Barke, H. C. Steinhausen, M. Thompson, and S. V. Faraone. 2008. 'Co-transmission of conduct problems with attention-deficit/hyperactivity disorder: familial evidence for a distinct disorder', *J Neural Transm (Vienna)*, 115: 163-75.

Coghill, D. R., S. Seth, S. Pedroso, T. Usala, J. Currie, and A. Gagliano. 2014. 'Effects of methylphenidate on cognitive functions in children and adolescents with attention-deficit/hyperactivity disorder: evidence from a systematic review and a meta-analysis', *Biol Psychiatry*, 76: 603-15.

Cole, J., H. A. Ball, N. C. Martin, J. Scourfield, and P. McGuffin. 2009. 'Genetic overlap between measures of hyperactivity/inattention and mood in children and adolescents', *J Am Acad Child Adolesc Psychiatry*, 48: 1094-101.

Colizza, Vittoria, Alessandro Flammini, M Angeles Serrano, and Alessandro Vespignani. 2006. 'Detecting rich-club ordering in complex networks', *Nature physics*, 2: 110-15.

Connaughton, Michael, Robert Whelan, Erik O'Hanlon, and Jane McGrath. 2022. 'White matter microstructure in children and adolescents with ADHD', *NeuroImage: Clinical*, 33: 102957.

Conners, C Keith. 2008. 'Conners 3-Parent Short Form', *North Tonawanda, NY: Multi-Health Systems Inc.[Google Scholar]*.

Cooper, M., A. Thapar, and D. K. Jones. 2015. 'ADHD severity is associated with white matter microstructure in the subgenual cingulum', *NeuroImage Clinical*, 7: 653-60.

Cortese, S., C. Kelly, C. Chabernaud, E. Proal, A. Di Martino, M. P. Milham, and F. X. Castellanos. 2012a. 'Toward systems neuroscience of ADHD: a meta-analysis of 55 fMRI studies', *Am J Psychiatry*, 169: 1038-55.

———. 2012b. 'Toward systems neuroscience of ADHD: A meta-analysis of 55 fMRI sudies', *American Journal of Psychiatry*, 169: 1038-55.

Costenbader, KH, and EW Karlson. 2006. 'Cigarette smoking and autoimmune disease: what can we learn from epidemiology?', *Lupus*, 15: 737-45.

Cuffe, Steven P, Charity G Moore, and Robert E McKeown. 2005. 'Prevalence and correlates of ADHD symptoms in the national health interview survey', *Journal of Attention Disorders*, 9: 392-401.

Currie, Stuart, Nigel Hoggard, Ian J Craven, Marios Hadjivassiliou, and Iain D Wilkinson. 2013. 'Understanding MRI: basic MR physics for physicians', *Postgraduate Medical Journal*, 89: 209-23.

Dark, Callum, Jihane Homman-Ludiye, and Robert J. Bryson-Richardson. 2018. 'The role of ADHD associated genes in neurodevelopment', *Developmental Biology*, 438: 69-83.

Das, S. K., J. L. Wang, L. Bing, A. Bhetuwal, and H. F. Yang. 2017. 'Regional Values of Diffusional Kurtosis Estimates in the Healthy Brain during Normal Aging', *Clinical Neuroradiology*, 27: 283-98.

Davenport, N. D., C. Karatekin, T. White, and K. O. Lim. 2010. 'Differential fractional anisotropy abnormalities in adolescents with ADHD or schizophrenia', *Psychiatry Research*, 181: 193-8.

Davidson, R. J., D. C. Jackson, and N. H. Kalin. 2000. 'Emotion, plasticity, context, and regulation: perspectives from affective neuroscience', *Psychol Bull*, 126: 890-909.

Davidson, R. J., K. M. Putnam, and C. L. Larson. 2000. 'Dysfunction in the neural circuitry of emotion regulation--a possible prelude to violence', *Science*, 289: 591-4.

De Pasquale, Francesco, S Della Penna, O Sporns, GL Romani, and Maurizio Corbetta. 2016. 'A dynamic core network and global efficiency in the resting human brain', *Cerebral Cortex*, 26: 4015-33.

De Rouvroit, Catherine Lambert, and André M Goffinet. 2001. 'Neuronal migration', *Mechanisms of development*, 105: 47-56.

de Zeeuw, P., R. C. Mandl, H. E. Hulshoff Pol, H. van Engeland, and S. Durston. 2012. 'Decreased frontostriatal microstructural organization in attention deficit/hyperactivity disorder', *Human Brain Mapping*, 33: 1941-51.

de Zeeuw, Patrick, Juliette Weusten, Sarai van Dijk, Janna van Belle, and Sarah Durston. 2012. 'Deficits in Cognitive Control, Timing and Reward Sensitivity Appear to be Dissociable in ADHD', *Plos One*, 7: e51416.

Demontis, Ditte, G. Bragi Walters, Georgios Athanasiadis, Raymond Walters, Karen Therrien, Trine Tollerup Nielsen, Leila Farajzadeh, Georgios Voloudakis, Jaroslav Bendl, Biau Zeng, Wen Zhang, Jakob Grove, Thomas D. Als, Jinjie Duan, F. Kyle Satterstrom, Jonas Bybjerg-Grauholm, Marie Bækved-Hansen, Olafur O. Gudmundsson, Sigurdur H. Magnusson, Gisli Baldursson, Katrin Davidsdottir, Gyda S. Haraldsdottir, Esben Agerbo, Gabriel E. Hoffman, Søren Dalsgaard, Joanna Martin, Marta Ribasés, Dorret I. Boomsma, Maria Soler Artigas, Nina Roth Mota, Daniel Howrigan, Sarah E. Medland, Tetyana Zayats, Veera M. Rajagopal, Alexandra Havdahl, Alysa Doyle, Andreas Reif, Anita Thapar, Bru Cormand, Calwing Liao, Christie Burton, Claiton H. D. Bau, Diego Luiz Rovaris, Edmund Sonuga-Barke, Elizabeth Corfield, Eugenio Horacio Grevet, Henrik Larsson, Ian R. Gizer, Irwin Waldman, Isabell Brikell, Jan Haavik, Jennifer Crosbie, James McGough, Jonna Kuntsi, Joseph Glessner, Kate Langley, Klaus-Peter Lesch, Luis Augusto Rohde, Mara H. Hutz, Marieke Klein, Mark Bellgrove, Martin Tesli, Michael C. O'Donovan, Ole Andreas Andreassen, Patrick W. L. Leung, Pedro M. Pan, Ridha Joober, Russel Schachar, Sandra Loo, Stephanie H. Witt, Ted Reichborn-Kjennerud, Tobias Banaschewski, Ziarih Hawi, Mark J. Daly, Ole Mors, Merete Nordentoft, Ole Mors, David M. Hougaard, Preben Bo Mortensen, Mark J. Daly, Stephen V. Faraone, Hreinn Stefansson, Panos Roussos, Barbara Franke,

Thomas Werge, Benjamin M. Neale, Kari Stefansson, Anders D. Børglum, Adhd Working Group of the Psychiatric Genomics Consortium, and Psych-Broad Consortium i. 2023. 'Genome-wide analyses of ADHD identify 27 risk loci, refine the genetic architecture and implicate several cognitive domains', *Nature Genetics*, 55: 198-208.

Demontis, Ditte, Raymond K. Walters, Joanna Martin, Manuel Mattheisen, Thomas D. Als, Esben Agerbo, Gísli Baldursson, Rich Belliveau, Jonas Bybjerg-Grauholm, Marie Bækvad-Hansen, Felecia Cerrato, Kimberly Chambert, Claire Churchhouse, Ashley Dumont, Nicholas Eriksson, Michael Gandal, Jacqueline I. Goldstein, Katrina L. Grasby, Jakob Grove, Olafur O. Gudmundsson, Christine S. Hansen, Mads Engel Hauberg, Mads V. Hollegaard, Daniel P. Howrigan, Hailiang Huang, Julian B. Maller, Alicia R. Martin, Nicholas G. Martin, Jennifer Moran, Jonatan Pallesen, Duncan S. Palmer, Carsten Bøcker Pedersen, Marianne Giørtz Pedersen, Timothy Poterba, Jesper Buchhave Poulsen, Stephan Ripke, Elise B. Robinson, F. Kyle Satterstrom, Hreinn Stefansson, Christine Stevens, Patrick Turley, G. Bragi Walters, Hyejung Won, Margaret J. Wright, Özgür Albayrak, Richard J. L. Anney, Maria Jesús Arranz, Tobias J. Banaschewski, Claiton Bau, Joseph Biederman, Jan K. Buitelaar, Miguel Casas, Alice Charach, Jennifer Crosbie, Astrid Dempfle, Alysa E. Doyle, Richard P. Ebstein, Josephine Elia, Christine Freitag, Manuel Föcker, Michael Gill, Eugenio Grevet, Ziarih Hawi, Johannes Hebebrand, Beate Herpertz-Dahlmann, Amaia Hervas, Anke Hinney, Sarah Hohmann, Peter Holmans, Mara Hutz, Abel Ickowitz, Stefan Johansson, Lindsey Kent, Sarah Kittel-Schneider, Nanda Lambregts-Rommelse, Gerd Lehmkuhl, Sandra K. Loo, James J. McGough, Jobst Meyer, Eric Mick, Frank Middletion, Ana Miranda, Nina Roth Mota, Fernando Mulas, Aisling Mulligan, Freimer Nelson, T. Trang Nguyen, Robert D. Oades, Michael C. O'Donovan, Michael J. Owen, Haukur Palmason, Josep Antoni Ramos-Quiroga, Tobias J. Renner, Marta Ribasés, Marcella Rietschel, Olga Rivero, Jasmin Romanos, Marcel Romanos, Aribert Rothenberger, Herbert Royers, Christina Sánchez-Mora, André Scherag, Benno G. Schimmelmann, Helmut Schäfer, Joseph Sergeant, Judith Sinzig, Susan L. Smalley, Hans-Christoph Steinhausen, Margaret Thompson, Alexandre Todorov, Alejandro Arias Vasquez, Susanne Walitza, Yufeng Wang, Andreas Warnke, Nigel Williams, Stephanie H. Witt, Li Yang, Tetyana Zayats, Yanli Zhang-James, George Davey Smith, Gareth E. Davies, Erik A. Ehli, David M. Evans, Iryna O. Fedko, Corina U. Greven, Maria M. Groen-Blokhuis, Monica Guxens, Anke R. Hammerschlag, Catharina A. Hartman, Joachim Heinrich, Jouke Jan Hottenga, James Hudziak, Astanand Jugessur, John P. Kemp, Eva Krapohl, Mario Murcia, Ronny Myhre, Ilja M. Nolte, Dale R. Nyholt, Johan Ormel, Klaasjan G. Ouwens, Irene Pappa, Craig E. Pennell, Robert Plomin, Susan Ring, Marie Standl, Evie Stergiakouli, Beate St Pourcain, Camilla Stoltenberg, Jordi Sunyer, Elisabeth Thiering, Henning Tiemeier, Carla M. T. Tiesler, Nicholas J. Timpson, Maciej Trzaskowski, Peter Johannes van der Most, Natalia Vilor-Tejedor, Carol A. Wang, Andrew J. O. Whitehouse, Huiying Zhao, Michelle Agee, Babak Alipanahi, Adam Auton, Robert K. Bell, Katarzyna Bryc, Sarah L. Elson, Pierre Fontanillas, Nicholas A. Furlotte, David A. Hinds, Bethann S. Hromatka, Karen E. Huber, Aaron Kleinman, Nadia K. Litterman, Matthew H. McIntyre, Joanna L. Mountain, Carrie A. M. Northover, Steven J. Pitts, J. Fah

Sathirapongsasuti, Olga V. Sazonova, Janie F. Shelton, Suyash Shringarpure, Chao Tian, Vladimir Vacic, Catherine H. Wilson, Ole A. Andreassen, Philip Asherson, Christie L. Burton, Dorret I. Boomsma, Bru Cormand, Søren Dalsgaard, Barbara Franke, Joel Gelernter, Daniel Geschwind, Hakon Hakonarson, Jan Haavik, Henry R. Kranzler, Jonna Kuntsi, Kate Langley, Klaus-Peter Lesch, Christel Middeldorp, Andreas Reif, Luis Augusto Rohde, Panos Roussos, Russell Schachar, Pamela Sklar, Edmund J. S. Sonuga-Barke, Patrick F. Sullivan, Anita Thapar, Joyce Y. Tung, Irwin D. Waldman, Sarah E. Medland, Kari Stefansson, Merete Nordentoft, David M. Hougaard, Thomas Werge, Ole Mors, Preben Bo Mortensen, Mark J. Daly, Stephen V. Faraone, Anders D. Børglum, Benjamin M. Neale, Adhd Working Group of the Psychiatric Genomics Consortium, Lifecourse Early, Consortium Genetic Epidemiology, and Team andMe Research. 2019. 'Discovery of the first genome-wide significant risk loci for attention deficit/hyperactivity disorder', *Nature Genetics*, 51: 63-75.

Dennis, Emily L, Neda Jahanshad, Arthur W Toga, Katie L McMahon, Greig I de Zubicaray, Ian Hickie, Margaret J Wright, and Paul M Thompson. 2013. "Development of the “rich club” in brain connectivity networks from 438 adolescents & adults aged 12 to 30." In *2013 IEEE 10th International Symposium on Biomedical Imaging*, 624-27. IEEE.

Dennis, Maureen, David J Francis, Paul T Cirino, Russell Schachar, Marcia A Barnes, and Jack M Fletcher. 2009. 'Why IQ is not a covariate in cognitive studies of neurodevelopmental disorders', *Journal of the International Neuropsychological Society*, 15: 331-43.

Descoteaux, Maxime. 'High Angular Resolution Diffusion Imaging (HARDI).' in, *Wiley Encyclopedia of Electrical and Electronics Engineering*.

Desikan, R. S., F. Ségonne, B. Fischl, B. T. Quinn, B. C. Dickerson, D. Blacker, R. L. Buckner, A. M. Dale, R. P. Maguire, B. T. Hyman, M. S. Albert, and R. J. Killiany. 2006a. 'An automated labeling system for subdividing the human cerebral cortex on MRI scans into gyral based regions of interest', *Neuroimage*, 31: 968-80.

Desikan, Rahul S., Florent Ségonne, Bruce Fischl, Brian T. Quinn, Bradford C. Dickerson, Deborah Blacker, Randy L. Buckner, Anders M. Dale, R. Paul Maguire, Bradley T. Hyman, Marilyn S. Albert, and Ronald J. Killiany. 2006b. 'An automated labeling system for subdividing the human cerebral cortex on MRI scans into gyral based regions of interest', *Neuroimage*, 31: 968-80.

Despotović, Ivana, Bart Goossens, and Wilfried Philips. 2015. 'MRI segmentation of the human brain: challenges, methods, and applications', *Computational and mathematical methods in medicine*, 2015.

Destrieux, Christophe, Bruce Fischl, Anders Dale, and Eric Halgren. 2010. 'Automatic parcellation of human cortical gyri and sulci using standard anatomical nomenclature', *Neuroimage*, 53: 1-15.

Dhollander, Thijs, Adam Clemente, Mervyn Singh, Frederique Boonstra, Oren Civier, Juan Dominguez Duque, Natalia Egorova, Peter Enticott, Ian Fuelscher, Sanuji Gajamange, Sila Genc, Elie Gottlieb, Christian Hyde, Phoebe Imms, Claire Kelly, Melissa Kirkovski, Scott Kolbe, Xiaoyun Liang, Atul Malhotra, Remika Mito, Govinda Poudel, Tim J. Silk, David N. Vaughan, Julien Zanin, David Raffelt, and

Karen Caeyenberghs. 2021. 'Fixel-based Analysis of Diffusion MRI: Methods, Applications, Challenges and Opportunities', *Neuroimage*, 241: 118417.

Dimond, Dennis, Christiane S. Rohr, Robert E. Smith, Thijs Dhollander, Ivy Cho, Catherine Lebel, Deborah Dewey, Alan Connelly, and Signe Bray. 2020. 'Early childhood development of white matter fiber density and morphology', *Neuroimage*, 210: 116552.

Does, M. D., E. C. Parsons, and J. C. Gore. 2003. 'Oscillating gradient measurements of water diffusion in normal and globally ischemic rat brain', *Magn Reson Med*, 49: 206-15.

Dorn, Lorah D. 2006. 'Measuring puberty', *Journal of Adolescent Health*, 39: 625-26.

Dorval, KM, KG Wigg, J Crosbie, R Tannock, JL Kennedy, A Ickowicz, T Pathare, M Malone, R Schachar, and CL Barr. 2007. 'Association of the glutamate receptor subunit gene GRIN2B with attention-deficit/hyperactivity disorder', *Genes, Brain and Behavior*, 6: 444-52.

Dosenbach, Nico UF, Jonathan M Koller, Eric A Earl, Oscar Miranda-Dominguez, Rachel L Klein, Andrew N Van, Abraham Z Snyder, Bonnie J Nagel, Joel T Nigg, and Annie L Nguyen. 2017. 'Real-time motion analytics during brain MRI improve data quality and reduce costs', *Neuroimage*, 161: 80-93.

Doyle, A. E., and S. V. Faraone. 2002. 'Familial links between attention deficit hyperactivity disorder, conduct disorder, and bipolar disorder', *Curr Psychiatry Rep*, 4: 146-52.

Drgonova, J., D. Walther, G. L. Hartstein, M. O. Bukhari, M. H. Baumann, J. Katz, F. S. Hall, E. R. Arnold, S. Flax, A. Riley, O. Rivero-Martin, K. P. Lesch, J. Troncoso, B. Ranscht, and G. R. Uhl. 2016. 'Cadherin 13: human cis-regulation and selectively-altered addiction phenotypes and cerebral cortical dopamine in knockout mice', *Mol Med*, 22: 537-47.

Dunn, G. A., J. T. Nigg, and E. L. Sullivan. 2019. 'Neuroinflammation as a risk factor for attention deficit hyperactivity disorder', *Pharmacol Biochem Behav*, 182: 22-34.

El-Sayed, E., J. O. Larsson, H. E. Persson, P. J. Santosh, and P. A. Rydelius. 2003. '"Maturational lag" hypothesis of attention deficit hyperactivity disorder: an update', *Acta Paediatr*, 92: 776-84.

Elhakeem, Ahmed, Rachael A. Hughes, Kate Tilling, Diana L. Cousminer, Stefan A. Jackowski, Tim J. Cole, Alex S. F. Kwong, Zheyuan Li, Struan F. A. Grant, Adam D. G. Baxter-Jones, Babette S. Zemel, and Deborah A. Lawlor. 2022. 'Using linear and natural cubic splines, SITAR, and latent trajectory models to characterise nonlinear longitudinal growth trajectories in cohort studies', *BMC Medical Research Methodology*, 22: 68.

Elia, J., X. Gai, H. M. Xie, J. C. Perin, E. Geiger, J. T. Glessner, M. D'Arcy, R. deBerardinis, E. Frackelton, C. Kim, F. Lantieri, B. M. Muganga, L. Wang, T. Takeda, E. F. Rappaport, S. F. A. Grant, W. Berrettini, M. Devoto, T. H. Shaikh, H. Hakonarson, and P. S. White. 2010. 'Rare structural variants found in attention-deficit hyperactivity disorder are preferentially associated with neurodevelopmental genes', *Molecular Psychiatry*, 15: 637-46.

Ellison-Wright, I., Z. Ellison-Wright, and E. Bullmore. 2008. 'Structural brain change in Attention Deficit Hyperactivity Disorder identified by meta-analysis', *Bmc Psychiatry*, 8: 51.

Ercan, Eyup Sabri, Serkan Suren, Ali Bacanlı, Kemal Utku Yazıcı, Cem Callı, Ulku Akyol Ardic, Duygu Aygunes, Buket Kosova, Onur Ozyurt, and Cahide Aydın. 2016. 'Altered structural connectivity is related to attention deficit/hyperactivity subtypes: A DTI study', *Psychiatry Research: Neuroimaging*, 256: 57-64.

Ercan, Eyup Sabri, Serkan Suren, Ali Bacanli, Kemal Utku Yazici, Cem Calli, Ulku Akyol Ardic, Duygu Aygunes, Buket Kosova, Onur Ozyurt, Cahide Aydin, and Luis Augusto Rohde. 2016. 'Altered structural connectivity is related to attention deficit/hyperactivity subtypes: A DTI study', *Psychiatry Research-Neuroimaging*, 256: 57-64.

Erskine, Holly E, Alize J Ferrari, Paul Nelson, Guilherme V Polanczyk, Abraham D Flaxman, Theo Vos, Harvey A Whiteford, and James G Scott. 2013. 'Research Review: Epidemiological modelling of attention-deficit/hyperactivity disorder and conduct disorder for the Global Burden of Disease Study 2010', *Journal of Child Psychology and Psychiatry*, 54: 1263-74.

Fair, Damien A., Deepti Bathula, Molly A. Nikolas, and Joel T. Nigg. 2012. 'Distinct neuropsychological subgroups in typically developing youth inform heterogeneity in children with ADHD', *Proceedings of the National Academy of Sciences*, 109: 6769-74.

Falangola, Maria F., David N. Guilfoyle, Ali Tabesh, Edward S. Hui, Xingju Nie, Jens H. Jensen, Scott V. Gerum, Caixia Hu, John LaFrancois, Heather R. Collins, and Joseph A. Helpern. 2014. 'Histological correlation of diffusional kurtosis and white matter modeling metrics in cuprizone-induced corpus callosum demyelination', *NMR in Biomedicine*, 27: 948-57.

Fall, S., L. Querne, A. G. Le Moing, and P. Berquin. 2015. 'Individual differences in subcortical microstructure organization reflect reaction time performances during a flanker task: a diffusion tensor imaging study in children with and without ADHD', *Psychiatry Research*, 233: 50-6.

Fallin, M Daniele, Virginia K Lasseter, Dimitrios Avramopoulos, Kristin K Nicodemus, Paula S Wolyniec, John A McGrath, Gary Steel, Gerald Nestadt, Kung-Yee Liang, and Richard L Huganir. 2005. 'Bipolar I disorder and schizophrenia: a 440–single-nucleotide polymorphism screen of 64 candidate genes among Ashkenazi Jewish case-parent trios', *The American Journal of Human Genetics*, 77: 918-36.

Farahani, Farzad V, Waldemar Karwowski, and Nichole R Lighthall. 2019. 'Application of graph theory for identifying connectivity patterns in human brain networks: a systematic review', *Frontiers in Neuroscience*, 13: 585.

Faraone, S. V., P. Asherson, T. Banaschewski, J. Biederman, J. K. Buitelaar, J. A. Ramos-Quiroga, L. A. Rohde, E. J. Sonuga-Barke, R. Tannock, and B. Franke. 2015. 'Attention-deficit/hyperactivity disorder', *Nat Rev Dis Primers*, 1: 15020.

Faraone, S. V., J. Biederman, and E. Mick. 2006. 'The age-dependent decline of attention deficit hyperactivity disorder: a meta-analysis of follow-up studies', *Psychol Med*, 36: 159-65.

Faraone, S. V., and H. Larsson. 2019. 'Genetics of attention deficit hyperactivity disorder', *Mol Psychiatry*, 24: 562-75.

Fassbender, Catherine, and Julie B. Schweitzer. 2006. 'Is there evidence for neural compensation in attention deficit hyperactivity disorder? A review of the functional neuroimaging literature', *Clinical Psychology Review*, 26: 445-65.

Fields, R. D. 2010. 'Neuroscience. Change in the brain's white matter', *Science*, 330: 768-9.

Fischl, B., D. H. Salat, E. Busa, M. Albert, M. Dieterich, C. Haselgrove, A. van der Kouwe, R. Killiany, D. Kennedy, S. Klaveness, A. Montillo, N. Makris, B. Rosen, and A. M. Dale. 2002. 'Whole brain segmentation: automated labeling of neuroanatomical structures in the human brain', *Neuron*, 33: 341-55.

Fischl, B., A. van der Kouwe, C. Destrieux, E. Halgren, F. Ségonne, D. H. Salat, E. Busa, L. J. Seidman, J. Goldstein, D. Kennedy, V. Caviness, N. Makris, B. Rosen, and A. M. Dale. 2004. 'Automatically parcellating the human cerebral cortex', *Cereb Cortex*, 14: 11-22.

Fitzmaurice, Garrett M, Nan M Laird, and James H Ware. 2012. *Applied longitudinal analysis* (John Wiley & Sons).

Francis, D. J., J. M. Fletcher, K. K. Stuebing, K. C. Davidson, and N. M. Thompson. 1991. 'Analysis of change: modeling individual growth', *J Consult Clin Psychol*, 59: 27-37.

Friedman, L. A., and J. L. Rapoport. 2015. 'Brain development in ADHD', *Current Opinion in Neurobiology*, 30: 106-11.

Frodl, T., and N. Skokauskas. 2012. 'Meta-analysis of structural MRI studies in children and adults with attention deficit hyperactivity disorder indicates treatment effects', *Acta Psychiatrica Scandinavica*, 125: 114-26.

Fuelscher, I., C. Hyde, V. Anderson, and T. Silk. 2021. 'White matter tract signatures of fiber density and morphology in ADHD', *Cortex*, 138: 329-40.

Fuelscher, I., C. Hyde, P. Thomson, N. Vijayakumar, E. Sciberras, D. Efron, V. Anderson, P. Hazell, and T. J. Silk. 2023. 'Longitudinal Trajectories of White Matter Development in Attention-Deficit/Hyperactivity Disorder', *Biol Psychiatry Cogn Neurosci Neuroimaging*.

Furukawa, Emi, Raquel Quimas Molina da Costa, Patricia Bado, Sebastian Hoefle, Paula Vigne, Myriam Monteiro, Jeff R Wickens, Jorge Moll, Gail Tripp, and Paulo Mattos. 2020. 'Methylphenidate modifies reward cue responses in adults with ADHD: an fMRI study', *Neuropharmacology*, 162: 107833.

Gallo, E. F., and J. Posner. 2016. 'Moving towards causality in attention-deficit hyperactivity disorder: Overview of neural and genetic mechanisms', *The Lancet Psychiatry*, 3: 555-67.

Gao, Y., D. Shuai, X. Bu, X. Hu, S. Tang, L. Zhang, H. Li, X. Hu, L. Lu, Q. Gong, and X. Huang. 2019. 'Impairments of large-scale functional networks in attention-deficit/hyperactivity disorder: a meta-analysis of resting-state functional connectivity', *Psychol Med*, 49: 2475-85.

Gareth Ball, Ph.D. ,, Charles B. Malpas, Ph.D. ,, Sila Genc, M.Sc. ,, Daryl Efron, M.D. , F.R.A.C.P. ,, Emma Sciberras, D.Psych. ,, Vicki Anderson, Ph.D. ,, Jan M. Nicholson, Ph.D. ,, and Timothy J. Silk, Ph.D. 2019. 'Multimodal Structural Neuroimaging Markers of Brain Development and ADHD Symptoms', *American Journal of Psychiatry*, 176: 57-66.

Gau, S. S., W. L. Tseng, W. YI. Tseng, Y. H. Wu, and Y. C. Lo. 2015. 'Association between microstructural integrity of frontostriatal tracts and school functioning: ADHD symptoms and executive function as mediators', *Psychological Medicine*, 45: 529-43.

Genc, Sila, Chantal M. W. Tax, Erika P. Raven, Maxime Chamberland, Greg D. Parker, and Derek K. Jones. 2020. 'Impact of b-value on estimates of apparent fibre density', *Human Brain Mapping*, 41: 2583-95.

Giedd, J. N. 2019. 'The enigma of neuroimaging in ADHD', *American Journal of Psychiatry*, 176: 503-04.

Glenn, G Russell, Joseph A Helpern, Ali Tabesh, and Jens H Jensen. 2015. 'Quantitative assessment of diffusional kurtosis anisotropy', *NMR in Biomedicine*, 28: 448-59.

Goddings, Anne-Lise, David Roalf, Catherine Lebel, and Christian K. Tamnes. 2021. 'Development of white matter microstructure and executive functions during childhood and adolescence: a review of diffusion MRI studies', *Developmental Cognitive Neuroscience*, 51: 101008.

Goddyn, Hannelore, Zsuzsanna Callaerts-Vegh, Stijn Stroobants, Trinette Dirikx, Debora Vansteenwegen, Dirk Hermans, Herman van der Putten, and Rudi D'Hooge. 2008. 'Deficits in acquisition and extinction of conditioned responses in mGluR7 knockout mice', *Neurobiology of learning and memory*, 90: 103-11.

Gold, A. L., R. A. Morey, and G. McCarthy. 2015. 'Amygdala-prefrontal cortex functional connectivity during threat-induced anxiety and goal distraction', *Biol Psychiatry*, 77: 394-403.

Goñi, Joaquín, Andrea Avena-Koenigsberger, Nieves Velez de Mendizabal, Martijn P. van den Heuvel, Richard F. Betzel, and Olaf Sporns. 2013. 'Exploring the Morphospace of Communication Efficiency in Complex Networks', *Plos One*, 8: e58070.

Goryawala, M. Z., D. O. Heros, R. J. Komotar, S. Sheriff, E. Saraf-Lavi, and A. A. Maudsley. 2018. 'Value of diffusion kurtosis imaging in assessing low-grade gliomas', *J Magn Reson Imaging*, 48: 1551-58.

Gratton, Caterina, Steven M Nelson, and Evan M Gordon. 2022. 'Brain-behavior correlations: Two paths toward reliability', *Neuron*, 110: 1446-49.

Groves, A. R., C. F. Beckmann, S. M. Smith, and M. W. Woolrich. 2011. 'Linked independent component analysis for multimodal data fusion', *Neuroimage*, 54: 2198-217.

Gu, Z., W. Liu, J. Wei, and Z. Yan. 2012. 'Regulation of N-methyl-D-aspartic acid (NMDA) receptors by metabotropic glutamate receptor 7', *J Biol Chem*, 287: 10265-75.

Guldberg-Kjär, Taina, and Boo Johansson. 2009. 'Old people reporting childhood AD/HD symptoms: Retrospectively self-rated AD/HD symptoms in a population-based Swedish sample aged 65–80', *Nordic Journal of Psychiatry*, 63: 375-82.

Haber, Suzanne N. 2011. '11 neuroanatomy of reward: A view from the ventral striatum', *Neurobiology of sensation and reward*: 235.

Hagmann, Patric, Leila Cammoun, Xavier Gigandet, Reto Meuli, Christopher J. Honey, Van J. Wedeen, and Olaf Sporns. 2008. 'Mapping the Structural Core of Human Cerebral Cortex', *PLOS Biology*, 6: e159.

Haines, D.E. 2008. *Neuroanatomy: An Atlas of Structures, Sections, and Systems* (Wolters Kluwer Health/Lippincott Williams & Wilkins).

Halperin, J. M., and K. P. Schulz. 2006. 'Revisiting the role of the prefrontal cortex in the pathophysiology of attention-deficit/hyperactivity disorder', *Psychol Bull*, 132: 560-81.

Hamilton, Liberty S., Jennifer G. Levitt, Joseph O'Neill, Jeffry R. Alger, Eileen Luders, Owen R. Phillips, Rochelle Caplan, Arthur W. Toga, James McCracken, and Katherine L.

Narr. 2008. 'Reduced white matter integrity in attention-deficit hyperactivity disorder', *Neuroreport*, 19: 1705-08.
Hansen, B. 2019. 'An introduction to kurtosis fractional anisotropy', *Ajnr: American Journal of Neuroradiology*, 40: 1638.
Hansen, Brian, and Sune Nørhøj Jespersen. 2016. 'Kurtosis fractional anisotropy, its contrast and estimation by proxy', *Scientific Reports*, 6: 23999.
Harrison, X. A., L. Donaldson, M. E. Correa-Cano, J. Evans, D. N. Fisher, C. E. D. Goodwin, B. S. Robinson, D. J. Hodgson, and R. Inger. 2018. 'A brief introduction to mixed effects modelling and multi-model inference in ecology', *PeerJ*, 6: e4794.
Hart, Elizabeth L, Benjamin B Lahey, Rolf Loeber, Brooks Applegate, and Paul J Frick. 1995. 'Developmental change in attention-deficit hyperactivity disorder in boys: a four-year longitudinal study', *Journal of abnormal child psychology*, 23: 729-49.
Hart, Heledd, Joaquim Radua, Tomohiro Nakao, David Mataix-Cols, and Katya Rubia. 2013. 'Meta-analysis of functional magnetic resonance imaging studies of inhibition and attention in attention-deficit/hyperactivity disorder: exploring task-specific, stimulant medication, and age effects', *Jama Psychiatry*, 70: 185-98.
Hassan, Waseem, Hamsa Noreen, Vitor Castro-Gomes, Imdadullah Mohammadzai, Joao Batista Teixeira da Rocha, and J Landeira-Fernandez. 2016. 'Association of oxidative stress with psychiatric disorders', *Current pharmaceutical design*, 22: 2960-74.
Henriques, R. N., S. N. Jespersen, D. K. Jones, and J. Veraart. 2021. 'Toward more robust and reproducible diffusion kurtosis imaging', *Magn Reson Med*, 86: 1600-13.
Henriques, Rafael Neto. 2012. 'Diffusion kurtosis imaging of the healthy human brain'.
Hernando, Kathleen A., Jerzy P. Szaflarski, Lawrence W. Ver Hoef, Seongtaek Lee, and Jane B. Allendorfer. 2015. 'Uncinate fasciculus connectivity in patients with psychogenic nonepileptic seizures: A preliminary diffusion tensor tractography study', *Epilepsy & Behavior*, 45: 68-73.
Herting, Megan M., Cory Johnson, Kathryn L. Mills, Nandita Vijayakumar, Meg Dennison, Chang Liu, Anne-Lise Goddings, Ronald E. Dahl, Elizabeth R. Sowell, Sarah Whittle, Nicholas B. Allen, and Christian K. Tamnes. 2018. 'Development of subcortical volumes across adolescence in males and females: A multisample study of longitudinal changes', *Neuroimage*, 172: 194-205.
Hillman, H. 2000. 'Limitations of clinical and biological histology', *Med Hypotheses*, 54: 553-64.
Hinshaw, Stephen P, Elizabeth B Owens, Christine Zalecki, Suzanne Perrigue Huggins, Adriana J Montenegro-Nevado, Emily Schrodek, and Erika N Swanson. 2012. 'Prospective follow-up of girls with attention-deficit/hyperactivity disorder into early adulthood: continuing impairment includes elevated risk for suicide attempts and self-injury', *Journal of consulting and clinical psychology*, 80: 1041.
Hoffman, L. J., C. T. Ngo, K. L. Canada, O. Pasternak, F. Zhang, T. Riggins, and I. R. Olson. 2022. 'The fornix supports episodic memory during childhood', *Cereb Cortex*, 32: 5388-403.
Hoffman, Lesa. 2015. *Longitudinal analysis: Modeling within-person fluctuation and change* (Routledge).
Hong, S. B., Andrew Zalesky, Alex Fornito, Subin Park, Young-Hui Yang, Min-Hyeon Park, In-Chan Song, Chul-Ho Sohn, Min-Sup Shin, Bung-Nyun Kim, Soo-Churl Cho, Doug

Hyun Han, Jae Hoon Cheong, and Jae-Won Kim. 2014. 'Connectomic Disturbances in Attention-Deficit/Hyperactivity Disorder: A Whole-Brain Tractography Analysis', *Biological Psychiatry*, 76: 656-63.

Hoogman, M., J. Bralten, D. P. Hibar, M. Mennes, M. P. Zwiers, L. S. J. Schweren, K. J. E. van Hulzen, S. E. Medland, E. Shumskaya, N. Jahanshad, P. D. Zeeuw, E. Szekely, G. Sudre, T. Wolfers, A. M. H. Onnink, J. T. Dammers, J. C. Mostert, Y. Vives-Gilabert, G. Kohls, E. Oberwelland, J. Seitz, M. Schulte-Rüther, S. Ambrosino, A. E. Doyle, M. F. Høvik, M. Dramsdahl, L. Tamm, T. G. M. van Erp, A. Dale, A. Schork, A. Conzelmann, K. Zierhut, R. Baur, H. McCarthy, Y. N. Yoncheva, A. Cubillo, K. Chantiluke, M. A. Mehta, Y. Paloyelis, S. Hohmann, S. Baumeister, I. Bramati, P. Mattos, F. Tovar-Moll, P. Douglas, T. Banaschewski, D. Brandeis, J. Kuntsi, P. Asherson, K. Rubia, C. Kelly, A. D. Martino, M. P. Milham, F. X. Castellanos, T. Frodl, M. Zentis, K. P. Lesch, A. Reif, P. Pauli, T. L. Jernigan, J. Haavik, K. J. Plessen, A. J. Lundervold, K. Hugdahl, L. J. Seidman, J. Biederman, N. Rommelse, D. J. Heslenfeld, C. A. Hartman, P. J. Hoekstra, J. Oosterlaan, G. V. Polier, K. Konrad, O. Vilarroya, J. A. Ramos-Quiroga, J. C. Soliva, S. Durston, J. K. Buitelaar, S. V. Faraone, P. Shaw, P. M. Thompson, and B. Franke. 2017a. 'Subcortical brain volume differences in participants with attention deficit hyperactivity disorder in children and adults: a cross-sectional mega-analysis', *The Lancet Psychiatry*, 4: 310-19.

Hoogman, M., J. Bralten, D. P. Hibar, M. Mennes, M. P. Zwiers, L. S. J. Schweren, K. J. E. van Hulzen, S. E. Medland, E. Shumskaya, N. Jahanshad, P. Zeeuw, E. Szekely, G. Sudre, T. Wolfers, A. M. H. Onnink, J. T. Dammers, J. C. Mostert, Y. Vives-Gilabert, G. Kohls, E. Oberwelland, J. Seitz, M. Schulte-Rüther, S. Ambrosino, A. E. Doyle, M. F. Høvik, M. Dramsdahl, L. Tamm, T. G. M. van Erp, A. Dale, A. Schork, A. Conzelmann, K. Zierhut, R. Baur, H. McCarthy, Y. N. Yoncheva, A. Cubillo, K. Chantiluke, M. A. Mehta, Y. Paloyelis, S. Hohmann, S. Baumeister, I. Bramati, P. Mattos, F. Tovar-Moll, P. Douglas, T. Banaschewski, D. Brandeis, J. Kuntsi, P. Asherson, K. Rubia, C. Kelly, A. D. Martino, M. P. Milham, F. X. Castellanos, T. Frodl, M. Zentis, K. P. Lesch, A. Reif, P. Pauli, T. L. Jernigan, J. Haavik, K. J. Plessen, A. J. Lundervold, K. Hugdahl, L. J. Seidman, J. Biederman, N. Rommelse, D. J. Heslenfeld, C. A. Hartman, P. J. Hoekstra, J. Oosterlaan, G. V. Polier, K. Konrad, O. Vilarroya, J. A. Ramos-Quiroga, J. C. Soliva, S. Durston, J. K. Buitelaar, S. V. Faraone, P. Shaw, P. M. Thompson, and B. Franke. 2017b. 'Subcortical brain volume differences in participants with attention deficit hyperactivity disorder in children and adults: a cross-sectional mega-analysis', *Lancet Psychiatry*, 4: 310-19.

Hoogman, M., R. Muetzel, J. P. Guimaraes, E. Shumskaya, M. Mennes, M. P. Zwiers, N. Jahanshad, G. Sudre, T. Wolfers, E. A. Earl, J. C. Soliva Vila, Y. Vives-Gilabert, S. Khadka, S. E. Novotny, C. A. Hartman, D. J. Heslenfeld, L. J. S. Schweren, S. Ambrosino, B. Oranje, P. de Zeeuw, T. M. Chaim-Avancini, P. G. P. Rosa, M. V. Zanetti, C. B. Malpas, G. Kohls, G. G. von Polier, J. Seitz, J. Biederman, A. E. Doyle, A. M. Dale, T. G. M. van Erp, J. N. Epstein, T. L. Jernigan, R. Baur-Streubel, G. C. Ziegler, K. C. Zierhut, A. Schrantee, M. F. Høvik, A. J. Lundervold, C. Kelly, H. McCarthy, N. Skokauskas, R. L. O'Gorman Tuura, A. Calvo, S. Lera-Miguel, R. Nicolau, K. C. Chantiluke, A. Christakou, A. Vance, M. Cercignani, M. C. Gabel, P.

Asherson, S. Baumeister, D. Brandeis, S. Hohmann, I. E. Bramati, F. Tovar-Moll, A. J. Fallgatter, B. Kardatzki, L. Schwarz, A. Anikin, A. Baranov, T. Gogberashvili, D. Kapilushniy, A. Solovieva, H. El Marroun, T. White, G. Karkashadze, L. Namazova-Baranova, T. Ethofer, P. Mattos, T. Banaschewski, D. Coghill, K. J. Plessen, J. Kuntsi, M. A. Mehta, Y. Paloyelis, N. A. Harrison, M. A. Bellgrove, T. J. Silk, A. I. Cubillo, K. Rubia, L. Lazaro, S. Brem, S. Walitza, T. Frodl, M. Zentis, F. X. Castellanos, Y. N. Yoncheva, J. Haavik, L. Reneman, A. Conzelmann, K. P. Lesch, P. Pauli, A. Reif, L. Tamm, K. Konrad, E. Oberwelland Weiss, G. F. Busatto, M. R. Louza, S. Durston, P. J. Hoekstra, J. Oosterlaan, M. C. Stevens, J. A. Ramos-Quiroga, O. Vilarroya, D. A. Fair, J. T. Nigg, P. M. Thompson, J. K. Buitelaar, S. V. Faraone, P. Shaw, H. Tiemeier, J. Bralten, and B. Franke. 2019. 'Brain Imaging of the Cortex in ADHD: A Coordinated Analysis of Large-Scale Clinical and Population-Based Samples', *Am J Psychiatry*, 176: 531-42.

Hosenbocus, Sheik, and Raj Chahal. 2012. 'A review of executive function deficits and pharmacological management in children and adolescents', *Journal of the Canadian Academy of Child and Adolescent Psychiatry*, 21: 223.

Howells, Fleur Margaret, and Vivienne Ann Russell. 2008. 'Glutamate-stimulated release of norepinephrine in hippocampal slices of animal models of attention-deficit/hyperactivity disorder (spontaneously hypertensive rat) and depression/anxiety-like behaviours (Wistar–Kyoto rat)', *Brain Research*, 1200: 107-15.

Hutchinson, A. D., J. L. Mathias, and M. T. Banich. 2008. 'Corpus callosum morphology in children and adolescents with attention deficit hyperactivity disorder: a meta-analytic review', *Neuropsychology*, 22: 341-9.

Hyde, C., E. Sciberras, D. Efron, I. Fuelscher, and T. Silk. 2021. 'Reduced fine motor competence in children with ADHD is associated with atypical microstructural organization within the superior longitudinal fasciculus', *Brain Imaging and Behavior*, 15: 727-37.

Ickowicz, A. 2002. *Hyperactivity and Attention Disorders of Childhood. Second Edition* (Can Child Adolesc Psychiatr Rev. 2004 Nov;13(4):121.).

Iglesias, J. E., J. C. Augustinack, K. Nguyen, C. M. Player, A. Player, M. Wright, N. Roy, M. P. Frosch, A. C. McKee, L. L. Wald, B. Fischl, and K. Van Leemput. 2015. 'A computational atlas of the hippocampal formation using ex vivo, ultra-high resolution MRI: Application to adaptive segmentation of in vivo MRI', *Neuroimage*, 115: 117-37.

Iglesias, Juan Eugenio, Ricardo Insausti, Garikoitz Lerma-Usabiaga, Martina Bocchetta, Koen Van Leemput, Douglas N Greve, Andre Van der Kouwe, Bruce Fischl, César Caballero-Gaudes, and Pedro M Paz-Alonso. 2018. 'A probabilistic atlas of the human thalamic nuclei combining ex vivo MRI and histology', *Neuroimage*, 183: 314-26.

Iglewicz, Boris, and David C Hoaglin. 1993. *Volume 16: how to detect and handle outliers* (Quality Press).

Ioannidis, J. P., M. R. Munafò, P. Fusar-Poli, B. A. Nosek, and S. P. David. 2014. 'Publication and other reporting biases in cognitive sciences: detection, prevalence, and prevention', *Trends Cogn Sci*, 18: 235-41.

Irfanoglu, M. O., L. Walker, J. Sarlls, S. Marenco, and C. Pierpaoli. 2012. 'Effects of image distortions originating from susceptibility variations and concomitant fields on diffusion MRI tractography results', *Neuroimage*, 61: 275-88.

Jacobson, Lisa A, Daniel J Peterson, Keri S Rosch, Deana Crocetti, Susumu Mori, and Stewart H Mostofsky. 2015. 'Sex-based dissociation of white matter microstructure in children with attention-deficit/hyperactivity disorder', *Journal of the American Academy of Child & Adolescent Psychiatry*, 54: 938-46.

Jakob, C. 1906. 'Nueva contribución á la fisio-patología de los lóbulos frontales', *La Semana Médica*, 13: 1325-29.

Janak, Patricia H, and Kay M Tye. 2015. 'From circuits to behaviour in the amygdala', *Nature*, 517: 284-92.

Jensen, Jens H., Joseph A. Helpern, Anita Ramani, Hanzhang Lu, and Kyle Kaczynski. 2005. 'Diffusional kurtosis imaging: The quantification of non-gaussian water diffusion by means of magnetic resonance imaging', *Magnetic Resonance in Medicine*, 53: 1432-40.

Jeurissen, B., A. Leemans, and J. Sijbers. 2014. 'Automated correction of improperly rotated diffusion gradient orientations in diffusion weighted MRI', *Med Image Anal*, 18: 953-62.

Jeurissen, B., J. D. Tournier, T. Dhollander, A. Connelly, and J. Sijbers. 2014. 'Multi-tissue constrained spherical deconvolution for improved analysis of multi-shell diffusion MRI data', *Neuroimage*, 103: 411-26.

Jeurissen, Ben, Alexander Leemans, Derek K Jones, Jacques-Donald Tournier, and Jan Sijbers. 2011. 'Probabilistic fiber tracking using the residual bootstrap with constrained spherical deconvolution', *Human Brain Mapping*, 32: 461-79.

Jones, D. K., K. F. Christiansen, R. J. Chapman, and J. P. Aggleton. 2013. 'Distinct subdivisions of the cingulum bundle revealed by diffusion MRI fibre tracking: implications for neuropsychological investigations', *Neuropsychologia*, 51: 67-78.

Jones, D. K., T. R. Knösche, and R. Turner. 2013. 'White matter integrity, fiber count, and other fallacies: the do's and don'ts of diffusion MRI', *Neuroimage*, 73: 239-54.

Jones, D. K., and A. Leemans. 2011. 'Diffusion tensor imaging', *Methods Mol Biol*, 711: 127-44.

Joseph Biederman, M.D. ,, Eric Mick, Sc.D. ,, Stephen V. Faraone, Ph.D. ,, Ellen Braaten, Ph.D. ,, Alysa Doyle, Ph.D. ,, Thomas Spencer, M.D. ,, Timothy E. Wilens, M.D. ,, Elizabeth Frazier, B.A. , and, and Mary Ann Johnson, R.N., M.S., C.S. 2002. 'Influence of Gender on Attention Deficit Hyperactivity Disorder in Children Referred to a Psychiatric Clinic', *American Journal of Psychiatry*, 159: 36-42.

Juraska, J. M., and J. Willing. 2017. 'Pubertal onset as a critical transition for neural development and cognition', *Brain Res*, 1654: 87-94.

Kamali, Arash, Caroline C. Zhang, Roy F. Riascos, Nitin Tandon, Eliana E. Bonafante-Mejia, Rajan Patel, John A. Lincoln, Pejman Rabiei, Laura Ocasio, Kyan Younes, and Khader M. Hasan. 2018. 'Diffusion tensor tractography of the mammillothalamic tract in the human brain using a high spatial resolution DTI technique', *Scientific Reports*, 8: 5229.

Kernbach, J. M., B. T. T. Yeo, J. Smallwood, D. S. Margulies, M. Thiebaut de Schotten, H. Walter, M. R. Sabuncu, A. J. Holmes, A. Gramfort, G. Varoquaux, B. Thirion, and

D. Bzdok. 2018. 'Subspecialization within default mode nodes characterized in 10,000 UK Biobank participants', *Proc Natl Acad Sci U S A*, 115: 12295-300.

Kesner, R. P., and E. T. Rolls. 2015. 'A computational theory of hippocampal function, and tests of the theory: new developments', *Neurosci Biobehav Rev*, 48: 92-147.

Kier, E. Leon, Lawrence H. Staib, Lawrence M. Davis, and Richard A. Bronen. 2004. 'MR Imaging of the Temporal Stem: Anatomic Dissection Tractography of the Uncinate Fasciculus, Inferior Occipitofrontal Fasciculus, and Meyer's Loop of the Optic Radiation', *American Journal of Neuroradiology*, 25: 677-91.

Kim, M Justin, and Paul J Whalen. 2009. 'The structural integrity of an amygdala–prefrontal pathway predicts trait anxiety', *Journal of Neuroscience*, 29: 11614-18.

Kim, S-Y, H Sun Chung, W Sun, and H Kim. 2007. 'Spatiotemporal expression pattern of non-clustered protocadherin family members in the developing rat brain', *Neuroscience*, 147: 996-1021.

King, Jace B., Deborah Yurgelun-Todd, Amanda Stoeckel, Jennifer M. DiMuzio, and Melissa P. Lopez-Larson. 2015. 'Sex differences in white matter integrity in youths with attention-deficit/hyperactivity disorder: a pilot study', *Frontiers in Neuroscience*, 9.

Kingsley, P. B., and W. G. Monahan. 2004. 'Selection of the optimum b factor for diffusion-weighted magnetic resonance imaging assessment of ischemic stroke', *Magn Reson Med*, 51: 996-1001.

Knutson, Brian, Scott Rick, G Elliott Wimmer, Drazen Prelec, and George Loewenstein. 2007. 'Neural predictors of purchases', *Neuron*, 53: 147-56.

Kobel, Maja, Nina Bechtel, Karsten Specht, Markus Klarhoefer, Peter Weber, Klaus Scheffler, Klaus Opwis, and Iris-Katharina Penner. 2010. 'Structural and functional imaging approaches in attention deficit/hyperactivity disorder: Does the temporal lobe play a key role?', *Psychiatry Research-Neuroimaging*, 183: 230-36.

Kong, Xiang-zhen, Zonglei Zhen, Xueting Li, Huan-hua Lu, Ruosi Wang, Ling Liu, Yong He, Yufeng Zang, and Jia Liu. 2014. 'Individual Differences in Impulsivity Predict Head Motion during Magnetic Resonance Imaging', *Plos One*, 9.

Konrad, Kerstin, and Simon B. Eickhoff. 2010. 'Is the ADHD Brain Wired Differently? A Review on Structural and Functional Connectivity in Attention Deficit Hyperactivity Disorder', *Human Brain Mapping*, 31: 904-16.

Kronfol, Ziad, and Daniel G Remick. 2000. 'Cytokines and the brain: implications for clinical psychiatry', *American Journal of Psychiatry*, 157: 683-94.

Kuder, Tristan A, Bram Stieltjes, Peter Bachert, Wolfhard Semmler, and Frederik B Laun. 2012. 'Advanced fit of the diffusion kurtosis tensor by directional weighting and regularization', *Magnetic Resonance in Medicine*, 67: 1401-11.

Kuntsi, J., R. Pinto, T. S. Price, J. J. van der Meere, A. C. Frazier-Wood, and P. Asherson. 2014. 'The separation of ADHD inattention and hyperactivity-impulsivity symptoms: pathways from genetic effects to cognitive impairments and symptoms', *J Abnorm Child Psychol*, 42: 127-36.

Lahey, Benjamin B, William E Pelham, Jan Loney, Steve S Lee, and Erik Willcutt. 2005. 'Instability of the DSM-IV subtypes of ADHD from preschool through elementary school', *Archives of General Psychiatry*, 62: 896-902.

Langberg, Joshua M, Jeffery N Epstein, Mekibib Altaye, Brooke SG Molina, L Eugene Arnold, and Benedetto Vitiello. 2008. 'The transition to middle school is

associated with changes in the developmental trajectory of ADHD symptomatology in young adolescents with ADHD', *Journal of Clinical Child & Adolescent Psychology*, 37: 651-63.

Larsson, H., P. Asherson, Z. Chang, T. Ljung, B. Friedrichs, J. O. Larsson, and P. Lichtenstein. 2013. 'Genetic and environmental influences on adult attention deficit hyperactivity disorder symptoms: a large Swedish population-based study of twins', *Psychol Med*, 43: 197-207.

Lasky-Su, Jessica, Benjamin M. Neale, Barbara Franke, Richard J.L. Anney, Kaixin Zhou, Julian B. Maller, Alejandro Arias Vasquez, Wai Chen, Philip Asherson, Jan Buitelaar, Tobias Banaschewski, Richard Ebstein, Michael Gill, Ana Miranda, Fernando Mulas, Robert D. Oades, Herbert Roeyers, Aribert Rothenberger, Joseph Sergeant, Edmund Sonuga-Barke, Hans Christoph Steinhausen, Eric Taylor, Mark Daly, Nan Laird, Christoph Lange, and Stephen V. Faraone. 2008. 'Genome-wide association scan of quantitative traits for attention deficit hyperactivity disorder identifies novel associations and confirms candidate gene associations', *American Journal of Medical Genetics Part B: Neuropsychiatric Genetics*, 147B: 1345-54.

Latora, V., and M. Marchiori. 2003. 'Economic small-world behavior in weighted networks', *The European Physical Journal B - Condensed Matter and Complex Systems*, 32: 249-63.

Latora, Vito, and Massimo Marchiori. 2001. 'Efficient behavior of small-world networks', *Physical review letters*, 87: 198701.

Lawrence, K. E., J. G. Levitt, S. K. Loo, R. Ly, V. Yee, J. O'Neill, J. Alger, and K. L. Narr. 2013. 'White matter microstructure in subjects with attention-deficit/hyperactivity disorder and their siblings', *J Am Acad Child Adolesc Psychiatry*, 52: 431-40.e4.

Lebel, Catherine, and Christian Beaulieu. 2011. 'Longitudinal Development of Human Brain Wiring Continues from Childhood into Adulthood', *The Journal of Neuroscience*, 31: 10937-47.

Lebel, Catherine, and Sean Deoni. 2018. 'The development of brain white matter microstructure', *Neuroimage*, 182: 207-18.

Lebel, Catherine, Myrlene Gee, Richard Camicioli, Marguerite Wieler, Wayne Martin, and Christian Beaulieu. 2012. 'Diffusion tensor imaging of white matter tract evolution over the lifespan', *Neuroimage*, 60: 340-52.

Lebel, Catherine, Sarah Treit, and Christian Beaulieu. 2019. 'A review of diffusion MRI of typical white matter development from early childhood to young adulthood', *NMR in Biomedicine*, 32: e3778.

LeDoux, Joseph. 1998. *The emotional brain: The mysterious underpinnings of emotional life* (Simon and Schuster).

Leemans, A., and D. K. Jones. 2009. 'The B-matrix must be rotated when correcting for subject motion in DTI data', *Magn Reson Med*, 61: 1336-49.

Leemans, Alexander, Ben Jeurissen, Jan Sijbers, and Derek K Jones. 2009. "ExploreDTI: a graphical toolbox for processing, analyzing, and visualizing diffusion MR data." In *Proc Intl Soc Mag Reson Med*, 3537.

Lemiere, Jurgen, Marina Danckaerts, Wim Van Hecke, Mitul A Mehta, Ronald Peeters, Stefan Sunaert, and Edmund Sonuga-Barke. 2012. 'Brain activation to cues

predicting inescapable delay in adolescent Attention Deficit/Hyperactivity Disorder: an fMRI pilot study', *Brain Research*, 1450: 57-66.

Lesch, K. P. 2019. 'Editorial: Can dysregulated myelination be linked to ADHD pathogenesis and persistence?', *J Child Psychol Psychiatry*, 60: 229-31.

Leung, Louis C., Vasja Urbančič, Marie-Laure Baudet, Asha Dwivedy, Timothy G. Bayley, Aih Cheun Lee, William A. Harris, and Christine E. Holt. 2013. 'Coupling of NF-protocadherin signaling to axon guidance by cue-induced translation', *Nature Neuroscience*, 16: 166-73.

Li, Mingfeng, Gabriel Santpere, Yuka Imamura Kawasawa, Oleg V Evgrafov, Forrest O Gulden, Sirisha Pochareddy, Susan M Sunkin, Zhen Li, Yurae Shin, and Ying Zhu. 2018. 'Integrative functional genomic analysis of human brain development and neuropsychiatric risks', *Science*, 362: eaat7615.

Li, Qianqian, Jinhua Sun, Lanting Guo, Yufeng Zang, Zhengzhi Feng, Xiaoqi Huang, Hong Yang, Yating Lv, Mingjin Huang, and Qiyong Gong. 2010. 'Increased fractional anisotropy in white matter of the right frontal region in children with attention-deficit/hyperactivity disorder: a diffusion tensor imaging study', *Neuroendocrinology Letters*, 31: 747.

Li, Ting, Daan van Rooij, Nina Roth Mota, Jan K. Buitelaar, The ENIGMA ADHD Working Group, Martine Hoogman, Alejandro Arias Vasquez, and Barbara Franke. 2021. 'Characterizing neuroanatomic heterogeneity in people with and without ADHD based on subcortical brain volumes', *Journal of Child Psychology and Psychiatry*, 62: 1140-49.

Liao, Xuhong, Athanasios V. Vasilakos, and Yong He. 2017. 'Small-world human brain networks: Perspectives and challenges', *Neuroscience & Biobehavioral Reviews*, 77: 286-300.

Lichenstein, Sarah D., Timothy Verstynen, and Erika E. Forbes. 2016. 'Adolescent brain development and depression: A case for the importance of connectivity of the anterior cingulate cortex', *Neuroscience & Biobehavioral Reviews*, 70: 271-87.

Lin, H. Y., S. S. F. Gau, S. L. Huang-Gu, C. Y. Shang, Y. H. Wu, and W. Y. I. Tseng. 2014. 'Neural substrates of behavioral variability in attention deficit hyperactivity disorder: based on ex-Gaussian reaction time distribution and diffusion spectrum imaging tractography', *Psychological Medicine*, 44: 1751-64.

Lin, Q., X. Bu, M. Wang, Y. Liang, H. Chen, W. Wang, Y. Yi, H. Lin, J. Zhou, L. Lu, X. Hu, C. Yang, and X. Huang. 2020. 'Aberrant white matter properties of the callosal tracts implicated in girls with attention-deficit/hyperactivity disorder', *Brain Imaging and Behavior*, 14: 728-35.

Lopez-Persem, Alizée, Lennart Verhagen, Céline Amiez, Michael Petrides, and Jérome Sallet. 2019. 'The human ventromedial prefrontal cortex: sulcal morphology and its influence on functional organization', *Journal of Neuroscience*, 39: 3627-39.

Lövblad, Karl-Olof, Karl Schaller, and Maria Isabel Vargas. 2014. 'The Fornix and Limbic System', *Seminars in Ultrasound, CT and MRI*, 35: 459-73.

Lu, You-Ming, Zhengping Jia, Christopher Janus, Jeffrey T. Henderson, Robert Gerlai, J. Martin Wojtowicz, and John C. Roder. 1997. 'Mice Lacking Metabotropic Glutamate Receptor 5 Show Impaired Learning and Reduced CA1 Long-Term Potentiation (LTP) But Normal CA3 LTP', *The Journal of Neuroscience*, 17: 5196-205.

Luo, T., W. H. Wu, and B. S. Chen. 2011. 'NMDA receptor signaling: death or survival?', *Front Biol (Beijing)*, 6: 468-76.

MacLean, Paul D. 1949. 'Psychosomatic Disease and the" Visceral Brain": Recent Developments Bearing on the Papez Theory of Emotion', *Psychosomatic Medicine*, 11: 338-53.

———. 1952. 'Some psychiatric implications of physiological studies on frontotemporal portion of limbic system (visceral brain)', *Electroencephalography and clinical neurophysiology*, 4: 407-18.

Maia, Tiago V., and James L. McClelland. 2004. 'A reexamination of the evidence for the somatic marker hypothesis: What participants really know in the Iowa gambling task', *Proceedings of the National Academy of Sciences*, 101: 16075-80.

Maiter, Ahmed, Frank Riemer, Kieren Allinson, Fulvio Zaccagna, Mireia Crispin-Ortuzar, Marcel Gehrung, Mary A. McLean, Andrew N. Priest, James Grist, Tomasz Matys, Martin J. Graves, and Ferdia A. Gallagher. 2021. 'Investigating the relationship between diffusion kurtosis tensor imaging (DKTI) and histology within the normal human brain', *Scientific Reports*, 11: 8857.

Marek, Scott, Brenden Tervo-Clemmens, Finnegan J. Calabro, David F. Montez, Benjamin P. Kay, Alexander S. Hatoum, Meghan Rose Donohue, William Foran, Ryland L. Miller, Timothy J. Hendrickson, Stephen M. Malone, Sridhar Kandala, Eric Feczko, Oscar Miranda-Dominguez, Alice M. Graham, Eric A. Earl, Anders J. Perrone, Michaela Cordova, Olivia Doyle, Lucille A. Moore, Gregory M. Conan, Johnny Uriarte, Kathy Snider, Benjamin J. Lynch, James C. Wilgenbusch, Thomas Pengo, Angela Tam, Jianzhong Chen, Dillan J. Newbold, Annie Zheng, Nicole A. Seider, Andrew N. Van, Athanasia Metoki, Roselyne J. Chauvin, Timothy O. Laumann, Deanna J. Greene, Steven E. Petersen, Hugh Garavan, Wesley K. Thompson, Thomas E. Nichols, B. T. Thomas Yeo, Deanna M. Barch, Beatriz Luna, Damien A. Fair, and Nico U. F. Dosenbach. 2022. 'Reproducible brain-wide association studies require thousands of individuals', *Nature*, 603: 654-60.

Margaret H. Sibley , Ph.D. ,, L. Eugene Arnold , M.D. ,, James M. Swanson , Ph.D. ,, Lily T. Hechtman , M.D. ,, Traci M. Kennedy , Ph.D. ,, Elizabeth Owens , Ph.D. ,, Brooke S.G. Molina , Ph.D. ,, Peter S. Jensen , M.D. ,, Stephen P. Hinshaw , Ph.D. ,, Arunima Roy , Ph.D. ,, Andrea Chronis-Tuscano , Ph.D. ,, Jeffrey H. Newcorn , M.D. ,, and Luis A. Rohde , M.D., Ph.D .,. 2022. 'Variable Patterns of Remission From ADHD in the Multimodal Treatment Study of ADHD', *American Journal of Psychiatry*, 179: 142-51.

Marquand, Andre F., Iead Rezek, Jan Buitelaar, and Christian F. Beckmann. 2016. 'Understanding Heterogeneity in Clinical Cohorts Using Normative Models: Beyond Case-Control Studies', *Biological Psychiatry*, 80: 552-61.

Marshall, Louise H, and Horace W Magoun. 2013. *Discoveries in the human brain: neuroscience prehistory, brain structure, and function* (Springer Science & Business Media).

Martinez-Heras, Eloy, Francesco Grussu, Ferran Prados, Elisabeth Solana, and Sara Llufriu. 2021. 'Diffusion-Weighted Imaging: Recent Advances and Applications', *Seminars in Ultrasound, CT and MRI*, 42: 490-506.

McAuley, Julian J, Luciano da Fontoura Costa, and Tibério S Caetano. 2007. 'Rich-club phenomenon across complex network hierarchies', *Applied Physics Letters*, 91: 084103.

McNaughton, Neil, and Seralynne D. Vann. 2022. 'Construction of complex memories via parallel distributed cortical–subcortical iterative integration', *Trends in Neurosciences*, 45: 550-62.

Merwood, A., W. Chen, F. Rijsdijk, C. Skirrow, H. Larsson, A. Thapar, J. Kuntsi, and P. Asherson. 2014. 'Genetic associations between the symptoms of attention-deficit/hyperactivity disorder and emotional lability in child and adolescent twins', *J Am Acad Child Adolesc Psychiatry*, 53: 209-20.e4.

Messina, Irene, Alessandro Grecucci, and Roberto Viviani. 2021. 'Neurobiological models of emotion regulation: a meta-analysis of neuroimaging studies of acceptance as an emotion regulation strategy', *Social Cognitive and Affective Neuroscience*, 16: 257-67.

Mesulam, M-Marsel. 2000. 'Behavioral neuroanatomy', *Principles of behavioral and cognitive neurology*, 2: 1-120.

Metzler-Baddeley, Claudia, Derek K. Jones, Boubakeur Belaroussi, John P. Aggleton, and Michael J. O'Sullivan. 2011. 'Frontotemporal Connections in Episodic Memory and Aging: A Diffusion MRI Tractography Study', *The Journal of Neuroscience*, 31: 13236-45.

Meys, Karlijn ME, Linda S de Vries, F Groenendaal, Seralynne D Vann, and Maarten H Lequin. 2022. 'The mammillary bodies: a review of causes of injury in infants and children', *American Journal of Neuroradiology*, 43: 802-12.

Michael-Titus, Adina, Patricia Revest, and Peter Shortland. 2010. '1 - ORGANIZATION OF THE NERVOUS SYSTEM.' in Adina Michael-Titus, Patricia Revest and Peter Shortland (eds.), *The Nervous System (Second Edition)* (Churchill Livingstone).

Michielsen, Marieke, Evert Semeijn, Hannie C Comijs, Peter van de Ven, Aartjan TF Beekman, Dorly JH Deeg, and JJ Sandra Kooij. 2012. 'Prevalence of attention-deficit hyperactivity disorder in older adults in The Netherlands', *The British Journal of Psychiatry*, 201: 298-305.

Moeller, Steen, Essa Yacoub, Cheryl A Olman, Edward Auerbach, John Strupp, Noam Harel, and Kâmil Uğurbil. 2010. 'Multiband multislice GE-EPI at 7 tesla, with 16-fold acceleration using partial parallel imaging with application to high spatial and temporal whole-brain fMRI', *Magnetic Resonance in Medicine*, 63: 1144-53.

Mohammadi, Siawoosh, Karsten Tabelow, Lars Ruthotto, Thorsten Feiweier, Jörg Polzehl, and Nikolaus Weiskopf. 2015. 'High-resolution diffusion kurtosis imaging at 3T enabled by advanced post-processing', *Frontiers in Neuroscience*, 8: 427.

Molina, Brooke SG, Stephen P Hinshaw, James M Swanson, L Eugene Arnold, Benedetto Vitiello, Peter S Jensen, Jeffery N Epstein, Betsy Hoza, Lily Hechtman, and Howard B Abikoff. 2009. 'The MTA at 8 years: prospective follow-up of children treated for combined-type ADHD in a multisite study', *Journal of the American Academy of Child & Adolescent Psychiatry*, 48: 484-500.

Mori, S., and P. C. van Zijl. 2002. 'Fiber tracking: principles and strategies - a technical review', *NMR Biomed*, 15: 468-80.

Mori, Susumu, Walter E Kaufmann, Godfrey D Pearlson, Barbara J Crain, Bram Stieltjes, Meiyappan Solaiyappan, and Peter CM Van Zijl. 2000. 'In vivo visualization of

human neural pathways by magnetic resonance imaging', *Annals of Neurology: Official Journal of the American Neurological Association and the Child Neurology Society*, 47: 412-14.

Mowlem, Florence, Jessica Agnew-Blais, Eric Taylor, and Philip Asherson. 2019. 'Do different factors influence whether girls versus boys meet ADHD diagnostic criteria? Sex differences among children with high ADHD symptoms', *Psychiatry Research*, 272: 765-73.

Mueller, A., D. S. Hong, S. Shepard, and T. Moore. 2017. 'Linking ADHD to the Neural Circuitry of Attention', *Trends Cogn Sci*, 21: 474-88.

Murillo, Lourdes García, Samuele Cortese, David Anderson, Adriana Di Martino, and Francisco Xavier Castellanos. 2015. 'Locomotor activity measures in the diagnosis of attention deficit hyperactivity disorder: Meta-analyses and new findings', *Journal of Neuroscience Methods*, 252: 14-26.

Nagel, B. J., D. Bathula, M. Herting, C. Schmitt, C. D. Kroenke, D. Fair, and J. T. Nigg. 2011. 'Altered white matter microstructure in children with attention-deficit/hyperactivity disorder', *Journal of the American Academy of Child & Adolescent Psychiatry*, 50: 283-92.

Nakao, T., J. Radua, K. Rubia, and D. Mataix-Cols. 2011. 'Gray matter volume abnormalities in ADHD: voxel-based meta-analysis exploring the effects of age and stimulant medication', *American Journal of Psychiatry*, 168: 1154-63.

Nigg, J. T., S. L. Karalunas, H. C. Gustafsson, P. Bhatt, P. Ryabinin, M. A. Mooney, S. V. Faraone, D. A. Fair, and B. Wilmot. 2020. 'Evaluating chronic emotional dysregulation and irritability in relation to ADHD and depression genetic risk in children with ADHD', *J Child Psychol Psychiatry*, 61: 205-14.

Nigg, J. T., E. G. Willcutt, A. E. Doyle, and E. J. Sonuga-Barke. 2005. 'Causal heterogeneity in attention-deficit/hyperactivity disorder: do we need neuropsychologically impaired subtypes?', *Biol Psychiatry*, 57: 1224-30.

Niida, R., B. Yamagata, A. Niida, A. Uechi, H. Matsuda, and M. Mimura. 2018. 'Aberrant Anterior Thalamic Radiation Structure in Bipolar Disorder: A Diffusion Tensor Tractography Study', *Front Psychiatry*, 9: 522.

Ning, Lipeng, Carl-Fredrik Westin, and Yogesh Rathi. 2015. 'Estimating diffusion propagator and its moments using directional radial basis functions', *Ieee Transactions on Medical Imaging*, 34: 2058-78.

Niswender, Colleen M, and P Jeffrey Conn. 2010. 'Metabotropic glutamate receptors: physiology, pharmacology, and disease', *Annual review of pharmacology and toxicology*, 50: 295-322.

Nolte, John, Todd Vanderah, and Douglas Gould. 2016. "Nolte's the Human Brain: An Introduction to Its Functional Anatomy." In.: Philadelphia, PA: Elsevier.

Norman, L. J., C. Carlisi, S. Lukito, H. Hart, D. Mataix-Cols, J. Radua, and K. Rubia. 2016. 'Structural and Functional Brain Abnormalities in Attention-Deficit/Hyperactivity Disorder and Obsessive-Compulsive Disorder: A Comparative Meta-analysis', *Jama Psychiatry*, 73: 815-25.

Noroozi, R., M. Taheri, M. D. Omrani, and S. Ghafouri-Fard. 2019. 'Glutamate receptor metabotropic 7 (GRM7) gene polymorphisms in mood disorders and attention deficit hyperactive disorder', *Neurochem Int*, 129: 104483.

Noroozi, Rezvan, Mohammad Taheri, Abolfazl Movafagh, Reza Mirfakhraie, Ghasem Solgi, Arezou Sayad, Mehrdokht Mazdeh, and Hossein Darvish. 2016. 'Glutamate receptor, metabotropic 7 (GRM7) gene variations and susceptibility to autism: a case–control study', *Autism Research*, 9: 1161-68.

Ochsner, Kevin N, and James J Gross. 2005. 'The cognitive control of emotion', *Trends in Cognitive Sciences*, 9: 242-49.

Onnink, A. Marten H., Marcel P. Zwiers, Martine Hoogman, Jeanette C. Mostert, Janneke Dammers, Cornelis C. Kan, Alejandro Arias Vasquez, Aart H. Schene, Jan Buitelaar, and Barbara Franke. 2015. 'Deviant white matter structure in adults with attention-deficit/hyperactivity disorder points to aberrant myelination and affects neuropsychological performance', *Progress in Neuro-Psychopharmacology and Biological Psychiatry*, 63: 14-22.

Organization, World Health. 2004. *International Statistical Classification of Diseases and related health problems: Alphabetical index* (World Health Organization).

Özarslan, Evren, Cheng Guan Koay, Timothy M Shepherd, Michal E Komlosh, M Okan İrfanoğlu, Carlo Pierpaoli, and Peter J Basser. 2013. 'Mean apparent propagator (MAP) MRI: a novel diffusion imaging method for mapping tissue microstructure', *Neuroimage*, 78: 16-32.

Pakpoor, J., R. Goldacre, K. Schmierer, G. Giovannoni, E. Waubant, and M. J. Goldacre. 2018. 'Psychiatric disorders in children with demyelinating diseases of the central nervous system', *Mult Scler*, 24: 1243-50.

Papez, James W. 1937. 'A proposed mechanism of emotion', *Archives of Neurology & Psychiatry*, 38: 725-43.

Pardoe, H. R., R. Kucharsky Hiess, and R. Kuzniecky. 2016. 'Motion and morphometry in clinical and nonclinical populations', *Neuroimage*, 135: 177-85.

Park, H. J., and K. Friston. 2013. 'Structural and functional brain networks: from connections to cognition', *Science*, 342: 1238411.

Parlatini, Valeria, Takashi Itahashi, Yeji Lee, Siwei Liu, Thuan T. Nguyen, Yuta Y. Aoki, Stephanie J. Forkel, Marco Catani, Katya Rubia, Juan H. Zhou, Declan G. Murphy, and Samuele Cortese. 2023. 'White matter alterations in Attention-Deficit/Hyperactivity Disorder (ADHD): a systematic review of 129 diffusion imaging studies with meta-analysis', *Molecular Psychiatry*.

Pastura, Giuseppe, Thomas Doering, Emerson Leandro Gasparetto, Paulo Mattos, and Alexandra Prüfer Araújo. 2016. 'Exploratory analysis of diffusion tensor imaging in children with attention deficit hyperactivity disorder: evidence of abnormal white matter structure', *ADHD Attention Deficit and Hyperactivity Disorders*, 8: 65-71.

Pattij, Tommy, and Louk JMJ Vanderschuren. 2008. 'The neuropharmacology of impulsive behaviour', *Trends in Pharmacological Sciences*, 29: 192-99.

Paus, T., M. Keshavan, and J. N. Giedd. 2008. 'Why do many psychiatric disorders emerge during adolescence?', *Nat Rev Neurosci*, 9: 947-57.

Pavuluri, M. N., S. Yang, K. Kamineni, A. M. Passarotti, G. Srinivasan, E. M. Harral, J. A. Sweeney, and X. J. Zhou. 2009. 'Diffusion tensor imaging study of white matter fiber tracts in pediatric bipolar disorder and attention-deficit/hyperactivity disorder', *Biological Psychiatry*, 65: 586-93.

Pergadia, Michele L, Anne L Glowinski, Naomi R Wray, Arpana Agrawal, Scott F Saccone, Anu Loukola, Ulla Broms, Tellervo Korhonen, Brenda WJH Penninx, and Julia D Grant. 2011. 'A 3p26-3p25 genetic linkage finding for DSM-IV major depression in heavy smoking families', *American Journal of Psychiatry*, 168: 848-52.

Perrone, Daniele, Jan Aelterman, Aleksandra Pižurica, Ben Jeurissen, Wilfried Philips, and Alexander Leemans. 2015. 'The effect of Gibbs ringing artifacts on measures derived from diffusion MRI', *Neuroimage*, 120: 441-55.

Peters, Bart D., and Katherine H. Karlsgodt. 2015. 'White matter development in the early stages of psychosis', *Schizophrenia Research*, 161: 61-69.

Peterson, D. J., M. Ryan, S. L. Rimrodt, L. E. Cutting, M. B. Denckla, W. E. Kaufmann, and E. M. Mahone. 2011. 'Increased regional fractional anisotropy in highly screened attention-deficit hyperactivity disorder (ADHD)', *Journal of Child Neurology*, 26: 1296-302.

Peterson, M. R., V. Cherukuri, J. N. Paulson, P. Ssentongo, A. V. Kulkarni, B. C. Warf, V. Monga, and S. J. Schiff. 2021. 'Normal childhood brain growth and a universal sex and anthropomorphic relationship to cerebrospinal fluid', *J Neurosurg Pediatr*, 28: 458-68.

Philip Shaw, M.B.B.Ch., Ph.D. ,, Argyris Stringaris, M.D., Ph.D. ,, Joel Nigg, Ph.D. , and, and Ellen Leibenluft, M.D. 2014. 'Emotion Dysregulation in Attention Deficit Hyperactivity Disorder', *American Journal of Psychiatry*, 171: 276-93.

Phillips, Mary L, Cecile D Ladouceur, and Wayne C Drevets. 2008. 'A neural model of voluntary and automatic emotion regulation: implications for understanding the pathophysiology and neurodevelopment of bipolar disorder', *Molecular Psychiatry*, 13: 833-57.

Pierpaoli, Carlo, Alan Barnett, Sinisa Pajevic, Robert Chen, LaRoy Penix, Anette Virta, and Peter Basser. 2001. 'Water diffusion changes in Wallerian degeneration and their dependence on white matter architecture', *Neuroimage*, 13: 1174-85.

Pineda, David A, M Adelaida Restrepo, Ruth J Sarmiento, Juan E Gutierrez, Sergio A Vargas, Yakel T Quiroz, and George W Hynd. 2002. 'Statistical analyses of structural magnetic resonance imaging of the head of the caudate nucleus in Colombian children with attention-deficit hyperactivity disorder', *Journal of Child Neurology*, 17: 97-105.

Pines, A. R., M. Cieslak, B. Larsen, G. L. Baum, P. A. Cook, A. Adebimpe, D. G. Dávila, M. A. Elliott, R. Jirsaraie, K. Murtha, D. J. Oathes, K. Piiwaa, A. F. G. Rosen, S. Rush, R. T. Shinohara, D. S. Bassett, D. R. Roalf, and T. D. Satterthwaite. 2020. 'Leveraging multi-shell diffusion for studies of brain development in youth and young adulthood', *Dev Cogn Neurosci*, 43: 100788.

Plaisier, A., K. Pieterman, M. H. Lequin, P. Govaert, A. M. Heemskerk, I. K. Reiss, G. P. Krestin, A. Leemans, and J. Dudink. 2014. 'Choice of diffusion tensor estimation approach affects fiber tractography of the fornix in preterm brain', *AJNR Am J Neuroradiol*, 35: 1219-25.

Plewes, Donald B., and Walter Kucharczyk. 2012. 'Physics of MRI: A primer', *Journal of Magnetic Resonance Imaging*, 35: 1038-54.

Plichta, Michael M, and Anouk Scheres. 2014. 'Ventral–striatal responsiveness during reward anticipation in ADHD and its relation to trait impulsivity in the healthy

population: A meta-analytic review of the fMRI literature', *Neuroscience & Biobehavioral Reviews*, 38: 125-34.

Pliszka, Steven R, M Lynn Crismon, Carroll W Hughes, C Keith Corners, Graham J Emslie, Peter S Jensen, JAMES T McCRACKEN, James M Swanson, Molly Lopez, and PHARMACOTHERAPY OF CHILDHOOD ATTENTION DEFICIT HYPERACTIVITY. 2006. 'The Texas Children's Medication Algorithm Project: revision of the algorithm for pharmacotherapy of attention-deficit/hyperactivity disorder', *Journal of the American Academy of Child & Adolescent Psychiatry*, 45: 642-57.

Polanczyk, G., M. S. de Lima, B. L. Horta, J. Biederman, and L. A. Rohde. 2007. 'The worldwide prevalence of ADHD: a systematic review and metaregression analysis', *Am J Psychiatry*, 164: 942-8.

Poot, D. H. J., A. J. den Dekker, E. Achten, M. Verhoye, and J. Sijbers. 2010. 'Optimal Experimental Design for Diffusion Kurtosis Imaging', *Ieee Transactions on Medical Imaging*, 29: 819-29.

Posner, J., G. V. Polanczyk, and E. Sonuga-Barke. 2020. 'Attention-deficit hyperactivity disorder', *Lancet*, 395: 450-62.

Posner, M. I., and M. K. Rothbart. 1998. 'Attention, self-regulation and consciousness', *Philos Trans R Soc Lond B Biol Sci*, 353: 1915-27.

Qian, L., Y. Li, Y. Wang, Y. Wang, X. Cheng, C. Li, X. Cui, G. Jiao, and X. Ke. 2021. 'Shared and Distinct Topologically Structural Connectivity Patterns in Autism Spectrum Disorder and Attention-Deficit/Hyperactivity Disorder', *Front Neurosci*, 15: 664363.

Qiu, A., S. Mori, and M. I. Miller. 2015. 'Diffusion tensor imaging for understanding brain development in early life', *Annu Rev Psychol*, 66: 853-76.

Qiu, M. G., Z. Ye, Q. Y. Li, G. J. Liu, B. Xie, and J. Wang. 2011. 'Changes of Brain Structure and Function in ADHD Children', *Brain Topography*, 24: 243-52.

Raffelt, D., J. D. Tournier, S. Rose, G. R. Ridgway, R. Henderson, S. Crozier, O. Salvado, and A. Connelly. 2012. 'Apparent Fibre Density: a novel measure for the analysis of diffusion-weighted magnetic resonance images', *Neuroimage*, 59: 3976-94.

Raffelt, David A, J-Donald Tournier, Robert E Smith, David N Vaughan, Graeme Jackson, Gerard R Ridgway, and Alan Connelly. 2017. 'Investigating white matter fibre density and morphology using fixel-based analysis', *Neuroimage*, 144: 58-73.

Rajmohan, V., and E. Mohandas. 2007. 'The limbic system', *Indian J Psychiatry*, 49: 132-9.

Ray, Siddharth, Meghan Miller, Sarah Karalunas, Charles Robertson, David S. Grayson, Robert P. Cary, Elizabeth Hawkey, Julia G. Painter, Daniel Kriz, Eric Fombonne, Joel T. Nigg, and Damien A. Fair. 2014. 'Structural and functional connectivity of the human brain in autism spectrum disorders and attention-deficit/hyperactivity disorder: A rich club-organization study', *Human Brain Mapping*, 35: 6032-48.

Reed, Geoffrey M, Michael B First, Cary S Kogan, Steven E Hyman, Oye Gureje, Wolfgang Gaebel, Mario Maj, Dan J Stein, Andreas Maercker, and Peter Tyrer. 2019. 'Innovations and changes in the ICD-11 classification of mental, behavioural and neurodevelopmental disorders', *World psychiatry*, 18: 3-19.

Reifman, Alan, and Kristina Garrett. 2010. 'Winsorize (2010)': 1636-38.

Réus, Gislaine Z, Gabriel R Fries, Laura Stertz, Marwa Badawy, IC Passos, Tatiana Barichello, Flavio Kapczinski, and Joao Quevedo. 2015. 'The role of inflammation

and microglial activation in the pathophysiology of psychiatric disorders', *Neuroscience*, 300: 141-54.
Roine, Timo, Ben Jeurissen, Daniele Perrone, Jan Aelterman, Wilfried Philips, Jan Sijbers, and Alexander Leemans. 2019. 'Reproducibility and intercorrelation of graph theoretical measures in structural brain connectivity networks', *Medical Image Analysis*, 52: 56-67.
Rolls, E. T. 2018a. 'The storage and recall of memories in the hippocampo-cortical system', *Cell Tissue Res*, 373: 577-604.
———. 2019a. 'The cingulate cortex and limbic systems for emotion, action, and memory', *Brain Struct Funct*, 224: 3001-18.
———. 2019b. 'The orbitofrontal cortex and emotion in health and disease, including depression', *Neuropsychologia*, 128: 14-43.
Rolls, E. T., and S. Wirth. 2018. 'Spatial representations in the primate hippocampus, and their functions in memory and navigation', *Prog Neurobiol*, 171: 90-113.
Rolls, Edmund T. 2018b. *The brain, emotion, and depression* (Oxford University Press).
———. 2019c. 'The cingulate cortex and limbic systems for action, emotion, and memory', *Handbook of clinical neurology*, 166: 23-37.
———. 2021. *Brain computations: what and how* (Oxford University Press, USA).
Rolls, Edmund T. 2015. 'Limbic systems for emotion and for memory, but no single limbic system', *Cortex*, 62: 119-57.
Rommelse, N. N., B. Franke, H. M. Geurts, C. A. Hartman, and J. K. Buitelaar. 2010. 'Shared heritability of attention-deficit/hyperactivity disorder and autism spectrum disorder', *Eur Child Adolesc Psychiatry*, 19: 281-95.
Rosch, Keri S, Deana Crocetti, Kathryn Hirabayashi, Martha B Denckla, Stewart H Mostofsky, and E Mark Mahone. 2018. 'Reduced subcortical volumes among preschool-age girls and boys with ADHD', *Psychiatry Research: Neuroimaging*, 271: 67-74.
Ross, Elliott D. 2008. 'Sensory-specific amnesia and hypoemotionality in humans and monkeys: gateway for developing a hodology of memory', *Cortex*, 44: 1010-22.
Roth, R. M., and A. J. Saykin. 2004. 'Executive dysfunction in attention-deficit/hyperactivity disorder: cognitive and neuroimaging findings', *Psychiatr Clin North Am*, 27: 83-96, ix.
Rubia, K. 2007. 'Neuro-anatomic evidence for the maturational delay hypothesis of ADHD', *Proc Natl Acad Sci U S A*, 104: 19663-4.
Rubia, Katya. 2011. '"Cool" Inferior Frontostriatal Dysfunction in Attention-Deficit/Hyperactivity Disorder Versus "Hot" Ventromedial Orbitofrontal-Limbic Dysfunction in Conduct Disorder: A Review', *Biological Psychiatry*, 69: e69-e87.
Rubinov, Mikail, and Olaf Sporns. 2010. 'Complex network measures of brain connectivity: Uses and interpretations', *Neuroimage*, 52: 1059-69.
Runge, K., C. Cardoso, and A. de Chevigny. 2020. 'Dendritic Spine Plasticity: Function and Mechanisms', *Front Synaptic Neurosci*, 12: 36.
Sabariego-Navarro, M., Á Fernández-Blanco, C. Sierra, and M. Dierssen. 2022. 'Neurodevelopmental disorders: 2022 update', *Free Neuropathol*, 3.
Sagvolden, Terje, Espen Borga Johansen, Heidi Aase, and Vivienne Ann Russell. 2005. 'A dynamic developmental theory of attention-deficit/hyperactivity disorder

(ADHD) predominantly hyperactive/impulsive and combined subtypes', *Behavioral and Brain Sciences*, 28: 397-418.

Sansig, Gilles, Trevor J Bushell, Vernon RJ Clarke, Andrei Rozov, Nail Burnashev, Chantal Portet, Fabrizio Gasparini, Markus Schmutz, Klaus Klebs, and Ryuichi Shigemoto. 2001. 'Increased seizure susceptibility in mice lacking metabotropic glutamate receptor 7', *Journal of Neuroscience*, 21: 8734-45.

Sarra, Scott A. 2006. 'Digital total variation filtering as postprocessing for Chebyshev pseudospectral methods for conservation laws', *Numerical Algorithms*, 41: 17-34.

Sarwar, Tabinda, Kotagiri Ramamohanarao, and Andrew Zalesky. 2019. 'Mapping connectomes with diffusion MRI: deterministic or probabilistic tractography?', *Magnetic Resonance in Medicine*, 81: 1368-84.

Scheffler, Richard M, Stephen P Hinshaw, Sepideh Modrek, and Peter Levine. 2007. 'The global market for ADHD medications', *Health affairs*, 26: 450-57.

Schermuly, I, A Fellgiebel, S Wagner, I Yakushev, P Stoeter, REEA Schmitt, RJ Knickenberg, F Bleichner, and ME Beutel. 2010. 'Association between cingulum bundle structure and cognitive performance: an observational study in major depression', *European Psychiatry*, 25: 355-60.

Schmahmann, Jeremy D, Eric E Smith, Florian S Eichler, and Christopher M Filley. 2008. 'Cerebral white matter: neuroanatomy, clinical neurology, and neurobehavioral correlates', *Annals of the New York Academy of Sciences*, 1142: 266.

Schönbrodt, Felix D, and Marco Perugini. 2013. 'At what sample size do correlations stabilize?', *Journal of Research in Personality*, 47: 609-12.

Schwartz, E. D., E. T. Cooper, C. L. Chin, S. Wehrli, A. Tessler, and D. B. Hackney. 2005. 'Ex vivo evaluation of ADC values within spinal cord white matter tracts', *AJNR Am J Neuroradiol*, 26: 390-7.

Sciberras, Emma, Daryl Efron, Elizabeth J Schilpzand, Vicki Anderson, Brad Jongeling, Philip Hazell, Obioha C Ukoumunne, and Jan M Nicholson. 2013. 'The Children's Attention Project: a community-based longitudinal study of children with ADHD and non-ADHD controls', *Bmc Psychiatry*, 13: 1-11.

Seiger, René, Fabian P. Hammerle, Godber M. Godbersen, Murray B. Reed, Benjamin Spurny-Dworak, Patricia Handschuh, Manfred Klöbl, Jakob Unterholzner, Gregor Gryglewski, Thomas Vanicek, and Rupert Lanzenberger. 2021. 'Comparison and Reliability of Hippocampal Subfield Segmentations Within FreeSurfer Utilizing T1- and T2-Weighted Multispectral MRI Data', *Frontiers in Neuroscience*, 15.

Sen, Srijan, Ronald Duman, and Gerard Sanacora. 2008. 'Serum brain-derived neurotrophic factor, depression, and antidepressant medications: meta-analyses and implications', *Biological Psychiatry*, 64: 527-32.

Senova, S., A. Fomenko, E. Gondard, and A. M. Lozano. 2020. 'Anatomy and function of the fornix in the context of its potential as a therapeutic target', *J Neurol Neurosurg Psychiatry*, 91: 547-59.

Sexton, Claire E., Kristine B. Walhovd, Andreas B. Storsve, Christian K. Tamnes, Lars T. Westlye, Heidi Johansen-Berg, and Anders M. Fjell. 2014. 'Accelerated Changes in White Matter Microstructure during Aging: A Longitudinal Diffusion Tensor Imaging Study', *The Journal of Neuroscience*, 34: 15425-36.

Seymour, K. E., S. P. Reinblatt, L. Benson, and S. Carnell. 2015. 'Overlapping neurobehavioral circuits in ADHD, obesity, and binge eating: evidence from neuroimaging research', *CNS Spectr*, 20: 401-11.

Seymour, K. E., X. Tang, D. Crocetti, S. H. Mostofsky, M. I. Miller, and K. S. Rosch. 2017. 'Anomalous subcortical morphology in boys, but not girls, with ADHD compared to typically developing controls and correlates with emotion dysregulation', *Psychiatry Research - Neuroimaging*, 261: 20-28.

Shaffer, D., P. Fisher, C. P. Lucas, M. K. Dulcan, and M. E. Schwab-Stone. 2000. 'NIMH Diagnostic Interview Schedule for Children Version IV (NIMH DISC-IV): description, differences from previous versions, and reliability of some common diagnoses', *J Am Acad Child Adolesc Psychiatry*, 39: 28-38.

Shang, C. Y., Y. H. Wu, S. S. Gau, and W. Y. Tseng. 2013. 'Disturbed microstructural integrity of the frontostriatal fiber pathways and executive dysfunction in children with attention deficit hyperactivity disorder', *Psychological Medicine*, 43: 1093-107.

Shankar, Kartik, Ying Zhong, Ping Kang, Franchesca Lau, Michael L Blackburn, Jin-Ran Chen, Sarah J Borengasser, Martin JJ Ronis, and Thomas M Badger. 2011. 'Maternal obesity promotes a proinflammatory signature in rat uterus and blastocyst', *Endocrinology*, 152: 4158-70.

Shaw, P., P. De Rossi, B. Watson, A. Wharton, D. Greenstein, A. Raznahan, W. Sharp, J. P. Lerch, and M. M. Chakravarty. 2014. 'Mapping the development of the basal ganglia in children with attention-deficit/hyperactivity disorder', *Journal of the American Academy of Child and Adolescent Psychiatry*, 53: 780-89.e11.

Shaw, P., K. Eckstrand, W. Sharp, J. Blumenthal, J. P. Lerch, D. Greenstein, L. Clasen, A. Evans, J. Giedd, and J. L. Rapoport. 2007. 'Attention-deficit/hyperactivity disorder is characterized by a delay in cortical maturation', *Proc Natl Acad Sci U S A*, 104: 19649-54.

Shaw, P., A. Stringaris, J. Nigg, and E. Leibenluft. 2014. 'Emotion dysregulation in attention deficit hyperactivity disorder', *Am J Psychiatry*, 171: 276-93.

Shaw, Philip, Meaghan Malek, Bethany Watson, Deanna Greenstein, Pietro de Rossi, and Wendy Sharp. 2013. 'Trajectories of Cerebral Cortical Development in Childhood and Adolescence and Adult Attention-Deficit/Hyperactivity Disorder', *Biological Psychiatry*, 74: 599-606.

Shaw, Philip, Meaghan Malek, Bethany Watson, Wendy Sharp, Alan Evans, and Deanna Greenstein. 2012. 'Development of Cortical Surface Area and Gyrification in Attention-Deficit/Hyperactivity Disorder', *Biological Psychiatry*, 72: 191-97.

Shaw, Philip, and Gustavo Sudre. 2021. 'Adolescent attention-deficit/hyperactivity disorder: understanding teenage symptom trajectories', *Biological Psychiatry*, 89: 152-61.

Shields, Ann, and Dante Cicchetti. 1997. 'Emotion regulation among school-age children: the development and validation of a new criterion Q-sort scale', *Developmental psychology*, 33: 906.

Silk, T. J., A. Vance, N. Rinehart, J. L. Bradshaw, and R. Cunnington. 2009a. 'Structural development of the basal ganglia in attention deficit hyperactivity disorder: a diffusion tensor imaging study', *Psychiatry Research*, 172: 220-5.

———. 2009b. 'White-matter abnormalities in attention deficit hyperactivity disorder: A diffusion tensor imaging study', *Human Brain Mapping*, 30: 2757-65.

Silk, T. J., V. Vilgis, C. Adamson, J. Chen, L. Smit, A. Vance, and M. A. Bellgrove. 2016. 'Abnormal asymmetry in frontostriatal white matter in children with attention deficit hyperactivity disorder', *Brain Imaging & Behavior*, 10: 1080-89.

Silk, Timothy J., Sila Genc, Vicki Anderson, Daryl Efron, Philip Hazell, Jan M. Nicholson, Michael Kean, Charles B. Malpas, and Emma Sciberras. 2016. 'Developmental brain trajectories in children with ADHD and controls: a longitudinal neuroimaging study', *Bmc Psychiatry*, 16: 59.

Silk, Timothy J., Charles B. Malpas, Richard Beare, Daryl Efron, Vicki Anderson, Philip Hazell, Brad Jongeling, Jan M. Nicholson, and Emma Sciberras. 2019. 'A network analysis approach to ADHD symptoms: More than the sum of its parts', *Plos One*, 14: e0211053.

Simon, Viktória, Pál Czobor, Sára Bálint, Agnes Mészáros, and István Bitter. 2009. 'Prevalence and correlates of adult attention-deficit hyperactivity disorder: meta-analysis', *The British Journal of Psychiatry*, 194: 204-11.

Simonds, Jennifer, and Mary K Rothbart. 2004. "The Temperament in Middle Childhood Questionnaire (TMCQ): A computerized self-report instrument for ages 7–10." In *Poster Sess Present Occas Temperament Conf Athens, GA*.

Sjöwall, D., L. Roth, S. Lindqvist, and L. B. Thorell. 2013. 'Multiple deficits in ADHD: executive dysfunction, delay aversion, reaction time variability, and emotional deficits', *J Child Psychol Psychiatry*, 54: 619-27.

Smith, Stephen M, Mark Jenkinson, Heidi Johansen-Berg, Daniel Rueckert, Thomas E Nichols, Clare E Mackay, Kate E Watkins, Olga Ciccarelli, M Zaheer Cader, and Paul M Matthews. 2006. 'Tract-based spatial statistics: voxelwise analysis of multi-subject diffusion data', *Neuroimage*, 31: 1487-505.

Solanto, Mary V, Howard Abikoff, Edmund Sonuga-Barke, Russell Schachar, Gordon D Logan, Tim Wigal, Lily Hechtman, Stephen Hinshaw, and Elihu Turkel. 2001. 'The ecological validity of delay aversion and response inhibition as measures of impulsivity in AD/HD: a supplement to the NIMH multimodal treatment study of AD/HD', *Journal of abnormal child psychology*, 29: 215-28.

Soman, Shania Mereen, Nandita Vijayakumar, Phoebe Thomson, Gareth Ball, Christian Hyde, and Timothy J. Silk. 2023. 'Cortical structural and functional coupling during development and implications for attention deficit hyperactivity disorder', *Translational Psychiatry*, 13: 252.

Song, J. M., M. Kang, D. H. Park, S. Park, S. Lee, and Y. H. Suh. 2021. 'Pathogenic GRM7 Mutations Associated with Neurodevelopmental Disorders Impair Axon Outgrowth and Presynaptic Terminal Development', *J Neurosci*, 41: 2344-59.

Song, S. K., Jun Yoshino, Tuan Q Le, Shiow-Jiuan Lin, Shu-Wei Sun, Anne H Cross, and Regina C Armstrong. 2005. 'Demyelination increases radial diffusivity in corpus callosum of mouse brain', *Neuroimage*, 26: 132-40.

Sonuga-Barke, E., P. Bitsakou, and M. Thompson. 2010. 'Beyond the dual pathway model: evidence for the dissociation of timing, inhibitory, and delay-related impairments in attention-deficit/hyperactivity disorder', *J Am Acad Child Adolesc Psychiatry*, 49: 345-55.

Sonuga-Barke, E. J. 2005. 'Causal models of attention-deficit/hyperactivity disorder: from common simple deficits to multiple developmental pathways', *Biol Psychiatry*, 57: 1231-8.

———. 2011. 'Editorial: ADHD as a reinforcement disorder - moving from general effects to identifying (six) specific models to test', *J Child Psychol Psychiatry*, 52: 917-8.

Sonuga-Barke, E. J., and F. X. Castellanos. 2007. 'Spontaneous attentional fluctuations in impaired states and pathological conditions: a neurobiological hypothesis', *Neurosci Biobehav Rev*, 31: 977-86.

Sonuga-Barke, E. J., J. A. Sergeant, J. Nigg, and E. Willcutt. 2008. 'Executive dysfunction and delay aversion in attention deficit hyperactivity disorder: nosologic and diagnostic implications', *Child Adolesc Psychiatr Clin N Am*, 17: 367-84, ix.

Sotiropoulos, Stamatios N., and Andrew Zalesky. 2019. 'Building connectomes using diffusion MRI: why, how and but', *NMR in Biomedicine*, 32: e3752.

Sporns, Olaf, Giulio Tononi, and Gerald M Edelman. 2000. 'Connectivity and complexity: the relationship between neuroanatomy and brain dynamics', *Neural networks*, 13: 909-22.

Sporns, Olaf, Giulio Tononi, and Rolf Kötter. 2005. 'The human connectome: a structural description of the human brain', *Plos Computational Biology*, 1: e42.

Stalnaker, T. A., N. K. Cooch, and G. Schoenbaum. 2015. 'What the orbitofrontal cortex does not do', *Nat Neurosci*, 18: 620-7.

Stephani, C. 2014. 'Limbic System.' in Michael J. Aminoff and Robert B. Daroff (eds.), *Encyclopedia of the Neurological Sciences (Second Edition)* (Academic Press: Oxford).

Steven, Andrew J., Jiachen Zhuo, and Elias R. Melhem. 2013. 'Diffusion Kurtosis Imaging: An Emerging Technique for Evaluating the Microstructural Environment of the Brain', *American Journal of Roentgenology*, 202: W26-W33.

Stibbe, T., J. Huang, M. Paucke, C. Ulke, and M. Strauss. 2020. 'Gender differences in adult ADHD: Cognitive function assessed by the test of attentional performance', *Plos One*, 15: e0240810.

Stikov, Nikola, Joshua D. Trzasko, and Matt A. Bernstein. 2019. 'Reproducibility and the future of MRI research', *Magnetic Resonance in Medicine*, 82: 1981-83.

Stiles, Joan, and Terry L. Jernigan. 2010. 'The Basics of Brain Development', *Neuropsychology Review*, 20: 327-48.

Stringaris, A., R. Goodman, S. Ferdinando, V. Razdan, E. Muhrer, E. Leibenluft, and M. A. Brotman. 2012. 'The Affective Reactivity Index: a concise irritability scale for clinical and research settings', *J Child Psychol Psychiatry*, 53: 1109-17.

Sudre, G., M. Bouyssi-Kobar, L. Norman, W. Sharp, S. Choudhury, and P. Shaw. 2021. 'Estimating the Heritability of Developmental Change in Neural Connectivity, and Its Association With Changing Symptoms of Attention-Deficit/Hyperactivity Disorder', 89: 443-50.

Sudre, Gustavo, Luke Norman, Marine Bouyssi-Kobar, Jolie Price, Gauri Ganesh Shastri, and Philip Shaw. 2023. 'A Mega-analytic Study of White Matter Microstructural Differences Across 5 Cohorts of Youths With Attention-Deficit/Hyperactivity Disorder', *Biological Psychiatry*, 94: 18-28.

Surman, C. B., J. Biederman, T. Spencer, D. Yorks, C. A. Miller, C. R. Petty, and S. V. Faraone. 2011. 'Deficient emotional self-regulation and adult attention deficit hyperactivity disorder: a family risk analysis', *Am J Psychiatry*, 168: 617-23.

Svatkova, Alena, Igor Nestrasil, Kyle Rudser, Jodene Goldenring Fine, Jesse Bledsoe, and Margaret Semrud-Clikeman. 2016. 'Unique White Matter Microstructural Patterns in ADHD Presentations-A Diffusion Tensor Imaging Study', *Human Brain Mapping*, 37: 3323-36.

Swartz, Johnna R, Melisa Carrasco, Jillian Lee Wiggins, Moriah E Thomason, and Christopher S Monk. 2014. 'Age-related changes in the structure and function of prefrontal cortex–amygdala circuitry in children and adolescents: A multi-modal imaging approach', *Neuroimage*, 86: 212-20.

Symms, M., H. R. Jäger, K. Schmierer, and T. A. Yousry. 2004. 'A review of structural magnetic resonance neuroimaging', *J Neurol Neurosurg Psychiatry*, 75: 1235-44.

Tabesh, Ali, Jens H Jensen, Babak A Ardekani, and Joseph A Helpern. 2011. 'Estimation of tensors and tensor-derived measures in diffusional kurtosis imaging', *Magnetic Resonance in Medicine*, 65: 823-36.

Tajima-Pozo, Kazuhiro, Miguel Yus, Gonzalo Ruiz-Manrique, Adrian Lewczuk, Juan Arrazola, and Francisco Montañes-Rada. 2016. 'Amygdala Abnormalities in Adults With ADHD', *Journal of Attention Disorders*, 22: 671-78.

Takahashi, M., D. B. Hackney, G. Zhang, S. L. Wehrli, A. C. Wright, W. T. O'Brien, H. Uematsu, F. W. Wehrli, and M. E. Selzer. 2002. 'Magnetic resonance microimaging of intraaxonal water diffusion in live excised lamprey spinal cord', *Proc Natl Acad Sci U S A*, 99: 16192-6.

Takeuchi, Tamotsu, Akiko Misaki, Sheng-Ben Liang, Akiko Tachibana, Nakanobu Hayashi, Hiroshi Sonobe, and Yuji Ohtsuki. 2000. 'Expression of T-cadherin (CDH13, H-Cadherin) in human brain and its characteristics as a negative growth regulator of epidermal growth factor in neuroblastoma cells', *Journal of Neurochemistry*, 74: 1489-97.

Tamm, L., N. Barnea-Goraly, and A. L. Reiss. 2012. 'Diffusion tensor imaging reveals white matter abnormalities in Attention-Deficit/Hyperactivity Disorder', *Psychiatry Research*, 202: 150-4.

Tamnes, C. K., M. M. Herting, A. L. Goddings, R. Meuwese, S. J. Blakemore, R. E. Dahl, B. Güroğlu, A. Raznahan, E. R. Sowell, E. A. Crone, and K. L. Mills. 2017. 'Development of the Cerebral Cortex across Adolescence: A Multisample Study of Inter-Related Longitudinal Changes in Cortical Volume, Surface Area, and Thickness', *J Neurosci*, 37: 3402-12.

Tang, Brady, Tricia Thornton-Wells, and Kathleen D Askland. 2011. 'Comparative linkage meta-analysis reveals regionally-distinct, disparate genetic architectures: application to bipolar disorder and schizophrenia', *Plos One*, 6: e19073.

Tax, C. M., B. Jeurissen, S. B. Vos, M. A. Viergever, and A. Leemans. 2014. 'Recursive calibration of the fiber response function for spherical deconvolution of diffusion MRI data', *Neuroimage*, 86: 67-80.

Tax, Chantal, Sjoerd Vos, and Alexander Leemans. 2016. 'Checking and Correcting DTI Data.' in.

Team, MuToss Coding, Gilles Blanchard, Thorsten Dickhaus, Niklas Hack, Frank Konietschke, Kornelius Rohmeyer, Jonathan Rosenblatt, Marsel Scheer, Wiebke

Werft, and Maintainer Kornelius Rohmeyer. 2017. 'Package ‘mutoss’', *Statistics in Medicine*, 9: 811-18.

Team, R Core. 2013. 'R: A language and environment for statistical computing'.

Terasaki, Laurne S, and Jaclyn M Schwarz. 2016. 'Effects of moderate prenatal alcohol exposure during early gestation in rats on inflammation across the maternal-fetal-immune interface and later-life immune function in the offspring', *Journal of Neuroimmune Pharmacology*, 11: 680-92.

Thapar, A., and M. Cooper. 2016. 'Attention deficit hyperactivity disorder', *Lancet*, 387: 1240-50.

Thelwall, P. E., T. M. Shepherd, G. J. Stanisz, and S. J. Blackband. 2006. 'Effects of temperature and aldehyde fixation on tissue water diffusion properties, studied in an erythrocyte ghost tissue model', *Magn Reson Med*, 56: 282-9.

Thomas, J. B., and S. Yoshikawa. 2009. 'Axon Guidance: Morphogens as Chemoattractants and Chemorepellants.' in Larry R. Squire (ed.), *Encyclopedia of Neuroscience* (Academic Press: Oxford).

Thomas, Rae, Sharon Sanders, Jenny Doust, Elaine Beller, and Paul Glasziou. 2015. 'Prevalence of attention-deficit/hyperactivity disorder: a systematic review and meta-analysis', *Pediatrics*, 135: e994-e1001.

Thompson, Ross A. 1994. 'Emotion regulation: A theme in search of definition', *Monographs of the society for research in child development*: 25-52.

Thomson, Phoebe, Katherine A Johnson, Charles B Malpas, Daryl Efron, Emma Sciberras, and Timothy J Silk. 2021. 'Head motion during MRI predicted by out-of-scanner sustained attention performance in attention-deficit/hyperactivity disorder', *Journal of Attention Disorders*, 25: 1429-40.

Tierney, A. L., and C. A. Nelson, 3rd. 2009. 'Brain Development and the Role of Experience in the Early Years', *Zero Three*, 30: 9-13.

Tisdall, M Dylan, Aaron T Hess, Martin Reuter, Ernesta M Meintjes, Bruce Fischl, and André JW van der Kouwe. 2012. 'Volumetric navigators for prospective motion correction and selective reacquisition in neuroanatomical MRI', *Magnetic Resonance in Medicine*, 68: 389-99.

Togashi, H., T. Sakisaka, and Y. Takai. 2009. 'Cell adhesion molecules in the central nervous system', *Cell Adh Migr*, 3: 29-35.

Tournier, J-Donald, Fernando Calamante, and Alan Connelly. 2007. 'Robust determination of the fibre orientation distribution in diffusion MRI: non-negativity constrained super-resolved spherical deconvolution', *Neuroimage*, 35: 1459-72.

Tournier, J-Donald, Fernando Calamante, David G Gadian, and Alan Connelly. 2004a. 'Direct estimation of the fiber orientation density function from diffusion-weighted MRI data using spherical deconvolution', *Neuroimage*, 23: 1176-85.

Tournier, J. D., F. Calamante, D. G. Gadian, and A. Connelly. 2004b. 'Direct estimation of the fiber orientation density function from diffusion-weighted MRI data using spherical deconvolution', *Neuroimage*, 23: 1176-85.

Tripp, G., and J. R. Wickens. 2008. 'Research review: dopamine transfer deficit: a neurobiological theory of altered reinforcement mechanisms in ADHD', *J Child Psychol Psychiatry*, 49: 691-704.

Tuch, David S. 2004. 'Q-ball imaging', *Magnetic Resonance in Medicine*, 52: 1358-72.

Tung, Y. H., H. Y. Lin, C. L. Chen, C. Y. Shang, L. Y. Yang, Y. C. Hsu, W. I. Tseng, and S. S. Gau. 2021. 'Whole Brain White Matter Tract Deviation and Idiosyncrasy From Normative Development in Autism and ADHD and Unaffected Siblings Link With Dimensions of Psychopathology and Cognition', *Am J Psychiatry*, 178: 730-43.

Turrigiano, Gina G, and Sacha B Nelson. 2004. 'Homeostatic plasticity in the developing nervous system', *Nature Reviews Neuroscience*, 5: 97-107.

Tuteja, N. 2009. 'Signaling through G protein coupled receptors', *Plant Signal Behav*, 4: 942-7.

Valera, E. M., S. V. Faraone, K. E. Murray, and L. J. Seidman. 2007. 'Meta-analysis of structural imaging findings in attention-deficit/hyperactivity disorder', *Biol Psychiatry*, 61: 1361-9.

Van Den Heuvel, Martijn P, and Olaf Sporns. 2011. 'Rich-club organization of the human connectome', *Journal of Neuroscience*, 31: 15775-86.

Van Den Heuvel, Martijn P, Cornelis J Stam, René S Kahn, and Hilleke E Hulshoff Pol. 2009. 'Efficiency of functional brain networks and intellectual performance', *Journal of Neuroscience*, 29: 7619-24.

Van Dessel, J., E. Sonuga-Barke, M. Moerkerke, S. Van der Oord, J. Lemiere, S. Morsink, and M. Danckaerts. 2020. 'The amygdala in adolescents with attention-deficit/hyperactivity disorder: Structural and functional correlates of delay aversion', *World Journal of Biological Psychiatry*, 21: 673-84.

Van Dessel, Jeroen, Edmund Sonuga-Barke, Gabry Mies, Jurgen Lemiere, Saskia Van der Oord, Sarah Morsink, and Marina Danckaerts. 2018. 'Delay aversion in attention deficit/hyperactivity disorder is mediated by amygdala and prefrontal cortex hyper-activation', *Journal of Child Psychology and Psychiatry*, 59: 888-99.

van Ewijk, Hanneke, Dirk J Heslenfeld, Marcel P Zwiers, Jan K Buitelaar, and Jaap Oosterlaan. 2012. 'Diffusion tensor imaging in attention deficit/hyperactivity disorder: a systematic review and meta-analysis', *Neuroscience & Biobehavioral Reviews*, 36: 1093-106.

Van Hecke, Wim, Louise Emsell, and Stefan Sunaert. 2016. *Diffusion tensor imaging: a practical handbook* (Springer).

Vanderah, T.W., and D.J. Gould. 2016. *Nolte's The Human Brain: An Introduction to Its Functional Anatomy* (Elsevier).

Vann, Seralynne D. 2010. 'Re-evaluating the role of the mammillary bodies in memory', *Neuropsychologia*, 48: 2316-27.

Vann, Seralynne D., Cornel Zachiu, Karlijn M. E. Meys, Sara Ambrosino, Sarah Durston, Linda S. de Vries, Floris Groenendaal, and Maarten H. Lequin. 2022. 'Normative mammillary body volumes: From the neonatal period to young adult', *Neuroimage: Reports*, 2: 100122.

Veraart, Jelle, Els Fieremans, Ileana O Jelescu, Florian Knoll, and Dmitry S Novikov. 2016. 'Gibbs ringing in diffusion MRI', *Magnetic Resonance in Medicine*, 76: 301-14.

Veraart, Jelle, Wim Van Hecke, and Jan Sijbers. 2011. 'Constrained maximum likelihood estimation of the diffusion kurtosis tensor using a Rician noise model', *Magnetic Resonance in Medicine*, 66: 678-86.

Verbeke, Geert. 1997. 'Linear mixed models for longitudinal data.' in, *Linear mixed models in practice* (Springer).

Vijayakumar, N., N. B. Allen, G. Youssef, M. Dennison, M. Yücel, J. G. Simmons, and S. Whittle. 2016. 'Brain development during adolescence: A mixed-longitudinal investigation of cortical thickness, surface area, and volume', *Hum Brain Mapp*, 37: 2027-38.

Vijayakumar, N., G. J. Youssef, N. B. Allen, V. Anderson, D. Efron, P. Hazell, L. Mundy, J. M. Nicholson, G. Patton, M. L. Seal, J. G. Simmons, S. Whittle, and T. Silk. 2021. 'A longitudinal analysis of puberty-related cortical development', *Neuroimage*, 228: 117684.

Vijayakumar, Nandita, Gareth Ball, Marc L. Seal, Lisa Mundy, Sarah Whittle, and Tim Silk. 2021. 'The development of structural covariance networks during the transition from childhood to adolescence', *Scientific Reports*, 11: 9451.

Vilgis, V., L. Sun, J. Chen, T. J. Silk, and A. Vance. 2016. 'Global and local grey matter reductions in boys with ADHD combined type and ADHD inattentive type', *Psychiatry Research - Neuroimaging*, 254: 119-26.

Vos, S. B., C. M. Tax, P. R. Luijten, S. Ourselin, A. Leemans, and M. Froeling. 2017. 'The importance of correcting for signal drift in diffusion MRI', *Magn Reson Med*, 77: 285-99.

Wakana, S., A. Caprihan, M. M. Panzenboeck, J. H. Fallon, M. Perry, R. L. Gollub, K. Hua, J. Zhang, H. Jiang, P. Dubey, A. Blitz, P. van Zijl, and S. Mori. 2007. 'Reproducibility of quantitative tractography methods applied to cerebral white matter', *Neuroimage*, 36: 630-44.

Wakana, Setsu, Hangyi Jiang, Lidia M. Nagae-Poetscher, Peter C. M. van Zijl, and Susumu Mori. 2004. 'Fiber Tract–based Atlas of Human White Matter Anatomy', *Radiology*, 230: 77-87.

Wang, C., A. Chen, B. Ruan, Z. Niu, Y. Su, H. Qin, Y. Zheng, B. Zhang, L. Gao, Z. Chen, H. Huang, X. Wang, and Q. Sun. 2020. 'PCDH7 Inhibits the Formation of Homotypic Cell-in-Cell Structure', *Front Cell Dev Biol*, 8: 329.

Wijetunge, Lasani S, Sally M Till, Thomas H Gillingwater, Cali A Ingham, and Peter C Kind. 2008. 'mGluR5 regulates glutamate-dependent development of the mouse somatosensory cortex', *Journal of Neuroscience*, 28: 13028-37.

Wilbertz, G., A. Trueg, E. J. Sonuga-Barke, J. Blechert, A. Philipsen, and L. Tebartz van Elst. 2013. 'Neural and psychophysiological markers of delay aversion in attention-deficit hyperactivity disorder', *Journal of Abnormal Psychology*, 122: 566-72.

Willcutt, Erik G. 2012. 'The prevalence of DSM-IV attention-deficit/hyperactivity disorder: a meta-analytic review', *Neurotherapeutics*, 9: 490-99.

Willis, Thomas. 1973. *Cerebri anatome: cui accessit nervorum descriptio et usus* (Apud Gerbrandum Schagen).

Winklewski, P. J., A. Sabisz, P. Naumczyk, K. Jodzio, E. Szurowska, and A. Szarmach. 2018. 'Understanding the Physiopathology Behind Axial and Radial Diffusivity Changes-What Do We Know?', *Front Neurol*, 9: 92.

Winstanley, Catharine A, David EH Theobald, Rudolf N Cardinal, and Trevor W Robbins. 2004. 'Contrasting roles of basolateral amygdala and orbitofrontal cortex in impulsive choice', *Journal of Neuroscience*, 24: 4718-22.

Witte, J. S. 2010. 'Genome-wide association studies and beyond', *Annu Rev Public Health*, 31: 9-20 4 p following 20.

Wood, Simon N. 2017. *Generalized additive models: an introduction with R* (CRC press).

Wu, W., G. McAnulty, H. M. Hamoda, K. Sarill, S. Karmacharya, B. Gagoski, L. Ning, P. E. Grant, M. E. Shenton, D. P. Waber, N. Makris, and Y. Rathi. 2020. 'Detecting microstructural white matter abnormalities of frontal pathways in children with ADHD using advanced diffusion models', *Brain Imaging & Behavior*, 14: 981-97.

Wu, Y. H., S. S. Gau, Y. C. Lo, and W. Y. Tseng. 2014. 'White matter tract integrity of frontostriatal circuit in attention deficit hyperactivity disorder: association with attention performance and symptoms', *Human Brain Mapping*, 35: 199-212.

Wu, Z. M., J. Bralten, Q. J. Cao, M. Hoogman, M. P. Zwiers, L. An, L. Sun, L. Yang, Y. F. Zang, and B. Franke. 2017. 'White matter microstructural alterations in children with ADHD: categorical and dimensional perspectives', *Neuropsychopharmacology*, 42: 572-80.

Wu, Zhao-Min, Peng Wang, Lu Liu, Juan Liu, Xiao-Lan Cao, Li Sun, Qing-Jiu Cao, Li Yang, Yu-Feng Wang, and Bin-Rang Yang. 2022. 'ADHD-inattentive versus ADHD-Combined subtypes: A severity continuum or two distinct entities? A comprehensive analysis of clinical, cognitive and neuroimaging data', *Journal of Psychiatric Research*, 149: 28-36.

Xia, S., X. Li, A. E. Kimball, M. S. Kelly, I. Lesser, and C. Branch. 2012. 'Thalamic shape and connectivity abnormalities in children with attention-deficit/hyperactivity disorder', *Psychiatry Research*, 204: 161-7.

Xie, Mingqiang, Jennifer E Tobin, Matthew D Budde, Chin-I Chen, Kathryn Trinkaus, Anne H Cross, Dennis P McDaniel, Sheng-Kwei Song, and Regina C Armstrong. 2010. 'Rostrocaudal analysis of corpus callosum demyelination and axon damage across disease stages refines diffusion tensor imaging correlations with pathological features', *Journal of Neuropathology & Experimental Neurology*, 69: 704-16.

Yakovlev, Paul I. 1948. 'MOTILITY, BEHAVIOR AND THE BRAIN*: STEREODYNAMIC ORGANIZATION AND NEURAL CO-ORDINATES OF BEHAVIOR', *The Journal of nervous and mental disease*, 107: 313-35.

Yeh, Chun-Hung, Derek K. Jones, Xiaoyun Liang, Maxime Descoteaux, and Alan Connelly. 2021. 'Mapping Structural Connectivity Using Diffusion MRI: Challenges and Opportunities', *Journal of Magnetic Resonance Imaging*, 53: 1666-82.

Yeh, Chun-Hung, Robert E. Smith, Xiaoyun Liang, Fernando Calamante, and Alan Connelly. 2016. 'Correction for diffusion MRI fibre tracking biases: The consequences for structural connectomic metrics', *Neuroimage*, 142: 150-62.

Yendiki, A., K. Koldewyn, S. Kakunoori, N. Kanwisher, and B. Fischl. 2014. 'Spurious group differences due to head motion in a diffusion MRI study', *Neuroimage*, 88: 79-90.

Yong-Hing, C. J., A. Obenaus, R. Stryker, K. Tong, and G. E. Sarty. 2005. 'Magnetic resonance imaging and mathematical modeling of progressive formalin fixation of the human brain', *Magn Reson Med*, 54: 324-32.

Yoo, S. W., M. G. Motari, K. Susuki, J. Prendergast, A. Mountney, A. Hurtado, and R. L. Schnaar. 2015. 'Sialylation regulates brain structure and function', *Faseb j*, 29: 3040-53.

Zaitsev, M., J. Maclaren, and M. Herbst. 2015. 'Motion artifacts in MRI: A complex problem with many partial solutions', *J Magn Reson Imaging*, 42: 887-901.

Zalesky, Andrew, Alex Fornito, Luca Cocchi, Leonardo L. Gollo, Martijn P. van den Heuvel, and Michael Breakspear. 2016. 'Connectome sensitivity or specificity: which is more important?', *Neuroimage*, 142: 407-20.

Zeman, Janice Lillian, Michael Cassano, Cynthia Suveg, and Kimberly Shipman. 2010. 'Initial Validation of the Children's Worry Management Scale', *Journal of Child and Family Studies*, 19: 381-92.

Zeman, Janice, Kimberly Shipman, and Susan Penza-Clyve. 2001. 'Development and Initial Validation of the Children's Sadness Management Scale', *Journal of Nonverbal Behavior*, 25: 187-205.

Zeman, Janice, Kimberly Shipman, and Cynthia Suveg. 2002. 'Anger and Sadness Regulation: Predictions to Internalizing and Externalizing Symptoms in Children', *Journal of Clinical Child & Adolescent Psychology*, 31: 393-98.

Zhang, H., T. Schneider, C. A. Wheeler-Kingshott, and D. C. Alexander. 2012. 'NODDI: practical in vivo neurite orientation dispersion and density imaging of the human brain', *Neuroimage*, 61: 1000-16.

Zhang, Yu, and Marc A Burock. 2020. 'Diffusion tensor imaging in Parkinson's disease and parkinsonian syndrome: a systematic review', *Frontiers in Neurology*, 11: 1091.

Zuur, Alain F, Elena N Ieno, Neil J Walker, Anatoly A Saveliev, and Graham M Smith. 2009. *Mixed effects models and extensions in ecology with R* (Springer).